DURBAN UNIVERSITY OF TECHNOLOGY
INYUVESI YASETHEKWINI YEZOBUCHWEPHESHE

Metagenomic fingerprinting of waterborne enteric viruses and their inhibition using phyto-nanomaterials

Adedayo Ayodeji Lanrewaju

22172511

Submitted in fulfilment of the requirements for the degree of Doctor of Philosophy (PhD) in Biotechnology in the Department of Biotechnology and Food Science, Faculty of Applied Sciences, Durban University of Technology, Durban, South Africa.

Supervisor: Prof. Feroz Mahomed Swalaha

Co-supervisor: Dr Abimbola Motunrayo Folami

Co-supervisor: Prof. Saheed Sabiu

July 2025

DECLARATION

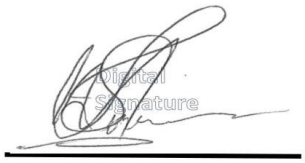
I, Adedayo Ayodeji Lanrewaju, hereby declare that this thesis titled "Metagenomic fingerprinting of waterborne enteric viruses and their inhibition using phyto-nanomaterials" submitted for the degree Doctor of Philosophy: Biotechnology at the Department of Biotechnology and Food Science, Faculty of Applied Science, Durban University of Technology is my original work and has not been previously submitted in any form to any other academic institution. The study presents original work by the author and all sources used or cited have been duly acknowledged. The research work described in the thesis was carried out in the Department of Biotechnology and Food Science, Durban University of Technology, Durban, South Africa, under the supervision of Prof. F. M. Swalaha, Dr A. M. Folami and Prof. S. Sabiu.



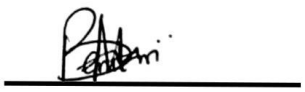
04/07/2025

A.A. Lanrewaju

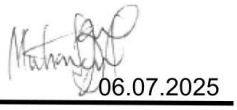
As the candidate's supervisors we agree to the submission of this thesis



Prof. F.M. Swalaha



Dr A.M. Folami



Prof. S. Sabiu

DEDICATION

I dedicate this work to the glory of God, the author of wisdom and the giver of every good and perfect gift.

In loving memory of my hero, my father, whose faith, strength, tutelage and unwavering belief in my potential continue to inspire me.

ACKNOWLEDGEMENTS

I am extremely grateful to my Supervisor, Prof. Feroz Mahomed Swalaha for your fatherly, supervisory and mentorship role and for ensuring that all resources needed for the research are made available. Thanks for all the lessons that extended beyond the laboratory.

I remain grateful to my co-supervisor, Dr Abimbola Motunrayo Folami, for your love, relentless support, invaluable guidance and encouragement.

I am very grateful to my co-supervisor, Prof. Saheed Sabiu, for your invaluable assistance, insightful suggestions, dedicated involvement, guidance and support throughout this study.

Altogether, your intellectual contributions and kind disposition towards me in all forms to ensure this degree is complete is quite appreciated. Thanks for believing in me all the way.

I extend my sincere gratitude to all the members of the Waterborne Pathogens Research Group and Computational and Systems Biology Research Group of the Department of Biotechnology and Food Science, Durban University of Technology, for their support and contributions at one time or another. I am indeed grateful to Dr Charlene Pillay for her friendly support and for always instilling confidence in me.

The lab technicians (Dr Adarsh and Mr Melvin), the lab assistants, the cleaners, and the postdoctoral fellows (Dr Alabi, Dr Kabange, Dr Ekundayo, Dr Balogun, Dr Aruwa, Dr Babalola, Dr Gyebi Dr Adedirin and Dr Mohammed).

I am exclusively grateful to Prof. Martins Nyaga of the University of the Free State next-generation sequencing unit (UFS-NGS-Unit) for the introduction and exposure to the NGS experience. Additionally, I would like to appreciate all the unit members for their support and training during my research visit to the UFS-NGS Laboratory. I am very thankful for the assistance and encouragement from Dr Ogunbayo, Dr Mogotsi, Ms. Sondlane, Ms. Shange, Ms Eyong and Ms Mpaxa while on the bench.

Special appreciation goes to my colleagues, including Happiness, Oga Jamiu, Vivian, Grace, Rukayat, Ayesha, Athika, Nosipho, Dweba, Halimah, Dunni, Betty, Abiola, Mordi, Naveen, Nikwando in the Department; your open doors, open hearts and willingness to help are duly appreciated.

I appreciate the Durban University of Technology for enabling a supportive research environment and the Department of Biotechnology and Food Science staff members. Furthermore, I would like to thank and acknowledge the Directorate of Research and Postgraduate Support for the Doctoral Scholarship awarded to me during my study.

My parents whose principles about life have been of great significance in my life. My Dad, your memory lingers on; your voice of encouragement echoes in my heart, reminding me never to give up. My mum, your love, faith, constant prayers, encouragement and sacrifices have sustained me; I remain grateful. May you live long in sound health, wealth and peace to enjoy the fruits of your labour.

My siblings and their families, your prayers, encouragements and support at every point of the research are duly acknowledged.

My in-laws, your support in all ramifications is also exclusively appreciated. You are the best.

At this juncture, it is imperative to convey my sincere and warmest gratitude to my dearest (Debola); your ever and uncommon accommodating love, care, endurance, understanding, and support are duly acknowledged and appreciated. Your prayers and encouragement lift my spirits and balance me throughout this journey. Thanks for holding the forth and having my back. May we live together till old age in good health and wealth, fulfilling purpose. To my daughter (Blessing), thank you for the joy and laughter you brought into our lives. We love you forever and ever…smiles.

RESEARCH OUTPUTS

Journal articles

LANREWAJU, A. A., ENITAN-FOLAMI, A. M., SABIU, S. & SWALAHA, F. M. 2024. Bioprospection for antiviral compounds from selected medicinal plants against RNA-dependent RNA polymerase of rotavirus A using molecular modelling and density-functional theory. *Chemical Physics Impact*, 9, 1-12. https://doi.org/10.1016/j.chphi.2024.100745

LANREWAJU, A. A., ENITAN-FOLAMI, A. M., SABIU, S. & SWALAHA, F. M. 2024. Computational bioprospection of selected plant secondary metabolites against VP7 (capsid protein) of rotavirus A. *Scientific African*, 23, 1-21. https://doi.org/10.1016/j.sciaf.2024.e02109

LANREWAJU, A. A., ENITAN-FOLAMI, A. M., NYAGA, M. M., SABIU, S. & SWALAHA, F. M. 2023. Cheminformatics bioprospection of selected medicinal-plant metabolites against trypsin-cleaved VP4 (spike protein) of rotavirus A. *Journal of Biomolecular Structure and Dynamics*, 42(20), 10652-10671. https://doi.org/10.1080/07391102.2023.2258405

LANREWAJU, A. A., ENITAN-FOLAMI, A. M., NYAGA, M. M., SABIU, S. & SWALAHA, F. M. 2023. Metabolite profiling and cheminformatics bioprospection of selected medicinal plants against the main protease and RNA-dependent RNA polymerase of SARS-CoV-2. *Journal of Biomolecular Structure and Dynamics*, 42(13), 6740-6760. https://doi.org/10.1080/07391102.2023.2236718

LANREWAJU, A. A., ENITAN-FOLAMI, A. M., SABIU, S. & SWALAHA, F. M. 2022. A review on disinfection methods for inactivation of waterborne viruses. *Frontiers in Microbiology*, 13, 1-19. https://doi.org/10.3389/fmicb.2022.991856

LANREWAJU, A. A., ENITAN-FOLAMI, A. M., SABIU, S., EDOKPAYI, J. N. & SWALAHA, F. M. 2022. Global public-health implications of human exposure to viral-contaminated water. *Frontiers in Microbiology*, 13, 1-18. https://doi.org/10.3389/fmicb.2022.981896

Conference papers (presented)

LANREWAJU, A. A., ENITAN-FOLAMI, A. M., SABIU, S. & SWALAHA, F. M. 2024. Computational bioprospection of selected plant secondary metabolites against VP7 (capsid protein) of rotavirus A. Oral presentation, *Computational and Systems Biology Conference 2024*, Coastlands Hotel, Durban, South Africa, 24–26 June 2024.

LANREWAJU, A. A., ENITAN-FOLAMI, A. M., SABIU, S. & SWALAHA, F. M. 2023c. Computational bioprospection of selected medicinal-plant metabolites against the main protease and RNA-dependent RNA polymerase of SARS-CoV-2. Oral presentation, *22nd Biennial Congress of the South African Society for Microbiology*, Stellenbosch, South Africa, 17–20 September 2023.

LANREWAJU, A. A., ENITAN-FOLAMI, A. M., SABIU, S. & SWALAHA, F. M. 2023d. Cheminformatics bioprospection of selected medicinal-plant metabolites against trypsin-cleaved VP4 of rotavirus A. Oral presentation, *56th Annual Conference of the South African*

Society for Basic and Clinical Pharmacology, Rhodes University, Grahamstown, South Africa, 24–27 August 2023.

LANREWAJU, A. A., ENITAN-FOLAMI, A. M., SABIU, S. & SWALAHA, F. M. 2023e. Cheminformatics bioprospection of selected medicinal-plant metabolites against VP1 (RNA-dependent RNA polymerase) of rotavirus A. Poster presentation, *14th African Rotavirus Symposium*, Abuja, Nigeria, 8–10 November 2023.

Academic awards during the study

1st Place Winner of the 2024 Three Minutes Flash Fact Competition of the Department of Biotechnology and Food Science

1st Position in the Oral Presentation Winners of the 2024 Computational and Systems Biology Conference

People's Choice Award Winner of the 2024 Computational and Systems Biology Conference

GENERAL ABSTRACT

Waterborne enteric viruses are major causes of diseases including gastroenteritis, hepatitis, encephalitis, meningitis, conjunctivitis, and respiratory disorders. Transmission occurs primarily through the faecal-oral channel via contaminated water or food, constituting significant public health risks. These viruses have been reported in South Africa following exposure to contaminated surface waters, dams, and wastewater. Nevertheless, limited data exist on their prevalence, diversity and abundance, especially in wastewater treatment plants (WWTPs) in eThekwini Municipality, Durban, KwaZulu-Natal, South Africa, necessitating metagenomic surveillance. In addition, the development of resistance to conventional drugs and high treatment costs necessitates the development of novel approaches to identify inexpensive and efficient antiviral medications. Interestingly, *Spondias mombin* and *Macaranga barteri* extracts have exhibited antiviral activity against several enteric viruses while *Dicerocaryum eriocarpum* with reported antibacterial activity remain unexplored as a reservoir of antiviral drug candidates. Accordingly, for the first time, this study profile the prevalence and diversity of viral families, including human and plant pathogenic viruses at the selected WWTPs and receiving rivers in eThekwini, Durban, Kwazulu-Natal, South Africa, using metagenomics next-generation sequencing (mNGS) approach and evaluates metabolites from *S. mombin*, *M. barteri* and *D. eriocarpum* against severe acute respiratory syndrome-coronavirus-2 (SARS-CoV-2) and rotavirus A (RVA) using *in silico* techniques.

The mNGS viral surveillance investigation identified viral families with a wide range of hosts including vertebrates (19.46%), plant (6.89%), insect (1.90%), fungal (0.13%), unclassified (7.25%) and phages (64.37%). Altogether, 30 viral families encompassing 26 different human pathogenic viral species were identified including enteroviruses, hepatovirus A, rotavirus A, norovirus, and astrovirus A. Conversely, plant viruses accounted for eight families dominated by the *Virgaviridae*. Most phytopathogenic reads belonged to the Tobamovirus genus, with additional representation from the family *Bromoviridae* detected across all sampling sites except RIVER4. These findings highlight the significance of wastewater surveillance in tracking known infections and unveiling possible emerging viral threats. RVA, one of the commonest waterborne enteric viruses detected in this study and SARS-CoV-2, although not detected in this study, probably due to low circulation within the communities at the time of sampling, were selected due to their clinical relevance and therapeutic limitations for *in silico* drug discovery from selected antiviral plants (*S. mombin, M. barteri* and *D. eriocarpum*).

Molecular docking identified top-ranked compounds with higher negative docking scores against SARS-CoV-2 and RVA targets from the 77 pooled metabolites identified from the three selected medicinal plants against each of the investigated targets [main protease and RNA-dependent RNA polymerase (RdRp)] of SARS-CoV-2 and RVA [capsid protein (VP7A, VP7C, VP7D), RdRp (VP1), spike protein (VP5*, VP8*)]. A minimum of three top-ranked compounds were subsequently identified owing to their physicochemical, pharmacokinetic and toxicological profiles suitable for drug development. The profiled top ranked compounds against the selected druggable targets of SARS-CoV-2 and RVA were subsequently subjected to 120-ns molecular dynamics (MD) simulations using the in-house HEAL1361 program with the Amber 18 package of the Centre for High Performance Computing (CHPC), South Africa.

At least three of the top-ranked compounds exhibited higher negative binding free energy across the evaluated targets, suggesting structural and thermodynamic compatibility of the ligands at the binding domain of the targets and their suitability for drug development thereby validating the antiviral potential of the selected medicinal plants. However, against SCMP, only quercetin 3-O-rhamnoside had a higher negative binding free energy, suggesting the need for optimization of other metabolites. Notably, chrysoeriol7-glucuronide and spiraeoside demonstrated broad-spectrum affinity for RdRp of SARS-CoV-2 and RVA. Furthermore, (2S)-6-(gamma,gamma-dimethylallyl)-3',4'-dimethoxy-6'',6''-dimethylpyran[2'',3'':7,8]flavanone (2SG) and sericetin had better broad-spectrum affinities for both RVA VP5* and VP8*, while 2SG, apigenin-4 ′-glucoside and gnetin L exhibited better broad-spectrum affinities for RVA VP7A, VP7C and VP7D, suggesting their potential as multitarget antiviral candidates. However, some compounds induce higher thermodynamic entropy within the proteins relative to the standard. For instance, against VP5*, 2SG (-20.98 kcal/mol, 1.88 Å), sericetin (-20.46 kcal/mol, 1.93 Å) and sacranoside (-16.96 kcal/mol, 1.50 Å), though having higher negative binding free energies, exhibited higher RMSD values compared to the standard (1.30 Å) and unbound VP5* (1.45 Å). A partly similar trend was illustrated against VP8*, where sericetin (-18.31 kcal/mol, 1.27 Å) and 2SG (-20.98 kcal/mol, 1.18 Å) exhibited higher negative binding free energies yet had higher RMSD and RMSF values respectively, compared to the standard (1.19 Å, 1.01 Å). This observation highlights the need for optimizing these leads to improve their thermodynamic stability while boosting their affinity for the target proteins. Thus, due to their critical role in viral entry and infection, silver complexation optimization was limited to VP5* and VP8* of RVA to block the first and most vulnerable stage of infection. Accordingly, the silver complexation approach was employed to model possible silver nanoparticle conjugates for each lead compound, treating the compound as the reducing and capping agent. Thereafter, the effect of the complexation was evaluated whether complexation of the lead compound with silver enhances their binding affinity *in silico*.

Improved binding affinity enhances drug activity through silver complexation which help mitigate drug resistance, broaden activity spectrum and enhance potency *in vitro* and *in vivo*. Thus, the study adopted silver complexation approach by conjugating silver with identified lead compounds against VP5* and VP8* via *in silico* modelling to achieve improved activity, reduced toxicity and maintain favorable pharmacokinetic profiles. To comprehend the effect of the complexation, quantum chemical calculations (density functional theory) were used to compare the molecular features of the silver-complexed leads against the lead compounds alongside assessment of drug-likeness and toxicity profiles. Thereafter, 12 and 19 silver-complexed leads were docked against VP5* and VP8* respectively, followed by comparative interaction analysis between lead and silver-complexed compounds. Notably, the silver-complexed leads exhibited enhanced molecular properties, suggesting better reactivity than their corresponding lead compounds without significantly altering their pharmacokinetic properties and toxicity profiles; hence, they remain suitable for drug development. Remarkably, higher negative docking scores were observed in all silver-complexed leads docked against VP5* compared to their corresponding lead compounds, except in the sacranoside A series. Conversely, lower negative docking scores were reported in the apigenin-4'-glucoside series,

gnetin L A-E, and sericetin B relative to their lead compounds, while the remaining silver-complexed leads exhibited improved binding affinity. Comparative interaction analysis identified 2SGC (-6.59 kcal/mol) and 2SGA (-6.77 kcal/mol) against VP5* and 2SGC (-8.06 kcal/mol) and SERA (-7.26 kcal/mol) against VP8* as promising candidates. Further computational investigation, including MD simulation, is recommended to elucidate the thermodynamics profile of the resulting protein and silver-complexed leads. Summarily, the observed enhanced binding capability of the silver-complexed leads could be attributed to their higher reactivity and increased interactions with essential amino acids at the binding pocket of the targets investigated. To validate the therapeutic potential of the profiled silver-complexed leads in combating viral infections, complementary *in vitro* and *in vivo* studies are strongly recommended.

Keywords: Antiviral drug candidates; Metagenomics; Molecular docking; Molecular dynamics simulation; Pathogenic viruses; Public health; River; Rotavirus A; Silver complexes; Wastewater surveillance

TABLE OF CONTENT

DECLARATION.....i

DEDICATION.....ii

ACKNOWLEDGMENTS……iii

RESEARCH OUTPUTS.....v

GENERAL ABSTRACT.....viii

CHAPTER ONE

1.0 General introduction……..1

1.1 Introduction…….…2

1.1.1 Detection of viruses in wastewater……..…4

1.1.2 Waterborne viral diseases……...7

1.1.3 Antiviral potentials of medicinal plants……10

1.1.4 *In silico* approaches in drug discovery and development…….……..11

1.1.5 Nanotechnology as a tool in enhancing potency and lead molecule delivery……..…..14

1.2 Research problem and justification…….……16

1.3 Aim and objectives…….…….18

1.4 Thesis outline…….…….19

References…….…….....20

CHAPTER TWO

2.0 Literature Review…….……40

2.1 Introduction……....41

2.2 A review on disinfection methods for inactivation of waterborne viruses ……..……...…….46

2.3 Global public health implications of human exposure to viral contaminated water……...…….…….……65

2.4 Unravelling viral diversity in wastewater treatment plants through metagenomics: An overview……...…….……...83

2.5 An overview of the advancements in antiviral drug discovery and development ……..…….....145

References…….…….....226

CHAPTER THREE

3.0 Viral landscape of selected wastewater treatment plants and receiving river in eThekwini Municipality, Durban, South Africa: A metagenomic approach……....231

CHAPTER FOUR

4.0 Metabolite profiling of selected medicinal plants and identification of lead compounds against selected druggable targets of SARS-CoV-2 and rotavirus A using computational techniques……..288

4.1 Introduction……..……289

4.2 Metabolites profiling and cheminformatics bioprospection of selected medicinal plants against the main protease and RNA-dependent RNA polymerase of SARS-CoV-2…….…….....293

4.3 Computational bioprospection of selected plant secondary metabolites against VP7 (capsid protein) of rotavirus A……..…….…….....…315

4.4 Bioprospection for antiviral compounds from selected medicinal plants against RNA polymerase of rotavirus A using molecular modelling and density functional theory……...……..…….....337

4.5 Cheminformatics bioprospection of selected medicinal plants metabolites against trypsin cleaved VP4 (spike protein) of rotavirus A..……...……350

References…….…….....372

CHAPTER FIVE

5.1 Computational bioprospection of silver-complexed leads against trypsin-cleaved spike protein of rotavirus A……..……...……...376

CHAPTER SIX

6.0 General discussion, conclusion and recommendations……....428

6.1 General discussion……..…..429

6.2 Conclusion and recommendation…….……..……...439

References…….…….....443

CHAPTER ONE

1.0 General introduction

1.1 Introduction……..….2

1.1.1 Detection of viruses in wastewater……..…4

1.1.2 Waterborne viral diseases……...7

1.1.3 Antiviral potentials of medicinal plants……11

1.1.4 *In silico* approaches in drug discovery and development…….…….12

1.1.5 Nanotechnology as a tool in enhancing potency and lead molecule delivery……..…..15

1.2 Research problem and justification…….……17

1.3 Aim and objectives…….…….19

1.4 Thesis outline…….…….20

Reference…….…….....21

1.1 Introduction

The provision of adequate and uncontaminated drinking water has continued to be a difficult task globally (Soller *et al*., 2019; Kaushal, 2016; Roberson, 2011). Although waterborne bacterial contaminants are routinely monitored, viruses are a persistent danger to human health that cause many infections, making them a significant concern among other water contaminants (Gerba *et al*., 2017; Fenwick, 2006). Insufficient sewage treatment and low standards of cleanliness significantly increase the risk of drinking contaminated water, which may subsequently result in human diseases. For instance, since late 2019, the emergence of COVID-19, caused by the severe acute respiratory syndrome-coronavirus-2 (SARS-CoV-2), has rapidly expanded worldwide, putting all nations and territories in danger of infection (Lu *et al*., 2020). Initially, the virus was mainly transmitted through contact with surfaces and inhalation of viral droplets and aerosols (Deng *et al*., 2020); however, the viral fragments have been detected in faeces (Van Doremalen *et al*., 2020) and water (La Rosa *et al*., 2020) raising concerns about their transmission via wastewater (WW).

Numerous pathogens, including bacteria, fungi, protozoans, toxins and viruses are prevalent in WW, a biologically diverse environment. Waterborne enteric viruses, which are mostly spread by the faecal-oral channel, either through direct contact between individuals or by consuming contaminated water or food, may provide a significant health risk to both workers at wastewater treatment plants (WWTPs) and the surrounding community (Stobnicka-Kupiec *et al*., 2022; Diaz, 2006). Enteric viruses enter WW systems from waste, faeces, vomit and urine of infected humans through infiltration and inflow (Bosch *et al*., 2006; Diaz, 2006). These viruses may be shed in very high numbers from the faeces of infected individuals (Upfold *et al*., 2021) and have been reported to subsist for an extended period in aquatic environments under a wide

range of pHs and temperatures (Sánchez and Bosch, 2016), and could exhibit resistance to the traditional disinfection techniques (Bleotu *et al*., 2024).

Different factors such as the water constituents, temperature and light exposure impact the viability of viruses in water. Precisely, ultraviolet light (UV) and temperature are important environmental elements that greatly impact the ability of viruses to survive in water, as sunlight exposure speeds up the process of inactivating viruses, while colder temperatures may extend their survival (Pinon and Vialette, 2019; Rzeżutka and Cook, 2004). Enteric viruses include non-enveloped viruses such as rotavirus (RV) and exhibit resistance to disinfection, including UV treatment, which is attributed to its structure, especially the double-stranded RNA and three-layered capsid protein (Li *et al*., 2009). Conversely, enveloped viruses are vulnerable to inactivation in WW relative to non-enveloped viruses as their lipid viral envelope or surface proteins become easily compromised due to the presence of solvents, detergents and disinfectants in WW (Paul *et al*., 2021). SARS-CoV-1, an enveloped virus, demonstrated persistence in raw sewage for two days at 20°C and 14 days at 4°C (Wang *et al*., 2005a; Wang *et al*., 2005b). Furthermore, Yang *et al*., (2022) reported that SARS-CoV-2 could persist in WW for about 17 days at 4°C and for 8 days at 26°C, suggesting that SARS-CoV's could persist in WW for about two weeks at lower temperatures. Different techniques adopted at WWTPs for viral removal include adsorption, sedimentation (Verbyla and Mihelcic, 2015), retention by membrane and biofilm layers, predation and enzymatic degradation within membrane bioreactors (Chaudhry *et al*., 2015), and inactivation through disinfection methods such as UV light, ozonation and chlorination (Xagoraraki *et al*., 2014), which is the commonest (Lanrewaju *et al*., 2022b).

Double-stranded viruses such as human adenovirus (HAdV), reovirus and RV have exhibited greater resistance to UV radiation compared to single-stranded viruses (Calgua *et al*., 2014; Li *et al*., 2009; Harris *et al*., 1987) and this could be due to their abilities to repair genomes during replication inside the host cells (Beck *et al*., 2014). Also, this increased resistance might be attributed to the double stranded genome structure allowing for effective repair of UV-induced damage as the complementary strand functions as a template for accurate repair during replication to replace lesions caused by UV radiation like pyrimidine dimers on one strand (Rastogi *et al*., 2010). In addition, viral adsorption onto solids aids in their removal from WW; nevertheless, it also prevents the viral particles from inactivation to a certain extent (Corpuz *et al*., 2020; Hejkal *et al*., 1981). Therefore, the occurrence of viruses in WW could differ based on factors such as geographical and climatic conditions, degree of development, population health status, and WW treatment techniques (Bleotu *et al*., 2024).

1.1.1 Detection of viruses in wastewater

Surveillance of pathogenic viruses in WW is used to monitor the prevalence of enteric viruses within a community and to forecast disease outbreaks via a concept referred to as wastewater-based epidemiology (Zahedi *et al*., 2021). This concept is based on the examination of community WW as an indicator of public health conditions. WW analysis is analogous to the collection and examination of urine and faecal samples within a community (Zahedi *et al*., 2021). Monitoring temporal variations in viral concentration and variety discharged in community WW and evaluation of metabolites and biomarkers facilitates the early detection of outbreaks shortly before the onset of an outbreak. Furthermore, meticulously structured geographical sampling facilitates site identification where an epidemic could begin and spread (Xagoraraki and O'Brien, 2020). Therefore, viral identification and quantification from WW is a crucial procedure for managing water quality and controlling the transmission of viral

infections (Dos Santos *et al*., 2024) with different techniques of detection based on the available technology and objectives of the investigation.

The common procedures of viral detection in WW entail sample collection from the WW source followed by concentration of viruses owing to the low viral content in WW (Zhang *et al*., 2022). The next step is viral nucleic acid extraction using methods like precipitation or mechanical resuspension and analysis of the extracted viral particles through specific techniques to characterize and quantify viral types with either polymerase chain reaction (PCR) or cell culture to determine viral infectivity (Haramoto *et al*., 2018). Thus, result interpretation can provide insights into the occurrence, concentration and types of viruses in WW (Bleotu *et al*., 2024).

Globally, viruses including hepatitis A viruses (HAV), adenoviruses (AdVs), astroviruses (AstVs), noroviruses (NVs), enteroviruses (EVs), rotaviruses (RVs), Aichi viruses (AiVs) and bacteriophages have been identified in different water matrices (Lanrewaju *et al*., 2022a; Chen *et al*., 2021; Corpuz *et al*., 2020). Specifically in South Africa, these viruses have been reported in surface waters (Altintas *et al*., 2015), treated effluent (Sibanda and Okoh, 2013; Okoh *et al*., 2010) and raw sewage (Onosi *et al*., 2019). Generally, PCR-based techniques have been preferred relative to other conventional identification techniques as a standard molecular technique for viral detection because of their short detection time and high sensitivity as it does not require cell culturing and are more effective. Unfortunately, PCR-based methods are often vulnerable to inhibitory substances, do not distinguish between infectious and non-infectious viruses and have limited capability in providing insights into the viral diversity or novel pathogens discovery within an ecosystem (Haramoto *et al*., 2018). Globally, the advent of

metagenomics next-generation sequencing (NGS), a high-throughput sequencing technique has transformed the use of molecular approaches for understanding intricate microbial communities (Garner *et al*., 2021).

Evaluating bacterial population diversity by metagenomics is simple because bacteria possess a common gene, 16S rRNA, which can be sequenced for phylogenetic analysis (Azaroual *et al*., 2022; D'Amore *et al*., 2016). Conversely, viruses do not uniformly share conserved genes, complicating the assessment of indices for viral population genetic diversity. Random amplification and high throughput sequencing accompanied by suitable bioinformatic analysis could significantly overcome these drawbacks, providing a chance to enhance the translatability of WW monitoring techniques (Li *et al*., 2024). Thus, high-throughput sequencing approaches have been efficient in elucidating environmental viromes (Breitwieser *et al*., 2019), as they enabled the concurrent identification of several viruses, both DNA and RNA, without bias towards specific genes; it also delineates the total microbial domain composition, functional analysis and potential pathogen characterization (Osunmakinde *et al*., 2021). For instance, Guajardo-Leiva *et al*., (2020) employed viral metagenomics to obtain a snapshot of the RNA virosphere in the WW of Santiago de Chile, America. Despite the predominance of dsRNA, they reported that RNA virosphere in Santiago's sewage mostly consisted of unidentified sequences (88%), while recognized viral sequences were primarily composed of bacteriophages (60%), invertebrate viruses (37%) and human viruses (2.4%). In addition, three new genogroups within the *Picobirnaviridae* family were identified, and this potentially addresses significant gaps in the evolutionary history of this taxon. Furthermore, they illustrated the prevalence of emerging RV genotypes, including G8 and G6, that have replaced other classical genotypes, which is in tandem with clinical data (Guajardo-Leiva *et al*., 2020).

Furthermore, the viral phytopathogen diversity in WW, freshwater and sludge from the southernmost tropical region in Mexico was studied by Lopez-Roblero *et al*. (2024) using a metagenomic approach. They identified 15 distinct phytopathogenic viruses under the family *Virgaviridae*, genus Tobamovirus, with the highest number of reads in pepper mild mottle virus, tomato brown rugose fruit virus and tropical soda apple mosaic virus. Notably, the large variety of phytoviruses in WW and rivers, together with their potential infectivity, raises concerns about the use of polluted freshwater and WW for agriculture in Mexico (Lopez-Roblero *et al*., 2024). Unfortunately, most studies conducted in South Africa over the years have concentrated primarily on the identification and surveillance of specific human pathogenic viruses and bacteriophages in WW and various environmental matrices via molecular methods thus, many of these investigations lack information on the diversity, functional analysis and insights on unknown pathogenic viruses (Osunmakinde *et al*., 2018; Osuolale and Okoh, 2017; Bolger *et al*., 2014; Ikner *et al*., 2011). Hence, there is a need to assess the various viral families, genetic diversity, plant, animal and waterborne enteric viruses at the different WWTPs in South Africa, which could be of public health importance. In this study, four WWTPs in the eThekwini Municipality (Durban, KwaZulu-Natal, South Africa) were assessed, including Amanzimtoti (mixed domestic and industrial influent) and Isipingo, Kingsburgh, and Shallcross (predominantly domestic influent). All plants operate activated sludge systems with chlorinated effluent discharge.

1.1.2 Waterborne viral diseases

The detection of these viruses in the treated effluent of WWTPs discharged into surrounding waters demonstrated their resistance to standard disinfection processes (Lanrewaju *et al*., 2022b) and further renders viral enteric infection a public health issue. Waterborne enteric viruses may cause several diseases, especially diarrhoea, which ranks as the third highest cause

of death in children under five years, with an annual mortality of approximately 443,832 primarily due to contaminated food and water sources (World Health Organization, 2024).

Although four WHO-approved vaccines are currently available, RV infection is the predominant cause of diarrhoea-related morbidity and mortality in children under the age of five. Specifically, RV infection has been associated with about 258 million diarrhoea cases and, consequently, 128,500 fatalities among children below five years globally in 2016 (Troeger *et al*., 2018). Also, EVs have infected millions of individuals globally and have been responsible for the irregular outbreak of illnesses in both developed and developing countries (Puenpa *et al*., 2019; Cassidy *et al*., 2018; Smuts *et al*., 2018; Lugo and Krogstad, 2016). Furthermore, NV is also a known cause of acute gastroenteritis, infecting about 685 million people and killing roughly 200,000 people annually, thus costing society about $60 billion globally (Giancotti *et al*., 2019; Lopman *et al*., 2016). Despite its public health significance, the mainstay for electrolyte imbalance and dehydration reversal associated with the infection is supportive care because no effective vaccine for NV has been developed yet (Dos Santos *et al*., 2024; Robilotti *et al*., 2015).

In 2015, about 1.34 million fatalities were linked to viral hepatitis, with 0.8% and 3.3% of deaths attributed to hepatitis A and E, respectively. Besides the faecal-oral transmission route for HAV infection prevalent in developing countries, most HAV outbreaks in developed countries have been linked to person-to-person contact (Migueres *et al*., 2021, Abutaleb and Kottilil, 2020). In addition, more than 150 million infections have been estimated to occur yearly (Van Damme *et al*., 2023) despite the implementation of vaccines for the prevention of infection.

Several illnesses, including pneumonia, respiratory tract infections, conjunctivitis, hemorrhagic cystitis, nephritis or meningoencephalitis and gastroenteritis, have been linked to human adenovirus (HAdV) (Huang *et al*., 2021). Another important cause of acute viral gastroenteritis is the human astrovirus and a common cause of diarrhoea in children (Lu *et al*., 2021; Bányai *et al*., 2018). In addition, they have been connected with central nervous system infections in humans, especially in immunocompromised individuals (Koukou *et al*., 2019; Cordey *et al*., 2016). While RV, NoV, AdV and AstV have been documented as the principal agents of gastroenteritis transmitted via water and food, AiV has recently emerged in association with gastroenteritis outbreaks linked with contaminated food and water (Rivadulla and Romalde, 2020, Yamashita *et al*., 2000). Regrettably, there are few broad-spectrum antiviral therapeutics available to manage diseases caused by enteric viruses (Gall *et al*., 2015).

All the highlighted viruses are pathogenic; however, this study will focus on identifying inhibitors for two viruses (SARS-CoV-2 and RVA) because of their public health importance. Since the emergence of the novel SARS-CoV-2 responsible for COVID-19 in December 2019, which became a global pandemic in a few months, over 776 million cases and more than 7 million fatalities have been reported globally as of September 15, 2024 (WHO, 2024). While WHO approved vaccines have been introduced, no vaccine offers 100% effectiveness (Vardhan and Sahoo, 2022). Unfortunately, no specialized drug has been approved yet for the treatment of COVID-19.

Furthermore, the RVA strain, being one of the three RV groups that could infect humans, is the leading cause of diarrhoea in children below the age of five (Kim *et al*., 2021), with a mortality rate of about 130 000 in 2016 globally (Troeger *et al*., 2018). Currently, four WHO pre-

qualified oral vaccines are in use, with effectiveness estimated to be 50-90% in preventing severe diarrhoea and with moderate efficacy in low-income nations (Troeger *et al*., 2018). Similar to SARS-CoV-2, there is no FDA-approved medication for the treatment of RVA-induced diarrhoea; hence, prioritizing the development of compounds that could be further developed as antiviral drugs against these viruses is a global imperative.

1.1.3 Antiviral potentials of medicinal plants

Medicinal plants have been used as treatment options for numerous diseases for centuries, and consequently, many drugs are either plant-derived natural products or their derivatives (Newman and Cragg, 2012). Historically, plants have been utilized for the management of diarrhoea and accompanying symptoms (Rawat *et al*., 2017; Semenya and Maroyi, 2012). Unfortunately, there are several reports of new viral illnesses (Kapoor *et al*., 2017) and have escalated into a principal global public health concern (Chen and Huang, 2018) owing to the propensity of viruses to become drug-resistant (Mohammadi Pour *et al*., 2019; Zitzmann and Kaderali, 2018). Developing effective antiviral therapies has become cumbersome in recent years because viruses can mutate their genome rapidly (Irwin *et al*., 2016). Interestingly, plants generate an extensive array of structurally diverse secondary metabolites with multiple functions; these metabolites have evolved for distinct biological roles and possess significant molecular scaffolds in plants, which make them useful for drug discovery (Grigalunas *et al*., 2020; Rodrigues *et al*., 2016). Plant metabolites have demonstrated potent antiviral activity (Kang *et al*., 2021, Li *et al*., 2020, Xu *et al*., 2020) and can be used with pre-existing medicines, as well as other delivery modalities, to improve antiviral efficiency and bioavailability (Kapoor *et al*., 2017).

Spondias mombin, commonly called hog plum, amra or cajazeira is of the family Anacardiaceae and has been used traditionally to treat cold sores, mouth inflammation, conjunctivitis, diarrhoea and dysentery as it is equally used to relieve stomach pain and treat wounds (Ayoka *et al*., 2008; De Albuquerque *et al*., 2007). Furthermore, the antiviral activity of *S. mombin* leaves against Coxsackie B2 and Herpes simplex type 1 has been demonstrated *in vitro* (Siqueira et al., 2020; Corthout et al., 1991). Similarly, *Macaranga barteri* (Agbasa or Aarasa) is another important plant belonging to the family Euphorbiaceae which has been used traditionally to treat cold sores, anaemia, bronchitis, cancer, cough, diabetes, fever, gonorrhoea, wounds, and diarrhoea linked to viruses, bacteria, or parasitic worm infestations (Segun *et al*., 2019; Ogbole *et al*., 2018; Segun *et al*., 2018). In addition, the antiviral activity of *M. barteri* extracts against Echoviruses E7 and E9 has been reported (Ogbole *et al*., 2018). Specifically, Vedelianin and Schweinfurthin compounds isolated from *M. barteri* exerted antiviral activity against Echoviruses E7 and E19 (Segun *et al*., 2019). Furthermore, *Diceriocaryum eriocarpum* (Devil's thorn) is a multipurpose plant with diverse ethnomedicinal benefits such as in wound care, retained placenta expulsion, antibacterial and anti-inflammatory ability (Luseba *et al*., 2007), abdominal pains (Du Preez and Mumbengegwi, 2014) and ethnoveterinary benefits (Van der Merwe *et al*., 2001). Due to the reported traditional use and antiviral properties of these plants, they may harbour essential bioactive metabolites that could be identified and developed against SARS-CoV-2 and RVA.

1.1.4 *In silico* approaches in drug discovery and development

The conventional drug discovery pipeline is a very expensive, risky and time-consuming procedure which could take about 15 years and almost US$2 billion (Doytchinova, 2022), with a high attrition rate (Waring *et al*., 2015) owing to poor drug efficacy and suboptimal drug absorption, distribution, metabolism, excretion and toxicity (ADMET) challenges (Giri and

Bader, 2015). Clinical trials have been acknowledged to be the costliest aspect of drug development; nevertheless, most time and cost-saving potentials are embedded in the early discovery and pre-clinical phases (Sadybekov and Katritch, 2023). Thus, emerging technologies, including modern and advanced high-throughput drug screening techniques, are being employed to mitigate the expenses, duration of drug discovery and the risk of failure (Berdigaliyev and Aljofan, 2020).

One of such technology is computer-aided drug design (CADD), which employs computer-based methods to identify, develop and assess active compounds with optimum druggability features. The major components of CADD include homology modelling, molecular docking, virtual screening, quantitative structure-activity relationship and three-dimensional (3D) pharmacophore mapping (Surabhi and Singh, 2018, Hassan Baig *et al*., 2016). Among the virtual screening techniques, molecular docking has become one of the most commonly used tools, especially in the structure-based approach (Liu *et al*., 2017), to predict a ligand's bound conformation at the binding domain of the protein. Nevertheless, molecular docking is ladened with limitations, including flexibility challenges, potential uncertainties in experimental structures in specific contexts, pseudo-positive binding conformations, constraints in precisely quantifying hydrogen bonds, directional interactions and the confounding effects of solvent and entropy (Kitchen *et al*., 2004, Taylor *et al*., 2002).

Accordingly, molecular dynamics simulation has been adopted as an advanced approach to complement molecular docking as it is mostly used to evaluate and corroborate the protein-ligand complex docking result, determine their stability, fluctuation rates, interatomic interactions and binding free energies (Menchon *et al*., 2018). For example, Uhomoibhi *et al*.,

(2022) used MD simulation to shed light on the mechanism responsible for the modulatory impact of metabolites from selected medicinal plants against the druggable targets of SARS-CoV-2. They reported higher affinity of the lead metabolites against the investigated proteins relative to the standard drugs coupled with their ability to form stable complexes upon binding to the proteins. Similarly, Aribisala *et al*., (2022) identified broad-spectrum plant secondary metabolites against spike proteins of the SARS-CoV-2 wild-type and omicron variants with better affinity compared to zafirlukast (standard drug). Except for kaempferol-7-glucoside, the top-ranked metabolites were shown to be thermodynamically stable with the spike proteins of both variants.

The least common method used to complement virtual screening is the density functional theory (DFT); however, this method is the most common and extensively used quantum theory technique for calculating the electronic properties such as lowest unoccupied molecular orbital (LUMO) and highest occupied molecular orbital (HOMO) of drug molecules and drug delivery systems (Sabe *et al*., 2021). This technique offers insight that molecular modelling cannot achieve, especially in describing the mechanism of reactions between drug molecules and receptor's binding sites. Consequently, DFT effectively interprets pharmacological properties and their inhibitory effects on therapeutic targets (Ye *et al*., 2022). The optimized geometry, which offers essential structural insights into the relaxed structure of drug molecules and their binding to the receptors in addition to the energy calculations derived from DFT, has been described across numerous studies (Rasool *et al*., 2021; Bui *et al*., 2020; Hagar *et al*., 2020).

About 40-80% of drug candidates are often excluded from further assessments at the pre-clinical stage due to ADMET issues (Myung *et al*., 2024; Kennedy, 1997). To access their

biological targets and produce therapeutic activity, drug molecules must traverse several physiological barriers, including the gastrointestinal barrier, blood-brain barrier and microcirculatory barriers. In the process, they could be altered to be activated or transformed into toxic substances with unfavourable outcomes (Gardiner and Begg, 2006). Nonetheless, conventional ADMET evaluation methods remain arduous and expensive (Shaker *et al*., 2021). SwissADME is an online web tool that has been used to predict the physicochemical and pharmacokinetic parameters (Daina *et al*., 2017), while protox-II has been used to predict various toxicity endpoints of drug molecules (Banerjee *et al*., 2018). In a bid to lessen the financial burden and timeframe of drug discovery and development and importantly, minimize candidate failure, lead optimization has been proposed as an approach for correcting identified defects (Barcelos *et al*., 2022). Recently, Machine Learning (ML) techniques have emerged as a complementary to conventional CADD techniques, especially in domains like protein structure prediction, virtual screening, and ADMET modeling (Vamathevan *et al*., 2019; Chen *et al*., 2018). Methods like AlphaFold and RoseTTAFold have shown significant progress in structural biology (Baek *et al*., 2021; Jumper *et al*., 2021). However, the present study focuses on established structure-based and ligand-based computational techniques that are widely utilized and validated in the drug discovery process.

1.1.5 Nanotechnology as a tool in enhancing potency and lead molecule delivery

Recently, nanotechnology has shown significant progress in the fight against viruses. Nanoscale particles have been used as antiviral agents owing to their physical (plasmonic resonance, fluorescence enhancement, similar size, surface roughness, surface charge) and chemical (catalytic activity augmentation, generation of reactive oxygen species) properties arising from a large surface area to volume ratio (Hussain *et al*., 2022; Ratan *et al*., 2021; Singh *et al*., 2017). Precisely, increasing microbial resistance against metal ions, antibiotics, and an

upsurge of resistant strains attracted scientists to metallic nanoparticles as a viable option, which have an enormous surface area to volume ratio (Hamouda, 2012).

Among metallic nanoparticles, silver nanoparticles (AgNPs) are the most intensively researched due to their remarkable broad-spectrum efficacy. Their size ranges between 10-100 nm and are characterized by distinctive physicochemical features such as size, shape, optical activity, electrical conductivity and large surface area. Plant-mediated AgNPs are safe, eco-friendly, cost-effective, rapidly synthesized and are good reducing, stabilizing and capping agents; thus, green synthesis of AgNPs is beneficial relative to the chemical and physical methods of synthesis (Jain *et al*., 2021). The antiviral activity of AgNPs against different viruses including feline coronavirus (FCoV) (Chen *et al*., 2016), Influenza virus (Kim *et al*., 2020), HIV (Elechiguerra *et al*., 2005), AdV (Chen et al., 2013), HSV (Hu *et al*., 2014), Dengue virus (Sujitha *et al*., 2015), Chikungunya virus (Sharma *et al*., 2019), NVs (Bekele *et al*., 2016), bovine Herpesvirus (El-Mohamady *et al*., 2018), Human parainfluenza virus type 3 (Gaikwad *et al*., 2013) have been reported.

Interestingly, bioactive metal ions may be combined with organic ligands to optimize their activity while preventing drug resistance, increasing their activity via synergism, broadening the range of action and decreasing the necessary doses number *in silico* (Kucuk *et al*., 2022). As a result, the expense of producing such medications and the possibility of adverse side effects may be reduced (Rizzotto, 2012). Previously, different metal complexes have been derived by combining organic ligands with different metal ions, including zinc, nickel, cobalt, iron, manganese and silver (Veena *et al*., 2024; da Silva *et al*., 2022; Kucuk *et al*., 2022), followed by computational investigations into their binding affinity via molecular docking

studies and molecular dynamics simulation accompanied with quantum chemical calculations to determine their molecular and electronic properties.

Silver is a broad-spectrum microbicide with significant pharmacological efficacy against challenges encountered in disease therapy; hence, there is strong interest in designing novel silver complexes (Kucuk *et al*., 2022). Considering the foregoing, for the first time, this study evaluated the viral diversity and abundance at the Amanzimtoti, Isipingo, Shallcross, and Kingsburgh WWTPs in Durban, South Africa using the NGS technique. Monitoring the selected WWTPs will provide a detailed understanding of the various viral families, plants, animals, and waterborne enteric viruses circulating within the WWTPs and could be of public health importance. Also, for the first time, the modulatory potential of the metabolites of the selected medicinal plants (*S. mombin*, *M. barteri*, and *D. eriocarpum*) was evaluated against selected druggable targets of SARS-CoV-2 (main protease and RNA dependent RNA polymerase) and RVA (spike protein, capsid protein and RNA dependent RNA polymerase) using computational techniques. Furthermore, the resulting lead compounds were complexed with silver metal to determine their combined antiviral potential against the druggable targets of SARS-CoV-2 and RVA *in silico*. Evaluating the antiviral ability of medicinal plants' metabolites complexed with silver metal via computational techniques will facilitate the identification of antiviral candidates for further *in vitro* and *in vivo* studies and subsequent development as novel antiviral drugs.

1.2 Research problem and justification

Waterborne enteric viruses are recognised as causative agents of many infections, such as gastroenteritis and hepatitis, among others (Bouseettine *et al*., 2020), which have been reported

in South Africa following exposure to contaminated surface waters, dams, and WW (Mans *et al*., 2014; Mans *et al*., 2010). Nevertheless, there is limited data on the prevalence, distribution, diversity and abundance of enteric viruses (Pang *et al*., 2019), especially WWTPs in eThekwini Durban, KwaZulu-Natal, South Africa. The persistence of these viruses in treated WW implies that treatment processes reduce but do not eliminate viral loads (Rusiñol *et al*., 2015), thus emphasizing the need for regular monitoring of viral communities. Due to the constraints of current molecular approaches which target specific viruses, advances in NGS now enable comprehensive metagenomic identification of known and novel viral genomes across diverse environmental matrices (Osunmakinde *et al*., 2021; Bibby *et al*., 2019; Haramoto *et al*., 2018).

Furthermore, viral infections are often self-limiting in healthy individuals but could lead to high morbidity in children below five, the aged, immunocompromised individuals and pregnant women, thus making surveillance of enteric viral diseases important for these groups. Only a limited range of broad-spectrum antiviral therapeutics is available for the treatment of these diseases (Gall *et al*., 2015). Regrettably, viral drug resistance and genomic variability further complicate the development of effective antiviral treatments (Mohammadi Pour *et al*., 2019; Chen and Huang, 2018; Zitzmann and Kaderali, 2018). To make matters worse, conventional drug discovery pipelines are constrained by high costs, labour demands and time requirements, although these limitations can be mitigated via computational approaches (Diakou *et al*., 2022). Thus, the development of novel, effective and cost-efficient therapeutics against enteric viral diseases remains a global priority.

Interestingly, bioactive plant secondary metabolites have demonstrated antiviral potential and can be integrated with existing therapeutic approaches to improve efficacy and bioavailability (Kapoor *et al*., 2017). Therefore, this study offers insights into the diverse viral families,

diversity of human and plant pathogenic viruses prevalent at the selected WWTPs in eThekwini Durban, KwaZulu-Natal, South Africa. In addition, this study forms part of the continuing efforts to develop antiviral drug candidates against selected enteric viruses (SARS-CoV-2 and RVA).

1.3 Aim and objectives

Aim

The overall aim of the study was to profile the metagenomic fingerprints of waterborne enteric viruses in selected WWTPs in eThekwini Municipality, Durban, South Africa and to evaluate the inhibitory potential of bioactive compounds and silver-complexed leads against selected viral pathogens using computational methods.

The specific objectives are:

- To assess the virome diversity in Amanzimtoti, Isipingo, Shallcross and Kingsburgh WWTPs and receiving rivers samples within the eThekwini Municipality, Durban, KwaZulu-Natal, South Africa using the Illumina Miseq NGS technique.
- To determine the phytochemical fingerprint of three selected plant (*S. mombin*, *M. barteri*, and *D. eriocarpum*) extracts using liquid chromatography-mass spectrometry (LCMS).
- To determine the modulatory potential of the bioactive compounds of the selected plants against the druggable targets of SARS-CoV-2 (main protease and RNA dependent RNA polymerase) and RVA (spike protein, capsid protein and RNA dependent RNA polymerase) and their pharmacokinetics properties using computational methods.

- To determine the antiviral potential of silver-complexed leads against (spike protein) of RVA *in silico*.

1.4 Thesis outline

The thesis is organized into six chapters, and the first chapter starts with a general introduction, the aim and objectives of the study and the outline of the thesis. Subsequent chapters (one to five) comprise contributions in the form of published articles and manuscripts that will be submitted for publication. Specifically, chapter two is a comprehensive literature review organized into four sections. To begin with, it surveys disinfection methods for the inactivation of waterborne viruses and examines the global public health implications of human exposure to viral contaminated water. Thereafter, it highlights the viral diversity in WWTPs profiled using metagenomics and reviews recent advancements in antiviral drug discovery and development. Furthermore, chapter three marks the commencement of the experimental work presenting an overview of the viral diversity in selected WWTPs in Durban using mNGS technology is presented in chapter three. This chapter provides the virological framework and guides the selection of pertinent viral targets for subsequent computational and antiviral studies. In chapter four, the phytochemical fingerprint of the selected medicinal plants investigated in this study and the modulatory potential of the identified plants' metabolites against the druggable targets of selected enteric viruses using *in silico* approaches were presented. This chapter represents an intermediate discovery phase whereby bioactive plant-derived chemicals are discovered and prioritized, establishing the foundation for their later integration into phyto-nanomaterials. Chapter five is a continuation of the preceding chapter, where the resulting lead compounds-conjugated silver nanoparticles were evaluated for their antiviral potential against the enteric virus's druggable targets using computational techniques. Thus, chapters four and five together provide a cohesive pathway, advancing from lead

identification to nano-enabled antiviral assessment. Chapter six concludes the study by providing a general discussion, conclusion and recommendations to summarize the overall findings of the study.

References

ABUTALEB, A. & KOTTILIL, S. 2020. Hepatitis A: epidemiology, natural history, unusual clinical manifestations, and prevention. *Gastroenterology Clinics,* 49**,** 191-199.

ALTINTAS, Z., GITTENS, M., POCOCK, J. & TOTHILL, I. E. 2015. Biosensors for waterborne viruses: Detection and removal. *Biochimie,* 115**,** 144-154.

ARIBISALA, J. O., ARUWA, C. E., UTHMAN, T. O., NURAIN, I. O., IDOWU, K. & SABIU, S. 2022. Cheminformatics bioprospection of broad spectrum plant secondary metabolites targeting the spike proteins of omicron variant and wild-type SARS-CoV-2. *Metabolites,* 12(982), 1-26.

AYOKA, A., AKOMOLAFE, R., AKINSOMISOYE, O. & UKPONMWAN, O. 2008. Medicinal and economic value of *Spondias mombin*. *African Journal of Biomedical Research,* 11, 129-136.

AZAROUAL, S. E., KASMI, Y., AASFAR, A., EL ARROUSSI, H., ZEROUAL, Y., EL KADIRI, Y., ZRHIDRI, A., ELFAHIME, E., SEFIANI, A. & MEFTAH KADMIRI, I. 2022. Investigation of bacterial diversity using 16S rRNA sequencing and prediction of its functionalities in Moroccan phosphate mine ecosystem. *Scientific Reports,* 12 (3741), 1-16.

BAEK, M., DIMAIO, F., ANISHCHENKO, I., DAUPARAS, J., OVCHINNIKOV, S., LEE, G. R., WANG, J., CONG, Q., KINCH, L. N., SCHAEFFER, R. D. & MILLÁN, C. 2021. Accurate prediction of protein structures and interactions using a three-track neural network. *Science*, 373(6557), 871-876.

BANERJEE, P., ECKERT, A. O., SCHREY, A. K. & PREISSNER, R. 2018. ProTox-II: a webserver for the prediction of toxicity of chemicals. *Nucleic Acids Research,* 46**,** W257-W263.

BÁNYAI, K., ESTES, M. K., MARTELLA, V. & PARASHAR, U. D. 2018. Viral gastroenteritis. *The Lancet,* 392**,** 175-186.

BARCELOS, M. P., GOMES, S. Q., FEDERICO, L. B., FRANCISCHINI, I. A. G., HAGE-MELIM, L. I. D. S., SILVA, G. M. & DE PAULA DA SILVA, C. H. T. 2022. Lead optimization in drug discovery. *Research Topics in Bioactivity, Environment and Energy: Experimental and Theoretical Tools,* 481-500.

BECK, S. E., RODRIGUEZ, R. A., LINDEN, K. G., HARGY, T. M., LARASON, T. C. & WRIGHT, H. B. 2014. Wavelength dependent UV inactivation and DNA damage of adenovirus as measured by cell culture infectivity and long range quantitative PCR. *Environmental Science & Technology,* 48**,** 591-598.

BEKELE, A. Z., GOKULAN, K., WILLIAMS, K. M. & KHARE, S. 2016. Dose and size-dependent antiviral effects of silver nanoparticles on feline calicivirus, a human norovirus surrogate. *Foodborne Pathogens and Disease,* 13**,** 239-244.

BERDIGALIYEV, N. & ALJOFAN, M. 2020. An overview of drug discovery and development. *Future Medicinal Chemistry,* 12**,** 939-947.

BIBBY, K., CRANK, K., GREAVES, J., LI, X., WU, Z., HAMZA, I. A. & STACHLER, E. 2019. Metagenomics and the development of viral water quality tools. *NPJ Clean Water,* 2(9), 1-13.

BLEOTU, C., MATEI, L., DRAGU, L. D., NECULA, L. G., PITICA, I. M., CHIVU-ECONOMESCU, M. & DIACONU, C. C. 2024. Viruses in wastewater-a concern for public health and the environment. *Microorganisms,* 12(1430), 1-30.

BOLGER, A. M., LOHSE, M. & USADEL, B. 2014. Trimmomatic: a flexible trimmer for Illumina sequence data. *Bioinformatics,* 30**,** 2114-2120.

BOSCH, A., PINTÓ, R. M. & ABAD, F. X. 2006. Survival and transport of enteric viruses in the environment. *Viruses in Foods.* 151-187.

BOUSEETTINE, R., HASSOU, N., BESSI, H. & ENNAJI, M. M. 2020. Waterborne transmission of enteric viruses and their impact on public health. *Emerging and Reemerging Viral Pathogens.* 907-932.

BREITWIESER, F. P., LU, J. & SALZBERG, S. L. 2019. A review of methods and databases for metagenomic classification and assembly. *Briefings in Bioinformatics,* 20**,** 1125-1136.

BUI, T. Q., LOAN, H. T. P., MY, T. T. A., QUANG, D. T., THUY, B. T. P., NHAN, V. D., QUY, P. T., VAN TAT, P., DAO, D. Q. & TRUNG, N. T. 2020. A density functional theory study on silver and bis-silver complexes with lighter tetrylene: are silver and bis-silver carbenes candidates for SARS-CoV-2 inhibition? Insight from molecular docking simulation. *RSC Advances,* 10**,** 30961-30974.

CALGUA, B., CARRATALÀ, A., GUERRERO-LATORRE, L., DE ABREU CORRÊA, A., KOHN, T., SOMMER, R. & GIRONES, R. 2014. UVC inactivation of dsDNA and ssRNA viruses in water: UV fluences and a qPCR-based approach to evaluate decay on viral infectivity. *Food and Environmental Virology,* 6**,** 260-268.

CASSIDY, H., POELMAN, R., KNOESTER, M., LEER-BUTER, V., CORETTA, C. & NIESTERS, H. G. 2018. Enterovirus D68–the new polio? *Frontiers in Microbiology,* 9**,** 1-11.

CHAUDHRY, R. M., NELSON, K. L. & DREWES, J. R. E. 2015. Mechanisms of pathogenic virus removal in a full-scale membrane bioreactor. *Environmental Science & Technology,* 49**,** 2815-2822.

CHEN, H., ENGKVIST, O., WANG, Y., OLIVECRONA, M. & BLASCHKE, T. 2018. The rise of deep learning in drug discovery. *Drug Discovery Today*, 23(6), 1241-1250.

CHEN, L. & HUANG, G. 2018. The antiviral activity of polysaccharides and their derivatives. *International Journal of Biological Macromolecules,* 115**,** 77-82.

CHEN, L., DENG, Y., DONG, S., WANG, H., LI, P., ZHANG, H. & CHU, W. 2021. The occurrence and control of waterborne viruses in drinking water treatment: a review. *Chemosphere***,** 281(130728), 1-11.

CHEN, N., ZHENG, Y., YIN, J., LI, X. & ZHENG, C. 2013. Inhibitory effects of silver nanoparticles against adenovirus type 3 in vitro. *Journal of Virological Methods,* 193**,** 470-477.

CHEN, Y. N., HSUEH, Y. H., HSIEH, C.-T., TZOU, D. Y. & CHANG, P. L. 2016. Antiviral activity of graphene–silver nanocomposites against non-enveloped and enveloped viruses. *International Journal of Environmental Research and Public Health,* 13(4)**,** 1-12.

CORDEY, S., BRITO, F., VU, D.-L., TURIN, L., KILOWOKO, M., KYUNGU, E., GENTON, B., ZDOBNOV, E. M., D'ACREMONT, V. & KAISER, L. 2016. Astrovirus VA1 identified by next-generation sequencing in a nasopharyngeal specimen of a febrile Tanzanian child with acute respiratory disease of unknown etiology. *Emerging Microbes & Infections,* 5**,** 1-3.

CORPUZ, M. V. A., BUONERBA, A., VIGLIOTTA, G., ZARRA, T., BALLESTEROS JR, F., CAMPIGLIA, P., BELGIORNO, V., KORSHIN, G. & NADDEO, V. 2020. Viruses in wastewater: occurrence, abundance and detection methods. *Science of the Total Environment,* 745(140910), 1-26.

CORTHOUT, J., PIETERS, L., CLAEYS, M., BERGHE, D. V. & VLIETINCK, A. 1991. Antiviral ellagitannins from *Spondias mombin*. *Phytochemistry,* 30**,** 1129-1130.

D'AMORE, R., IJAZ, U. Z., SCHIRMER, M., KENNY, J. G., GREGORY, R., DARBY, A. C., SHAKYA, M., PODAR, M., QUINCE, C. & HALL, N. 2016. A comprehensive benchmarking study of protocols and sequencing platforms for 16S rRNA community profiling. *BMC Genomics,* 17**,** 1-20.

DA SILVA, T. U., DA SILVA, E. T., DE CARVALHO POUGY, K., DA SILVA LIMA, C. H. & DE PAULA MACHADO, S. 2022. Molecular modeling of indazole-3-carboxylic acid and its metal complexes (Zn, Ni, Co, Fe and Mn) as NO synthase inhibitors: DFT calculations, docking studies and molecular dynamics simulations. *Inorganic Chemistry Communications,* 135**,** 1-9.

DAINA, A., MICHIELIN, O. & ZOETE, V. 2017. SwissADME: a free web tool to evaluate pharmacokinetics, drug-likeness and medicinal chemistry friendliness of small molecules. *Scientific Reports,* 7**,** 1-13.

DE ALBUQUERQUE, U. P., DE MEDEIROS, P. M., DE ALMEIDA, A. L. S., MONTEIRO, J. M., NETO, E. M. D. F. L., DE MELO, J. G. & DOS SANTOS, J. P. 2007. Medicinal plants of the caatinga (semi-arid) vegetation of NE Brazil: a quantitative approach. *Journal of Ethnopharmacology,* 114**,** 325-354.

DENG, Y., LI, B., NADAGOUDA, M. N. & TARABARA, V. V. 2020. Virus monitoring and removal in natural and built systems. *Journal of Environmental Engineering*, 146(10), 01820001-3

DIAKOU, I., PAPAKONSTANTINOU, E., PAPAGEORGIOU, L., PIEROULI, K., DRAGOUMANI, K., SPANDIDOS, D. A., BACOPOULOU, F., CHROUSOS, G. P., ELIOPOULOS, E. & VLACHAKIS, D. 2022. Novel computational pipelines in antiviral structure-based drug design. *Biomedical Reports,* 17**,** 1-5.

DIAZ, L. F. 2006. MH Gerardi, MC Zimmerman, Wastewater pathogens, in: Wastewater Microbiology Series, Wiley-Interscience, John Wiley & Sons, Hoboken, New Jersey,

USA (2004), price: US $49.95. Soft cover, 179 pages, ISBN: 0-471-20692-X. Pergamon.

DONGDEM, J. T., SOYIRI, I. & OCLOO, A. 2009. Public health significance of viral contamination of drinking water. *African Journal of Microbiology Research,* 3**,** 856-861.

DOS SANTOS, M. C., SILVA, A. C. C., DOS REIS TEIXEIRA, C., PRAZERES, F. P. M., DOS SANTOS, R. F., DE ARAÚJO ROLO, C., DE SOUZA SANTOS, E., DA FONSECA, M. S., VALENTE, C. O. & HODEL, K. V. S. 2024. Wastewater surveillance for viral pathogens: A tool for public health. *Heliyon,* 10, 1-23.

DOYTCHINOVA, I. 2022. Drug design—past, present, future. *Molecules,* 27(5)**,** 1-9.

DU PREEZ, I. C. & MUMBENGEGWI, D. R. 2014. Phytochemical investigation on Namibian plants for anti-malaria compounds. *Journal for Studies in Humanities and Social Sciences***,** 147-158.

EL-MOHAMADY, R. S., GHATTAS, T., ZAWRAH, M. & ABD EL-HAFEIZ, Y. 2018. Inhibitory effect of silver nanoparticles on bovine herpesvirus-1. *International Journal of Veterinary Science and Medicine,* 6**,** 296-300.

ELECHIGUERRA, J. L., BURT, J. L., MORONES, J. R., CAMACHO-BRAGADO, A., GAO, X., LARA, H. H. & YACAMAN, M. J. 2005. Interaction of silver nanoparticles with HIV-1. *Journal of Nanobiotechnology,* 3**,** 1-10.

FENWICK, A. 2006. Waterborne infectious diseases could they be consigned to history? *Science,* 313**,** 1077-1081.

GAIKWAD, S., INGLE, A., GADE, A., RAI, M., FALANGA, A., INCORONATO, N., RUSSO, L., GALDIERO, S. & GALDIERO, M. 2013. Antiviral activity of mycosynthesized silver nanoparticles against herpes simplex virus and human parainfluenza virus type 3. *International Journal of Nanomedicine,* 8**,** 4303-4314.

GALL, A. M., MARIÑAS, B. J., LU, Y. & SHISLER, J. L. 2015. Waterborne viruses: a barrier to safe drinking water. *PLoS Pathogens,* 11(6)**,** 1-7.

GARDINER, S. J. & BEGG, E. J. 2006. Pharmacogenetics, drug-metabolizing enzymes, and clinical practice. *Pharmacological Reviews,* 58**,** 521-590.

GARNER, E., DAVIS, B. C., MILLIGAN, E., BLAIR, M. F., KEENUM, I., MAILE-MOSKOWITZ, A., PAN, J., GNEGY, M., LIGUORI, K. & GUPTA, S. 2021. Next generation sequencing approaches to evaluate water and wastewater quality. *Water Research,* 194**,** 1-24.

GERBA, C. P., BETANCOURT, W. Q. & KITAJIMA, M. 2017. How much reduction of virus is needed for recycled water: A continuous changing need for assessment? *Water Research,* 108**,** 25-31.

GIANCOTTI, G., RIGO, I., PASQUALETTO, G., YOUNG, M. T., NEYTS, J., ROCHA-PEREIRA, J., BRANCALE, A., FERLA, S. & BASSETTO, M. 2019. A new antiviral scaffold for human norovirus identified with computer-aided approaches on the viral polymerase. *Scientific Reports,* 9**,** 1-20.

GIBSON, K. E. 2014. Viral pathogens in water: occurrence, public health impact, and available control strategies. *Current Opinion in Virology,* 4**,** 50-57.

GIRI, S. & BADER, A. 2015. A low-cost, high-quality new drug discovery process using patient-derived induced pluripotent stem cells. *Drug Discovery Today,* 20**,** 37-49.

GRIGALUNAS, M., BURHOP, A., CHRISTOFOROW, A. & WALDMANN, H. 2020. Pseudo-natural products and natural product-inspired methods in chemical biology and drug discovery. *Current Opinion in Chemical Biology,* 56**,** 111-118.

GUAJARDO-LEIVA, S., CHNAIDERMAN, J., GAGGERO, A. & DÍEZ, B. 2020. Metagenomic insights into the sewage RNA virosphere of a large city. *Viruses,* 12(9)**,** 1-15.

HAGAR, M., AHMED, H. A., ALJOHANI, G. & ALHADDAD, O. A. 2020. Investigation of some antiviral N-heterocycles as COVID-19 drug: molecular docking and DFT calculations. *International Journal of Molecular Sciences,* 21(11)**,** 1-13.

HAMOUDA, I. M. 2012. Current perspectives of nanoparticles in medical and dental biomaterials. *Journal of Biomedical Research,* 26**,** 143-151.

HARAMOTO, E., KITAJIMA, M., HATA, A., TORREY, J. R., MASAGO, Y., SANO, D. & KATAYAMA, H. 2018. A review on recent progress in the detection methods and prevalence of human enteric viruses in water. *Water Research,* 135**,** 168-186.

HARRIS, G. D., ADAMS, V. D., SORENSEN, D. L. & CURTIS, M. S. 1987. Ultraviolet inactivation of selected bacteria and viruses with photoreactivation of the bacteria. *Water Research,* 21**,** 687-692.

HASSAN BAIG, M., AHMAD, K., ROY, S., MOHAMMAD ASHRAF, J., ADIL, M., HARIS SIDDIQUI, M., KHAN, S., AMJAD KAMAL, M., PROVAZNÍK, I. & CHOI, I. 2016. Computer aided drug design: success and limitations. *Current Pharmaceutical Design,* 22**,** 572-581.

HEJKAL, T. W., WELLINGS, F. M., LEWIS, A. L. & LAROCK, P. A. 1981. Distribution of viruses associated with particles in waste water. *Applied and Environmental Microbiology,* 41**,** 628-634.

HU, R., LI, S., KONG, F., HOU, R., GUAN, X. & GUO, F. 2014. Inhibition effect of silver nanoparticles on herpes simplex virus 2. *Genetics and Molecular Research,* 13**,** 7022-7028.

HUANG, D., WANG, Z., ZHANG, G. & SAI, L. 2021. Molecular and epidemiological characterization of human adenoviruses infection among children with acute diarrhea in Shandong Province, China. *Virology Journal,* 18**,** 1-7.

HUSSAIN, F.S., ABRO, N.Q., AHMED, N., MEMON, S.Q. & MEMON, N. 2022. Nano-antivirals: A comprehensive review. *Frontiers in Nanotechnology*, 4(1064615), 1-27.

IKNER, L. A., SOTO-BELTRAN, M. & BRIGHT, K. R. 2011. New method using a positively charged microporous filter and ultrafiltration for concentration of viruses from tap water. *Applied and Environmental Microbiology,* 77**,** 3500-3506.

IRWIN, K. K., RENZETTE, N., KOWALIK, T. F. & JENSEN, J. D. 2016. Antiviral drug resistance as an adaptive process. *Virus Evolution,* 2, 1-10.

JAIN, N., JAIN, P., RAJPUT, D. & PATIL, U. K. 2021. Green synthesized plant-based silver nanoparticles: Therapeutic prospective for anticancer and antiviral activity. *Micro and Nano Systems Letters,* 9**(**5), 1-24.

JUMPER, J., EVANS, R., PRITZEL, A., GREEN, T., FIGURNOV, M., RONNEBERGER, O., TUNYASUVUNAKOOL, K., BATES, R., ŽÍDEK, A., POTAPENKO, A. & BRIDGLAND, A. 2021. Highly accurate protein structure prediction with AlphaFold. *Nature*, 596(7873), 583-589.

KANG, N., GAO, H., HE, L., LIU, Y., FAN, H., XU, Q. & YANG, S. 2021. Ginsenoside Rb1 is an immune-stimulatory agent with antiviral activity against enterovirus 71. *Journal of Ethnopharmacology*, 266, 1-9

KAPOOR, R., SHARMA, B. & KANWAR, S. 2017. Antiviral phytochemicals: an overview. *Biochemistry & Physiology,* 6**,** 1-7.

KAUSHAL, S. S. 2016. Increased salinization decreases safe drinking water. *Environmental Science & Technology*, 50(6), 2765–2766

KENNEDY, T. 1997. Managing the drug discovery/development interface. *Drug Discovery Today,* 2**,** 436-444.

KIM, A. H., HOGARTY, M. P., HARRIS, V. C. & BALDRIDGE, M. T. 2021. The complex interactions between rotavirus and the gut microbiota. *Frontiers in Cellular and Infection Microbiology,* 10, 1-9.

KIM, M., NGUYEN, D.-V., HEO, Y., PARK, K. H., PAIK, H.-D. & KIM, Y. B. 2020. Antiviral activity of fritillaria thunbergii extract against human influenza virus H1N1 (PR8) in vitro, in ovo and in vivo. *Journal of Microbiology and Biotechnology,* 30(172), 1-9.

KITCHEN, D. B., DECORNEZ, H., FURR, J. R. & BAJORATH, J. 2004. Docking and scoring in virtual screening for drug discovery: methods and applications. *Nature reviews Drug Discovery,* 3**,** 935-949.

KOUKOU, G., NIENDORF, S., HORNEI, B., SCHLUMP, J.-U., JENKE, A. C. & JACOBSEN, S. 2019. Human astrovirus infection associated with encephalitis in an immunocompetent child: a case report. *Journal of Medical Case Reports,* 13**,** 1-5.

KUCUK, C., YURDAKUL, S., CELIK, S. & ERDEM, B. 2022. Experimental and DFT studies of 2-methyl-quinoxaline and its silver (I) complex: Non-covalent interaction analysis, antimicrobial activity and molecular docking study. *Inorganic Chemistry Communications,* 145**,** 1-17.

KUMAR, S., AHLAWAT, W., BHANJANA, G., HEYDARIFARD, S., NAZHAD, M. M. & DILBAGHI, N. 2014. Nanotechnology-based water treatment strategies. *Journal of Nanoscience and Nanotechnology,* 14**,** 1838-1858.

LA ROSA, G., FRATINI, M., DELLA LIBERA, S., IACONELLI, M. & MUSCILLO, M. 2012. Emerging and potentially emerging viruses in water environments. *Annali dell'Istituto Superiore di Sanità,* 48**,** 397-406.

LA ROSA, G., IACONELLI, M., MANCINI, P., FERRARO, G. B., VENERI, C., BONADONNA, L., LUCENTINI, L. & SUFFREDINI, E. 2020. First detection of

SARS-CoV-2 in untreated wastewaters in Italy. *Science of The Total Environment,* 736**,** 139652.

LANREWAJU, A. A., ENITAN-FOLAMI, A. M., SABIU, S., EDOKPAYI, J. N. & SWALAHA, F. M. 2022a. Global public health implications of human exposure to viral contaminated water. *Frontiers in Microbiology,* 13, 1-18.

LANREWAJU, A. A., ENITAN-FOLAMI, A. M., SABIU, S. & SWALAHA, F. M. 2022b. A review on disinfection methods for inactivation of waterborne viruses. *Frontiers in Microbiology,* 13, 1-19.

LI, D., GU, A. Z., HE, M., SHI, H.-C. & YANG, W. 2009. UV inactivation and resistance of rotavirus evaluated by integrated cell culture and real-time RT-PCR assay. *Water Research,* 43**,** 3261-3269.

LI, W., XU, C., HAO, C., ZHANG, Y., WANG, Z., WANG, S. & WANG, W. 2020. Inhibition of herpes simplex virus by myricetin through targeting viral gD protein and cellular EGFR/PI3K/Akt pathway. *Antiviral Research*, 177, 1-11.

LI, Y., MIYANI, B., FAUST, R. A., DAVID, R. E. & XAGORARAKI, I. 2024. A broad wastewater screening and clinical data surveillance for virus-related diseases in the metropolitan Detroit area in Michigan. *Human Genomics,* 18(14), 1-18.

LIU, Z., CHEN, H., WOLD, E. & ZHOU, J. 2017. Small-molecule inhibitors of protein-protein interactions. *Drug Discovery Technologies,* 2-8, 329-353.

LOPEZ-ROBLERO, A., MARTÍNEZ CANO, D. J., DIEGO-GARCÍA, E., GUILLÉN-NAVARRO, G. K., IŠA, P. & ZARZA, E. 2024. Metagenomic analysis of plant viruses in tropical fresh and wastewater. *Environmental DNA,* 6**,** 1-13.

LOPMAN, B. A., STEELE, D., KIRKWOOD, C. D. & PARASHAR, U. D. 2016. The vast and varied global burden of norovirus: prospects for prevention and control. *PLoS Medicine,* 13**,** 1-12.

LU, L., ZHONG, H., XU, M., SU, L., CAO, L., JIA, R. & XU, J. 2021. Molecular and epidemiological characterization of human adenovirus and classic human astrovirus in children with acute diarrhea in Shanghai, 2017–2018. *BMC Infectious Diseases,* 21**,** 1-10.

LU, R., ZHAO, X., LI, J., NIU, P., YANG, B., WU, H., WANG, W., SONG, H., HUANG, B. & ZHU, N. 2020. Genomic characterisation and epidemiology of 2019 novel coronavirus: implications for virus origins and receptor binding. *The Lancet,* 395**,** 565-574.

LUGO, D. & KROGSTAD, P. 2016. Enteroviruses in the early 21st century: new manifestations and challenges. *Current Opinion in Pediatrics,* 28**,** 101-113.

LUSEBA, D., ELGORASHI, E., NTLOEDIBE, D. & VAN STADEN, J. 2007. Antibacterial, anti-inflammatory and mutagenic effects of some medicinal plants used in South Africa for the treatment of wounds and retained placenta in livestock. *South African Journal of Botany,* 73**,** 378-383.

MANS, J., DE VILLIERS, J. C., DU PLESSIS, N. M., AVENANT, T. & TAYLOR, M. B. 2010. Emerging norovirus GII. 4 2008 variant detected in hospitalised paediatric patients in South Africa. *Journal of Clinical Virology,* 49**,** 258-264.

MANS, J., MURRAY, T. Y. & TAYLOR, M. B. 2014. Novel norovirus recombinants detected in South Africa. *Virology Journal,* 11**,** 1-9.

MENCHON, G., MAVEYRAUD, L. & CZAPLICKI, G. 2018. Molecular dynamics as a tool for virtual ligand screening. *Computational Drug Discovery and Design***,** 145-178.

MIGUERES, M., LHOMME, S. & IZOPET, J. 2021. Hepatitis A: epidemiology, high-risk groups, prevention and research on antiviral treatment. *Viruses,* 13**,** 1-12.

MOHAMMADI POUR, P., FAKHRI, S., ASGARY, S., FARZAEI, M. H. & ECHEVERRIA, J. 2019. The signaling pathways, and therapeutic targets of antiviral agents: focusing

on the antiviral approaches and clinical perspectives of anthocyanins in the management of viral diseases. *Frontiers in Pharmacology,* 10**,** 1-23.

MYUNG, Y., DE SÁ, A.G. & ASCHER, D.B. 2024. Deep-PK: deep learning for small molecule pharmacokinetic and toxicity prediction. *Nucleic Acids Research*, 52, 469-475.

NEWMAN, D. J. & CRAGG, G. M. 2012. Natural products as sources of new drugs over the 30 years from 1981 to 2010. *Journal of Natural Products,* 75**,** 311-335.

OGBOLE, O. O., AKINLEYE, T. E., SEGUN, P. A., FALEYE, T. C. & ADENIJI, A. J. 2018. In vitro antiviral activity of twenty-seven medicinal plant extracts from Southwest Nigeria against three serotypes of echoviruses. *Virology Journal,* 15**,** 1-8.

OKOH, A. I., SIBANDA, T. & GUSHA, S. S. 2010. Inadequately treated wastewater as a source of human enteric viruses in the environment. *International Journal of Environmental Research and Public Health,* 7**,** 2620-2637.

ONOSI, O., UPFOLD, N. S., JUKES, M. D., LUKE, G. A. & KNOX, C. 2019. The first molecular detection of aichi virus 1 in raw sewage and mussels collected in South Africa. *Food and Environmental Virology,* 11**,** 96-100.

OSUNMAKINDE, C. O., SELVARAJAN, R., MAMBA, B. & MSAGATI, T. A. 2021. Viral communities distribution and diversity in wastewater treatment plants using high-throughput sequencing analysis. *Polish Journal of Environmental Studies,* 30, 3189-3201.

OSUNMAKINDE, C. O., SELVARAJAN, R., SIBANDA, T., MAMBA, B. B. & MSAGATI, T. A. 2018. Overview of trends in the application of metagenomic techniques in the analysis of human enteric viral diversity in Africa's environmental regimes. *Viruses,* 10**,** 1-25.

OSUOLALE, O. & OKOH, A. 2017. Human enteric bacteria and viruses in five wastewater treatment plants in the Eastern Cape, South Africa. *Journal of Infection and Public Health,* 10**,** 541-547.

PANG, X., QIU, Y., GAO, T., ZURAWELL, R., NEUMANN, N. F., CRAIK, S. & LEE, B. E. 2019. Prevalence, levels and seasonal variations of human enteric viruses in six major rivers in Alberta, Canada. *Water Research,* 153**,** 349-356.

PAUL, D., KOLAR, P. & HALL, S.G. 2021. A review of the impact of environmental factors on the fate and transport of coronaviruses in aqueous environments. *NPJ Clean Water*, 4(1), 1-13.

PINON, A. & VIALETTE, M. 2019. Survival of viruses in water. *Intervirology*, 61(5), 214-222.

PUENPA, J., WANLAPAKORN, N., VONGPUNSAWAD, S. & POOVORAWAN, Y. 2019. The history of enterovirus A71 outbreaks and molecular epidemiology in the Asia-Pacific region. *Journal of Biomedical Science,* 26**,** 1-11.

RASOOL, N., YASMIN, F., SAHAI, S., HUSSAIN, W., INAM, H. & ARSHAD, A. 2021. Biological perspective of thiazolide derivatives against Mpro and MTase of SARS-CoV-2: Molecular docking, DFT and MD simulation investigations. *Chemical Physics Letters,* 771**,** 1-14.

RASTOGI, R.P., RICHA, N., KUMAR, A., TYAGI, M.B. & SINHA, R.P. 2010. Molecular mechanisms of ultraviolet radiation-induced DNA damage and repair. *Journal of Nucleic Acids*, (1), 1-32.

RATAN, Z. A., MASHRUR, F. R., CHHOAN, A. P., SHAHRIAR, S. M., HAIDERE, M. F., RUNA, N. J., KIM, S., KWEON, D.-H., HOSSEINZADEH, H. & CHO, J. Y. 2021. Silver nanoparticles as potential antiviral agents. *Pharmaceutics,* 13**,** 1-25.

RAWAT, P., SINGH, P. K. & KUMAR, V. 2017. Evidence based traditional anti-diarrheal medicinal plants and their phytocompounds. *Biomedicine & Pharmacotherapy,* 96**,** 1453-1464.

RIVADULLA, E. & ROMALDE, J. L. 2020. A comprehensive review on human Aichi virus. *Virologica Sinica***,** 35, 501-516.

RIZZOTTO, M. 2012. Metal complexes as antimicrobial agents. *A search for antibacterial agents,* 10**,** 73-88.

ROBERSON, J. A. 2011. What's next after 40 years of drinking water regulations? *Environmental Science & Technology*, 45, 154-160.

ROBILOTTI, E., DERESINSKI, S. & PINSKY, B. A. 2015. Norovirus. *Clinical Microbiology Reviews,* 28**,** 134-164.

RODRIGUES, T., REKER, D., SCHNEIDER, P. & SCHNEIDER, G. 2016. Counting on natural products for drug design. *Nature Chemistry,* 8**,** 531-541.

RUSIÑOL, M., FERNANDEZ-CASSI, X., TIMONEDA, N., CARRATALÀ, A., ABRIL, J. F., SILVERA, C., FIGUERAS, M. J., GELATI, E., RODÓ, X. & KAY, D. 2015. Evidence of viral dissemination and seasonality in a Mediterranean river catchment: implications for water pollution management. *Journal of Environmental Management,* 159**,** 58-67.

RZEŻUTKA, A. & COOK, N. 2004. Survival of human enteric viruses in the environment and food. *FEMS Microbiology Reviews,* 28**,** 441-453.

SABE, V. T., NTOMBELA, T., JHAMBA, L. A., MAGUIRE, G. E., GOVENDER, T., NAICKER, T. & KRUGER, H. G. 2021. Current trends in computer aided drug design and a highlight of drugs discovered via computational techniques: A review. *European Journal of Medicinal Chemistry,* 224**,**1-21.

SADYBEKOV, A. V. & KATRITCH, V. 2023. Computational approaches streamlining drug discovery. *Nature,* 616**,** 673-685.

SÁNCHEZ, G. & BOSCH, A. 2016. Survival of enteric viruses in the environment and food. *Viruses in Foods*, 367-392.

SEGUN, P. A., OGBOLE, O. O. & AJAIYEOBA, E. O. 2018. Medicinal plants used in the management of cancer among the Ijebus of Southwestern Nigeria. *Journal of Herbal Medicine,* 14, 68-75.

SEGUN, P. A., OGBOLE, O. O., AKINLEYE, T. E., FALEYE, T. O. & ADENIJI, A. J. 2019. In vitro anti-enteroviral activity of stilbenoids isolated from the leaves of *Macaranga barteri*. *Natural Product Research*, 1909-1913.

SEMENYA, S. & MAROYI, A. 2012. Medicinal plants used by the Bapedi traditional healers to treat diarrhoea in the Limpopo Province, South Africa. *Journal of Ethnopharmacology,* 144, 395-401.

SHAKER, B., AHMAD, S., LEE, J., JUNG, C. & NA, D. 2021. In silico methods and tools for drug discovery. *Computers in Biology and Medicine,* 137, 1-15.

SHARMA, V., KAUSHIK, S., PANDIT, P., DHULL, D., YADAV, J. P. & KAUSHIK, S. 2019. Green synthesis of silver nanoparticles from medicinal plants and evaluation of their antiviral potential against chikungunya virus. *Applied Microbiology and Biotechnology,* 103, 881-891.

SIBANDA, T. & OKOH, A. I. 2013. Real-time PCR quantitative assessment of hepatitis A virus, rotaviruses and enteroviruses in the Tyume River located in the Eastern Cape Province, South Africa. *Water SA,* 39, 295-304.

SINGH, L., KRUGER, H.G., MAGUIRE, G.E., GOVENDER, T. & PARBOOSING, R. 2017. The role of nanotechnology in the treatment of viral infections. *Therapeutic Advances in Infectious Disease*, 4(4), 105-131.

SIQUEIRA, E. M. D. S., LIMA, T. L., BOFF, L., LIMA, S. G., LOURENÇO, E. M., FERREIRA, É. G., BARBOSA, E. G., MACHADO, P. R., FARIAS, K. J. &

FERREIRA, L. D. S. 2020. Antiviral potential of *Spondias mombin* L. leaves extract against herpes simplex virus type-1 replication using *in vitro* and *in silico* approaches. *Planta Medica,* 86**,** 505-515.

SMUTS, H., CRONJE, S., THOMAS, J., BRINK, D., KORSMAN, S. & HARDIE, D. 2018. Molecular characterization of an outbreak of enterovirus-associated meningitis in Mossel Bay, South Africa, December 2015–January 2016. *BMC Infectious Diseases,* 18**,** 1-11.

SOLLER, J. A., EFTIM, S. E. & NAPPIER, S. P. 2019. Comparison of predicted microbiological human health risks associated with de facto, indirect, and direct potable water reuse. *Environmental Science & Technology,* 53**,** 13382-13389.

STOBNICKA-KUPIEC, A., GOŁOFIT-SZYMCZAK, M., CYPROWSKI, M. & GÓRNY, R.L. 2022. Detection and identification of potentially infectious gastrointestinal and respiratory viruses at workplaces of wastewater treatment plants with viability qPCR/RT-qPCR. *Scientific Reports*, 12(1), 1-16.

SUJITHA, V., MURUGAN, K., PAULPANDI, M., PANNEERSELVAM, C., SURESH, U., RONI, M., NICOLETTI, M., HIGUCHI, A., MADHIYAZHAGAN, P. & SUBRAMANIAM, J. 2015. Green-synthesized silver nanoparticles as a novel control tool against dengue virus (DEN-2) and its primary vector Aedes aegypti. *Parasitology Research,* 114**,** 3315-3325.

SURABHI, S. & SINGH, B. 2018. Computer aided drug design: an overview. *Journal of Drug Delivery and Therapeutics,* 8**,** 504-509.

TAYLOR, R. D., JEWSBURY, P. J. & ESSEX, J. W. 2002. A review of protein-small molecule docking methods. *Journal of Computer-Aided Molecular Design,* 16**,** 151-166.

TROEGER, C., KHALIL, I. A., RAO, P. C., CAO, S., BLACKER, B. F., AHMED, T., ARMAH, G., BINES, J. E., BREWER, T. G. & COLOMBARA, D. V. 2018. Rotavirus

vaccination and the global burden of rotavirus diarrhea among children younger than 5 years. *JAMA Pediatrics,* 172**,** 958-965.

UHOMOIBHI, J., IDOWU, K., SHODE, F. & SABIU, S. 2022. Molecular modeling identification of potential drug candidates from selected African plants against SARS-CoV-2 key druggable proteins. *Scientific African,* 17**,** 1-11.

UPFOLD, N. S., LUKE, G. A. & KNOX, C. 2021. Occurrence of human enteric viruses in water sources and shellfish: A focus on Africa. *Food and Environmental Virology***,** 13, 1-31.

VAMATHEVAN, J., CLARK, D., CZODROWSKI, P., DUNHAM, I., FERRAN, E., LEE, G., LI, B., MADABHUSHI, A., SHAH, P., SPITZER, M. & ZHAO, S. 2019. Applications of machine learning in drug discovery and development. *Nature Reviews Drug Discovery*, 18(6), 463-477.

VAN DAMME, P., PINTÓ, R. M., FENG, Z., CUI, F., GENTILE, A. & SHOUVAL, D. 2023. Hepatitis A virus infection. *Nature Reviews Disease Primers,* 9**,** 1-18.

VAN DER MERWE, D., SWAN, G. & BOTHA, C. 2001. Use of ethnoveterinary medicinal plants in cattle by Setswana-speaking people in the Madikwe area of the North West Province of South Africa. *Journal of the South African Veterinary Association,* 72**,** 189-196.

VAN DOREMALEN, N., BUSHMAKER, T., MORRIS, D., HOLBROOK, M. & GAMBLE, A. 2020. BN 9 Williamson, A. Tamin, JL Harcourt, NJ Thornburg, SI Gerber, JO Lloyd-Smith, E. 10 De Wit, VJ Munster, Aerosol and surface stability of SARS-CoV-2 as compared with 11 SARS-CoV-1. *New England Journal of Med*icine, 382, 1564-1567.

VARDHAN, S. & SAHOO, S. K. 2022. Computational studies on the interaction of SARS-CoV-2 Omicron SGp RBD with human receptor ACE2, limonin and glycyrrhizic acid. *Computers in Biology and Medicine,* 144**,** 1-8.

VEENA, V., SHIVAPRASAD, K., SHARANAGOUDA, H. & LAGASHETTY, A. 2024. Facile synthesis, characterization, *in silico* modelling, and bioinformatic study of dimercapto-triazole functionalized silver nanoparticles. *Results in Chemistry,* 7**,** 1-12.

VERBYLA, M. E. & MIHELCIC, J. R. 2015. A review of virus removal in wastewater treatment pond systems. *Water Research,* 71**,** 107-124.

WANG, X.-W., LI, J.-S., GUO, T.-K., ZHEN, B., KONG, Q.-X., YI, B., LI, Z., SONG, N., JIN, M. & XIAO, W.-J. 2005a. Concentration and detection of SARS coronavirus in sewage from Xiao Tang Shan Hospital and the 309th Hospital. *Journal of Virological Methods,* 128**,** 156-161.

WANG, X.-W., LI, J.-S., JIN, M., ZHEN, B., KONG, Q.-X., SONG, N., XIAO, W.-J., YIN, J., WEI, W. & WANG, G.-J. 2005b. Study on the resistance of severe acute respiratory syndrome-associated coronavirus. *Journal of Virological Methods,* 126**,** 171-177.

WARING, M.J., ARROWSMITH, J., LEACH, A.R., LEESON, P.D., MANDRELL, S., OWEN, R.M., PAIRAUDEU, G., PENNIE, W.D., PICKETT, S.D., WANG, J. & WALLACE, O. 2015. An analysis of the attrition of drug candidates from four major pharmaceutical companies. *Nature Reviews Drug Discovery*, 14(7), 475-486.

WORLD HEALTH ORGANIZATION 2024. COVID-19 epidemiological update – 9 October 2024. https://www.who.int/publications/m/item/covid-19-epidemiological-update-edition-172 (Accessed 11 October 2024).

WORLD HEALTH ORGANIZATION 2024. Diarrhoeal disease, Available online: https://www.who.int/news-room/fact-sheets/detail/diarrhoeal-disease. (Accessed 20 September 2024).

XAGORARAKI, I. & O'BRIEN, E. 2020. Wastewater-based epidemiology for early detection of viral outbreaks. *Women in Water Quality.* 75-97

XAGORARAKI, I., YIN, Z. & SVAMBAYEV, Z. 2014. Fate of viruses in water systems. *Journal of Environmental Engineering,* 140**,** 04014021-040140218.

XU, H.Y., REN, J.H., SU, Y., REN, F., ZHOU, Y.J., JIANG, H., CHENG, S.T., ZHANG, C.R. & CHEN, J. 2020. Anti-hepatitis B virus activity of swertisin isolated from *Iris tectorum* Maxim. *Journal of Ethnopharmacology*, 257, 1-9.

YAMASHITA, T., SUGIYAMA, M., TSUZUKI, H., SAKAE, K., SUZUKI, Y. & MIYAZAKI, Y. 2000. Application of a reverse transcription-PCR for identification and differentiation of Aichi virus, a new member of the Picornavirus family associated with gastroenteritis in humans. *Journal of Clinical Microbiology,* 38**,** 2955-2961.

YANG, S., DONG, Q., LI, S., CHENG, Z., KANG, X., REN, D., XU, C., ZHOU, X., LIANG, P. & SUN, L. 2022. Persistence of SARS-CoV-2 RNA in wastewater after the end of the COVID-19 epidemics. *Journal of Hazardous Materials,* 429**,** 1-9.

YE, N., YANG, Z. & LIU, Y. 2022. Applications of density functional theory in COVID-19 drug modeling. *Drug Discovery Today,* 27**,** 1411-1419.

ZAHEDI, A., MONIS, P., DEERE, D. & RYAN, U. 2021. Wastewater-based epidemiology—surveillance and early detection of waterborne pathogens with a focus on SARS-CoV-2, Cryptosporidium and Giardia. *Parasitology Research***,** 1-22.

ZHANG, D., DURAN, S. S. F., LIM, W. Y. S., TAN, C. K. I., CHEONG, W. C. D., SUWARDI, A. & LOH, X. J. 2022. SARS-CoV-2 in wastewater: From detection to evaluation. *Materials Today Advances,* 13**,** 1-14.

ZITZMANN, C. & KADERALI, L. 2018. Mathematical analysis of viral replication dynamics and antiviral treatment strategies: from basic models to age-based multi-scale modeling. *Frontiers in Microbiology,* 9**,** 1-18.

CHAPTER TWO

2.0 Literature Review

2.1 Introduction……41

2.2 A review on disinfection methods for inactivation of waterborne viruses **(Published in Frontiers in Microbiology)** ……...……46

2.3 Global public health implications of human exposure to viral contaminated water **(Published in Frontiers in Microbiology)**.…….……65

2.4 Unravelling viral diversity in wastewater treatment plants through metagenomics: An overview **(has been formatted for submission to Science of the Total Environment)** …....83

2.5 An overview of the advancements in antiviral drug discovery and development **(has been formatted for submission to Bioorganic & Medicinal Chemistry)** ……...……145

References……..226

Two of the four review articles in this section have been published in Frontiers in Microbiology. The third and the fourth review articles has been formatted for submission to Science of the Total Environment and Bioorganic & Medicinal Chemistry, respectively.

2.1 Introduction

Globally, there is a pressing need for safe drinking water as about 25% of the global population lacking access to safe drinking water as of 2020 (WHO, UNICEF, 2021). At the onset of the COVID-19 pandemic, approximately 30% of the global population lacked access to soap and clean water for handwashing in their homes. Unfortunately, it is projected that by the year 2030, about 19% of the global population equating 1.6 billion individuals will lack access to safe water (WHO, UNICEF, 2021). Contaminated water may harbour pathogenic bacteria, protozoa and viruses associated with diverse debilitating human diseases. The prevalence and survival rates of waterborne viruses contrast with those of bacteria and other waterborne microorganisms. Moreover, viruses contribute to more severe waterborne diseases including gastroenteritis, myocarditis and encephalitis among others. This underscores the necessity for focused efforts on viral inactivation. Importantly, the effectiveness of viral disinfection approaches in fundamentally dependent on accurate identification and characterizations of the viral populations in environmental systems informing the selection of relevant viral targets for control and intervention.

Viral contamination presents a substantial problem when the effluent is released into freshwater environments or when viral removal is insufficient during planned or unplanned water reuse (Chen *et al*., 2021). Conventional water and wastewater treatment processes encounter limitations associated with reduced removal efficiency owing to the diminutive size of viruses (Ibrahim *et al*., 2021). In addition, free chlorine, a commonly used disinfectant, has been linked with the formation of regulated toxic disinfection by-products (DBPs). This has led to the adoption of other disinfectants, such as monochloramine, chlorine dioxide, and ozone among others by some drinking water utilities. Recently, there has been a search for holistic

disinfection techniques with much lower health risks. Unfortunately, this ongoing search comes with costs and operational challenges (Gall *et al*., 2015). Thus, the conventional disinfection approaches alongside emerging disinfection technologies were examined in this section of the study.

According to Clemente *et al*., (2012), individuals experiencing gastroenteritis may release approximately 10^5–10^{11} virus particles per gram of faeces, which subsequently migrate into environmental matrices when contaminated wastewater is released (Wu *et al*., 2020; Yeo *et al*., 2020). Though enteric viruses are the smallest enteric pathogens and require only a minimal infectious dose, they are resilient and challenging to detect and deactivate (Gonzales-Gustavson *et al*., 2019; Zitzmann and Kaderali, 2018); consequently, even low-level exposures pose a notable health risk (Zhu *et al*., 2018; Zwart *et al*., 2009). Hence, the spread of human enteric viruses through waterborne pathways is now increasingly recognised as a likely contributor to human illnesses including gastroenteritis, encephalitis, meningitis, and hepatitis, among others (Tang *et al*., 2020; WHO, 2014). Detecting and quantifying the diverse human viruses in environmental water is pivotal to public health, enhancing both disease prevention and rapid outbreak response. Hence, routine viral surveillance of treated wastewater discharged into the environment is essential for preventing illnesses arising from exposure to virus-contaminated water. As a result, this section delineates the prevalence of enteric viruses in water and wastewater sources, their public-health consequences, the diseases linked to human exposure to waterborne enteric viruses, and strategies for mitigating the identified concerns.

Viral detection through the conventional culture methods enables the separation of pure viral stock and are very efficient in assessing both infectivity and concentration. Nevertheless, these

techniques are constrained by the extended time required for incubation and the inability to cultivate most viruses (McCall and Xagoraraki, 2019). Therefore, polymerase chain reaction (PCR) emerged as the conventional standard for viral identification and quantification because it circumvents the need for cell culture, delivers rapid results, and proves highly effective when analyzing environmental samples (Xagoraraki *et al*., 2014). Unfortunately, these molecular techniques still depend on already known primers and a pre-existing understanding of the microbiome in the sample, hence limiting a thorough understanding of viral populations or the identification of novel viruses in wastewater and other environmental matrices (Fancello *et al*., 2012). Therefore, the need for immediate human pathogen characterization and the evaluation of viral diversity in different environments has prompted the creation of a new generation of technologies.

Interestingly, the advent of next-generation sequencing (NGS) technology is revolutionising the use of molecular approaches in comprehending intricate microbial ecosystems as it overcomes the constraints of conventional techniques by employing sophisticated platforms to sequence the genes or genomes of organisms or microbial communities (Garner *et al*., 2021). This technique is used without the requirement of culturing the organisms or possess prior insight into the sample's microbial composition. Furthermore, metagenomics, which entails sequencing and analysing the genetic material present in a sample, has provided unparalleled insight into viral diversity (Fancello *et al*., 2012). Therefore, this section evaluated different viral characterization techniques, sequencing technologies, viral diversity in WWTPs using metagenomics, viral metagenomics workflow, constraints and prospects of viral metagenomics in wastewater.

Beyond the fatalities linked to a lack of safe drinking water and inadequate sanitation, the World Bank has placed the resulting global economic loss at roughly US$260 billion annually (WHO, 2012). Infections arising from contaminated water and enteric-virus outbreaks are believed to be under reported globally regardless of a nation's socioeconomic status because symptoms are generally mild and people seldom seek medical attention for self-limiting conditions (Control and Prevention, 2013). In most healthy individuals these viral infections resolve on their own; however, greater morbidity can occur in children under five, the elderly, pregnant women, and immunocompromised patients. Thus, surveillance of diseases associated with enteric viruses remains challenging (Cortez *et al*., 2017; Li *et al*., 2017). Unfortunately, only a limited selection of broad-spectrum antiviral drugs is currently available to treat such enteric viral diseases (Gall *et al*., 2015).

Additionally, viruses are renowned for the molecular manipulations that enable them to proliferate and endure in all species owing to their capability to undermine the defense mechanisms of the cells they infect, to guarantee the survival, reproduction, and spread of their genetic materials in the host (Li *et al*., 2024). In addition, viruses present obstacles to broad-spectrum antiviral medications that target both RNA and DNA viruses, which can be attributed to factors like the structure of the virus's genetic material (single or double genomic structure), site of replication (cytoplasmic or nuclear), and the extent to which the virus relies on host proteins for its survival (Schoeman and Fielding, 2019).

The fact that more than 220 identified human viruses are in circulation, yet only a small number of antiviral medications have received clinical approvals is a matter of significant concern (Cheung *et al*., 2024; Adamson *et al*., 2021), which becomes worrisome, especially in low-

income countries where expensive drugs are not easily accessible. To make matters worse, each virus needs specialized pharmaceutical interventions or therapies owing to the distinct characteristics and behaviours of each virus, hence necessitating customized treatments (Kausar *et al*., 2021). The problem is worsened by drug-resistant mutants, particularly when utilizing inhibitors that target specific viral enzymes, which greatly reduces the effectiveness of the antiviral agents (Geretti *et al*., 2012; Locarnini and Yuen, 2010). Therefore, the discovery of novel antiviral drugs that are both efficient and economical to effectively manage and control viral infections in cases when vaccines and conventional treatments are insufficient becomes imperative. Consequently, in this section of the study, different challenges associated with conventional antiviral drugs, alongside recent approaches in antiviral drug discovery and development, were assessed.

This chapter of the thesis is divided into four parts with each section presented as a review article: (1) a review on disinfection methods for inactivation of waterborne viruses, (2) global public health implications of human exposure to viral contaminated water, (3) unravelling viral diversity in wastewater treatment plants through metagenomics; an overview and (4) an overview of the advancements in antiviral drug discovery and development.

frontiers | Frontiers in Microbiology

TYPE Review
PUBLISHED 23 September 2022
DOI 10.3389/fmicb.2022.991856

Check for updates

OPEN ACCESS

EDITED BY
Anthony Ayodeji Adegoke,
University of Uyo,
Nigeria

REVIEWED BY
Kshama Balapure,
National Chemical Laboratory (CSIR), India
Richard M. Mariita,
Crystal IS Inc., United States
Rajul Randive,
Asahi Kasei America, United States

*CORRESPONDENCE
Abimbola Motunrayo Enitan-Folami
enitanabimbola@gmail.com

SPECIALTY SECTION
This article was submitted to Infectious Agents and Disease, a section of the journal Frontiers in Microbiology

RECEIVED 12 July 2022
ACCEPTED 29 August 2022
PUBLISHED 23 September 2022

CITATION
Lanrewaju AA, Enitan-Folami AM, Sabiu S and Swalaha FM (2022) A review on disinfection methods for inactivation of waterborne viruses. *Front. Microbiol.* 13:991856. doi: 10.3389/fmicb.2022.991856

COPYRIGHT
© 2022 Lanrewaju, Enitan-Folami, Sabiu and Swalaha. This is an open-access article distributed under the terms of the Creative Commons Attribution License (CC BY). The use, distribution or reproduction in other forums is permitted, provided the original author(s) and the copyright owner(s) are credited and that the original publication in this journal is cited, in accordance with accepted academic practice. No use, distribution or reproduction is permitted which does not comply with these terms.

A review on disinfection methods for inactivation of waterborne viruses

Adedayo Ayodeji Lanrewaju, Abimbola Motunrayo Enitan-Folami*, Saheed Sabiu and Feroz Mahomed Swalaha

Department of Biotechnology and Food Science, Durban University of Technology, Durban, South Africa

Water contamination is a global health problem, and the need for safe water is ever-growing due to the public health implications of unsafe water. Contaminated water could contain pathogenic bacteria, protozoa, and viruses that are implicated in several debilitating human diseases. The prevalence and survival of waterborne viruses differ from bacteria and other waterborne microorganisms. In addition, viruses are responsible for more severe waterborne diseases such as gastroenteritis, myocarditis, and encephalitis among others, hence the need for dedicated attention to viral inactivation. Disinfection is vital to water treatment because it removes pathogens, including viruses. The commonly used methods and techniques of disinfection for viral inactivation in water comprise physical disinfection such as membrane filtration, ultraviolet (UV) irradiation, and conventional chemical processes such as chlorine, monochloramine, chlorine dioxide, and ozone among others. However, the production of disinfection by-products (DBPs) that accompanies chemical methods of disinfection is an issue of great concern due to the increase in the risks of harm to humans, for example, the development of cancer of the bladder and adverse reproductive outcomes. Therefore, this review examines the conventional disinfection approaches alongside emerging disinfection technologies, such as photocatalytic disinfection, cavitation, and electrochemical disinfection. Moreover, the merits, limitations, and log reduction values (LRVs) of the different disinfection methods discussed were compared concerning virus removal efficiency. Future research needs to merge single disinfection techniques into one to achieve improved viral disinfection, and the development of medicinal plant-based materials as disinfectants due to their antimicrobial and safety benefits to avoid toxicity is also highlighted.

KEYWORDS

chlorination, disinfection, disinfection by-products, viral inactivation, waterborne viruses

Introduction

Worldwide, there is an urgent demand for potable water as approximately 1 in 4 people of the global population have no access to safe drinking water in the year 2020 (WHO, UNICEF, 2021). At the beginning of the COVID-19 pandemic, three out of 10 individuals in the world could not wash their hands with soap and clean water in their homes.

Unfortunately, it has been estimated that by the year 2030, about 19% of the global population (1.6 billion persons) will not have access to safe water (WHO, UNICEF, 2021).

Waterborne diarrhea is a prominent global morbidity and mortality source, with an estimated 4 billion instances of sickness and 1.8 million deaths annually (Manetu and Karanja, 2021). Approximately 90% of death associated with diarrhea globally resulted from poor hygiene, inadequate sanitation, and, more importantly consumption of unsafe water. Apart from the loss of lives linked with poor access to safe water, it also leads to a global economic loss of about US$260 billion *per annum* (WHO, 2012). Unsafe water could contain bacteria, protozoa, and viruses which are implicated in several human diseases with gastroenteritis being the most notable among them (Gall et al., 2015). Unfortunately, waterborne viruses, which are more persistent in the environment than bacteria, are frequently the source of diarrheal sickness in drinking, recreational, and groundwaters (Magana-Arachchi and Wanigatunge, 2020). However, less attention is given to these viruses despite their huge negative impact on public health (Gall et al., 2015; Lanrewaju et al., 2022).

Most viruses are linked to gastroenteritis resulting in diarrhea and other symptoms such as abdominal cramping, vomiting, and fever (Magana-Arachchi and Wanigatunge, 2020). Furthermore, they could be responsible for more severe health conditions such as encephalitis, myocarditis, meningitis, cancer, and hepatitis among others (WHO, 2016; Magana-Arachchi and Wanigatunge, 2020; Lanrewaju et al., 2022). Unfortunately, few antiviral drugs with a broad spectrum of action to treat these diseases are available. Both symptomatic and asymptomatic patients can excrete a significant quantity of viruses. Clinical observations have shown that infected individuals with symptomatic infection may shed viruses for a few weeks after infection (Albinana-Gimenez et al., 2006; Wu et al., 2020; Yeo et al., 2020).

Primarily, waterborne enteric viruses are transmitted through the fecal-oral route (Sánchez and Bosch, 2016; Bouseettine et al., 2020) which could be from person to person or *via* drinking contaminated water with its accompanying health hazard (Diaz, 2006; Upfold et al., 2021). Discharge of influents generated from faeces, vomit, and urine of infected animals and humans could introduce viruses into wastewater sources (Bosch et al., 2006; Diaz, 2006). Viruses that could be detected in wastewater include adenoviruses (AdVs), enterovirus (EVs), polioviruses (PVs), hepatitis A viruses (HAV), hepatitis E viruses (HEV), rotaviruses (RVs), reoviruses, noroviruses (NoVs), and coronaviruses (including SARS-CoV-2) among others (Diaz, 2006; Kitajima et al., 2014; Farkas et al., 2018; Gormley et al., 2020; Buonerba et al., 2021; Hasan et al., 2021; Lanrewaju et al., 2022). Virus genome copies (GC) L^{-1} approximately range from 10^5 to 10^7 in raw domestic wastewater (Albinana-Gimenez et al., 2006). The ongoing global outbreak of SARS-CoV-2 which is responsible for COVID-19 has raised the urgency of elucidating the fate and prevalence of coronaviruses as well as other viruses in sewage and drinking water sources.

Viruses can be reduced by 3-4log with traditional primary and secondary wastewater treatment (Sidhu et al., 2018); however, several viruses may survive in treated effluent and then contaminate natural water sources when discharged into it. The minimum requirement for the water treatment method to be considered efficient for viral disinfection is to achieve a 99.99% (4log) reduction of viral concentrations in water after treatment as recommended by the United States Environmental Protection Agency and Health Canada (Monteiro et al., 2015). Hence, viral contamination is a major concern when the effluent is discharged into freshwater sources, or when insufficient viral elimination occurs during planned or accidental water recycling (Chen et al., 2021b). One of the challenges of the traditional water/wastewater treatment processes is the low removal efficiency due to virus sizes; however, adopting membrane-based technologies helps overcome this challenge (Ibrahim et al., 2021). Furthermore, free chlorine, a commonly used disinfectant, has been linked with the formation of regulated toxic disinfection by-products (DBPs). This has led to the adoption of other disinfectants such as monochloramine, chlorine dioxide, and ozone among others by some drinking water utilities. Recently, there has been a search for holistic disinfection techniques with much lower health risks. Unfortunately, this ongoing search comes with costs and operational challenges (Gall et al., 2015). Therefore, the objective of this study is to critically review different disinfection methods, and highlight some of their merits and limitations associated with the inactivation of waterborne viruses.

Disinfection methods for the inactivation of waterborne viruses

Effective disinfection strategies are vital in water treatment procedures because they ensure the elimination of pathogenic microorganisms responsible for waterborne illnesses. The commonly used techniques of disinfection for viral inactivation in water comprise conventional chemical processes such as chlorine, monochloramine, chlorine dioxide, and ozone (Figure 1). Furthermore, membrane filtration and UV irradiation which are physical methods have also been utilized for disinfection in the treatment of water (Collivignarelli et al., 2018). Many parameters, including water, pH, temperature, type of microorganisms, type of disinfection, disinfectant dose, contact time, and inorganic and organic material in water, are known to influence disinfection (Tsitsifli and Kanakoudis, 2018). Even though disinfection entails the process of pathogen inactivation, the use of chemical disinfectants can result in the production of inorganic and organic DBPs (Sadiq and Rodriguez, 2004). Interestingly, the introduction of improved disinfection technologies such as advanced oxidation processes (AOPs) is a viable strategy for enhancing the water and wastewater treatment processes (Feitz, 2005; Kokkinos et al., 2021).

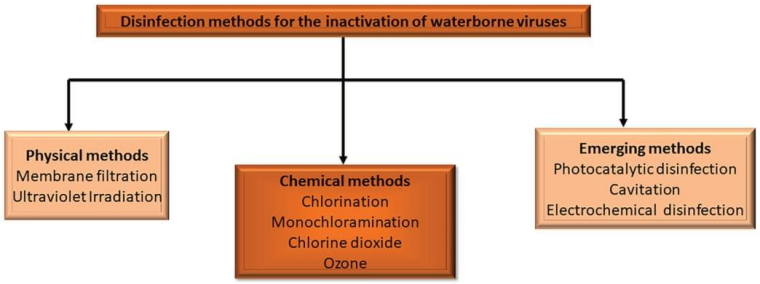


FIGURE 1
Disinfection methods for the inactivation of waterborne viruses (adapted from Chen et al., 2021b).

Advanced oxidation processes have been considered a potential, environmentally acceptable, and effective alternative to the traditional disinfection approaches for controlling the microbiological quality of water. Water disinfection and degradation of different toxic pollutants are achieved through the on-site production of chemical oxidants (Shabat-Hadas et al., 2017; Giannakis et al., 2017b; Marjanovic et al., 2018; Rekhate and Srivastava, 2020). Generally, AOPs are redox technologies that involve various oxidation processes, including ozonation, ozonation coupled with hydrogen peroxide (H_2O_2) and/or UV radiation, photocatalysis activated by semiconductors such as TiO_2, and electrochemical oxidation among others (Figure 1). Their mechanism of action is a function of the formation of very reactive oxygen species (ROS) that are not target-specific and can be utilized as a pre-or post-treatment to a biological procedure (Galeano et al., 2017; Kokkinos et al., 2020). Therefore, photocatalytic, cavitation, and electrochemical methods of disinfection are highlighted as emerging methods of disinfection in this review.

Meanwhile, the safety of treatment plant operators should be considered whenever disinfectants are used because some of the disinfectants are harmful; hence, compliance with safety precautions by the operators handling the disinfectants is important. For instance, UV radiation is considered a "complete carcinogen" because it is both a mutagen and a nonspecific damaging agent. In addition, it can initiate and promotes tumor formation (D'Orazio et al., 2013; Raeiszadeh and Adeli, 2020). Likewise, ozone can harm the lungs when inhaled. In relatively little doses, chest pain, coughing, shortness of breath, and throat irritation can occur. Additionally, ozone may weaken the body's defenses against respiratory infections and aggravate chronic respiratory conditions like asthma (USEPA, 2008). Therefore, appropriate personal protective equipment (PPE), such as goggles, gloves, long-sleeved shirts, long pants, and masks should be worn while applying disinfectants (Dhama et al., 2021). Using a suitable mask for a given purpose is preferable to using any non-specific mask (Agrawal et al., 2020).

Physical methods

Membrane filtration

Membrane filtration is a highly efficient technique for the removal of suspended particles, bacteria, and organic materials from drinking water and wastewater. This method enables the separation of contaminants present in water by passing it through a physical barrier. Commonly used technologies are microfiltration (MF), ultrafiltration (UF), nanofiltration (NF), and reverse osmosis (RO; Chen et al., 2021a). The basic mechanism of virus removal by membrane filtration is size exclusion, as ultrafiltration with a nominal pore size of 10^{-2} µm is suitable for the removal of most viruses (Zhang et al., 2016). Apart from the principle of size exclusion which operates on the surface of the membrane, other mechanisms involving electrostatic interactions are linked with the virus and membrane charge, adsorption retention, and hydrophilic-hydrophobic reactions. They are also associated with the physicochemical parameters of the membranes as well as the viruses. These properties facilitate the movement of the viruses through the surface of the membrane and their deposition on the internal matrix of the membrane (Van Voorthuizen et al., 2001; Schaldach et al., 2006; ElHadidy et al., 2013; Gentile et al., 2018; Chen et al., 2021a). However, the effectiveness of the membrane is affected by the quality of water, the content of solid particles in the water, and fouling formation during the water treatment process (Collivignarelli et al., 2018). Therefore, several membrane modifications have been made to enhance its efficiency, and consequently, this has resulted in the inactivation of viruses as the modifications facilitate the incorporation of materials with enhanced antiviral properties (Sinclair et al., 2018).

Membranes have been modified with different materials such as polymers and in the field of antimicrobial polymers, polyethylenimine (PEI) is one of the most investigated amine-containing polymers (Jarach et al., 2020). Sinclair et al. (2018) modified a commercial polyether sulfone (PES) microfiltration membrane using cationic polyethylenimine (PEI) for virus removal through gravity filtration. The virus removal rate was

enhanced as the membrane modification weakened the virus build-up on the membrane surface *via* surface repulsion. In addition, the utilization of the modified membrane required additional force at a reduced cost yet increased the rate of virus removal. In another study, cross-linked multilayers on model surfaces and commercial PES MF membranes were created using a cross-linking agent; terephthalaldehyde (TA), for the formation of a positively charged membrane for trapping and inactivation of viruses. Furthermore, silver and copper nanoparticles (Ag and CuNPs) with antiviral activity were coated on the substrates and stabilized with PEI. These resulted in a 4.5-5log unit reduction of MS2 bacteriophages through the viral particle inactivation and adsorption (Sinclair et al., 2019). Therefore, the incorporation of nanoparticles has enhanced the virus removal efficiency as well as the reinforcement of the structural integrity, membrane hydrophilicity, and electrostatic interaction between the viruses and the membrane for increased water flux (Khin et al., 2012; Liu et al., 2019; Németh et al., 2019; Kuo et al., 2020; Chen et al., 2021a).

Two major challenges in water treatment using membrane filtration are biofouling and virus penetration, as the membrane's permeability decreases with increased biofouling. Consequently, it results in high energy costs and a reduction in the membrane's durability (Zodrow et al., 2009). Furthermore, virus separation is increased to some extent by membrane fouling (Chen et al., 2021a); however, the membrane surface could become weakened accompanied by increased penetrability and then compromised virus retention (Wang et al., 2017). Membranes have been modified with different materials such as polymers; however, polymer leaching is a problem associated with this technology (Sinclair et al., 2018) which could lead to a loss of the antiviral ability of the material when the substance is leached into the environment (Koplin et al., 2008; Sinclair et al., 2019). Another material that has been incorporated into the membrane for its modification is nanoparticles due to their proven antimicrobial properties; however, the loss of nanoparticles is a major drawback (Zodrow et al., 2009). Therefore, further research is needed in this regard to concentrate on the encapsulation of the nanoparticles in a bid to control their release.

Ultraviolet irradiation

One of the physical techniques used for the inactivation of microorganisms is ultraviolet radiation (Oguma and Rattanakul, 2021). The International Commission on Illumination has described the UV region of the electromagnetic spectrum as radiation with wavelengths that ranges from 100 to 400 nm (CIE, 2003; ASHRAE, 2019). Furthermore, the UV spectrum is categorized into UVA (wavelengths of 400–315 nm), UVB (315–280 nm), UVC (280–200 nm), and vacuum UV (VUV; 200–100 nm; IESNA, 2000). A relatively high energy level is associated with radiation in the UV range, and microbes absorb protons with a high absorption coefficient between 200 and 300 nm (Chen et al., 2021a). Exposure of microorganisms to UV light damages their nucleic acids (DNA or RNA; Ibrahim et al., 2021). In other words, the process entails running water through UV disinfection tubes, which damages the nucleic acids resulting in the non-viability of the bacteria and viruses, thus, become incapable of reproduction (Wigginton et al., 2012; Sigstam et al., 2013). This disinfection method has been proven effective for the inactivation of cysts of *Cryptosporidium* and *Giardia* in water (Chen et al., 2021b). The UV disinfection is considered an efficient and competitive alternative for the disinfection of secondary effluent because it does not make use of chemical agents, is non-corrosive, easy to install and operate, and produces no DBPs, hence no toxic residue after disinfection (Tondera et al., 2015; Zhang et al., 2016). Short contact time is required for disinfection due to the rapid-reacting nature of the radicals, and there is no odor or taste when it is used. Therefore, UV radiation is appropriate for drinking water treatment plants (Ibrahim et al., 2021).

The most frequently used UV sources are low-pressure (LP) and medium-pressure (MP) UV. They are mercury lamps for monochromatic UV at 254 nm and polychromatic UV with a broad spectrum, respectively, (Song et al., 2019). Germicidal lamps produce UVC energy by emitting radiation mostly at a wavelength of 253.7 nm, which kills or inactivates microorganisms (ASHRAE, 2019). Viruses are inactivated differently due to the morphological and genomic varieties (enveloped or non-enveloped; DNA or RNA viruses) of the different viral species as well as the wavelength of the germicidal UV applied (Oguma and Rattanakul, 2021). For instance, DNA replication in viruses is generally inhibited by UV at 254 nm and 280 nm irradiation. However, UV at 224 nm irradiation has little effect on the viability of the human adenovirus-2 (HAdV-2) genome. Nevertheless, the impact of capsid alterations may impede the virus's genome ability to enter the nucleus in host cells (Vazquez-Bravo et al., 2018). Conversely, 3log inactivation can be attained for poliovirus, coxsackievirus, and echovirus using UV at 254 nm in the range of 14 to 27 mJ/cm^2 (Gerba et al., 2002; Shin et al., 2005).

In a bid to enhance viral inactivation using UV, H_2O_2, ozone, sodium hypochlorite, and chlorine dioxide, among others, have been incorporated into the UV disinfection process. Mamane et al. (2007), incorporated 25 mgl^{-1} dose of H_2O_2 to filtered UV irradiation for 15 min, which led to a 2.5log increase inactivation effect on MS2, whereas MS2 was resistant to only UV irradiation at >295 nm. The authors opined that hydroxyl radicals produced from the photolysis of H_2O_2 could be responsible for the observed effect and could have destroyed the cell membranes of MS2 with a simple but rigid structure. Similarly, combining UV treatment with chlorine resulted in 3-5log_{10} reductions for chlorine-resistant coliphages coupled with reduced DBPs formation (Zyara et al., 2016).

Ultraviolet C (UVC) light with wavelength between 207 and 222 nm has been reported to be effective for the inactivation of microorganisms. Specifically, far UVC light is considered safe for human health compared to the traditional germicidal UV light

because it does not damage mammalian cells (Buonanno et al., 2017; Ponnaiya et al., 2018; Buonanno et al., 2020; Narita et al., 2020). Sequential UVA and UVC irradiation using light-emitting diodes (UV-LED) were applied for *Escherichia coli* and MS2 inactivation in a study carried out by Song et al. (2019). There was no improvement in the inactivation of MS2 as compared to *E. coli* following UVA pre-treatment accompanied by UVC treatment. The observed inactivation of MS2 in their study was attributed to its composition as being void of a cellular metabolic system (Song et al., 2019).

The efficiency of 222 nm UVC light for the inactivation of alpha HCoV-229E and beta HCoV-OC43 was evaluated using an aerosol irradiation chamber. Aerosolized coronavirus 229E and OC43 were inactivated by UVC with low doses of 1.7 and 1.2 mJ/cm^2, respectively, (Buonanno et al., 2020). Biasin et al. (2021), investigated the ability of UVC irradiation at different doses to inactivate SARS-CoV-2 (Virus Human 2019-nCoV strain 2019-nCoV/Italy-INMI1, Rome, Italy) at a multiplicity of infection (MOI) of 1000, 5, and 0.05. The authors reported that UVC dose of just 3.7 mJ/cm^2 was adequate to attain above 3log inactivation without viral replication. All the viral concentrations evaluated at a UVC dose of 16.9 mJ/cm^2 were inactivated completely. Mariita et al. (2022), inactivated Feline calicivirus (FCV) ATCC VR-782; a surrogate of norovirus with a UVC light-emitting diode (LED) array (KL265-50 V-SM-WD). A 99.9% virus reduction (3log reduction) was achieved at a UVC dose of 22.5 mJ cm^{-2}; hence, the authors posited that NoVs can be inactivated effectively using UVC LED array (Mariita et al., 2022).

Disinfection methods, especially UV light, have repeatedly been found ineffective against adenovirus (Prado et al., 2019); hence, optimizing this method for the inactivation of adenovirus is a necessity. The use of UV-LEDs for viral inactivation just got into the limelight recently (Rattanakul and Oguma, 2018; Keshavarzfathy et al., 2021); therefore, more research is needed in this regard. Although UV disinfection is known for not resulting in the formation of DBPs compared to chlorine, turbid and colored particles in the secondary effluent may reduce UV light penetration which affects its disinfection ability (Zhang et al., 2016). In addition, incorporation of H_2O_2 into UV irradiation for improved viral inactivation is less efficient when applied to wastewater with increased absorbance and its utilization is affected by the high cost of operation (Rasalingam et al., 2014).

Chemical methods

Chlorination

For several decades, chlorination has been used in both developing and advanced countries as the most economical, traditional, and versatile disinfectant for water disinfection processes (Lim et al., 2010; Hu et al., 2019; Martino, 2019; Luo et al., 2020; Rachmadi et al., 2020). The slower decay rate of chlorine in comparison to many other chemical disinfectants is responsible for its capacity to retain disinfection activity for longer periods; hence, its preference for use in drinking water distribution systems and water reservoirs avoids subsequent replication of the microorganisms (WHO, 1996; Xiao et al., 2020).

Chlorine interacts with organic chemicals in the water to generate several secondary products that are more hazardous than the parental components (Anand et al., 2014). Chlorine gas combines with water to generate aqueous HOCl and HCl (Equation 1), and then HOCl dissociates further to form OCl^- and H^+ (Equation 2; Lin and Lee, 2007; Collivignarelli et al., 2018). The use of aqueous chlorine for disinfection is a function of contact time and concentration (Kumar et al., 2020).

$$Cl_2 + H_2O \leftrightarrow HOCl + HCl \quad (1)$$

$$HOCl \leftrightarrow OCl^- + H^+ \quad (2)$$

Chlorine gas and water have a reversible and pH-dependent chemical interaction in nature (Hung et al., 2017). The presence of OCl^- and HOCl in large quantities in water aids in the oxidation, hydrolysis, and disintegration of cell membranes. These reactions between the chlorine compounds and membrane proteins of the microorganisms in water result in the formation of chloro-nitrogen compounds. Proteins, DNA, lipids, and cholesterol are all biological targets that HOCl is known to interact within the body (Hawkins et al., 2003). The purine and pyrimidine sequences of the DNA of the microorganisms are altered by HOCl as this is expressed in its negative effect on the genetic sequence mutation, metabolism, synthesis of protein, and transport of glucose (Kumar et al., 2020).

Chlorine exhibits its potent bactericidal effect by blocking metabolic activities through a variety of complex processes. The modus operandi it adopts alters the chemical composition of the enzymes at the center of bacteria's nutrition systems, rendering them inactive thereby preventing their growth and survival (Collivignarelli et al., 2018). However, some endospore-forming bacteria such as *Bacillus* and *Clostridium* are not inactivated by chlorine disinfection. At the same time, protozoa, including *Entamoeba histolytica* and *Giardia lamblia*, require a high dose (mgL^{-1}) and considerable contact time to be inactivated (Kumar et al., 2020).

The destruction of viral capsid protein and the inhibition of genome replication can both be achieved toward the inactivation of viruses using free chlorine (Fuzawa et al., 2019). At a pH of 7.4, room temperature, 5 mM PO_4^{2-}, and 10 mM NaCl, it was reported that no undamaged capsid protein was detected after 5log inactivation of MS2 with chlorination having caused significant damage to the genome and capsid protein. The considerable capsid protein degradation led to a substantial loss of protein-mediated binding or injection capabilities, and the treatments hindered replication functions and causes significant genome damage (Wigginton et al., 2012).

The efficiency of free chlorine in the inactivation of waterborne viruses has been expressed to be temperature and pH-dependent (Lim et al., 2010) as well as the type of virus involved. Table 1 shows the estimated Ct values for 4log reduction of waterborne viruses using the efficiency factor hom (EFH) model. This method has been utilized to evaluate disinfection kinetics in drinking water to ensure conformity with the Surface Water Treatment Rules for microbiological reduction requirements (Haas and Joffe, 1994). The idea of disinfectant dose and contact time is essential to comprehending disinfection kinetics and using the Ct concept (Collivignarelli et al., 2018). The Ct values are the product of the disinfectant dose C (in mgL^{-1}) and the contact time *t* (in minutes; Haas and Joffe, 1994; Girones et al., 2014; Rachmadi et al., 2020). They are an important metric for practical disinfection evaluation and system design (Collivignarelli et al., 2018; Chen et al., 2021b). Under similar conditions, Echovirus (E), Coxsackievirus B (CVB), and PV are more resistant to inactivation using chlorination. However, pH dependence for disinfection of CVB5, CVB6, PV, E-1, and E-12 was revealed to occur at pH 9 or higher, resulting in a remarkable increase in the required Ct values for the inactivation of these viruses when compared to pH 7 or lower without a change in the time (Black et al., 2009; Cromeans et al., 2010). In addition, it has been documented that reoviruses are more sensitive to chlorine compared to enteroviruses (Betancourt and Gerba, 2016). It has not been reported that chlorine effectively controls all waterborne viruses as Norovirus suspension remained infectious after 30 min of contact with 3.75 mgl^{-1} free chlorine (Keswick et al., 1985).

In the presence of naturally occurring organic molecules, chlorine produces trihalomethane and acetoacetic, which are recognized to be carcinogenic to humans with the most frequent being the trihalomethanes (THMs; Rebhun et al., 1997; Guay et al., 2005; Sun et al., 2009; Badawy et al., 2012; Wu et al., 2013; Sorlini et al., 2015; Sorlini et al., 2016). While chloroform, bromodichloromethane (BDCM), chlorodibromomethane (CDBM), and bromoform comprise the volatile compound category. The THMs, haloacetic acids (HAAs), chlorophenols, chloral hydrate, and haloacetonitriles (HANs) are some of the undesired halogenated organic compounds formed when chlorine combines with natural organic molecules (humic and fulvic acids). Although brominated THMs can be produced in large quantities when waters with high bromide content are chlorinated, chloroform is generally the most common by-product generated, while the majority of other DBPs are found in trace amounts, typically less than 1 μgl^{-1} (Nieuwenhuijsen et al., 2000). Production of DBPs that accompanies chlorine disinfection is an issue of great concern due to the increase in significant human health risks, such as cancer of the bladder and adverse associated reproductive outcomes (EPA, 2005; Richardson et al., 2007). This has made the development of alternative disinfectants a necessity due to the mutagenicity, carcinogenicity, and teratogenicity of the DBPs formed during chlorine disinfection in a bid to meet up with the regulation of DBPs (Gall et al., 2016).

TABLE 1 Estimated Ct values for 4-logs reduction of waterborne viruses using the efficiency factor hom (EFH) model (adapted from Chen et al., 2021b).

Enteric virus	CT value (mg min L^{-1})	Disinfectant dose (mg L^{-1})	Conditions	References
Adenovirus-40	0.22	1.0	pH 6, 5°C	Thurston-Enriquez et al. (2003)
	0.75		pH 7, 5°C	
	0.27		pH 8, 5°C	
Poliovirus-1	6.36		pH 6, 5°C	
	5.3		pH 7.5, 5°C	
	5.3	1.0	pH 7.5, 5°C	Black et al. (2009)
	22.9	1.0	pH 9, 5°C	
Coxsackievirus B5	11.5	1.0	pH 7.5, 5°C	
	22.9	1.0	pH 9, 5°C	
Echovirus 1	6.2	1.0	pH 7.5, 5°C	
	16.6	1.0	pH 9, 5°C	
Echovirus 12	7.4	1.0	pH 7.5, 5°C	
	32.3	1.0	pH 9, 5°C	
Coxsackievirus B3	2.9	0.2	pH 7, 5°C	Cromeans et al. (2010)
	1.7	0.2	pH 8, 5°C	
Coxsackievirus B5	7.4	0.2	pH 7, 5°C	
	10	0.2	pH 8, 5°C	
MS2	0.435	0.172	pH 7.2, 5°C	Lim et al. (2010)
	0.183	0.172	pH 7.2, 20°C	
Rotavirus	5.55	0.4	pH 7.2, 20°C	Xue et al. (2013)
Adenovirus-2	1.65	2.7	pH 8, 25–26°C	Girones et al. (2014)

Monochloramination

Many chemical reactions occur from the interaction between chlorine and the aqueous solution of ammonia (Equations 3 and 4), which depends on the concentration, temperature, and pH of the aqueous solution. The mechanism of the formation of chloramine from the reaction between chlorine and aqueous ammonia is a function of the molar concentration of ammonia and chlorine (Equations 5 and 6; Kumar et al., 2020).

$$Cl_2 + H_2O \leftrightarrow HOCl \quad (3)$$

$$HOCl + NH_3 \rightarrow NH_2Cl + H_2O \quad (4)$$

$$HOCl + NH_2Cl \rightarrow NHCl_2 + H_2O \quad (5)$$

$$HOCl + NHCl_2 \rightarrow NCl_3 + H_2O \quad (6)$$

Organic chloramine is the end-product of the reaction between chloramine and several amino acids. At a suitable temperature and pH, the organochlorine compound is formed at the interaction of chloramine and cell component which include alanine, tyrosine, and glycine. Monochloramine (NH_2Cl) is a desirable disinfectant because; unlike free chlorine, it does not readily interact with natural organic matter to produce controlled DBPs [total trihalomethanes (TTHM) and haloacetic acids (HAA5); Lytle et al., 2021]. On the contrary, NH_2Cl has been used by many drinking water systems in the United States as a secondary disinfectant to reduce the generation of DBPs and the growth of biofilms (Cromeans et al., 2010). The inactivation of bacteria by NH_2Cl as well as their resistance to NH_2Cl has been reported when extra and intracellular antibiotic resistance genes (eARG and iARG) were employed in both intracellular and extracellular components (He et al., 2019).

The inactivation rates of NH_2Cl disinfection on AdV2, 40, and 41, E-1 and E-2, CVB3 and B5, and Murine Norovirus (MNV) have been compared by Cromeans et al. (2010). Disinfection with NH_2Cl was most effective against E-1 and least effective against E-2 and AdV 2. However, to attain 4log inactivation of CVB5 and E-2, Ct values of 900 mg × min L^{-1} and 1,500 mg × min L^{-1} were required. At pH 7, the authors reported that NH_2Cl was the most effective against AdV2, CVB5, and E-1. Unlike chlorine disinfection, NH_2Cl disinfection showed more variation in virus inactivation rates (Cromeans et al., 2010). The outcome of the investigation revealed that NH_2Cl efficacy data for different viruses should be integrated into the NH_2Cl inactivation modeling and system design. In addition, no single disinfection method is effective in the inactivation of all types of viruses.

Kahler et al. (2011) examined the disinfection efficiency of NH_2Cl on CVB5, E-11, MNV, and HAdV2 in untreated groundwater and two partially treated surface water. The authors reported that this method was most effective for MNV, followed by CVB5, while it was least effective for HAdV2 and E-11. The study indicated that the water quality impacts the inactivation of viruses; hence, this should be considered while developing monochloramination designs. According to Gall et al. (2016), at pH 9, Ct values of approximately 13,000 mg × min L^{-1} at 5°C and above 5,000 mg × min L^{-1} at 15°C are sufficient to attain 4log inactivation of HAdV. The examination of the different stages in the replication cycle of HAdV was conducted to understand the mechanism of inhibition of NH_2Cl by Gall et al. (2016). Therefore, the authors concluded that there is a possibility of the inhibition of a replication cycle action after binding, although it was claimed that this would have occurred before the early viral protein synthesis.

Likewise, the effect of NH_2Cl was examined in human norovirus (hNoV) GI, and GII, in secondary wastewater and phosphate buffer (PB). Using RT-qPCR as a method of detection, <0.5log_{10} reductions of all viruses at *C*t values were up to 450 mg × min L^{-1} except for hNoV GI, where 1log_{10} reductions at *C*t values of <50 mg × min L^{-1} for NH_2Cl in wastewater were recorded. There was a comparable resistance to monochloramine by hNoVGI and MNV with 2log_{10} RT-qPCR reductions ranging from 300 to 360 mg × min L^{-1} in PB (Dunkin et al., 2017). The results revealed that there is an occurrence of genogroup dependent resistance pattern in hNoVs.

Because of poor disinfection properties and ineffectiveness against spore-forming waterborne pathogens like *Cryptosporidium*, chloramine is not utilized as a primary disinfectant (Kumar et al., 2020). When compared with chlorine, it is less virucidal (Dunkin et al., 2017), and a longer contact time is needed to attain similar disinfection efficiency because the active ingredient in chloramine, which is hypochlorite, is released slowly (Chen et al., 2021b). In other words, it is a less effective disinfectant than chlorine because it requires more exposure time to inactivate many waterborne pathogens, including enteric viruses.

Chlorine dioxide

In recent years, there has been a significant increase in the usage of gaseous chlorine dioxide as a disinfectant for drinking water. Chlorine dioxide (ClO_2) is typically utilized for water disinfection at 0.1 and 5.0 mgl^{-1} concentrations. It is a volatile gas created *in situ* by mechanical generators utilizing acid-based or electrolytic processes (Ma et al., 2017). It is employed as an oxidizing agent (Symons, 1981) to break down biofilm in pipes and tanks (Michael et al., 1981), and it can only react in water *via* oxidation with a low generation of THM. It oxidizes organic components derived primarily from oxidized by-products and a small quantity of chloro-organic molecules, whereas chlorine interacts with substances through oxidation and electrophilic substitution (WHO, 2002; Totaro et al., 2021). Furthermore,

chlorine dioxide lowers the development of harmful halogenated disinfection by-products; however, at concentrations of 0.5 mgl^{-1}, it also produces the organic halides chlorite/chlorate as well as tastes and odors (Thurston-Enriquez et al., 2005).

The disinfection impact of chlorine oxide on algae, protozoa, biofilms, bacteria, and viruses was also examined (Aieta and Berg, 1986). The inactivation process of viruses is not like other cells because the time of inactivation is shorter than that of bacteria even under similar conditions. This could be attributed to the less complex structure of viruses compared to bacteria. Chlorine oxide gas acts on the genome of the non-enveloped viruses, whereas in enveloped viruses, it interacts with one or more of the cysteine, tyrosine, and tryptophan amino acid residues of the spike proteins as it does not need to invade the enclosed viral surface (Noss et al., 1986; Noszticzius et al., 2013; Kály-Kullai et al., 2020). Factors that have significant effects on the inactivation rates of viruses using ClO_2 include dosage, time, pH, and temperature (Berman and Hoff, 1984). When they are treated with 1.0 mg/l of chlorine oxide, enveloped viruses are inactivated readily compared to non-enveloped viruses (Sanekata et al., 2010). The adherence of the virus to the host cell is prevented *via* the disinfection action on the proteins of the viral envelope, and consequently, cell invasion and infection were prevented (Li et al., 2004). According to Noss et al. (1986), the premise of the disinfection process is a viral protein component; inactivating the coat viral protein results in the inhibition of the virus capacity to attack the host cells. Table 2 shows the inactivation efficiency of selected viruses by chlorine dioxide.

Furthermore, Thurston-Enriquez et al. (2005), examined the inactivation efficiency of ClO_2 within the range of 0.67–1.28 mgl^{-1} on AdV40 under pH values of 6 and 8 at 5°C and 15°C. The disinfection effectiveness of chlorine oxide improved at higher temperatures and pH values. Higher inactivation rates were reported at 15°C and pH 8 compared to other investigated conditions (Thurston-Enriquez et al., 2005). The effect of ClO_2 at an initial concentration of 5 mgl^{-1} was elucidated on HAV, and the disinfectant could not eliminate the infectivity after 60 min; however, the virus was completely inactivated after 10 min having increased the concentration to 7.5 mgl^{-1}. The 5′-non-translated region (5'NTR) of the virus's genome was damaged by the disinfectant, which hindered the replication, and interaction with viral proteins and prevented adherence to the host's cells (Li et al., 2004). A faster inactivation rate of 30 s at 0.8 mgl^{-1} and 5 min at 0.4 mgl^{-1}, respectively, for HAV was reported by the Department of Public Health of Parma (Li et al., 2004; Zoni et al., 2007).

Feline Calicivirus (FCV) was inactivated completely by ClO_2 in 30 min at 0.2 mgl^{-1} as reported by Alvarez and O'Brien (1982). In the same vein, at the same concentration and contact time, CVB5 was inactivated completely. Interestingly, at 0.2 mgl^{-1} of ClO_2 and a reduced contact time of 4 min, complete inactivation of CVB5 was reported (Alvarez and O'Brien, 1982). Thurston-Enriquez et al. (2005) discovered that treating EV71 with ClO_2 for more than 30 min (0.5 mgl^{-1}), 25 min (1.5 mgl^{-1}), and 15 min (2.0 mgl^{-1}) resulted in complete inactivation of the virus. Similarly, at 4.92 mgl^{-1} of ClO_2 for 1 min, higher rate of inactivation was reported at pH 8.2 compared to pH 5.6 while inactivation occurred rapidly at 36°C compared to 4°C or 20°C. The effectiveness of ClO_2 for the inactivation of EV71 was dependent on both temperature and pH. Likewise, it has been found that the inactivation of AdV40 and FCV by ClO_2 is more significant at 15°C than at 5°C (Thurston-Enriquez et al., 2005).

Chlorine dioxide is connected with DBPs such as chlorite and chlorate formation during water disinfection. As a disinfectant, ClO_2 is commonly used for pre-oxidation followed by post-chlor(am)ination to reduce the production of chlorite and chlorate as neurotoxicity could result from a high dose of ClO_2 (Chen et al., 2021b). The unstable nature of ClO_2 prevents its storage; hence, it must be manufactured on-site and then added to water (Collivignarelli et al., 2018). Also, ClO_2 is more biocidal when compared with chlorine and chloramines; however, it causes organoleptic abnormalities in treated water (Ngwenya et al., 2013), which makes this disinfectant less suitable for purification.

Ozonation

For over a century, ozone (O_3) has been used in drinking water treatment and chemical oxidation. It is used to substitute chlorine for disinfection in some parts of the world (Choudhury et al., 2018). Ozone is a bluish gas with a strong odor. It is an exceedingly reactive and unstable allotrope of oxygen (Rekhate and Srivastava, 2020). It is one of the most potent disinfectants available, and effective against practically all sorts of waterborne infections (Wolf et al., 2018). It is partially soluble in water and interacts with organic particles found in bacteria, viruses, and protozoa cells. The development of the organism's cytoplasmic protein is inhibited as a result of the reaction between the ozone and the cell's plasma membrane (Kumar et al., 2020).

Bacteria, viruses, protozoa, and prion protein as well as other pathogens such as *Cryptosporidium*, *Giardia* cysts, parvum oocysts, and *Legionella* that are resistant to chlorine are known to be effectively inactivated by ozone (Von Gunten, 2003; Betancourt and Rose, 2004; Passos et al., 2014; Li et al., 2017; Xi et al., 2017). More specifically, the effectiveness of ozone for the removal of viruses in water has been documented (Tondera et al., 2015; Wolf et al., 2018; Wang et al., 2018b), and this is usually through the oxidation of nucleic acids or promotion of protein coagulation in the viral particle (Tyrrell et al., 1995; Gomes et al., 2019b). Besides the inactivation of waterborne pathogens, O_3 is employed to control taste and odor and the chemical oxidation of contaminants in drinking water (Chen et al., 2021b).

According to the Environmental Protection Agency (Agency, 1999), O_3 at 0.1 mgl^{-1} outperforms chlorine at 2.0 mgl^{-1} due to faster reaction times in terms of disinfection with no regrowth of microorganisms. Ozone has been adopted recently in wastewater treatment with the primary goal of reducing micropollutants in secondary wastewater effluent and their impact on the aquatic environment (Wolf et al., 2018). Many potable reuse systems

TABLE 2 Inactivation efficiency of selected viruses by chlorine dioxide.

Enteric virus	*Ct* value	Inactivation efficiency	Conditions	Reference
Feline calicivirus	0.18 mg min L^{-1}	4log	pH 8, 15°C	Thurston-Enriquez et al. (2005)
Feline calicivirus	9.59 min	4log	0.4 mg/l, pH 7.0, 20°C	Zoni et al. (2007)
Feline calicivirus	2 min	0.25log	1.0 mg L^{-1} ClO_2	Sanekata et al. (2010)
Murine norovirus	0.25 mg min L^{-1}	4log	pH 7.2, 5°C	Lim et al. (2010)
Coxsackievirus B5	2.41 min	4log	0.4 mg L^{-1} ClO_2, pH 7.0, 20°C	Zoni et al. (2007)
Hepatitis A virus	19.58 min	4log	0.4 mg L^{-1} ClO_2, pH 7.0, 20°C	Zoni et al. (2007)
Enterovirus 71	3.93 mg min L^{-1}	4log	pH 7.2, 20°C	Jin et al. (2013)
Echovirus 11	1.0 mg min L^{-1}	6log	pH 7.4	Zhong et al. (2017)
Human rotavirus	1.21 mg min L^{-1}	4log	pH 7.2, 20°C	Xue et al. (2013)
Adenovirus type 40	0.12 mg min L^{-1}	4log	pH 8, 15°C	Thurston-Enriquez et al. (2005)
Human Adenovirus	2 min	1.5log	1.0 mg L^{-1} ClO_2	Sanekata et al. (2010)

incorporate ozone as an essential component, for pre-oxidation of organic materials in the effluent, micropollutant reduction, and disinfection (Gerrity et al., 2013). In addition, due to its ability to reduce membrane fouling (Stanford et al., 2011), ozonation is commonly employed for membrane pre-treatment (Cheng et al., 2016).

In a bid to achieve improved disinfection using ozone, biologically activated carbon, free chlorine, or other catalysts have been incorporated with ozone. Gomes et al. (2019a), integrated volcanic rocks as catalysts into ozone, resulting in the complete removal of NoV GI, GII, and JC Polyomavirus (JCPyV). However, after 150 min, JCPyV remains inactivated. Also, an increase in the amount of ozone led to a surge in the disinfection of MS2 from 2.1 to 6.8log when ozone, coagulation, and ceramic membrane filtration were combined for the removal of viruses for water reclamation (Im et al., 2018).

Ozone can be used more effectively for viral inactivation in water than traditional water treatments such as mechanical treatment, aerated grit chamber, activated sludge, and reactors (Wang et al., 2018b). However, there could be a reduction in the inactivation with changes in some operational parameters, such as a lower temperature or an increase in pH. In clearer terms, ozone's attenuation rate and oxidation ability are affected by a rise in pH and vice versa. In addition, other factors that could reduce the inactivation of viruses in water using ozone include the presence of particles, organic matter, and co-existing ions (Cai et al., 2014). Thus, the movement of ozone molecules is enhanced by an increase in temperature, resulting in the attachment of organic particles to the virus, which shields the viruses from ozone molecules and affects inactivation. In essence, the efficiency of ozone disinfection is reduced when a substantial quantity of ozone is consumed due to the presence of dissolved organic matters (Chen et al., 2021a).

The formation of bromate during disinfection from the oxidation of bromide ions in water (Chen et al., 2021a) a kind of DBPs is a major concern when significant ozone exposures are needed for pathogen inactivation (Gomes et al., 2019b). The instability and poor solubility of ozone in water is a setback for its application in practice; hence, its on-site production is required for its utilization (Rekhate and Srivastava, 2020). Therefore, there is a high operation cost associated with using ozone for disinfection in addition to maintenance costs linked to the use of ozonation equipment (Collivignarelli et al., 2018).

Emerging methods

Photocatalytic disinfection

The interaction between a photocatalyst (reaction initiator) and the aquatic medium (disinfection target) is known as photocatalytic disinfection; hence, both components of the photocatalyst and the properties of the aqueous medium are important factors in the reaction (Schneider et al., 2014; Smith and Rodrigues, 2015). The process of photocatalytic oxidation entails the production of electron–hole pairs by the irradiation of a semiconductor (such as TiO_2) with appropriate light. As a result of the irradiation, electrons (e-) are stimulated into the conduction band (CB), leaving a hole (h+) in the valence band (VB). Thereafter, the duo of e−/h+, which are the charge carriers, migrates to the photocatalyst's surface/interface and takes part in the redox processes. These charge carriers start a chain of events that result in the production of ROS. The ROS formed include singlet oxygen, superoxide radicals, hydrogen peroxide, hydroxyl radicals, and perhydroxyl radicals. These highly reactive chemicals are particularly important because they can engage in cellular

component oxidation, microbial cell content release, and other activities (Cabiscol Català et al., 2000; Reddy et al., 2016).

Photocatalytic disinfection is very effective for the inactivation of bacterial species. TiO_2 nanotubes were used for the inactivation of *E. coli* at the rate of 10^6 CFU/ml under 10 min (Baram et al., 2009). Daels et al. (2015) also reported the effective inactivation of 76% of the overall bacterial colonies within 6 h of exposure time using TiO_2-functionalized membranes. Also, Li et al. (2015) utilized Ag-TiO_2 to disinfect *Pseudomonas aeruginosa*. Similarly, photocatalytic disinfection was also used to inactivate fungus and algae (Tatlıdil et al., 2011; Lee et al., 2015).

Over the last few years, nanostructured TiO_2, the most notable studied photocatalyst, has been actively investigated for photocatalytic viral disinfection. Degussa P25 was the most preferred photocatalyst in all these investigations because of its strong photoactivity, long-term stability, relatively low toxicity, and inexpensive cost (Zhang et al., 2015; Wang et al., 2018a). Viral inactivation kinetics is affected by TiO_2 crystalline structures which are either anatase or rutile. Sjogren and Sierka (1994) began the pioneering work on the inactivation of MS2 through photocatalytic viral disinfection by using TiO_2 photocatalyst. Thereafter, TiO_2 and TiO_2 -based photocatalysts, metal-containing photocatalysts apart from TiO_2, and metal-free green photocatalysts have been employed to achieve improved antiviral disinfection effects (Table 3). Sato and Taya (2006) studied the impact of TiO_2 particle crystalline structures on their virucidal ability. The authors achieved a maximum viral inactivation efficacy when both anatase and rutile TiO_2 particles were combined with a 70% anatase ratio, having anatase and rutile phases that is 2 and 11 times more than TiO_2, respectively.

To achieve increased viral inactivation in drinking water, researchers have embarked on enhancing both metal and metal oxides. TiO_2 photocatalysis was improved by loading the photocatalyst with nano-sized silver (nAg) by Liga et al. (2011), as a result of the several benefits attached, which include suppressed charge recombination in TiO_2 by trapping the excited electrons, increased surface area for virus adsorption, and Ag^+ release for viral inactivation. The combination of TiO_2 and nAg facilitated increased viral disinfection efficiency, as 6.2-log MS2 was inactivated within 2 min of UV irradiation using nAg/TiO_2 and was > 6 times quicker compared to the unmodified TiO_2.

Furthermore, a variety of effective, metal-containing, visible-light-active photocatalysts, as well as TiO_2-based photocatalysts, for instance, plasmon-induced viral disinfection by Ag-AgI/Al_2O_3 (Hu et al., 2010) and platinum-tungsten oxide (Pt-WO_3; Takehara et al., 2010), have been developed to enable solar-driven inactivation of waterborne viruses. Bacteriophage MS2 titer of 2×10^6 PFU/mL was reduced to <5 PFU/mL under visible-light radiation for 3 h when graphene oxide (GO) sheets were integrated into WO_3 films to give graphene-WO_3(G-WO_3) films (Akhavan et al., 2012). Wustite, Maghemite, and nano-Maghemite which are iron oxides were explored for their photocatalytic antiviral activity using solar irradiation. Wustite demonstrated the highest disinfection efficiency with a record of 5log MS2 under 30 min, while 2.6log MS2 inactivation was achieved within 120 min (Giannakis et al., 2017a). Some of the distinct advantages of using iron ore minerals to inactivate microbial contaminants include low-cost material, availability, earth abundance, visible-light reaction owing to the presence of iron components, and simple magnetic recovery from water. Therefore, natural photocatalysts based on iron have a potential for industrial manufacture and real-time utilization for waterborne viruses' disinfection (Zhang et al., 2019a).

Moreover, fullerene-based photocatalysts have been developed to improve the disinfection and inactivation of waterborne viruses. Novel C_{60} derivatives with diverse functional groups such as eNH_3^+, –COOH, or –OH-terminals were developed, with improved water stability. There is a possibility that the electrostatic bond between positively charged C_{60} derivatives and negatively charged MS2 viruses was responsible for the outstanding viral inactivation activity demonstrated by the cationic aminoC_{60} when compared to the commercial TiO_2 P25 (Lee et al., 2009; Cho et al., 2010; Lee et al., 2010; Moor and Kim, 2014; Moor et al., 2015). In addition, aminoC_{60} was found to be reactive when exposed to visible light from fluorescent lamps as well as sunlight (Cho et al., 2010). Furthermore, an organic linker with an amide group was utilized to link the C_{60} derivatives onto functionalized SiO_2 surface all in a bid to reduce their accidental discharge to water (Lee et al., 2010), leading to a significant improvement of the viral inactivation.

To develop an outstanding photocatalyst with a very high viral disinfection efficiency, Hu et al. (2012) introduced aptamers on the edge of GO and the composite novel antiviral material through energy transform/electron transfer efficiently inactivated viruses as it damaged nucleic acids and viral proteins using visible-light radiation. Aptamers that were integrated into GO increased the GO nanosheets' stability and bind to targets precisely. Graphitic carbon nitride (g-C_3N_4) became an attractive candidate for photocatalytic viral inactivation due to its biocompatibility with insignificant toxicity, resistance to photo-corrosion, air oxidation at increased temperature, and chemical stability in solvents such as acids and bases (Cao et al., 2015; Zheng et al., 2017).

Matsuura et al. (2021) examined the ability of light-emitting diode (LED)-activated TiO_2 fixed on a glass sheet to inactivate SARS-CoV-2 in aerosol and liquid. They reported that SARS-CoV-2 was inactivated with a reduction in its infectivity by 99% after 20 min and 120 min of interaction in aerosol and liquid, respectively. Hence, it was deduced that the photocatalytic interaction mediated by TiO_2 with the SARS-CoV-2 virus was dependent on time. The impacts of TiO_2 photocatalyst on SARS-CoV-2 virion include reduced virion count, increased virion size, decreased particle surface spike structure, and destruction of viral proteins and genome. The authors believed that the degradation of the spike protein of SARS-CoV-2 by the photocatalytic reaction of TiO_2 could inactivate the virus irrespective of the mutation in the protein.

However, one of the major limitations of using TiO_2 in water disinfection is the reaction kinetics; therefore, more studies should focus on improving the TiO_2 inactivation efficiency and the rate of solar energy utilization toward viral inactivation. Furthermore, magnetically separable materials that facilitate the removal of used

TABLE 3 Summary of parameters, inactivation efficiency, and photocatalysts used for viral disinfection in water.

Virus	Photocatalyst	Catalyst loading ($mg\,L^{-1}$)	Virus level (PFU/ml)	Light source	Inactivation efficiency/time	References
Murine norovirus	TiO_2	10	1×10^8	UV lamp	3.3log/ 24 h	Lee et al. (2008)
MS-2 bacteriophage	TiO_2	–	2×10^5	4 W BLB lamp	2log/109 min	Cho et al. (2011)
Phage f2	TiO_2	1,000	10^{10}–10^{11}	6 W black light Lamp	6log/15 min	Zuo et al. (2015)
Phage MS2	Mn-TiO_2	100	1×10^5	150 W Xe ozone-free lamp	4log/60 min	Venieri et al. (2015)
Phage MS2	g-C_3N_4	150	1×10^8	300 W Xe lamp	8log/300 min	Li et al. (2016)
Phage Qβ	Rh-$SrTiO_3$	3,000	5×10^7	Vis	5log/120 min	Yamaguchi et al. (2017)
Phage MS2	FeO	5	1×10^6	Simulated solar	5log/30 min	Giannakis et al. (2017a)
Phage f2	TiO_2	100	>20	4 W UV-lamp	5-6log/160 min	Cheng et al. (2018b)
Bacteriophage f2	Cu - TiO_2 Nanofibers	50	1×10^4	Xe lamp	4.0log/120 min	Zheng et al. (2018)
Bacteriophage f2	Ag_3PO4/g-C_3N_4	100	3×10^7	8 W UVA lamp	6.5log/80 min	Cheng et al. (2018a)
Phage MS2	g-C_3N_4	135.4	1×10^8	Xe lamp	8log/240 min	Zhang et al. (2018b)
MS2	g-C_3N_4/EP	0.06	1×10^8	300 W Xe lamp	8log/240 min	Zhang et al. (2018a)
Bacteriophage f2	Cu - TiO_2 Nanofibers	10	1×10^8	Xe lamp	>5log/240 min	Cheng et al. (2019)
HAdV-2	O-g-C_3N_4/HTCC	3	–	7 W white LED Lamp	5log/120 min	Zhang et al. (2019b)
Norovirus	Cu- TiO_2	–	2.89 ± 0.11 log 10	UVA-LED	5log/60 min	Moon et al. (2020)
HAdV-2	g-C_3N_4/H_2O_2	100	1×10^5	300 W Xe lamp	2.6log/150 min	Zhang et al. (2021)
MNV	TiO_2	300	1×10^6	4 W Blacklight Blue Lamps	1.4×10^{-5}/32 min	Kim et al. (2021)

photocatalysts from aquatic environments are another obstacle for the semiconductor-based photocatalytic viral disinfection method. Thus, floating photocatalysts are interesting candidates for enhancing the use of light/oxygen to generate more ROS (Habibi-Yangjeh et al., 2020).

Another significant drawback of the photocatalytic disinfection method for the inactivation of waterborne viruses is the high level of charge recombination in TiO_2 and low photocatalytic activity. In addition, the broad bandgap of TiO_2 (3.2 eV for anatase and 3.0 eV for rutile) enables the material to operate solely on UV light accounting for approximately 4% of solar energy used for photocatalytic disinfection. The majority of photocatalysts that have been shown to have outstanding antiviral action contain (heavy) metals, and the accidental release of hazardous metals (e.g., Cu, Ag) into treated water presents serious health issues (Zhang et al., 2019a).

Cavitation

Cavitation is the production of tiny vapor bubbles (cavities) within a liquid that was originally uniform and an abrupt drop in pressure causes this quick physical process. Cavities are formed due to the disruption of the liquid medium at one or more sites and their shapes are majorly influenced by the flow structure. The unstable vapor structures frequently collapse suddenly as they approach a section of elevated pressure. Strong shear flows, jets, high local temperatures, shock waves, rapid depressurization, and supersonic flow are all possible outcomes of the collapse (Shamsborhan et al., 2010; Kosel et al., 2017). In general, there are two types of cavitation: hydrodynamic cavitation (HC) and acoustic cavitation (AC). The process which results in a drop in the local pressure differentiates the two; however, the mechanisms that regulate the hydrodynamic bubble and the acoustic bubble are essentially similar. In AC, the propagation of acoustic waves achieves the required low pressures to cause the disruption of the liquid and lead to cavitation. In contrast, the liquid's current speed in HC will generate a reduced local pressure below saturation point for a liquid temperature, resulting in cavitation formation (Zupanc et al., 2019).

The precise mechanism by which cavitation inactivates viruses is not fully comprehended yet as few studies have evaluated the impact of cavitation on waterborne viruses (Filipić et al., 2022). The inactivation of viruses was known to be caused by heat and

high pressure, and OH^- was linked to damage of viral capsid proteins (Chen et al., 2021b). According to Su et al. (2010), virus inactivation could be due to the damage caused during cavitation either to the exterior protein capsid or the recognition sites situated on the exterior of the capsid. Kosel et al. (2017), opined that the alteration of the viral capsid or genome by OH^- produced during cavitation combined with mechanical impacts could be attributed to virus inactivation.

Dular et al. (2016), assessed the effect of HC on the decrease of rotavirus (RV), in a Venturi cavitation chamber using a pulsating system. The treatment reduced the RV concentration by 75% using RT-qPCR. In a similar Venturi constriction, the effect of HC on MS2 infectivity was investigated by Kosel et al. (2017), and it was reported that there was a 4.8log reduction per litre. The authors also mentioned that the viral inactivation could be linked to the damage of the host's recognition receptors situated on the virus surface due to the OH^- radicals generated from cavitation. Also, they posited that OH^- radicals were formed because cavitation could be responsible for the observed damage. Furthermore, they suggested that high shear forces inside the cavity could be another factor responsible for additional damage to the virus. Filipić et al. (2022), recently evaluated the inactivation of potato virus Y (PVY) in a liter of water using HC where inactivation was achieved after about 125 to 500 HC passes. It was observed that there was rapid and severe damage to the protein capsid of the virus compared to the genomic RNA, and this could be a major contributory factor to the virus inactivation. The authors further observed that strong oxidants such as O_2, OH^-, and H_2O_2 were not really involved in the virus inactivation; hence, this suggested that mechanical effects are possibly responsible for the inactivation.

Although hydrodynamic cavitation is a less expensive form of disinfection than AC, it costs more than chlorination and ozonation (Holkar et al., 2019). Also, it requires a continuous energy supply, and there is a limit to how much water can be treated using this process (Dular et al., 2016). Due to significant operational expenses, HC disinfection technology is currently in the laboratory stage (Pichel et al., 2019), and is yet to be implemented in large-scale applications (Sun et al., 2020).

Electrochemical disinfection

The primary basis of the electrochemical disinfection method is the oxidation ability of disinfectants in the electrode layer or the bulk of the electrode (Bruguera-Casamada et al., 2016; Ghernaout, 2017). This disinfection method is characterized by the production of intermediates, and it is grouped into two categories: direct anode oxidization, and indirect product oxidation. The transfer of electrons between the electrode and the target material without using poisonous chemicals and other organic molecules is the basis of inactivation when direct anode oxidation is performed. In contrast, concentrated saline solution is needed for anode oxidation, and therefore the accumulated molecules and ions (e.g., H_2O and Cl) at the electrode are oxidized for the formation of chlorine-active substances (for instance, Cl_2, HOCl, and ClO_3) as well as oxygen-active substances (e.g., oscillation of $[O(3P)]$, H_2O_2, O_3). To oxidize and remove the target substance, intermediate products are critical in transporting the electrons from the target material to the surface of the electrode (Panizza and Cerisola, 2005; Santana et al., 2005; Yang et al., 2018; Jung et al., 2020). The main cause of the inactivation of microorganisms when electrochemical disinfection is employed is damage to the intracellular enzyme system of the microbes (Long et al., 2015).

Boron-doped diamond electrodes have also been employed as a disinfectant in a sequential electrocoagulation-electro-oxidation treatment system for the removal of viruses in water. Bacteriophages MS2, ΦX174, and human echovirus were reduced from the positive simulation effect in the physical decrease of coagulation-filtration, ferrous iron-based disinfection, and electro-oxidation disinfection (Heffron et al., 2019). Tu et al. (2021) reported the inactivation of SARS-CoV-2 virus in Na_2CO_3 aqueous solution using nickel foam as both cathode and anode. Inactivation rates of 95, 99, and 99.99% at 5 V were recorded within just 30s, 2 min, and 5 min, respectively. The inactivation rates were attributed to oxidation and degradation of the receptor binding domain (RBD) of the SARS-CoV-2 spike glycoprotein by the NiOOH anode surface formed *in situ* during the electrolysis.

Even though viruses are smaller and less complex physically than bacteria, they resist electrochemical treatment more strongly, limiting the method's utilization, thereby necessitating further research (Drees et al., 2003; Chen et al., 2021b). Much attention has not been given to DBPs formation from electrochemical disinfection; however, some researchers now explore the possibility of by-products generation from electrochemical disinfectants and their possible toxicity levels (Jasper et al., 2017; García-Espinoza and Nacheva, 2019). Disinfection by-products that are produced during chemical disinfection processes might also be produced during electrochemical disinfection treatment depending on the electrode material used and applied voltage (Ghernaout, 2017).

Comparison of disinfection methods

Common disinfection methods involve membrane filters, ultraviolet irradiation, chlorine, monochloramine, chlorine dioxide, ozone, and emerging disinfection treatments such as photocatalytic and electrochemical disinfection. The mechanism of disinfection for virus mitigation and inactivation is based on the contact between the viruses and disinfectants to break down the virus's capsid protein and nucleic acid. This makes it impossible for viruses to spread to host cells and reproduce, while membrane filtration employs the size exclusion principle. The kind and primary concentration of the disinfectant and virus, as well as the

TABLE 4 Virus removal/inactivation range and the merits and limitations of the various disinfection method (adapted from Chen et al., 2021a).

Method	Removal/ inactivation log	Merits	Limitations
Membrane filtration	0.5–5.9	Low energy cost, the potential for mobile treatment unit, does not require chemicals	Removal efficiency is unstable, a potential health risk for humans
Ultraviolet irradiation	0.09–5	No DBPs formation, less susceptible to pH and temperature, non-corrosive, ease of installation and operation, short contact time	Relatively high energy consumption, inefficient in turbid water
Chlorination	1- > 5	Simple to handle, cost-effective, residual in distribution	DBPs production, residual toxicity
Monochloramination	0.5–4	Stable residual, less odor, and taste issues	Weak disinfectant, less virucidal, long contact time
Chlorine dioxide	0.25–6	More effective than chlorine at higher pH, lowers DBPs formation	DBPs formation, organoleptic abnormalities
Ozonation	0.6–7.7	Effective disinfectant, short contact time, possible combination with various catalysts	DBPs formation, high operation and maintenance cost, non-stable and poor solubility, effectiveness is affected by water turbidity
Photocatalytic disinfection	1–8	Low cost of operation, possible reuse of catalysts, favorable catalytic performance	Accidental leaching of hazardous metals into treated water
Cavitation	<4	No DBPs formation, possible for incorporation into a continuous flow process	Energy-intensive and high operating cost, still at the developmental stage
Electrochemical disinfection	3.4–5	Easy to control, environment friendly	Possibility of DBPs formation, low selectivity, the high operating cost associated with electricity consumption

pH, temperature, and treated water matrix (particles, dissolved oxygen, coexisting ions, and dissolved organic matter), remain the major factors militating against water disinfection.

Each disinfection method reviewed reduces the viral load before the effluent is discharged into the environment. However, the rate of viral inactivation differs, for instance, ozonation and UV irradiation are more effective for viral inactivation when compared with chlorination. Interestingly, UV irradiation is considered a clean disinfection technology due to its viral inactivation efficiency without forming DBPs. Furthermore, studies have revealed that RVs (Betancourt and Gerba, 2016), JC PyV, and echoviruses are better inactivated using chlorine compared to other waterborne viruses (Chen et al., 2021a). SARS-CoV-2 is inactivated by both chlorine and chlorine oxide (Brown et al., 2021; Hatanaka et al., 2021), as well as the emerging methods: photocatalytic disinfection (Khaiboullina et al., 2020), and electrochemical disinfection (Tu et al., 2021). However, the efficiency of cavitation for the disinfection of SARS-CoV-2 has not been investigated. Adenoviruses which have been reported to be resistant to UV irradiation (Augsburger et al., 2021), and monochloramination (Gall et al., 2016), are inactivated by both ozonation and photocatalysis disinfection (Chen et al., 2021a). Furthermore, Chen et al. (2021b) mentioned that inactivation of *E. coli*, *Clostridium perfringens*, *Vibrio cholerae*, and MS2 was faster using chlorine-active substances produced on-site compared to chlorine. Table 4 further summarized the virus removal/inactivation range, merits, and limitations of various disinfection methods discussed in this article. The log reduction value (LRV) shows the relative number of inactivated pathogens during the disinfection process (Equation 7).

$$\log \text{reduction values}(\text{LRV}) = \log_{10}(\text{A} / \text{B}) \quad (7)$$

where A is the number of viable pathogens before treatment while B is the number of pathogens after treatment (Mariita and Randive, 2021).

Conclusion and perspectives

Disinfection is critical in the elimination of waterborne microorganisms for the discharge of safe water to the environment. However, viruses differ from other pathogens in that they react differently in treatment processes, resulting in differences in their fate and behavior in water. Therefore, this has led to the adoption of different disinfection techniques, all in a bid to achieve safe water that is void of viruses. Unfortunately, secondary pollution caused by the formation of DBPs associated with chemical disinfectants cannot be overemphasized; hence, it should be avoided during viral disinfection. Interestingly, single techniques of disinfection can be sequentially merged into one and utilized as one method.

Emerging disinfection technologies have the potential to significantly increase virus inactivation in water by utilizing synergistic effects of different disinfection methods to solve the problem of the persistence of waterborne viruses. Nevertheless, they are not void of toxicity issues and accompanying high cost of operation. For example, to reduce DBPs formation yet increase viral inactivation, UV irradiation could precede chlorination, and

this would reduce the quantity of chlorine that is required. On the other hand, there could be formation of more DBPs if already chlorinated water is exposed to UV radiation. Furthermore, the feasibility of the application of these merged technologies to large-scale water treatment plants still hinders the adoption of these techniques on an industrial scale despite their undeniable benefits. Therefore, these techniques should be investigated on a pilot scale to ascertain their feasibility. Considering the foregoing, it could be logically proposed that natural biomaterials such as medicinal plants that are biocompatible, biodegradable, abundant, readily available, and cost-efficient with intrinsic health and safety benefits coupled with their significant antimicrobial attributes should be explored as potential novel disinfectants, and adapted for the inactivation of waterborne viruses.

Author contributions

AL, AE, and FS conceived the review idea. AL wrote the first draft. AL, AE, and SS reviewed and edited the manuscript. All authors approved the final manuscript.

Funding

This work was funded by the Water Research Commission (WRC) of South Africa (project no. K5/C2020-2021-00181). We were also supported by our institution, the Durban University of Technology, South Africa.

Conflict of interest

The authors declare that they have no known competing financial interests or personal relationships that could have appeared to influence the work reported in this paper.

Publisher's note

All claims expressed in this article are solely those of the authors and do not necessarily represent those of their affiliated organizations, or those of the publisher, the editors and the reviewers. Any product that may be evaluated in this article, or claim that may be made by its manufacturer, is not guaranteed or endorsed by the publisher.

References

Agency, U. E. P., 1999. *Wastewater Technology Fact Sheet: Ozone D*. Washington, DC: US Environmental Protection Agency.

Agrawal, H., Singh, S., and Gupta, N. (2020). What all we should know about masks in COVID-19 pandemic. *Indian J. Surg.* 82, 295–296. doi: 10.1007/s12262-020-02469-4

Aieta, E. M., and Berg, J. D. (1986). A review of chlorine dioxide in drinking water treatment. *J. Am. Water Works Ass.* 78, 62–72. doi: 10.1002/j.1551-8833.1986.tb05766.x

Akhavan, O., Choobtashani, M., and Ghaderi, E. (2012). Protein degradation and RNA efflux of viruses photocatalyzed by graphene–tungsten oxide composite under visible light irradiation. *J. Phys. Chem. C* 116, 9653–9659. doi: 10.1021/jp301707m

Albinana-Gimenez, N., Clemente-Casares, P., Bofill-Mas, S., Hundesa, A., Ribas, F., and Girones, R. (2006). Distribution of human polyoma-viruses, adenoviruses, and hepatitis E virus in the environment and in a drinking-water treatment plant. *Environ. Sci. Technol.* 40, 7416–7422. doi: 10.1021/es060343i

Alvarez, M. E., and O'Brien, R. (1982). Mechanisms of inactivation of poliovirus by chlorine dioxide and iodine. *Appl. Environ. Microbiol.* 44, 1064–1071. doi: 10.1128/aem.44.5.1064-1071.1982

American Society of Heating, Refrigerating and Air Conditioning Engineers (ASHRAE), 2019. Ultraviolet air and surface treatment. ASHRAE Handbook-HVAC Appl. (SI) 1–18.

Anand, S., Philip, B., and Mehendale, H. (2014). *Chlorination byproducts in Encyclopedia of Toxicology: Third Edition*. Elsevier. doi: 10.1016/B978-0-12-386454-3.00276-1.

Augsburger, N., Rachmadi, A. T., Zaouri, N., Lee, Y., and Hong, P. Y. (2021). Recent update on UV disinfection to fulfill the disinfection credit value for enteric viruses in water. *Environ. Sci. Technol.* 55, 16283–16298. doi: 10.1021/acs.est.1c03092

Badawy, M. I., Gad-Allah, T. A., Ali, M. E., and Yoon, Y. (2012). Minimization of the formation of disinfection by-products. *Chemosphere* 89, 235–240. doi: 10.1016/j.chemosphere.2012.04.025

Baram, N., Starosvetsky, D., Starosvetsky, J., Epshtein, M., Armon, R., and Ein-Eli, Y. (2009). Enhanced inactivation of E. coli bacteria using immobilized porous TiO_2 photoelectrocatalysis. *Electrochim. Acta* 54, 3381–3386. doi: 10.1016/j.electacta.2008.12.033

Berman, D., and Hoff, J. C. (1984). Inactivation of simian rotavirus SA11 by chlorine, chlorine dioxide, and monochloramine. *Appl. Environ. Microbiol.* 48, 317–323. doi: 10.1128/aem.48.2.317-323.1984

Betancourt, W. Q., and Gerba, C. P. (2016). Rethinking the significance of reovirus in water and wastewater. *Food Environ. Virol.* 8, 161–173. doi: 10.1007/s12560-016-9250-8

Betancourt, W. Q., and Rose, J. B. (2004). Drinking water treatment processes for removal of cryptosporidium and giardia. *Vet. Parasitol.* 126, 219–234. doi: 10.1016/j.vetpar.2004.09.002

Biasin, M., Bianco, A., Pareschi, G., Cavalleri, A., Cavatorta, C., Fenizia, C., et al. (2021). UV-C irradiation is highly effective in inactivating SARS-CoV-2 replication. *Sci. Rep.* 11, 1–7.

Black, S., Thurston, J. A., and Gerba, C. P. (2009). Determination of Ct values for chlorine of resistant enteroviruses. *J. Environ. Sci. Health Part A.* 44, 336–339. doi: 10.1080/10934520802659653

Bosch, A., Pintó, R. M., and Abad, F. X. (2006). Survival and transport of enteric viruses in the environment. Viruses in foods. *Springer*, 151–187. doi: 10.1007/0-387-29251-9_6

Bouseettine, R., Hassou, N., Bessi, H., and Ennaji, M. M. (2020). Waterborne transmission of enteric viruses and their impact on public health. Emerging and reemerging viral pathogens. *Elsevier*, 907–932. doi: 10.1016/B978-0-12-819400-3.00040-5

Brown, J. C., Moshe, M., Blackwell, A., and Barclay, W. S. (2021). Inactivation of SARS-CoV-2 in chlorinated swimming pool water. *Water Res.* 205:117718. doi: 10.1016/j.watres.2021.117718

Bruguera-Casamada, C., Sirés, I., Prieto, M. J., Brillas, E., and Araujo, R. M. (2016). The ability of electrochemical oxidation with a BDD anode to inactivate gram-negative and gram-positive bacteria in low conductivity sulfate medium. *Chemosphere* 163, 516–524. doi: 10.1016/j.chemosphere.2016.08.042

Buonanno, M., Ponnaiya, B., Welch, D., Stanislauskas, M., Randers-Pehrson, G., Smilenov, L., et al. (2017). Germicidal efficacy and mammalian skin safety of 222-nm UV light. *Radiat. Res.* 187, 493–501. doi: 10.1667/RR0010CC.1

Buonanno, M., Welch, D., Shuryak, I., and Brenner, D. J. (2020). Far-UVC light (222 nm) efficiently and safely inactivates airborne human coronaviruses. *Sci. Rep.* 10, 1–8.

Buonerba, A., Corpuz, M. V. A., Ballesteros, F., Choo, K. H., Hasan, S. W., Korshin, G. V., et al. (2021). Coronavirus in water media: analysis, fate, disinfection and epidemiological applications. *J. Hazard. Mater.* 415:125580.

Cabiscol Català, E., Tamarit Sumalla, J., and Ros Salvador, J. (2000). Oxidative stress in bacteria and protein damage by reactive oxygen species. *Int. Microbiol.* 3, 3–8.

Cai, X., Han, J. C., Li, R., Zhang, Y., Liu, Y., Liu, X., et al. (2014). Phage MS2 inactivation in pure and filtered water: effect of pseudo-kinetics and other factors. *Ozone Sci. Eng.* 36, 86–93. doi: 10.1080/01919512.2013.836953

Cao, S., Low, J., Yu, J., and Jaroniec, M. (2015). Polymeric photocatalysts based on graphitic carbon nitride. *Adv. Mater.* 27, 2150–2176. doi: 10.1002/adma.201500033

Chen, L., Deng, Y., Dong, S., Wang, H., Li, P., Zhang, H., et al. (2021b). The occurrence and control of waterborne viruses in drinking water treatment: a review. *Chemosphere* 130728, 1–11.

Chen, C., Guo, L., Yang, Y., Oguma, K., and Hou, L. A. (2021a). Comparative effectiveness of membrane technologies and disinfection methods for virus elimination in water: a review. *Sci. Total Environ.* 801:149678. doi: 10.1016/j.scitotenv.2021.149678

Cheng, R., Kang, M., Shen, Z. P., Shi, L., and Zheng, X. (2019). Visible-light-driven photocatalytic inactivation of bacteriophage f2 by cu-TiO_2 nanofibers in the presence of humic acid. *J. Environ. Sci.* 77, 383–391. doi: 10.1016/j.jes.2018.09.017

Cheng, X., Liang, H., Ding, A., Qu, F., Shao, S., Liu, B., et al. (2016). Effects of pre-ozonation on the ultrafiltration of different natural organic matter (NOM) fractions: membrane fouling mitigation, prediction and mechanism. *J. Membr. Sci.* 505, 15–25. doi: 10.1016/j.memsci.2016.01.022

Cheng, R., Shen, L., Wang, Q., Xiang, S., Shi, L., Zheng, X., et al. (2018b). Photocatalytic membrane reactor (PMR) for virus removal in drinking water: effect of humic acid. *Catalysts* 8:284. doi: 10.3390/catal8070284

Cheng, R., Shen, L. J., Yu, J. H., Xiang, S. Y., and Zheng, X. (2018a). Photocatalytic inactivation of bacteriophage f2 with Ag_3PO_4/g-C_3N_4 composite under visible light irradiation: performance and mechanism. *Catalysts* 8:406. doi: 10.3390/catal8100406

Cho, M., Cates, E. L., and Kim, J. H. (2011). Inactivation and surface interactions of MS-2 bacteriophage in a TiO_2 photoelectrocatalytic reactor. *Water Res.* 45, 2104–2110. doi: 10.1016/j.watres.2010.12.017

Cho, M., Lee, J., Mackeyev, Y., Wilson, L. J., Alvarez, P. J., Hughes, J. B., et al. (2010). Visible light sensitized inactivation of MS-2 bacteriophage by a cationic amine-functionalized C60 derivative. *Environ. Sci. Technol.* 44, 6685–6691. doi: 10.1021/es1014967

Choudhury, B., Portugal, S., Mastanaiah, N., Johnson, J. A., and Roy, S. (2018). Inactivation of *Pseudomonas aeruginosa* and methicillin-resistant *Staphylococcus aureus* in an open water system with ozone generated by a compact, atmospheric DBD plasma reactor. *Sci. Rep.* 8, 1–11. doi: 10.1038/s41598-018-36003-0

Collivignarelli, M. C., Abbà, A., Benigna, I., Sorlini, S., and Torretta, V. (2018). Overview of the main disinfection processes for wastewater and drinking water treatment plants. *Sustainability* 10:86.

Commission Internationale de L'Eclairage, 2003. Ultraviolet air disinfection. Publication 155, Vienna.

Cromeans, T. L., Kahler, A. M., and Hill, V. R. (2010). Inactivation of adenoviruses, enteroviruses, and murine norovirus in water by free chlorine and monochloramine. *Appl. Environ. Microbiol.* 76, 1028–1033. doi: 10.1128/AEM.01342-09

D'Orazio, J., Jarrett, S., Amaro-Ortiz, A., and Scott, T. (2013). UV radiation and the skin. *Int. J. Mol. Sci.* 14, 12222–12248. doi: 10.3390/ijms140612222

Daels, N., Radoicic, M., Radetic, M., De Clerck, K., and Van Hulle, S. W. (2015). Electrospun nanofibre membranes functionalised with TiO_2 nanoparticles: evaluation of humic acid and bacterial removal from polluted water. *Sep. Purif. Technol.* 149, 488–494. doi: 10.1016/j.seppur.2015.06.016

Dhama, K., Patel, S. K., Kumar, R., Masand, R., Rana, J., Yatoo, M., et al. (2021). The role of disinfectants and sanitizers during COVID-19 pandemic: advantages and deleterious effects on humans and the environment. *Environ. Sci. Pollut. Res.* 28, 34211–34228. doi: 10.1007/s11356-021-14429-w

Diaz, L. F. (2006). "Wastewater pathogens," in *Wastewater Microbiology Series*. eds. M. H. Gerardi and M. C. Zimmerman (Hoboken, NJ: Wiley-Interscience, John Wiley & Sons).

Drees, K. P., Abbaszadegan, M., and Maier, R. M. (2003). Comparative electrochemical inactivation of bacteria and bacteriophage. *Water Res.* 37, 2291–2300. doi: 10.1016/S0043-1354(03)00009-5

Dular, M., Griessler-Bulc, T., Gutierrez-Aguirre, I., Heath, E., Kosjek, T., Klemenčič, A. K., et al. (2016). Use of hydrodynamic cavitation in (waste) water treatment. *Ultrason. Sonochem.* 29, 577–588. doi: 10.1016/j.ultsonch.2015.10.010

Dunkin, N., Weng, S., Coulter, C. G., Jacangelo, J. G., and Schwab, K. J. (2017). Reduction of human norovirus GI, GII, and surrogates by peracetic acid and monochloramine in municipal secondary wastewater effluent. *Environ. Sci. Technol.* 51, 11918–11927. doi: 10.1021/acs.est.7b02954

ElHadidy, A. M., Peldszus, S., and Van Dyke, M. I. (2013). An evaluation of virus removal mechanisms by ultrafiltration membranes using MS2 and φX174 bacteriophage. *Sep. Purif. Technol.* 120, 215–223. doi: 10.1016/j.seppur.2013.09.026

EPA, N., 2005. Membrane filtration guidance manual. Agency, Office of Water, Cincinnati, OH.

Farkas, K., Cooper, D. M., McDonald, J. E., Malham, S. K., de Rougemont, A., and Jones, D. L. (2018). Seasonal and spatial dynamics of enteric viruses in wastewater and in riverine and estuarine receiving waters. *Sci. Total Environ.* 634, 1174–1183. doi: 10.1016/j.scitotenv.2018.04.038

Feitz, A. (2005). Advanced oxidation processes and industrial wastewater treatment. *Water* 32, 59–65.

Filipić, A., Lukežič, T., Bačnik, K., Ravnikar, M., Ješelnik, M., Košir, T., et al. (2022). Hydrodynamic cavitation efficiently inactivates potato virus Y in water. *Ultrason. Sonochem.* 82:105898. doi: 10.1016/j.ultsonch.2021.105898

Fuzawa, M., Araud, E., Li, J., Shisler, J. L., and Nguyen, T. H. (2019). Free chlorine disinfection mechanisms of rotaviruses and human norovirus surrogate Tulane virus attached to fresh produce surfaces. *Environ. Sci. Technol.* 53, 11999–12006. doi: 10.1021/acs.est.9b03461

Galeano, L.A., Guerrero-Flórez, M., Sánchez, C.A., Gil, A., and Vicente, M.Á., 2017. *Disinfection by Chemical Oxidation Methods, Applications of Advanced Oxidation Processes (AOPs) in Drinking Water Treatment*. New York: Springer, 257–295.

Gall, A. M., Mariñas, B. J., Lu, Y., and Shisler, J. L. (2015). Waterborne viruses: a barrier to safe drinking water. *PLoS Pathog.* 11:e1004867. doi: 10.1371/journal.ppat.1004867

Gall, A. M., Shisler, J. L., and Mariñas, B. J. (2016). Inactivation kinetics and replication cycle inhibition of adenovirus by monochloramine. *Environ. Sci. Technol. Lett.* 3, 185–189. doi: 10.1021/acs.estlett.6b00079

García-Espinoza, J. D., and Nacheva, P. M. (2019). Degradation of pharmaceutical compounds in water by oxygenated electrochemical oxidation: parametric optimization, kinetic studies and toxicity assessment. *Sci. Total Environ.* 691, 417–429. doi: 10.1016/j.scitotenv.2019.07.118

Gentile, G. J., Cruz, M. C., Rajal, V. B., and de Cortalezzi, M. M. F. (2018). Electrostatic interactions in virus removal by ultrafiltration membranes. *J. Environ. Chem. Eng.* 6, 1314–1321. doi: 10.1016/j.jece.2017.11.041

Gerba, C. P., Gramos, D. M., and Nwachuku, N. (2002). Comparative inactivation of enteroviruses and adenovirus 2 by UV light. *Appl. Environ. Microbiol.* 68, 5167–5169. doi: 10.1128/AEM.68.10.5167-5169.2002

Gerrity, D., Pecson, B., Trussell, R. S., and Trussell, R. R. (2013). Potable reuse treatment trains throughout the world. *J. Water Supply Res. T.* 62, 321–338. doi: 10.2166/aqua.2013.041

Ghernaout, D. (2017). Microorganisms' electrochemical disinfection phenomena. *EC Microbiol.* 9, 60–169.

Giannakis, S., Liu, S., Carratalà, A., Rtimi, S., Amiri, M. T., Bensimon, M., et al. (2017a). Iron oxide-mediated semiconductor photocatalysis vs. heterogeneous photo-Fenton treatment of viruses in wastewater. Impact of the oxide particle size. *J. Hazard. Mater.* 339, 223–231. doi: 10.1016/j.jhazmat.2017.06.037

Giannakis, S., Liu, S., Carratalà, A., Rtimi, S., Bensimon, M., and Pulgarin, C. (2017b). Effect of Fe (II)/Fe (III) species, pH, irradiance and bacterial presence on viral inactivation in wastewater by the photo-Fenton process: kinetic modeling and mechanistic interpretation. *Appl Catal B* 204, 156–166. doi: 10.1016/j.apcatb.2016.11.034

Girones, R., Carratalà, A., Calgua, B., Calvo, M., Rodriguez-Manzano, J., and Emerson, S. (2014). Chlorine inactivation of hepatitis E virus and human adenovirus 2 in water. *J. Water Health* 12, 436–442. doi: 10.2166/wh.2014.027

Gomes, J., Frasson, D., Quinta-Ferreira, R. M., Matos, A., and Martins, R. C. (2019a). Removal of enteric pathogens from real wastewater using single and catalytic ozonation. *Water* 11:127. doi: 10.3390/w11010127

Gomes, J., Matos, A., Gmurek, M., Quinta-Ferreira, R. M., and Martins, R. C. (2019b). Ozone and photocatalytic processes for pathogens removal from water: a review. *Catalysts* 9:46. doi: 10.3390/catal9010046

Gormley, M., Aspray, T. J., and Kelly, D. A. (2020). COVID-19: mitigating transmission via wastewater plumbing systems. *Lancet Glob. Health* 8:e643. doi: 10.1016/S2214-109X(20)30112-1

Guay, C., Rodriguez, M., and Serodes, J. (2005). Using ozonation and chloramination to reduce the formation of trihalomethanes and haloacetic acids in drinking water. *Desalination* 176, 229–240. doi: 10.1016/j.desal.2004.10.015

Haas, C. N., and Joffe, J. (1994). Disinfection under dynamic conditions: modification of Hom's model for decay. *Environ. Sci. Technol.* 28, 1367–1369. doi: 10.1021/es00056a028

Habibi-Yangjeh, A., Asadzadeh-Khaneghah, S., Feizpoor, S., and Rouhi, A. (2020). Review on heterogeneous photocatalytic disinfection of waterborne, airborne, and foodborne viruses: can we win against pathogenic viruses? *J. Colloid Interface Sci.* 580, 503–514. doi: 10.1016/j.jcis.2020.07.047

Hasan, S. W., Ibrahim, Y., Daou, M., Kannout, H., Jan, N., Lopes, A., et al. (2021). Detection and quantification of SARS-CoV-2 RNA in wastewater and treated effluents: surveillance of COVID-19 epidemic in the United Arab Emirates. *Sci. Total Environ.* 764:142929. doi: 10.1016/j.scitotenv.2020.142929

Hatanaka, N., Xu, B., Yasugi, M., Morino, H., Tagishi, H., Miura, T., et al. (2021). Chlorine dioxide is a more potent antiviral agent against SARS-CoV-2 than sodium hypochlorite. *J. Hosp. Infect.* 118, 20–26. doi: 10.1016/j.jhin.2021.09.006

Hawkins, C., Pattison, D., and Davies, M. (2003). Hypochlorite-induced oxidation of amino acids, peptides and proteins. *Amino Acids* 25, 259–274. doi: 10.1007/s00726-003-0016-x

He, H., Zhou, P., Shimabuku, K. K., Fang, X., Li, S., Lee, Y., et al. (2019). Degradation and deactivation of bacterial antibiotic resistance genes during exposure to free chlorine, monochloramine, chlorine dioxide, ozone, ultraviolet light, and hydroxyl radical. *Environ. Sci. Technol.* 53, 2013–2026. doi: 10.1021/acs.est.8b04393

Heffron, J., Ryan, D. R., and Mayer, B. K. (2019). Sequential electrocoagulation-electrooxidation for virus mitigation in drinking water. *Water Res.* 160, 435–444. doi: 10.1016/j.watres.2019.05.078

Holkar, C. R., Jadhav, A. J., Pinjari, D. V., and Pandit, A. B. (2019). Cavitationally driven transformations: a technique of process intensification. *Ind. Eng. Chem. Res.* 58, 5797–5819. doi: 10.1021/acs.iecr.8b04524

Hu, C. Y., Deng, Y. G., Lin, Y. L., and Hou, Y. Z. (2019). Chlorination of bromacil: kinetics and disinfection by-products. *Sep. Purif. Technol.* 212, 913–919. doi: 10.1016/j.seppur.2018.12.002

Hu, X., Hu, C., Peng, T., Zhou, X., and Qu, J. (2010). Plasmon-induced inactivation of enteric pathogenic microorganisms with Ag–AgI/Al_2O_3 under visible-light irradiation. *Environ. Sci. Technol.* 44, 7058–7062. doi: 10.1021/es1012577

Hu, X., Mu, L., Wen, J., and Zhou, Q. (2012). Covalently synthesized graphene oxide-aptamer nanosheets for efficient visible-light photocatalysis of nucleic acids and proteins of viruses. *Carbon* 50, 2772–2781. doi: 10.1016/j.carbon.2012.02.038

Hung, Y. C., Waters, B. W., Yemmireddy, V. K., and Huang, C. H. (2017). pH effect on the formation of THM and HAA disinfection byproducts and potential control strategies for food processing. *J. Integr. Agric.* 16, 2914–2923. doi: 10.1016/S2095-3119(17)61798-2

Ibrahim, Y., Ouda, M., Kadadou, D., Banat, F., Naddeo, V., Alsafar, H., et al. (2021). Detection and removal of waterborne enteric viruses from wastewater: a comprehensive review. *J. Environ. Chem. Eng.* 9:105613. doi: 10.1016/j.jece.2021.105613

Illuminating Engineering Society of North America (2000). "Ch. 5: Nonvisual effects of optical radiation," in *The IESNA Lighting Handbook*. ed. M. S. Rea. *9th* ed (New York: Illuminating Engineering Society of North America).

Im, D., Nakada, N., Fukuma, Y., Kato, Y., and Tanaka, H. (2018). Performance of combined ozonation, coagulation and ceramic membrane process for water reclamation: effects and mechanism of ozonation on virus coagulation. *Sep. Purif. Technol.* 192, 429–434. doi: 10.1016/j.seppur.2017.10.044

Jarach, N., Dodiuk, H., and Kenig, S. (2020). Polymers in the medical antiviral front-line. *Polymers* 12:1727. doi: 10.3390/polym12081727

Jasper, J. T., Yang, Y., and Hoffmann, M. R. (2017). Toxic byproduct formation during electrochemical treatment of latrine wastewater. *Environ. Sci. Technol.* 51, 7111–7119. doi: 10.1021/acs.est.7b01002

Jin, M., Shan, J., Chen, Z., Guo, X., Shen, Z., Qiu, Z., et al. (2013). Chlorine dioxide inactivation of enterovirus 71 in water and its impact on genomic targets. *Environ. Sci. Technol.* 47, 4590–4597. doi: 10.1021/es305282g

Jung, E., Shin, H., Hooch Antink, W., Sung, Y. E., and Hyeon, T. (2020). Recent advances in electrochemical oxygen reduction to H_2O_2: catalyst and cell design. *ACS Energy Lett.* 5, 1881–1892. doi: 10.1021/acsenergylett.0c00812

Kahler, A. M., Cromeans, T. L., Roberts, J. M., and Hill, V. R. (2011). Source water quality effects on monochloramine inactivation of adenovirus, coxsackievirus, echovirus, and murine norovirus. *Water Res.* 45, 1745–1751. doi: 10.1016/j.watres.2010.11.026

Kály-Kullai, K., Wittmann, M., Noszticzius, Z., and Rosivall, L. (2020). Can chlorine dioxide prevent the spreading of coronavirus or other viral infections? Medical hypotheses. *Physiol. Int.* 107, 1–11. doi: 10.1556/2060.2020.00015

Keshavarzfathy, M., Hosoi, Y., Oguma, K., and Taghipour, F. (2021). Experimental and computational evaluation of a flow-through UV-LED reactor for MS2 and adenovirus inactivation. *Chem. Eng. J.* 407:127058. doi: 10.1016/j.cej.2020.127058

Keswick, B., Satterwhite, T. K., Johnson, P. C., DuPont, H. L., Secor, S. L., Bitsura, J. A., et al. (1985). Inactivation of Norwalk virus in drinking water by chlorine. *Appl. Environ. Microbiol.* 50, 261–264. doi: 10.1128/aem.50.2.261-264.1985

Khaiboullina, S., Uppal, T., Dhabarde, N., Subramanian, V. R., and Verma, S. C. (2020). Inactivation of human coronavirus by titania nanoparticle coatings and UVC radiation: throwing light on SARS-CoV-2. *Viruses* 13:19. doi: 10.3390/v13010019

Khin, M. M., Nair, A. S., Babu, V. J., Murugan, R., and Ramakrishna, S. (2012). A review on nanomaterials for environmental remediation. *Energy Environ. Sci.* 5, 8075–8109. doi: 10.1039/c2ee21818f

Kim, M. G., Kang, J. M., Lee, J. E., Kim, K. S., Kim, K. H., Cho, M., et al. (2021). Effects of calcination temperature on the phase composition, photocatalytic degradation, and virucidal activities of TiO_2 nanoparticles. *ACS Omega* 6, 10668–10678. doi: 10.1021/acsomega.1c00043

Kitajima, M., Iker, B. C., Pepper, I. L., and Gerba, C. P. (2014). Relative abundance and treatment reduction of viruses during wastewater treatment processes—identification of potential viral indicators. *Sci. Total Environ.* 488, 290–296.

Kokkinos, P., Mantzavinos, D., and Venieri, D. (2020). Current trends in the application of nanomaterials for the removal of emerging micropollutants and pathogens from water. *Molecules* 25:2016. doi: 10.3390/molecules25092016

Kokkinos, P., Venieri, D., and Mantzavinos, D. (2021). Advanced oxidation processes for water and wastewater viral disinfection. A systematic review. *Food Environ. Virol.* 13, 283–302. doi: 10.1007/s12560-021-09481-1

Koplin, S. A., Lin, S., and Domanski, T. (2008). Evaluation of the antimicrobial activity of cationic polyethylenimines on dry surfaces. *Biotechnol. Prog.* 24, 1160–1165. doi: 10.1002/btpr.32

Kosel, J., Gutiérrez-Aguirre, I., Rački, N., Dreo, T., Ravnikar, M., and Dular, M. (2017). Efficient inactivation of MS-2 virus in water by hydrodynamic cavitation. *Water Res.* 124, 465–471. doi: 10.1016/j.watres.2017.07.077

Kumar, S., Gupta, A. K., Maurya, A., and Singh, M. K. (2020). Chemical treatment for removal of waterborne pathogens. *Waterborne Pathog.*, 205–218. doi: 10.1016/B978-0-12-818783-8.00011-6

Kuo, D., Liu, M., Kumar, K. S., Hamaguchi, K., Gan, K. P., Sakamoto, T., et al. (2020). High virus removal by self-organized nanostructured 2D liquid-crystalline Smectic membranes for water treatment. *Small* 16:2001721. doi: 10.1002/smll.202001721

Lanrewaju, A. A., Enitan-Folami, A. M., Sabiu, S., Edokpayi, J. N., and Swalaha, F. M. (2022). Global public health implications of human exposure to viral contaminated water. *Front. Microbiol.* 13:981896. doi: 10.3389/fmicb.2022.981896

Lee, J., Mackeyev, Y., Cho, M., Li, D., Kim, J. H., Wilson, L. J., et al. (2009). Photochemical and antimicrobial properties of novel C60 derivatives in aqueous systems. *Environ. Sci. Technol.* 43, 6604–6610. doi: 10.1021/es901501k

Lee, J., Mackeyev, Y., Cho, M., Wilson, L. J., Kim, J. H., and Alvarez, P. J. (2010). C60 aminofullerene immobilized on silica as a visible-light-activated photocatalyst. *Environ. Sci. Technol.* 44, 9488–9495. doi: 10.1021/es1028475

Lee, S. W., Obregón, S., and Rodríguez-González, V. (2015). The role of silver nanoparticles functionalized on TiO_2 for photocatalytic disinfection of harmful algae. *RSC Adv.* 5, 44470–44475. doi: 10.1039/C5RA08313C

Lee, J., Zoh, K., and Ko, G. (2008). Inactivation and UV disinfection of murine norovirus with TiO2 under various environmental conditions. *Appl. Environ. Microbiol.* 74, 2111–2117. doi: 10.1128/AEM.02442-07

Li, J., Li, K., Zhou, Y., Li, X., and Tao, T. (2017). Kinetic analysis of *legionella* inactivation using ozone in wastewater. *Chemosphere* 168, 630–637. doi: 10.1016/j.chemosphere.2016.11.014

Li, G., Nie, X., Chen, J., Jiang, Q., An, T., Wong, P. K., et al. (2015). Enhanced visible-light-driven photocatalytic inactivation of *Escherichia coli* using g-C_3N_4/TiO_2 hybrid photocatalyst synthesized using a hydrothermal-calcination approach. *Water Res.* 86, 17–24. doi: 10.1016/j.watres.2015.05.053

Li, J. W., Xin, Z. T., Wang, X. W., Zheng, J. L., and Chao, F. H. (2004). Mechanisms of inactivation of hepatitis a virus in water by chlorine dioxide. *Water Res.* 38, 1514–1519. doi: 10.1016/j.watres.2003.12.021

Li, Y., Zhang, C., Shuai, D., Naraginti, S., Wang, D., and Zhang, W. (2016). Visible-light-driven photocatalytic inactivation of MS2 by metal-free g-C_3N_4: virucidal performance and mechanism. *Water Res.* 106, 249–258. doi: 10.1016/j.watres.2016.10.009

Liga, M. V., Bryant, E. L., Colvin, V. L., and Li, Q. (2011). Virus inactivation by silver doped titanium dioxide nanoparticles for drinking water treatment. *Water Res.* 45, 535–544. doi: 10.1016/j.watres.2010.09.012

Lim, M. Y., Kim, J. M., and Ko, G. (2010). Disinfection kinetics of murine norovirus using chlorine and chlorine dioxide. *Water Res.* 44, 3243–3251. doi: 10.1016/j.watres.2010.03.003

Lin, S.D., and Lee, C.C., 2007. *Water and Wastewater Calculations Manual*. New York: McGraw-Hill.

Liu, Z., Tang, Y., Zhao, K., and Chen, W. (2019). Self-assembly of positively charged SiO2/Y2O3 composite nanofiber membranes with plum-flower-like structures for the removal of water contaminants. *Appl. Surf. Sci.* 489, 717–724. doi: 10.1016/j.apsusc.2019.06.013

Long, Y., Ni, J., and Wang, Z. (2015). Subcellular mechanism of *Escherichia coli* inactivation during electrochemical disinfection with boron-doped diamond anode: a comparative study of three electrolytes. *Water Res.* 84, 198–206. doi: 10.1016/j.watres.2015.07.035

Luo, P., Wang, F., Krasner, S. W., Fang, C., Chen, S., and Chu, W. (2020). Emerging investigator series: formation of brominated haloacetamides from trihalomethanes during zero-valent iron reduction and subsequent booster chlorination in drinking water distribution. *Environ. Sci. Water Res. Technol.* 6, 1244–1255. doi: 10.1039/C9EW00977A

Lytle, D. A., Pfaller, S., Muhlen, C., Struewing, I., Triantafyllidou, S., White, C., et al. (2021). A comprehensive evaluation of monochloramine disinfection on water

quality, *legionella* and other important microorganisms in a hospital. *Water Res.* 189:116656. doi: 10.1016/j.watres.2020.116656

Ma, J. W., Huang, B. S., Hsu, C. W., Peng, C. W., Cheng, M. L., Kao, J. Y., et al. (2017). Efficacy and safety evaluation of a chlorine dioxide solution. *Int. J. Environ. Res.* 14:329.

Magana-Arachchi, D., and Wanigatunge, R. (2020). Ubiquitous waterborne pathogens. *Elsevier*, 15–42. doi: 10.1016/B978-0-12-818783-8.00002-5

Mamane, H., Shemer, H., and Linden, K. G. (2007). Inactivation of *E. coli*, *B. subtilis* spores, and MS2, T4, and T7 phage using UV/H_2O_2 advanced oxidation. *J. Hazard. Mater.* 146, 479–486. doi: 10.1016/j.jhazmat.2007.04.050

Manetu, W. M., and Karanja, A. M. (2021). Waterborne disease risk factors and intervention practices: a review. *Open Access Libr.* 8, 1–11.

Mariita, R. M., Miller, A. C. W., and Randive, R. V. (2022). Evaluation of the virucidal efficacy of Klaran UVC LEDs against surface-dried norovirus. *Access Microbiol.* 4:000323. doi: 10.1099/acmi.0.000323

Mariita, R. M., and Randive, R. V. (2021). Disinfection of methicillin-resistant *Staphylococcus aureus*, vancomycin-resistant *enterococcus faecium* and *Acinetobacter baumannii* using Klaran WD array system. *Access Microbiol.* 3:194. doi: 10.1099/acmi.0.000194

Marjanovic, M., Giannakis, S., Grandjean, D., de Alencastro, L. F., and Pulgarin, C. (2018). Effect of μM Fe addition, mild heat and solar UV on sulfate radical-mediated inactivation of bacteria, viruses, and micropollutant degradation in water. *Water Res.* 140, 220–231. doi: 10.1016/j.watres.2018.04.054

Martino, D. (2019). The effects of chlorinated drinking water on the assembly of the intestinal microbiome. *Challenges* 10:10. doi: 10.3390/challe10010010

Matsuura, R., Lo, C. W., Wada, S., Somei, J., Ochiai, H., Murakami, T., et al. (2021). SARS-CoV-2 disinfection of air and surface contamination by tio 2 photocatalyst-mediated damage to viral morphology, RNA, and protein. *Viruses* 13:942. doi: 10.3390/v13050942

Michael, G. E., Miday, R. K., Bercz, J. P., Miller, R. G., Greathouse, D. G., Kraemer, D. F., et al. (1981). Chlorine dioxide water disinfection: a prospective epidemiology study. *Arch. Environ. Health* 36, 20–27. doi: 10.1080/00039896.1981.10667601

Monteiro, G. S., Staggemeier, R., Klauck, C. R., Bernardes, A. M., Rodrigues, M. A. S., and Spilki, F. R. (2015). Degradation and inactivation of adenovirus in water by photo-electro-oxidation. *Braz. J. Biol.* 75, S37–S42.

Moon, E. W., Lee, H. W., Rok, J. H., and Ha, J. H. (2020). Photocatalytic inactivation of viral particles of human norovirus by cu-doped TiO_2 non-woven fabric under UVA-LED wavelengths. *Sci. Total Environ.* 749:141574. doi: 10.1016/j.scitotenv.2020.141574

Moor, K. J., and Kim, J. H. (2014). Simple synthetic method toward solid supported C60 visible light-activated photocatalysts. *Environ. Sci. Technol.* 48, 2785–2791. doi: 10.1021/es405283w

Moor, K. J., Valle, D. C., Li, C., and Kim, J. H. (2015). Improving the visible light photoactivity of supported fullerene photocatalysts through the use of [C70] fullerene. *Environ. Sci. Technol.* 49, 6190–6197. doi: 10.1021/es505888d

Narita, K., Asano, K., Naito, K., Ohashi, H., Sasaki, M., Morimoto, Y., et al. (2020). Ultraviolet C light with wavelength of 222 nm inactivates a wide spectrum of microbial pathogens. *J. Hosp. Infect.* 105, 459–467. doi: 10.1016/j.jhin.2020.03.030

Németh, Z., Szekeres, G. P., Schabikowski, M., Schrantz, K., Traber, J., Pronk, W., et al. (2019). Enhanced virus filtration in hybrid membranes with MWCNT nanocomposite. *R. Soc. Open Sci.* 6:181294. doi: 10.1098/rsos.181294

Ngwenya, N., Ncube, E. J., and Parsons, J. (2013). Recent advances in drinking water disinfection: successes and challenges. *Rev. Environ. Contam. Toxicol.* 222, 111–170.

Nieuwenhuijsen, M. J., Toledano, M. B., Eaton, N. E., Fawell, J., and Elliott, P. (2000). Chlorination disinfection byproducts in water and their association with adverse reproductive outcomes: a review. *Occup. Environ. Med.* 57, 73–85. doi: 10.1136/oem.57.2.73

Noss, C. I., Hauchman, F. S., and Olivieri, V. P. (1986). Chlorine dioxide reactivity with proteins. *Water Res.* 20, 351–356. doi: 10.1016/0043-1354(86)90083-7

Noszticzius, Z., Wittmann, M., Kály-Kullai, K., Beregvári, Z., Kiss, I., Rosivall, L., et al. (2013). Chlorine dioxide is a size-selective antimicrobial agent. *PLoS One* 8:e79157. doi: 10.1371/journal.pone.0079157

Oguma, K., and Rattanakul, S. (2021). UV inactivation of viruses in water: its potential to mitigate current and future threats of viral infectious diseases. *Jpn. J. Appl. Phys.* 60:110502. doi: 10.35848/1347-4065/ac2b4f

Panizza, M., and Cerisola, G. (2005). Application of diamond electrodes to electrochemical processes. *Electrochim. Acta* 51, 191–199. doi: 10.1016/j.electacta.2005.04.023

Passos, T. M., da Silva, L. H. M., Moreira, L. M., Zângaro, R. A., da Silva Santos, R., Fernandes, F. B., et al. (2014). Comparative analysis of ozone and ultrasound effect on the elimination of giardia spp. cysts from wastewater. *Ozone Sci. Eng.* 36, 138–143. doi: 10.1080/01919512.2013.864227

Pichel, N., Vivar, M., and Fuentes, M. (2019). The problem of drinking water access: a review of disinfection technologies with an emphasis on solar treatment methods. *Chemosphere* 218, 1014–1030. doi: 10.1016/j.chemosphere.2018.11.205

Ponnaiya, B., Buonanno, M., Welch, D., Shuryak, I., Randers-Pehrson, G., and Brenner, D. J. (2018). Far-UVC light prevents MRSA infection of superficial wounds in vivo. *PLoS One* 13:e0192053. doi: 10.1371/journal.pone.0192053

Prado, T., de Castro Bruni, A., Barbosa, M. R. F., Garcia, S. C., de Jesus Melo, A. M., and Sato, M. I. Z. (2019). Performance of wastewater reclamation systems in enteric virus removal. *Sci. Total Environ.* 678, 33–42. doi: 10.1016/j.scitotenv.2019.04.435

Rachmadi, A. T., Kitajima, M., Kato, T., Kato, H., Okabe, S., and Sano, D. (2020). Required chlorination doses to fulfill the credit value for disinfection of enteric viruses in water: a critical review. *Environ. Sci. Technol.* 54, 2068–2077. doi: 10.1021/acs.est.9b01685

Raeiszadeh, M., and Adeli, B. (2020). A critical review on ultraviolet disinfection systems against COVID-19 outbreak: applicability, validation, and safety considerations. *Acs Photonics* 7, 2941–2951. doi: 10.1021/acsphotonics.0c01245

Rasalingam, S., Peng, R., and Koodali, R. T. (2014). Removal of hazardous pollutants from wastewaters: applications of TiO_2-SiO_2 mixed oxide materials. *J. Nanomater.* 2014, 1–42. doi: 10.1155/2014/617405

Rattanakul, S., and Oguma, K. (2018). Inactivation kinetics and efficiencies of UV-LEDs against *Pseudomonas aeruginosa*, *legionella pneumophila*, and surrogate microorganisms. *Water Res.* 130, 31–37. doi: 10.1016/j.watres.2017.11.047

Rebhun, M., Heller-Grossman, L., and Manka, J. (1997). Formation of disinfection byproducts during chlorination of secondary effluent and renovated water. *Water Environ. Res.* 69, 1154–1162. doi: 10.2175/106143097X125902

Reddy, P. A. K., Reddy, P. V. L., Kwon, E., Kim, K. H., Akter, T., and Kalagara, S. (2016). Recent advances in photocatalytic treatment of pollutants in aqueous media. *Environ. Int.* 91, 94–103. doi: 10.1016/j.envint.2016.02.012

Rekhate, C. V., and Srivastava, J. K. (2020). Recent advances in ozone-based advanced oxidation processes for treatment of wastewater-a review. *Chem. Eng. J. Adv.* 3:100031. doi: 10.1016/j.ceja.2020.100031

Richardson, S. D., Plewa, M. J., Wagner, E. D., Schoeny, R., and DeMarini, D. M. (2007). Occurrence, genotoxicity, and carcinogenicity of regulated and emerging disinfection by-products in drinking water: a review and roadmap for research. *Mutat. Res. Rev. Mutat. Res.* 636, 178–242. doi: 10.1016/j.mrrev.2007.09.001

Sadiq, R., and Rodriguez, M. J. (2004). Disinfection by-products (DBPs) in drinking water and predictive models for their occurrence: a review. *Sci. Total Environ.* 321, 21–46. doi: 10.1016/j.scitotenv.2003.05.001

Sánchez, G., and Bosch, A. (2016). Survival of enteric viruses in the environment and food. *Viruses Foods*, 367–392. doi: 10.1007/978-3-319-30723-7_13

Sanekata, T., Fukuda, T., Miura, T., Morino, H., Lee, C., Maeda, K., et al. (2010). Evaluation of the antiviral activity of chlorine dioxide and sodium hypochlorite against feline calicivirus, human influenza virus, measles virus, canine distemper virus, human herpesvirus, human adenovirus, canine adenovirus and canine parvovirus. *Biocontrol Sci.* 15, 45–49. doi: 10.4265/bio.15.45

Santana, M. H., De Faria, L. A., and Boodts, J. F. (2005). Electrochemical characterisation and oxygen evolution at a heavily boron doped diamond electrode. *Electrochim. Acta* 50, 2017–2027. doi: 10.1016/j.electacta.2004.08.050

Sato, T., and Taya, M. (2006). Enhancement of phage inactivation using photocatalytic titanium dioxide particles with different crystalline structures. *Biochem. Eng. J.* 28, 303–308. doi: 10.1016/j.bej.2006.01.004

Schaldach, C., Bourcier, W. L., Shaw, H. F., Viani, B. E., and Wilson, W. (2006). The influence of ionic strength on the interaction of viruses with charged surfaces under environmental conditions. *J. Colloid Interface Sci.* 294, 1–10. doi: 10.1016/j.jcis.2005.06.082

Schneider, J., Matsuoka, M., Takeuchi, M., Zhang, J., Horiuchi, Y., Anpo, M., et al. (2014). Understanding TiO_2 photocatalysis: mechanisms and materials. *Chem. Rev.* 114, 9919–9986. doi: 10.1021/cr5001892

Shabat-Hadas, E., Mamane, H., and Gitis, V. (2017). Rhodamine B in dissolved and nano-bound forms: indicators for light-based advanced oxidation processes. *Chemosphere* 184, 1020–1027. doi: 10.1016/j.chemosphere.2017.06.076

Shamsborhan, H., Coutier-Delgosha, O., Caignaert, G., and Abdel Nour, F. (2010). Experimental determination of the speed of sound in cavitating flows. *Exp. Fluids* 49, 1359–1373. doi: 10.1007/s00348-010-0880-6

Shin, G. A., Linden, K. G., and Sobsey, M. D. (2005). Low pressure ultraviolet inactivation of pathogenic enteric viruses and bacteriophages. *J. Environ. Eng. Sci.* 4, S7–S11. doi: 10.1139/s04-036

Sidhu, J., Sena, K., Hodgers, L., Palmer, A., and Toze, S. (2018). Comparative enteric viruses and coliphage removal during wastewater treatment processes in a sub-tropical environment. *Sci. Total Environ.* 616, 669–677.

Sigstam, T., Gannon, G., Cascella, M., Pecson, B. M., Wigginton, K. R., and Kohn, T. (2013). Subtle differences in virus composition affect disinfection kinetics and mechanisms. *Appl. Environ. Microbiol.* 79, 3455–3467. doi: 10.1128/AEM.00663-13

Sinclair, T., Patil, A., Raza, B., Reurink, D., Van den Hengel, S., Rutjes, S., et al. (2019). Cationically modified membranes using covalent layer-by-layer assembly for antiviral applications in drinking water. *J. Membr. Sci.* 570, 494–503.

Sinclair, T., Robles, D., Raza, B., Van den Hengel, S., Rutjes, S., de Roda Husman, A., et al. (2018). Virus reduction through microfiltration membranes modified with a cationic polymer for drinking water applications. *Colloids Surf. A Physicochem. Eng. Asp.* 551, 33–41. doi: 10.1016/j.colsurfa.2018.04.056

Sjogren, J. C., and Sierka, R. A. (1994). Inactivation of phage MS2 by iron-aided titanium dioxide photocatalysis. *Appl. Environ. Microbiol.* 60, 344–347. doi: 10.1128/aem.60.1.344-347.1994

Smith, S. C., and Rodrigues, D. F. (2015). Carbon-based nanomaterials for removal of chemical and biological contaminants from water: a review of mechanisms and applications. *Carbon* 91, 122–143. doi: 10.1016/j.carbon.2015.04.043

Song, K., Mohseni, M., and Taghipour, F. (2019). Mechanisms investigation on bacterial inactivation through combinations of UV wavelengths. *Water Res.* 163:114875. doi: 10.1016/j.watres.2019.114875

Sorlini, S., Biasibetti, M., Gialdini, F., and Collivignarelli, M. C. (2016). How can drinking water treatments influence chlorine dioxide consumption and by-product formation in final disinfection? *Water Sci. Technol. Water Supply* 16, 333–346.

Sorlini, S., Collivignarelli, M. C., and Canato, M. (2015). Effectiveness in chlorite removal by two activated carbons under different working conditions: a laboratory study. *J. Water Supply Res. Tech.* 64, 450–461. doi: 10.2166/aqua.2015.132

Stanford, B. D., Pisarenko, A. N., Holbrook, R. D., and Snyder, S. A. (2011). Preozonation effects on the reduction of reverse osmosis membrane fouling in water reuse. *Ozone Sci. Eng.* 33, 379–388. doi: 10.1080/01919512.2011.607385

Su, X., Zivanovic, S., and D'Souza, D. H. (2010). Inactivation of human enteric virus surrogates by high-intensity ultrasound. *Foodborne Pathog. Dis.* 7, 1055–1061. doi: 10.1089/fpd.2009.0515

Sun, X., Liu, J., Ji, L., Wang, G., Zhao, S., Yoon, J. Y., et al. (2020). A review on hydrodynamic cavitation disinfection: the current state of knowledge. *Sci. Total Environ.* 737:139606. doi: 10.1016/j.scitotenv.2020.139606

Sun, Y. X., Wu, Q. Y., Hu, H. Y., and Tian, J. (2009). Effect of ammonia on the formation of THMs and HAAs in secondary effluent chlorination. *Chemosphere* 76, 631–637. doi: 10.1016/j.chemosphere.2009.04.041

Symons, J. M., 1981. Treatment techniques for controlling trihalomethanes in drinking water. Drinking Water Research Division, Municipal Environmental Research Laboratory, Office of Research and Development, US Environmental Protection Agency.

Takehara, K., Yamazaki, K., Miyazaki, M., Yamada, Y., Ruenphet, S., Jahangir, A., et al. (2010). Inactivation of avian influenza virus H1N1 by photocatalyst under visible light irradiation. *Virus Res.* 151, 102–103. doi: 10.1016/j.virusres.2010.03.006

Tatlıdil, İ., Sökmen, M., Breen, C., Clegg, F., Buruk, C. K., and Bacaksız, E. (2011). Degradation of *Candida albicans* on TiO_2 and Ag-TiO_2 thin films prepared by sol–gel and nanosuspensions. *J. Solgel Sci. Technol.* 60, 23–32. doi: 10.1007/s10971-011-2546-0

Thurston-Enriquez, J. A., Haas, C. N., Jacangelo, J., and Gerba, C. P. (2003). Chlorine inactivation of adenovirus type 40 and feline calicivirus. *Appl. Environ. Microbiol.* 69, 3979–3985. doi: 10.1128/AEM.69.7.3979-3985.2003

Thurston-Enriquez, J. A., Haas, C. N., Jacangelo, J., and Gerba, C. P. (2005). Inactivation of enteric adenovirus and feline calicivirus by chlorine dioxide. *Appl. Environ. Microbiol.* 71, 3100–3105. doi: 10.1128/AEM.71.6.3100-3105.2005

Tondera, K., Klaer, K., Gebhardt, J., Wingender, J., Koch, C., Horstkott, M., et al. (2015). Reducing pathogens in combined sewer overflows using ozonation or UV irradiation. *Int. J. Hyg. Environ. Health* 218, 731–741. doi: 10.1016/j.ijheh.2015.09.002

Totaro, M., Badalucco, F., Costa, A. L., Tuvo, B., Casini, B., Privitera, G., et al. (2021). Effectiveness of disinfection with chlorine dioxide on respiratory transmitted, enteric, and Bloodborne viruses: a narrative synthesis. *Pathogens* 10:1017. doi: 10.3390/pathogens10081017

Tsitsifli, S., and Kanakoudis, V. (2018). Disinfection impacts to drinking water safety: a review. *Multidiscip. Digi. Pub. Ins. Proc.* 2:603.

Tu, Y., Tang, W., Yu, L., Liu, Z., Liu, Y., Xia, H., et al. (2021). Inactivating SARS-CoV-2 by electrochemical oxidation. *Sci. Bull.* 66, 720–726.

Tyrrell, S. A., Rippey, S. R., and Watkins, W. D. (1995). Inactivation of bacterial and viral indicators in secondary sewage effluents, using chlorine and ozone. *Water Res.* 29, 2483–2490. doi: 10.1016/0043-1354(95)00103-R

United States Environmental Protection Agency (US EPA), 2008. Ozone generators that are sold as air cleaners. Available at: https://www.epa.gov/indoor-air-quality-iaq/ozone-generators-are-sold-air-cleaners (accessed September 02, 2022).

Upfold, N. S., Luke, G. A., and Knox, C. (2021). Occurrence of human enteric viruses in water sources and shellfish: a focus on Africa. *Food Environ. Virol.* 13, 1–31. doi: 10.1007/s12560-020-09456-8

Van Voorthuizen, E., Ashbolt, N., and Schäfer, A. (2001). Role of hydrophobic and electrostatic interactions for initial enteric virus retention by MF membranes. *J. Membr. Sci.* 194, 69–79. doi: 10.1016/S0376-7388(01)00522-1

Vazquez-Bravo, B., Gonçalves, K., Shisler, J. L., and Mariñas, B. J. (2018). Adenovirus replication cycle disruption from exposure to polychromatic ultraviolet irradiation. *Environ. Sci. Technol.* 52, 3652–3659. doi: 10.1021/acs.est.7b06082

Venieri, D., Gounaki, I., Binas, V., Zachopoulos, A., Kiriakidis, G., and Mantzavinos, D. (2015). Inactivation of MS2 coliphage in sewage by solar photocatalysis using metal-doped TiO_2. *Appl Catal B* 178, 54–64. doi: 10.1016/j.apcatb.2014.10.052

Von Gunten, U. (2003). Ozonation of drinking water: part II. Disinfection and by-product formation in presence of bromide, iodide or chlorine. *Water Res.* 37, 1469–1487. doi: 10.1016/S0043-1354(02)00458-X

Wang, K., Abdalla, A. A., Khaleel, M. A., Hilal, N., and Khraisheh, M. K. (2017). Mechanical properties of water desalination and wastewater treatment membranes. *Desalination* 401, 190–205. doi: 10.1016/j.desal.2016.06.032

Wang, D., Pillai, S. C., Ho, S. H., Zeng, J., Li, Y., and Dionysiou, D. D. (2018a). Plasmonic-based nanomaterials for environmental remediation. *Appl. Catal. B* 237, 721–741. doi: 10.1016/j.apcatb.2018.05.094

Wang, H., Sikora, P., Rutgersson, C., Lindh, M., Brodin, T., Björlenius, B., et al. (2018b). Differential removal of human pathogenic viruses from sewage by conventional and ozone treatments. *Int. J. Hyg. Environ. Health* 221, 479–488. doi: 10.1016/j.ijheh.2018.01.012

Wigginton, K. R., Pecson, B. M., Sigstam, T., Bosshard, F., and Kohn, T. (2012). Virus inactivation mechanisms: impact of disinfectants on virus function and structural integrity. *Environ. Sci. Technol.* 46, 12069–12078. doi: 10.1021/es3029473

Wolf, C., von Gunten, U., and Kohn, T. (2018). Kinetics of inactivation of waterborne enteric viruses by ozone. *Environ. Sci. Technol.* 52, 2170–2177. doi: 10.1021/acs.est.7b05111

World Health Organization 1996. Fact sheets on environmental sanitation. Available at: https://www.who.int/publications/i/item/WHO-EOS-96.4 (accessed September 02, 2022).

World Health Organization 2002. *The World Health Report 2002: Reducing Risks, Promoting Healthy Life*. Geneva, Switzerland: World Health Organization.

World Health Organization 2012. *Global Costs and Benefits of Drinking-Water Supply and Sanitation Interventions to Reach the MDG Target and Universal Coverage*. Geneva, Switzerland: World Health Organization.

World Health Organization 2016. *Guidelines for Drinking-Water Quality. 4th ed.* Geneva, Switzerland: World Health Organization; 2011.

World Health Organization/United Nations Children Emergency Fund 2021. Progress on household drinking water, sanitation, and hygiene 2000–2020: five years into the SDGs, Geneva, Switzerland. Retrieved from https://data.unicef.org/resources/progress-on-household-drinking-water-sanitation-and-hygiene-2000-2020/ (accessed September 02, 2022).

Wu, Y., Guo, C., Tang, L., Hong, Z., Zhou, J., Dong, X., et al. (2020). Prolonged presence of SARS-CoV-2 viral RNA in faecal samples. *Lancet Gastroenterol. Hepatol.* 5, 434–435. doi: 10.1016/S2468-1253(20)30083-2

Wu, M. N., Wang, X. C., and Ma, X. Y. (2013). Characteristics of THMFP increase in secondary effluent and its potential toxicity. *J. Hazard. Mater.* 261, 325–331. doi: 10.1016/j.jhazmat.2013.07.022

Xi, J., Zhang, F., Lu, Y., and Hu, H. Y. (2017). A novel model simulating reclaimed water disinfection by ozonation. *Sep. Purif. Technol.* 179, 45–52. doi: 10.1016/j.seppur.2017.01.027

Xiao, R., Duan, Y., and Chu, W. (2020). The effectiveness of household water treatment and safe storage in improving drinking water quality: a disinfection by-product (DBP) perspective. *J. Water Supply Res Technol.* 69, 785–806. doi: 10.2166/aqua.2020.052

Xue, B., Jin, M., Yang, D., Guo, X., Chen, Z., Shen, Z., et al. (2013). Effects of chlorine and chlorine dioxide on human rotavirus infectivity and genome stability. *Water Res.* 47, 3329–3338. doi: 10.1016/j.watres.2013.03.025

Yamaguchi, Y., Usuki, S., Kanai, Y., Yamatoya, K., Suzuki, N., Katsumata, K. I., et al. (2017). Selective inactivation of bacteriophage in the presence of bacteria by use of ground Rh-doped $SrTiO_3$ photocatalyst and visible light. *ACS Appl. Mater. Interfaces* 9, 31393–31400. doi: 10.1021/acsami.7b07786

Yang, S., Verdaguer-Casadevall, A., Arnarson, L., Silvioli, L., Čolić, V., Frydendal, R., et al. (2018). Toward the decentralized electrochemical production of H_2O_2: a focus on the catalysis. *ACS Catal.* 8, 4064–4081. doi: 10.1021/acscatal.8b00217

Yeo, C., Kaushal, S., and Yeo, D. (2020). Enteric involvement of coronaviruses: is faecal–oral transmission of SARS-CoV-2 possible? *Lancet Gastroenterol. Hepatol.* 5, 335–337. doi: 10.1016/S2468-1253(20)30048-0

Zhang, C., Li, Y., Shuai, D., Shen, Y., and Wang, D. (2019a). Progress and challenges in photocatalytic disinfection of waterborne viruses: a review to fill current knowledge gaps. *Chem. Eng. J.* 355, 399–415. doi: 10.1016/j.cej.2018.08.158

Zhang, C., Li, Y., Shuai, D., Zhang, W., Niu, L., Wang, L., et al. (2018a). Visible-light-driven, water-surface-floating antimicrobials developed from graphitic carbon nitride and expanded perlite for water disinfection. *Chemosphere* 208, 84–92. doi: 10.1016/j.chemosphere.2018.05.163

Zhang, C., Li, Y., Wang, D., Zhang, W., Wang, Q., Wang, Y., et al. (2015). Ag@ helical chiral TiO_2 nanofibers for visible light photocatalytic degradation of 17α-ethinylestradiol. *Environ. Sci. Pollutn. Res.* 22, 10444–10451. doi: 10.1007/s11356-015-4251-y

Zhang, C., Li, Y., Wang, C., and Zheng, X. (2021). Different inactivation behaviors and mechanisms of representative pathogens (*Escherichia coli* bacteria, human adenoviruses and Bacillus subtilis spores) in g-C_3N_4-based metal-free visible-light-enabled photocatalytic disinfection. *Sci. Total Environ.* 755:142588. doi: 10.1016/j.scitotenv.2020.142588

Zhang, C., Li, Y., Zhang, W., Wang, P., and Wang, C. (2018b). Metal-free virucidal effects induced by g-C3N4 under visible light irradiation: statistical analysis and parameter optimization. *Chemosphere* 195, 551–558. doi: 10.1016/j.chemosphere.2017.12.122

Zhang, C. M., Xu, L. M., Xu, P. C., and Wang, X. C. (2016). Elimination of viruses from domestic wastewater: requirements and technologies. *World J. Microbiol. Biotechnol.* 32, 1–9.

Zhang, C., Zhang, M., Li, Y., and Shuai, D. (2019b). Visible-light-driven photocatalytic disinfection of human adenovirus by a novel heterostructure of oxygen-doped graphitic carbon nitride and hydrothermal carbonation carbon. *Appl. Catal. B* 248, 11–21. doi: 10.1016/j.apcatb.2019.02.009

Zheng, X., Shen, Z. P., Cheng, C., Shi, L., Cheng, R., and Yuan, D. H. (2018). Photocatalytic disinfection performance in virus and virus/bacteria system by cu-TiO_2 nanofibers under visible light. *Environ. Pollut.* 237, 452–459. doi: 10.1016/j.envpol.2018.02.074

Zheng, Q., Shen, H., and Shuai, D. (2017). Emerging investigators series: advances and challenges of graphitic carbon nitride as a visible-light-responsive photocatalyst for sustainable water purification. *Environ. Sci. Water Res. Technol.* 3, 982–1001.

Zhong, Q., Carratalà, A., Ossola, R., Bachmann, V., and Kohn, T. (2017). Cross-resistance of UV-or chlorine dioxide-resistant echovirus 11 to other disinfectants. *Front. Microbiol.* 8:1928. doi: 10.3389/fmicb.2017.01928

Zodrow, K., Brunet, L., Mahendra, S., Li, D., Zhang, A., Li, Q., et al. (2009). Polysulfone ultrafiltration membranes impregnated with silver nanoparticles show improved biofouling resistance and virus removal. *Water Res.* 43, 715–723. doi: 10.1016/j.watres.2008.11.014

Zoni, R., Zanelli, R., Riboldi, E., Bigliardi, L., and Sansebastiano, G. (2007). Investigation on virucidal activity of chlorine dioxide. Experimental data on feline calicivirus, HAV and Coxsackie B5. *J. Prev. Med. Hyg.* 48, 91–95.

Zuo, X., Chu, X., and Hu, J. (2015). Effects of water matrix on virus inactivation using common virucidal techniques for condensate urine disinfection. *Chemosphere* 136, 118–124. doi: 10.1016/j.chemosphere.2015.04.083

Zupanc, M., Pandur, Ž., Perdih, T. S., Stopar, D., Petkovšek, M., and Dular, M. (2019). Effects of cavitation on different microorganisms: the current understanding of the mechanisms taking place behind the phenomenon. A review and proposals for further research. *Ultrason. Sonochem.* 57, 147–165. doi: 10.1016/j.ultsonch.2019.05.009

Zyara, A. M., Torvinen, E., Veijalainen, A. M., and Heinonen-Tanski, H. (2016). The effect of chlorine and combined chlorine/UV treatment on coliphages in drinking water disinfection. *J. Water Health* 14, 640–649. doi: 10.2166/wh.2016.144

frontiers | Frontiers in Microbiology

TYPE Review
PUBLISHED 30 August 2022
DOI 10.3389/fmicb.2022.981896

Check for updates

OPEN ACCESS

EDITED BY
Anthony Ayodeji Adegoke,
University of Uyo,
Nigeria

REVIEWED BY
Timothy Sibanda,
University of Namibia,
Namibia
Abdennaceur Hassen,
Centre de Recherches et des Technologies des Eaux, Tunisia

*CORRESPONDENCE
Abimbola Motunrayo Enitan-Folami
enitanabimbola@gmail.com

SPECIALTY SECTION
This article was submitted to Infectious Agents and Disease, a section of the journal Frontiers in Microbiology

RECEIVED 29 June 2022
ACCEPTED 05 August 2022
PUBLISHED 30 August 2022

CITATION
Lanrewaju AA, Enitan-Folami AM, Sabiu S, Edokpayi JN and Swalaha FM (2022) Global public health implications of human exposure to viral contaminated water. *Front. Microbiol.* 13:981896. doi: 10.3389/fmicb.2022.981896

COPYRIGHT
© 2022 Lanrewaju, Enitan-Folami, Sabiu, Edokpayi and Swalaha. This is an open-access article distributed under the terms of the Creative Commons Attribution License (CC BY). The use, distribution or reproduction in other forums is permitted, provided the original author(s) and the copyright owner(s) are credited and that the original publication in this journal is cited, in accordance with accepted academic practice. No use, distribution or reproduction is permitted which does not comply with these terms.

Global public health implications of human exposure to viral contaminated water

Adedayo Ayodeji Lanrewaju[1], Abimbola Motunrayo Enitan-Folami[1]*, Saheed Sabiu[1], Joshua Nosa Edokpayi[2] and Feroz Mahomed Swalaha[1]

[1]Department of Biotechnology and Food Science, Durban University of Technology, Durban, South Africa, [2]Water and Environmental Management Research Group, Engineering and Agriculture, University of Venda, Thohoyandou, South Africa

Enteric viruses are common waterborne pathogens found in environmental water bodies contaminated with either raw or partially treated sewage discharge. Examples of these viruses include adenovirus, rotavirus, noroviruses, and other caliciviruses and enteroviruses like coxsackievirus and polioviruses. They have been linked with gastroenteritis, while some enteric viruses have also been implicated in more severe infections such as encephalitis, meningitis, hepatitis (hepatitis A and E viruses), cancer (polyomavirus), and myocarditis (enteroviruses). Therefore, this review presents information on the occurrence of enteric viruses of public health importance, diseases associated with human exposure to enteric viruses, assessment of their presence in contaminated water, and their removal in water and wastewater sources. In order to prevent illnesses associated with human exposure to viral contaminated water, we suggest the regular viral monitoring of treated wastewater before discharging it into the environment. Furthermore, we highlight the need for more research to focus on the development of more holistic disinfection methods that will inactivate waterborne viruses in municipal wastewater discharges, as this is highly needed to curtail the public health effects of human exposure to contaminated water. Moreover, such a method must be devoid of disinfection by-products that have mutagenic and carcinogenic potential.

KEYWORDS

enteric viruses, gastroenteritis, outbreak, wastewater, wastewater-based epidemiology

Introduction

The world is increasingly faced with daunting challenges in meeting the expanding requirements for clean water as the existing supplies of freshwater are in short supply owing to (i) prolonged droughts; (ii) population growth; (iii) strict health-based guidelines; and (iv) contending demands from diverse users (Mancosu et al., 2015). Due to these facts and many others, water protection against possible biological and chemical contaminants is becoming

critical in water resources management. Enteric viruses are one of the emerging biological contaminants responsible for the sporadic outbreak of waterborne illnesses worldwide (La Rosa et al., 2012; Upfold et al., 2021). Compared with bacteria and protozoa, viruses are smaller, measuring between 20 and 350 nm in diameter (Health Canada, 2019). Viruses are obligate intracellular parasites containing bundles of gene strands of either RNA or DNA as a core nucleic acid surrounded by a protective coat called protein capsid (Clemente et al., 2012). Sometimes, the capsid protein is enclosed in an additional spikey envelope. In an enveloped virus, the nucleocapsid is bounded by a lipid bilayer which results from the modified host cell membrane with an outer layer of virus envelope glycoproteins (Zwart et al., 2009; Lázaro et al., 2018). Unlike bacterial cells, which are free-living entities, viruses employ the host cell environment to multiply. Studies have shown that viruses can latch onto host cells, as seen in several outbreaks including the current coronavirus (COVID-19) pandemic caused by the severe acute respiratory syndrome coronavirus 2 (SARS-CoV-2) (Shang et al., 2020).

According to Clemente et al. (2012), patients suffering from gastroenteritis may defecate about 10^5–10^{11} virus particles per gram of stool which in turn gain entrance into environmental media through the discharge of contaminated wastewater (Wu et al., 2020; Yeo et al., 2020). Though enteric viruses are the smallest enteric pathogens with a low infective dose, they are robust and difficult to detect and inactivate (Gonzales-Gustavson et al., 2019; Farkas et al., 2020a) hence, they serve as a route of potential health risk at a low exposure dose (Zwart et al., 2009; Zhu et al., 2018). Thus, the transmission of human enteric viruses *via* the water route is becoming more widely recognized as a potential cause of human diseases such as gastroenteritis, encephalitis, meningitis, and hepatitis, among others (World Health Organization, 2014; Tang et al., 2020).

There are several cases where viruses are detected in water deemed compliant with bacterial indicators, and the consumption of such water has been reported to result in waterborne diseases (Umesha et al., 2008; Chen et al., 2021). Even when subjected to conventional wastewater treatments, only about 20–80% of the enteric viruses get inactivated due to their resistance to chemical disinfectants (Jiang et al., 2001; La Rosa et al., 2012), thus leading to the discharge of viruses into the aquatic environment. They can survive unfavorable conditions such as temperature and pH among others for an extended period in environmental waters owing to their small size (Bertrand et al., 2012; Meixell et al., 2013), inertness, and the presence of viral capsid.

Several studies have detected enteric viruses in seawater, surface and groundwater, municipal wastewater influent, and inadequately treated wastewater effluent (Saxena et al., 2015; Shih et al., 2017; Hendriksen et al., 2019; Pang et al., 2019; Verani et al., 2019; Shaheen et al., 2020; Tang et al., 2020; Farkas et al., 2020a). However, their occurrence is not limited to those water matrices, but they have also been found in drinking water systems and recreational water (Umesha et al., 2008; Upfold et al., 2021). Another route of enteric virus transmission is food products contaminated with irrigation water (Benko et al., 2002; Bouseettine et al., 2020). They could be transmitted *via* food, such as shellfish grown in contaminated water, wastewater irrigated farm produce, open defecation, untreated contaminated surface water, and exposure to inadequately treated wastewater due to poor infrastructure (Umesha et al., 2008; Haramoto et al., 2018). Therefore, this review focuses on the occurrence of enteric viruses in water and wastewater sources, their public health implications, and associated diseases due to human exposure to waterborne enteric viruses. Finally, we examined how the identified public health concerns can be minimized.

Enteric viruses of public health importance

Worldwide, more than 150 enteric viruses are associated with waterborne diseases. The prevalence of Hepatitis A Virus (HAV), Adenovirus (AdV), Rotaviruses (RV) and Enteroviruses (EVs), Astroviruses (AstVs), Noroviruses (NoVs), and bacteriophages in surface waters (Radin, 2014), dams and treated drinking water (Fernandez-Cassi et al., 2018; Opere, 2019), treated effluent from wastewater treatment plants (WWTPs; Gonzales-Gustavson et al., 2019) and the detection in post chlorinated water is not exempted (La Rosa et al., 2012). Figure 1 shows both enveloped (e.g., coronaviruses) and non-enveloped viruses found in treated and untreated wastewater. In the recent SARS-CoV-2 outbreak, scientists discovered that the virus responsible for the pandemic; SARS-CoV-2 is shed in feces, detected in the sewerage system, and treated effluent (Ahmed et al., 2020; Haramoto et al., 2020; Randazzo et al., 2020). Furthermore, NoV, AdV, AstV, EV, HAV, RV, and hepatitis E virus (HEV) are transmitted *via* water (Gibson, 2014; Bouseettine et al., 2020).

Adenovirus

Human adenoviruses (HAdV) are icosahedral capsid structures, non-segmented, non-enveloped, and double-stranded DNA viruses with a diameter between 90 and 100 nm (Opere, 2019). The family Adenoviridae is divided into five genera: Genus Mastadenovirus, which infects mammals; Aviadenovirus, which infects birds; Siadenovirus, which infects birds and frogs and Atadenovirus, which infects a wide variety of hosts such as aves, reptiles, and marsupial hosts (Arnold and MacMahon, 2017) and lastly, the newly proposed genera, Ichtadenovirus (Benko et al., 2002). Human adenovirus (HAdV) is a nonlinear envelope single-stranded DNA in the Adenoviridae family and genus Mastadenoviruses (Crenshaw et al., 2019). Within the Mastadenovirus genus, there are presently 103 HAdV serotypes, categorized into seven species (A–G) (Kosulin, 2019; Mennechet et al., 2019).

Many adenoviruses are shed in high amounts with more than 10^{11} particles per gram of faeces, urine, or respiratory

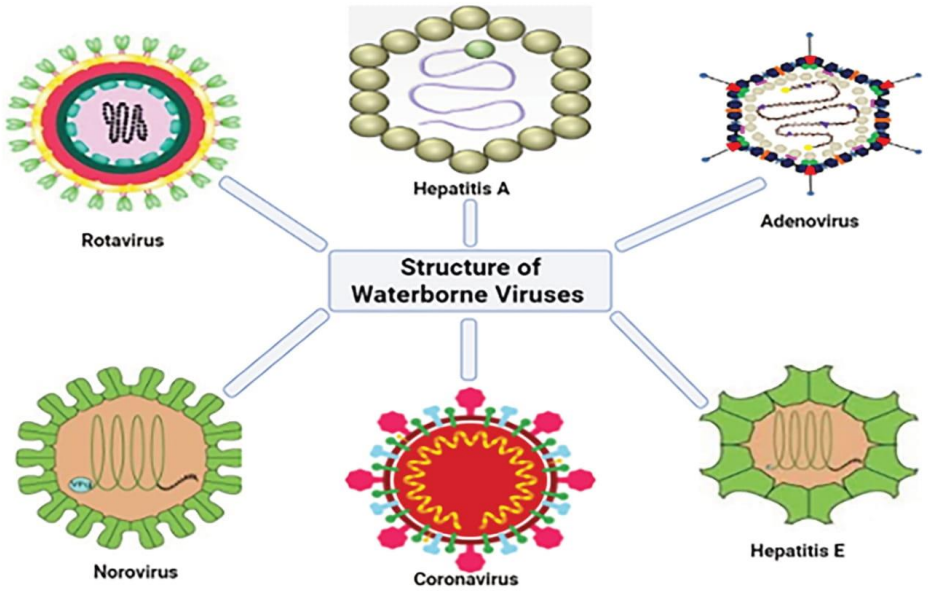


FIGURE 1
Structures of some of the viruses that have been detected in water sources (adapted from Altintas et al., 2015).

excretions (Hewitt et al., 2013). Across the world, these viruses have been found in wastewater, both influent and effluent (Mena and Gerba, 2008; Iaconelli et al., 2017a). Specifically, many HAdV species have been detected in surface water (Sibanda and Okoh, 2012; Opere, 2019) and wastewater (Osuolale and Okoh, 2015; Iaconelli et al., 2017b). Generally, they can survive as extra circular chromosomes or through integration into the DNA of the host (Fu et al., 2019).

In general, HAdVs are prevalent etiological agents of intestinal, respiratory, and ophthalmic diseases. Several clinical features are caused in the respiratory tract, eyes, gastrointestinal tract, and other organs due to the initial propagation, which may occur in the mucosa of the pharynx, conjunctiva, or intestinal mucosa (Howley and Lowy, 2007). Symptoms of infection include gastroenteritis, upper and lower respiratory tract infection, conjunctivitis, pneumonia, myocarditis, and encephalitis (Russell, 2009; Akello et al., 2020). They are generally mild and self-limiting, but in immunocompromised individuals, they can evolve into severe infections with unique manifestations (Khanal et al., 2018). In both developed and developing nations, the occurrence of enteric HAdVs in childhood diarrhea range from 1 to 8% and 2 to 31%, respectively (Meqdam and Thwiny, 2007; Hassou et al., 2020). Between 2007 and 2019, HAdV was found in about 10.8% of all gastroenteritis incidents among children below five in Sub-Saharan Africa (Oppong et al., 2020).

Rotavirus

Rotavirus (RV), belonging to the Reoviridae family, is a relevant and significant waterborne pathogen (Atabakhsh et al., 2021). The genus comprises five species (A–E), two tentative species (F and G) as well as an unassigned species (ADRV-N) which is referred to as RVH (Desselberger, 2014). The rotavirus genome has 11 segments of dsRNA with a size that ranges from 0.6 to 33 kilobase pairs (Bouseettine et al., 2020). Segmentation in the RV genome allows the rearrangement mechanism and production of new strains with different combinations of genome segments resulting in genetic diversity, boosting the evolution, and emerging new strains of RVs each year (Esona et al., 2010; Menezes et al., 2020).

In humans, serogroups A–C cause gastroenteritis, while group A causes severe diarrhea in young children (Bouseettine et al., 2020). Group A is the most common cause of gastrointestinal disease in children below the age of 5, with severe outcomes such as hospitalization and death (Prez et al., 2015; Magana-Arachchi and Wanigatunge, 2020). The principal agents of infectious dehydrating diarrhea in infants are the rotavirus group A [RVA], which is linked to most human RV infections. RVA genotypes G1 P[8], G2 P[4], G3 P[8], and G9 P[8] are associated with most human gastroenteritis and easily undergo genetic recombination (Leite et al., 2008; Tate et al., 2010). Wa-like (G1-P[8]-I1-R1-C1- M1-A1-N1- T1-E1-H1) and DS-1-like

(G2-P[4]-I2-R2-C2-M2-A2- N2-T2-E2-H2) are the two main genogroups identified from the analyses of the complete genome sequences of human rotavirus (HRV) strains to contain the majority of wild-type HRV strains (Tate et al., 2010). The G1P [8] strain is the most predominant in Europe, with about 69.4% of infections in America and some Asian countries (Fongaro et al., 2015). However, there has been a wide level of reduction in the cases of severe childhood diarrhea in countries where routine childhood vaccination against rotavirus has been entrenched. In the same vein, there seems to be a reduction in the number of unvaccinated children due to the protection already offered to vaccinated children, thereby suggesting herd protection because of the vaccination (Fongaro et al., 2015).

Rotavirus infection has been linked to about 258 million cases of diarrhea in children under 5 years worldwide (Troeger et al., 2018). Nevertheless, RV continues to be the leading cause of annual childhood deaths associated with diarrhea worldwide despite the effective introduction of vaccines in more than 106 countries (Kim et al., 2021). The virus has been estimated to be responsible for 122,000–215,000 diarrheic child deaths between 2013 and 2017 annually (Tate et al., 2016; Troeger et al., 2018). In a study conducted to investigate the link between the contaminated water source and rotaviral infection among 184 children under 5 years with acute watery diarrhea, the highest rotaviral infection was observed in children that consume contaminated pond water (94.44%). It was followed by children that were not breastfed exclusively (83.87%) and 64.00% in children living in areas with lower socio-economic conditions (Habib et al., 2021).

Enterovirus

Enterovirus (EV) is a spherical non-enveloped virus containing a 7,500-nucleotide positive-sense single-stranded RNA genome. They are 7.3–7.4 kb in length and are protected by an icosahedral capsid (Opere, 2019). Enteroviruses belong to the family Picornaviridae and are extremely small, with diameters ranging from 22 to 30 nm (Magana-Arachchi and Wanigatunge, 2020). The genus enterovirus has more than 300 known serotypes and 15 species (Chen et al., 2020). The different species include polioviruses, coxsackieviruses A and B, enteroviruses, and echoviruses and they have been linked with human infections (Table 1; Bouseettine et al., 2020).

Millions of people worldwide have been infected with enteroviruses, which have caused the irregular outbreak of illnesses in both advanced and evolving nations (Lugo and Krogstad, 2016; Cassidy et al., 2018; Smuts et al., 2018; Puenpa et al., 2019). Of the seven species to which human EVs belong, only four species (A–D) infect the gastrointestinal tract (Baggen et al., 2018). Enterovirus 71 (EV-A71) is a human enteric virus linked with hand-foot-and-mouth disease (HFMD), while EV-D68 is associated with acute flaccid paralysis (Lee and Chi, 2014; Baggen et al., 2018). A total of 2,967 cases of EV and Parechovirus infections were documented in the United States of America between 2014 and 2016. The most frequently reported enterovirus is the EV-D68 which is responsible for 68% of identified types in 2014 and accounted for 56% of all documented types between 2014 and 2016. Other enteroviruses that were also frequently reported include echovirus 30 (13.1%), coxsackievirus A6 (12.5%), echovirus 18 (9.5%), and coxsackievirus B3 (9%) (Abedi et al., 2018).

TABLE 1 Species of human enteroviruses and associated pathologies (adapted from Bouseettine et al., 2020).

Species	Serotypes	Associated pathologies
Enteroviruses	68–71	Encephalitis, conjunctivitis, meningitis, and paralysis
Echovirus	1–9, 11–21, 24–27, 29–34	Encephalitis, conjunctivitis, meningitis, paralysis, and gastroenteritis
Coxsackievirus A	1–22, 24	Encephalitis, fever, meningitis, and paralysis
Coxsackievirus B	1–6	Encephalitis, gastroenteritis, myalgia, meningitis, paralysis, and pericarditis
Poliovirus	1–3	Encephalitis, gastroenteritis, and pericarditis

The mode of transmission of enterovirus is the faecal-oral route through different sources, such as contaminated water, food, or person-to-person contact. The faecal-oral route becomes problematic when there is exposure to aerosols that are transmitted from any surface or groundwater sources (Gao et al., 2012). Enteroviruses are robust organisms as they can survive critical changes in both pH and temperature (Okoh et al., 2010). Therefore, they have been proposed as a criterion for assessing viral contamination of environmental waters because they are common and shed for an extended period in the environment (La Rosa et al., 2010a). Studies that focused on their removal at WWTPs revealed that they are more resistant to treatment when compared to some other enteric viruses such as adenoviruses and noroviruses (La Rosa et al., 2010b). Several studies have identified them in both raw and treated sewage (La Rosa et al., 2010b; Simmons et al., 2011).

Norovirus

Noroviruses, which were initially referred to as Norwalk or Norwalk-like viruses, are small non-enveloped single-stranded RNA viruses of 27–38 nm in diameter (Rani et al., 2021). They are members of the family Caliciviridae (Upfold et al., 2021). Norwalk virus is composed of a single strand of RNA and bounded by

many copies of a single protein organized into a protective capsid (Wang et al., 2018b). According to Thorne and Goodfellow (2014), it has been frequently revealed that Norovirus is widespread and that infections occur more in the human population. Noroviruses are classified into 10 different genogroups (GI–GX; Laconi et al., 2020). Generally, NoVs GI, GII, and GIV infect man, while GI is less found in patients with acute gastroenteritis across the globe than in GII strains (Koopmans et al., 2002). The most common genogroup in man is the three distinct clusters in GII to which the porcine NoVs belong. This has raised public health concerns regarding the potential NoVs recombinant strains in causing zoonotic transmission (Shen et al., 2012; Okada et al., 2019; Laconi et al., 2020). Generally, gastroenteritis linked with NoVs is self-limiting, although young children, the elderly, and immunocompromised individuals could experience long-term symptoms (Trivedi et al., 2013; Petrignani et al., 2018). Norovirus GI and GII are majorly responsible for human infections; however, for about 10 years now, the genogroup GII.4 has been linked with most human NoVs diseases (Siebenga et al., 2009; Vinjé, 2015; Mans et al., 2016). A novel strain of genotype GII.17 (GII.P17-GII.17) was reported in Asia to be responsible for gastroenteritis linked with NoV in the year 2014 and has subsequently been documented worldwide (Chan et al., 2015, 2017; Lu et al., 2015; Hoa-Tran et al., 2017; Zhou et al., 2019).

The transmission of noroviruses is primarily *via* the faecal-oral route. It transpires through the intake of contaminated water or by direct contact with persons already infected and on environmental surfaces (Zhou et al., 2016; Boonchan et al., 2017; Kittigul et al., 2019). Drinking water and recreational water polluted from sewage are the sources of several outbreaks of NoVs (Kittigul et al., 2019; Prado et al., 2019; Tryfinopoulou et al., 2019). According to de Graaf et al. (2016), GI variants are more linked with transmission through the water route than variant GII.4, which relates to person–person contact. The GI strains of Norovirus are believed to be stable in water compared to the GII strains because they are more likely to be transmitted through water than other transmission routes. Across the globe, NoVs have been detected in different water bodies, including sewages, rivers, recreational waters, municipal water, and groundwater (La Rosa et al., 2007, 2008, 2010a; Miura et al., 2019).

Astrovirus

Human astroviruses (HAstVs) are the third most frequent cause of gastroenteritis, and they were first detected in 1975 (Vu et al., 2017). They are small with sizes ranging from 28 to 30 nm and are non-enveloped viruses having single-stranded RNA (+ssRNA) genomes with about 6,400–7,900 nucleotides. Genera Mamastrovirus (MAstV) and Avastrovirus (AAstV) make up the family Astroviridae (Appleton, 1975; De Benedictis et al., 2011; Donato and Vijaykrishna, 2017). Human astroviruses (HAstVs) are a vital cause of gastroenteritis in infants and young children (De Benedictis et al., 2011). They are found in surface and groundwaters meant for drinking purposes, marine waters, and wastewater effluents (Magana-Arachchi and Wanigatunge, 2020). A study on the molecular detection of gastroenteritis viruses reported that HAstV had a lesser occurrence than EV, RV, NoV, and AdV (Chitambar et al., 2012). The aged and individuals with weak immune system are susceptible to gastroenteritis linked with HAstV (Vu et al., 2017; Wohlgemuth et al., 2019). This could be credited to the pathogenic role of the virus being performed in immunocompromised individuals. In addition, HAstVs have been linked to central nervous system (CNS) infections including encephalitis and acute flaccid paralysis in people with compromised immunity (Cordey et al., 2016; Vu et al., 2016). It could also be due to the inability of the individuals to mount an active inflammatory response to the virus hence a reflection of their highly immunocompromised state.

Hepatitis A virus

Hepatitis A virus (HAV), which is a member of the Hepatovirus genus belonging to the family Picornaviridae, is non-enveloped with an icosahedral structure of an average of 30 nm in diameter and a naked RNA genome (Smith and Simmonds, 2018; Bouseettine et al., 2020). The capsid contains a densely packed icosahedral configuration of 60 protomers, each of which includes three polypeptides VP1, VP2, and VP3 (McKnight and Lemon, 2018). Studies have reported that about 1.5 million people are infected with HAV annually, which is underestimated due to the asymptomatic presentation of the virus and limited epidemiologic information on the virus (World Health Organization, 2017b; Lemon et al., 2018).

As the major causative agent of non-parenteral hepatitis in developing nations as well as endemic infections in developing countries, the primary mechanism of transmission of the HAV is the faecal-oral route and direct contact with an infected person (Mehta and Reddivari, 2021). The outbreaks of HAV infection are mostly associated with water supplies (Jothikumar et al., 2005). The consumption of raw or improperly cooked oysters and clams from sewage-contaminated water has led to many outbreaks of HAV infection (Elbashir et al., 2018). Fever, anorexia, malaise, abdominal discomfort, nausea, and jaundice are some of the numerous symptoms that equally result from HAV infection and could to liver damage (La Rosa et al., 2012).

Hepatitis A virus is found in the feces and urine of diseased individuals through which it contaminates the soil and water. The virus is detected in water and wastewater globally; however, an area's sanitary conditions determine the virus's prevalence (World Health Organization, 2012c). People living in areas with poor sanitation infrastructure are more prone to contracting the virus, especially among children (World Health Organization, 2012b). According to Rodriguez-Lazaro et al. (2012), HAV can subsist for about 60 days in tap water, while it can stay alive for more than 6 weeks in river water, can stay above 8 weeks in groundwater, and for about 30 weeks in seawater. The virus has been found in

different water environments such as raw wastewaters (Osuolale and Okoh, 2015), treated effluents (Van Zyl et al., 2019), surface waters (Marie and Lin, 2017; Shaheen et al., 2019), and drinking waters (Moreno et al., 2009).

Hepatitis E virus

Hepatitis E virus (HEV) is a member of the family Hepeviridae and belongs to the Orthohepevirus genus and the Orthohepevirus A species. HEV is a non-enveloped, positive sense, ssRNA virus (Denner, 2019) that causes significant acute hepatitis worldwide thereby resulting in sporadic infections and epidemics (Raji et al., 2021). The infection is usually asymptomatic in the general population (Khuroo and Kamili, 2003). The virus is regarded as zoonotic with swine and other animals such as rabbits serving as the reservoir for human infections (Ruggeri et al., 2013; Syed et al., 2018). Hepatitis E virus is another waterborne pathogen threatening global health in developing and developed countries (Raji et al., 2021). Currently, eight HEV genotypes have been identified (Upfold et al., 2021), and genotypes 1–4 and 7 are known to be the main threats to humans. They are transmitted through the ingestion of contaminated water, causing acute hepatitis (Purdy et al., 2017).

Ruggeri et al. (2013), posited that HEV strains that belong to genotypes 1 and 2 are the cause of the most sporadic outbreak of hepatitis in developing countries of Africa, Asia, and Mexico (Smith and Simmonds, 2018). Genotypes 3, 4, and 7 are basically associated with zoonotic transmission (Marek et al., 2010) and are generally connected with irregular and grouped infections in advanced countries (Nimgaonkar et al., 2018). It is transmitted *via* the faecal-oral pathway and spreads readily through water bodies polluted with human faeces. Globally, the virus has been detected in different water bodies including rivers (Iaconelli et al., 2015), and raw wastewater (Iaconelli et al., 2017a; Wang et al., 2018a), among others.

Aichivirus

Aichivirus (AiV) belongs to the Kobuvirus genus and the family Picornaviridae (Rivadulla and Romalde, 2020). It is one of the significant causative organisms of gastroenteritis in humans and is transmitted *via* the faecal-oral route from contaminated food or water (Yamashita et al., 2000; Adams et al., 2013; Kebe et al., 2021). Aichivirus consists of Human AiV (HAiV) 1, Murine Kobuvirus (MuKV) 1, and Canine Kobuvirus (CaKV) 1. Human AiV is composed of three genotypes (A–C; Yamashita et al., 2000; Shaheen et al., 2020; Kebe et al., 2021), and the infection rate of AiV in gastroenteritis cases worldwide is low between 0.4 and 6.5% (Rivadulla and Romalde, 2020; Taghinejad et al., 2020; Upfold et al., 2021). However, specific antibodies produced against the virus are found in about 80–90% of adults (Kitajima and Gerba, 2015; Rivadulla and Romalde, 2020), which is a pointer to the asymptomatic condition of most infections (Bergallo et al., 2017). Furthermore, this virus is often detected in connection with other enteric pathogens (Oh et al., 2006; Ambert-Balay et al., 2008; Kaikkonen et al., 2010; Japhet et al., 2019). Diarrhea, abdominal pain, vomiting, and fever are some clinical signs and symptoms of human AiV virus infection (Yamashita et al., 2000). Aichivirus has been reported in Africa, Asia, South America, and Europe (Oh et al., 2006; Lodder et al., 2013). The virus is normally passed out in the faeces of humans directly or after discharge of treated or untreated sewage (Lodder et al., 2013; Kebe et al., 2021), and can be adopted as a potential indicator of wastewater reclamation system (Kitajima et al., 2014; Farkas et al., 2020b).

Coronaviruses

Coronaviruses (CoVs) are positive-sense single-stranded RNA viruses (Qu et al., 2020; Yeo et al., 2020) with more than 30 different species and have the biggest genome of RNA viruses of 30 kb (Amirian, 2020; Amoah et al., 2020). Coronaviruses are classified into four types: Alphacoronavirus (Alpha-CoV), Betacoronavirus (Beta-CoV), Gammacoronavirus (Gamma-CoV), and Deltacoronavirus (Delta-CoV; Delta-CoV; Qu et al., 2020). The coronavirus virion is typically spherical, with a diameter of 60–140 nm, and is enclosed by an outer viral envelope covered by projections (9–12 nm; Zhu et al., 2020). CoVs were thought to be insignificant human pathogens until the beginning of this century. The latest outbreak in Wuhan, China toward the end of 2019 was the emergence of a novel coronavirus (Lu et al., 2020). It was initially referred to as HCoV-19 but later officially named Severe Acute Respiratory Syndrome Coronavirus 2 (SARS-CoV-2); because the novel virus is most closely linked to the SARS-CoV virus that was implicated in the 2003 SARS outbreak (Lu et al., 2020; World Health Organization, 2020).

The SARS-CoV-2 is responsible for a variety of common cold-like and acute respiratory diseases (Qu et al., 2020; Yeo et al., 2020). COVID-19 is the respiratory disease induced by SARS-CoV-2 (World Health Organization, 2020), with clinical symptoms including diarrhea, nausea, fever, cough, rhinorrhea, dyspnea, or severe pneumonia and myalgia (Guan et al., 2020; Liu et al., 2020; Yeo et al., 2020). Nevertheless, a considerable proportion of individuals remain symptomless despite testing positive for SARS-CoV-2 (Bai et al., 2020; Lai et al., 2020; Liu et al., 2020; Rothe et al., 2020). Evidence from the present COVID-19 outbreak proposes that about 2–35% of patients develop gastrointestinal (GI) symptoms such as diarrhea, abdominal discomfort, and vomiting; however, this is less common than respiratory symptoms (Yeo et al., 2020; Wang et al., 2020a), and this has resulted in the presence of the virus in feces and sewage (Amirian, 2020; Pan et al., 2020). Therefore, this virus has been detected in untreated wastewater and rivers (La Rosa et al., 2020; Medema et al., 2020; Rimoldi et al., 2020; Sherchan et al., 2020; Pillay et al., 2021), as well as in treated wastewaters (Haramoto et al., 2020; Randazzo et al., 2020).

Prevalence of enteric viruses in freshwater and wastewater sources

Critical tools for detection and prevention of the further spread of diseases and outbreaks include clinical surveillance and monitoring of waterborne pathogens. However, disease prevalence is under-reported through clinical testing because it is typically restricted to those who are ill to the extent of seeking treatment and testing (Cacciò and Chalmers, 2016). Hence, there is a lag indicator for predicting an outbreak in a community. Therefore, there is a desperate need for cost-effective and improved monitoring methods to detect numerous waterborne diseases in a community, preferably in real-time. To this end, wastewater-based epidemiology (WBE) has recently garnered much attention as an early warning technique for a range of waterborne infectious diseases (Zahedi et al., 2021).

Wastewater-based epidemiology (WBE) has been employed before now to monitor drug abuse within a community (Castiglioni et al., 2006) and other chemical pollutants (Choi et al., 2018), as well as the prevalence of poliovirus (Pöyry et al., 1988; Berchenko et al., 2017). Broadly, it entails the detection of nucleic acids or other biomarkers excreted in feces and urine in wastewater to offer detailed health information about a community (Mao et al., 2020). The approaches encompass the detection of pathogens released in saliva, sputum, mucus, vomitus, and phlegm that are frequently trapped in wastewater (Zahedi et al., 2021). Accordingly, WBE is thus equal to the collection and analysis of a large community-based combined sample of faeces, saliva, vomitus, sputum, urine, shed skin, and other substances released during personal cleansing, washing, bathing, and excretion. Hence, it provides a sensitive technique for tracking temporal alterations and variety in pathogen concentrations within a community (Xagoraraki and O'Brien, 2020). Another benefit of the direct analysis of wastewater samples is the presence of higher populations of pathogens in wastewater compared to environments where inadequately treated wastewater is discharged (Zahedi et al., 2021).

Wastewater passes through a series of treatment processes, including oxidation ponds, coagulation, activated sludge, chlorination, and ozonation until good effluent quality is achieved. However, about 50–90% of the waterborne viruses can only be removed *via* different treatment processes, thereby releasing a significantly high viral load into the environment that humans become exposed to with accompanying public health diseases (Gersberg et al., 1988; Zhu et al., 2005; Charles et al., 2008; Okoh et al., 2010; La Rosa et al., 2012; Sano et al., 2016). Supplementary Table 1 shows the prevalence of selected waterborne enteric viruses across different countries in various water environments, which portends the potential risk of the transmission of the virus. The employment of bacterial indicator species to assess the quantity of the virus load in wastewater effluents is one of such limitations. This has been faulted as an inefficient technique for monitoring the quality of wastewater (Gersberg et al., 1988; Hunter, 1997; Zhu et al., 2005; Bofill-Mas et al., 2006; Charles et al., 2008; Karmakar et al., 2008; Okoh et al., 2010; Farkas et al., 2020b).

The prevalence of HAdV in both 60 stool samples from children with acute gastroenteritis and 96 sewage samples collected from the Zenin wastewater treatment plant was investigated within a community in Egypt from January to December 2017 (Elmahdy et al., 2019). The virus was detected in 17 (28.3%) of stool, 27 (84.4%) of raw sewage, 16 (50%) of treated sewage, and 25 (78%) of sludge samples throughout a whole year of sample collection. According to Elmahdy et al. (2019), the occurrence of HAdV in the treated effluent of the WWTP portends a serious public health problem. Similarly, the prevalence of AdVs in treated wastewater in Brazil was reported by Quintão et al. (2021). The study reported the occurrence of AdVs in 27.2% (61/224) of the investigated samples. It was observed that the occurrence of the virus was higher in downstream samples than that in upstream samples. In another study, F species HAdVs serotype 41 (79.2%) and C species PAdVs serotype 5 (18.1%) were higher than other serotypes in the water samples collected from Puzi River, Taiwan. On the other hand, the prevalence of NoV GII was more than GI in the same river. Specifically, GII.4 (21.2%) and GII.17 (18.2%) were reported as the predominant genotypes. The occurrence of both AdVs and NoVs was higher in the winter compared to the spring, summer, and autumn seasons.

Furthermore, Iaconelli et al. (2017a), reported the prevalence of EV, AdV, HAV, HEV, and NoV in raw and treated wastewater. Adenovirus was the most frequently detected virus in raw wastewater (81%) compared to 33% in treated effluents, followed by EV, with 13 samples detected in raw sewage and 3 samples in treated effluents. Norovirus GI or GII were detected in 10 raw wastewater and 4 treated effluents. Likewise, HEV was detected in one sewage sample, while HAV was 33% in raw sewage and 19% in treated effluents (Iaconelli et al., 2017a). Conversely, Hepatitis A and E virus outbreaks were linked to contaminated drinking water in 72% (109/151) and 49 (38%) of the 128 outbreaks (Kumar et al., 2015). Also, Miao et al. (2018), assessed the prevalence of EV, RV, AstV, NoV GII, and AdV in Jinhe River, China. The detection frequency differs as follows; 91.7% for AdV, 81.3% for NoV GII, 79.2% for EV and AstV, and 70.8% for RV. In addition, the authors reported a seasonal pattern concerning the prevalence of the detected viruses in which there was an abundance of EVs in summer whereas RVs, AstVs, NoV GII, and AdVs showed opposite seasonal trends.

The prevalence of different astrovirus strains in different water matrices such as wastewater in the US, groundwater, and river in Nepal has also been reported (Hata et al., 2018). The identified strains include types 6 and 7 classical human astroviruses, emerging type 5 VA-astroviruses, and putative recombinants. The prevalence of classical and VA-astroviruses was reported during the cooler months while it was during the warmer months that MLB-astroviruses were detected (Hata et al., 2018). Aichivirus was found in Nepal in different water sources such as sewage pipes, rivers, groundwater, and a house that received its water from a

tanker (Haramoto and Kitajima, 2017). Variations in AiV detection with a significant prevalence of AiV B were reported in the study. When compared to shallow tube wells, where AiV was detected in 1 out of 15 samples (7%), the frequency of AiV detection was substantially higher in shallow dug wells, where it was discovered in 10 out of 22 samples (45%). This variation could be attributed to the fragile structure of dug wells often composed of stone or brick compared to that of tube wells. Conversely, AiV was detected in 50% of river water samples examined in a study conducted in Iran (Azhdar et al., 2019). According to a survey carried out by Moreira and Bondelind (2017), *Cryptosporidium*, norovirus, *Giardia*, *Campylobacter*, and rotavirus were the waterborne pathogens responsible for drinking waterborne outbreaks during 2000–2014. Authors further reported that contamination of surface water sources affected most consumers which led to gastrointestinal diseases, while the distribution network was responsible for most individual incidents (Moreira and Bondelind, 2017).

Also, rotaviruses in surface water and wastewater have been reported in different parts of the world, especially in developing countries (Taylor et al., 2001; Verheyen et al., 2009; Rezaeinejad et al., 2014). Nevertheless, they are less often detected in environmental samples compared to AdVs (Spilki et al., 2013). The distribution of RV infection is seasonal, with the incidence reaching the peak during winter (Suzuki et al., 2005). However, it has been reported all year round worldwide (Osuolale and Okoh, 2016). The RV strains are linked with diseases like acute diarrhea in humans and animals (Almeida et al., 2018; Menezes et al., 2020). The transmission of rotavirus is majorly *via* the ingestion of food and water that has been contaminated with human wastes. In most cases, newborns or young children with gastroenteritis are infected with subclinical illness from an older sibling or mother. The shedding of the virus from the intestinal tract occurs before diarrhea sets in or even after it has been reported (Mukhopadhya et al., 2013).

During the global COVID-19 outbreak in Japan, Hata et al. (2021) investigated the presence of SARS-CoV-2 RNA in wastewater samples and the number of confirmed COVID-19 cases in the study area was compared. During the study period, a total of 45 influent samples were collected from five wastewater treatment plants in Ishikawa and Toyama regions in Japan. The virus was detected in 21 out of the 45 influent samples. There was an increase in the frequency of detection as the total number of confirmed cases in 100,000 people surpassed 10 in each region; however, SARS-CoV-2 RNA could still be detected even when there was a reduction in the number of confirmed cases. This could be attributed to the continuous shedding of the virus from discharged asymptomatic individuals. Hata et al. (2021), opined that the viral monitoring of wastewater could be adopted as an early warning signal of COVID-19 outbreaks in Japan.

Considering the occurrence of these viruses in water bodies, there is a need to carefully monitor treated wastewater before discharge; however, the employed methods have some drawbacks. The number of viruses contained in environmental media can vary significantly; however, it is a function of the type of sample being examined. High viral concentration could be detected and quantified in wastewater or sludge from treatment plants using a very small sample volume (Haramoto et al., 2018). Nevertheless, a significantly small volume which could be less than 1 ml that will be concentrated from the wastewater sample is required for the downstream detection experiments. Ultrafiltration, adsorption/elution, flocculation, and ultracentrifugation, among other techniques, have been utilized to concentrate viruses from wastewater (Prata et al., 2012; Haramoto et al., 2018). A dependable and appropriate method of concentration should have a capacity for high viral recovery, repeatable results, be suitable for detecting a wide array of viruses, create a minimal volume of viral concentrate, be rapid and cost-effective to operate (Bosch, 1998).

Unfortunately, all these criteria have not been found in any single technique for the concentration of viruses in water. This has made the concentration of viruses in water considerably more difficult. Hence, rapid action is necessary to track viruses in fresh and wastewater sources. Even though no strict standards have been set in addressing the concentration of viruses in treated wastewater effluents before disposal. Their elimination before discharge into environmental media is critical to minimize potential outbreaks and accompanying diseases due to exposure to humans (Haramoto et al., 2018). It is crucial to optimize and evaluate the available concentration techniques to improve virus recovery and build a highly effective process that will go a long way in combating virus outbreaks in the future hence, research should be geared toward achieving this goal (Ibrahim et al., 2021).

Public health implications of waterborne enteric viral diseases

The genomic content and capsid proteins of enteric viruses differ, nevertheless, they share some similar attributes making them more of public health threat regarding the risk of drinking contaminated water. The non-enveloped virus can remain active in water bodies for extended periods (Reynolds et al., 2008). Considering those attributes, drinking inadequately disinfected water contaminated with faeces could lead to waterborne disease outbreaks (Gall et al., 2015a; Sano et al., 2016; Adelodun et al., 2021). It is also noteworthy that viruses could be transmitted through three major routes; ingestion, inhalation, and direct contact *via* interaction with skin and eyes (swimming) leading to respiratory and ocular infections (Gall et al., 2015a).

Usually, waterborne enteric viruses are associated with gastrointestinal diseases, epidemics, and acute hepatitis. Adenovirus, AstVs, HAV, HEV, RVs, NoVs, and other caliciviruses, and enteroviruses, including coxsackieviruses and polioviruses are classified by WHO as waterborne viral pathogens with modest to high health importance (WHO, 2017c). These viruses are linked with gastroenteritis and diarrhea coupled with the severity of other symptoms such as fever and abdominal cramps among others. Table 2 shows the different waterborne

enteric viruses and related diseases. Gastroenteritis is the most frequent pathology connected with enteric virus' infections (Bányai et al., 2018). Various gastroenteritis outbreaks have been associated with drinking sewage-contaminated water containing some of these enteric viruses which include AdVs, EVs, NoVs, RVs, AstVs, AiVs among others (Maunula et al., 2009; Räsänen et al., 2010; Kauppinen et al., 2019). For instance, a minimum of 33 outbreaks were connected to drinking contaminated water between 2009 and 2014 in the United States of America (Control and Prevention, 2013). The most important cause of gastrointestinal illness across the world is human noroviruses. Due to increased environmental robustness, human noroviruses genogroup I is usually involved in waterborne cases (Matthews et al., 2012), while genogroup II with the large majority of cases is transmitted from person to person and presumed to be connected with food (Ahmed et al., 2014).

Likewise, diarrhea has also emerged as the world's second-biggest cause of death in children under 5 years (Murray and Newby, 2012). It is one of the major recurrent waterborne infections, with 1.7 billion cases recorded each year (WHO, 2017a), and 525,000 children's deaths (Pooi and Ng, 2018). According to the global burden of disease investigated in 2015, 1.2 million deaths and 71.7 million disability-adjusted life years (DALYs) coupled with 1.1 million deaths and 61.1 million DALYs from diarrheal diseases all resulted from contaminated water sources (Forouzanfar et al., 2016). The primary cause of diarrhea contracted by drinking contaminated water is bacteria; however, little or no attention is being paid to viral pathogens in water sources as well as their impact on public health. Gibney et al. (2017), conducted a study in 2010 on the disease burden of cryptosporidiosis, campylobacteriosis, giardiasis, nontyphoidal salmonellosis, and norovirus ascribed to the waterborne transmission of selected enteric pathogens in Australia. Most waterborne disease cases were linked to norovirus, a waterborne enteric virus (479,632; 95% confidence interval [UI]: 0–1,111,874), followed by giardiasis and campylobacteriosis. Based on a global study of groundwater-related enteric illness outbreaks survey, an alarming rise in groundwater-related acute gastrointestinal infections (AGI) was reported between 1948 and 2015, with 649 incidents identified (Murphy et al., 2017).

Recently, Carol et al. (2021) investigated the causative agent responsible for an outbreak of acute gastroenteritis (AGE) among 174 pupils that were involved in a school trip between 30 January and 3 February 2017 at a holiday camp in Catalonia. The authors discovered about 41 episodes of AGE with symptoms ranging from abdominal pain (73.8%), nausea (64.3%), vomiting (54.8%), diarrhea (45.2%), and headache (42.9%). The outbreak also was linked to the consumption of NoV GII contaminated water samples (crude RR: 1.72, 95% CI: 1.01–2.92; adjusted RR: 1.88, 95% CI 1.03–3.56). According to the World Health Organization/United Nations Children Emergency Fund, (2015) reports, untreated water is used by 663 million people worldwide. Although, individuals living in poverty-stricken or rural areas and developing regions are affected by a lack of access to safe drinking water. Notwithstanding, even people living in developed countries with advanced water and wastewater treatment facilities are not spared from waterborne diseases (Adelodun et al., 2021). Furthermore, it has been estimated that by the year 2030, approximately 1.6 billion people (19% of the global population) will lack clean water, leading to more waterborne outbreaks and illnesses (World Health Organization/United Nations Children Emergency Fund, 2021).

The Integrated Disease Surveillance Programme (IDSP) reported 804,782 hepatitis cases and 291 outbreaks in India between 2011 and 2013. Hepatitis A testing revealed 44,663 (7.4%) positive cases out of 599,605 total cases, and HEV testing revealed 19,508 (10.4%) positive cases out of 187,040 total cases. Hepatitis E virus accounted for 78 (48%) out of 163 (56%) outbreaks with known etiologies as hepatitis A accounted for 54 (33%), while hepatitis A and E accounted for 19 (12%), (Kumar et al., 2015). In a hepatitis A and E surveillance carried out between 2015 and 2017 in India, 23 disease outbreaks were reported of which 4 outbreaks occurred in 2015, 12 in 2016, and 7 in 2017 (Kadri et al., 2018). Twelve of the total outbreaks were related to hepatitis A infection, 10 to hepatitis E infection, while 1–8 cases of jaundice with no hepatitis A or hepatitis E virus were identified. During the study period, a total of 393 cases of hepatitis A or E were detected. Of the 50 water samples that were examined, 38 were unsuitable for human consumption

TABLE 2 Enteric viruses and related diseases.

Enteric viruses	Related diseases	References
Adenoviruses	Gastroenteritis, respiratory disease, and conjunctivitis	Gibson, 2014; Kumar et al., 2014; La Rosa et al., 2012
Enteroviruses	Gastroenteritis, meningitis, myocarditis, respiratory disease, encephalitis, and conjunctivitis	Bouseettine et al., 2020; Gibson, 2014; Kumar et al., 2014; La Rosa et al., 2012
Poliovirus	Poliomyelitis, meningitis, and encephalitis	Bouseettine et al., 2020; Kumar et al., 2014
Coxsackievirus	Meningitis, encephalitis, paralysis, and myocarditis	Bouseettine et al., 2020; Kumar et al., 2014
Astroviruses	Gastroenteritis	Gibson, 2014; Kumar et al., 2014
Hepatitis viruses A, E	Hepatitis	Gibson, 2014; Kumar et al., 2014
Noroviruses	Gastroenteritis	Gibson, 2014; Kumar et al., 2014
Sapoviruses	Gastroenteritis	Kumar et al., 2014
Rotavirus	Gastroenteritis	Gibson, 2014; Kumar et al., 2014
Aichivirus	Gastroenteritis	Bouseettine et al., 2020
Coronavirus	Gastroenteritis and respiratory disease	Dongdem et al., 2009; La Rosa et al., 2012

hence the authors opined that both HAV and HEV outbreaks were due to human exposure to contaminated water (Kadri et al., 2018).

In addition, there was an increase in diarrhea cases reported in Mgcawu District, Northern Cape province, and eThekwini Metropolitan Municipality, KwaZulu-Natal province, South Africa (Shonhiwa et al., 2020). The reported diarrhea outbreaks that affected children under age 5 coincided with the yearly South Africa rotavirus season in 2013 (Shonhiwa et al., 2020). In the same vein, a gastroenteritis outbreak linked to swimming in the lagoon in KwaZulu-Natal Coast, South Africa, resulted in more than 600 cases within 3 weeks in December 2016/January 2017 (Sekwadi et al., 2018). Also, RVs, AstVs, NoVs GI.6, GII.3, and GII.6, were the waterborne viruses identified in the lagoon water samples. The prevalence of the viruses is due to the discharge from WWTPs effluent into the river that feeds the lagoon (Sekwadi et al., 2018). Similarly, in 2017, there was a rotavirus outbreak in India, with a 22.8% attack rate due to drinking water from contaminated wells (Joshi et al., 2019). The Hepatitis E virus was also linked with the largest viral waterborne outbreak in India in which about 80,000 people were affected (Naik et al., 1992; Farkas et al., 2020b).

With above 6 million deaths worldwide as of March 2022, COVID-19, the highly contagious infectious disease caused by SARS-CoV-2, had a devastating impact on the world's demographics and is emerging as the most significant global health crisis since the period of the influenza pandemic of 1918 (Cascella et al., 2022). The COVID-19 pandemic has resulted in the emergence of significant health challenges owing to its contagious nature and the absence of efficient medical treatment (Coccia, 2021). Respiratory symptoms are the most common in COVID-19 individuals. However, research suggests that gastrointestinal (GI) symptoms such as diarrhea, nausea/vomiting, and abdominal discomfort are common in COVID-19 patients, with a frequency of up to 31.9% (Cholankeril et al., 2020; Remes-Troche et al., 2020). The possibility of the waterborne transmission of SARS-CoV-2 began to draw increasing attention due to the detection of its genetic marker in different water matrices as highlighted earlier. However, there is currently no scientific evidence that the viral RNA is infectious in water and wastewater and can be contacted in water. This gives room for more future studies to look comprehensively into this.

Apart from the loss of lives associated with the unavailability of safe drinking water and poor sanitation, the World Bank estimated an annual economic loss of US$260 billion globally (World Health Organization, 2012a). The infections associated with contaminated water and enteric viral outbreaks are considered under-reported irrespective of the country's socio-economic condition because the symptoms are generally mild, and people rarely seek medical treatment for self-limiting illnesses (Control and Prevention, 2013). Generally, in healthy individuals, viral infections are self-limiting; however, in children under the age of five, the aged, pregnant women, and immunocompromised patients, greater morbidity could result. Hence, it makes the surveillance of diseases associated with enteric viruses challenging (Cortez et al., 2017; Li et al., 2017). Unfortunately, few broad-spectrum antiviral drugs exist for the treatment of those diseases (Gall et al., 2015a).

Strategies for the removal of waterborne viruses

Detecting and quantifying the various types of viruses in wastewater are critical for preventing diseases and creating strategic responses to outbreaks. Nevertheless, removing enteric viruses from wastewater is equally essential to avert their spread through food, water, or other pathways. However, the transmission of waterborne viruses is common in developing countries due to their poor sanitation. For instance, there has been a threat to global polio eradication. This is due to the possible movement of indigenous wild poliovirus (WPV) into polio-free countries. Also, it could be through the importation of WPV from polio-endemic countries as well as the release of WPV into the environment from laboratory stocks (Sharma et al., 2015). Hence, every country must detect WPV circulation and other waterborne viruses *via* a sensitive surveillance system.

Although, physical removal of pathogens *via* conventional methods, ultraviolet light or chemical oxidants like chlorine, chloramines, and ozone have been employed, unfortunately, the capacity to resist disinfection due to viral particle size (Ibrahim et al., 2021), and the presence of viral capsid make virus removal a challenging task for most available technologies as well as wastewater epidemiologist. Till date, chlorine disinfectant is being used for water treatment to enhance the deactivation of pathogens and maintain a residual concentration in the distribution line (Crittenden et al., 2012). The availability of chlorine made it a common disinfectant in water purification (Rosario-Ortiz et al., 2016); however, it raises the risk of creating possibly mutagenic and carcinogenic disinfection by-products like bromate and chlorite (Sharma et al., 2014; Gall et al., 2015b) that could pose major health risks to humans (Agency, 2006; Richardson and Postigo, 2011).

Generally, the side effects and limitations associated with the use of conventional techniques for the disinfection of water made it inappropriate in the long run. As highlighted, harmful disinfection by-products are formed when chlorine reacts with natural organic matter found in water sources (Hrudey and Charrois, 2012). The by-products released from the use of those conventional oxidants as disinfectants have been reported to be harmful to human health. Another danger for humans that is associated with the use of conventional disinfectants is their non-specificity as higher doses are needed for disinfection (Kumar et al., 2020). Specifically, studies have shown that the reoviruses may be more sensitive to chlorine disinfection than enteroviruses (Betancourt and Gerba, 2016). Unfortunately, attaining complete sterilization and disinfection has not been confirmed to be achieved by any conventional wastewater treatment procedures (Sano et al., 2016). Hence, finding solutions to reduce this problem has become an issue of keen interest. Therefore, research should be geared toward the development of an effective method of disinfection for the removal of waterborne enteric viruses. In addition, such

methods must be devoid of the formation of disinfection by-products which characterizes the chemical methods of disinfection owing to the reaction of residual chlorine with organic matter to form possible mutagenic and carcinogenic by-products.

Conclusion

This article reviews the public health implications of human exposure to viral contaminated water. The presence of enteric viruses in water comes with accompanying public health implications that cannot be ignored. Although the presence of other microbes in wastewater has been the focus of research before now, the risk of diseases associated with the presence of viruses in water is by far greater than that of other microbes as just an insignificant quantity of viruses is adequate to cause diseases when compared to other microorganisms.

The detection and quantification of the various human viruses in environmental water are critical for public health concerning the prevention of diseases as well as response to outbreaks. Hence, conducting regular viral monitoring of treated wastewater discharged into the environment is important for the prevention of diseases associated with exposure to viral contaminated water. Meanwhile, the presence of viral particles in water and wastewater does not mean that the particles are infectious but are pointers to potential infections and health risk burdens that could emanate from the matrices. Hence, there is an urgent need for further studies to highlight infectious fractions of viral particles disseminated *via* wastewater and water resources for effective risk assessment and epidemiologic purposes. Nevertheless, removing viruses from wastewater using other alternative treatment methods in a bid to stop their transmission *via* the ingestion of contaminated water should be considered. Therefore, a search for a more holistic and cost-effective disinfection method that will inactivate waterborne viruses in water is highly needed to curtail the public health effects of human exposure to contaminated water.

Author contributions

AL, AE-F, and FS conceived the review idea. AL wrote the first draft. AL, AE-F, SS, and JE reviewed and edited the manuscript. All authors contributed to the article and approved the submitted version.

Funding

This work was funded by the Water Research Commission (WRC) of South Africa (Project no. K5/C2020-2021-00181). We were also supported by our institution, the Durban University of Technology, South Africa.

Conflict of interest

The authors declare that the research was conducted in the absence of any commercial or financial relationships that could be construed as a potential conflict of interest.

Publisher's note

All claims expressed in this article are solely those of the authors and do not necessarily represent those of their affiliated organizations, or those of the publisher, the editors and the reviewers. Any product that may be evaluated in this article, or claim that may be made by its manufacturer, is not guaranteed or endorsed by the publisher.

Supplementary material

The Supplementary material for this article can be found online at: https://www.frontiersin.org/articles/10.3389/fmicb.2022.981896/full#supplementary-material

References

Abedi, G. R., Watson, J. T., Nix, W. A., Oberste, M. S., and Gerber, S. I. (2018). Enterovirus and parechovirus surveillance—United States, 2014–2016. *Morb. Mortal. Wkly Rep.* 67, 515–518. doi: 10.15585/mmwr.mm6718a2

Adams, M., King, A., and Carstens, E. (2013). Ratification vote on taxonomic proposals to the international committee on taxonomy of viruses (2013). *Arch. Virol.* 158, 2023–2030. doi: 10.1007/s00705-013-1688-5

Adelodun, B., Ajibade, F. O., Ighalo, J. O., Odey, G., Ibrahim, R. G., Kareem, K. Y., et al. (2021). Assessment of socioeconomic inequality based on virus-contaminated water usage in developing countries: a review. *Environ. Res.* 192:110309. doi: 10.1016/j.envres.2020.110309

Agency, U. E. P. (2006). National primary drinking water regulations: stage 2 disinfectants and disinfection byproducts rule. *Fed. Regist.* 71, 387–493.

Ahmed, W., Angel, N., Edson, J., Bibby, K., Bivins, A., O'Brien, J. W., et al. (2020). First confirmed detection of SARS-CoV-2 in untreated wastewater in Australia: a proof of concept for the wastewater surveillance of COVID-19 in the community. *Sci. Total Environ.* 728:138764. doi: 10.1016/j.scitotenv.2020.138764

Ahmed, S. M., Hall, A. J., Robinson, A. E., Verhoef, L., Premkumar, P., Parashar, U. D., et al. (2014). Global prevalence of norovirus in cases of gastroenteritis: a systematic review and meta-analysis. *Lancet Infect. Dis.* 14, 725–730. doi: 10.1016/S1473-3099(14)70767-4

Akello, J. O., Kamgang, R., Barbani, M. T., Suter-Riniker, F., Leib, S. L., and Ramette, A. (2020). Epidemiology of human adenoviruses: a 20-year retrospective observational study in hospitalized patients in Bern, Switzerland. *Clin. Epidemiol.* 12, 353–366. doi: 10.2147/CLEP.S246352

Almeida, P. R., Lorenzetti, E., Cruz, R. S., Watanabe, T. T., Zlotowski, P., Alfieri, A. A., et al. (2018). Diarrhea caused by rotavirus A, B, and C in suckling piglets from southern Brazil: molecular detection and histologic and immunohistochemical characterization. *J. Vet. Diagn. Investig.* 30, 370–376. doi: 10.1177/1040638718756050

Altintas, Z., Gittens, M., Pocock, J., and Tothill, I. E. (2015). Biosensors for waterborne viruses: detection and removal. *Biochimie* 115, 144–154. doi: 10.1016/j.biochi.2015.05.010

Ambert-Balay, K., Lorrot, M., Bon, F., Giraudon, H., Kaplon, J., Wolfer, M., et al. (2008). Prevalence and genetic diversity of Aichi virus strain in stool samples from

community and hospitalized patients. *J. Clin. Microbiol.* 46, 1252–1258. doi: 10.1128/JCM.02140-07

Amirian, E. S. (2020). Potential fecal transmission of SARS-CoV-2: current evidence and implications for public health. *Int. J. Infect. Dis.* 95, 363–370. doi: 10.1016/j.ijid.2020.04.057

Amoah, I. D., Kumari, S., and Bux, F. (2020). Coronaviruses in wastewater processes: source, fate and potential risks. *Environ. Int.* 143:105962. doi: 10.1016/j.envint.2020.105962

Appleton, H. (1975). Viruses and gastroenteritis in infants. *Lancet* 305:1297. doi: 10.1016/S0140-6736(75)92581-7

Arnold, A., and MacMahon, E. (2017). Adenovirus infections. *Medicine* 45, 777–780. doi: 10.1016/j.mpmed.2017.09.016

Assis, A. S. F., Fumian, T. M., Miagostovich, M. P., Drumond, B. P., and da Rosa e Silva, M. L. (2018). Adenovirus and rotavirus recovery from a treated effluent through an optimized skimmed-milk flocculation method. *Environ. Sci. Pollut. Res.* 25, 17025–17032. doi: 10.1007/s11356-018-1873-x

Atabakhsh, P., Kargar, M., and Doosti, A. (2021). Detection and evaluation of rotavirus surveillance methods as viral indicator in the aquatic environments. *Braz. J. Microbiol.* 52, 811–820. doi: 10.1007/s42770-020-00417-8

Azhdar, Z., Ghaderi, M., and Mousavi-Nasab, S. D. (2019). Optimization of RT-qPCR for detection of Aichi virus in sewage and river water samples in Karaj, Iran. *Arch. Iran. Med.* 22, 242–246.

Baggen, J., Thibaut, H. J., Strating, J. R., and van Kuppeveld, F. J. (2018). The life cycle of non-polio enteroviruses and how to target it. *Nat. Rev. Microbiol.* 16, 368–381. doi: 10.1038/s41579-018-0005-4

Bai, Y., Yao, L., Wei, T., Tian, F., Jin, D. Y., Chen, L., et al. (2020). Presumed asymptomatic carrier transmission of COVID-19. *JAMA* 323, 1406–1407. doi: 10.1001/jama.2020.2565

Bányai, K., Estes, M. K., Martella, V., and Parashar, U. D. (2018). Viral gastroenteritis. *Lancet* 392, 175–186. doi: 10.1016/S0140-6736(18)31128-0

Benko, M., Élo, P., Ursu, K., Ahne, W., LaPatra, S. E., Thomson, D., et al. (2002). First molecular evidence for the existence of distinct fish and snake adenoviruses. *J. Virol.* 76, 10056–10059. doi: 10.1128/JVI.76.19.10056-10059.2002

Berchenko, Y., Manor, Y., Freedman, L. S., Kaliner, E., Grotto, I., Mendelson, E., et al. (2017). Estimation of polio infection prevalence from environmental surveillance data. *Sci. Transl. Med.* 9, 1–8. doi: 10.1126/scitranslmed.aaf6786

Bergallo, M., Galliano, I., Montanari, P., Rassu, M., and Daprà, V. (2017). Aichivirus in children with diarrhea in northern Italy. *Intervirology* 60, 196–200. doi: 10.1159/000487051

Bertrand, I., Schijven, J., Sánchez, G., Wyn-Jones, P., Ottoson, J., Morin, T., et al. (2012). The impact of temperature on the inactivation of enteric viruses in food and water: a review. *J. Appl. Microbiol.* 112, 1059–1074. doi: 10.1111/j.1365-2672.2012.05267.x

Betancourt, W. Q., and Gerba, C. P. (2016). Rethinking the significance of reovirus in water and wastewater. *Food Environ. Virol.* 8, 161–173. doi: 10.1007/s12560-016-9250-8

Beyer, S., Szewzyk, R., Gnirss, R., Johne, R., and Selinka, H. C. (2020). Detection and characterization of hepatitis E virus genotype 3 in wastewater and urban surface waters in Germany. *Food Environ. Virol.* 12, 137–147. doi: 10.1007/s12560-020-09424-2

Bofill-Mas, S., Albinana-Gimenez, N., Clemente-Casares, P., Hundesa, A., Rodriguez-Manzano, J., Allard, A., et al. (2006). Quantification and stability of human adenoviruses and polyomavirus JCPyV in wastewater matrices. *Appl. Environ. Microbiol.* 72, 7894–7896. doi: 10.1128/AEM.00965-06

Boonchan, M., Motomura, K., Inoue, K., Ode, H., Chu, P. Y., Lin, M., et al. (2017). Distribution of norovirus genotypes and subtypes in river water by ultra-deep sequencing-based analysis. *Lett. Appl. Microbiol.* 65, 98–104. doi: 10.1111/lam.12750

Bortagaray, V., Girardi, V., Pou, S., Lizasoain, A., Tort, L. F. L., Spilki, F. R., et al. (2020). Detection, quantification, and microbial risk assessment of group A rotavirus in rivers from Uruguay. *Food Environ. Virol.* 12, 89–98. doi: 10.1007/s12560-019-09416-x

Bosch, A. (1998). Human enteric viruses in the water environment: a minireview. *Int. Microbiol.* 1, 191–196.

Bouseettine, R., Hassou, N., Bessi, H., and Ennaji, M. M. (2020). "Waterborne transmission of enteric viruses and their impact on public health" in *Emerging and Reemerging Viral Pathogens*. ed. M. M. Ennaji (London: Elsevier), 907–932.

Cacciò, S., and Chalmers, R. (2016). Human cryptosporidiosis in Europe. *Clin. Microbiol. Infect.* 22, 471–480. doi: 10.1016/j.cmi.2016.04.021

Carol, M., Guadalupe-Fernández, V., Rius, C., Soldevila, N., Razquin, E., Guix, S., et al. (2021). A waterborne gastroenteritis outbreak caused by a GII Norovirus in a holiday camp in Catalonia (Spain), 2017. *Viruses* 13:1792. doi: 10.3390/v13091792

Cascella, M., Rajnik, M., Aleem, A., Dulebohn, S. C., and Di Napoli, R. (2022). *Features, Evaluation, and Treatment of Coronavirus (COVID-19),* United States: Statpearls Publishing.

Cassidy, H., Poelman, R., Knoester, M., Leer-Buter, V., Coretta, C., and Niesters, H. G. (2018). Enterovirus D68–the new polio? *Front. Microbiol.* 9:2677. doi: 10.3389/fmicb.2018.02677

Castiglioni, S., Zuccato, E., Crisci, E., Chiabrando, C., Fanelli, R., and Bagnati, R. (2006). Identification and measurement of illicit drugs and their metabolites in urban wastewater by liquid chromatography-tandem mass spectrometry. *Anal. Chem.* 78, 8421–8429. doi: 10.1021/ac061095b

Chan, M. C., Hu, Y., Chen, H., Podkolzin, A. T., Zaytseva, E. V., Komano, J., et al. (2017). Global spread of norovirus GII. 17 Kawasaki 308, 2014–2016. *Emerg. Infect. Dis.* 23, 1359–1364. doi: 10.3201/eid2308.161138

Chan, M. C., Lee, N., Hung, T. N., Kwok, K., Cheung, K., Tin, E. K., et al. (2015). Rapid emergence and predominance of a broadly recognizing and fast-evolving norovirus GII. 17 variant in late 2014. Nature. *Communications* 6, 1–9. doi: 10.1038/ncomms10061

Charles, K. J., Souter, F. C., Baker, D. L., Davies, C. M., Schijven, J. F., Roser, D. J., et al. (2008). Fate and transport of viruses during sewage treatment in a mound system. *Water Res.* 42, 3047–3056. doi: 10.1016/j.watres.2008.02.032

Chen, L., Deng, Y., Dong, S., Wang, H., Li, P., Zhang, H., et al. (2021). The occurrence and control of waterborne viruses in drinking water treatment: a review. *Chemosphere* 281:130728. doi: 10.1016/j.chemosphere.2021.130728

Chen, B. S., Lee, H. C., Lee, K. M., Gong, Y. N., and Shih, S. R. (2020). Enterovirus and encephalitis. *Front. Microbiol.* 11:261. doi: 10.3389/fmicb.2020.00261

Chitambar, S., Gopalkrishna, V., Chhabra, P., Patil, P., Verma, H., Lahon, A., et al. (2012). Diversity in the enteric viruses detected in outbreaks of gastroenteritis from Mumbai, Western India. *Int. J. Environ. Res. Public Health* 9, 895–915. doi: 10.3390/ijerph9030895

Choi, P. M., Tscharke, B. J., Donner, E., O'Brien, J. W., Grant, S. C., Kaserzon, S. L., et al. (2018). Wastewater-based epidemiology biomarkers: past, present and future. *TrAC Trends Anal. Chem.* 105, 453–469. doi: 10.1016/j.trac.2018.06.004

Cholankeril, G., Podboy, A., Aivaliotis, V. I., Tarlow, B., Pham, E. A., Spencer, S. P., et al. (2020). High prevalence of concurrent gastrointestinal manifestations in patients with severe acute respiratory syndrome coronavirus 2: early experience from California. *Gastroenterology* 159, 775–777. doi: 10.1053/j.gastro.2020.04.008

Cioffi, B., Ianiro, G., Iaccarino, D., D'Apice, F., Ferraro, A., Race, M., et al. (2021). A potential risk assessment tool to monitor pathogens circulation in coastal waters. *Environ. Res.* 200:111748. doi: 10.1016/j.envres.2021.111748

Clemente, J. C., Ursell, L. K., Parfrey, L. W., and Knight, R. (2012). The impact of the gut microbiota on human health: an integrative view. *Cell* 148, 1258–1270. doi: 10.1016/j.cell.2012.01.035

Coccia, M. (2021). Pandemic prevention: lessons from COVID-19. *Encyclopedia* 1, 433–444. doi: 10.3390/encyclopedia1020036

Control and Prevention (2013). Prevention and control of seasonal influenza with vaccines. Recommendations of the advisory committee on immunization practices--United States, 2013-2014. *MMWR* 62, 1–43.

Cooksey, E. M., Singh, G., Scott, L. C., and Aw, T. G. (2019). Detection of coliphages and human adenoviruses in a subtropical estuarine lake. *Sci. Total Environ.* 649, 1514–1521. doi: 10.1016/j.scitotenv.2018.08.322

Cordey, S., Brito, F., Vu, D.-L., Turin, L., Kilowoko, M., Kyungu, E., et al. (2016). Astrovirus VA1 identified by next-generation sequencing in a nasopharyngeal specimen of a febrile Tanzanian child with acute respiratory disease of unknown etiology. *Emerg. Microb. Infect.* 5, 1–3. doi: 10.1038/emi.2016.67

Cortez, V., Meliopoulos, V. A., Karlsson, E. A., Hargest, V., Johnson, C., and Schultz-Cherry, S. (2017). Astrovirus biology and pathogenesis. *Ann. Rev. Virol.* 4, 327–348. doi: 10.1146/annurev-virology-101416-041742

Crenshaw, B. J., Jones, L. B., Bell, C. R., Kumar, S., and Matthews, Q. L. (2019). Perspective on adenoviruses: epidemiology, pathogenicity, and gene therapy. *Biomedicine* 7:61. doi: 10.3390/biomedicines7030061

Crittenden, J. C., Trussell, R. R., Hand, D. W., Howe, K. J., and Tchobanoglous, G. (2012). *MWH's Water Treatment: Principles and Design*. United States: John Wiley & Sons.

De Benedictis, P., Schultz-Cherry, S., Burnham, A., and Cattoli, G. (2011). Astrovirus infections in humans and animals–molecular biology, genetic diversity, and interspecies transmissions. *Infect. Genet. Evol.* 11, 1529–1544. doi: 10.1016/j.meegid.2011.07.024

de Graaf, M., van Beek, J., and Koopmans, M. P. (2016). Human norovirus transmission and evolution in a changing world. *Nat. Rev. Microbiol.* 14, 421–433. doi: 10.1038/nrmicro.2016.48

Denner, J. (2019). Hepatitis E virus (HEV)—The future. *Viruses* 11:251. doi: 10.3390/v11030251

Desselberger, U. (2014). Rotaviruses. *Virus Res.* 190, 75–96. doi: 10.1016/j.virusres.2014.06.016

Dias, J., Pinto, R. N., Vieira, C. B., and de Abreu Corrêa, A. (2018). Detection and quantification of human adenovirus (HAdV), JC polyomavirus (JCPyV) and hepatitis A virus (HAV) in recreational waters of Niterói, Rio de Janeiro, Brazil. *Mar. Pollut. Bull.* 133, 240–245. doi: 10.1016/j.marpolbul.2018.05.031

Donato, C., and Vijaykrishna, D. (2017). The broad host range and genetic diversity of mammalian and avian astroviruses. *Viruses* 9:102. doi: 10.3390/v9050102

Dongdem, J. T., Soyiri, I., and Ocloo, A. (2009). Public health significance of viral contamination of drinking water. *Afr. J. Microbiol. Res.* 3, 856–861. doi: 10.5897/AJMR.9000610

Elbashir, S., Parveen, S., Schwarz, J., Rippen, T., Jahncke, M., and DePaola, A. (2018). Seafood pathogens and information on antimicrobial resistance: a review. *Food Microbiol.* 70, 85–93. doi: 10.1016/j.fm.2017.09.011

Elmahdy, E. M., Ahmed, N. I., Shaheen, M. N., Mohamed, E. C. B., and Loutfy, S. A. (2019). Molecular detection of human adenovirus in urban wastewater in Egypt and among children suffering from acute gastroenteritis. *J. Water Health* 17, 287–294. doi: 10.2166/wh.2019.303

Elmahdy, E. M., Shaheen, M. N., Rizk, N. M., and Saad-Hussein, A. (2020). Quantitative detection of human adenovirus and human rotavirus group A in wastewater and el-Rahawy drainage canal influencing River Nile in the north of Giza, Egypt. *Food Environ. Virol.* 12, 218–225. doi: 10.1007/s12560-020-09429-x

Esona, M. D., Mijatovic-Rustempasic, S., Conrardy, C., Tong, S., Kuzmin, I. V., Agwanda, B., et al. (2010). Reassortant group A rotavirus from straw-colored fruit bat (Eidolon helvum). *Emerg. Infect. Dis.* 16, 1844–1852. doi: 10.3201/eid1612.101089

Farkas, K., Cooper, D. M., McDonald, J. E., Malham, S. K., de Rougemont, A., and Jones, D. L. (2018). Seasonal and spatial dynamics of enteric viruses in wastewater and in riverine and estuarine receiving waters. *Sci. Total Environ.* 634, 1174–1183. doi: 10.1016/j.scitotenv.2018.04.038

Farkas, K., Hillary, L. S., Malham, S. K., McDonald, J. E., and Jones, D. L. (2020a). Wastewater and public health: the potential of wastewater surveillance for monitoring COVID-19. *Curr. Opinion Environ. Sci. Health* 17, 14–20. doi: 10.1016/j.coesh.2020.06.001

Farkas, K., Walker, D. I., Adriaenssens, E. M., McDonald, J. E., Hillary, L. S., Malham, S. K., et al. (2020b). Viral indicators for tracking domestic wastewater contamination in the aquatic environment. *Water Res.* 181:115926. doi: 10.1016/j.watres.2020.115926

Fernandez-Cassi, X., Timoneda, N., Martínez-Puchol, S., Rusinol, M., Rodriguez-Manzano, J., Figuerola, N., et al. (2018). Metagenomics for the study of viruses in urban sewage as a tool for public health surveillance. *Sci. Total Environ.* 618, 870–880. doi: 10.1016/j.scitotenv.2017.08.249

Fongaro, G., Silva, H. D. D., Ibrahim, E. M. E., Schissi, C. D., Moreira, M., Lanna, M. C. D. S., et al. (2015). Enteric viruses as contaminants and bioindicators in environmental samples. *Virus Rev. Res.* 20, 1–20. doi: 10.17525/vrrjournal.v20i2.255

Forouzanfar, M. H., Afshin, A., Alexander, L. T., Anderson, H. R., Bhutta, Z. A., Biryukov, S., et al. (2016). Global, regional, and national comparative risk assessment of 79 behavioural, environmental and occupational, and metabolic risks or clusters of risks, 1990–2015: a systematic analysis for the global burden of disease study 2015. *Lancet* 388, 1659–1724. doi: 10.1016/S0140-6736(16)31679-8

Fu, Y., Tang, Z., Ye, Z., Mo, S., Tian, X., Ni, K., et al. (2019). Human adenovirus type 7 infection causes a more severe disease than type 3. *BMC Infect. Dis.* 19, 36–11. doi: 10.1186/s12879-018-3651-2

Gall, A. M., Mariñas, B. J., Lu, Y., and Shisler, J. L. (2015a). Waterborne viruses: a barrier to safe drinking water. *PLoS Pathog.* 11:e1004867. doi: 10.1371/journal.ppat.1004867

Gall, A. M., Shisler, J. L., and Mariñas, B. J. (2015b). Analysis of the viral replication cycle of adenovirus serotype 2 after inactivation by free chlorine. *Environ. Sci. Technol.* 49, 4584–4590. doi: 10.1021/acs.est.5b00301

Gao, F., Wang, Y. P., Mao, Q. Y., Yao, X., Liu, S., Li, F. X., et al. (2012). Enterovirus 71 viral capsid protein linear epitopes: identification and characterization. *Virol. J.* 9, 1–7. doi: 10.1186/1743-422X-9-26

Gersberg, R., Lyon, S., Brenner, R., and Elkins, B. (1988). Performance of a clay-alum flocculation (CCBA) process for virus removal from municipal wastewater. *Water Res.* 22, 1449–1454. doi: 10.1016/0043-1354(88)90103-0

Gibney, K. B., O'Toole, J., Sinclair, M., and Leder, K. (2017). Burden of disease attributed to waterborne transmission of selected enteric pathogens, Australia, 2010. *Am. J. Trop. Med. Hygiene* 96, 1400–1403. doi: 10.4269/ajtmh.16-0907

Gibson, K. E. (2014). Viral pathogens in water: occurrence, public health impact, and available control strategies. *Curr. Opin. Virol.* 4, 50–57. doi: 10.1016/j.coviro.2013.12.005

Girardi, V., Demoliner, M., Rigotto, C., Schneider, V. E., Paesi, S., and Spilki, F. R. (2018). Assessment of diversity of adenovirus DNA polymerase gene in recreational waters facilitated by ultracentrifugal concentration. *J. Water Health* 16, 102–111. doi: 10.2166/wh.2017.144

Goh, S. G., Saeidi, N., Gu, X., Vergara, G. G. R., Liang, L., Fang, H., et al. (2019). Occurrence of microbial indicators, pathogenic bacteria and viruses in tropical surface waters subject to contrasting land use. *Water Res.* 150, 200–215. doi: 10.1016/j.watres.2018.11.058

Gonzales-Gustavson, E., Rusiñol, M., Medema, G., Calvo, M., and Girones, R. (2019). Quantitative risk assessment of norovirus and adenovirus for the use of reclaimed water to irrigate lettuce in Catalonia. *Water Res.* 153, 91–99. doi: 10.1016/j.watres.2018.12.070

Guan, W. J., Ni, Z. Y., Hu, Y., Liang, W. H., Ou, C. Q., He, J. X., et al. (2020). Clinical characteristics of coronavirus disease 2019 in China. *N. Engl. J. Med.* 382, 1708–1720. doi: 10.1056/NEJMoa2002032

Habib, F. B., Rahman, M. M., Choudhury, R., Ahmed, N., Chowdhury, S., Tanni, N. N., et al. (2021). Relation between water source and Rotaviral infection: An observational study. *Archiv. Microbiol. Immunol.* 5, 353–361. doi: 10.26502/ami.93650068

Haramoto, E., and Kitajima, M. (2017). Quantification and genotyping of Aichi virus 1 in water samples in the Kathmandu Valley, Nepal. *Food Environ. Virol.* 9, 350–353. doi: 10.1007/s12560-017-9283-7

Haramoto, E., Kitajima, M., Hata, A., Torrey, J. R., Masago, Y., Sano, D., et al. (2018). A review on recent progress in the detection methods and prevalence of human enteric viruses in water. *Water Res.* 135, 168–186. doi: 10.1016/j.watres.2018.02.004

Haramoto, E., Malla, B., Thakali, O., and Kitajima, M. (2020). First environmental surveillance for the presence of SARS-CoV-2 RNA in wastewater and river water in Japan. *Sci. Total Environ.* 737:140405. doi: 10.1016/j.scitotenv.2020.140405

Hassou, N., Bouseettine, R., Abouchoaib, N., and Ennaji, M. M. (2020). "Enteric adenoviruses: emerging of a public health threat" in *Emerging and Reemerging Viral Pathogens*. ed. M. M. Ennaji (London: Elsevier), 879–905.

Hata, A., Hara-Yamamura, H., Meuchi, Y., Imai, S., and Honda, R. (2021). Detection of SARS-CoV-2 in wastewater in Japan during a COVID-19 outbreak. *Sci. Total Environ.* 758:143578. doi: 10.1016/j.scitotenv.2020.143578

Hata, A., Kitajima, M., Haramoto, E., Lee, S., Ihara, M., Gerba, C. P., et al. (2018). Next-generation amplicon sequencing identifies genetically diverse human astroviruses, including recombinant strains, in environmental waters. *Sci. Rep.* 8, 11837–11839. doi: 10.1038/s41598-018-30217-y

Health Canada (2019). Guidelines for Canadian Drinking Water Quality: Guideline Technical Document—Enteric Viruses. Water and Air Quality Bureau, Healthy Environments and Consumer Safety Branch, Health Canada, Ottawa, Ontario.

Hendriksen, R. S., Lukjancenko, O., Munk, P., Hjelmsø, M. H., Verani, J. R., Ng'eno, E., et al. (2019). Pathogen surveillance in the informal settlement, Kibera, Kenya, using a metagenomics approach. *PLoS One* 14:e0222531. doi: 10.1371/journal.pone.0222531

Hewitt, J., Greening, G. E., Leonard, M., and Lewis, G. D. (2013). Evaluation of human adenovirus and human polyomavirus as indicators of human sewage contamination in the aquatic environment. *Water Res.* 47, 6750–6761. doi: 10.1016/j.watres.2013.09.001

Hoa-Tran, T., Nakagomi, O., Dao, A., Nguyen, A., Agbemabiese, C., Vu, H., et al. (2017). Molecular epidemiology of noroviruses detected in Vietnamese children with acute gastroenteritis from 2012 to 2015. *J. Med. Microbiol.* 66, 34–45. doi: 10.1099/jmm.0.000417

Howley, P. M., and Lowy, D. (2007). "Papillomaviridae" in *Fields Virology*. eds. D. M. Knipe and P. M. Howley (Philadelphia: Lippincott Williams and Wilkins).

Hrudey, S. E., and Charrois, J. W. (2012). *Disinfection By-Products and Human Health*. United Kingdom: IWA publishing.

Hunter, P. (1997). *Waterborne Disease: Epidemiology and Ecology*. United States: John Wiley & Sons.

Iaconelli, M., Muscillo, M., Della Libera, S., Fratini, M., Meucci, L., De Ceglia, M., et al. (2017a). One-year surveillance of human enteric viruses in raw and treated wastewaters, downstream river waters, and drinking waters. *Food Environ. Virol.* 9, 79–88. doi: 10.1007/s12560-016-9263-3

Iaconelli, M., Purpari, G., Della Libera, S., Petricca, S., Guercio, A., Ciccaglione, A., et al. (2015). Hepatitis A and E viruses in wastewaters, in river waters, and in bivalve molluscs in Italy. *Food Environ. Virol.* 7, 316–324. doi: 10.1007/s12560-015-9207-3

Iaconelli, M., Valdazo-González, B., Equestre, M., Ciccaglione, A., Marcantonio, C., Della Libera, S., et al. (2017b). Molecular characterization of human adenoviruses in urban wastewaters using next generation and sanger sequencing. *Water Res.* 121, 240–247. doi: 10.1016/j.watres.2017.05.039

Ibrahim, C., Hammami, S., Mejri, S., Mehri, I., Pothier, P., and Hassen, A. (2017a). Detection of Aichi virus genotype B in two lines of wastewater treatment processes. *Microb. Pathog.* 109, 305–312. doi: 10.1016/j.micpath.2017.06.001

Ibrahim, C., Mehri, I., Hammami, S., Mejri, S., Hassen, A., and Pothier, P. (2017b). Removal of human astroviruses from hospital wastewater by two biological treatment methods: natural oxidizing lagoons and rotating biodisks. *Desalin. Water Treat.* 89, 287–296. doi: 10.5004/dwt.2017.21356

Ibrahim, Y., Ouda, M., Kadadou, D., Banat, F., Naddeo, V., Alsafar, H., et al. (2021). Detection and removal of waterborne enteric viruses from wastewater: a comprehensive review. *J. Environ. Chem. Eng.* 9:105613. doi: 10.1016/j.jece.2021.105613

Jahne, M. A., Brinkman, N. E., Keely, S. P., Zimmerman, B. D., Wheaton, E. A., and Garland, J. L. (2020). Droplet digital PCR quantification of norovirus and adenovirus in decentralized wastewater and graywater collections: implications for onsite reuse. *Water Res.* 169:115213. doi: 10.1016/j.watres.2019.115213

Janahi, E. M., Mustafa, S., Parkar, S. F., Naser, H. A., and Eisa, Z. M. (2020). Detection of enteric viruses and bacterial indicators in a sewage treatment center and shallow Water Bay. *Int. J. Environ. Res. Public Health* 17:6483. doi: 10.3390/ijerph17186483

Japhet, M., Famurewa, O., Adesina, O., Opaleye, O., Wang, B., Höhne, M., et al. (2019). Viral gastroenteritis among children of 0-5 years in Nigeria: characterization of the first Nigerian aichivirus, recombinant noroviruses and detection of a zoonotic astrovirus. *J. Clin. Virol.* 111, 4–11. doi: 10.1016/j.jcv.2018.12.004

Jiang, S., Noble, R., and Chu, W. (2001). Human adenoviruses and coliphages in urban runoff-impacted coastal waters of Southern California. *Appl. Environ. Microbiol.* 67, 179–184. doi: 10.1128/AEM.67.1.179-184.2001

Joshi, M. S., Lole, K. S., Barve, U. S., Salve, D. S., Ganorkar, N. N., Chavan, N. A., et al. (2019). Investigation of a large waterborne acute gastroenteritis outbreak caused by group B rotavirus in Maharashtra state, India. *J. Med. Virol.* 91, 1877–1881. doi: 10.1002/jmv.25523

Jothikumar, N., Cromeans, T., Sobsey, M., and Robertson, B. (2005). Development and evaluation of a broadly reactive TaqMan assay for rapid detection of hepatitis A virus. *Appl. Environ. Microbiol.* 71, 3359–3363. doi: 10.1128/AEM.71.6.3359-3363.2005

Kadri, S. M., Rehana, K., Benetou, D. R., Ahmad, D. F., Abdullah, A., and Chattu, V. K. (2018). Hepatitis A and E outbreak surveillance during 2015–2017 in Kashmir, India: is the water to blame? *J. Epidemiol. Global Health* 8, 203–207. doi: 10.2991/j.jegh.2018.04.101

Kaikkonen, S., Räsänen, S., Rämet, M., and Vesikari, T. (2010). Aichi virus infection in children with acute gastroenteritis in Finland. *Epidemiol. Infect.* 138, 1166–1171. doi: 10.1017/S0950268809991300

Karmakar, S., Rathore, A. S., Kadri, S. M., Dutt, S., Khare, S., and Lal, S. (2008). Post-earthquake outbreak of rotavirus gastroenteritis in Kashmir (India): An epidemiological analysis. *Public Health* 122, 981–989. doi: 10.1016/j.puhe.2008.01.006

Kauppinen, A., Pitkänen, T., Al-Hello, H., Maunula, L., Hokajärvi, A. M., Rimhanen-Finne, R., et al. (2019). Two drinking water outbreaks caused by wastewater intrusion including Sapovirus in Finland. *Int. J. Environ. Res. Public Health* 16:4376. doi: 10.3390/ijerph16224376

Kebe, O., Fernandez-Garcia, M. D., Fall, A., Dia, H., Bidalot, M., Ambert-Balay, K., et al. (2021). Prevalence and genetic diversity of Aichi virus 1 from urban wastewater in Senegal. *Intervirology* 64, 96–101. doi: 10.1159/000512130

Keller, R., Pratte-Santos, R., Scarpati, K., Martins, S. A., Loss, S. M., Fumian, T. M., et al. (2019). Surveillance of enteric viruses and thermotolerant coliforms in surface water and bivalves from a mangrove estuary in southeastern Brazil. *Food Environ. Virol.* 11, 288–296. doi: 10.1007/s12560-019-09391-3

Khanal, S., Ghimire, P., and Dhamoon, A. S. (2018). The repertoire of adenovirus in human disease: the innocuous to the deadly. *Biomedicine* 6:30. doi: 10.3390/biomedicines6010030

Khuroo, M., and Kamili, S. (2003). Aetiology, clinical course and outcome of sporadic acute viral hepatitis in pregnancy. *J. Viral Hepat.* 10, 61–69. doi: 10.1046/j.1365-2893.2003.00398.x

Kim, A. H., Hogarty, M. P., Harris, V. C., and Baldridge, M. T. (2021). The complex interactions between rotavirus and the gut microbiota. *Front. Cell. Infect. Microbiol.* 10:586751. doi: 10.3389/fcimb.2020.586751

Kitajima, M., and Gerba, C. P. (2015). Aichi virus 1: environmental occurrence and behavior. *Pathogens* 4, 256–268. doi: 10.3390/pathogens4020256

Kitajima, M., Iker, B. C., Pepper, I. L., and Gerba, C. P. (2014). Relative abundance and treatment reduction of viruses during wastewater treatment processes—identification of potential viral indicators. *Sci. Total Environ.* 488-489, 290–296. doi: 10.1016/j.scitotenv.2014.04.087

Kittigul, L., Rupprom, K., Che-arsae, M., Pombubpa, K., Thongprachum, A., Hayakawa, S., et al. (2019). Occurrence of noroviruses in recycled water and sewage sludge: emergence of recombinant norovirus strains. *J. Appl. Microbiol.* 126, 1290–1301. doi: 10.1111/jam.14201

Kiulia, N. M., Gonzalez, R., Thompson, H., Aw, T. G., and Rose, J. B. (2021). Quantification and trends of rotavirus and Enterovirus in untreated sewage using reverse transcription droplet digital PCR. *Food Environ. Virol.* 13, 154–169. doi: 10.1007/s12560-020-09455-9

Koopmans, M., von Bonsdorff, C. H., Vinjé, J., de Medici, D., and Monroe, S. (2002). Foodborne viruses. *FEMS Microbiol. Rev.* 26, 187–205. doi: 10.1111/j.1574-6976.2002.tb00610.x

Kosulin, K. (2019). Intestinal HAdV infection: tissue specificity, persistence, and implications for antiviral therapy. *Viruses* 11:804. doi: 10.3390/v11090804

Kumar, S., Ahlawat, W., Bhanjana, G., Heydarifard, S., Nazhad, M. M., and Dilbaghi, N. (2014). Nanotechnology-based water treatment strategies. *J. Nanosci. Nanotechnol.* 14, 1838–1858. doi: 10.1166/jnn.2014.9050

Kumar, S., Gupta, A. K., Maurya, A., and Singh, M. K. (2020). "Chemical treatment for removal of waterborne pathogens," in *Waterborne pathogens*. eds. M. N. Prasad and A. Grobelak (United Kingdom: Elsevier), 205–218.

Kumar, T., Shrivastava, A., Kumar, A., Laserson, K. F., Narain, J. P., Venkatesh, S., et al. (2015). Viral hepatitis surveillance—India, 2011–2013. *Morb. Mortal. Wkly Rep.* 64, 758–762. doi: 10.15585/mmwr.mm6428a3

La Rosa, G., Fontana, S., Di Grazia, A., Iaconelli, M., Pourshaban, M., and Muscillo, M. (2007). Molecular identification and genetic analysis of norovirus genogroups I and II in water environments: comparative analysis of different reverse transcription-PCR assays. *Appl. Environ. Microbiol.* 73, 4152–4161. doi: 10.1128/AEM.00222-07

La Rosa, G., Fratini, M., Della Libera, S., Iaconelli, M., and Muscillo, M. (2012). Emerging and potentially emerging viruses in water environments. *Ann. Ist. Super. Sanita* 48, 397–406. doi: 10.4415/ANN_12_04_07

La Rosa, G., Iaconelli, M., Mancini, P., Ferraro, G. B., Veneri, C., Bonadonna, L., et al. (2020). First detection of SARS-CoV-2 in untreated wastewaters in Italy. *Sci. Total Environ.* 736:139652. doi: 10.1016/j.scitotenv.2020.139652

La Rosa, G., Iaconelli, M., Pourshaban, M., and Muscillo, M. (2010a). Detection and molecular characterization of noroviruses from five sewage treatment plants in Central Italy. *Water Res.* 44, 1777–1784. doi: 10.1016/j.watres.2009.11.055

La Rosa, G., Pourshaban, M., Iaconelli, M., and Muscillo, M. (2008). Recreational and drinking waters as a source of norovirus gastroenteritis outbreaks: a review and update. *Environ. Biotechnol.* 1, 15–22. doi: 10.1007/s12560-008-9002-5

La Rosa, G., Pourshaban, M., Iaconelli, M., and Muscillo, M. (2010b). Quantitative real-time PCR of enteric viruses in influent and effluent samples from wastewater treatment plants in Italy. *Ann. Ist. Super. Sanita* 46, 266–273. doi: 10.4415/ANN_10_03_07

La Rosa, G., Proroga, Y., De Medici, D., Capuano, F., Iaconelli, M., Della Libera, S., et al. (2018). First detection of hepatitis E virus in shellfish and in seawater from production areas in southern Italy. *Food Environ. Virol.* 10, 127–131. doi: 10.1007/s12560-017-9319-z

Laconi, A., Cavicchio, L., Tassoni, L., Cunial, G., Milani, A., Ustulin, M., et al. (2020). Identification of two divergent swine Noroviruses detected at the slaughterhouse in north East Italy. *Porcine Health Manag.* 6, 9–6. doi: 10.1186/s40813-020-00147-1

Lai, C. C., Liu, Y. H., Wang, C. Y., Wang, Y. H., Hsueh, S. C., Yen, M. Y., et al. (2020). Asymptomatic carrier state, acute respiratory disease, and pneumonia due to severe acute respiratory syndrome coronavirus 2 (SARS-CoV-2): facts and myths. *J. Microbiol. Immunol. Infect.* 53, 404–412. doi: 10.1016/j.jmii.2020.02.012

Lázaro, G. R., Mukhopadhyay, S., and Hagan, M. F. (2018). Why enveloped viruses need cores—the contribution of a nucleocapsid core to viral budding. *Biophys. J.* 114, 619–630. doi: 10.1016/j.bpj.2017.11.3782

Lee, H. F., and Chi, C. S. (2014). Enterovirus 71 infection–associated acute flaccid paralysis: a case series of long-term neurologic follow-up. *J. Child Neurol.* 29, 1283–1290. doi: 10.1177/0883073813516193

Leite, J. P. G., Carvalho-Costa, F. A., and Linhares, A. C. (2008). Group A rotavirus genotypes and the ongoing Brazilian experience: a review. *Mem. Inst. Oswaldo Cruz* 103, 745–753. doi: 10.1590/S0074-02762008000800001

Lemon, S. M., Ott, J. J., Van Damme, P., and Shouval, D. (2018). Type A viral hepatitis: A summary and update on the molecular virology, epidemiology, pathogenesis and prevention. *J. Hepatol.* 68, 167–184. doi: 10.1016/j.jhep.2017.08.034

Li, L. L., Liu, N., Yu, J. M., Ao, Y. Y., Li, S., Stine, O. C., et al. (2017). Analysis of Aichi virus and Saffold virus association with pediatric acute gastroenteritis. *J. Clin. Virol.* 87, 37–42. doi: 10.1016/j.jcv.2016.12.003

Liu, R., Ma, Q., Han, H., Su, H., Liu, F., Wu, K., et al. (2020). The value of urine biochemical parameters in the prediction of the severity of coronavirus disease 2019. *Clin. Chem. Lab. Med.* 58, 1121–1124. doi: 10.1515/cclm-2020-0220

Lizasoain, A., Burlandy, F. M., Victoria, M., Tort, L. F. L., da Silva, E. E., and Colina, R. (2018). An environmental surveillance in Uruguay reveals the presence of highly divergent types of human enterovirus species C and a high frequency of species a and B types. *Food Environ. Virol.* 10, 343–352. doi: 10.1007/s12560-018-9351-7

Lodder, W. J., Rutjes, S. A., Takumi, K., and de Roda Husman, A. M. (2013). Aichi virus in sewage and surface water, the Netherlands. *Emerg. Infect. Dis.* 19, 1222–1230. doi: 10.3201/eid1908.130312

Lu, J., Sun, L., Fang, L., Yang, F., Mo, Y., Lao, J., et al. (2015). Gastroenteritis outbreaks caused by norovirus GII. 17, Guangdong Province, China, 2014–2015. *Emerg. Infect. Dis.* 21, 1240–1242. doi: 10.3201/eid2107.150226

Lu, R., Zhao, X., Li, J., Niu, P., Yang, B., Wu, H., et al. (2020). Genomic characterisation and epidemiology of 2019 novel coronavirus: implications for virus origins and receptor binding. *Lancet* 395, 565–574. doi: 10.1016/S0140-6736(20)30251-8

Lugo, D., and Krogstad, P. (2016). Enteroviruses in the early 21st century: new manifestations and challenges. *Curr. Opin. Pediatr.* 28, 107–113. doi: 10.1097/MOP.0000000000000303

Magana-Arachchi, D., and Wanigatunge, R. (2020). "Ubiquitous waterborne pathogens" in *Waterborne Pathogens*. eds. M. N. Prasad and A. Grobelak (United Kingdom: Elsevier), 15–42.

Malla, B., Ghaju Shrestha, R., Tandukar, S., Bhandari, D., Thakali, O., Sherchand, J. B., et al. (2019). Detection of pathogenic viruses, pathogen indicators, and fecal-source markers within tanker water and their sources in the Kathmandu Valley, Nepal. *Pathogens* 8:81. doi: 10.3390/pathogens8020081

Mancosu, N., Snyder, R. L., Kyriakakis, G., and Spano, D. (2015). Water scarcity and future challenges for food production. *WaterSA* 7, 975–992. doi: 10.3390/w7030975

Mans, J., Armah, G. E., Steele, A. D., and Taylor, M. B. (2016). Norovirus epidemiology in Africa: a review. *PLoS One* 11:e0146280. doi: 10.1371/journal.pone.0146280

Mao, K., Zhang, K., Du, W., Ali, W., Feng, X., and Zhang, H. (2020). The potential of wastewater-based epidemiology as surveillance and early warning of infectious disease outbreaks. *Curr. Opinion Environ. Sci. Health* 17, 1–7. doi: 10.1016/j.coesh.2020.04.006

Marek, A., Bilic, I., Prokofieva, I., and Hess, M. (2010). Phylogenetic analysis of avian hepatitis E virus samples from European and Australian chicken flocks supports the existence of a different genus within the Hepeviridae comprising at least three different genotypes. *Vet. Microbiol.* 145, 54–61. doi: 10.1016/j.vetmic.2010.03.014

Marie, V., and Lin, J. (2017). Viruses in the environment–presence and diversity of bacteriophage and enteric virus populations in the Umhlangane River, Durban, South Africa. *J. Water Health* 15, 966–981. doi: 10.2166/wh.2017.066

Masachessi, G., Pisano, M. B., Prez, V. E., Martínez, L., Michelena, J., Martínez-Wassaf, M., et al. (2018). Enteric viruses in surface waters from Argentina: molecular and viable-virus detection. *Appl. Environ. Microbiol.* 84, e02327–e02317. doi: 10.1128/AEM.02327-17

Matthews, J., Dickey, B., Miller, R., Felzer, J., Dawson, B., Lee, A., et al. (2012). The epidemiology of published norovirus outbreaks: a review of risk factors associated with attack rate and genogroup. *Epidemiol. Infect.* 140, 1161–1172. doi: 10.1017/S0950268812000234

Maunula, L., Klemola, P., Kauppinen, A., Söderberg, K., Nguyen, T., Pitkänen, T., et al. (2009). Enteric viruses in a large waterborne outbreak of acute gastroenteritis in Finland. *Food Environ. Virol.* 1, 31–36. doi: 10.1007/s12560-008-9004-3

McCall, C., Wu, H., Miyani, B., and Xagoraraki, I. (2020). Identification of multiple potential viral diseases in a large urban center using wastewater surveillance. *Water Res.* 184:116160. doi: 10.1016/j.watres.2020.116160

McKnight, K. L., and Lemon, S. M. (2018). Hepatitis A virus genome organization and replication strategy. *Cold Spring Harb. Perspect. Med.* 8:a033480. doi: 10.1101/cshperspect.a033480

Medema, G., Heijnen, L., Elsinga, G., Italiaander, R., and Brouwer, A. (2020). Presence of SARS-Coronavirus-2 RNA in sewage and correlation with reported COVID-19 prevalence in the early stage of the epidemic in the Netherlands. *Environ. Sci. Technol. Lett.* 7, 511–516. doi: 10.1021/acs.estlett.0c00357

Mehta, P., and Reddivari, A. K. R. (2021). Hepatitis. StatPearls [Internet].

Meixell, B. W., Borchardt, M. A., and Spencer, S. K. (2013). Accumulation and inactivation of avian inluenza virus by filter-feeding invertebrate Daphnia magna. *Appl. Environ. Microbiol.* 79, 7249–7255. doi: 10.1128/AEM.02439-13

Mena, K. D., and Gerba, C. P. (2008). Waterborne adenovirus. *Rev. Environ. Contam. Toxicol.* 133-167. doi: 10.1007/978-0-387-09647-6_4

Menezes, P. Q., Silva, T. T., Simas, F. B., Brauner, R. K., Bandarra, P., Demoliner, M., et al. (2020). Molecular detection of human adenovirus and rotavirus in Faeces of white-eared opossums. *EcoHealth* 17, 326–332. doi: 10.1007/s10393-020-01497-6

Mennechet, F. J., Paris, O., Ouoba, A. R., Salazar Arenas, S., Sirima, S. B., Takoudjou Dzomo, G. R., et al. (2019). A review of 65 years of human adenovirus seroprevalence. *Expert Rev. Vaccines* 18, 597–613. doi: 10.1080/14760584.2019.1588113

Meqdam, M. M., and Thwiny, I. R. (2007). Prevalence of group a rotavirus, enteric adenovirus, norovirus and astrovirus infections among children with acute gastroenteritis in Al-Qassim, Saudi Arabia. *Pakistan J. Med. Sci.* 23:551.

Miao, J., Guo, X., Liu, W., Yang, D., Shen, Z., Qiu, Z., et al. (2018). Total coliforms as an indicator of human enterovirus presence in surface water across Tianjin city. *BMC Infect. Dis.* 18, 1–9. doi: 10.1186/s12879-018-3438-5

Miura, T., Gima, A., and Akiba, M. (2019). Detection of norovirus and rotavirus present in suspended and dissolved forms in drinking water sources. *Food Environ. Virol.* 11, 9–19. doi: 10.1007/s12560-018-9361-5

Moazeni, M., Nikaeen, M., Hadi, M., Moghim, S., Mouhebat, L., Hatamzadeh, M., et al. (2017). Estimation of health risks caused by exposure to enteroviruses from agricultural application of wastewater effluents. *Water Res.* 125, 104–113. doi: 10.1016/j.watres.2017.08.028

Moreira, N. A., and Bondelind, M. (2017). Safe drinking water and waterborne outbreaks. *J. Water Health* 15, 83–96. doi: 10.2166/wh.2016.103

Moreno, S., Alvarado, M. V., Bermúdez, A., and Gutiérrez, M. F. (2009). DNA sequence analysis indicates human origin of rotavirus and hepatitis A virus strains from western Colombia. *Biomedica* 29, 209–217. doi: 10.7705/biomedica.v29i2.23

Mukhopadhya, I., Sarkar, R., Menon, V. K., Babji, S., Paul, A., Rajendran, P., et al. (2013). Rotavirus shedding in symptomatic and asymptomatic children using reverse transcription-quantitative PCR. *J. Med. Virol.* 85, 1661–1668. doi: 10.1002/jmv.23641

Murphy, H. M., Prioleau, M. D., Borchardt, M. A., and Hynds, P. D. (2017). Review: epidemiological evidence of groundwater contribution to global enteric disease, 1948–2015. *Hydrogeol. J.* 25, 981–1001. doi: 10.1007/s10040-017-1543-y

Murray, C., and Newby, H. (2012). Data resource profile: United Nations children's fund (UNICEF). *Int. J. Epidemiol.* 41, 1595–1601. doi: 10.1093/ije/dys185

Naik, S., Aggarwal, R., Salunke, P., and Mehrotra, N. (1992). A large waterborne viral hepatitis E epidemic in Kanpur, India. *Bull. World Health Organ.* 70, 597–604. PMID: 1464145

Nasiri, M., Ghalejoogh, Z. Y., Ataei-Pirkooh, A., Bokharaei-Salim, F., Monavari, S. H., Tavakoli, A., et al. (2021). Detection and phylogenetic analysis of hepatitis A virus in the wastewater treatment Plant of Ekbatan Town in Tehran, Iran. *Hepat. Mon.* 21:121270. doi: 10.5812/hepatmon.121270

Nimgaonkar, I., Ding, Q., Schwartz, R. E., and Ploss, A. (2018). Hepatitis E virus: advances and challenges. *Nat. Rev. Gastroenterol. Hepatol.* 15, 96–110. doi: 10.1038/nrgastro.2017.150

Nour, I., Hanif, A., Zakri, A. M., Al-Ashkar, I., Alhetheel, A., and Eifan, S. (2021). Human adenovirus molecular characterization in various water environments and seasonal impacts in Riyadh, Saudi Arabia. *Int. J. Environ. Res. Public Health* 18:4773. doi: 10.3390/ijerph18094773

Oh, D. Y., Silva, P., Hauroeder, B., Diedrich, S., Cardoso, D., and Schreier, E. (2006). Molecular characterization of the first Aichi viruses isolated in Europe and in South America. *Arch. Virol.* 151, 1199–1206. doi: 10.1007/s00705-005-0706-7

Okada, A., Kobayashi, S., and Inoshima, Y. (2019). Detection frequency of porcine noroviruses in healthy pigs in Japan. *Jpn. Agric. Res. Q.* 53, 305–310. doi: 10.6090/jarq.53.305

Okoh, A. I., Sibanda, T., and Gusha, S. S. (2010). Inadequately treated wastewater as a source of human enteric viruses in the environment. *Int. J. Environ. Res. Public Health* 7, 2620–2637. doi: 10.3390/ijerph7062620

Onosi, O., Upfold, N. S., Jukes, M. D., Luke, G. A., and Knox, C. (2019). The first molecular detection of Aichi virus 1 in raw sewage and mussels collected in South Africa. *Food Environ. Virol.* 11, 96–100. doi: 10.1007/s12560-018-9362-4

Opere, W. M. (2019). *Detection of Pathogenic Human Adenoviruses in water Samples Collected from Lake Victoria along Homa Bay Town*, Homa Bay Country: Kenya Kenyatta University

Opere, W. M., John, M., and Ombori, O. (2021). Molecular detection of human enteric adenoviruses in water samples collected from Lake Victoria waters Along Homa Bay town, Homa Bay County, Kenya. *Food Environ. Virol.* 13, 32–43. doi: 10.1007/s12560-020-09444-y

Oppong, T., Yang, H., Amponsem-Boateng, C., Kyere, E. D., Abdulai, T., Duan, G., et al. (2020). Enteric pathogens associated with gastroenteritis among children under 5 years in sub-Saharan Africa: a systematic review and meta-analysis. *Epidemiol. Infect.* 148:e64. doi: 10.1017/S0950268820000618

Osuolale, O., and Okoh, A. (2015). Incidence of human adenoviruses and hepatitis A virus in the final effluent of selected wastewater treatment plants in eastern Cape Province, South Africa. *Virol. J.* 12, 1–8. doi: 10.1186/s12985-015-0327-z

Osuolale, O., and Okoh, A. (2016). Human enteric bacteria and viruses in five wastewater treatment plants in the eastern cape, South Africa. *J. Infect. Public Health* 10, 541–547. doi: 10.1016/j.jiph.2016.11.012

Pan, Y., Zhang, D., Yang, P., Poon, L. L., and Wang, Q. (2020). Viral load of SARS-CoV-2 in clinical samples. *Lancet Infect. Dis.* 20, 411–412. doi: 10.1016/S1473-3099(20)30113-4

Pang, X., Qiu, Y., Gao, T., Zurawell, R., Neumann, N. F., Craik, S., et al. (2019). Prevalence, levels and seasonal variations of human enteric viruses in six major rivers in Alberta, Canada. *Water Res.* 153, 349–356. doi: 10.1016/j.watres.2019.01.034

Petrignani, M., Verhoef, L., de Graaf, M., Richardus, J. H., and Koopmans, M. (2018). Chronic sequelae and severe complications of norovirus infection: a systematic review of literature. *J. Clin. Virol.* 105, 1–10. doi: 10.1016/j.jcv.2018.05.004

Pillay, L., Amoah, I. D., Deepnarain, N., Pillay, K., Awolusi, O. O., Kumari, S., et al. (2021). Monitoring changes in COVID-19 infection using wastewater-based epidemiology: a south African perspective. *Sci. Total Environ.* 786:147273. doi: 10.1016/j.scitotenv.2021.147273

Pooi, C. K., and Ng, H. Y. (2018). Review of low-cost point-of-use water treatment systems for developing communities. *NPJ Clean Water* 1:11. doi: 10.1038/s41545-018-0011-0

Pöyry, T., Stenvik, M., and Hovi, T. (1988). Viruses in sewage waters during and after a poliomyelitis outbreak and subsequent nationwide oral poliovirus vaccination campaign in Finland. *Appl. Environ. Microbiol.* 54, 371–374. doi: 10.1128/aem.54.2.371-374.1988

Prado, T., de Castro Bruni, A., Barbosa, M. R. F., Garcia, S. C., Moreno, L. Z., and Sato, M. I. Z. (2019). Noroviruses in raw sewage, secondary effluents and reclaimed water produced by sand-anthracite filters and membrane bioreactor/reverse osmosis system. *Sci. Total Environ.* 646, 427–437. doi: 10.1016/j.scitotenv.2018.07.301

Prata, C., Ribeiro, A., Cunha, Â., Gomes, N. C., and Almeida, A. (2012). Ultracentrifugation as a direct method to concentrate viruses in environmental waters: virus-like particle enumeration as a new approach to determine -the efficiency of recovery. *J. Environ. Monit.* 14, 64–70. doi: 10.1039/C1EM10603A

Prez, V. E., Gil, P. I., Temprana, C. F., Cuadrado, P. R., Martinez, L. C., Giordano, M. O., et al. (2015). Quantification of human infection risk caused by rotavirus in surface waters from Cordoba, Argentina. *Sci. Total Environ.* 538, 220–229. doi: 10.1016/j.scitotenv.2015.08.041

Prez, V. E., Poma, H. R., Giordano, G. G., Victoria, M., Nates, S. V., Rajal, V. B., et al. (2020). Rotavirus contamination of surface waters from the northwest of Argentina. *J. Water Health* 18, 409–415. doi: 10.2166/wh.2020.005

Puenpa, J., Wanlapakorn, N., Vongpunsawad, S., and Poovorawan, Y. (2019). The history of enterovirus A71 outbreaks and molecular epidemiology in the Asia-Pacific region. *J. Biomed. Sci.* 26, 75–11. doi: 10.1186/s12929-019-0573-2

Purdy, M. A., Harrison, T. J., Jameel, S., Meng, X. J., Okamoto, H., Van der Poel, W., et al. (2017). ICTV virus taxonomy profile: Hepeviridae. *J. Gen. Virol.* 98, 2645–2646. doi: 10.1099/jgv.0.000940

Purpari, G., Macaluso, G., Di Bella, S., Gucciardi, F., Mira, F., Di Marco, P., et al. (2019). Molecular characterization of human enteric viruses in food, water samples, and surface swabs in Sicily. *Int. J. Infect. Dis.* 80, 66–72. doi: 10.1016/j.ijid.2018.12.011

Qu, G., Li, X., Hu, L., and Jiang, G. (2020). An imperative need for research on the role of environmental factors in transmission of novel coronavirus (COVID-19). *Environ. Sci. Technol.* 54, 3730–3732. doi: 10.1021/acs.est.0c01102

Quintão, T. S. C., Silva, F. G., Pereira, A. L., Araújo, W. N., Oliveira, P. M., Souza, M. B. L. D., et al. (2021). Detection and molecular characterization of enteric adenovirus in treated wastewater in the Brazilian Federal District. *SN Appl. Sci.* 3, 1–11. doi: 10.1007/s42452-021-04678-2

Radin, D. (2014). New trends in food-and waterborne viral outbreaks. *Arch. Biol. Sci.* 66, 1–9. doi: 10.2298/ABS1401001R

Raji, Y. E., Toung, O. P., Taib, N. M., and Sekawi, Z. B. (2021). Hepatitis E virus: An emerging enigmatic and underestimated pathogen. *Saudi J. Biol. Sci.* 29, 499–512. doi: 10.1016/j.sjbs.2021.09.003

Randazzo, W., Truchado, P., Cuevas-Ferrando, E., Simón, P., Allende, A., and Sánchez, G. (2020). SARS-CoV-2 RNA in wastewater anticipated COVID-19 occurrence in a low prevalence area. *Water Res.* 181:115942. doi: 10.1016/j.watres.2020.115942

Rani, M., Rajyalakshmi, S., Pakalapaty, S., and Kammilli, N. (2021). "Norovirus structure and classification" in *Norovirus*, vol. 31

Räsänen, S., Lappalainen, S., Kaikkonen, S., Hämäläinen, M., Salminen, M., and Vesikari, T. (2010). Mixed viral infections causing acute gastroenteritis in children in a waterborne outbreak. *Epidemiol. Infect.* 138, 1227–1234. doi: 10.1017/S0950268809991671

Remes-Troche, J. M., Ramos-de-la-Medina, A., Manríquez-Reyes, M., Martínez-Pérez-Maldonado, L., Lara, E. L., and Solís-González, M. A. (2020). Initial gastrointestinal manifestations in patients with severe acute respiratory syndrome coronavirus 2 infection in 112 patients from Veracruz in southeastern Mexico. *Gastroenterology* 159, 1179–1181. doi: 10.1053/j.gastro.2020.05.055

Reynolds, K. A., Mena, K. D., and Gerba, C. P. (2008). Risk of waterborne illness via drinking water in the United States. *Rev. Environ. Contam. Toxicol.* 192, 117–158. doi: 10.1007/978-0-387-71724-1_4

Rezaeinejad, S., Vergara, G., Woo, C., Lim, T., Sobsey, M., and Gin, K. (2014). Surveillance of enteric viruses and coliphages in a tropical urban catchment. *Water Res.* 58, 122–131. doi: 10.1016/j.watres.2014.03.051

Richardson, S. D., and Postigo, C. (2011). "Drinking water disinfection by-products" in *Emerging Organic Contaminants and Human Health*. ed. D. Barcelo (Berlin, Heidelberg: Springer), 93–137.

Rimoldi, S. G., Stefani, F., Gigantiello, A., Polesello, S., Comandatore, F., Mileto, D., et al. (2020). Presence and infectivity of SARS-CoV-2 virus in wastewaters and rivers. *Sci. Total Environ.* 744:140911. doi: 10.1016/j.scitotenv.2020.140911

Rivadulla, E., and Romalde, J. L. (2020). A comprehensive review on human Aichi virus. *Virol. Sin.* 35, 501–516. doi: 10.1007/s12250-020-00222-5

Rodriguez-Lazaro, D., Cook, N., Ruggeri, F. M., Sellwood, J., Nasser, A., Nascimento, M. S. J., et al. (2012). Virus hazards from food, water and other contaminated environments. *FEMS Microbiol. Rev.* 36, 786–814. doi: 10.1111/j.1574-6976.2011.00306.x

Rosario-Ortiz, F., Rose, J., Speight, V., Von Gunten, U., and Schnoor, J. (2016). How do you like your tap water? *Science* 351, 912–914. doi: 10.1126/science.aaf0953

Rosiles-González, G., Ávila-Torres, G., Moreno-Valenzuela, O. A., Cháidez-Quiroz, C., Hernández-Flores, C. I., Acosta-González, G., et al. (2019). Norovirus and human adenovirus occurrence and diversity in recreational water in a karst aquifer in the Yucatan peninsula, Mexico. *J. Appl. Microbiol.* 127, 1255–1269. doi: 10.1111/jam.14385

Rothe, C., Schunk, M., Sothmann, P., Bretzel, G., Froeschl, G., Wallrauch, C., et al. (2020). Transmission of 2019-nCoV infection from an asymptomatic contact in Germany. *N. Engl. J. Med.* 382, 970–971. doi: 10.1056/NEJMc2001468

Ruggeri, F. M., Di Bartolo, I., Ponterio, E., Angeloni, G., Trevisani, M., and Ostanello, F. (2013). Zoonotic transmission of hepatitis E virus in industrialized countries. *New Microbiol.* 36, 331–344. PMID: 24177295

Russell, W. (2009). Adenoviruses: update on structure and function. *J. Gen. Virol.* 90, 1–20. doi: 10.1099/vir.0.003087-0

Salvador, D., Caeiro, M. F., Serejo, F., Nogueira, P., Carneiro, R. N., and Neto, C. (2020). Monitoring waterborne pathogens in surface and drinking waters. Are water treatment plants (WTPs) simultaneously efficient in the elimination of enteric viruses and fecal indicator bacteria (FIB)? *WaterSA* 12:2824. doi: 10.3390/w12102824

Sano, D., Amarasiri, M., Hata, A., Watanabe, T., and Katayama, H. (2016). Risk management of viral infectious diseases in wastewater reclamation and reuse. *Environ. Int.* 91, 220–229. doi: 10.1016/j.envint.2016.03.001

Santiso-Bellón, C., Randazzo, W., Pérez-Cataluña, A., Vila-Vicent, S., Gozalbo-Rovira, R., Muñoz, C., et al. (2020). Epidemiological surveillance of norovirus and rotavirus in sewage (2016–2017) in Valencia (Spain). *Microorganisms* 8:458. doi: 10.3390/microorganisms8030458

Saxena, G., Bharagava, R. N., Kaithwas, G., and Raj, A. (2015). Microbial indicators, pathogens and methods for their monitoring in water environment. *J. Water Health* 13, 319–339. doi: 10.2166/wh.2014.275

Sedji, M. I., Varbanov, M., Meo, M., Colin, M., Mathieu, L., and Bertrand, I. (2018). Quantification of human adenovirus and norovirus in river water in the north-east of France. *Environ. Sci. Pollut. Res.* 25, 30497–30507. doi: 10.1007/s11356-018-3045-4

Sekwadi, P., Ravhuhali, K., Mosam, A., Essel, V., Ntshoe, G., Shonhiwa, A., et al. (2018). Waterborne outbreak of gastroenteritis on the KwaZulu-natal coast, South Africa, december 2016/january 2017. *Epidemiol. Infect.* 146, 1318–1325. doi: 10.1017/S095026881800122X

Shaheen, M. N., El-Daim, A., Sahar, E., Ahmed, N. I., and Elmahdy, E. M. (2020). Environmental monitoring of Aichi virus and human bocavirus in samples from wastewater treatment plant, drain, and River Nile in Egypt. *J. Water Health* 18, 30–37. doi: 10.2166/wh.2019.075

Shaheen, M. N., Elmahdy, E. M., and Chawla-Sarkar, M. (2019). Quantitative PCR-based identification of enteric viruses contaminating fresh produce and surface water used for irrigation in Egypt. *Environ. Sci. Pollut. Res.* 26, 21619–21628. doi: 10.1007/s11356-019-05435-0

Shang, J., Wan, Y., Luo, C., Ye, G., Geng, Q., Auerbach, A., et al. (2020). Cell entry mechanisms of SARS-CoV-2. *Proc. Natl. Acad. Sci.* 117, 11727–11734. doi: 10.1073/pnas.2003138117

Sharma, D. K., Nalavade, U. P., and Deshpande, J. M. (2015). Real-time reverse transcription-polymerase chain reaction assays for identification of wild poliovirus 1 & 3. *Indian J. Med. Res.* 142, 471–478. doi: 10.4103/0971-5916.169216

Sharma, V. K., Zboril, R., and McDonald, T. J. (2014). Formation and toxicity of brominated disinfection byproducts during chlorination and chloramination of water: a review. *J. Environ. Sci. Health B* 49, 212–228. doi: 10.1080/03601234.2014.858576

Shen, Q., Zhang, W., Yang, S., Yang, Z., Chen, Y., Cui, L., et al. (2012). Recombinant porcine norovirus identified from piglet with diarrhea. *BMC Vet. Res.* 8:155. doi: 10.1186/1746-6148-8-155

Sherchan, S. P., Shahin, S., Ward, L. M., Tandukar, S., Aw, T. G., Schmitz, B., et al. (2020). First detection of SARS-CoV-2 RNA in wastewater in North America: a study in Louisiana, USA. *Sci. Total Environ.* 743:140621. doi: 10.1016/j.scitotenv.2020.140621

Shih, Y. J., Tao, C. W., Tsai, H. C., Huang, W. C., Huang, T. Y., Chen, J. S., et al. (2017). First detection of enteric adenoviruses genotype 41 in recreation spring areas of Taiwan. *Environ. Sci. Pollut. Res.* 24, 18392–18399. doi: 10.1007/s11356-017-9513-4

Shonhiwa, A. M., Ntshoe, G., Crisp, N., Olowolagba, A. J., Mbuthu, V., Taylor, M. B., et al. (2020). Investigation of two suspected diarrhoeal-illness outbreaks in northern cape and KwaZulu-Natal provinces, South Africa, April–July 2013: The role of rotavirus. *South. Afr. J. Infect. Dis.* 35, 159. doi: 10.4102/sajid.v35i1.159

Sibanda, T., and Okoh, A. I. (2012). Assessment of the incidence of enteric adenovirus species and serotypes in surface waters in the eastern cape province of South Africa: Tyume River as a case study. *Sci. World J.* 2012:949216. doi: 10.1100/2012/949216

Siebenga, J. J., Vennema, H., Zheng, D. P., Vinjé, J., Lee, B. E., Pang, X. L., et al. (2009). Norovirus illness is a global problem: emergence and spread of norovirus GII. 4 variants, 2001–2007. *J. Infect. Dis.* 200, 802–812. doi: 10.1086/605127

Simmons, F. J., Kuo, D. H. W., and Xagoraraki, I. (2011). Removal of human enteric viruses by a full-scale membrane bioreactor during municipal wastewater processing. *Water Res.* 45, 2739–2750. doi: 10.1016/j.watres.2011.02.001

Smith, D. B., and Simmonds, P. (2018). Classification and genomic diversity of enterically transmitted hepatitis viruses. *Cold Spring Harb. Perspect. Med.* 8:a031880. doi: 10.1101/cshperspect.a031880

Smuts, H., Cronje, S., Thomas, J., Brink, D., Korsman, S., and Hardie, D. (2018). Molecular characterization of an outbreak of enterovirus-associated meningitis in Mossel Bay, South Africa, December 2015–January 2016. *BMC Infect. Dis.* 18, 709–711. doi: 10.1186/s12879-018-3641-4

Spilki, F. R., Luz, R. B. D., Fabres, R. B., Soliman, M. C., Kluge, M., Fleck, J. D., et al. (2013). Detection of human adenovirus, rotavirus and enterovirus in water samples collected on dairy farms from Tenente Portela, northwest of Rio Grande do Sul, Brazil. *Braz. J. Microbiol.* 44, 953–957. doi: 10.1590/S1517-83822013000300046

Staggemeier, R., Heck, T. M., Demoliner, M., Ritzel, R. G., Röhnelt, N. M., Girardi, V., et al. (2017). Enteric viruses and adenovirus diversity in waters from 2016 Olympic venues. *Sci. Total Environ.* 586, 304–312. doi: 10.1016/j.scitotenv.2017.01.223

Suzuki, H., Sakai, T., Tanabe, N., and Okabe, N. (2005). Peak rotavirus activity shifted from winter to early spring in Japan. *Pediatr. Infect. Dis. J.* 24, 257–260. doi: 10.1097/01.inf.0000154327.00232.4d

Syed, S. F., Zhao, Q., Umer, M., Alagawany, M., Ujjan, I. A., Soomro, F., et al. (2018). Past, present and future of hepatitis E virus infection: zoonotic perspectives. *Microb. Pathog.* 119, 103–108. doi: 10.1016/j.micpath.2018.03.051

Sylvestre, É., Prévost, M., Burnet, J.-B., Pang, X., Qiu, Y., Smeets, P., et al. (2021). Demonstrating the reduction of enteric viruses by drinking water treatment during snowmelt episodes in urban areas. *Water Res. X* 11:100091. doi: 10.1016/j.wroa.2021.100091

Taghinejad, M., Ghaderi, M., and Mousavi-Nasab, S. D. (2020). Aichivirus with acute gastroenteritis in Iran. *Pediatr. Infect. Dis. J.* 39, 576–579. doi: 10.1097/INF.0000000000002638

Tang, A., Bi, X., Li, X., Li, F., Liao, X., Zou, J., et al. (2020). The inactivation of bacteriophage MS2 by sodium hypochlorite in the presence of particles. *Chemosphere* 266:129191. doi: 10.1016/j.chemosphere.2020.129191

Tate, J. E., Burton, A. H., Boschi-Pinto, C., Parashar, U. D., World Health Organization–Coordinated Global Rotavirus Surveillance NetworkAgocs, M., et al. (2016). Global, regional, and national estimates of rotavirus mortality in children <5 years of age, 2000–2013. *Clin. Infect. Dis.* 62, S96–S105. doi: 10.1093/cid/civ1013

Tate, J. E., Patel, M. M., Steele, A. D., Gentsch, J. R., Payne, D. C., Cortese, M. M., et al. (2010). Global impact of rotavirus vaccines. *Expert Rev. Vaccines* 9, 395–407. doi: 10.1586/erv.10.17

Taylor, M., Cox, N., Vrey, M., and Grabow, W. (2001). The occurrence of hepatitis A and astroviruses in selected river and dam waters in South Africa. *Water Res.* 35, 2653–2660. doi: 10.1016/S0043-1354(00)00551-0

Thorne, L. G., and Goodfellow, I. G. (2014). Norovirus gene expression and replication. *J. Gen. Virol.* 95, 278–291. doi: 10.1099/vir.0.059634-0

Trivedi, T. K., Desai, R., Hall, A. J., Patel, M., Parashar, U. D., and Lopman, B. A. (2013). Clinical characteristics of norovirus-associated deaths: a systematic literature review. *Am. J. Infect. Control* 41, 654–657. doi: 10.1016/j.ajic.2012.08.002

Troeger, C., Khalil, I. A., Rao, P. C., Cao, S., Blacker, B. F., Ahmed, T., et al. (2018). Rotavirus vaccination and the global burden of rotavirus diarrhea among children younger than 5 years. *JAMA Pediatr.* 172, 958–965. doi: 10.1001/jamapediatrics.2018.1960

Tryfinopoulou, K., Kyritsi, M., Mellou, K., Kolokythopoulou, F., Mouchtouri, V. A., Potamiti-Komi, M., et al. (2019). Norovirus waterborne outbreak in Chalkidiki, Greece, 2015: detection of GI.P2_GI.2 and GII.P16_GII.13 unusual strains. *Epidemiol. Infect.* 147, e227. doi: 10.1017/S0950268819000852

Umesha, K. R., Bhavani, N. C., Venugopal, M. N., Karunasagar, I., Krohne, G., and Karunasagar, I. (2008). Prevalence of human pathogenic enteric viruses in bivalve molluscan shellfish and cultured shrimp in south west coast of India. *Int. J. Food Microbiol.* 122, 279–286. doi: 10.1016/j.ijfoodmicro.2007.12.024

Upfold, N. S., Luke, G. A., and Knox, C. (2021). Occurrence of human enteric viruses in water sources and shellfish: A focus on Africa. *Food Environ. Virol.* 13, 1–31. doi: 10.1007/s12560-020-09456-8

Van Zyl, W. B., Zhou, N. A., Wolfaardt, M., Matsapola, P. N., Ngwana, F. B., Symonds, E. M., et al. (2019). Detection of potentially pathogenic enteric viruses in environmental samples from Kenya using the bag-mediated filtration system. *Water Supply* 19, 1668–1676. doi: 10.2166/ws.2019.046

Verani, M., Federigi, I., Donzelli, G., Cioni, L., and Carducci, A. (2019). Human adenoviruses as waterborne index pathogens and their use for quantitative microbial risk assessment. *Sci. Total Environ.* 651, 1469–1475. doi: 10.1016/j.scitotenv.2018.09.295

Verheyen, J., Timmen-Wego, M., Laudien, R., Boussaad, I., Sen, S., Koc, A., et al. (2009). Detection of adenoviruses and rotaviruses in drinking water sources used in rural areas of Benin, West Africa. *Appl. Environ. Microbiol.* 75, 2798–2801. doi: 10.1128/AEM.01807-08

Vinjé, J. (2015). Advances in laboratory methods for detection and typing of norovirus. *J. Clin. Microbiol.* 53, 373–381. doi: 10.1128/JCM.01535-14

Vu, D. L., Bosch, A., Pintó, R. M., and Guix, S. (2017). Epidemiology of classic and novel human astrovirus: gastroenteritis and beyond. *Viruses* 9:33. doi: 10.3390/v9020033

Vu, D. L., Cordey, S., Brito, F., and Kaiser, L. (2016). Novel human astroviruses: novel human diseases? *J. Clin. Virol.* 82, 56–63. doi: 10.1016/j.jcv.2016.07.004

Wang, Y., Hao, L., Pan, L., Xue, C., Liu, Q., Zhao, X., et al. (2018b). Age, primary symptoms, and genotype characteristics of norovirus outbreaks in Shanghai schools in 2017. *Sci. Rep.* 8:15238. doi: 10.1038/s41598-018-33724-0

Wang, D., Hu, B., Hu, C., Zhu, F., Liu, X., Zhang, J., et al. (2020a). Clinical characteristics of 138 hospitalized patients with 2019 novel coronavirus–infected pneumonia in Wuhan, China. *JAMA* 323, 1061–1069. doi: 10.1001/jama.2020.1585

Wang, H., Kjellberg, I., Sikora, P., Rydberg, H., Lindh, M., Bergstedt, O., et al. (2020b). Hepatitis E virus genotype 3 strains and a plethora of other viruses detected in raw and still in tap water. *Water Res.* 168:115141. doi: 10.1016/j.watres.2019.115141

Wang, H., Sikora, P., Rutgersson, C., Lindh, M., Brodin, T., Björlenius, B., et al. (2018a). Differential removal of human pathogenic viruses from sewage by conventional and ozone treatments. *Int. J. Hyg. Environ. Health* 221, 479–488. doi: 10.1016/j.ijheh.2018.01.012

WHO (2017a). Diarrhoeal disease. Fact Sheets.1–4. Available at: https://www.who.int/en/news-room/fact-sheets/detail/diarrhoeal-disease (December 7, 2020).

WHO (2017c). *Guidelines for Drinking-Water Quality: Fourth Edition Incorporating the First Addendum*. Geneva, Switzerland: WHO

Wohlgemuth, N., Honce, R., and Schultz-Cherry, S. (2019). Astrovirus evolution and emergence. *Infect. Genet. Evol.* 69, 30–37. doi: 10.1016/j.meegid.2019.01.009

World Health Organization (2012a). *Global Costs and Benefits of Drinking-water Supply and Sanitation Interventions to reach the MDG Target and universal Coverage*. Geneva: WHO

World Health Organization (2012b). Position paper on hepatitis A vaccines. *Weekly Epidemiol. Rec.* 87, 261–276.

World Health Organization (2012c). WHO position paper on hepatitis A vaccines–June 2012. *Weekly Epidemiol. Rec.* 87, 261–276.

World Health Organization (2014). Waterborne Outbreaks of Hepatitis E: Recognition, Investigation and Control. World Health Organization.

World Health Organization (2017b). Global Hepatitis Report 2017. World Health Organization.

World Health Organization (2020). Naming the coronavirus disease (COVID-19) and the virus that causes it. *Braz. J. Implantol. Health Sci.* 2, 1–4.

World Health Organization/United Nations Children Emergency Fund (2015). Progress on sanitation and drinking water: 2015 update and MDG assessment.

World Health Organization/United Nations Children Emergency Fund (2021). Progress on Household Drinking water, Sanitation, and Hygiene 2000–2020: Five Years into the SDGs. Geneva, Switzerland.

Wu, Y., Guo, C., Tang, L., Hong, Z., Zhou, J., Dong, X., et al. (2020). Prolonged presence of SARS-CoV-2 viral RNA in faecal samples. *Lancet Gastroenterol. Hepatol.* 5, 434–435. doi: 10.1016/S2468-1253(20)30083-2

Xagoraraki, I., and O'Brien, E. (2020). "Wastewater-based epidemiology for early detection of viral outbreaks" in *Women in Water Quality*. ed. D. O'Bannon (Switzerland: Springer), 75–97.

Yamashita, T., Sugiyama, M., Tsuzuki, H., Sakae, K., Suzuki, Y., and Miyazaki, Y. (2000). Application of a reverse transcription-PCR for identification and differentiation of Aichi virus, a new member of the Picornavirus family associated with gastroenteritis in humans. *J. Clin. Microbiol.* 38, 2955–2961. doi: 10.1128/JCM.38.8.2955-2961.2000

Yang, Q., Rivailler, P., Zhu, S., Yan, D., Xie, N., Tang, H., et al. (2021). Detection of multiple viruses potentially infecting humans in sewage water from Xinjiang Uygur autonomous region, China. *Sci. Total Environ.* 754:142322. doi: 10.1016/j.scitotenv.2020.142322

Yeo, C., Kaushal, S., and Yeo, D. (2020). Enteric involvement of coronaviruses: is faecal–oral transmission of SARS-CoV-2 possible? *Lancet Gastroenterol. Hepatol.* 5, 335–337. doi: 10.1016/S2468-1253(20)30048-0

Zahedi, A., Monis, P., Deere, D., and Ryan, U. (2021). Wastewater-based epidemiology—surveillance and early detection of waterborne pathogens with a focus on SARS-CoV-2, cryptosporidium and giardia. *Parasitol. Res.* 120, 4167–4188. doi: 10.1007/s00436-020-07023-5

Zhou, X., Kong, D. G., Li, J., Pang, B. B., Zhao, Y., Zhou, J. B., et al. (2019). An outbreak of gastroenteritis associated with GII. 17 Norovirus-contaminated secondary water supply system in Wuhan, China, 2017. *Food Environ. Virol.* 11, 126–137. doi: 10.1007/s12560-019-09371-7

Zhou, N., Lin, X., Wang. S., Tao, Z., Xiong, P., Wang, H., et al. (2016). Molecular epidemiology of GI and GII noroviruses in sewage: 1-year surveillance in eastern China. *J. Appl. Microbiol.* 121, 1172–1179. doi: 10.1111/jam.13218

Zhu, B., Clifford, D. A., and Chellam, S. (2005). Virus removal by iron coagulation–microfiltration. *Water Res.* 39, 5153–5161. doi: 10.1016/j.watres.2005.09.035

Zhu, H., Yuan, F., Yuan, Z., Liu, R., Xie, F., Huang, L., et al. (2018). Monitoring of Poyang lake water for sewage contamination using human enteric viruses as an indicator. *Virol. J.* 15, 3–9. doi: 10.1186/s12985-017-0916-0

Zhu, N., Zhang, D., Wang, W., Li, X., Yang, B., Song, J., et al. (2020). A novel coronavirus from patients with pneumonia in China, 2019. *N. Engl. J. Med.* 382, 727–733. doi: 10.1056/NEJMoa2001017

Zwart, M. P., Hemerik, L., Cory, J. S., de Visser, J. A. G., Bianchi, F. J., Van Oers, M. M., et al. (2009). An experimental test of the independent action hypothesis in virus–insect pathosystems. *Proc. R. Soc. B Biol. Sci.* 276, 2233–2242. doi: 10.1098/rspb.2009.0064

Unravelling viral diversity in wastewater treatment plants through metagenomics: a review

Adedayo Ayodeji Lanrewaju, Abimbola Motunrayo Folami, Saheed Sabiu and Feroz Mahomed Swalaha*

Department of Biotechnology and Food Science, Faculty of Applied Science, Durban University of Technology, P. O. Box 1334, Durban 4000, South Africa

*Correspondence: fswalaha@dut.ac.za

Abstract

Wastewater is a biologically diverse environment that harbours a wide range of pathogens including bacteria, fungi, protozoans and viruses which enters the wastewater from waste, vomit and urine of infected humans and animals via the inflow. Viruses unlike bacteria and other microorganisms are highly resilient in wastewater environments, easily evade the treatment processes and subsequently contaminate water sources into which they are discharged and have potential to cause widespread outbreaks. Therefore, to monitor the prevalence of these viruses in water which could be an early warning signal to predict epidemics, different methods are being used. However, the conventional methods have several shortcomings including extended time of incubation and the use of known primers to target already known viruses, which limits detection to only those primers, and reduces the scope of disinfection leading to a lack of understanding of total viral populations or the identification of novel viruses in wastewater and other environmental matrices. Notably, metagenomics characterizes known and unknown microbial assemblies in a genetic material and overcomes the challenges associated with the conventional techniques used for viral identification in water matrices. Hence, this review will examine various viral characterization techniques in water, different sequencing technologies and studies in which viral diversity in wastewater has been

investigated using metagenomics while highlighting the commonly profiled viruses and the essence of their occurrence. Furthermore, the different stages in viral metagenomics workflow in wastewater will be evaluated. The drawbacks and prospects associated with the use of metagenomics for assessing viral diversity in wastewater were highlighted. Therefore, a need for more research to focus on the identified constraints, such as high costs, the requirement for specialized knowledge and equipment, difficulties in data analysis and interpretation, the absence of standardized methods and the rapid advancements in technology to improve viral metagenomics in wastewater was recommended.

Keywords: Bioinformatics analysis; Sequencing technologies; Standardized methods; Viral metagenomics; Wastewater

1.0 Introduction

Given the recent global outbreaks of diseases such as COVID-19 and cholera, there is growing recognition of the risks posed by human exposure to emerging pathogens in wastewater treatment. These pathogens may enter wastewater via multiple routes including the release of pathogens in human waste, treated or untreated effluent, illegal activities (illegal dump of medical waste, unauthorized slaughterhouses and meat processing, improper discharge of livestock waste), animal rearing, hospital waste, or surface water run off after a wide-area biological event (Lahrich *et al*., 2021). Wastewater is a highly biodiverse habitat that harbours diverse pathogens, including bacteria, fungi, protozoans and viruses. Among these, enteric viruses, typically transmitted via the faecal-oral route through contaminated water, food, or direct contact, pose a significant health risk to wastewater treatment plants (WWTPs) workers and nearby communities (Gerardi and Zimmerman, 2004). These treatment plants are designed to remove contaminants protect ecosystems and public health (Wang *et al*., 2012). However,

enteric viruses remain difficult to detect and inactivate due to their low infectious dose and persistence (Gonzales-Gustavson *et al*., 2019), and they have been detected in the effluent of WWTPs (Wang *et al*., 2020), and may still pose health risks even at low concentrations (Zhu *et al*., 2018). The transmission of enteric viruses through water has been linked to diseases including gastroenteritis, encephalitis, meningitis, and hepatitis (Tang *et al*., 2021). Therefore, continuous monitoring of treated wastewater is essential for viral surveillance and disease prevention (Lanrewaju *et al*., 2022).

Viral detection through culture methods enables the separation of pure viral stock and is effective for assessing concentration and infectivity. Nevertheless, these techniques are constrained by long incubation times and limited cultivability (McCall and Xagoraraki, 2019). Therefore, polymerase chain reaction (PCR) has become a standard method for viral identification and quantification due to its rapid detection and independence from cell culture (Xagoraraki *et al*., 2014). However, these molecular techniques rely on known primers and prior microbiome knowledge limiting detection of novel viruses (Fancello *et al*., 2012). Therefore, this has driven the development of advanced approaches for broader viral characterization.

The advent of next-generation sequencing (NGS) technology is transforming the use of molecular approaches in comprehending intricate microbial ecosystems as it overcomes the constraints of conventional techniques by employing sophisticated technologies to sequence the genes or genomes of organisms or microbial communities (Garner *et al*., 2021). This technique is used without the requirement of culturing the organisms or having prior knowledge of the microbial composition of a sample. Furthermore, metagenomics, which involves

sequencing and analysing the genetic material present in a sample, has provided unparalleled insight into viral diversity (Fancello *et al*., 2012).

At first, the technologies used in metagenomics were specifically developed for the analysis of bacterial metagenomes, but the rise in viral metagenomic investigations has resulted in improvements in existing bioinformatics tools and the development of new tools and standardized approaches to analyze viral metagenomes (viromes) (Roux *et al*., 2021). Several reviews have documented the use of metagenomics to unveil viral diversity in different water matrices (McCall and Xagoraraki, 2019, Osunmakinde *et al*., 2018), with only a few focusing on wastewater directly. Therefore, reviewing studies in this regard will further advance environmental and public health and provide a comprehensive oversight of viral diversity in WWTPs. To this end, this review examines the different techniques used for viral characterization and sequencing technologies, viral diversity in WWTPs using metagenomics and the viral metagenomics workflow, constraints and prospects of viral metagenomics in wastewater.

2.0 Techniques for viral characterization in water samples

Various techniques used to identify and measure viruses in wastewater include epifluorescence microscopy, transmission electron microscopy, pulsed-field gel electrophoresis, immunofluorescence test, flow cytometry, classic cell-culture, and molecular approaches. These detection techniques provide both distinct information on the presence of viruses in wastewater samples as some methods offer qualitative data, while others yield quantitative data. Specifically, molecular techniques quantify virus based on certain portions of the virus's genetic material hence, the virus may be identified even when it has been inactivated while

viral viability is assessed using cell-culture based and immunological techniques (Corpuz *et al*., 2020).

2.1 Transmission electron microscopy

Transmission electron microscopy (TEM), an imaging approach that offers high resolution at the nanoscale range, was among the earliest methods used to detect and quantify viruses. This approach enables identification, classification and quantification of viruses based on their morphology (Roingeard *et al*., 2019). This approach employs negative staining in which the viral particles adhere to a pre-treated specimen support. Following the adsorption process, the particles are treated with heavy metals such as uranyl acetate and phosphotungstic acid (PTA) used as electron-dense stains. Thereafter, the samples are examined using an electron microscope, providing valuable information on the size, structures and counts of stained virus particles (Laue, 2010).

Using TEM, Wu and Liu (2009), investigated the viral morphology in activated sludge and anaerobic digestion sludge samples obtained from a municipal WWTP. The identified structures were then used to classify viral particles based on the International Committee on Taxonomy of Virus (ICTV) procedures. The TEM findings revealed a wide range of morphological types in the sludge samples, suggesting a diversified viral community. Viruses in developing illnesses could possibly be detected using TEM owing to the stability of viral morphology even after nucleic acids mutation (Laue, 2010). Nevertheless, drawbacks of this technique include its strong preference for host-specific infectious viruses, resulting in a lower viral count than the true population (Brown *et al*., 2015). In addition, analysing many samples

with TEM is challenging due to the need for skilled workers, advanced equipment and its lack of automation (Barreto-Vieira and Barth, 2015).

2.2 Staining nucleic acid with fluorescent dyes

This viral quantification approach uses nucleic acid dyes with a high level of fluorescence (Wen *et al*., 2004) and requires filtering water samples using the 0.22 μm filter (Otawa *et al*., 2007, Wu and Liu, 2009). The viral particles' nucleic acids are then labelled with a fluorescent dye to enable luminous dots formation bigger than the virus particles. Excitation of the fluorescent dye attached to nucleic acids results in the formation of fluorescent dots. The viral particles can then be quantified by counting the fluorescent dots using an epifluorescence microscope (Ortmann and Suttle, 2009). The commonest staining dye used in this approach is SYBR Green I. Wu and Liu (2009) quantified viral particles in the influent, effluent and sludge samples while Otawa *et al*., (2007), counted viral particles in mixed liquor activated sludge samples using same dye. This technique is better compared to TEM in that it can used to quantify non-cultivable viruses and stained viral particles even at lower magnifications (Ortmann and Suttle, 2009). Also, viral particles with nucleic acids can be distinguished from viral-like particles void of nucleic acids using the DNase treatment. Nevertheless, this approach is hindered by its limited efficacy in identifying RNA viruses or single-stranded DNA viruses (Forterre *et al*., 2013).

2.3 Flow cytometry (FCM)

Fluorescent nucleic acid-specific dyes have been integrated into FCM to quantify viruses in wastewater samples. The process of viral quantification using FCM entails diluting viral samples with buffer solutions and subsequent staining with fluorescent dyes before injecting

into the flow cytometer. The surrounding sheath fluid facilitates the entry of the viral particles in a single file as the discrete particles interact with a beam of light from an argon-ion laser. Detectors gather and evaluate the scattering and fluorescence intensity resulting from the interactions between each particle and the incoming laser beam (Brown and Wittwer, 2000). In this approach, the fluorescent dye specifically binds to the DNA or RNA with the fluorescence intensity of the DNA/dye and RNA/dye complexes directly proportional to the DNA/RNA concentration of the sample (Adan *et al*., 2017, Brown and Wittwer, 2000). According to Ma *et al*., (2013), one of the main benefits of FCM is its rapid quantification and high accuracy. Influent, primary and secondary settling water, activated sludge, and effluent samples were analysed using FCM to quantify the viral abundance in a municipal wastewater plant (Ma *et al*., 2013). More sensitivity and rapid quantification were observed when viral quantification evaluated using FCM and EPM were compared. Specifically, a 2.7-fold increase in sensitivity from the FCM technique was observed relative to TEM in the viral quantification of activated sludge samples (Brown *et al*., 2015).

2.4 Immunofluorescence assay (IFA)

This approach involves the adsorption of a sample taken from an infected cell culture onto a microscope slide. The presence of the viral protein antigen is identified by consecutively exposing the sample, which is attached to a slide, to a particular antibody and a secondary antibody that is chemically linked to a fluorescent compound that can recognise the first antibody. The fluorophore-conjugated antibody exhibits fluorescence when stimulated by light. When observed with a fluorescent microscope, the antigen-antibody combination is visible as a fluorescent particle (Im *et al*., 2019; Dowd *et al*., 2009).

This technique has been used to measure the levels of human adenovirus (HAdV) and JC polyomavirus (JCPyV) in untreated sewage that flows into WWTPs (Calgua *et al*., 2011), showing that the sensitivity of IFA is higher than that of the other cell culture techniques. Schlindwein *et al*., (2010), confirmed that HAdV 2 in activated sludge samples and effluent samples from a wastewater treatment facility are viable using IFA. This technique was found to be better, compared to other detection methods due to its virus infectivity analysis (Calgua *et al*., 2011), however, it could be time-consuming and necessitates the use of a costly fluorescence microscope and the expertise of qualified individuals for interpretation.

2.5 Enzyme linked immunosorbent assay (ELISA)

The technique depends on the binding of an antigen to its corresponding antibody resulting in a colour or fluorescence change because of the enzyme activity. The first stage of the procedure involves the attachment of an antigen to a particular antibody that is fixed in place on a surface; in 96-well microtiter plates. A second enzyme-linked antibody, which targets the same antigen, is used to create a sandwich structure consisting of an antibody, an antigen, and another antibody. The enzyme-linked antibody binds to a substrate that undergoes a colour change upon modification by the enzyme. The change in colour or fluorescence is directly linked to the concentration of the probed antigens in the sample (Gan and Patel, 2013). This technique has been used for detecting RVA in the raw sewage and tertiary treated samples obtained from municipal and hospital WWTPs and to equally analyze the efficiency of the WWTPs in the removal of RV (Kargar *et al*., 2013). Nevertheless, this technique is becoming outdated due to its time-consuming procedures and poor sensitivity which could yield false-negative results at low viral concentrations (Pilevar *et al*., 2021).

2.6 Pulsed-field gel electrophoresis (PFGE)

Using a pulsating electric field, the PFGE technique separates DNA fragments with high molecular weights based on their molecular sizes (Nassonova, 2008, Díez *et al*., 2000). This technique involves creating alternating electric vectors between two independent electrodes forcing molecules to undergo periodic re-orientation to match the shifting field (Tang et al., 2006). A fragment's size and charge determine how readily it can realign with the modulated electric field. Smaller molecules may move quickly and re-orient by threading through a gel matrix's pores and toward each new anode while the re-orientation of larger DNA molecules is more time-consuming. DNA molecules that cannot re-align within the preset pulse duration typically move through the gel as a single band (Lopez-Canovas *et al*., 2019; Tang *et al*., 2006). The viral community forms a visible band pattern serving as its fingerprint while the number of bands generated provides an estimate of the viral diversity in the sample (Díez *et al*., 2000).

According to Otawa *et al*., (2007), the predominant sizes of viral DNA detected in activated sludge samples obtained from 14 WWTPs ranged from 40 – 70 kb. The PFGE technique revealed that the viral species found in the activated sludge of the WWTPs were similar as indicated by their nearly identical band patterns. In their investigation on the viral diversity of a municipal WWTP, Wu and Liu (2009) adopted the PFGE method to analyze influent, primary settling tank, effluent, and sludge samples. Consequently, they reported the highest abundance of bands in the activated sludge, anaerobic digestion sludge, and effluent exhibited the greatest abundance of bands while the influent and primary settling tank samples exhibited similar band patterns. The PFGE approach demonstrated that the prevailing sizes of viral DNAs were between 30 - 80 kb and 200 - 350 kb. This method offers a rapid and simple means of observing

variations in the composition of viral assemblages however, its application is restricted for viral assemblages' analysis owing to the extreme genetic diversity among viruses (Steward, 2001).

2.7 Molecular methods

Molecular techniques have greatly reduced the time needed to identify viruses, while enhancing sensitivity by focusing on distinct, exclusive, and conserved viral genomic areas. Several water quality guideline standards use molecular approaches because of their quicker turnaround times (Fernández-Baca *et al*., 2021; Donaldson *et al*., 2002), as they enable faster decision-making and perhaps, reduces the dangers associated with exposure to water sources contaminated with faecal matter. Polymerase chain reaction (PCR) is a very sensitive traditional test method used to amplify specific viral DNA or RNA, resulting in the production of thousands or millions of copies (Rodríguez *et al*., 2009; Fong and Lipp, 2005). PCR procedures are specifically intended to exponentially increase the amount of a certain nucleic acid sequence by a factor of one million via three unique steps: denaturation, annealing, and extension. To induce denaturation, the target DNA is exposed to elevated temperatures, causing the DNA strands to split. By subjecting the primers to annealing with the target DNA, the DNA polymerase can amplify that sequence selectively at a lower temperature (Fong and Lipp, 2005). PCR tests are characterized by their high sensitivity, specificity, and attractiveness for detecting non-cultivable infectious organisms making them an appealing approach for detecting target pathogens (Fong and Lipp, 2005).

There are several PCR techniques available that can quickly identify and confirm the occurrence of viral fragment in various water samples. Quantitative PCR (qPCR) allows for the simultaneous detection, quantification of DNA and subsequent calculation of its

concentration based on a standard curve with the use of sequence-specific probes enhancing the precision of DNA amplification. Quantitative reverse transcription (RT-qPCR) is similar to qPCR but involves the conversion of RNA into complementary DNA (cDNA) using reverse transcriptase and may subsequently be used as a template for qPCR. An additional benefit of using qPCR or RT-qPCR relative to the traditional approach is the elimination of the agarose gel electrophoresis step after amplification (Corpuz *et al*., 2020). Furthermore, by incorporating several primer sets within a single reaction, multiplex PCR enables the simultaneous detection of many viruses in a single reaction (Newby *et al*., 2009). Similarly, multiplex qPCR enables the identification of many distinct viruses by using multiple fluorescent reporters in a single reaction (Haramoto *et al*., 2018). In addition to its sensitivity, another benefit of the multiplex assay is the speed connected to the use of simultaneous detection as well as reduced expenses for reagents and labour, relative to single plex PCR-based tests (Hamza *et al*., 2014; Fumian *et al*., 2010). Moreover, an enhanced version of the qPCR technique has been developed to provide more precise measurement by incorporating it with a digital system, which could be droplet-based (emulsion) or chip-based (microfluidic) (Barceló i Cullerés, 2020). Studies have shown that digital PCR offers higher sensitivity and lower variability in detecting trace viral loads (2.4×10^3 gene copies per litres of wastewater) (de la Cruz Barron *et al*., 2023; Huggett *et al*., 2015), and it does not need any external calibration, hence enabling absolute quantification (Barceló i Cullerés, 2020).

Quantitative PCR methods have been used for viral characterization in different water matrices including water sediments (Farkas *et al*., 2017; Staggemeier *et al*., 2015), WWTP (Okoh *et al*., 2010, Schlindwein *et al*., 2010), treated and untreated sewage (Schlindwein *et al*., 2010, Pinto *et al*., 2009), groundwater (Abbaszadegan *et al*., 1993), and surface water (Chigor and Okoh, 2012, Chapron *et al*., 2000). However, a major drawback of PCR methods is their inability to

differentiate between viable and non-viable targets. Additionally, they are susceptible to inhibition caused by DNA contact or interference with the DNA polymerase, leading to an increased risk of false negative findings (Osunmakinde *et al*., 2018). Furthermore, the use of distinct primer sequences renders it unsuitable, considering the identification of novel viruses as prior knowledge of the viral sequence is essential for each PCR reaction. Moreover, the need for direct identification of human pathogens and evaluation of viral diversity in different environments has resulted in the emergence of advanced technologies (Fancello *et al*., 2013). Thus, viral metagenomics has been the subject of a growing numbers of research to determine the viral diversity in different environments.

2.8 Viral metagenomics

Viral metagenomics is simply the process of sequencing and analysing the viral genetic material (DNA and/or RNA). In 2002, the first study documenting viral metagenomics application to analyse marine viromes was published (Breitbart *et al*., 2002), with several significant findings emanating from the application of viral metagenomics thereafter in the last two decades. Furthermore, the utilization of viral metagenomics has facilitated the advancement of diverse applications encompassing diagnostics, microbiological source tracing, monitoring and surveillance (Santiago-Rodriguez and Hollister, 2022). In the last 20 years, sequencing technology has advanced at a remarkable pace with three distinct generations which have emerged as a direct result of this fast advancement (Satam *et al*., 2023).

2.8.1 First generation sequencing

Initially, the process of sequencing nucleic acids entailed breaking down the molecules by chemical or enzymatic techniques, resulting in smaller pieces that could be examined

separately. Robert Holley achieved the pioneering feat of sequencing Alanine tRNA in 1964 with ribonuclease from *Saccharomyces cerevisiae* (Holley *et al*., 1965). Likewise, Walter Gilbert and Allan Maxam developed a chemical degradation technique to sequence the entire genome of bacteriophage PhiX174 (Heather and Chain, 2016). The chain termination-based sequencing technique of Fredrick Sanger in 1975 laid a proper bedrock for the sequencing technology (Sanger *et al*., 1977). This method employed dideoxynucleotides, which stop DNA strands elongation during replication, facilitating the generation of sequence reads with ranges of up to several hundred nucleotides in length. The adoption of Sanger's technique had a significant impact on molecular biology because it enabled the speedy sequencing of nucleic acids (Heather and Chain, 2016).

Different fields of biology and medicine have witnessed a significant transformation owing to the capacity to sequence both DNA and RNA which has subsequently resulted in diverse findings and progress in comprehending genetics and molecular biology (Satam *et al*., 2023). Specifically, different groups of HAdVs have been characterized from the environment using this approach (Ogorzaly *et al*., 2015), however, low throughput, labour intensity, and slow processing speed include the primary drawbacks associated with this approach hence a limitation for its adoption as a diagnostic tool (Heather and Chain, 2016, Zhang *et al*., 2011).

2.8.2 Second generation sequencing (SGS)

The challenges associated with the first-generation sequencing technology especially Sanger sequencing paved the way for the advent of the SGS technology after 2005 with features fashioned to overcome the drawbacks of the previous sequencers. The basic distinguishing features of the SGS technology included the simultaneous generation of numerous short reads,

accelerated sequencing process, cost-effective sequencing and direct detection of sequencing output without electrophoresis (Kchouk *et al*., 2017). Broadly, SGS techniques were divided into two principal groups: sequencing by ligation and sequencing by synthesis. The SGS platform included Roche 454 platform introduced in 2005, followed by the Illumina Solexa sequencers in 2006, which was succeeded in 2007 by the AB SOLiD and in 2010 emerged the Ion Torrent Personal Genome Machine (Ambardar *et al*., 2016).

2.8.2.1 454 pyrosequencing

Pyrosequencing exemplified by the Roche 454 platform advanced sequencing technology by employing the luminescent features of pyrophosphate where a nucleotide is integrated into a complementary strand (Simner *et al*., 2015). This platform was an upgrade regarding its high throughput reading relative to Sanger due to its capacity to generate the longest reads of about 700 bp compared to other second-generation platforms (Weirather *et al*., 2017). Four distinct viral types were identified in Lake Needwood; a freshwater lake in Maryland, USA in a study conducted to elucidate RNA viral diversity using this sequencing platform (Djikeng *et al*., 2009). Similarly, this platform has been used for the detection of both DNA and RNA viruses in reclaimed water while it revealed that both reclaimed and portable water were densely populated by phages (Rosario *et al*., 2009a). In addition, viruses responsible for plant, animal and human diseases have been identified in freshwater samples using the 454 platform (Rooks *et al*., 2010). Nonetheless, a few downsides associated with this platform include high cost per run, shorter nucleotide sequences and increased error rates owing to light intensity build-up in repetitive complex regions specifically in homopolymer sections (White III *et al*., 2016). In 2013, Roche folded its 454 sequencing operations because Illumina (San Diego, CA, USA)

and Ion Torrent (Thermo Fisher, MA, USA) developed more advanced and complex NGS platforms with more precise and speedy sequencing applications (Genome Web 2013, 2015).

2.8.2.2 Illumina sequencing

The Illumina sequencing platform which rely on the sequencing by synthesis (SBS) technique uses advanced systems versions and is often regarded as the most preferred relative to other second-generation sequencing platforms (Ambardar *et al*., 2016; Van Dijk *et al*., 2014; Liu *et al*., 2012a), as it provides approximately 1 gigabase (Gb) of data per run hence, it is used globally for different sequencing studies (Akacin *et al*., 2022). On this platform, nucleotides identification is accomplished by excitation of fluorophores and DNA polymerase incorporates modified deoxyribonucleotide triphosphates (dNTPs) labelled with fluorescent tags during DNA synthesis. Illumina sequencers can read millions of DNA fragments by using microscopic imaging to monitor synthesis on fragments immobilised on a chip (Cox *et al*., 2010). Viral metagenomics of both clinical and environmental samples has been conducted using the Illumina technology (Hjelmsø *et al*., 2017; Iaconelli *et al*., 2017). The short-read lengths of this technology often range from 100 - 300 bp (Table 1) which makes species-level bias and novel species identification in microbial investigations difficult specifically in environmental and ecological studies relative to long-read technologies is a significant limitation of this technique (Fujiyoshi *et al*., 2020). Furthermore, another constraint of this technology is overlapping clusters and poor sequencing quality (overall error rate of 1%) which could result from its high need for sample loading control. The most prevalent error in this technology is nucleotide substitutions (Dohm *et al*., 2008), owing to the inaccurate identification of the integrated nucleotide (Kchouk *et al*., 2017).

2.8.2.3 ABI/SOLiD sequencing

The Supported Oligonucleotide Ligation and Detection (SOLiD) is an NGS sequencing platform from Life Technologies and, after the 2007 acquisition by Applied Biosystems (ABI), it subsequently became a merged sequencer platform referred to as ABI/SOLiD sequencing (Shendure and Ji, 2008). Using a DNA ligase, this sequencing method ligates four bases that are fluorescently labelled, which are contending to attach to a complementary oligonucleotide to the template being sequenced. The process involves repeating the steps of ligation, detection, and cleavage several times, with the number of cycles defining the final read length. The ABI/SOLiD platform is characterized by its excellent precision owing to its ability to read each base twice, while its weakness includes relatively short reads and long-run durations. In addition, the primary kind of error in this technology is substitution leading to inaccurate identification of bases owing to noise during the ligation cycle (Kchouk *et al*., 2017).

2.8.2.4 Ion torrent sequencing

Ion torrent sequencing technology uses the ion semiconductor technology integrated in the Ion Personal Genome Machine (PGM™), a benchtop sequencer. Unlike other NGS platforms using optical sensing technology, PGM™ distinctly adopts semiconductor chips and used H^+ ions during dNTP integration for gene sequencing. Specifically, this platform utilises the pH alteration caused by the buildup of H^+ ions (Goodwin *et al*., 2016). The short run time of the Ion Torrent sequencer has made it become acceptable for its efficient and cost-effective sequencing capabilities, particularly in the clinical and diagnostics field. The new Ion Torrent instruments, including PMG™ Dx and Ion S5, are basically designed for clinical and diagnostic sequencing applications with a special focus on oncology, genetic and infectious diseases and complex disease genomics (Goodwin *et al*., 2016). Nevertheless, numerous viral families from

the Athabasca River sediments and animal samples have been sequenced and profiled using this sequencing platform (Neill *et al*., 2014; Yergeau *et al*., 2012). Challenges associated with this platform include its high-cost relative to Illumina (Bragg *et al*., 2013), and the homopolymer run errors due to variation in cumulative light intensity (Akacin *et al*., 2022).

Generally, the SGS systems have remarkable data processing abilities and offer precise results nevertheless, they are unable to generate long read lengths. Limited taxonomic precision emanates from short read lengths ranging from 100 - 500 bp hence they are inadequate for detailed microorganisms' identification at the species level in 16S rRNA gene sequencing relative to log-read technologies like Oxford Nanopore Technologies (Loit *et al*., 2019).

2.8.3 Third generation sequencing (TGS)

To proffer solutions to the challenges connected with the SGS technologies, TGS technologies emerged with the capacity to offer a faster, less expensive sequencing process and simplified sample preparation, eliminating the requirement for PCR amplification, generate long reads beyond several kilobases to resolve the assembling complicated genomes and repetitive areas challenges (Kchouk *et al*., 2017). PacBio Sequencing, for example employs a single-molecule, real-time (SMRT) approach through fluorescently labelled nucleotides facilitating the sequencing of lengthy DNA fragments, as long as tens of kilobases. Oxford Nanopore sequencing is another method which utilizes the nanopore technology in which a single-stranded DNA molecule threads through a nanopore and variations in the electrical current are measured to decipher the nucleotide sequence (Satam *et al*., 2023).

2.8.3.1 Pacific Biosciences' (PacBio) single molecule real time (SMRT) sequencing

The PacBio® sequencer (PacBio®, Menlo Park, CA, USA), like other SGS technologies, is a high-throughput platform released in 2012, although with a distinct capacity to produce full-length gene sequences of about 10 - 25 kbp relative to other sequencing platforms. Therefore, it generates a higher quantity of information with a library preparation technique that maximizes the use of genomic data and enables data consistency (Fujiyoshi *et al*., 2020). This sequencing platform adopts the SMRT technology which comprises a vast number of zero-mode waveguides (ZMWs) to immobilise individual DNA molecules as templates (Gupta, 2008). Adapters are attached to both ends of the target DNA strand to sequence a DNA molecule followed by the binding of a DNA polymerase leading to a circular DNA molecule formation. Subsequently, this molecule undergoes many sequencing cycles as DNA polymerase integrates DNA bases that are marked with distinct fluorescent dyes which is detected by Zero Mode Waveguides (ZMWs), enabling the direct and instantaneous identification of nucleotides (Pacific Biosciences, 2020a; 2020b).

Increased sensitivity of the technology is enhanced by multiple readings even in sequences with large error numbers thus enabling attaining precise long reads known as "HiFi reads". Therefore, PacBio® together with its long reads provide an effective remedy to the poor taxonomic resolution due to short reads in second-generation sequencers (Akacin *et al*., 2022). Large microbial communities can be comprehensively characterized and analysed effectively especially for novel genes identification within these communities. Additionally, this platform is a valuable tool in epigenetic investigations because it enables real time DNA identification using SMRT void of previous amplification (Akacin *et al*., 2022). Nevertheless, its inherent limitations include intricate sample preparation workflows and lower throughputs relative to

NGS include its inherent limitations (Fujiyoshi *et al*., 2020; Weirather *et al*., 2017; White III *et al*., 2016).

2.8.3.2 Oxford Nanopore MinION sequencing

The Nanopore MinION™ sequencer released in 2014 by Oxford Nanopore Technologies (ONT) is the latest advancement in the TGS (Mikheyev and Tin, 2014) and categorized as TGS due to its ability to sequence lengthy DNA samples longer than 50 kbp. Meanwhile, its most significant advancement compared to the NGS platforms is the fast creation of libraries and the ability to acquire genomic data in real-time. Interestingly, its distinct capacity to sequence single molecules enables the analysis of nanopore sequencing before completing the sequencing run (Charalampous *et al*., 2019).

This sequencing process entails the linkage of the first strand of a DNA molecule to its complementary strand through a hairpin structure. A protein nanopore, which is a tiny opening formed of protein or synthetic material (Kchouk *et al*., 2017; Heo, 2015), is used to transport the DNA fragment. There is a variation in the ionic current due to the differences in the nucleotides travelling through the pore when the DNA fragment is translated via it by means of a motor protein linked to the pore. The sequential recording of this ionic current change is detailed on a graphic model and then analysed to determine the sequence. The sequencing is performed on the direct strand, leading to the generation of the "template read"; afterward, the hairpin structure is read, followed by the sequencing of the inverse strand, which generates the "complement read". These readings are referred to as "$1D^2$" or 1D squared as both template and complement strands are sequenced in a single read (Logsdon et al., 2020; Jain et al., 2018).

A combination of the "template" and "complement" reads will result in a consensus sequence, improving the accuracy compared to single-strand sequencing (Wang et al., 2021).

The ONT system is an exceptional instrument for field studies, enabling the sequencing of environmental genetic materials and data collection in anywhere owing to its quick and real-time sequencing features (Fujiyoshi *et al*., 2020). Furthermore, its portability, lack of need for complex library preparation equipment, its required use of just a single computer void of any bulky laboratory apparatus made its application area unrestricted gave it a vast application scope spanning from orbital missions to tropical rainforests and from surgical theatres to deep ocean bottoms (Oliva *et al*., 2020). Nonetheless, modest throughputs and elevated error rates include the existing constraints that must be addressed in further improvements (Weirather *et al*., 2017). Generally, viral metagenomics allows for the identification of viruses that cannot be cultured however, one limitation of this method is that the findings may be restricted to viruses that are already documented in databases, which mostly consist of model bacteriophages and pathogenic viruses (Santiago-Rodriguez and Hollister, 2020).

3.0 Viral diversity in WWTPs using metagenomics

Wastewater has been investigated as a potential reservoir of viruses with the detection of diverse viruses such as human enteric viruses, which have equally been identified in faecal material subsequently discharged in wastewater systems (Xiao *et al*., 2020; Chan *et al*., 2011; Vicente *et al*., 2007). Viral metagenomics has been evaluated as an approach for monitoring enteric viruses in wastewater. Specifically, NGS-dependent metagenomic investigations of untreated sewage and reclaimed water have revealed a significant abundance of viral species in both the untreated and treated effluents (Cantalupo *et al*., 2011; Rosario *et al*., 2009a).

Broadly, the viral metagenomes of wastewater are composed of the DNA viral families that include the *Adenoviridae*, *Papillomaviridae*, *Parvoviridae*, and *Polyomaviridae*, as well as RNA viral families such as *Astroviridae*, *Caliciviridae*, *Hepeviridae*, *Picobirnaviridae*, *Picornaviridae*, and *Reoviridae* as previously reported (Aw *et al*., 2014; Ng *et al*., 2012; Cantalupo *et al*., 2011). However, results from these investigations indicate that most of the recovered sequence reads or contigs obtained failed to match entries in the International Nucleotide Sequence Database (GenBank database), suggesting that a vast variety of the viruses present in wastewater remain unidentified. Furthermore, Ng *et al*., (2012) used fragments of sequence reads to build whole genome sequences of new viruses, including one named Picalivirus, belonging to the picorna-like virus family. Besides identifying human enteric viruses, metagenomic investigations revealed a significant presence of plant viruses, particularly pepper mild mottle virus (PMMoV) in raw and treated effluents (Hamza et al., 2011; Rosario et al., 2009b).

Shotgun viral metagenomics was used to assess 10 sewage sludge samples from five WWTPs in the United States of America (Bibby and Peccia, 2013). The NGS analysis revealed that, in addition to the viruses often linked to gastrointestinal infections, the analysed sludge samples included a significant number of viruses associated with respiratory disorders (coronavirus HKU1, klassevirus, and cosavirus), whereas enteroviruses (EVs) are considerably less abundant and occur less often. Current pathogen monitoring standards for sludge concentrate

Table 1: Merits and limitations of second and third-generation sequencing

Platform	Amplification technique	Chemistry	Read length	Merits	Limitations	References
Roche 454	Emulsion PCR	Pyro-sequencing	400-700 bp	Long read length, short run times	High error rate	(Ambardar *et al*., 2016; Bleidorn, 2016; Reuter *et al*., 2015; Barba *et al*., 2014; Liu *et al*., 2012b; Cheval *et al*., 2011; Gupta, 2008)
Illumina	Bridge PCR	Reversible terminators	100-300 bp	High throughput, cost-effective, time-efficient, reduced error rate	Short reads Decrease in quality of reads towards the ends	(Reuter *et al*., 2015; Liu *et al*., 2012a; Gupta, 2008)
ABI/SOLiD	Emulsion PCR	Ligation	35 bp	Low error rate	Short reads, homopolymer errors	(Ambardar *et al*., 2016; Bleidorn, 2016; Bayley, 2015; Reuter *et al*., 2015; Van Dijk *et al*., 2014; Liu *et al*., 2012b; Gupta, 2008)
Ion Torrent	Emulsion PCR	Proton detection	100-400	Reduced sequencing time, cost-effective	Short reads, homopolymer errors	(Reuter *et al*., 2015; Liu *et al*., 2012a; Gupta, 2008)
Pacific Bioscience	Single molecule real time	Fluorescently labelled nucleotides	4000-5000 nts	Data generation is monitored in real-time, Accurate	Costly, high error rates	(Ambardar *et al*., 2016; Bleidorn, 2016; Bayley, 2015; Reuter *et al*., 2015; Gupta, 2008)
Oxford Nanopore (MinION)	Single molecule real time	Fluorescently labelled nucleotides	90 Mbp of data with 16,000 reads	Accurate	Costly, high error rate, low throughput	(Ambardar *et al*., 2016; Bleidorn, 2016; Bayley, 2015; Reuter *et al*., 2015; Gupta, 2008)

Note: PCR: Polymerase chain reaction; ABI/SOLiD: Applied Biosystems Inc/Sequencing by Oligonucleotide Ligation and Detection (Adapted from Osunmakinde *et al*., (2018)).

on the surveillance of EV and faecal coliform levels however, the prevalence of emerging viruses, apart from EV, suggests that current guidelines should be revisited.

Using viral metagenomics, the abundance and variety of human and vertebrate viruses in wastewater and surface water samples in Kampala and Uganda was investigated (O'Brien *et al*., 2017b). Several viruses of the family *Herpesviridae*, *Iridoviridae*, *Poxviridae*, *Circoviridae*, *Parvoviridae*, and *Bunyaviridae* were detected in the effluent discharge with temporal variation in the viral diversity of the WWTPs. The metagenomic evaluation suggests that the viral community exhibits temporal variation as samples obtained from different locations during same sampling period display greater similarity to each other relative to samples obtained from same point across different sampling periods. The observed temporal variation further suggests that wastewater monitoring may serve as a robust epidemiological tool for identifying and predicting disease outbreaks within a community. A similar study adopted NGS technique to identify the specific Norovirus GII genotypes present in the influent, primary effluent, and secondary effluent samples obtained from a WWTPs in Rio de Janeiro, Brazil (Fumian *et al*., 2019). The results indicated that there were six main genotypes of NoV GII circulating in wastewater over one year study period with a high prevalence of two strains, namely GII.5 and GII.7, although these strains were absent in the clinical samples. This suggests that these strains have the potential to cause asymptomatic infections or minor symptoms, which often go unreported.

Martínez-Puchol *et al*., (2020), used NGS methods to assess the prevalence of human pathogenic viruses in three WWTPs in Barcelona City, Spain. *Virgaviridae, Tombusviridae* and *Solemoviridae* include the identified viral plant families and accounted for 30% of the total

reads. The prevalence of these viral families holds significant relevance owing to their potential economic implications as plant pathogens. Additionally, JC polyomavirus, mamastrovirus 1, aichivirus A, non-human circoviruses and parvoviruses were identified from vertebrate families and accounted for 2.75% of the total reads. Consequently, viral metagenomics can be regarded as a valuable reference for examining the entire virome in sewage encompassing vertebrates, invertebrates, bacteria, plants and fungi viruses.

Furthermore, viral metagenomics was applied by assembling the metagenome, prediction of coding regions, and mapping against the NCBI non-redundant (nr) database to profile the RNA virome in the wastewater samples of a big Latin American metropolis with the detection of a significant concentration of dsRNA viruses which may infect humans, invertebrates, and bacteria in the investigated wastewater samples (Guajardo-Leiva *et al*., 2020). Specifically, an abundance of emerging rotaviruses (RVs) genotypes and the family *Picobirnaviridae* were reported in the sewage samples suggesting the efficacy of sewage viral metagenomics in public health surveillance because this virome could serve as a reservoir for human pathogens (Guajardo-Leiva *et al*., 2020).

Moreover, in a bid to identify novel or emerging infectious diseases within a community, Li *et al*., (2024b) conducted periodic metagenomics-based wastewater screening to evaluate the variety of possible human viral infections during the COVID-19 pandemic. Apart from betacoronavirus, the occurrence of other potential pathogenic virus genera detected in the investigated wastewater include orthopoxvirus, rhadinovirus, parapoxvirus, varicellovirus, hepatovirus, simplexvirus, bocaparvovirus, molluscipoxvirus, parechovirus, roseolovirus, lymphocryptovirus, alphavirus, spumavirus, lentivirus, deltaretrovirus, enterovirus, kobuvirus,

gammaretrovirus, cardiovirus, erythroparvovirus, salivirus, rubivirus, orthohepevirus, cytomegalovirus, norovirus, and mamastrovirus. They opined that the integration of advanced techniques such as metagenomic sequencing with viral epidemiology provides a robust pathway to enhance pathogenic viral surveillance and prediction from wastewater (Li *et al*., 2024b).

Recently, Lopez-Roblero *et al*., (2024), adopted a metagenomic technique to examine the viral phytopathogen diversity in wastewater, freshwater and sludge from the southernmost tropical region in Mexico. Of the 15 phytopathogenic viruses identified in the study, all of which are of the family *Virgaviridae*, genus tobamovirus, sequence reads were most abundant for pepper mild mottle virus, tomato brown rugose fruit virus and tropical soda apple mosaic virus. Interestingly, the phylogenetic study of the coat protein amino acid sequence indicated a strong correlation between solanaceous plant-infecting viruses and their GenBank reference counterparts. Meanwhile, the large diversity of phyto-viruses detected in wastewater and rivers accompanied with their likely infectivity, raises concerns about using polluted freshwater and wastewater in Mexican agriculture (Lopez-Roblero et al., 2024). Table 2 gives information on the adopted sample processing techniques, bioinformatics approaches, significant human viruses identified and other findings in viral metagenomics studies conducted in WWTPs.

4.0 Viral metagenomics workflow

Broadly, the viral metagenomics workflow pipelines can be divided into pre-sequencing and post-sequencing stages (Figure 1). The pre-sequencing procedures entail sample collection and processing (viral concentration, enrichment and nucleic acids extraction), which greatly influence the diversity of sequenced viral metagenomes (McCall and Xagoraraki, 2019) and

library preparation. Sample storage parameters, such as storage temperature, medium and buffer types, and whether samples are subjected to freeze-thaw cycling, are the primary determinants of viral nucleic acid recovery and viral community information (Santiago-Rodriguez and Hollister, 2020). Post-sequencing comprises of passing raw reads intended for viral metagenomics analyses through quality control, followed by assembling into longer contigs, matching against reference viromes databases and annotating with taxonomic labels based on their alignments. The reliability of the annotation workflow is a function of the sequencing platform, assembly software, alignment technique, and reference databases; hence posing challenges to diversity studies, rendering them arduous and often inadequate (McCall and Xagoraraki, 2019).

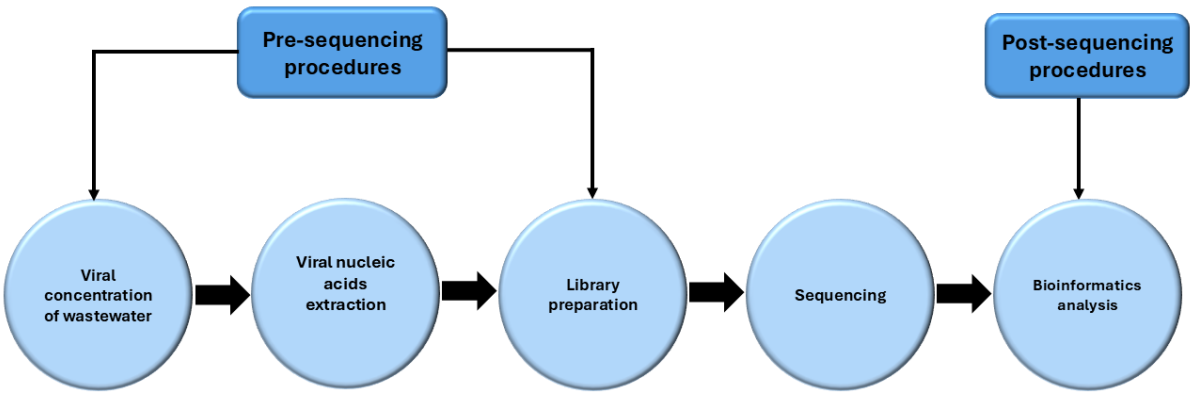


Figure 1: Viral metagenomics pipeline in wastewater.

Table 2: Viral metagenomic studies in WWTPs

Concentration method	Sequencing platform	Assembler	Aligner/annotator	Database	Significant human virus	References
TFF; filtration (0.22 μm); PEG; chloroform treatment; CsCl density gradient ultracentrifugation; nuclease treatment	454/Roche	Seqman	BLAST	Genbank nonredundant protein (non-viral-specific)	Rhinovirus	(Rosario *et al*., 2009a)
Flocculation with skim milk solution; ultracentrifugation; nuclease treatment	454/Roche	Phrap	BLAST	NCBI RefSeq (viral)	Klassevirus	(Cantalupo *et al*., 2011)
TFF; sucrose density gradient centrifugation; nuclease treatment	454/Roche	NR	BLAST	Genbank nonredundant protein and nucleotide (non-viral-specific)	Aichivirus	(Ng *et al*., 2012)
Glass fiber prefiltration; nitrocellulose filtration (1.2 μm); TFF; CsCl density gradient ultracentrifugation; nuclease treatment	454/Roche	Newbler	MG-RAST (BLAST)	SEED (non-viral-specific)	NR	(Tamaki *et al*., 2012)
Flocculation with glycine; filtration (0.45 μm); PEG	Illumina	Velvet	MG-RAST (BLAST); BLAST	NCBI RefSeq (viral) - amended	Herpesvirus	(Bibby and Peccia, 2013)
Filtration (0.22 μm)	454/Roche	NR	BLAST	NCBI Genbank (viral)	Circoviruses	(Alhamlan *et al*., 2013)
PEG; chloroform treatment; filtration (0.45 and 0.2 μm); nuclease treatment	Illumina	Velvet	BLAST	NCBI RefSeq (viral)	Adenovirus	(Aw *et al*., 2014)

Electropositive filtration (NanoCeram); flocculation with beef extract; filtration (0.22 µm)	Illumina	IDBA-UD	BLAST	NCBI RefSeq (viral)	Rotavirus	(O'Brien *et al*., 2017b)
Electropositive filtration (NanoCeram); flocculation with beef extract; filtration (0.22 µm)	Illumina	IDBA-UD	MetaVir2 (BLAST); Bowtie2	NCBI RefSeq (viral)	Herpesvirus	(O'Brien *et al*., 2017a)
Flocculation with skim milk solution; ultracentrifugation; filtration (0.45 µm); nuclease treatment	Illumina	CLC Genomics	BLAST	NCBI RefSeq (viral); NCBI Genbank (viral); UniProt (viral)	Mamastrovirus	(Fernandez-Cassi *et al*., 2018)
Membrane filtration; nuclease treatment	Illumina	Velvet	MG-RAST, MetaVir2	NCBI RefSeq	Adenovirus	(Brinkman *et al*., 2018)
Filtration (1.6 and 0.2 µm)	Illumina	IDBA-UD	BLAST; Bowtie2	NCBI RefSeq (viral)	NR	(Petrovich *et al*., 2019)
Electropositive filtration (NanoCeram); flocculation with beef extract; filtration (0.45 and 0.22 µm)	Illumina	IDBA-UD	BLAST	NCBI RefSeq (viral)	Coronavirus	(McCall *et al*., 2020)
Electropositive filtration (NanoCeram); flocculation with beef extract; filtration (0.45 and 0.22 µm)	Illumina	IDBA-UD	MG-RAST,	Viral RefSeq	Hepatitis A Virus	(McCall *et al*., 2021)
NetoVIR, filtration (0.8 µm); nuclease treatment	Illumina	Ray 2.3.1.	BLAST	NCBI	Adenovirus	(Perez-Cataluna *et al*., 2021)

PEG; Flocculation with glycine; filtration (0.45 μm)	Illumina	metaSPAdes	BLAST; Bowtie2	NCBI	Mamaastrovirus	(Schaeffer *et al*., 2023)
Electropositive filtration (NanoCeram); flocculation with beef extract; filtration (0.45 and 0.22 μm)	Illumina	MEGAHIT	MEGAN	NCBI RefSeq (viral); UniProt (viral)	Mamastrovirus	(Li *et al*., 2024b)
Virus Adsorption-Elution; PEG; filtration (0.22 and 0.45 μm)	Illumina	IDBA-UD; MEGAHIT	BLAST	NCBI	Betacoronavirus	(Li *et al*., 2024a)

Note: TFF: Tangential flow filtration; PEG: Polyethylene glycol; NR: Not reported; NCBI: National Center for Biotechnology Information; NetoVIR: Novel Enrichment Technique of Viromes; MEGAN: Metagenome analyzer; RefSeq: Reference Sequence; BLAST searches: BLASTx, BLASTn, and tBLASTx) are denoted as BLAST.

4.1 Viral concentration techniques

Viral concentration in water can vary due to the matrix type as viruses may be readily detected in a small sample volume (<100 ml) of wastewater or sludge from WWTPs (Haramoto *et al*., 2018). Specifically, influents often have a higher viral concentration, greater turbidity levels (Falman *et al*., 2019; Qiu *et al*., 2016; Sidhu *et al*., 2013), higher levels of suspended solids (Prado *et al*., 2019), increased organic matter content (Falman *et al*., 2019), larger amounts of humic substances and heavy metals (Prado *et al*., 2019) relative to most other aquatic matrices (Haramoto *et al*., 2018). Sludge, by contrast is an heterogenous sample type where viruses frequently adsorb to the surfaces of floc particles (Symonds *et al*., 2014). These different attributes affect the accuracy of viral detection, hence the need for concentration techniques, including primary and secondary concentration procedures. Therefore, to exclude bacteria and other untargeted substances, it is essential to conduct viral concentration after sample collection. Several techniques have been employed to concentrate viruses from wastewater, such as adsorption/elution, ultrafiltration, polyethylene glycol (PEG) precipitation, flocculation, and ultracentrifugation (Haramoto *et al*., 2018; Prata *et al*., 2012).

Features of an effective and acceptable viral concentration method should include high recovery, reproducible outcomes, suitability for different kinds of viruses, a minimal amount of viral concentrate, rapid and economical procedure (Bosch, 1998). Unfortunately, no universally acceptable method meets these requirements, and it becomes more difficult during pandemics because rapid measures to track viruses in wastewater and assess the effectiveness of viral removal methods must be ensured (Ibrahim *et al*., 2021). Presently, there is inadequate data to support the adoption of a certain technique over another as these procedures are not adequately evaluated utilising a diverse array of viruses to establish their overall effectiveness.

Moreover, a significant obstacle to the concentration procedures is the existence of organic inhibitors, including humic and fulvic acids, as well as Mg^{2+} cations which can prevent the enzymes required for the amplification of the genome during the detection process. Thus, it is crucial to prioritize the optimization and thorough evaluation of existing concentration techniques to improve viral recovery and set more efficient process standards as this will assist in combating future viral outbreaks instead of developing another concentration procedure (Lanrewaju *et al*., 2022; Ibrahim *et al*., 2021).

4.2 Nucleic acids extraction

Viruses possess genetic material that may be either RNA or DNA (Artika *et al*., 2020), and may be classified as either single-stranded or double-stranded with distinct polarities, either positive (+) or negative (−). Viral genomes may exist in two primary structures: linear or circular which could either be segmented or complete genomes (O'Carroll and Rein, 2016; Lennette *et al*., 1988). Extraction and purification of viral DNA/RNA involves three main steps: lysis, purification, and recovery. Various DNA extraction techniques include boiling, column method, magnetic beads, and the use of FTA cards (Barbosa *et al*., 2016). Recently, commercially accessible DNA and RNA kits have been widely used to investigate the presence of viruses in wastewater samples, with column-containing membranes made of silica being the DNA extraction kits that are frequently used (Barbosa *et al*., 2016). In addition, magnetic nanoparticles have been used to coat the silica particles, enabling purification without the need of a centrifuge (Wang *et al*., 2015).

The column-based extraction approach is categorized as a solid phase-DNA isolation technique in which the water sample is first lysed before being loaded onto the column. The lysate is

introduced into the column containing chaotropic salts, such as guanidine hydrochloride, guanidine isothiocyanate, sodium iodide, and sodium perchlorate which facilitate the specific adsorption of nucleic acids to the silica support by inhibiting their attraction to water. After adsorption, purification is achieved by washing with reagents such as ethanol and the final phase is to elute the bound nucleic acids with an appropriate buffer (Barbosa *et al*., 2016). The binding capacity and extraction effectiveness are two of the many variables introduced by the different processes and techniques used by extraction kit manufacturers. The sample type and post-concentration viral integrity have a significant impact on the total effectiveness of the kit's ability to extract viral nucleic acids (Seah *et al*., 1995). Furthermore, viral nucleic acids have been extracted from influent and effluent wastewater samples using automated extractors (Di Bonito *et al*., 2017; Ibrahim *et al*., 2017), which depend largely on the adherence of the nucleic acids to the magnetic beads hence leaving contaminants in the solution. Subsequently, the magnetic beads-attached DNA is retrieved via elution (Barbosa *et al*., 2016). The capacity of this approach to process a large volume of samples quickly and consistently, resulting in less variation in the data, includes the advantages associated with the use of automated extractors (Dundas *et al*., 2008).

Taken together, the range of viral metagenomes retrieved through sequencing is greatly influenced by the adopted pre-sequencing techniques, virus concentration and extraction method. Hall *et al*., (2014), examined the effects of routinely used techniques to enhance RNA viruses on the levels of influenza A and human enterovirus. The use of centrifugation, syringe filtering, and nuclease digestion resulted in a 10-fold and 20-fold increase in the relative abundance of influenza and enterovirus, respectively, in the metagenomic data set. Also, in a viral metagenomics study, (Hjelmsø *et al*., 2017), assessed different techniques for virus concentration and extraction kits and reported that both concentration and extraction

procedures had a substantial influence on viral richness and were mutually dependent in affecting viral specificity. Therefore, extracted viral particles are generally treated with DNase or RNase to deplete free DNA and/or RNA. Ultimately, adhering to optimal methods throughout sample handling and analysis may enhance the precision of viral identification in metagenomics research.

4.3 Library preparation and sequencing

Following sample processing and nucleic acid extraction, the resulting nucleic acids undergo library preparation before the sequencing procedures. Specifically, library preparation methods are mostly influenced by the sequencing platforms (Section 2.8) being used. The commonly used sequencing technologies could be the second-generation technology that offers short reads at a very cheap cost or the third-generation platforms with longer reads, however, with trade-offs in terms of cost and accuracy (Table 1). Short-read platforms are usually adopted for applications in which accurate measurement or higher sensitivity is required via deeper sequencing, while long-read technologies enhance *de novo assembly* significantly. Additional factors that could impact the selection of a surveillance platform include its mobility, acquisition and maintenance costs (Table 1).

4.4 Bioinformatics analysis

Sequences obtained from the sequencing platforms must be processed with bioinformatics pipelines that combine high specificity and sensitivity in order to correctly detect and identify viruses present. Essentially, the bioinformatics analysis method consists of four main steps: (i) quality control (QC) (ii) read trimming, adaptor excision and additional filtering, (iii) viral genome detection and (iv) results interpretation (Lapidus and Korobeynikov, 2021). Quality

control (QC) is a very important stage in the processing of sequencing data and entails the elimination or reduction of low-quality reads and the removal of undesired sequences such as adapters and host contamination that may cause issues in subsequent analysis. The QC technique should be tailored to a particular dataset, including the inherent variations between various sequencing technologies, as short-read platforms QC protocols will be unsuitable for long-read platforms (Fukasawa *et al*., 2020).

The next step which is genome identification involves using read alignment tools to annotate genomic or metagenomic data and doing a similarity search against a reference sequence using a best-hit strategy (Wilke *et al*., 2013). High-quality reads can now be utilized to identify viral genomes using two distinct approaches: (i) aligning the reads to a reference sequence database such as the NCBI nucleotide database (nt), the non-redundant protein database (nr), or the Reference Viral Database (RVDB) (Goodacre *et al*., 2018); (ii) performing a new de novo assembly, where overlapping reads are used to construct reference genomes instead of simply mapping the reads. The fundamental idea is based on the notion that genes with homology have comparable activities. Nevertheless, a mere alteration of a single base pair in a sequence might modify the function of a protein; hence, the level of strictness used in homology-based annotation can significantly impact the interpretation and repeatability of the results (Randle-Boggis *et al*., 2016).

Although the best hit technique is often used for annotation, it tends to generate a significant number of false positives (Randle-Boggis *et al*., 2016). *De novo assembly*, which involves assembling overlapping reads rather than mapped directly to reference genomes can reduce the elevated false positive rates that often accompany best-hit strategy when short reads are

analysed. However, there are several assemblers for processing sequencing data, there is a need to be cautious in the choice of the appropriate assembler owing to the problems posed by distinct datasets (Shakya *et al*., 2019). Furthermore, the assembly process is computationally demanding, albeit constrained by the challenge of achieving enough coverage at the genome level, and has potential for several applications. These include the capacity to create genomes of species that cannot be cultivated and establishing connections between metabolism, function, and phylogeny (Quince *et al*., 2017). The large volume of sequencing data generated also poses issues in terms of processing requirements and data storage. While public repositories like the NCBI Sequence Read Archive and the European Nucleotide Archive are commonly used for storing and sharing metagenomic data, in-house analyses still demand significant computational resources; hence an easily accessible cloud-based infrastructure can be adopted to solve this challenge.

Taken together, the reviewed studies indicate that wastewater treatment facilities encompass a diverse and dynamic viral ecosystem, including both well-documented and recently unidentified viruses pertinent to public health. Although, conventional detection approaches are restricted to known targets, metagenomics enables a more comprehensive evaluation of viral diversity without prior information. Advances in sequencing technology have enhanced the identification of low-abundance viral genomes, reinforcing the use of wastewater as an effective instrument for community-level monitoring. In addition, literature suggests that further progress will depend on improved methodological consistency, enhanced bioinformatics capabilities, and more comprehensive reference databases to facilitate relaible interpretation and broader application.

5.0 Limitations and prospects in the use of metagenomics for viral identification in wastewater

Although the application of metagenomics for unveiling the viral diversity in the WWTPs has recorded significant accomplishments just like other microbes, it is not exempted from constraints. In viral metagenomics investigations, the probability of sequencing the genome of a virus in a metagenome is not limited to its size (Bibby *et al*., 2011), but encompasses the intricate interplay of viral abundance (Lewandowska *et al*., 2017), nucleic acid characteristics and adopted techniques (Jurasz *et al*., 2021), host interactions (Iša *et al*., 2022), as well as sequencing technologies (Buddle *et al*., 2024). Viral genomes are often compact, relatively tiny in size and less prevalent, particularly RNA viruses, which pose a common difficulty in identifying and quantifying them in metagenomes (Marz *et al*., 2014).

An effective strategy to address this obstacle is the collection of huge sample volumes (Rodriguez-Brito *et al*., 2010; Rosario *et al*., 2009a; Breitbart *et al*., 2002), which is time-consuming and must be completed within a certain timeframe. Furthermore, the sample matrix could affect the most effective extraction technique because the process of separating nucleic acids from complex organic matrices and carrier materials can differ depending on the specific matrix (Sanz and Köchling, 2019). Moreover, the sample biomass varies significantly depending on the matrix, and low-biomass samples like the effluent would probably need more thorough concentration compared to samples with higher microbial density like the influent. This poses difficulties for comparing different samples (influent, effluent, sludge). Therefore, the standardization of pre-processing procedures for collecting and preparing samples for viral metagenomics is crucial to avoid biasness across different wastewater systems. Unfortunately, despite taking appropriate measures throughout the sampling, concentration and nucleic acid

extraction process, there is a possibility of introducing contaminants that could degrade the genetic material.

Furthermore, a significant number of viruses possess RNA as their genetic material, which undergoes degradation at a considerably faster rate relative to DNA. In the event of RNA degradation prior to sequencing, the virome analysis runs the risk of false negatives, potentially resulting in the omission of several significant viruses. To circumvent this constraint, sequencing technologies like Illumina enhance the likelihood of detecting genomes with lower abundance by generating short reads at greater sequencing depths (Nieuwenhuijse and Koopmans, 2017). As a result, the practical implications of the research should be considered in the choice of a suitable sequencing platform. In the same vein, web-based annotation tools such as viral informatics resource for metagenome exploration (VIROME) (Wommack *et al*., 2012) and Metavir (Roux *et al*., 2014), have been developed to streamline viral annotation and support comparative analyses of viral communities across varied sample matrices.

Currently, there is no universally accepted and user-friendly pipeline specifically designed for viromes, similar to that of bacterial/archaeal 16S rRNA genes, such as QIIME, hence, extensive bioinformatics and/or computational biology expertise is often necessary for most virome processes. Furthermore, efforts have been made to address sequencing bias, the scarcity of reference databases relative to bacteria and fungi remains a major challenge.

The large volume of sequencing data generated also poses issues in terms of processing requirements and data storage. While public repositories like the NCBI Sequence Read Archive and the European Nucleotide Archive are commonly used for storing and sharing metagenomic

data, in-house analyses still demand significant computational resources hence an easily accessible cloud-based infrastructure can be adopted to solve this challenge. Fewer than 1% of viruses had been analysed and added to databases; hence more than 75% of viruses found in sewage sludge cannot be identified (Bibby and Peccia, 2013), owing to their vast unexplored viral diversity and shortcomings of existing reference databases (Gholipour *et al*., 2022).

To improve viral databases, it is necessary to isolate and cultivate viruses and then expose them to whole genome sequencing (WGS) so that a greater number of viruses can contribute to the increased diversity within databases (Prussin *et al*., 2014; Rohwer and Edwards, 2002). Unfortunately, viral cultivation remains a very cumbersome process owing to their need for a host organism, such as bacteria, for bacteriophages, while many viruses are deemed 'unculturable' utilising existing methods and techniques. Thus, metagenomic sequencing and computational methods are essential for a detailed comprehension of the viral diversity in water owing to the overwhelming majority of viruses that are unculturable (Bassi *et al*., 2022; Roux *et al*., 2021).

The quantification of viral assemblages is often constrained by the process of sample and library preparation and the need to normalize samples to ensure consistent sequencing depth while preserving community composition. Additionally, the quantity of reads acquired across different samples during sequencing naturally varies. Therefore, quantitative evaluation in metagenomics, metatranscriptomics and targeted amplicon sequencing is typically limited to a comparative approach involving normalising NGS data to a secondary metric specific to each sample such as the number of reads, percentage of total reads, or number of reads annotated as a reference gene to determine the relative abundance (Weiss *et al*., 2017; Nayfach and Pollard,

2016). Although, relative abundances offer useful insights into the composition and functional capabilities of microbial communities, risk assessments require microbial targets to be expressed as absolute counts. One way to obtain such data is to merge NGS read numbers with independent estimates of the total cell population (Vandeputte *et al*., 2017; Garner *et al*., 2016); nevertheless, further validation is conducted using qPCR. Furthermore, determining viral viability remains challenging although metatranscriptomics offered as a solution target only mRNA produced by live cells connected with actively transcribed genes which is difficult to analyze in low biomass water samples like effluents containing very low RNA concentrations that are unfortunately prone to degradation and contamination (Garner *et al*., 2021). Therefore, metagenomics may have more applicability in evaluating treated wastewater samples because, after a disinfection procedure, a significant amount of the genetic material is expected to be contained in deactivated cells or float freely outside the cells. Despite its limitations, metagenomics has offered deep insights into the viral diversity of different environments via the use of modern bioinformatics tools to overcome the drawbacks of sequencing techniques, resulting in better accuracy.

6.0 Conclusion

The conventional molecular approaches for viral identification have limitations in their ability to detect just known viruses hence the need to adopt metagenomics with the potential for unveiling novel viruses for wastewater surveillance. However, the limited quantitative capabilities and infectivity determination of viral metagenomics techniques necessitate the use of conventional confirmatory techniques like qPCR and cell culture to quantify and confirm the infectivity of detected viruses. Additionally, other challenges, such as high costs, the requirement for specialized knowledge and equipment, difficulties in data analysis and

interpretation, absence of standardized methods, and rapid advancements in technology, the compilation of different applications of viral metagenomics presented calls for more research towards improving viral metagenomics. Therefore, with proper consideration of its current limitations, viral metagenomics could be a very successful approach for unearthing both known and unknown viral diversity in wastewater when combined with other confirmatory techniques to quantity and determine their infectivity status. This could further reduce the risks associated with human exposure to these viruses which could be pathogenic because understanding the metavirome of wastewater is important for public health as it reveals the viral strains that are currently spreading in a community and serves as a sophisticated system in the discovery of novel viruses.

References

ABBASZADEGAN, M., HUBER, M. S., GERBA, C. P. & PEPPER, I. L. 1993. Detection of enteroviruses in groundwater with the polymerase chain reaction. *Applied and Environmental Microbiology,* 59**,** 1318-1324.

ADAN, A., ALIZADA, G., KIRAZ, Y., BARAN, Y. & NALBANT, A. 2017. Flow cytometry: basic principles and applications. *Critical Reviews in Biotechnology,* 37**,** 163-176.

AKACIN, I., ERSOY, Ş., DOLUCA, O. & GÜNGÖRMÜŞLER, M. 2022. Comparing the significance of the utilization of next generation and third generation sequencing technologies in microbial metagenomics. *Microbiological Research,* 264**,** 1-14.

ALHAMLAN, F., EDERER, M., BROWN, C., COATS, E. & CRAWFORD, R. 2013. Metagenomics-based analysis of viral communities in dairy lagoon wastewater. *Journal of Microbiological Methods,* 92**,** 183-188.

AMBARDAR, S., GUPTA, R., TRAKROO, D., LAL, R. & VAKHLU, J. 2016. High throughput sequencing: an overview of sequencing chemistry. *Indian Journal of Microbiology,* 56**,** 394-404.

ARTIKA, I. M., WIYATNO, A. & MA'ROEF, C. N. 2020. Pathogenic viruses: molecular detection and characterization. *Infection, Genetics and Evolution,* 81**,** 1-14.

AW, T. G., HOWE, A. & ROSE, J. B. 2014. Metagenomic approaches for direct and cell culture evaluation of the virological quality of wastewater. *Journal of Virological Methods,* 210**,** 15-21.

BARBA, M., CZOSNEK, H. & HADIDI, A. 2014. Historical perspective, development and applications of next-generation sequencing in plant virology. *Viruses,* 6**,** 106-136.

BARBOSA, C., NOGUEIRA, S., GADANHO, M. & CHAVES, S. 2016. DNA extraction: finding the most suitable method. *Molecular Microbial Diagnostic Methods.* Elsevier.

BARCELÓ I CULLERÉS, D. 2020. Wastewater-based pidemiology to monitor COVID-19 outbreak: present and future diagnostic methods to be in your radar. *Case Studies in Chemical and Environmental Engineering,* 2, 1-6.

BARRETO-VIEIRA, D. F. & BARTH, O. M. 2015. Negative and positive staining in transmission electron microscopy for virus diagnosis. *Microbiology in Agriculture and Human Health***,** 45-56.

BASSI, C., GUERRIERO, P., PIERANTONI, M., CALLEGARI, E. & SABBIONI, S. 2022. Novel virus identification through metagenomics: a systematic review. *Life*, 12(12), 1-28.

BAYLEY, H. 2015. Nanopore sequencing: from imagination to reality. *Clinical chemistry,* 61**,** 25-31.

BIBBY, K. & PECCIA, J. 2013. Identification of viral pathogen diversity in sewage sludge by metagenome analysis. *Environmental Science & Technology,* 47**,** 1945-1951.

BIBBY, K., VIAU, E. & PECCIA, J. 2011. Viral metagenome analysis to guide human pathogen monitoring in environmental samples. *Letters in Applied Microbiology,* 52**,** 386-392.

BLEIDORN, C. 2016. Third generation sequencing: technology and its potential impact on evolutionary biodiversity research. *Systematics and Biodiversity,* 14**,** 1-8.

BOSCH, A. 1998. Human enteric viruses in the water environment: a mini review. *International Microbiology,* 1**,** 191-6.

BRAGG, L. M., STONE, G., BUTLER, M. K., HUGENHOLTZ, P. & TYSON, G. W. 2013. Shining a light on dark sequencing: characterising errors in Ion Torrent PGM data. *PLoS Computational Biology,* 9(4)**,** 1-18.

BREITBART, M., SALAMON, P., ANDRESEN, B., MAHAFFY, J. M., SEGALL, A. M., MEAD, D., AZAM, F. & ROHWER, F. 2002. Genomic analysis of uncultured marine viral communities. *Proceedings of the National Academy of Sciences,* 99**,** 14250-14255.

BRINKMAN, N. E., VILLEGAS, E. N., GARLAND, J. L. & KEELY, S. P. 2018. Reducing inherent biases introduced during DNA viral metagenome analyses of municipal wastewater. *PloS one,* 13**,** e0195350.

BROWN, M., CAMÉZULI, S., DAVENPORT, R. J., PETELENZ-KURDZIEL, E., ØVREÅS, L. & CURTIS, T. 2015. Flow cytometric quantification of viruses in activated sludge. *Water Research,* 68**,** 414-422.

BROWN, M. & WITTWER, C. 2000. Flow cytometry: principles and clinical applications in hematology. *Clinical Chemistry,* 46**,** 1221-1229.

BUDDLE, S., FORREST, L., AKINSUYI, N., MARTIN BERNAL, L. M., BROOKS, T., VENTURINI, C., MILLER, C., BROWN, J. R., STOREY, N., ATKINSON, L. & BEST, T. 2024. Evaluating metagenomics and targeted approaches for diagnosis and surveillance of viruses. *Genome Medicine*, 16(1), 1–20.

CALGUA, B., BARARDI, C. R. M., BOFILL-MAS, S., RODRIGUEZ-MANZANO, J. & GIRONES, R. 2011. Detection and quantitation of infectious human adenoviruses and JC polyomaviruses in water by immunofluorescence assay. *Journal of Virological Methods,* 171**,** 1-7.

CANTALUPO, P. G., CALGUA, B. & ZHAO, G. 2011. Raw sewage harbors diverse viral populations. *mBio*, 1-11.

CHAN, M. C., LEE, N., CHAN, P. K., TO, K., WONG, R. Y., HO, W.-S., NGAI, K. L. & SUNG, J. J. 2011. Seasonal influenza A virus in feces of hospitalized adults. *Emerging Infectious Diseases,* 17(11), 2038–2042.

CHAPRON, C. D., BALLESTER, N. A., FONTAINE, J. H., FRADES, C. N. & MARGOLIN, A. B. 2000. Detection of astroviruses, enteroviruses, and adenovirus types 40 and 41 in surface waters collected and evaluated by the information collection rule and an integrated cell culture-nested PCR procedure. *Applied and Environmental Microbiology,* 66**,** 2520-2525.

CHARALAMPOUS, T., KAY, G. L., RICHARDSON, H., AYDIN, A., BALDAN, R., JEANES, C., RAE, D., GRUNDY, S., TURNER, D. J. & WAIN, J. 2019. Nanopore metagenomics enables rapid clinical diagnosis of bacterial lower respiratory infection. *Nature Biotechnology,* 37**,** 783-792.

CHEVAL, J., SAUVAGE, V., FRANGEUL, L., DACHEUX, L., GUIGON, G., DUMEY, N., PARIENTE, K., ROUSSEAUX, C., DORANGE, F. & BERTHET, N. 2011. Evaluation of high-throughput sequencing for identifying known and unknown viruses in biological samples. *Journal of Clinical Microbiology,* 49**,** 3268-3275.

CHIGOR, V. N. & OKOH, A. I. 2012. Quantitative RT-PCR detection of hepatitis A virus, rotaviruses and enteroviruses in the Buffalo River and source water dams in the Eastern

Cape Province of South Africa. *International Journal of Environmental Research and Public Health,* 9**,** 4017-4032.

CORPUZ, M. V. A., BUONERBA, A., VIGLIOTTA, G., ZARRA, T., BALLESTEROS JR, F., CAMPIGLIA, P., BELGIORNO, V., KORSHIN, G. & NADDEO, V. 2020. Viruses in wastewater: occurrence, abundance and detection methods. *Science of the Total Environment,* 745**,** 1-26.

COX, M. P., PETERSON, D. A. & BIGGS, P. J. 2010. SolexaQA: At-a-glance quality assessment of Illumina second-generation sequencing data. *BMC Bioinformatics,* 11**,** 1-6.

de la CRUZ BARRON, M., KNEIS, D., GEISSLER, M., DUMKE, R., DALPKE, A. & BERENDONK, T. U. 2023. Evaluating the sensitivity of droplet digital PCR for the quantification of SARS-CoV-2 in wastewater. *Frontiers in Public Health*, 11, 1–7.

DI BONITO, P., IACONELLI, M., GHEIT, T., TOMMASINO, M., DELLA LIBERA, S., BONADONNA, L. & LA ROSA, G. 2017. Detection of oncogenic viruses in water environments by a Luminex-based multiplex platform for high throughput screening of infectious agents. *Water Research,* 123**,** 549-555.

DÍEZ, B., ANTÓN, J., GUIXA-BOIXEREU, N., PEDRÓS-ALIÓ, C. & RODRÍGUEZ-VALERA, F. 2000. Pulsed-field gel electrophoresis analysis of virus assemblages present in a hypersaline environment. *International Microbiology,* 3**,** 159-164.

DJIKENG, A., KUZMICKAS, R., ANDERSON, N. G. & SPIRO, D. J. 2009. Metagenomic analysis of RNA viruses in a fresh water lake. *PLOS One,* 4**,** 1-14.

DOHM, J. C., LOTTAZ, C., BORODINA, T. & HIMMELBAUER, H. 2008. Substantial biases in ultra-short read data sets from high-throughput DNA sequencing. *Nucleic Acids Research,* 36(16)**,** 1-10.

DONALDSON, K., GRIFFIN, D. W. & PAUL, J. 2002. Detection, quantitation and identification of enteroviruses from surface waters and sponge tissue from the Florida Keys using real-time RT–PCR. *Water Research,* 36**,** 2505-2514.

DOWD, S. E., HALONEN, M. J. & MAIER, R. M. 2009. Immunological methods. *Environmental Microbiology.* Elsevier, 225-241.

DUNDAS, N., LEOS, N. K., MITUI, M., REVELL, P. & ROGERS, B. B. 2008. Comparison of automated nucleic acid extraction methods with manual extraction. *The Journal of Molecular Diagnostics,* 10**,** 311-316.

FALMAN, J. C., FAGNANT-SPERATI, C. S., KOSSIK, A. L., BOYLE, D. S. & MESCHKE, J. S. 2019. Evaluation of secondary concentration methods for poliovirus detection in wastewater. *Food and Environmental Virology,* 11**,** 20-31.

FANCELLO, L., RAOULT, D. & DESNUES, C. 2012. Computational tools for viral metagenomics and their application in clinical research. *Virology,* 434**,** 162-174.

FANCELLO, L., TRAPE, S., ROBERT, C., BOYER, M., POPGEORGIEV, N., RAOULT, D. & DESNUES, C. 2013. Viruses in the desert: a metagenomic survey of viral communities in four perennial ponds of the Mauritanian Sahara. *The ISME journal,* 7**,** 359-369.

FARKAS, K., HASSARD, F., MCDONALD, J. E., MALHAM, S. K. & JONES, D. L. 2017. Evaluation of molecular methods for the detection and quantification of pathogen-derived nucleic acids in sediment. *Frontiers in Microbiology,* 8**,** 1-12.

FERNÁNDEZ-BACA, C. P., SPIRITO, C. M., BAE, J. S., SZEGLETES, Z. M., BAROTT, N., SAUSELE, D. J., BROOKS, Y. M., WELLER, D. L. & RICHARDSON, R. E. 2021. Rapid qPCR-based water quality monitoring in New York state recreational waters. *Frontiers in Water,* 3**,** 1-19.

FERNANDEZ-CASSI, X., TIMONEDA, N., MARTÍNEZ-PUCHOL, S., RUSIÑOL, M., RODRIGUEZ-MANZANO, J., FIGUEROLA, N., BOFILL-MAS, S., ABRIL, J. F. & GIRONES, R. 2018. Metagenomics for the study of viruses in urban sewage as a tool for public health surveillance. *Science of the Total Environment,* 618**,** 870-880.

FONG, T.-T. & LIPP, E. K. 2005. Enteric viruses of humans and animals in aquatic environments: health risks, detection, and potential water quality assessment tools. *Microbiology and Molecular Biology Reviews,* 69**,** 357-371.

FORTERRE, P., SOLER, N., KRUPOVIC, M., MARGUET, E. & ACKERMANN, H.-W. 2013. Fake virus particles generated by fluorescence microscopy. *Trends in Microbiology,* 21**,** 1-5.

FUJIYOSHI, S., MUTO-FUJITA, A. & MARUYAMA, F. 2020. Evaluation of PCR conditions for characterizing bacterial communities with full-length 16S rRNA genes using a portable nanopore sequencer. *Scientific Reports,* 10**,** 1-10.

FUKASAWA, Y., ERMINI, L., WANG, H., CARTY, K. & CHEUNG, M.-S. 2020. LongQC: a quality control tool for third generation sequencing long read data. *G3: Genes, Genomes, Genetics,* 10**,** 1193-1196.

FUMIAN, T. M., FIORETTI, J. M., LUN, J. H., DOS SANTOS, I. A., WHITE, P. A. & MIAGOSTOVICH, M. P. 2019. Detection of norovirus epidemic genotypes in raw sewage using next generation sequencing. *Environment International,* 123**,** 282-291.

FUMIAN, T. M., LEITE, J. P. G., CASTELLO, A. A., GAGGERO, A., DE CAILLOU, M. S. L. & MIAGOSTOVICH, M. P. 2010. Detection of rotavirus A in sewage samples using multiplex qPCR and an evaluation of the ultracentrifugation and adsorption-elution methods for virus concentration. *Journal of Virological Methods,* 170**,** 42-46.

GAN, S. D. & PATEL, K. R. 2013. Enzyme immunoassay and enzyme-linked immunosorbent assay. *Journal of Investigative Dermatology,* 133**,** 1-3.

GARNER, E., DAVIS, B. C., MILLIGAN, E., BLAIR, M. F., KEENUM, I., MAILE-MOSKOWITZ, A., PAN, J., GNEGY, M., LIGUORI, K. & GUPTA, S. 2021. Next generation sequencing approaches to evaluate water and wastewater quality. *Water Research,* 194**,** 1-24.

GARNER, E., WALLACE, J. S., ARGOTY, G. A., WILKINSON, C., FAHRENFELD, N., HEATH, L. S., ZHANG, L., ARABI, M., AGA, D. S. & PRUDEN, A. 2016. Metagenomic profiling of historic Colorado Front Range flood impact on distribution of riverine antibiotic resistance genes. *Scientific Reports,* 6**,** 1-10.

GENOME WEB, 2013. Roche Shutting Down 454 Sequencing Business. 〈https://www.genomeweb.com/sequencing/roche-shutting-down-454-sequencing business#.YGb1v-gzbIV (Accessed 23 October 2024).

GENOME WEB, 2015. Thermo Fisher Launches New Systems to Focus on Plug and Play Targeted Sequencing. 〈https://www.genomeweb.com/sequencing-technology/thermo-fisher-launches-new-systems-focus-plug-and-play-targeted-sequencing〉 (Accessed 24 October 2024).

GERARDI, M. H. & ZIMMERMAN, M. C. 2004. *Wastewater pathogens*, John Wiley & Sons, 1-177.

GHOLIPOUR, S., GHALHARI, M. R., NIKAEEN, M., RABBANI, D., PAKZAD, P. & MIRANZADEH, M. B. 2022. Occurrence of viruses in sewage sludge: a systematic review. *Science of the Total Environment*, 824, 1–9.

GONZALES-GUSTAVSON, E., RUSIÑOL, M., MEDEMA, G., CALVO, M. & GIRONES, R. 2019. Quantitative risk assessment of norovirus and adenovirus for the use of reclaimed water to irrigate lettuce in Catalonia. *Water Research,* 153**,** 91-99.

GOODACRE, N., ALJANAHI, A., NANDAKUMAR, S., MIKAILOV, M. & KHAN, A. S. 2018. A reference viral database (RVDB) to enhance bioinformatics analysis of high-throughput sequencing for novel virus detection. *MSphere,* 3**,** 1-18.

GOODWIN, S., MCPHERSON, J. D. & MCCOMBIE, W. R. 2016. Coming of age: ten years of next-generation sequencing technologies. *Nature Reviews Genetics,* 17**,** 333-351.

GUAJARDO-LEIVA, S., CHNAIDERMAN, J., GAGGERO, A. & DÍEZ, B. 2020. Metagenomic insights into the sewage RNA virosphere of a large city. *Viruses,* 12(9)**,** 1-15.

GUPTA, P. K. 2008. Single-molecule DNA sequencing technologies for future genomics research. *Trends in Biotechnology,* 26**,** 602-611.

HALL, R. J., WANG, J., TODD, A. K., BISSIELO, A. B., YEN, S., STRYDOM, H., MOORE, N. E., REN, X., HUANG, Q. S. & CARTER, P. E. 2014. Evaluation of rapid and simple techniques for the enrichment of viruses prior to metagenomic virus discovery. *Journal of Virological Methods,* 195**,** 194-204.

HAMZA, I. A., JURZIK, L., ÜBERLA, K. & WILHELM, M. 2011. Evaluation of pepper mild mottle virus, human picobirnavirus and Torque teno virus as indicators of fecal contamination in river water. *Water Research,* 45**,** 1358-1368.

HAMZA, I. A., JURZIK, L. & WILHELM, M. 2014. Development of a Luminex assay for the simultaneous detection of human enteric viruses in sewage and river water. *Journal of Virological Methods,* 204**,** 65-72.

HARAMOTO, E., KITAJIMA, M., HATA, A., TORREY, J. R., MASAGO, Y., SANO, D. & KATAYAMA, H. 2018. A review on recent progress in the detection methods and prevalence of human enteric viruses in water. *Water Research,* 135**,** 168-186.

HEATHER, J. M. & CHAIN, B. 2016. The sequence of sequencers: The history of sequencing DNA. *Genomics,* 107**,** 1-8.

HEO, Y. 2015. Improving quality of high-throughput sequencing reads. *Doctoral dissertation at the University of Illinois, Urbana-Champaign*, 1-109.

HJELMSØ, M. H., HELLMÉR, M., FERNANDEZ-CASSI, X., TIMONEDA, N., LUKJANCENKO, O., SEIDEL, M., ELSÄSSER, D., AARESTRUP, F. M., LÖFSTRÖM, C. & BOFILL-MAS, S. 2017. Evaluation of methods for the concentration and extraction of viruses from sewage in the context of metagenomic sequencing. *PloS One,* 12**,** 1-17.

HOLLEY, R. W., APGAR, J., EVERETT, G. A., MADISON, J. T., MARQUISEE, M., MERRILL, S. H., PENSWICK, J. R. & ZAMIR, A. 1965. Structure of a ribonucleic acid. *Science,* 147**,** 1462-1465.

HUGGETT, J. F., COWEN, S. & FOY, C. A. 2015. Considerations for digital PCR as an accurate molecular diagnostic tool. *Clinical Chemistry,* 61**,** 79-88.

IACONELLI, M., VALDAZO-GONZÁLEZ, B., EQUESTRE, M., CICCAGLIONE, A., MARCANTONIO, C., DELLA LIBERA, S. & LA ROSA, G. 2017. Molecular characterization of human adenoviruses in urban wastewaters using next generation and Sanger sequencing. *Water Research,* 121**,** 240-247.

IBRAHIM, C., HAMMAMI, S., MEJRI, S., MEHRI, I., POTHIER, P. & HASSEN, A. 2017. Detection of Aichi virus genotype B in two lines of wastewater treatment processes. *Microbial Pathogenesis,* 109**,** 305-312.

IBRAHIM, Y., OUDA, M., KADADOU, D., BANAT, F., NADDEO, V., ALSAFAR, H., YOUSEF, A. F., BARCELÓ, D. & HASAN, S. W. 2021. Detection and removal of waterborne enteric viruses from wastewater: A comprehensive review. *Journal of Environmental Chemical Engineering***,** 9, 1-25.

IM, K., MARENINOV, S., DIAZ, M. F. P. & YONG, W. H. 2019. An introduction to performing immunofluorescence staining. Yong, W. (eds) Biobanking. *Methods in Molecular Biology*, 299-311.

IŠA, P., TABOADA, B., GARCÍA-LÓPEZ, R., BOUKADIDA, C., RAMÍREZ-GONZÁLEZ, J. E., VÁZQUEZ-PÉREZ, J. A., HERNÁNDEZ-TERÁN, A., ROMERO-ESPINOZA, J. Á., MUÑOZ-MEDINA, J. E., GRAJALES-MUÑIZ, C. & RINCÓN-RUBIO, A. 2022. Metagenomic analysis reveals differences in the co-occurrence and abundance of viral species in SARS-CoV-2 patients with different severity of disease. *BMC Infectious Diseases*, 22(1), 1–12.

JAIN, M., KOREN, S., MIGA, K. H., QUICK, J., RAND, A. C., SASANI, T. A., TYSON, J. R., BEGGS, A. D., DILTHEY, A. T., FIDDES, I. T. & MALLA, S. 2018. Nanopore sequencing and assembly of a human genome with ultra-long reads. *Nature Biotechnology*, 36(4), 338–345.

JURASZ, H., PAWŁOWSKI, T. & PERLEJEWSKI, K. 2021. Contamination issue in viral metagenomics: problems, solutions, and clinical perspectives. *Frontiers in Microbiology*, 12, 1–13.

KARGAR, M., JAVDANI, N., NAJAFI, A. & TAHAMTAN, Y. 2013. First molecular detection of group A rotavirus in urban and hospital sewage systems by nested-RT PCR in Shiraz, Iran. *Journal of Environmental Health Science and Engineering,* 11**,** 1-6.

KCHOUK, M., GIBRAT, J.-F. & ELLOUMI, M. 2017. Generations of sequencing technologies: from first to next generation. *Biology and Medicine,* 9(3), 1-8.

LAHRICH, S., LAGHRIB, F., FARAHI, A., BAKASSE, M., SAQRANE, S. & EL MHAMMEDI, M. 2021. Review on the contamination of wastewater by COVID-19 virus: impact and treatment. *Science of the Total Environment,* 751**,** 1-9.

LANREWAJU, A. A., ENITAN-FOLAMI, A. M., SABIU, S., EDOKPAYI, J. N. & SWALAHA, F. M. 2022. Global public health implications of human exposure to viral contaminated water. *Frontiers in microbiology,* 13**,** 1-18.

LAPIDUS, A. L. & KOROBEYNIKOV, A. I. 2021. Metagenomic data assembly–the way of decoding unknown microorganisms. *Frontiers in Microbiology,* 12**,** 1-16.

LAUE, M. 2010. Electron microscopy of viruses. *Methods in cell biology.* 96, 1-20.

LENNETTE, E., HALONEN, P., MURPHY, F., BALOWS, A., HAUSLER, W. & MURPHY, F. A. 1988. Virus Taxonomy and Nomenclature. *Laboratory Diagnosis of Infectious Diseases Principles and Practice: VOLUME II Viral, Rickettsial, and Chlamydial Diseases***,** 153-176.

LEWANDOWSKA, D. W., ZAGORDI, O., GEISSBERGER, F. D., KUFNER, V., SCHMUTZ, S., BÖNI, J., METZNER, K. J., TRKOLA, A. & HUBER, M. 2017. Optimization and validation of sample preparation for metagenomic sequencing of viruses in clinical samples. *Microbiome*, 5, 1–13.

LI, Y., MIYANI, B., CHILDS, K. L., SHIU, S.-H. & XAGORARAKI, I. 2024a. Effect of wastewater collection and concentration methods on assessment of viral diversity. *Science of The Total Environment,* 908**,** 1-10.

LI, Y., MIYANI, B., FAUST, R. A., DAVID, R. E. & XAGORARAKI, I. 2024b. A broad wastewater screening and clinical data surveillance for virus-related diseases in the metropolitan Detroit area in Michigan. *Human Genomics,* 18(14)**,** 1-18.

LIU, L., LI, Y., LI, S., HU, N., HE, Y., PONG, R., LIN, D., LU, L. & LAW, M. 2012a. Comparison of next-generation sequencing systems. *BioMed Research International,* 2012(1)**,** 1-11.

LIU, Y., XU, Z.-Q., ZHANG, Q., JIN, M., YU, J.-M., LI, J.-S., LIU, N., CUI, S. X., KONG, X.-Y. & WANG, H. 2012b. Simultaneous detection of seven enteric viruses associated

with acute gastroenteritis by a multiplexed Luminex-based assay. *Journal of Clinical Microbiology,* 50**,** 2384-2389.

LOGSDON, G. A., VOLLGER, M. R. & EICHLER, E. E. 2020. Long-read human genome sequencing and its applications. *Nature Reviews Genetics*, 21(10), 597–614.

LOIT, K., ADAMSON, K., BAHRAM, M., PUUSEPP, R., ANSLAN, S., KIIKER, R., DRENKHAN, R. & TEDERSOO, L. 2019. Relative performance of MinION (Oxford Nanopore Technologies) versus Sequel (Pacific Biosciences) third-generation sequencing instruments in identification of agricultural and forest fungal pathogens. *Applied and Environmental Microbiology,* 85(21)**,** 1-20.

LOPEZ-CANOVAS, L., BENITEZ, M. B. M., ISIDRON, J. A. H. & SOTO, E. F. 2019. Pulsed field gel electrophoresis: past, present, and future. *Analytical Biochemistry,* 573**,** 17-29.

LOPEZ-ROBLERO, A., MARTÍNEZ CANO, D. J., DIEGO-GARCÍA, E., GUILLÉN-NAVARRO, G. K., IŠA, P. & ZARZA, E. 2024. Metagenomic analysis of plant viruses in tropical fresh and wastewater. *Environmental DNA,* 6(416), 1-13.

MA, L., MAO, G., LIU, J., YU, H., GAO, G. & WANG, Y. 2013. Rapid quantification of bacteria and viruses in influent, settled water, activated sludge and effluent from a wastewater treatment plant using flow cytometry. *Water Science and Technology,* 68**,** 1763-1769.

MARTÍNEZ-PUCHOL, S., RUSIÑOL, M., FERNÁNDEZ-CASSI, X., TIMONEDA, N., ITARTE, M., ANDRÉS, C., ANTÓN, A., ABRIL, J. F., GIRONES, R. & BOFILL-MAS, S. 2020. Characterisation of the sewage virome: comparison of NGS tools and occurrence of significant pathogens. *Science of the Total Environment,* 713**,** 1-9.

MARZ, M., BEERENWINKEL, N., DROSTEN, C., FRICKE, M., FRISHMAN, D., HOFACKER, I. L., HOFFMANN, D., MIDDENDORF, M., RATTEI, T. & STADLER, P. F. 2014. Challenges in RNA virus bioinformatics. *Bioinformatics,* 30**,** 1793-1799.

MCCALL, C., WU, H., MIYANI, B. & XAGORARAKI, I. 2020. Identification of multiple potential viral diseases in a large urban center using wastewater surveillance. *Water Research,* 184**,** 1-13.

MCCALL, C., WU, H., O'BRIEN, E. & XAGORARAKI, I. 2021. Assessment of enteric viruses during a hepatitis outbreak in Detroit MI using wastewater surveillance and metagenomic analysis. *Journal of Applied Microbiology,* 131**,** 1539-1554.

MCCALL, C. & XAGORARAKI, I. 2019. Metagenomic approaches for detecting viral diversity in water environments. *Journal of Environmental Engineering,* 145(8)**,** 1-9.

MIKHEYEV, A. S. & TIN, M. M. 2014. A first look at the Oxford Nanopore MinION sequencer. *Molecular Ecology Resources,* 14**,** 1097-1102.

NASSONOVA, E. 2008. Pulsed field gel electrophoresis: theory, instruments and application. *Cell and Tissue Biology,* 2**,** 557-565.

NAYFACH, S. & POLLARD, K. S. 2016. Toward accurate and quantitative comparative metagenomics. *Cell,* 166**,** 1103-1116.

NEILL, J. D., BAYLES, D. O. & RIDPATH, J. F. 2014. Simultaneous rapid sequencing of multiple RNA virus genomes. *Journal of Virological Methods,* 201**,** 68-72.

NEWBY, D. T., MARLOWE, E. M. & MAIER, R. M. 2009. Nucleic acid–based methods of analysis. *Environmental Microbiology.* 243-284.

NG, T. F. F., MARINE, R., WANG, C., SIMMONDS, P., KAPUSINSZKY, B., BODHIDATTA, L., ODERINDE, B. S., WOMMACK, K. E. & DELWART, E. 2012. High variety of known and new RNA and DNA viruses of diverse origins in untreated sewage. *Journal of Virology,* 86**,** 12161-12175.

NIEUWENHUIJSE, D. F. & KOOPMANS, M. P. 2017. Metagenomic sequencing for surveillance of food-and waterborne viral diseases. *Frontiers in Microbiology,* 8**,** 1-11.

O'BRIEN, E., MUNIR, M., MARSH, T., HERAN, M., LESAGE, G., TARABARA, V. V. & XAGORARAKI, I. 2017a. Diversity of DNA viruses in effluents of membrane bioreactors in Traverse City, MI (USA) and La Grande Motte (France). *Water Research,* 111**,** 338-345.

O'BRIEN, E., NAKYAZZE, J., WU, H., KIWANUKA, N., CUNNINGHAM, W., KANEENE, J. B. & XAGORARAKI, I. 2017b. Viral diversity and abundance in polluted waters in Kampala, Uganda. *Water Research,* 127**,** 41-49.

O'CARROLL, I. P. & REIN, A. 2016. Viral nucleic acids. *Encyclopedia of Cell Biology***,** 517.

OGORZALY, L., WALCZAK, C., GALLOUX, M., ETIENNE, S., GASSILLOUD, B. & CAUCHIE, H.-M. 2015. Human adenovirus diversity in water samples using a next-generation amplicon sequencing approach. *Food and Environmental Virology,* 7**,** 112-121.

OKOH, A. I., SIBANDA, T. & GUSHA, S. S. 2010. Inadequately treated wastewater as a source of human enteric viruses in the environment. *International Journal of Environmental Research and Public Health,* 7**,** 2620-2637.

OLIVA, M., MILICCHIO, F., KING, K., BENSON, G., BOUCHER, C. & PROSPERI, M. 2020. Portable nanopore analytics: are we there yet? *Bioinformatics,* 36**,** 4399-4405.

ORTMANN, A. C. & SUTTLE, C. A. 2009. Determination of virus abundance by epifluorescence microscopy. *Bacteriophages: Methods and Protocols, Volume 1: Isolation, Characterization, and Interactions***,** 87-95.

OSUNMAKINDE, C. O., SELVARAJAN, R., SIBANDA, T., MAMBA, B. B. & MSAGATI, T. A. 2018. Overview of trends in the application of metagenomic techniques in the analysis of human enteric viral diversity in Africa's environmental regimes. *Viruses,* 10**,** 1-25.

OTAWA, K., LEE, S. H., YAMAZOE, A., ONUKI, M., SATOH, H. & MINO, T. 2007. Abundance, diversity, and dynamics of viruses on microorganisms in activated sludge processes. *Microbial Ecology,* 53**,** 143-152.

PACIFIC BIOSCIENCES, 2020a. Sequencing 101: The Evolution of DNA Sequencing Tools. 〈https://www.pacb.com/blog/the-evolution-of-dna-sequencing-tools/〉(Accessed 23 March 2021).

PACIFIC BIOSCIENCES, 2020b. Smrt Sequencing, Delivering Highly Accurate Long Reads To Drive Discovery In Life Science. 〈https://www.pacb.com/smrt-science/smrt-sequen cing/〉(Accessed 23 March 2021).

PEREZ-CATALUNA, A., CUEVAS-FERRANDO, E., RANDAZZO, W. & SANCHEZ, G. 2021. Bias of library preparation for virome characterization in untreated and treated wastewaters. *Science of The Total Environment,* 767**,** 1-8.

PETROVICH, M. L., BEN MAAMAR, S., HARTMANN, E. M., MURPHY, B. T., PORETSKY, R. S. & WELLS, G. F. 2019. Viral composition and context in metagenomes from biofilm and suspended growth municipal wastewater treatment plants. *Microbial Biotechnology,* 12**,** 1324-1336.

PILEVAR, M., KIM, K. T. & LEE, W. H. 2021. Recent advances in biosensors for detecting viruses in water and wastewater. *Journal of Hazardous Materials,* 410**,** 1-13.

PINTO, R. M., COSTAFREDA, M. I. & BOSCH, A. 2009. Risk assessment in shellfish-borne outbreaks of hepatitis A. *Applied and Environmental Microbiology,* 75**,** 7350-7355.

PRADO, T., DE CASTRO BRUNI, A., BARBOSA, M. R. F., GARCIA, S. C., DE JESUS MELO, A. M. & SATO, M. I. Z. 2019. Performance of wastewater reclamation systems in enteric virus removal. *Science of the Total Environment,* 678**,** 33-42.

PRATA, C., RIBEIRO, A., CUNHA, Â., GOMES, N. C. & ALMEIDA, A. 2012. Ultracentrifugation as a direct method to concentrate viruses in environmental waters:

virus-like particle enumeration as a new approach to determine the efficiency of recovery. *Journal of Environmental Monitoring,* 14**,** 64-70.

PRUSSIN, A. J., MARR, L. C. & BIBBY, K. J. 2014. Challenges of studying viral aerosol metagenomics and communities in comparison with bacterial and fungal aerosols. *FEMS Microbiology Letters,* 357**,** 1-9.

QIU, Y., LEE, B. E., RUECKER, N. J., NEUMANN, N., ASHBOLT, N. & PANG, X. 2016. A one-step centrifugal ultrafiltration method to concentrate enteric viruses from wastewater. *Journal of Virological Methods,* 237**,** 150-153.

QUINCE, C., WALKER, A. W., SIMPSON, J. T., LOMAN, N. J. & SEGATA, N. 2017. Shotgun metagenomics, from sampling to analysis. *Nature Biotechnology,* 35**,** 833-844.

RANDLE-BOGGIS, R. J., HELGASON, T., SAPP, M. & ASHTON, P. D. 2016. Evaluating techniques for metagenome annotation using simulated sequence data. *FEMS Microbiology Ecology,* 92(7)**,** 1-15.

REUTER, J. A., SPACEK, D. V. & SNYDER, M. P. 2015. High-throughput sequencing technologies. *Molecular Cell,* 58**,** 586-597.

RODRIGUEZ-BRITO, B., LI, L., WEGLEY, L., FURLAN, M., ANGLY, F., BREITBART, M., BUCHANAN, J., DESNUES, C., DINSDALE, E. & EDWARDS, R. 2010. Viral and microbial community dynamics in four aquatic environments. *The ISME Journal,* 4**,** 739-751.

RODRÍGUEZ, R. A., PEPPER, I. L. & GERBA, C. P. 2009. Application of PCR-based methods to assess the infectivity of enteric viruses in environmental samples. *Applied and Environmental Microbiology,* 75**,** 297-307.

ROHWER, F. & EDWARDS, R. 2002. The Phage Proteomic Tree: a genome-based taxonomy for phage. *Journal of Bacteriology,* 184**,** 4529-4535.

ROINGEARD, P., RAYNAL, P. I., EYMIEUX, S. & BLANCHARD, E. 2019. Virus detection by transmission electron microscopy: still useful for diagnosis and a plus for biosafety. *Reviews in Medical Virology,* 29(1)**,** 1-9.

ROOKS, D. J., SMITH, D. L., MCDONALD, J. E., WOODWARD, M. J., MCCARTHY, A. J. & ALLISON, H. E. 2010. 454-pyrosequencing: a molecular battiscope for freshwater viral ecology. *Genes,* 1**,** 210-226.

ROSARIO, K., NILSSON, C., LIM, Y. W., RUAN, Y. & BREITBART, M. 2009a. Metagenomic analysis of viruses in reclaimed water. *Environmental Microbiology,* 11**,** 2806-2820.

ROSARIO, K., SYMONDS, E. M., SINIGALLIANO, C., STEWART, J. & BREITBART, M. 2009b. Pepper mild mottle virus as an indicator of fecal pollution. *Applied and Environmental Microbiology,* 75**,** 7261-7267.

ROUX, S., MATTHIJNSSENS, J. & DUTILH, B. E. 2021. Metagenomics in virology. *Encyclopedia of Virology***,** 133-140.

ROUX, S., TOURNAYRE, J., MAHUL, A., DEBROAS, D. & ENAULT, F. 2014. Metavir 2: new tools for viral metagenome comparison and assembled virome analysis. *BMC Bioinformatics,* 15**,** 1-12.

SANGER, F., NICKLEN, S. & COULSON, A. R. 1977. DNA sequencing with chain-terminating inhibitors. *Proceedings of the National Academy of Sciences,* 74**,** 5463-5467.

SANTIAGO-RODRIGUEZ, T. M. & HOLLISTER, E. B. 2020. Potential applications of human viral metagenomics and reference materials: considerations for current and future viruses. *Applied and Environmental Microbiology,* 86**,** e01794-20.

SANTIAGO-RODRIGUEZ, T. M. & HOLLISTER, E. B. 2022. Unraveling the viral dark matter through viral metagenomics. *Frontiers in Immunology,* 13**,** 1-13.

SANZ, J. L. & KÖCHLING, T. 2019. Next-generation sequencing and waste/wastewater treatment: a comprehensive overview. *Reviews in Environmental Science and Bio/Technology,* 18**,** 635-680.

SATAM, H., JOSHI, K., MANGROLIA, U., WAGHOO, S., ZAIDI, G., RAWOOL, S., THAKARE, R. P., BANDAY, S., MISHRA, A. K. & DAS, G. 2023. Next-generation sequencing technology: current trends and advancements. *Biology,* 12**,** 1-25.

SCHAEFFER, J., DESDOUITS, M., BESNARD, A. & LE GUYADER, F. S. 2023. Looking into sewage: how far can metagenomics help to detect human enteric viruses? *Frontiers in Microbiology,* 14**,** 1-17.

SCHLINDWEIN, A., RIGOTTO, C., SIMÕES, C. & BARARDI, C. 2010. Detection of enteric viruses in sewage sludge and treated wastewater effluent. *Water Science and Technology,* 61**,** 537-544.

SEAH, C., CHOW, V., CHAN, Y. & DORAISINGHAM, S. 1995. A comparative, prospective study of serological, virus isolation and PCR amplification techniques for the laboratory diagnosis of dengue infection. *Serodiagnosis and Immunotherapy in Infectious Disease,* 7**,** 55-58.

SHAKYA, M., LO, C.-C. & CHAIN, P. S. 2019. Advances and challenges in metatranscriptomic analysis. *Frontiers in Genetics,* 10**,** 1-10.

SHENDURE, J. & JI, H. 2008. Next-generation DNA sequencing. *Nature Biotechnology,* 26**,** 1135-1145.

SIDHU, J. P., AHMED, W. & TOZE, S. 2013. Sensitive detection of human adenovirus from small volume of primary wastewater samples by quantitative PCR. *Journal of Virological Methods,* 187**,** 395-400.

SIMNER, P. J., KHARE, R. & WENGENACK, N. L. 2015. Rapidly growing mycobacteria. *Molecular Medical Microbiology.* 1679-1690.

STAGGEMEIER, R., BORTOLUZZI, M., HECK, T. M. D. S., SPILKI, F. R. & ALMEIDA, S. E. D. M. 2015. Quantitative vs. conventional PCR for detection of human adenoviruses in water and sediment samples. *Revista do Instituto de Medicina Tropical de São Paulo,* 57**,** 299-303.

STEWARD, G. F. 2001. Fingerprinting viral assemblages by pulsed field gel electrophoresis (PFGE). *Methods in Microbiology.* 30, 85-103.

SYMONDS, E., VERBYLA, M., LUKASIK, J., KAFLE, R., BREITBART, M. & MIHELCIC, J. 2014. A case study of enteric virus removal and insights into the associated risk of water reuse for two wastewater treatment pond systems in Bolivia. *Water Research,* 65**,** 257-270.

TAMAKI, H., ZHANG, R., ANGLY, F. E., NAKAMURA, S., HONG, P. Y., YASUNAGA, T., KAMAGATA, Y. & LIU, W. T. 2012. Metagenomic analysis of DNA viruses in a wastewater treatment plant in tropical climate. *Environmental Microbiology,* 14**,** 441-452.

TANG, A., BI, X., LI, X., LI, F., LIAO, X., ZOU, J., SUN, W. & YUAN, B. 2021. The inactivation of bacteriophage MS2 by sodium hypochlorite in the presence of particles. *Chemosphere,* 266**,** 1-8.

TANG, Y.-W., STRATTON, C. W., WU, F. & DELLA-LATTA, P. 2006. Pulsed-field gel electrophoresis. *Advanced Techniques in Diagnostic Microbiology***,** 143-157.

VAN DIJK, E. L., AUGER, H., JASZCZYSZYN, Y. & THERMES, C. 2014. Ten years of next-generation sequencing technology. *Trends in Genetics,* 30**,** 418-426.

VANDEPUTTE, D., KATHAGEN, G., D'HOE, K., VIEIRA-SILVA, S., VALLES-COLOMER, M., SABINO, J., WANG, J., TITO, R. Y., DE COMMER, L. & DARZI, Y. 2017. Quantitative microbiome profiling links gut community variation to microbial load. *Nature,* 551**,** 507-511.

VICENTE, D., CILLA, G., MONTES, M., PÉREZ-YARZA, E. G. & PÉREZ-TRALLERO, E. 2007. Human bocavirus, a respiratory and enteric virus. *Emerging Infectious Diseases,* 13(4), 636–637.

WANG, H., NEYVALDT, J., ENACHE, L., SIKORA, P., MATTSSON, A., JOHANSSON, A., LINDH, M., BERGSTEDT, O. & NORDER, H. 2020. Variations among viruses in influent water and effluent water at a wastewater plant over one year as assessed by quantitative PCR and metagenomics. *Applied and Environmental Microbiology,* 86(24)**,** 1-14.

WANG, J., ALI, Z., WANG, N., LIANG, W., LIU, H., LI, F., YANG, H., HE, L., NIE, L. & HE, N. 2015. Simultaneous extraction of DNA and RNA from Escherichia coli BL 21 based on silica-coated magnetic nanoparticles. *Science China Chemistry,* 58**,** 1774-1778.

WANG, X., LIU, J., REN, N.-Q. & DUAN, Z. 2012. Environmental profile of typical anaerobic/anoxic/oxic wastewater treatment systems meeting increasingly stringent treatment standards from a life cycle perspective. *Bioresource Technology,* 126**,** 31-40.

WANG, Y., ZHAO, Y., BOLLAS, A., WANG, Y. & AU, K. F. 2021. Nanopore sequencing technology, bioinformatics and applications. *Nature Biotechnology*, 39(11), 1348–1365.

WEIRATHER, J. L., DE CESARE, M., WANG, Y., PIAZZA, P., SEBASTIANO, V., WANG, X.-J., BUCK, D. & AU, K. F. 2017. Comprehensive comparison of Pacific Biosciences and Oxford Nanopore Technologies and their applications to transcriptome analysis. *F1000Research,* 6, 1-32.

WEISS, S., XU, Z. Z., PEDDADA, S., AMIR, A., BITTINGER, K., GONZALEZ, A., LOZUPONE, C., ZANEVELD, J. R., VÁZQUEZ-BAEZA, Y. & BIRMINGHAM, A.

2017. Normalization and microbial differential abundance strategies depend upon data characteristics. *Microbiome,* 5**,** 1-18.

WEN, K., ORTMANN, A. C. & SUTTLE, C. A. 2004. Accurate estimation of viral abundance by epifluorescence microscopy. *Applied and Environmental Microbiology,* 70**,** 3862-3867.

WHITE III, R. A., CALLISTER, S. J., MOORE, R. J., BAKER, E. S. & JANSSON, J. K. 2016. The past, present and future of microbiome analyses. *Nature Protocols,* 11**,** 2049-2053.

WILKE, A., GLASS, E., BISCHOF, J., BRAITHWAITE, D., SOUZA, M. & GERLACH, W. 2013. MG-RAST technical report and manual for version 3.3. 6–Rev 1. *Lemont, IL: Argonne National Laboratory*.

WOMMACK, K. E., BHAVSAR, J., POLSON, S. W., CHEN, J., DUMAS, M., SRINIVASIAH, S., FURMAN, M., JAMINDAR, S. & NASKO, D. J. 2012. VIROME: a standard operating procedure for analysis of viral metagenome sequences. *Standards in Genomic Sciences,* 6**,** 421-433.

WU, Q. & LIU, W.-T. 2009. Determination of virus abundance, diversity and distribution in a municipal wastewater treatment plant. *Water Research,* 43**,** 1101-1109.

XAGORARAKI, I., YIN, Z. & SVAMBAYEV, Z. 2014. Fate of viruses in water systems. *Journal of Environmental Engineering,* 140, 04014021-040140218.

XIAO, F., SUN, J., XU, Y., LI, F., HUANG, X., LI, H., ZHAO, J., HUANG, J. & ZHAO, J. 2020. Infectious SARS-CoV-2 in feces of patient with severe COVID-19. *Emerging Infectious Diseases,* 26(8), 1920–1922.

YERGEAU, E., LAWRENCE, J. R., SANSCHAGRIN, S., WAISER, M. J., KORBER, D. R. & GREER, C. W. 2012. Next-generation sequencing of microbial communities in the Athabasca River and its tributaries in relation to oil sands mining activities. *Applied and Environmental Microbiology,* 78**,** 7626-7637.

ZHANG, J., CHIODINI, R., BADR, A. & ZHANG, G. 2011. The impact of next-generation sequencing on genomics. *Journal of Genetics and Genomics,* 38**,** 95-109.

ZHU, H., YUAN, F., YUAN, Z., LIU, R., XIE, F., HUANG, L., LIU, X., JIANG, X., WANG, J. & XU, Q. 2018. Monitoring of Poyang lake water for sewage contamination using human enteric viruses as an indicator. *Virology Journal,* 15**,** 1-9.

An overview of the advancements in antiviral drug discovery and development

Adedayo Ayodeji Lanrewaju, Abimbola Motunrayo Folami, Saheed Sabiu* and Feroz Mahomed Swalaha

Department of Biotechnology and Food Science, Faculty of Applied Science, Durban University of Technology, P. O. Box 1334, Durban 4000, South Africa

*Correspondence: sabius@dut.ac.za

Abstract

Viral infectious diseases pose a persistent threat to human survival and quality of life, hindering the stability and progress of human society at large. Thus, constant efforts are being directed toward developing effective, low-toxicity therapeutics for viral diseases. Unfortunately, the limited number of clinically approved antiviral medications raises significant concerns, particularly in developing countries with reduced access to costly drugs. The unique features and behaviours of each virus require specialized pharmaceutical interventions or therapies, thereby necessitating customized treatments. The challenge is further heightened by the emergence of increasing drug-resistant variants while vaccines often provide inadequate protection against newly mutated or novel viruses. Consequently, the identification of novel antiviral agents that are both effective and cost-efficient via innovative strategies for antiviral drug discovery is essential to manage and control viral infections, as the currently available vaccines and conventional therapies are inadequate. Therefore, this review examines the different challenges associated with conventional antiviral drugs alongside recent strategies in antiviral drug discovery and development, such as the exploitation of plants' secondary metabolites with antiviral properties, advanced microscopy technologies, computer-aided drug design, artificial intelligence and machine learning, gene-editing technologies, drug combination therapy and nanotechnology-enhanced drug delivery system. Arising from the

data garnered in this review, future research needs to harness combination of emerging technologies to enhance the development of novel and effective antiviral therapeutics to address the current viral infections and be stage-ready to mitigate the emergence of new viral pandemics in the future.

Keywords: Antivirals, Drug discovery, Drug resistance, Novel drugs, Viruses

1.0 Introduction

Among the many instances of infectious disease outbreaks that humanity has faced, viral infections as demonstrated by the COVID-19 pandemic undeniably provide the most significant risk of a global pandemic in the present era (Ali *et al*., 2021). Viruses are known for their molecular mechanisms that allow them to proliferate in their host cells. Natural selection has provided them with the genetic ability to circumvent the host's defense mechanisms, ensuring the dissemination of their genetic materials and consequently their survival (Su *et al*., 2024). In addition, viruses present obstacles to broad-spectrum antiviral medications that target both RNA and DNA viruses, which can be attributed to factors such as their genomic structure (single or double genomic structure), site of replication (cytoplasm or nucleus), and the extent to which the virus relies on host proteins for its survival (Schoeman and Fielding, 2019). Unfortunately, the occurrence of epidemic outbreaks caused by newly identified and recurring viruses poses a significant risk to public health, particularly in situations when vaccines and antiviral medications are unavailable.

Antiviral therapy continues to be the fundamental approach to treatment, with a wide variety of medicines such as amantadine, oseltamivir, nevirapine, tenofovir, acyclovir (Richman and Nathanson, 2016) and vaccines such as twinrix, cervarix, fluzone, rotarix, imovax, varivax

(Ellebedy and Ahmed, 2016), which are accessible for some viral infections. Nevertheless, contemporary antiviral treatment encounters certain obstacles that hinder the efficient control of infections. The fact that more than 220 identified human viruses are in circulation, yet only few antiviral drugs have secured clinical approvals is a shortfall that raises significant concern (Cheung *et al*., 2024; Adamson *et al*., 2021), which becomes worrisome, especially in low-income countries where expensive drugs are not easily accessible. To make matters worse, each virus needs specialized pharmaceutical interventions or therapies owing to their distinct characteristics and behaviours, hence necessitating customized treatments (Kausar *et al*., 2021). Examples include antiretroviral drugs (HIV), neuraminidase inhibitors (influenza), hepatitis C (sofosbuvir, ledipasvir), herpes (acyclovir) among others. Unfortunately, the problem is worsened by drug-resistant mutants, particularly when utilizing inhibitors that target specific viral enzymes, which greatly reduces the effectiveness of the antiviral agents (Geretti *et al*., 2012; Locarnini and Yuen, 2010). Therefore, the discovery of novel antiviral drugs that are both efficient and economical to effectively manage and control viral infections in cases when vaccines and conventional treatments are insufficient becomes imperative.

The development of effective drugs for new viral diseases has required the use of very sophisticated molecules, yet the process of antiviral drug discovery development has been slow and hindered by several obstacles (Desselberger, 2000), as it took over six decades for antiviral research to reach its present widespread status in contrast to antibiotics which achieved a targeted therapeutic level within three decades (Ali *et al*., 2021). In recent decades, extensive scientific research has identified several synthetic antiviral medicines that demonstrate efficacy against a wide range of viral infectious illnesses. Regrettably, these artificial substances have been shown to generate several detrimental consequences. These consequences may include neuropsychiatric complications, comprising a continuum of mild symptoms like irritability and

sleep disruptions such as depression, psychosis, painful neuropathy and side effects that may necessitate terminating the therapy (Zareifopoulos *et al*., 2020). Occasionally, they may lose their effectiveness against newly developing virus strains that have developed resistance (Kurokawa *et al*., 2010). Given the worldwide prevalence of viral infections, development of resistance to conventional drugs and the high expense of treatment, it is imperative to urgently devise novel approaches to identify inexpensive and efficient antiviral medications.

Previously, updates in antiviral drug discovery and development have been published (Saxena *et al*., 2010; Saxena *et al*., 2009; Hangyu *et al*., 2024), however less attention has been given to cutting edge techniques like computer-aided drug design, artificial intelligence and machine learning. Not only that, advanced microscopy techniques and gene editing technologies were not sufficiently evaluated in previous reviews. Therefore, this review examines the different challenges associated with conventional antiviral drugs, alongside recent approaches in antiviral drug discovery and development, such as the exploitation of plants' secondary metabolites with antiviral properties, advanced microscopy technologies, computer-aided drug design, artificial intelligence and machine learning, gene-editing technologies, drug combination therapy and nanotechnology-enhanced drug delivery system.

2.0 Challenges associated with conventional antiviral drugs

The advent of antiviral drug resistance due to the fast genetic modification of viruses remains a major issue (Ghaebi *et al*., 2020). Viral genomes are characterized by high multiplication inside the host cell, which could result in the formation of an expanded gene pool, from which mutations could arise. The presence of antiviral drugs in these conditions exerts selection pressure, leading to the multiplication and spread of resistant viruses and consequently the

vulnerable population being replaced by the resistant viruses (Saxena *et al*., 2010). For instance, the K22 compound: (Z)-N-(3-(4-(4-bromophenyl)-4-hydroxypiperidin-1-yl)-3-oxo-1-phenylprop-1-en-2-yl)-benzamide which exhibited strong anti-CoV activity by reducing endoplasmic reticulum zippering of the virus (Bills *et al*., 2023, Ricciardi *et al*., 2022), was later reported to be ineffective against some variants of the human coronavirus 229E (HCoV-229E), known as escape mutants due to their resistance which is attributed to specific changes in the non-structural protein-6 (nsp6) of the virus (Lundin *et al*., 2014). In addition to its use for SARS and MERS, lopinavir-ritonavir which has been investigated for coronavirus disease 2019 (COVID-19) has also exhibited resistance in its initial use for treating human immunodeficiency virus (HIV) infection (Nastri *et al*., 2023; Zumla *et al*., 2016). Research has shown that although adamantanes and neuraminidase inhibitors (NAIs) are useful in the treatment of influenza, medication resistance resulting from I223V and S247 mutations renders them inappropriate for usage during the pandemic (Leung *et al*., 2024; Monto, 2006). The H274Y/H1N1 influenza A virus strain acquired resistance to oseltamivir, a commonly used antiviral medication for influenza and this resistance contributed to the spread of the H1N1 pandemic caused by the subtype hemagglutinin1 neuraminidase 1 (H1N1) (Ait-Aissa *et al*., 2018; Renzette *et al*., 2014). Lim (2017) opined that the therapy for chronic hepatitis B has significantly advanced following the introduction of nucleoside analogue therapies. Nevertheless, the extensive utilization of less powerful nucleoside analogues with lower genetic thresholds, such as lamivudine and adefovir, has resulted in the emergence of substantial resistance in the hepatitis B virus (HBV), as demonstrated by the cumulative occurrence of HBV resistance (Liver, 2012, Papatheodoridis *et al*., 2005).

Another significant challenge is viral latency. According to Speck and Ganem (2010), viral latency is characterized by the virus's ability to persist and be reversed because most antivirals

are virustatic rather than virucidal (Saxena *et al*., 2010). The tiny, enclosed RNA viral genome can integrate into the host genome and remain as archived copies without causing any symptoms due to its replicative competence. These duplicates provide the templates that might trigger a recurrence of infection when ideal circumstances are realized, generating a state of persistence. De Leo *et al*., (2020), opined that viral episome maintenance proteins (EMPs) are crucial and contribute substantially to the continuous viral life cycle. For instance, HIV-1 can create a latent infection state that is unaffected by antiretroviral drugs or immunological defences, and its latency can be reversed once the infected cell is exposed to activating stimuli (Siliciano and Greene, 2011).

Moreover, the replication and transcription processes of positive-stranded RNA viruses are intricate; hence, while designing drugs against viral infections, it is necessary to analyse their targets in detail. For instance, antiviral drug design often centres on critical core enzymes encoded by the virus, such as those linked to the replication-transcription complex (RTC) and RNA-dependent RNA polymerase (RdRp). Thus, to create novel and useful antiviral control techniques, a thorough grasp of the viral biochemistry enabled by characterizing RTCs, namely their structure and activities. In developed nations, the effectiveness of antiretroviral therapy for viral suppression is determined at the time of diagnosis by the HIV-1 genotype test, which differentiates between the various drug resistance mutations (DRMs) and transmitted DRMs (Bills *et al*., 2023; Saag *et al*., 2018; Ryom *et al*., 2016). Thus, understanding every potential target and the mechanism of action would provide researchers with information to concentrate on managing, curing, and ultimately avoiding viral infections.

Another significant drawback in the development of antiviral drugs is the elevated cost, which is expected to have a negative effect on patients in low-income nations. For instance, Iyengar *et al*., (2016), conducted a study on the pricing and affordability of hepatitis C drugs in 30 countries and reported a global variation and unaffordability. Unfortunately, developed nations are not left out of this problem; for example, when sofosbuvir was licenced for the treatment of Hepatitis C in the United Kingdom in 2014, it took one year for UK patients to get access to it owing to disputes over the price (Henry, 2018; Trooskin *et al*., 2015). Benzaken *et al*., (2019), discovered that the long-term viability of providing effective antiretroviral medication for HIV in Brazil is compromised by the unsustainably high expense cost associated with the advanced technology needed for its production and distribution, which could consequently impede patients' ability to get treated thereby impacting the global endeavour to enhance the healthcare system.

Generally, high toxicity is frequently associated with conventional drugs, of which antiviral drugs are not exempted. The lack of selectivity in antiviral medications is a significant issue as it might lead to toxicity by interfering with the activity of normal cellular enzymes and DNA synthesis (Saxena *et al*., 2010). For the treatment of human cytomegalovirus (HCMV), Minces *et al*., (2014), examined cidofovir and foscarnet in which different toxicities, including kidney injury, electrolyte imbalances, and glycaemic index (GI) disturbances were identified to be linked with foscarnet while kidney damage and neutropenia related to cidofovir (Biron, 2006). In their study, Mishima *et al*., (2020), noted that favipiravir, an antiviral medication authorized for treating influenza in Japan and investigated as a possible therapy for COVID-19, was observed to increase uric acid levels in the bloodstream. Thus, there is a significant demand for inexpensive alternative medications with minimal adverse effects, easily accessible and less toxic profiles globally.

3.0 Recent approaches in antiviral drug discovery and development

3.1 Exploitation of plants' secondary metabolites with antiviral properties

Plant secondary metabolites (PSMs) are small molecules with considerable structural diversity and biological functions (Yeshi *et al*., 2022) generated through the secondary metabolic pathways in plants (Pang *et al*., 2021). They have diverse roles in plant growth, development, innate immunity (Piasecka *et al*., 2015), defense response signalling (Isah, 2019), and response to environmental challenges (Yang *et al*., 2018). Furthermore, PSMs possess significant roles, such as deterring pests and diseases, serving as communication signals for the mutualistic relationship between plants and microbes, and altering the microbial communities that are linked to hosts (Guerrieri *et al*., 2019). Additionally, they are accountable for the pigmentation, aroma and taste of plant-based products. Throughout the years, they have shown remarkable pharmacological potential and have been used as reservoirs of lead compounds with various biological activities for managing diverse diseases (Thirumurugan *et al*., 2018). PSMs could induce therapeutic effects in humans by functioning as neurotransmitters, hormones, endogenous metabolites, signalling molecules and ligands among others (Bilal *et al*., 2017). Based on their biosynthetic origins, PSMs fall into major chemical groups including phenolics, terpenes, steroids, alkaloids, and flavonoids. Presently, approximately 200,000 distinct PSMs have been catalogued and isolated (Kessler and Kalske, 2018). Furthermore, the antiviral activity of some PSMs has been reported as an alternative therapy for the treatment or management of viral diseases owing to their reduced or minimal toxicity relative to conventional antiviral drugs. Figure 1 shows the chemical structures of some PSMs with antiviral activities. These metabolites have adopted different mechanisms of action against viruses which include: (1) preventing virus entry and attachment (Derksen *et al*., 2016; Helfer *et al*., 2014), (2) inhibiting viral replication (Manivannan *et al*., 2019), (3) inhibiting protein synthesis (Oloche *et al*., 2023; Mansouri *et al*., 2012), (4) modulating the host's immune system

(Alhazmi *et al*., 2021), (5) modulating cellular signalling pathways (Bhuiyan *et al*., 2020), and (6) directly killing of the viruses (Bhuiyan *et al*., 2020; Perez, 2003).

Specifically, sodium ferulate was reported to inhibit the influenza virus replication by triggering toll-like receptors TLR7 and TLR9 which in turn drive interferon regulatory factor 7 (IRF7) into the nucleus enhancing type-1 interferons production (Zhu *et al*., 2019). Also, chicoric acid inhibited the viral integrase enzyme essential for incorporating HIV DNA into the host genome (Robinson *et al*., 2000). Conversely, gallic acid exhibits anti-HSV-2 activity by blocking the virus the virus from attaching to host cell receptors thereby limiting its spread (Kratz *et al*., 2008). Furthermore, the immunomodulatory activities of glycyrrhizin via interferon-gamma induction and its anti-inflammatory mechanisms have been reported (Richard, 2021; Fiore *et al*., 2008). Also, it inhibits severe acute respiratory syndrome-associated coronavirus (SARS-CoV) replication and prevents the adsorption and penetration of the virus (Cinatl *et al*., 2003). Interestingly, at a minimal concentration of 0.06%, isoborneol was reported to have completely halt herpes simplex virus (HSV-1) replication. In addition, β-pinene and limonene showed potent anti-HSV-1 effects, producing a 100% loss of viral infectivity via direct contact with free virions (Astani and Schnitzler, 2014). Remarkably, celastrol reportedly inhibits the replication of dengue virus (Yu *et al*., 2017), human immunodeficiency virus (Narayan *et al*., 2011) and hepatitis C virus (Tseng *et al*., 2017). Table 1 gives a summary of different PSMs and the corresponding mode of action through which their antiviral activity was exerted against viruses.

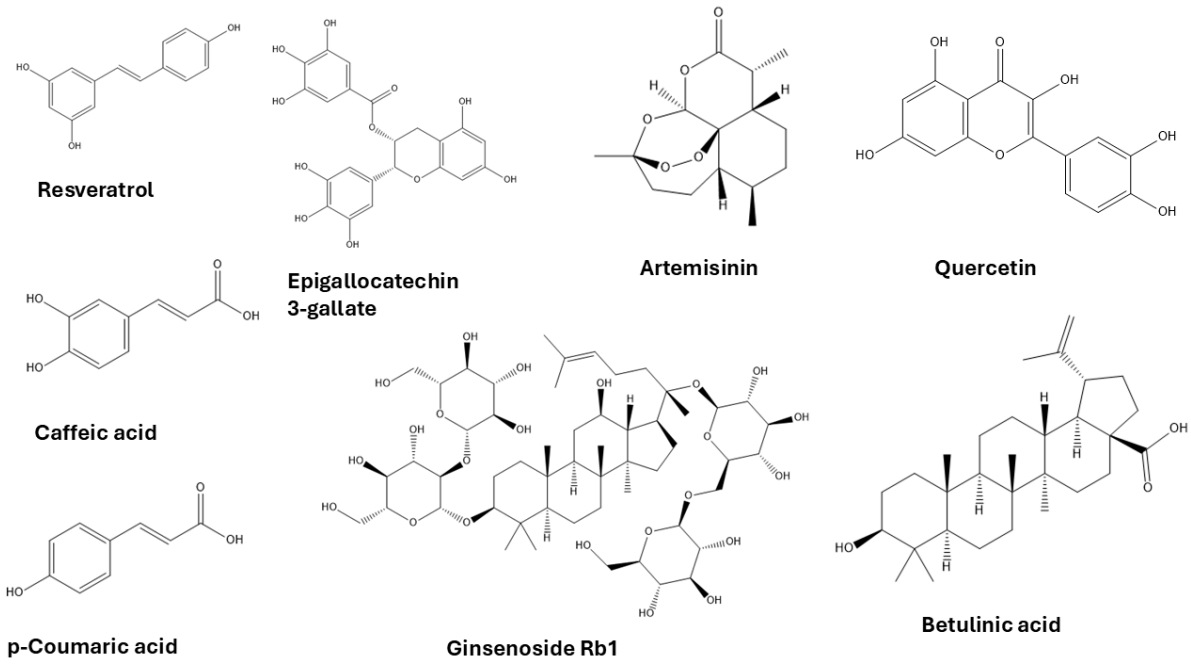


Figure 1: Chemical structures of some plant secondary metabolites with antiviral activities

Table 1: Plant secondary metabolites with antiviral activity

PSM	Virus	Mode of action	References
Caffeic acid	Influenza A virus (IAV)	Caffeic acid suppresses the growth of the virus *in vitro* by binding to viral proteins involved in replication	(Utsunomiya *et al*., 2014)
	Herpes simplex virus type 1 (HSV-1)	Caffeic acid exhibits an inhibitory effect on viral multiplication *in vitro* during the first phase of viral DNA replication via its interaction with the key replication proteins	(Zhou *et al*., 2023; Ikeda *et al*., 2011)
	Ilheus virus	From a molecular docking study, caffeic acid interacts with the allosteric site on the envelope protein of Ilheus virus potentially disrupting its function	(Saivish *et al*., 2023)
Oleanolic acid	Hepatitis C virus (HCV)	Oleanolic acid demonstrates antiviral effects by partially inhibiting the activity of HCV NS5B RNA-dependent RNA polymerase as a noncompetitive inhibitor	(Kong *et al*., 2013)
	IAV	Oleanolic acid inhibits the contact between the virus and host cells, probably by disrupting the connection between hemagglutinin and its sialic acid receptor	(Shao *et al*., 2023)

	Dengue virus (DENV)	Oleanolic acid exhibits marked affinity for the dengue virus non-structural proteins NS1 and NS5 as illustrated in a molecular docking analysis	(Kaushik *et al*., 2021)
	HSV-1	Oleanolic acid disrupts the helicase-primase machinery essential for genome replication by destabilising UL8, an important component of that complex	(Shan *et al*., 2021)
Betulinic acid	DENV	Betulinic acid restrains a post-entry phase in the replication cycle of DENV by suppressing the viral RNA synthesis and protein production	(Loe *et al*., 2020)
Dammarenolic acid	Human immunodeficiency virus type 1 (HIV-1)	Dammarenolic acid inhibits HIV-1 replication and viral infectivity	(Esimone *et al*., 2010)
Quercetin	HSV, Influenza virus, Severe acute respiratory syndrome coronavirus 2 (SARS-CoV-2)	Quercetin hinders the early phases of infection, binds with proteases critical for replication and reduce infection-induced inflammation	(Di Petrillo *et al*., 2022)
	HCV	Quercetin inhibits the virus replication by hindering oxidative/nitrosative stress and modifying PI3K-LXRα-driven lipogenesis associated with the development of steatosis and progression of the virus	(Septembre-Malaterre *et al*., 2022; Pisonero-Vaquero *et al*., 2014)
	DENV	Quercetin inhibits the activity of viral RNA polymerase, hence obstructing the replication of dengue virus 2 (DENV-2)	(Singh *et al*., 2023)
Artemisinin	SARS-CoV-2	Artemisinin binds to the Mpro of the virus through one of the catalytic residues, Cys145, thereby hindering the activity of the protein *in silico*	(Badraoui *et al*., 2022)
	IAV	Artemisinin and its derivatives inhibit the activity of PDE4, leading to an accumulation of intracellular cAMP and subsequently reducing the ERK/MAPK signalling and preventing the nuclear export of IAV viral ribonucleoprotein (vRNP).	(Yang *et al*., 2023)

Taxifolin	HCV	Taxifolin has the potential to prevent HCV entry by targeting the hepatocyte CD81 receptor; an essential gateway for viral uptake into cells as detailed in a molecular docking study	(Dey *et al*., 2023; Liu *et al*., 2023)
	HIV	Taxifolin suppresses HIV-1 during the earliest attachment/entry phase, thereby suppressing initial infection events	(Yang *et al*., 2021, Zheng *et al*., 2021)
	SARS-CoV-2	Taxifolin functions as a promising inhibitor of the Mpro of SARS-CoV-2	(Selim *et al*., 2023; Fischer *et al*., 2020)
	Ebola virus	Taxifolin binds strongly to the Ebola virus VP35 protein, establishing numerous hydrogen bonds in molecular docking and simulation analysis	(Badshah *et al*., 2021)
Kaempferol	Hepatitis B virus (HBV)	From a molecular docking analysis, kaempferol interfered with HBV by disabling the activity of HBV polymerase and core proteins	(Parvez *et al*., 2021)
	Varicella-zoster virus (VZV)	Kaempferol inhibits the virus's life cycle at the DNA replication stage, thereby stopping the infection	(Park *et al*., 2022)
	SARS-CoV-2	Kaempferol inhibits viral membrane fusion via binding to the heptad repeat (HR) segment of SARS-CoV-2 S2 subunits. Kaempferol binds to the SARS-CoV-2 protein 5R84 by forming hydrogen bonds with the amino acid residues	(Gao *et al*., 2023, Sun *et al*., 2023)
Naringenin	SARS-CoV-2	Naringenin has the potential to fight against COVID-19 by inhibiting the main viral protease 3CLpro, suppresses angiotensin-converting enzyme–mediated entry, displays notable anti-inflammatory activity, and can further impede the virus by targeting its RNA-dependent RNA polymerase	(Aleebrahim-Dehkordi *et al*., 2023, Tutunchi *et al*., 2020)
	Hepatitis C virus (HCV)	Naringenin hinders HCV proliferation by obstructing the formation of infectious viral particles inside cells before viral egress	(Goldwasser *et al*., 2011)

	Zika virus	Naringenin may interfere with the late stage of the Zika virus life cycle, perhaps serving as a non-competitive blocker of the non-structural NS2B-NS3 protease	(Cataneo *et al*., 2019)
Rosmarinic acid	Japanese encephalitis virus (JEV)	Rosmarinic acid inhibits the multiplication of JEV in the brain and dampen secondary inflammation responses driven by microglial activation.	(Swarup *et al*., 2007)
	Enterovirus A71	Rosmarinic acid inhibits EnterovirusA71 by disrupting virion engagement with the host receptor: virus-P-selectin glycoprotein ligand-1 (PSGL1) and with heparan sulphate chains on the cell surface	(Hsieh *et al*., 2020)
	IAV	Rosmarinic acid blocks IAV entry and replication by lowering GSK3β and phosphorylated AKT levels	(Jheng *et al*., 2022)
	DENV	Rosmarinic acid binds strongly to the envelope domain III (EDIII) protein, present in all four serotypes of DENV	(Panchal *et al*., 2022)
p-Coumaric acid	H1N1 influenza virus	H1N1 influenza virus was prevented from attaching to the host cells during the adsorption stage by hindering viral surface proteins from engaging their host-cell receptors thereby stopping attachment and accompanying infection	(Kim and Chung, 2018; Chojnacka *et al*., 2021,)
Baicalein	JEV	Baicalein may inhibit JEV multiplication by accumulating within host cells. Additionally, it has the potential to hinder the attachment and entrance of viruses, attach to viral RNA or engage with key JEV proteins	(Johari *et al*., 2012)
	DENV	Baicalein impedes intracellular replication of the virus, deactivating unbound DENV particles by blocking their attachment to host membranes	(Moghaddam *et al*., 2014)
	SARS-CoV-2	Baicalein suppresses the activity of Main protease (Mpro) and 3-chymotrypsin-like proteases (3CLpro)	(Liu *et al*., 2021; Song *et al*., 2021)
Excoecarianin	HSV-2, HCV	Impedes the first stage of HSV-2 replication and diminishes the virus's ability to infect, hence preventing HSV-2 infection	(Cheng *et al*., 2011)
Resveratrol	H1N1 influenza virus, Respiratory syncytial virus (RSV), SARS-CoV-2, Middle East respiratory syndrome coronavirus (MERS-CoV), Human	Resveratrol demonstrates anti-inflammatory properties and regulates the immune system via activating sirtuin-1 (Sirt-1)	(Meng *et al*., 2021; Filardo *et al*., 2020)

	rhinovirus (HRV)-16, Human metapneumovirus (HMPV)

Despite their remarkable potential antiviral activities, their advancement as medicines is frequently limited by their low solubility, bioavailability and toxicity, which results after their bioactivation (Giordano *et al*., 2023; Ponticelli *et al*., 2023). The biotransformation of PSMs has led to debate over the years with high molecules along with tannins, flavonoids and their glycosides have the potential to be adsorbed and bio-transformed by intestinal microbiota. Interestingly, various derivatizations have demonstrated effectiveness in enhancing their solubility and minimizing toxicity (Owen *et al*., 2022). Additionally, metabolic activation of various terpenoids can yield toxic intermediates making it essential to assess the safety of PSMs and their biotransformation products (Wen and Gorycki, 2019). Moreover, polyphenols have been reported to interact with multiple protein targets exhibiting broad-spectrum properties leading to an inaccurate characterization of their mechanisms of action and has been attributed to their nonspecific and promiscuous activities. This characteristic is basically attributed to chemical-photo reactivity, redox cycling, metal chelation, assay technology interferences, membrane disruption and other factors contingent upon the presence of many substructures within the interfering molecules classified as PAINS (pan-assay interference compounds). Consequently, several guidelines have been outlined to assist researchers in minimizing both financial and time loss towards investigating their bioactivity (Bisson *et al*., 2016; Baell and Walters, 2014). Obviously, PAINS is a significant concern; hence non-critical assays should not be embarked upon prior to proceeding with investigations involving these compounds. Conversely, some reports opined that some molecules categorized as PAINS do not necessarily exhibit high assay promiscuity (Capuzzi *et al*., 2017; Dimova *et al*., 2017); thus, the concept should be validated using data from different orthogonal assays rather than being applied indiscriminately (Aldrich *et al*., 2017).

3.2 Advanced microscopy technologies

Microscopy is an essential tool in contemporary bio-medical research as the only technique capable of accurately analysing the intricate spatial and temporal changes in living systems by providing the highest resolution necessary to depict biological systems in the most realistic manner (Cortese and Laketa, 2021). The primary benefit of high-throughput microscopy in drug discovery, as opposed to traditional biochemical methods, is its ability to utilize cellular assays that are more accurate in predicting *in vivo* conditions, especially compound uptake and susceptibility to intracellular metabolism. Furthermore, the capacity to multiplex several read-outs in a single test enables the evaluation of toxicity, mechanisms of action, and multiple drug profiling, thereby eliminating the need for secondary and tertiary assays (Simm *et al*., 2018). Electron microscopy (EM) has traditionally been the preferred technique for direct viral visualization. Although, super-resolution microscopy now enables nanoscale mapping of viral-protein distribution on the virion surface (Muranyi *et al*., 2013; Chojnacki *et al*., 2012), EM remains unrivalled for detailed structural and morphological insights and has played a crucial role in viral research, particularly during the COVID-19 pandemic in 2020 to investigate SARS-CoV-2 infection and pathogenesis (Cortese and Laketa, 2021). Specifically, Cryo-EM's high resolution may provide insights into the interplay between the structure and function of the viral components, leading to a better understanding of viral infection and pathogenesis. For instance, the first cryo-EM structure of the trimeric spike ectodomain of SARS-CoV-2, with a resolution of 3.5 Å was deposited in the Protein Data Bank (PDB) in late February 2020, within a span of less than 2 months following the publication of the first genome sequence of SARS-CoV-2 (Wrapp *et al*., 2020).

Precise high-resolution structures perform critical responsiblities in directing, facilitating rational drug design and elucidating the biological roles of bioactive molecules. The structure

of the SARS-CoV-2 replication and transcription complex (RTC) consisting of the viral RNA-dependent RNA polymerase (RdRp) nsp12 and several non-structural proteins, was determined using Cryo-EM by analysing the compound formed between an RNA template and the nucleoside analogue remdesivir; an antiviral drug that can block viral replication (Yin *et al*., 2020b). Therefore, this technique has facilitated drug design guided by the viral structure and the development of therapeutic antibodies that bind in the femtomolar range and the ability to neutralize the virus at picomolar concentrations (Schoof *et al*., 2020). Research on the cellular ultrastructural alterations triggered by SARS-CoV-2 has been crucial in comprehending the virus's effects on infected cells and has offered insights into possible treatment approaches (Cortese *et al*., 2020; Ogando *et al*., 2020; Wolff *et al*., 2020). Remarkably, the advanced microscopy techniques that have been developed are not specifically designed for SARS-CoV-2; instead, they can illuminate the pathophysiology of any virus with a distinct advantage for being able to act as a first line investigative tool when novel pathogens emerge. However, the main obstacle preventing the widespread use of microscopy technologies is a need for highly skilled technical experts to accurately identify the ultrastructural morphologies of viruses, while the resulting images need to be interpreted carefully as well to avoid ambiguity.

3.3 Computer-aided drug design (CADD)

Currently, there has been a growing interest in CADD methods due to their ability to address the challenges of scale, time, and cost associated with traditional experimental techniques. CADD encompasses the adoption of computational techniques to identify potential druggable targets, virtually screen massive chemical libraries for potent hits, optimize lead compounds, and analyse their potential toxicity. Therefore, it narrows the pool of compounds requiring laboratory validation while raising the odds of success by excluding candidates likely to be

inactive or harmful at an early stage (Segall and Barber, 2014). So far, CADD has already contributed to new therapeutics multiple diseases such as HIV-1 protease inhibitors such as atazanavir (Robinson *et al*., 2000), saquinavir (Krohn *et al*., 1991), indinavir (Chen *et al*., 1994), and ritonavir (Kempf *et al*., 1995), anti-cancer agent raltitrexed (Anderson, 2003)), and the antibiotic norfloxacin (Rutenber and Stroud, 1996)).

In order to make CADD methods more efficient and accurate, many methods have been designed and combined (Vamathevan *et al*., 2019) as structure-based drug discovery (SBDD) (Jhoti and Leach, 2007) and ligand-based drug discovery (LBDD) (Vidal *et al*., 2011) which are the two distinct methodologies adopted in CADD. The choice of an appropriate CADD method depends on whether detailed structural information for the target protein is available. To use the SBDD methodology, it is necessary to have structural data on the target protein, often derived from experimental methods such as nuclear magnetic resonance or X-ray crystallography (Jhoti and Leach, 2007). Predicting the three-dimensional structure of the target protein is possible using *in silico* prediction techniques, including homology modelling (Cavasotto and Phatak, 2009) or *ab initio* modelling (Wu *et al*., 2007), when the target protein is not obtainable from any of the experimental methods. Thereafter, molecular docking and structure-based virtual screening are conducted once the structure is obtained (Kitchen *et al*., 2004). When a dependable three-dimensional structure cannot be produced, either through computational modelling or experimental determination, the LBDD approach is frequently utilized as a substitute.

Using an optimized homology model of the CHIKV NSP2 protease alongside a pharmacophore model Bassetto *et al*., (2013), virtually screened a library of commercially available molecules

which resulted in several promising drug candidates that inhibited CHIKV-induced cytopathic effect formation in vero cells effectively, even at low micromolar concentrations.

Furthermore, a recent *in silico* investigation docked metabolites from corn silk and *Crescentia cujete* against spike glycoproteins of wild-type and omicron SARS-CoV-2 strains (Aribisala *et al*., 2022). The five best scoring ligands were subsequently carried forward into 100 ns molecular dynamics (MD) simulation, which confirmed that several PSMs display broader spectrum activity and stronger binding than the reference drug zafirlukast. Also, identified leads formed stable complexes with the investigated targets except kaempferol-7-glucoside. Table 2 shows a summary of commercialized antiviral drugs into which some form of computational technique was integrated into their discovery process.

Table 2: Antiviral drugs that adopted computer-aided drug design (CADD) in the discovery process

Drug	**Target**	**CAAD contribution to the discovery**	**Reference**
Saquinavir	Human immunodeficiency virus (HIV) protease	SBDD (Transition-state mimetic concept)	(Leelananda and Lindert, 2016; Van Drie, 2007)
Indinavir	HIV protease	SBDD (Transition-state mimetic concept driven by molecular modelling and X-ray crystal structure)	(Van Drie, 2007)
Ritonavir	HIV protease	SBDD, LBDD, SAR and lead optimization	(Lyle, 2007; Van Drie, 2007; Kempf *et al*., 1998,)
Delavirdine	HIV reverse transcriptase	SBDD (Virtual screening against HIV-1 RT) and LBDD (Lead optimization and SAR)	(Adams *et al*., 1998)

Nelfinavir	HIV-1 protease	LBDD (Iterative protein cocrystal structure analysis and lead optimization), Iterative SBDD and transition-state mimetic concept	(Lyle, 2007; Wlodawer and Vondrasek, 1998; Kaldor *et al*., 1997)
Efavirenz	Non-nucleoside HIV reverse transcriptase inhibitor	SBDD (Screening compounds against HIV-1 RT through computational dissimilarity analysis and lead structure optimization)	(Lyle, 2007)
Amprenavir	Antiretroviral (HIV-1) protease	SBDD, LBDD, protein modelling and molecular dynamics	(Batool *et al*., 2019; Leelananda and Lindert, 2016; Lyle, 2007)
Oseltamivir	Influenza A and B neuraminidase	Rational drug design via high-resolution X-ray crystal structures and the transition state analogue SBDD	(Lew *et al*., 2000)
Zanamivir	Influenza neuraminidase	SBDD (Active site modelling)	(Talele *et al*., 2010; Clark, 2006; Von Itzstein *et al*., 1993)
Lopinavir	HIV-1 protease	SBDD (Transition-state mimetic concept) [3D modelling and docking]	(Sham *et al*., 1998)
Atazanavir	HIV-1 protease	Computational mapping of protein binding sites and ligands docking	(Athanasiou and Cournia, 2018)
Enfuvirtide	HIV-1 protease	Homology modelling	(Athanasiou and Cournia, 2018)
Fosamprenavir	HIV-1 protease	Structure-based design	(Lyle, 2007)
Tipranavir	Nonpeptidic HIV-1 protease	Monte Carlo based automatic docking, X-ray crystallography, lead optimization	(Lyle, 2007)
Darunavir	Nonpeptidic HIV-1 protease	SBDD and LBDD	(Ghosh *et al*., 2007)
Raltegravir	HIV-1 integrase	MD and flexible ligand docking	(Schames *et al*., 2004)

Boceprevir	Hepatitis C virus (HCV)	SBDD (transition-state mimetics and SAR) using X-ray crystal structures and SAR optimization	(Njoroge *et al*., 2008)
Rilpivirine	HIV Non-nucleoside reverse transcriptase	SBDD ((homology modelling, compound screening, docking, mechanistic studies and transition state isostere modelling)	(Lyle, 2007)
Telaprevir	HCV NS3/4 A protease	Substrate-based inhibitor design and structure-based inhibitor optimization	(Rao *et al*., 2015)
Dolutegravir	HIV-1 Integrase	PBDD (two-metal binding pharmacophore structural-based design)	(Bailly and Cotelle, 2015; Kawasuji *et al*., 2013,)
Grazoprevir	HCV NS3/4 A protease	Molecular modelling and docking	(Athanasiou and Cournia, 2018)

Note: HTS: High Throughput Screening; MD: Molecular Dynamics; LBDD: Ligand-Based Drug Design; PBDD: Pharmacophore-Based Drug Design; SBDD: Structure-Based Drug Design; SAR: Structural Activity Relationship.

Generally, the influence of computational drug discovery is significant with increasing utilization and advancements in virtual screening and docking workflows, which still offers rough approximations. Consequently, molecular dynamics (MD) simulation, which offers binding affinity for protein-ligand systems, has been adopted to complement the initial screening studies. This technique applies force fields uniformly across the entire system with favourable binding energy values, which may not always align with experimental observations. Thus, quantum mechanics methods, especially density functional theory (DFT), which considers the electronic effects of interacting atoms within the systems, enable the partitioning of the system to facilitate more robust and precise quantum mechanical calculations has been integrated. This technique offers a more precise characterization of the mechanisms yielding more dependable approximations, which might be consistent with *in vitro* validations.

3.4 Artificial intelligence (AI) and machine learning (ML)

Recent physics-driven computational techniques including docking and MD simulations, capture ligand and target contacts with atomic details however, translating these atomic snapshots into reliable predictions of compound behaviour at cellular and organism level remains an enduring hurdle (Namba-Nzanguim *et al*., 2022). This is necessary to improve the translation of computational findings to *in vivo* studies, where effectiveness and ADMET liabilities could arise (Cherkasov *et al*., 2014). Several factors still limit predictive accuracy as most modelling workflows rely on relatively small, sometimes noisy datasets that span only a narrow slice of chemical space and may carry forward experimental measurement errors (Zhao, 2017; Fourches *et al*., 2010; Stouch *et al*., 2003), while only a fraction of the resulting predictions are ever validated prospectively in the wet lab (Tropsha, 2010). Also, an assumption suggesting that molecules with comparable chemical structures and target activity would have similar activities could be a drawback (Zhang *et al*., 2017), as it may not accurately predict the activities of compounds in the presence of activity cliffs (Stumpfe *et al*., 2019). To overcome these hurdles, researchers are embracing data-centric discovery pipelines enabled by AI and ML tools to model compound effects that cannot be accurately simulated using physics-based methods alone (Jayatunga *et al*., 2022; Schneider *et al*., 2020) and in developing advanced and biologically relevant similarity metrics between compounds (Fernández-Torras *et al*., 2022).

Algorithms are an integral part of ML performance in drug development; hence, selecting a learning algorithm that is best suited for the specific application is pivotal to achieving this. Artificial neural networks (ANN) (Deng *et al*., 2022; Jiménez-Luna *et al*., 2020), decision trees (DT) (Schöning and Hammann, 2018; Blower and Cross, 2006), support vector machines (SVM) (Rodríguez-Pérez and Bajorath, 2022), and cluster analysis (CA) (Jaeger and Banks,

2023; Lund and Ma, 2021; Ma *et al*., 2019), include the notable algorithms being used in machine learning. For instance, recently, Rajput and Kumar (2022) used SVM, random forest and AAN assessing each with tenfold cross-validation. The study indicated that the most accurate prediction model achieved a Pearson's correlation coefficient between 0.83 and 0.98 on the training/testing (T274) dataset. Afterwards, these models were re-validated for robustness with William's plot and were subsequently incorporated into a web server.

Five algorithms, random forest (RF), SVM, naïve Bayes (NB), k-nearest neighbour (kNN), and logistic regression, were employed to create predictive models for identifying possible inhibitors of EBOV glycoprotein and VP40, which are effective against the anti-Ebola virus (Adams *et al*., 2022). In this investigation, EBOV cell entry inhibitors from PubChem were adopted as training data RF, LR, and SVM models, achieving an overall accuracy value of 0.89, 0.84, and 0.86 respectively. The three models were then deployed as the web tool EBOLApred where a confidence metric was assigned to the projected bioactivity confirmed with the idea of applicability domain (Adams *et al*., 2022). Together, these results emphasise the essential significance of machine learning in the identification of drugs for Ebola virus (EBOV), indicating the need for more investigation.

Currently, deep learning has emerged as the predominant aspect of machine learning and is a developing method for speeding up the prediction of small molecules that are therapeutically relevant (Nag *et al*., 2022; Carpenter *et al*., 2018; Goh *et al*., 2017; Unterthiner *et al*., 2014). Deep learning techniques are often used in pattern recognition problems for their strong resilience, impressive performance, and straightforward structure, making them very effective in addressing nonlinear classification difficulties (Kwofie *et al*., 2023; Chen *et al*., 2018). Deep

learning algorithms have been leveraged to forecast inhibitors of pathogens' targets (Karki *et al*., 2021, Zhang *et al*., 2021) with the emergence of SARS-CoV-2, which has increased the urgency and importance of finding highly effective drugs to suppress the virus's activity (Beck *et al*., 2020; Bung *et al*., 2020; Zhang *et al*., 2020). Ton *et al*., (2020) introduced a new deep learning platform named Deep Docking (DD) for structure-based virtual screening to sift through 1.3 billion molecules to discover 1000 prospective inhibitors of the SARS-CoV-2 main protease (Mpro). While experimental confirmation is necessary for these anticipated molecules, they form a priority list for subsequent development. Another study used HIV-1 genomic sequence data with resistance profiles for 18 antiretroviral treatment (ART) medicines to train three deep learning models for resistance prediction in which a convolutional neural network outperformed both the multilayer perceptron and bidirectional recurrent neural networks (Steiner *et al*., 2020).

Deep learning models are successful in predicting viral inhibitors; however, they have certain limitations, such as the absence of standardised, open-source workflows for repeatability. Owing to their intricate and difficult architectures, reproducing the results of a previously conducted study are often difficult (Isdahl and Gundersen, 2019) and validating the conclusions of a study or replicate a comparable study in a different setting could be a notable obstacle for forecasting inhibitors because precise and consistent outcomes are essential. In addition, deep learning models are computationally demanding, necessitating substantial computer resources and time-consuming training (Thompson *et al*., 2020). Choosing the appropriate machine learning (ML) model from a range of predictive models may be a challenging endeavour as the effectiveness of a model might fluctuate based on the objective and dataset. Several models may exhibit strong performance on several criteria, including accuracy, precision, recall, F1 score, and AUC-ROC (Dinga *et al*., 2019). Certain models may exhibit strong performance on

a certain subset of the data but demonstrate inadequate performance on the other portions, highlighting the need to account for the underlying data distribution and feature characteristics. Additionally, it is crucial to consider the potential trade-offs between various metrics, such as a model that has a high level of precision but a poor level of recall. Therefore, when choosing a model, it is vital to carefully analyze the requirements and objectives of the work at hand (Dinga *et al*., 2019) and have comprehensive details of the data and job at hand and the specific metrics pertinent to the task.

3.5 The emergence of gene-editing technologies

Developing drugs from therapeutic compounds is difficult because viruses often exploit the host cellular machinery to replicate and spread; hence, therapeutic agents that hinder virus replication are likely to disrupt the host's normal biological processes (Rotondo *et al*., 2021). Moreover, the considerable variations in molecular features across viruses have posed substantial challenges in the development of comprehensive antiviral treatment medicines (Mehta *et al*., 2021; Adalja and Inglesby, 2019). Due to these reasons, the current development of antiviral drugs has switched its attention towards alternative tactics, namely the use of RNA interference (RNAi)-based approach (Aghamiri *et al*., 2019; Levanova and Poranen, 2018). Aside from structural proteins, the presence of nucleic acid is essential for the assembly of an infectious virion. Consequently, the successful completion of the virus life cycle within the host cell relies on the effective duplication of the viral genome. Therefore, the elimination of viral genetic components could potentially be one of the most effective antiviral approaches.

Interestingly, genome editing technologies enable the modification of specific sections in the genome. These tools provide novel strategies for treating viral infectious illnesses by manipulating DNA sequences in the genome via addition, removal, or alteration (Zhang and

Li, 2021). The primary genome editing techniques include zinc finger nucleases (ZFNs), transcriptional activator-like effector nucleases (TALENs), and clustered regularly interspersed short palindromic repeats (CRISPR) and CRISPR-associated proteins (CRISPR/Cas) (Li *et al*., 2014). However, the CRISPR/Cas system has garnered significant interest due to its ease of use, specificity and relative adaptability (Lee, 2019; Kaminski *et al*., 2016a; Kaminski *et al*., 2016b; Liao *et al*., 2015). This system has six different versions (Mohanraju *et al*., 2016), with the most significant being the type II CRISPR/Cas9 system isolated from *Streptococcus pyogenes*. Specifically, the CRISPR/Cas9 system has been proposed as a viable method for disabling target genes and inserting genetic material at precise locations in several animal models, including nonhuman primates, mice, Drosophila, and zebrafish (Sternberg and Doudna, 2015; Hsu *et al*., 2014).

Nucleases were first identified as a defensive mechanism in archaeal and bacterial species and have subsequently been repurposed as precise genome-editing instruments for manipulating nucleic acid sequences in different organisms (Mojica and Rodriguez-Valera, 2016). They have the capability to alter both viral and host genomes by modifying the sequences in DNA as well as RNA (Escalona-Noguero *et al*., 2021) and can alter many genes concurrently with high-efficiency rates (Zhou *et al*., 2014). However, relative to other sequence-specific endonucleases like TALENs and zinc-finger nucleases (ZFNs), the CRISPR-Cas system does not require the engineering, selection and validation of target site-specific protein pairs (Janusz *et al*., 2020). Instead, it utilizes tiny RNAs, which are simpler to design and more cost-effective to manufacture, for its targeted cutting ability, together with its high specificity and adaptability, making it an optimal therapeutic choice for viral infections (Najafi *et al*., 2022).

Viral infections could be lytic, latent or chronic. During the lytic phase, the virus undergoes active replication and generates virions. After the viral genomes are enclosed within protein shells (capsids), the particles are released from the host cell via lytic rupture, a process that ultimately kills that cell. Some viruses instead establish latency, entering a dormant state in which they remain transcriptionally silent for prolonged periods (Nehme *et al*., 2019; Traylen *et al*., 2011). Several human viruses, including HSV-1, Epstein-Barr virus (EBV), cytomegalovirus (CMV), human herpesvirus 6 (HHV-6), and HBV, can cause latent infections (De Leo *et al*., 2020). Chronic infection is distinguished by continuous, long-term viral replication at a low level, leading to gradual organ damage. Features of chronic infection are exhibited in significant human viruses such as HBV and HIV-1 (Tsukuda and Watashi, 2020; Fenwick *et al*., 2019).

The elimination of viruses in latent and chronic infections is challenging because the viral genome remains within host cell, either as independent minichromosomes or integrated into the host DNA. Interestingly, CRISPR-based tools can accurately target the intracellular viral genome, preventing the virus from transcribing and replicating. Thus, the CRISPR-Cas9 system has been extensively used to specifically target both human DNA [HSV-1, EBV, human papillomavirus (HPV)] and RNA [HIV, SARS-CoV-2] viruses. Scott *et al*., (2017) effectively deactivated the covalently closed circular DNA (cccDNA) in HBV-infected hNTCP-HepG2 cells by using the CRISPR/Cas system to specifically target the S open reading frame (ORF) of HBV. Also, CRISPR/Cas9 technology has been employed to cleave a 2,175-bp HBV DNA fragment that had been incorporated into the genome of infected cells (Li *et al*., 2017). Adeno-associated viral (AAV) vectors, such as AAV8 and its variants, have shown a strong affinity for the liver in these trials, thereby making them a very favourable choice for delivering the CRISPR/Cas anti-HBV treatment.

Furthermore, CRISPR-Cas complexes have the capability to hone in on RNA viruses and at least two RNA-directed CRISPR-Cas approaches are now available, one of which utilizes the Cas9 protein, though it does not naturally target RNA. Nevertheless, if a specific DNA oligomer containing the protospacer adjacent motif (PAM) may bind with the target RNA sequence to form a double-stranded target that is necessary for Cas9-mediated cleavage (O'Connell *et al*., 2014). The second platform employs Cas13, an RNase-active effector that cleaves RNA directly (Kim, 2018; Abudayyeh *et al*., 2017), and is under investigation as a therapeutic countermeasure against RNA viruses (Nguyen *et al*., 2020). Table 3 highlights present developments in the use of genome editing technologies for antiviral therapy.

Obviously, there have been notable advancements in genome editing for antiviral therapy; however, there are still considerable obstacles that need to be overcome before its practical usage. These drawbacks encompass precise DNA site targeting, off-target outcomes, selective sgRNA design, the efficacy of Cas9 cutting activity, the occurrence of HDR against NHEJ repair mechanisms, viral escape through mutation acquisition, resistance to Cas9/sgRNA system, and the choice of delivery tool (Lino *et al*., 2018; Xiao-Jie *et al*., 2015). The main obstacle in carrying out a clinical study of the CRISPR/Cas system is the unintended consequences, known as off-target effects, that may occur; hence, considering this factor while conducting *in vivo* examinations to establish the safety profile of viral vectors is imperative (Lin *et al*., 2021; Kim *et al*., 2015). Additional significant challenge for *in vivo* applications is achieving high editing fidelity while simultaneously ensuring efficient, targeted deployment of the CRISPR/Cas9 machinery.

Table 3: Summary of recent studies in the use of genome editing tools for antiviral therapy

Virus	Genome editing tool	Targets	References
Epstein-Barr Virus	CRISPR/Cas9	BART, LMP1, LMP2A	(Huo and Hu, 2019; van Diemen *et al*., 2016; Yuen *et al*., 2015)
Hepatitis B Virus	CRISPR/Cas9	cccDNA	(Seeger and Sohn, 2014)
	CRISPR/Cas9	HBV core and surface proteins	(Lin *et al*., 2014)
	CRISPR/Cas9	Core, polymerase and X ORFs	(Ramanan *et al*., 2015)
	CRISPR/Cas9	Conserved regions of the virus	(Dong *et al*., 2015)
	CRISPR/Cas9	Surface antigen (HBsAg)-encoding region of the virus	(Zhen *et al*., 2015)
	CRISPR/Cas9	DNA fragment	(Li *et al*., 2017)
	CRISPR/Cas9	S open reading frame of HBV	(Scott *et al*., 2017)
Human immunodeficiency virus (HIV)	ZFN	CCR5 gene	(Tebas *et al*., 2014)
	CRISPR/Cas9	LTR, Gag	(Kaminski *et al*., 2016a)
	CRISPR/Cas9	Proviral DNA fragment	(Bella *et al*., 2018)
	CRISPR/Cas9	Proviral SIV DNA fragment	(Mancuso *et al*., 2020)
	CRISPR/Cas12a	Relatively conserved HIV sequences including LTRs	(Gao *et al*., 2020)
	CRISPR/Cas13a	Conserved regions	(Yin *et al*., 2020a)
Human Papillomavirus HPV	CRISPR/Cas9	E6 and E7 oncogenes	(Kennedy *et al*., 2014)
	CRISPR/Cas9	HPV16 E7 gene	(Hu *et al*., 2014)

	CRISPR/Cas9	HPV16 promoter and E6 and E7 transcripts	(Zhen *et al*., 2014)
	CRISPR/Cas9	HPV16 E6 gene	(Yu *et al*., 2015)
	CRISPR/Cas9	E7 gene	(Liu *et al*., 2016)
	CRISPR/Cas9	E6 and E7	(Jubair *et al*., 2019)
SARS-CoV-2	CRISPR/Cas13d	Conserved viral regions	(Abbott *et al*., 2020)
	CRISPR/Cas13d	Peptide-coding regions of the ORF1ab and S genes	(Nguyen *et al*., 2020)

3.6 Drug combination therapy

Basically, combination therapy entails the combination of two or more drugs for the treatment of a disease condition. However, drug combinations can result in contrasting pharmacodynamic outcomes ranging from antagonistic interference or amplified toxicity to synergistic or additive therapeutic benefits (Bobrowski *et al*., 2021). While drug combinations could result in adverse effects owing to drug-drug interactions, their careful usage can yield positive outcomes. Combination therapy can facilitate targeting numerous pathways to enhance medication synergy, resulting in beneficial effects that outweigh simple additive effects. Besides therapeutic effectiveness, synergistic drug combinations enable the reduction of individual drug dosages, hence enhancing patient tolerability and reducing drug toxicity. Combination therapy has been employed against heterogeneous and multifactorial disorders that are difficult to manage including cancer, hypertension and intractable bacterial or fungal infections.

HIV infection remains a chronic disease with no curative therapies or licensed vaccines; nevertheless, major advances in treatment have enabled sustained reductions in viral load and

in AIDS-related mortality. In 1987, azidothymidine, a nucleoside reverse transcriptase inhibitor (NRTI), was the first approved antiretroviral for HIV treatment with reduced death and infection rates among patient with AIDS (Fischl *et al*., 1987). From 1987 to 1995, mono or dual NRTI therapy was the common mode of treatment; nevertheless, this treatment mode was either suboptimal or ineffective (Akanbi *et al*., 2012; Peters and Conway, 2011). Precisely, the ineffectiveness of monotherapy resulted from the development of resistance to the medication owing to the high HIV mutation rates common in RNA viruses borne out of viral genome mutations and lack of proofreading (Peters and Conway, 2011). Consequently, protease inhibitors (PI) were introduced into the HIV treatment regimen, resulting in a significant shift in the standard of care therapy. Therefore, the recognized standard treatment for HIV infections is the combination antiretroviral therapy (cART) consisting of two NRTIs and a PI has resulted in substantial reductions in HIV infection, progression to AIDS, secondary infections and death rates (Cihlar and Fordyce, 2016; Akanbi *et al*., 2012; Peters and Conway, 2011). HIV infection has become manageable with life expectancies comparable to the general population because of cART (Samji *et al*., 2013).

Just like HIV, there are no effective vaccines against HCV; nevertheless, antiviral medications have enabled a cure rate of about 95% of HCV infections, thereby lowering mortality risk due to HCV-related comorbidities (WHO, 2024). In the last two decades, HCV has been managed with non-PEGylated and subsequently PEGylated interferon (IFN), either in combination with or without the protease inhibitor ribavirin (Parlati *et al*., 2021). Unfortunately, poor clinical results were the outcomes of IFN/RBV treatment with a less than 50% cure rate contingent upon HCV genotypes and other comorbidities (Parlati *et al*., 2021; Kish *et al*., 2017). In 2011, the standard shifted to a triple regimen that added first-generation NS3/4A protease inhibitors such as telaprevir or boceprevir, lifting SVR rates to about 75 % (Pawlotsky, 2013).

Furthermore, cure rates rose to roughly 95% without an uptick in noticeable side effects after direct acting antivirals (DAAs) were introduced, notably sofosbuvir, a uridine nucleotide prodrug that targets the HCV NS5B polymerase and daclatasvir, an NS5A inhibitor (Parlati *et al*., 2021). Consequently, combination therapy shortens treatment courses while sustaining efficacy and limiting adverse events. It also offers a practical means to combat drug resistant HCV in patients presenting with additional comorbidities. Recent reports show improved response rates when novel drug cocktails were given to DAA experienced individuals who had relapsed (Belperio *et al*., 2019; Sarrazin *et al*., 2018; Bourlière *et al*., 2017). Remarkably, co-administering antiretrovirals devised for HIV/HCV coinfection produced robust HIV viral suppression and elevated HCV SVR without discernible toxicity (Huhn *et al*., 2020).

The rapid mutation rate of influenza viruses makes drug resistance possible and poses therapeutic difficulties. During the 1980s and early 2000s, extensive resistance to the adamantanes amantadine and rimantadine emerged, resulting in worldwide resistance in 45% of influenza A infections (Nguyen *et al*., 2010). While most influenza strains remain vulnerable to several neuraminidase inhibitors (Melville *et al*., 2018; Hussain *et al*., 2017), nearly universal oseltamivir resistance (98–100%) was reported among circulating viruses in the 2008–2009 season (Melville *et al*., 2018). To address this problem, multidrug regimens may be explored as the simultaneous evolution of resistance to multiple antivirals is comparatively unlikely (Perelson *et al*., 2012). Recently, Wang *et al*., (2020) showed that combination treatment may expedite recovery relative to oseltamivir only after evaluating the efficacy of the combination of favipiravir and oseltamivir against severe influenza. Generally, significant progress has been reported in the combination of free drugs for disease treatment (Komarova and Boland, 2013); however, different pharmacokinetic profiles and membrane transport properties of various active drugs coupled with the complexities of dosing and scheduling

optimization present challenges in drug combination therapy that may lead to outcomes insufficient to achieve therapeutic effects (Hu *et al*., 2010). However, significant adverse side effects could result from the concurrent use of highly potent drugs (Aditya *et al*., 2013).

3.7 Nanotechnology-enhanced drug delivery system for antiviral development

The primary causes of drug resistance are non-specific cell targeting and inadequate drug concentration at the target location, hence the renewed interest in nanotechnology, which has resulted in the formation of a smart nanotechnology-enhanced drug delivery system as an alternative for maintaining optimal drug concentration at the target site, reducing dosage frequency, enhancing drug bioavailability, mitigating drug metabolism, inhibiting cellular efflux mechanisms and improving targeted drug delivery to cells (Pradhan *et al*., 2021). The unique features that make it a promising drug delivery system include its nano dimensional configuration's improved permeability and retention effect, increased surface-area-to-volume ratio, ease of surface functionalization for cell targeting, conjugation with biocompatible molecules for prolonged circulation time (Pradhan *et al*., 2021).

Basically, antiviral medications are loaded within or adsorbed onto the nanoparticle matrices, protecting the drugs from immune clearance and have extended systemic residence period, hence improving their bioavailability and therapeutic effectiveness (Zeng *et al*., 2022; Ma *et al*., 2020; Kulkarni *et al*., 2019). Once nanoparticles (NPs) reach their target tissues, they interact with cell membranes and promote uptake through receptor engagement or targeting ligands (Donahue *et al*., 2019, Cullis *et al*., 2017; Lara *et al*., 2017; Xin *et al*., 2017; Blanco *et al*., 2015; Verma *et al*., 2008). After internalization, drug release occurs via matrix degradation, receptor-triggered unloading, or stimulus-responsive mechanisms dictated by the local

microenvironment (Chen and Feng, 2022; Islam *et al*., 2021; Vaughan *et al*., 2020; Dadfar *et al*., 2019; Ghorbani and Hamishehkar, 2017; Uva *et al*., 2015). Furthermore, the NPs delivery approach could facilitate the simultaneous delivery of multiple antiviral compounds, enabling combination delivery to boost potency and curb resistance (Li *et al*., 2022).

NPs can disrupt the interaction between viruses and host receptors by incorporating specific ligands or antibodies via surface functionalization or modification, thereby obstructing viral entry into host cells. The surface binding sites of NPs can be used to interact with target molecules to inactivate viruses. In addition, inorganic materials such as gold, silver, copper and zinc are readily assimilated by host immune cells including macrophages and dendritic cells and induce their activation to protect the host cell. The broad-spectrum virucidal activities of metal NPs against several viruses, including HIV-1, influenza virus, hepatitis B virus and herpes simplex virus, have been demonstrated (Galdiero *et al*., 2011). The molecular basis for the antiviral action of transition metals entails several pathways ranging from blocking viral entry to chemically inactivating intact virions (Singh *et al*., 2017). Specifically, metal NPs bind viral surface proteins via Kazimir forces, van der Waals interactions and disulphide exchange (Demchenko and Rusinchuk, 2019; Yadavalli and Shukla, 2017). For instance, silver nanoparticles (AgNPs) and gold nanoparticles (AuNPs) can break viral surface proteins disulphide bonds on the sulfhydryl groups, thereby blocking viral entry (Jeremiah *et al*., 2020; Kim *et al*., 2020). Cagno *et al*., (2018) developed NPs equipped with long flexible linkers that mimic heparan-sulfate proteoglycans; the multivalent attachment of these repeating motifs exerts forces of 190 pN, irreversibly deforming virions (Reina *et al*., 2020). Likewise, porous gold nanoparticles covalently tethered to hyaluronic acid via Au–Sulphide bonds hinder membrane fusion and subsequent internalization, rendering influenza virus non-infectious (Kim *et al*., 2020).

In addition, NPs can exert intracellular antiviral activity by directly associating with viral DNA or RNA. For instance, AgNPs inhibit viral reverse transcription by complexing with sulphur and oxygen bearing thiol, phosphate, and amino groups on nucleic acids or by attaching directly to the genome itself (Galdiero *et al*., 2011). Glutathione (GSH)-capped Ag_2S inhibits the synthesis of viral negative-sense RNA and the antiparasitic ivermectin has likewise been shown to impede viral genome replication. A clinical study indicates that the topical application of an ivermectin mucosal adhesion nano-suspension nasal spray is safe and effective for treating patients with mild COVID-19. Respiratory manifestations, including loss of olfactory sensation, coughing and dyspnoea, can be swiftly restored in patients after treatment (Aref *et al*., 2021).

Furthermore, NPs facilitate the induction of IFN-stimulated genes (ISGs) and pro-inflammatory cytokines, blocking porcine epidemic diarrhoea virus infection (Du *et al*., 2018). Nanovectors can obstruct the virus-receptors encounter, thus preventing viral entry using mechanisms like receptor mimicry, steric hindrance and chemical competition. Receptor mimicry involves the design of a nanocarrier that possesses structural or surface properties like those of the viral ligand, facilitating the nanocarrier's binding to the virus and stimulating its interaction with the receptor. The nanocarrier can inhibit normal interaction by binding to the virus competitively. For example, AgNPs inhibit the HIV gp 120-CD4 association and curb infection by interacting with sulphur and oxygen-bearing thiol and phosphate groups on nucleic acids and proteins or binding to DNA or RNA directly to slow viral reverse transcription rate (Galdiero *et al*., 2011).

Similar to nucleic acid inhibitors, ribavirin NPs exhibit prolonged (>4 months) suppression of HIV replication in the rectal tissue, as evidenced by a Phase 1 study ($p<0.0001$) (NCT01656018) (McGowan *et al*., 2016). Positively charged ZnO NPs, in turn block SARS-CoV-2 and host cell receptors, thereby disrupting virus-host attachment (Alavi *et al*., 2022; Hamdi *et al*., 2021). The nano carrier's presence can result in the formation of additional space, enabling competition with the virus for binding sites on the cell receptor; consequently, the virus cannot bind effectively with the host's cell receptor. NPs can trigger targeted immune responses to enhance viral identification and elimination by immune cells and are capable of activating pattern recognition receptors (PRRs) and inducing interferon (IFN) production. The surface structure and composition of NPs can directly interact with PPRs, thereby activating their signalling pathways. Montague *et al*., (2021), observed that surface-charged NPs can interact via charge dynamics, facilitating their binding and activation of platelet glycoprotein receptors, allowing them to operate as PPRs for both host and pathogen derived charged ligands. Conversely, some nanocarriers are also internalized by immune cells; once inside, their released components engage intracellular PRRs and trigger signalling cascades that activate the cells and amplify immune responses. Remarkably, certain nanomaterials stimulate PRRs without the need for phagocytic uptake. For example, Yazdi *et al.,* (2010), showed that titanium-dioxide NPs directly activate the NLRP3 inflammasome, driving intracellular IL-1α and IL-1β release and contributing to pulmonary inflammation.

Furthermore, NPs may regulate immune responses by inhibiting and overproduction of reactive oxygen species (ROS). Viral infection-induced intracellular ROS inhibits natural immunity; thus, inhibitors that reduce ROS levels may effectively halt viral proliferation. Glycyrrhizic-acid-based carbon dots regulate intracellular ROS levels to hinder porcine reproductive and respiratory syndrome virus (PRRSV) replication (Tong *et al*., 2020). Also, oseltamivir-

modified AgNPs reduced phosphorylated p53 and total p53 levels in MDCK cells significantly via the activation of ROS-mediated AKT and p53 phosphorylation pathways when its ability to inhibit virus activity was investigated (Li *et al*., 2016). Therefore, the utilization of nanotechnology in antiviral research extends beyond enhancing the delivery of antiviral drugs; it also involves the obstruction of viral infections and stimulation of immune responses, offering new strategies and approaches and bringing renewed hope for the treatment of viral diseases.

Despite numerous advantages linked with the application of nanotechnology for antiviral therapy, some challenges need to be addressed for optimal application of this technology. Toxicity is one of the topical issues that must not be disregarded as metal NPs exhibit toxicity, resulting in mitochondrial and DNA damage (Xiong *et al*., 2022; Bhargava *et al*., 2021; Buchman *et al*., 2019). Organs characterized by rapid perfusion, including the kidneys, liver, lungs and spleen, are vulnerable to NP accumulation and resultant damage (Mitchell *et al*., 2021, Li *et al*., 2020). Particle size has been demonstrated as a crucial factor affecting nanotoxicity (Liu *et al*., 2022; Egbuna *et al*., 2021); hence, manipulating the size and morphology of NPs can reduce their toxicity and subsequently influence their biodistribution, biodegradability and cellular uptake capabilities.

Another challenge is the existence of various barriers in humans, such as blood circulation, immune system clearance and cell membrane blockage, all of which may restrict the delivery efficiency and targeting of NPs. For instance, the most utilized method of drug administration is oral delivery; unfortunately, the acidic environment and several degradative enzymes residing in the gastrointestinal tract (GI) might impede the absorption of certain drugs resulting

in low stability and bioavailability (Ejazi *et al*., 2023; Wang *et al*., 2023; Beatty and Lewis, 2019; Poon *et al*., 2019; Desai, 2012). Consequently, it becomes cumbersome for such drugs to reach therapeutic levels in the bloodstream; thus, there is a need for dedicated research on non-intrusive or less intrusive techniques for their administration.

The stability of nanomaterials during preparation, storage and application influenced by the preparation method, environmental conditions such as temperature, humidity and light and *in vivo* factors like pH and enzyme is a significant concern (Ruan *et al*., 2022; Verma *et al*., 2021; Chen *et al*., 2019). The instability of the nanomaterials could result in increased toxicity and other negative effects as they accumulate or deteriorate in the environment, thereby impacting their efficacy and long-term effects. Specifically, ivermectin exhibits significant antiviral action against the zika virus; however, further progress on its nano drug is hindered due to its poor water solubility and the potential impact of specific formulations on its pharmacokinetic profile, which may alter plasma kinetics (Caparco *et al*., 2023; Surnar *et al*., 2019). Additionally, some NPs not toxic in the short term could become toxic with prolonged exposure; hence, modifying the production procedure or developing a stabilizer could address these issues (Tian *et al*., 2022; Kang *et al*., 2018).

Due to their distinctive features and accompanying risks, the application of nanomaterials encounters regulatory and ethical challenges; robust oversight frameworks must therefore be established to guarantee safety and compliance with standards. In light of prospective clinical translation efforts, drugs incorporating NPs must be produced in strict accordance with established specifications (Yu *et al*., 2019). Consequently, rigorous, standardised evaluations

of nanodrug efficacy, safety, and quality benchmarked against conventional medicines are essential to secure comparable therapeutic outcomes.

4.0 Conclusion and future perspectives

Taken together, this study highlights that, despite substantial progress in antiviral drug discovery, current therapeutic options remain limited relative to the diversity and rapid evolution of viral pathogens, with drug resistance and virus-specific treatment strategies posing persistent challenges. Emerging approaches, including plant-derived compounds, computer-aided drug design, artificial intelligence, gene-editing technologies and nanotechnology-based delivery systems, show considerable promise but are often constrained by limited clinical validation and fragmented application. Collectively, the evidence indicates that future progress in antiviral development will depend on the coordinated application of these strategies, alongside the prioritisation of broad-spectrum antiviral targets, improved standardisation of evaluation frameworks and increased focus on cost-effective therapies to enhance global accessibility.

The recent COVID-19 pandemic underscores the urgency of advancing antiviral development to effectively address emerging viral threats. In this context, multidisciplinary approaches will be essential to overcome current barriers and accelerate therapeutic innovation. This study outlines the challenges associated with conventional antiviral drugs and examines several emerging strategies for the development of novel antiviral agents aimed at enhancing anti-drug resistance profiles and potency. While these approaches offer significant potential, further validation and optimisation are required to support their clinical translation. The integration of medicinal chemistry with bioinformatics, artificial intelligence, gene-editing technology and

nanotechnology may facilitate the exploration of new drug indications. The establishment of rapid drug screening systems, along with reliable safety and effective evaluation systems, will accelerate the development of antiviral drugs. Future research should prioritise the systematic combination of these technologies to improve both efficacy and accessibility of antiviral therapeutics.

References

ABBOTT, T. R., DHAMDHERE, G., LIU, Y., LIN, X., GOUDY, L., ZENG, L., CHEMPARATHY, A., CHMURA, S., HEATON, N. S. & DEBS, R. 2020. Development of CRISPR as an antiviral strategy to combat SARS-CoV-2 and influenza. *Cell,* 181**,** 865-876.

ABUDAYYEH, O. O., GOOTENBERG, J. S., ESSLETZBICHLER, P., HAN, S., JOUNG, J., BELANTO, J. J., VERDINE, V., COX, D. B., KELLNER, M. J. & REGEV, A. 2017. RNA targeting with CRISPR–Cas13. *Nature,* 550**,** 280-284.

ADALJA, A. & INGLESBY, T. 2019. Broad-spectrum antiviral agents: a crucial pandemic tool. *Expert review of Anti-infective Therapy,* 17**,** 467-470.

ADAMS, J., AGYENKWA-MAWULI, K., AGYAPONG, O., WILSON, M. D. & KWOFIE, S. K. 2022. EBOLApred: A machine learning-based web application for predicting cell entry inhibitors of the Ebola virus. *Computational Biology and Chemistry,* 101**,** 1-10.

ADAMS, W. J., ARISTOFF, P. A., JENSEN, R. K., MOROZOWICH, W., ROMERO, D. L., SCHINZER, W. C., TARPLEY, W. G. & THOMAS, R. C. 1998. Discovery and development of the BHAP nonnucleoside reverse transcriptase inhibitor delavirdine mesylate. *Integration of Pharmaceutical Discovery and Development: Case Histories***,** 285-312.

ADAMSON, C. S., CHIBALE, K., GOSS, R. J., JASPARS, M., NEWMAN, D. J. & DORRINGTON, R. A. 2021. Antiviral drug discovery: preparing for the next pandemic. *Chemical Society Reviews,* 50**,** 3647-3655.

ADITYA, N., VATHSALA, P., VIEIRA, V., MURTHY, R. & SOUTO, E. 2013. Advances in nanomedicines for malaria treatment. *Advances in Colloid and Interface Science,* 201**,** 1-17.

AGHAMIRI, S., JAFARPOUR, A., MALEKSHAHI, Z. V., MAHMOUDI GOMARI, M. & NEGAHDARI, B. 2019. Targeting siRNA in colorectal cancer therapy: nanotechnology comes into view. *Journal of Cellular Physiology,* 234**,** 14818-14827.

AIT-AISSA, A., DERRAR, F., HANNOUN, D., GRADI, E. A., SCARAVELLI, D. & BOUSLAMA, Z. 2018. Surveillance for antiviral resistance among influenza viruses circulating in Algeria during five consecutive influenza seasons (2009-2014). *Journal of Medical Virology,* 90**,** 844-853.

AKANBI, M. O., SCARSI, K., TAIWO, B. & MURPHY, R. L. 2012. Combination nucleoside/nucleotide reverse transcriptase inhibitors for treatment of HIV infection. *Expert Opinion on Pharmacotherapy,* 13**,** 65-79.

ALAVI, M., KAMARASU, P., MCCLEMENTS, D. J. & MOORE, M. D. 2022. Metal and metal oxide-based antiviral nanoparticles: Properties, mechanisms of action, and applications. *Advances in Colloid and Interface Science,* 306**,** 1-16.

ALDRICH, C., BERTOZZI, C., GEORG, G. I., KIESSLING, L., LINDSLEY, C., LIOTTA, D., MERZ JR, K. M., SCHEPARTZ, A. & WANG, S. 2017. The ecstasy and agony of assay interference compounds. *ACS Chemical Neuroscience*, 8(3), 420–423.

ALEEBRAHIM-DEHKORDI, E., GHOSHOUNI, H., KOOCHAKI, P., ESMAILI-DEHKORDI, M., ALEEBRAHIM, E., CHICHAGI, F., JAFARI, A., HANAEI, S., HEIDARI-SOURESHJANI, E. & REZAEI, N. 2023. Targeting the vital non-structural

proteins (NSP12, NSP7, NSP8 and NSP3) from SARS-CoV-2 and inhibition of RNA polymerase by natural bioactive compound naringenin as a promising drug candidate against COVID-19. *Journal of Molecular Structure,* 1287**,** 1-14.

ALHAZMI, H. A., NAJMI, A., JAVED, S. A., SULTANA, S., AL BRATTY, M., MAKEEN, H. A., MERAYA, A. M., AHSAN, W., MOHAN, S. & TAHA, M. M. 2021. Medicinal plants and isolated molecules demonstrating immunomodulation activity as potential alternative therapies for viral diseases including COVID-19. *Frontiers in Immunology,* 12**,** 1-24.

ALI, S. I., SHEIKH, W. M., RATHER, M. A., VENKATESALU, V., MUZAMIL BASHIR, S. & NABI, S. U. 2021. Medicinal plants: treasure for antiviral drug discovery. *Phytotherapy Research,* 35**,** 3447-3483.

ANDERSON, A. C. 2003. The process of structure-based drug design. *Chemistry & Biology,* 10**,** 787-797.

AREF, Z. F., BAZEED, S. E. E. S., HASSAN, M. H., HASSAN, A. S., RASHAD, A., HASSAN, R. G. & ABDELMAKSOUD, A. A. 2021. Clinical, biochemical and molecular evaluations of ivermectin mucoadhesive nanosuspension nasal spray in reducing upper respiratory symptoms of mild COVID-19. *International Journal of Nanomedicine***,** 4063-4072.

ARIBISALA, J. O., ARUWA, C. E., UTHMAN, T. O., NURAIN, I. O., IDOWU, K. & SABIU, S. 2022. Cheminformatics bioprospection of broad spectrum plant secondary metabolites targeting the spike proteins of omicron variant and wild-type SARS-CoV-2. *Metabolites,* 12(982), 1-26.

ASTANI, A. & SCHNITZLER, P. 2014. Antiviral activity of monoterpenes beta-pinene and limonene against herpes simplex virus *in vitro*. *Iranian Journal of Microbiology,* 6(3), 149–155.

ATHANASIOU, C. & COURNIA, Z. 2018. From computers to bedside: Computational chemistry contributing to FDA approval. *Biomolecular Simulations in Structure-Based Drug Discovery***,** 163-203.

BADRAOUI, R., SAOUDI, M., HAMADOU, W. S., ELKAHOUI, S., SIDDIQUI, A. J., ALAM, J. M., JAMAL, A., ADNAN, M., SULIEMEN, A. M. & ALRESHIDI, M. M. 2022. Antiviral effects of artemisinin and its derivatives against SARS-CoV-2 main protease: Computational evidences and interactions with ACE2 allelic variants. *Pharmaceuticals,* 15**,** 1-14.

BADSHAH, S. L., FAISAL, S., MUHAMMAD, A., POULSON, B. G., EMWAS, A. H. & JAREMKO, M. 2021. Antiviral activities of flavonoids. *Biomedicine & Pharmacotherapy,* 140**,** 1-29.

BAELL, J. & WALTERS, M. A. 2014. Chemistry: Chemical con artists foil drug discovery. *Nature,* 513**,** 481-483.

BAILLY, F. & COTELLE, P. 2015. The preclinical discovery and development of dolutegravir for the treatment of HIV. *Expert Opinion on Drug Discovery,* 10**,** 1243-1253.

BASSETTO, M., DE BURGHGRAEVE, T., DELANG, L., MASSAROTTI, A., COLUCCIA, A., ZONTA, N., GATTI, V., COLOMBANO, G., SORBA, G. & SILVESTRI, R. 2013. Computer-aided identification, design and synthesis of a novel series of compounds with selective antiviral activity against chikungunya virus. *Antiviral Research,* 98**,** 12-18.

BATOOL, M., AHMAD, B. & CHOI, S. 2019. A structure-based drug discovery paradigm. *International Journal of Molecular Sciences,* 20(11)**,** 1-18.

BEATTY, P. H. & LEWIS, J. D. 2019. Cowpea mosaic virus nanoparticles for cancer imaging and therapy. *Advanced Drug Delivery Reviews,* 145**,** 130-144.

BECK, B. R., SHIN, B., CHOI, Y., PARK, S. & KANG, K. 2020. Predicting commercially available antiviral drugs that may act on the novel coronavirus (SARS-CoV-2) through a drug-target interaction deep learning model. *Computational and Structural Biotechnology Journal,* 18**,** 784-790.

BELLA, R., KAMINSKI, R., MANCUSO, P., YOUNG, W.-B., CHEN, C., SARIYER, R., FISCHER, T., AMINI, S., FERRANTE, P. & JACOBSON, J. M. 2018. Removal of HIV DNA by CRISPR from patient blood engrafts in humanized mice. *Molecular Therapy-Nucleic Acids,* 12**,** 275-282.

BELPERIO, P. S., SHAHOUMIAN, T. A., LOOMIS, T. P. & BACKUS, L. I. 2019. Real-world effectiveness of sofosbuvir/velpatasvir/voxilaprevir in 573 direct-acting antiviral experienced hepatitis C patients. *Journal of Viral Hepatitis,* 26**,** 980-990.

BENZAKEN, A. S., PEREIRA, G. F., COSTA, L., TANURI, A., SANTOS, A. F. & SOARES, M. A. 2019. Antiretroviral treatment, government policy and economy of HIV/AIDS in Brazil: is it time for HIV cure in the country? *AIDS Research and Therapy,* 16**,** 1-7.

BHARGAVA, A., DEV, A., MOHANBHAI, S. J., PAREEK, V., JAIN, N., CHOUDHURY, S. R., PANWAR, J. & KARMAKAR, S. 2021. Pre-coating of protein modulate patterns of corona formation, physiological stability and cytotoxicity of silver nanoparticles. *Science of the Total Environment,* 772**,** 1-12.

BHUIYAN, F. R., HOWLADER, S., RAIHAN, T. & HASAN, M. 2020. Plants metabolites: possibility of natural therapeutics against the COVID-19 pandemic. *Frontiers in Medicine,* 7**,** 1-26.

BILAL, M., RASHEED, T., IQBAL, H. M., HU, H., WANG, W. & ZHANG, X. 2017. Macromolecular agents with antimicrobial potentialities: A drive to combat antimicrobial resistance. *International Journal of Biological Macromolecules,* 103**,** 554-574.

BILLS, C., XIE, X. & SHI, P.-Y. 2023. The multiple roles of nsp6 in the molecular pathogenesis of SARS-CoV-2. *Antiviral Research,* 213**,** 1-10.

BIRON, K. K. 2006. Antiviral drugs for cytomegalovirus diseases. *Antiviral Research,* 71**,** 154-163.

BISSON, J., MCALPINE, J. B., FRIESEN, J. B., CHEN, S.-N., GRAHAM, J. & PAULI, G. F. 2016. Can invalid bioactives undermine natural product-based drug discovery? *Journal of Medicinal Chemistry,* 59**,** 1671-1690.

BLANCO, E., SHEN, H. & FERRARI, M. 2015. Principles of nanoparticle design for overcoming biological barriers to drug delivery. *Nature Biotechnology,* 33**,** 941-951.

BLOWER, P. E. & CROSS, K. P. 2006. Decision tree methods in pharmaceutical research. *Current Topics in Medicinal Chemistry,* 6**,** 31-39.

BOBROWSKI, T., CHEN, L., EASTMAN, R. T., ITKIN, Z., SHINN, P., CHEN, C. Z., GUO, H., ZHENG, W., MICHAEL, S. & SIMEONOV, A. 2021. Synergistic and antagonistic drug combinations against SARS-CoV-2. *Molecular Therapy,* 29**,** 873-885.

BOURLIÈRE, M., GORDON, S. C., FLAMM, S. L., COOPER, C. L., RAMJI, A., TONG, M., RAVENDHRAN, N., VIERLING, J. M., TRAN, T. T. & PIANKO, S. 2017. Sofosbuvir, velpatasvir, and voxilaprevir for previously treated HCV infection. *New England Journal of Medicine,* 376**,** 2134-2146.

BUCHMAN, J. T., HUDSON-SMITH, N. V., LANDY, K. M. & HAYNES, C. L. 2019. Understanding nanoparticle toxicity mechanisms to inform redesign strategies to reduce environmental impact. *Accounts of Chemical Research,* 52**,** 1632-1642.

BUNG, N., KRISHNAN, S. R., BULUSU, G. & ROY, A. 2020. De novo design of new chemical entities (NCEs) for SARS-CoV-2 using artificial intelligence. *Future Medicinal Chemistry*, 13, 575–585.

CAGNO, V., ANDREOZZI, P., D'ALICARNASSO, M., SILVA, P. J., MUELLER, M., GALLOUX, M., LE GOFFIC, R., JONES, S. T., VALLINO, M. & HODEK, J. 2018. Broad-spectrum non-toxic antiviral nanoparticles with a virucidal inhibition mechanism. *Nature Materials,* 17**,** 195-203.

CAPARCO, A. A., GONZÁLEZ-GAMBOA, I., HAYS, S. S., POKORSKI, J. K. & STEINMETZ, N. F. 2023. Delivery of nematicides using TMGMV-derived spherical nanoparticles. *Nano Letters,* 23**,** 5785-5793.

CAPUZZI, S. J., MURATOV, E. N. & TROPSHA, A. 2017. Phantom PAINS: problems with the utility of alerts for Pan-Assay INterference compounds. *Journal of Chemical Information and Modeling,* 57**,** 417-427.

CARPENTER, K. A., COHEN, D. S., JARRELL, J. T. & HUANG, X. 2018. Deep learning and virtual drug screening. *Future Medicinal Chemistry,* 10**,** 2557-2567.

CATANEO, A. H. D., KUCZERA, D., KOISHI, A. C., ZANLUCA, C., SILVEIRA, G. F., ARRUDA, T. B. D., SUZUKAWA, A. A., BORTOT, L. O., DIAS-BARUFFI, M. & VERRI JR, W. A. 2019. The citrus flavonoid naringenin impairs the *in vitro* infection of human cells by Zika virus. *Scientific Reports,* 9**,** 1-15.

CAVASOTTO, C. N. & PHATAK, S. S. 2009. Homology modeling in drug discovery: current trends and applications. *Drug Discovery Today,* 14**,** 676-683.

CHEN, H., ENGKVIST, O., WANG, Y., OLIVECRONA, M. & BLASCHKE, T. 2018. The rise of deep learning in drug discovery. *Drug Discovery Today,* 23**,** 1241-1250.

CHEN, X., CHEN, Y., ZOU, L., ZHANG, X., DONG, Y., TANG, J., MCCLEMENTS, D. J. & LIU, W. 2019. Plant-based nanoparticles prepared from proteins and phospholipids consisting of a core–multilayer-shell structure: fabrication, stability, and foamability. *Journal of Agricultural and Food Chemistry,* 67**,** 6574-6584.

CHEN, Y. & FENG, X. 2022. Gold nanoparticles for skin drug delivery. *International Journal of Pharmaceutics,* 625**,** 1-14.

CHEN, Z., LI, Y., CHEN, E., HALL, D. L., DARKE, P. L., CULBERSON, C., SHAFER, J. A. & KUO, L. C. 1994. Crystal structure at 1.9-A resolution of human immunodeficiency virus (HIV) II protease complexed with L-735,524, an orally bioavailable inhibitor of the HIV proteases. *Journal of Biological Chemistry,* 269**,** 26344-26348.

CHENG, H. Y., YANG, C. M., LIN, T. C., LIN, L. T., CHIANG, L. C. & LIN, C. C. 2011. Excoecarianin, isolated from Phyllanthus urinaria Linnea, inhibits herpes simplex virus type 2 infection through inactivation of viral particles. *Evidence-Based Complementary and Alternative Medicine,* 2011(1)**,** 1-10.

CHERKASOV, A., MURATOV, E. N., FOURCHES, D., VARNEK, A., BASKIN, I. I., CRONIN, M., DEARDEN, J., GRAMATICA, P., MARTIN, Y. C. & TODESCHINI, R. 2014. QSAR modeling: where have you been? Where are you going to? *Journal of Medicinal Chemistry,* 57**,** 4977-5010.

CHEUNG, Y. Y. H., LAU, E. H. Y., YIN, G., LIN, Y., COWLING, B. J. & LAM, K. F. 2024. Effectiveness of vaccines and antiviral drugs in preventing severe and fatal COVID-19, Hong Kong. *Emerging Infectious Diseases,* 30(1), 70–78.

CHOJNACKA, K., SKRZYPCZAK, D., IZYDORCZYK, G., MIKULA, K., SZOPA, D. & WITEK-KROWIAK, A. 2021. Antiviral properties of polyphenols from plants. *Foods,* 10**,** 1-28.

CHOJNACKI, J., STAUDT, T., GLASS, B., BINGEN, P., ENGELHARDT, J., ANDERS, M., SCHNEIDER, J., MÜLLER, B., HELL, S. W. & KRÄUSSLICH, H. G. 2012. Maturation-dependent HIV-1 surface protein redistribution revealed by fluorescence nanoscopy. *Science,* 338**,** 524-528.

CIHLAR, T. & FORDYCE, M. 2016. Current status and prospects of HIV treatment. *Current Opinion in Virology,* 18**,** 50-56.

CINATL, J., MORGENSTERN, B., BAUER, G., CHANDRA, P., RABENAU, H. & DOERR, H. 2003. Glycyrrhizin, an active component of liquorice roots, and replication of SARS-associated coronavirus. *The Lancet,* 361**,** 2045-2046.

CLARK, D. E. 2006. What has computer-aided molecular design ever done for drug discovery? *Expert Opinion on Drug Discovery,* 1**,** 103-110.

CORTESE, M. & LAKETA, V. 2021. Advanced microscopy technologies enable rapid response to SARS-CoV-2 pandemic. *Cellular Microbiology,* 23(7)**,** 1-10.

CORTESE, M., LEE, J.-Y., CERIKAN, B., NEUFELDT, C. J., OORSCHOT, V. M., KÖHRER, S., HENNIES, J., SCHIEBER, N. L., RONCHI, P. & MIZZON, G. 2020. Integrative imaging reveals SARS-CoV-2-induced reshaping of subcellular morphologies. *Cell Host & Microbe,* 28**,** 853-866.

CULLIS, J., SIOLAS, D., AVANZI, A., BARUI, S., MAITRA, A. & BAR-SAGI, D. 2017. Macropinocytosis of nab-paclitaxel drives macrophage activation in pancreatic cancer. *Cancer Immunology Research,* 5**,** 182-190.

DADFAR, S. M., ROEMHILD, K., DRUDE, N. I., VON STILLFRIED, S., KNÜCHEL, R., KIESSLING, F. & LAMMERS, T. 2019. Iron oxide nanoparticles: Diagnostic, therapeutic and theranostic applications. *Advanced Drug Delivery Reviews,* 138**,** 302-325.

DE LEO, A., CALDERON, A. & LIEBERMAN, P. M. 2020. Control of viral latency by episome maintenance proteins. *Trends in Microbiology,* 28**,** 150-162.

DEMCHENKO, H. O. & RUSINCHUK, N. M. 2019. Evaluation of the efficiency of interparticle interactions in nanosystems. *Journal of Nanotechnology,* 1, 1-8.

DENG, J., YANG, Z., OJIMA, I., SAMARAS, D. & WANG, F. 2022. Artificial intelligence in drug discovery: applications and techniques. *Briefings in Bioinformatics,* 23(1), 1–19.

DERKSEN, A., KÜHN, J., HAFEZI, W., SENDKER, J., EHRHARDT, C., LUDWIG, S. & HENSEL, A. 2016. Antiviral activity of hydroalcoholic extract from Eupatorium perfoliatum L. against the attachment of influenza A virus. *Journal of Ethnopharmacology,* 188**,** 144-152.

DESAI, N. 2012. Challenges in development of nanoparticle-based therapeutics. *The AAPS Journal,* 14**,** 282-295.

DESSELBERGER, U. 2000. Emerging and re-emerging infectious diseases. *Journal of Infection,* 40**,** 3-15.

DEY, D., BISWAS, P., PAUL, P., MAHMUD, S., EMA, T. I., KHAN, A. A., AHMED, S. Z., HASAN, M. M., SAIKAT, A. S. M. & FATEMA, B. 2023. Natural flavonoids effectively block the CD81 receptor of hepatocytes and inhibit HCV infection: A computational drug development approach. *Molecular Diversity,* 27**,** 1309-1322.

DI PETRILLO, A., ORRÙ, G., FAIS, A. & FANTINI, M. C. 2022. Quercetin and its derivates as antiviral potentials: A comprehensive review. *Phytotherapy Research,* 36**,** 266-278.

DIMOVA, D., GILBERG, E. & BAJORATH, J. 2017. Identification and analysis of promiscuity cliffs formed by bioactive compounds and experimental implications. *RSC Advances,* 7**,** 58-66.

DINGA, R., PENNINX, B. W., VELTMAN, D. J., SCHMAAL, L. & MARQUAND, A. F. 2019. Beyond accuracy: Measures for assessing machine learning models, pitfalls and guidelines. *BioRxiv***,** 1-20.

DONAHUE, N. D., ACAR, H. & WILHELM, S. 2019. Concepts of nanoparticle cellular uptake, intracellular trafficking, and kinetics in nanomedicine. *Advanced Drug Delivery Reviews,* 143**,** 68-96.

DONG, C., QU, L., WANG, H., WEI, L., DONG, Y. & XIONG, S. 2015. Targeting hepatitis B virus cccDNA by CRISPR/Cas9 nuclease efficiently inhibits viral replication. *Antiviral Research,* 118**,** 110-117.

DU, T., LIANG, J., DONG, N., LU, J., FU, Y., FANG, L., XIAO, S. & HAN, H. 2018. Glutathione-capped Ag2S nanoclusters inhibit coronavirus proliferation through blockage of viral RNA synthesis and budding. *ACS Applied Materials & Interfaces,* 10**,** 4369-4378.

EGBUNA, C., PARMAR, V. K., JEEVANANDAM, J., EZZAT, S. M., PATRICK-IWUANYANWU, K. C., ADETUNJI, C. O., KHAN, J., ONYEIKE, E. N., UCHE, C. Z. & AKRAM, M. 2021. Toxicity of nanoparticles in biomedical application: nanotoxicology. *Journal of Toxicology,* 2021**,** 1-21.

EJAZI, S. A., LOUISTHELMY, R. & MAISEL, K. 2023. Mechanisms of nanoparticle transport across intestinal tissue: an oral delivery perspective. *ACS Nano,* 17**,** 13044-13061.

ELLEBEDY, A.H. AND AHMED, R. 2016. Antiviral vaccines: challenges and advances. The *Vaccine Book*, 283-310.

ESCALONA-NOGUERO, C., LÓPEZ-VALLS, M. & SOT, B. 2021. CRISPR/Cas technology as a promising weapon to combat viral infections. *BioEssays,* 43(4)**,** 1-16.

ESIMONE, C. O., ECK, G., NWORU, C. S., HOFFMANN, D., ÜBERLA, K. & PROKSCH, P. 2010. Dammarenolic acid, a secodammarane triterpenoid from Aglaia sp. shows potent anti-retroviral activity in vitro. *Phytomedicine,* 17**,** 540-547.

FENWICK, C., JOO, V., JACQUIER, P., NOTO, A., BANGA, R., PERREAU, M. & PANTALEO, G. 2019. T-cell exhaustion in HIV infection. *Immunological Reviews,* 292**,** 149-163.

FERNÁNDEZ-TORRAS, A., COMAJUNCOSA-CREUS, A., DURAN-FRIGOLA, M. & ALOY, P. 2022. Connecting chemistry and biology through molecular descriptors. *Current Opinion in Chemical Biology,* 66**,** 1-12.

FILARDO, S., DI PIETRO, M., MASTROMARINO, P. & SESSA, R. 2020. Therapeutic potential of resveratrol against emerging respiratory viral infections. *Pharmacology & Therapeutics,* 214**,** 1-9.

FIORE, C., EISENHUT, M., KRAUSSE, R., RAGAZZI, E., PELLATI, D., ARMANINI, D. & BIELENBERG, J. 2008. Antiviral effects of Glycyrrhiza species. *Phytotherapy Research: An International Journal Devoted to Pharmacological and Toxicological Evaluation of Natural Product Derivatives,* 22**,** 141-148.

FISCHER, A., SELLNER, M., NERANJAN, S., SMIEŠKO, M. & LILL, M. A. 2020. Potential inhibitors for novel coronavirus protease identified by virtual screening of 606 million compounds. *International Journal of Molecular Sciences,* 21(10)**,** 1-17.

FISCHL, M. A., RICHMAN, D. D., GRIECO, M. H., GOTTLIEB, M. S., VOLBERDING, P. A., LASKIN, O. L., LEEDOM, J. M., GROOPMAN, J. E., MILDVAN, D. & SCHOOLEY, R. T. 1987. The efficacy of azidothymidine (AZT) in the treatment of patients with AIDS and AIDS-related complex. *New England Journal of Medicine,* 317**,** 185-191.

FOURCHES, D., MURATOV, E. & TROPSHA, A. 2010. Trust, but verify: on the importance of chemical structure curation in cheminformatics and QSAR modeling research. *Journal of Chemical Information and Modeling,* 50(7), 1189-1204.

GALDIERO, S., FALANGA, A., VITIELLO, M., CANTISANI, M., MARRA, V. & GALDIERO, M. 2011. Silver nanoparticles as potential antiviral agents. *Molecules,* 16**,** 8894-8918.

GAO, J., CAO, C., SHI, M., HONG, S., GUO, S., LI, J., LIANG, T., SONG, P., XU, R. & LI, N. 2023. Kaempferol inhibits SARS-CoV-2 invasion by impairing heptad repeats-mediated viral fusion. *Phytomedicine,* 118**,** 1-12.

GAO, Z., FAN, M., DAS, A. T., HERRERA-CARRILLO, E. & BERKHOUT, B. 2020. Extinction of all infectious HIV in cell culture by the CRISPR-Cas12a system with only a single crRNA. *Nucleic Acids Research,* 48**,** 5527-5539.

GERETTI, A. M., ARMENIA, D. & CECCHERINI-SILBERSTEIN, F. 2012. Emerging patterns and implications of HIV-1 integrase inhibitor resistance. *Current Opinion in Infectious Diseases,* 25**,** 677-686.

GHAEBI, M., OSALI, A., VALIZADEH, H., ROSHANGAR, L. & AHMADI, M. 2020. Vaccine development and therapeutic design for 2019-nCoV/SARS-CoV-2: Challenges and chances. *Journal of Cellular Physiology,* 235**,** 9098-9109.

GHORBANI, M. & HAMISHEHKAR, H. 2017. Decoration of gold nanoparticles with thiolated pH-responsive polymeric (PEG-bp (2-dimethylamio ethyl methacrylate-co-itaconic acid) shell: A novel platform for targeting of anticancer agent. *Materials Science and Engineering: C,* 81**,** 561-570.

GHOSH, A. K., DAWSON, Z. L. & MITSUYA, H. 2007. Darunavir, a conceptually new HIV-1 protease inhibitor for the treatment of drug-resistant HIV. *Bioorganic & Medicinal Chemistry,* 15**,** 7576-7580.

GIORDANO, D., FACCHIANO, A. & CARBONE, V. 2023. Food plant secondary metabolites antiviral activity and their possible roles in SARS-CoV-2 treatment: an overview. *Molecules,* 28(6)**,** 1-29.

GOH, G. B., HODAS, N. O. & VISHNU, A. 2017. Deep learning for computational chemistry. *Journal of Computational Chemistry,* 38**,** 1291-1307.

GOLDWASSER, J., COHEN, P. Y., LIN, W., KITSBERG, D., BALAGUER, P., POLYAK, S. J., CHUNG, R. T., YARMUSH, M. L. & NAHMIAS, Y. 2011. Naringenin inhibits the assembly and long-term production of infectious hepatitis C virus particles through a PPAR-mediated mechanism. *Journal of Hepatology,* 55**,** 963-971.

GUERRIERI, A., DONG, L. & BOUWMEESTER, H. J. 2019. Role and exploitation of underground chemical signaling in plants. *Pest Management Science,* 75**,** 2455-2463.

HAMDI, M., ABDEL-BAR, H. M., ELMOWAFY, E., EL-KHOULY, A., MANSOUR, M. & AWAD, G. A. 2021. Investigating the internalization and COVID-19 antiviral computational analysis of optimized nanoscale zinc oxide. *ACS Omega,* 6**,** 6848-6860.

HANGYU, W., PANPAN, L., JIE, S., HONGYAN, W., LINMIAO, W., KANGNING, H., YICHEN, S., SHUAI, W. AND CHENG, W. 2024. Advancements in Antiviral Drug Development: Comprehensive Insights into Design Strategies and Mechanisms Targeting Key Viral Proteins. *Journal of Microbiology and Biotechnology*, 34(7),1376–1384.

HELFER, M., KOPPENSTEINER, H., SCHNEIDER, M., REBENSBURG, S., FORCISI, S., MÜLLER, C., SCHMITT-KOPPLIN, P., SCHINDLER, M. & BRACK-WERNER, R. 2014. The root extract of the medicinal plant *Pelargonium sidoides* is a potent HIV-1 attachment inhibitor. *PloS One,* 9(1)**,** 1-12.

HENRY, B. 2018. Drug pricing & challenges to hepatitis C treatment access. *Journal of Health & Biomedical Law,* 14, 265-283.

HSIEH, C. F., JHENG, J. R., LIN, G. H., CHEN, Y. L., HO, J. Y., LIU, C. J., HSU, K. Y., CHEN, Y. S., CHAN, Y. F. & YU, H. M. 2020. Rosmarinic acid exhibits broad anti-enterovirus A71 activity by inhibiting the interaction between the five-fold axis of capsid VP1 and cognate sulfated receptors. *Emerging Microbes & Infections,* 9**,** 1194-1205.

HSU, P. D., LANDER, E. S. & ZHANG, F. 2014. Development and applications of CRISPR-Cas9 for genome engineering. *Cell,* 157**,** 1262-1278.

HU, C.-M. J., ARYAL, S. & ZHANG, L. 2010. Nanoparticle-assisted combination therapies for effective cancer treatment. *Therapeutic Delivery,* 1**,** 323-334.

HU, Z., YU, L., ZHU, D., DING, W., WANG, X., ZHANG, C., WANG, L., JIANG, X., SHEN, H. & HE, D. 2014. Disruption of HPV16-E7 by CRISPR/Cas system induces apoptosis and growth inhibition in HPV16 positive human cervical cancer cells. *BioMed Research International,* 2014(1)**,** 1-9.

HUHN, G. D., RAMGOPAL, M., JAIN, M. K., HINESTROSA, F., ASMUTH, D. M., SLIM, J., GOLDSTEIN, D., APPLIN, S., RYU, J. H. & JIANG, S. 2020. HIV/HCV therapy with ledipasvir/sofosbuvir after randomized switch to emtricitabine-tenofovir alafenamide-based single-tablet regimens. *PloS One,* 15(1)**,** 1-16.

HUO, H. & HU, G. 2019. CRISPR/Cas9-mediated LMP1 knockout inhibits Epstein-Barr virus infection and nasopharyngeal carcinoma cell growth. *Infectious Agents and Cancer,* 14**,** 1-10.

HUSSAIN, M., GALVIN, H. D., HAW, T. Y., NUTSFORD, A. N. & HUSAIN, M. 2017. Drug resistance in influenza A virus: the epidemiology and management. *Infection and Drug Resistance***,** 121-134.

IKEDA, K., TSUJIMOTO, K., UOZAKI, M., NISHIDE, M., SUZUKI, Y., KOYAMA, A. H. & YAMASAKI, H. 2011. Inhibition of multiplication of herpes simplex virus by caffeic acid. *International Journal of Molecular Medicine,* 28**,** 595-598.

ISAH, T. 2019. Stress and defense responses in plant secondary metabolites production. *Biological Research,* 52(39), 1-25.

ISDAHL, R. & GUNDERSEN, O. E. Out-of-the-box reproducibility: A survey of machine learning platforms. 2019 15th international conference on eScience (eScience), 2019. IEEE, 86-95.

ISLAM, Y., LEACH, A. G., SMITH, J., PLUCHINO, S., COXON, C. R., SIVAKUMARAN, M., DOWNING, J., FATOKUN, A. A., TEIXIDÒ, M. & EHTEZAZI, T. 2021. Physiological and pathological factors affecting drug delivery to the brain by nanoparticles. *Advanced Science,* 8(11)**,** 1-45.

IYENGAR, S., TAY-TEO, K., VOGLER, S., BEYER, P., WIKTOR, S., DE JONCHEERE, K. & HILL, S. 2016. Prices, costs, and affordability of new medicines for hepatitis C in 30 countries: an economic analysis. *PLoS Medicine,* 13(5)**,** 1-22.

JAEGER, A. & BANKS, D. 2023. Cluster analysis: A modern statistical review. *Wiley Interdisciplinary Reviews: Computational Statistics,* 15(3)**,** 1-17.

JANUSZ, G., PAWLIK, A., ŚWIDERSKA-BUREK, U., POLAK, J., SULEJ, J., JAROSZ-WILKOŁAZKA, A. & PASZCZYŃSKI, A. 2020. Laccase properties, physiological functions, and evolution. *International Journal of Molecular Sciences,* 21(3)**,** 1-25.

JAYATUNGA, M. K., XIE, W., RUDER, L., SCHULZE, U. & MEIER, C. 2022. AI in small-molecule drug discovery: a coming wave. *Nature Reviews Drug Discovery,* 21**,** 175-176.

JEREMIAH, S. S., MIYAKAWA, K., MORITA, T., YAMAOKA, Y. & RYO, A. 2020. Potent antiviral effect of silver nanoparticles on SARS-CoV-2. *Biochemical and Biophysical Research Communications,* 533**,** 195-200.

JHENG, J.-R., HSIEH, C.-F., CHANG, Y.-H., HO, J.-Y., TANG, W.-F., CHEN, Z.-Y., LIU, C.-J., LIN, T.-J., HUANG, L.-Y. & CHERN, J.-H. 2022. Rosmarinic acid interferes with influenza virus A entry and replication by decreasing GSK3β and phosphorylated AKT expression levels. *Journal of Microbiology, Immunology and Infection,* 55**,** 598-610.

JHOTI, H. & LEACH, A. R. 2007. Structure-based drug discovery, *Springer*, 1-249.

JIMÉNEZ-LUNA, J., GRISONI, F. & SCHNEIDER, G. 2020. Drug discovery with explainable artificial intelligence. *Nature Machine Intelligence,* 2**,** 573-584.

JOHARI, J., KIANMEHR, A., MUSTAFA, M. R., ABUBAKAR, S. & ZANDI, K. 2012. Antiviral activity of baicalein and quercetin against the Japanese encephalitis virus. *International Journal of Molecular Sciences,* 13**,** 16785-16795.

JUBAIR, L., FALLAHA, S. & MCMILLAN, N. A. 2019. Systemic delivery of CRISPR/Cas9 targeting HPV oncogenes is effective at eliminating established tumors. *Molecular Therapy,* 27**,** 2091-2099.

KALDOR, S. W., KALISH, V. J., DAVIES, J. F., SHETTY, B. V., FRITZ, J. E., APPELT, K., BURGESS, J. A., CAMPANALE, K. M., CHIRGADZE, N. Y. & CLAWSON, D. K. 1997. Viracept (nelfinavir mesylate, AG1343): a potent, orally bioavailable inhibitor of HIV-1 protease. *Journal of Medicinal Chemistry,* 40**,** 3979-3985.

KAMINSKI, R., BELLA, R., YIN, C., OTTE, J., FERRANTE, P., GENDELMAN, H. E., LI, H., BOOZE, R., GORDON, J. & HU, W. 2016a. Excision of HIV-1 DNA by gene editing: a proof-of-concept *in vivo* study. *Gene Therapy,* 23**,** 690-695.

KAMINSKI, R., CHEN, Y., FISCHER, T., TEDALDI, E., NAPOLI, A., ZHANG, Y., KARN, J., HU, W. & KHALILI, K. 2016b. Elimination of HIV-1 genomes from human T-lymphoid cells by CRISPR/Cas9 gene editing. *Scientific Reports,* 6**,** 1-15.

KANG, H., BUCHMAN, J. T., RODRIGUEZ, R. S., RING, H. L., HE, J., BANTZ, K. C. & HAYNES, C. L. 2018. Stabilization of silver and gold nanoparticles: preservation and improvement of plasmonic functionalities. *Chemical Reviews,* 119**,** 664-699.

KARKI, N., VERMA, N., TROZZI, F., TAO, P., KRAKA, E. & ZOLTOWSKI, B. 2021. Predicting potential SARS-COV-2 drugs—In depth drug database screening using deep

neural network framework SSnet, classical virtual screening and docking. *International Journal of Molecular Sciences,* 22(4)**,** 1-17.

KAUSAR, S., SAID KHAN, F., ISHAQ MUJEEB UR REHMAN, M., AKRAM, M., RIAZ, M., RASOOL, G., HAMID KHAN, A., SALEEM, I., SHAMIM, S. & MALIK, A. 2021. A review: mechanism of action of antiviral drugs. *International Journal of immunopathology and Pharmacology,* 35**,** 1-12.

KAUSHIK, S., DAR, L., KAUSHIK, S. & YADAV, J. P. 2021. Anti-dengue activity of super critical extract and isolated oleanolic acid of *Leucas cephalotes* using *in vitro* and *in silico* approach. *BMC Complementary Medicine and Therapies,* 21**,** 1-15.

KAWASUJI, T., JOHNS, B. A., YOSHIDA, H., WEATHERHEAD, J. G., AKIYAMA, T., TAISHI, T., TAODA, Y., MIKAMIYAMA-IWATA, M., MURAI, H. & KIYAMA, R. 2013. Carbamoyl pyridone HIV-1 integrase inhibitors. 2. Bi-and tricyclic derivatives result in superior antiviral and pharmacokinetic profiles. *Journal of Medicinal Chemistry,* 56**,** 1124-1135.

KEMPF, D. J., MARSH, K. C., DENISSEN, J. F., MCDONALD, E., VASAVANONDA, S., FLENTGE, C. A., GREEN, B. E., FINO, L., PARK, C. H. & KONG, X.-P. 1995. ABT-538 is a potent inhibitor of human immunodeficiency virus protease and has high oral bioavailability in humans. *Proceedings of the National Academy of Sciences,* 92**,** 2484-2488.

KEMPF, D. J., SHAM, H. L., MARSH, K. C., FLENTGE, C. A., BETEBENNER, D., GREEN, B. E., MCDONALD, E., VASAVANONDA, S., SALDIVAR, A. & WIDEBURG, N. E. 1998. Discovery of ritonavir, a potent inhibitor of HIV protease with high oral bioavailability and clinical efficacy. *Journal of Medicinal Chemistry,* 41**,** 602-617.

KENNEDY, E. M., KORNEPATI, A. V., GOLDSTEIN, M., BOGERD, H. P., POLING, B. C., WHISNANT, A. W., KASTAN, M. B. & CULLEN, B. R. 2014. Inactivation of the

human papillomavirus E6 or E7 gene in cervical carcinoma cells by using a bacterial CRISPR/Cas RNA-guided endonuclease. *Journal of Virology,* 88**,** 11965-11972.

KESSLER, A. & KALSKE, A. 2018. Plant secondary metabolite diversity and species interactions. *Annual Review of Ecology, Evolution, and Systematics,* 49**,** 115-138.

KIM, D., BAE, S., PARK, J., KIM, E., KIM, S., YU, H. R., HWANG, J., KIM, J.-I. & KIM, J.-S. 2015. Digenome-seq: genome-wide profiling of CRISPR-Cas9 off-target effects in human cells. *Nature Methods,* 12**,** 237-243.

KIM, H. & CHUNG, M. S. 2018. Antiviral activities of mulberry (Morus alba) juice and seed against influenza viruses. *Evidence-Based Complementary and Alternative Medicine,*1, 1-10.

KIM, J., YEOM, M., LEE, T., KIM, H.-O., NA, W., KANG, A., LIM, J.-W., PARK, G., PARK, C. & SONG, D. 2020. Porous gold nanoparticles for attenuating infectivity of influenza A virus. *Journal of Nanobiotechnology,* 18**,** 1-11.

KIM, V. N. 2018. RNA-targeting CRISPR comes of age. *Nature Biotechnology,* 36**,** 44-45.

KISH, T., AZIZ, A. & SORIO, M. 2017. Hepatitis C in a new era: a review of current therapies. *Pharmacy and Therapeutics,* 42(5), 316–329.

KITCHEN, D. B., DECORNEZ, H., FURR, J. R. & BAJORATH, J. 2004. Docking and scoring in virtual screening for drug discovery: methods and applications. *Nature reviews Drug Discovery,* 3**,** 935-949.

KOMAROVA, N. L. & BOLAND, C. R. 2013. Calculated treatment. *Nature,* 499**,** 291-292.

KONG, L., LI, S., LIAO, Q., ZHANG, Y., SUN, R., ZHU, X., ZHANG, Q., WANG, J., WU, X. & FANG, X. 2013. Oleanolic acid and ursolic acid: novel hepatitis C virus antivirals that inhibit NS5B activity. *Antiviral Research,* 98**,** 44-53.

KRATZ, J. M., ANDRIGHETTI-FRÖHNER, C. R., LEAL, P. C., NUNES, R. J., YUNES, R. A., TRYBALA, E., BERGSTRÖM, T., BARARDI, C. R. M. & SIMÕES, C. M. O.

2008. Evaluation of anti-HSV-2 activity of gallic acid and pentyl gallate. *Biological and Pharmaceutical Bulletin,* 31**,** 903-907.

KROHN, A., REDSHAW, S., RITCHIE, J. C., GRAVES, B. J. & HATADA, M. H. 1991. Novel binding mode of highly potent HIV-proteinase inhibitors incorporating the (R)-hydroxyethylamine isostere. *Journal of Medicinal Chemistry,* 34**,** 3340-3342.

KULKARNI, J. A., WITZIGMANN, D., CHEN, S., CULLIS, P. R. & VAN DER MEEL, R. 2019. Lipid nanoparticle technology for clinical translation of siRNA therapeutics. *Accounts of Chemical Research,* 52**,** 2435-2444.

KUROKAWA, M., SHIMIZU, T., WATANABE, W. & SHIRAKI, K. 2010. Development of new antiviral agents from natural products. *The Open Antimicrobial Agents Journal,* 2, 49-57.

KWOFIE, S. K., ADAMS, J., BRONI, E., ENNINFUL, K. S., AGONI, C., SOLIMAN, M. E. & WILSON, M. D. 2023. Artificial Intelligence, machine learning, and big data for Ebola virus drug discovery. *Pharmaceuticals,* 16(3)**,** 1-12.

LARA, S., ALNASSER, F., POLO, E., GARRY, D., LO GIUDICE, M. C., HRISTOV, D. R., ROCKS, L., SALVATI, A., YAN, Y. & DAWSON, K. A. 2017. Identification of receptor binding to the biomolecular corona of nanoparticles. *ACS nano,* 11**,** 1884-1893.

LEE, C. 2019. CRISPR/Cas9-based antiviral strategy: current status and the potential challenge. *Molecules,* 24(7)**,** 1-28.

LEELANANDA, S. P. & LINDERT, S. 2016. Computational methods in drug discovery. *Beilstein Journal of Organic Chemistry,* 12**,** 2694-2718.

LEUNG, R. C.-Y., IP, J. D., CHEN, L.-L., CHAN, W.-M. & TO, K. K.-W. 2024. Global emergence of neuraminidase inhibitor-resistant influenza A (H1N1) pdm09 viruses with I223V and S247N mutations: implications for antiviral resistance monitoring. *The Lancet Microbe,* 5, 627-628.

LEVANOVA, A. & PORANEN, M. M. 2018. RNA interference as a prospective tool for the control of human viral infections. *Frontiers in Microbiology,* 9**,** 1-9.

LEW, W., CHEN, X. & KIM, C. U. 2000. Discovery and development of GS 4104 (oseltamivir) an orally active influenza neuraminidase inhibitor. *Current Medicinal Chemistry,* 7**,** 663-672.

LI, H., SHENG, C., WANG, S., YANG, L., LIANG, Y., HUANG, Y., LIU, H., LI, P., YANG, C. & YANG, X. 2017. Removal of integrated hepatitis B virus DNA using CRISPR-Cas9. *Frontiers in Cellular and Infection Microbiology,* 7**,** 1-9.

LI, M., SUZUKI, K., KIM, N. Y., LIU, G.-H. & BELMONTE, J. C. I. 2014. A cut above the rest: targeted genome editing technologies in human pluripotent stem cells. *Journal of Biological Chemistry,* 289**,** 4594-4599.

LI, X., WANG, B., ZHOU, S., CHEN, W., CHEN, H., LIANG, S., ZHENG, L., YU, H., CHU, R. & WANG, M. 2020. Surface chemistry governs the sub-organ transfer, clearance and toxicity of functional gold nanoparticles in the liver and kidney. *Journal of Nanobiotechnology,* 18**,** 1-16.

LI, Y., JIANG, Y., ZHENG, Z., DU, N., GUAN, S., GUO, W., TANG, X., CUI, J., ZHANG, L. & LIU, K. 2022. Co-delivery of precisely prescribed multi-prodrug combination by an engineered nanocarrier enables efficient individualized cancer chemotherapy. *Advanced Materials,* 34(12)**,** 1-12.

LI, Y., LIN, Z., ZHAO, M., XU, T., WANG, C., HUA, L., WANG, H., XIA, H. & ZHU, B. 2016. Silver nanoparticle based codelivery of oseltamivir to inhibit the activity of the H1N1 influenza virus through ROS-mediated signaling pathways. *ACS Applied Materials & Interfaces,* 8**,** 24385-24393.

LIAO, H.-K., GU, Y., DIAZ, A., MARLETT, J., TAKAHASHI, Y., LI, M., SUZUKI, K., XU, R., HISHIDA, T. & CHANG, C.-J. 2015. Use of the CRISPR/Cas9 system as an

intracellular defense against HIV-1 infection in human cells. *Nature Communications,* 6**,** 1-10.

LIM, Y.-S. 2017. Management of antiviral resistance in chronic hepatitis B. *Gut and Liver,* 11(2), 189–195.

LIN, H., LI, G., PENG, X., DENG, A., YE, L., SHI, L., WANG, T. & HE, J. 2021. The use of CRISPR/Cas9 as a tool to study human infectious viruses. *Frontiers in Cellular and Infection Microbiology,* 11**,** 1-14.

LIN, S.-R., YANG, H.-C., KUO, Y.-T., LIU, C.-J., YANG, T.-Y., SUNG, K.-C., LIN, Y.-Y., WANG, H.-Y., WANG, C.-C. & SHEN, Y.-C. 2014. The CRISPR/Cas9 system facilitates clearance of the intrahepatic HBV templates *in vivo*. *Molecular Therapy-Nucleic Acids,* 3, 1-7.

LINO, C. A., HARPER, J. C., CARNEY, J. P. & TIMLIN, J. A. 2018. Delivering CRISPR: a review of the challenges and approaches. *Drug Delivery,* 25**,** 1234-1257.

LIU, H., YE, F., SUN, Q., LIANG, H., LI, C., LI, S., LU, R., HUANG, B., TAN, W. & LAI, L. 2021. Scutellaria baicalensis extract and baicalein inhibit replication of SARS-CoV-2 and its 3C-like protease *in vitro*. *Journal of Enzyme Inhibition and Medicinal Chemistry,* 36**,** 497-503.

LIU, Y.-C., CAI, Z.-M. & ZHANG, X.-J. 2016. Reprogrammed CRISPR-Cas9 targeting the conserved regions of HPV6/11 E7 genes inhibits proliferation and induces apoptosis in E7-transformed keratinocytes. *Asian Journal of Andrology,* 18**,** 475-479.

LIU, Y., SHI, X., TIAN, Y., ZHAI, S., LIU, Y., XIONG, Z. & CHU, S. 2023. An insight into novel therapeutic potentials of taxifolin. *Frontiers in Pharmacology,* 14**,** 1-17.

LIU, Y., ZHU, S., GU, Z., CHEN, C. & ZHAO, Y. 2022. Toxicity of manufactured nanomaterials. *Particuology,* 69**,** 31-48.

LIVER, E. A. F. T. S. O. T. 2012. EASL clinical practice guidelines: management of chronic hepatitis B virus infection. *Journal of Hepatology,* 57**,** 167-185.

LOCARNINI, S. A. & YUEN, L. 2010. Molecular genesis of drug-resistant and vaccine-escape HBV mutants. *Antiviral Therapy,* 15**,** 451-461.

LOE, M. W. C., HAO, E., CHEN, M., LI, C., LEE, R. C. H., ZHU, I. X. Y., TEO, Z. Y., CHIN, W.-X., HOU, X. & DENG, J. 2020. Betulinic acid exhibits antiviral effects against dengue virus infection. *Antiviral Research,* 184**,** 1-15.

LUND, B. & MA, J. 2021. A review of cluster analysis techniques and their uses in library and information science research: k-means and k-medoids clustering. *Performance Measurement and Metrics,* 22**,** 161-173.

LUNDIN, A., DIJKMAN, R., BERGSTRÖM, T., KANN, N., ADAMIAK, B., HANNOUN, C., KINDLER, E., JONSDOTTIR, H. R., MUTH, D. & KINT, J. 2014. Targeting membrane-bound viral RNA synthesis reveals potent inhibition of diverse coronaviruses including the middle East respiratory syndrome virus. *PLoS Pathogens,* 10(5)**,** 1-15.

LYLE, T. 2007. Ribonucleic acid viruses: antivirals for human immunodeficiency virus. *Comprehensive Medicinal Chemistry II***,** 329-371.

MA, J., WANG, J., GHORAIE, L. S., MEN, X., HAIBE-KAINS, B. & DAI, P. 2019. A comparative study of cluster detection algorithms in protein–protein interaction for drug target discovery and drug repurposing. *Frontiers in Pharmacology,* 10**,** 1-15.

MA, M., ZHU, H., LING, J., GONG, S., ZHANG, Y., XIA, Y. & TANG, Z. 2020. Quasi-amorphous and hierarchical Fe2O3 supraparticles: active T 1-weighted magnetic resonance imaging *in vivo* and renal clearance. *ACS Nano,* 14**,** 4036-4044.

MANCUSO, P., CHEN, C., KAMINSKI, R., GORDON, J., LIAO, S., ROBINSON, J. A., SMITH, M. D., LIU, H., SARIYER, I. K. & SARIYER, R. 2020. CRISPR based editing

of SIV proviral DNA in ART treated non-human primates. *Nature Communications,* 11**,** 1-11.

MANIVANNAN, R., PUNNIYAMOORTHY, A. & TAMILSELVAN, C. 2019. Plant secondary metabolites of antiviral properties a rich medicinal source for drug discovery: a mini review. *Journal of Drug Delivery and Therapeutics,* 9**,** 161-167.

MANSOURI, S., KUTKY, M. & HUDAK, K. A. 2012. Pokeweed antiviral protein increases HIV-1 particle infectivity by activating the cellular mitogen activated protein kinase pathway. *PloS One,* 7(5)**,** 1-9.

MCGOWAN, I., DEZZUTTI, C. S., SIEGEL, A., ENGSTROM, J., NIKIFOROV, A., DUFFILL, K., SHETLER, C., RICHARDSON-HARMAN, N., ABEBE, K. & BACK, D. 2016. Long-acting rilpivirine as potential pre-exposure prophylaxis for HIV-1 prevention (the MWRI-01 study): an open-label, phase 1, compartmental, pharmacokinetic and pharmacodynamic assessment. *The Lancet HIV,* 3**,** e569-e578.

MEHTA, A., MICHLER, T. & MERKEL, O. M. 2021. siRNA therapeutics against respiratory viral infections—What have we learned for potential COVID-19 therapies? *Advanced Healthcare Materials,* 10(7)**,** 1-16.

MELVILLE, K., RODRIGUEZ, T. & DOBROVOLNY, H. M. 2018. Investigating different mechanisms of action in combination therapy for influenza. *Frontiers in Pharmacology,* 9**,** 1-13.

MENG, T., XIAO, D., MUHAMMED, A., DENG, J., CHEN, L. & HE, J. 2021. Anti-inflammatory action and mechanisms of resveratrol. *Molecules,* 26(1)**,** 1-15.

MINCES, L. R., NGUYEN, M. H., MITSANI, D., SHIELDS, R. K., KWAK, E. J., SILVEIRA, F. P., ABDEL-MASSIH, R., PILEWSKI, J. M., CRESPO, M. M. & BERMUDEZ, C. 2014. Ganciclovir-resistant cytomegalovirus infections among lung transplant

recipients are associated with poor outcomes despite treatment with foscarnet-containing regimens. *Antimicrobial Agents and Chemotherapy,* 58**,** 128-135.

MISHIMA, E., ANZAI, N., MIYAZAKI, M. & ABE, T. 2020. Uric acid elevation by favipiravir, an antiviral drug. *The Tohoku Journal of Experimental Medicine,* 251**,** 87-90.

MITCHELL, M. J., BILLINGSLEY, M. M., HALEY, R. M., WECHSLER, M. E., PEPPAS, N. A. & LANGER, R. 2021. Engineering precision nanoparticles for drug delivery. *Nature Reviews Drug Discovery,* 20**,** 101-124.

MOGHADDAM, E., TEOH, B.-T., SAM, S.-S., LANI, R., HASSANDARVISH, P., CHIK, Z., YUEH, A., ABUBAKAR, S. & ZANDI, K. 2014. Baicalin, a metabolite of baicalein with antiviral activity against dengue virus. *Scientific Reports,* 4**,** 1-8.

MOHANRAJU, P., MAKAROVA, K. S., ZETSCHE, B., ZHANG, F., KOONIN, E. V. & VAN DER OOST, J. 2016. Diverse evolutionary roots and mechanistic variations of the CRISPR-Cas systems. *Science,* 353(6299)**,** aad5147-12.

MOJICA, F. J. & RODRIGUEZ-VALERA, F. 2016. The discovery of CRISPR in archaea and bacteria. *The FEBS Journal,* 283**,** 3162-3169.

MONTAGUE, S. J., PATEL, P., MARTIN, E. M., SLATER, A., QUINTANILLA, L. G., PERRELLA, G., KARDEBY, C., NAGY, M., MEZZANO, D. & MENDES, P. M. 2021. Platelet activation by charged ligands and nanoparticles: platelet glycoprotein receptors as pattern recognition receptors. *Platelets,* 32**,** 1018-1030.

MONTO, A. S. 2006. Vaccines and antiviral drugs in pandemic preparedness. *Emerging Infectious Diseases,* 12(1), 55–60.

MURANYI, W., MALKUSCH, S., MÜLLER, B., HEILEMANN, M. & KRÄUSSLICH, H.-G. 2013. Super-resolution microscopy reveals specific recruitment of HIV-1 envelope

proteins to viral assembly sites dependent on the envelope C-terminal tail. *PLoS Pathogens,* 9(2)**,** 1-13.

NAG, S., BAIDYA, A. T., MANDAL, A., MATHEW, A. T., DAS, B., DEVI, B. & KUMAR, R. 2022. Deep learning tools for advancing drug discovery and development. *3 Biotech,* 12(110), 1-21.

NAJAFI, S., TAN, S. C., AGHAMIRI, S., RAEE, P., EBRAHIMI, Z., JAHROMI, Z. K., RAHMATI, Y., NAHAND, J. S., PIROOZMAND, A. & JAJARMI, V. 2022. Therapeutic potentials of CRISPR-Cas genome editing technology in human viral infections. *Biomedicine & Pharmacotherapy,* 148**,** 1-17.

NAMBA-NZANGUIM, C. T., TURON, G., SIMOBEN, C. V., TIETJEN, I., MONTANER, L. J., EFANGE, S. M., DURAN-FRIGOLA, M. & NTIE-KANG, F. 2022. Artificial intelligence for antiviral drug discovery in low resourced settings: A perspective. *Frontiers in Drug Discovery,* 2**,** 1-12.

NARAYAN, V., RAVINDRA, K. C., CHIARO, C., CARY, D., AGGARWAL, B. B., HENDERSON, A. J. & PRABHU, K. S. 2011. Celastrol inhibits Tat-mediated human immunodeficiency virus (HIV) transcription and replication. *Journal of Molecular Biology,* 410**,** 972-983.

NASTRI, B. M., PAGLIANO, P., ZANNELLA, C., FOLLIERO, V., MASULLO, A., RINALDI, L., GALDIERO, M. & FRANCI, G. 2023. HIV and drug-resistant subtypes. *Microorganisms,* 11(1)**,** 1-15.

NEHME, Z., PASQUEREAU, S. & HERBEIN, G. 2019. Control of viral infections by epigenetic-targeted therapy. *Clinical Epigenetics,* 11**,** 1-17.

NGUYEN, J. T., HOOPES, J. D., LE, M. H., SMEE, D. F., PATICK, A. K., FAIX, D. J., BLAIR, P. J., DE JONG, M. D., PRICHARD, M. N. & WENT, G. T. 2010. Triple

combination of amantadine, ribavirin, and oseltamivir is highly active and synergistic against drug resistant influenza virus strains in vitro. *PloS One,* 5(2)**,** 1-12.

NGUYEN, T. M., ZHANG, Y. & PANDOLFI, P. P. 2020. Virus against virus: a potential treatment for 2019-nCov (SARS-CoV-2) and other RNA viruses. *Cell Research,* 30**,** 189-190.

NJOROGE, F. G., CHEN, K. X., SHIH, N.-Y. & PIWINSKI, J. J. 2008. Challenges in modern drug discovery: a case study of boceprevir, an HCV protease inhibitor for the treatment of hepatitis C virus infection. *Accounts of Chemical Research,* 41**,** 50-59.

O'CONNELL, M. R., OAKES, B. L., STERNBERG, S. H., EAST-SELETSKY, A., KAPLAN, M. & DOUDNA, J. A. 2014. Programmable RNA recognition and cleavage by CRISPR/Cas9. *Nature,* 516**,** 263-266.

OGANDO, N. S., DALEBOUT, T. J., ZEVENHOVEN-DOBBE, J. C., LIMPENS, R. W., VAN DER MEER, Y., CALY, L., DRUCE, J., DE VRIES, J. J., KIKKERT, M. & BÁRCENA, M. 2020. SARS-coronavirus-2 replication in Vero E6 cells: replication kinetics, rapid adaptation and cytopathology. *Journal of General Virology,* 101**,** 925-940.

OLOCHE, J. J., OLUREMI, B. B., ARUWA, C. E. & SABIU, S. 2023. Molecular modeling identification of key secondary metabolites from *Xylopia aethiopica* as promising therapeutics targeting essential measles viral proteins. *Evidence-Based Complementary and Alternative Medicine,* 1, 1-13.

OWEN, L., LAIRD, K. & SHIVKUMAR, M. 2022. Antiviral plant-derived natural products to combat RNA viruses: Targets throughout the viral life cycle. *Letters in Applied Microbiology,* 75**,** 476-499.

PANCHAL, R., GHOSH, S., MEHLA, R., RAMALINGAM, J., GAIROLA, S., MUKHERJEE, S. & CHOWDHARY, A. 2022. Antiviral activity of rosmarinic acid against four serotypes of dengue virus. *Current Microbiology,* 79(203), 1-7.

PANG, Z., CHEN, J., WANG, T., GAO, C., LI, Z., GUO, L., XU, J. & CHENG, Y. 2021. Linking plant secondary metabolites and plant microbiomes: a review. *Frontiers in Plant Science,* 12**,** 1-22.

PAPATHEODORIDIS, G. V., DIMOU, E., DIMAKOPOULOS, K., MANOLAKOPOULOS, S., RAPTI, I., KITIS, G., TZOURMAKLIOTIS, D., MANESIS, E. & HADZIYANNIS, S. J. 2005. Outcome of hepatitis B e antigen–negative chronic hepatitis B on long-term nucleos(t)ide analog therapy starting with lamivudine. *Hepatology,* 42**,** 121-129.

PARK, S., KIM, N.-E., PARK, B. J., KWON, H. C. & SONG, Y.-J. 2022. Kaempferol interferes with varicella-zoster virus replication in human foreskin fibroblasts. *Pharmaceuticals,* 15(12)**,** 1-9.

PARLATI, L., HOLLANDE, C. & POL, S. 2021. Treatment of hepatitis C virus infection. *Clinics and Research in Hepatology and Gastroenterology,* 45(4)**,** 1-8.

PARVEZ, M. K., AHMED, S., AL-DOSARI, M. S., ABDELWAHID, M. A., ARBAB, A. H., AL-REHAILY, A. J. & AL-OQAIL, M. M. 2021. Novel anti-hepatitis B virus activity of *Euphorbia schimperi* and its quercetin and kaempferol derivatives. *ACS Omega,* 6**,** 29100-29110.

PAWLOTSKY, J.-M. 2013. Hepatitis C virus: standard-of-care treatment. *Advances in Pharmacology,* 67**,** 169-215.

PERELSON, A. S., RONG, L. & HAYDEN, F. G. 2012. Combination antiviral therapy for influenza: predictions from modeling of human infections. *The Journal of Infectious Diseases,* 205**,** 1642-1645.

PEREZ, R. 2003. Antiviral activity of compounds isolated from plants. *Pharmaceutical Biology,* 41**,** 107-157.

PETERS, B. & CONWAY, K. 2011. Therapy for HIV: past, present, and future. *Advances in Dental Research,* 23**,** 23-27.

PIASECKA, A., JEDRZEJCZAK-REY, N. & BEDNAREK, P. 2015. Secondary metabolites in plant innate immunity: conserved function of divergent chemicals. *New Phytologist,* 206**,** 948-964.

PISONERO-VAQUERO, S., GARCÍA-MEDIAVILLA, M. V., JORQUERA, F., MAJANO, P. L., BENET, M., JOVER, R., GONZÁLEZ-GALLEGO, J. & SÁNCHEZ-CAMPOS, S. 2014. Modulation of PI3K-LXRα-dependent lipogenesis mediated by oxidative/nitrosative stress contributes to inhibition of HCV replication by quercetin. *Laboratory Investigation,* 94**,** 262-274.

PONTICELLI, M., BELLONE, M. L., PARISI, V., IANNUZZI, A., BRACA, A., DE TOMMASI, N., RUSSO, D., SILEO, A., QUARANTA, P. & FREER, G. 2023. Specialized metabolites from plants as a source of new multi-target antiviral drugs: a systematic review. *Phytochemistry Reviews,* 22**,** 615-693.

POON, W., ZHANG, Y.-N., OUYANG, B., KINGSTON, B. R., WU, J. L., WILHELM, S. & CHAN, W. C. 2019. Elimination pathways of nanoparticles. *ACS Nano,* 13**,** 5785-5798.

PRADHAN, D., BISWASROY, P., GOYAL, A., GHOSH, G. & RATH, G. 2021. Recent advancement in nanotechnology-based drug delivery system against viral infections. *Aaps Pharmscitech,* 22**,** 1-19.

RAJPUT, A. & KUMAR, M. 2022. Anti-Ebola: An initiative to predict Ebola virus inhibitors through machine learning. *Molecular Diversity,* 26**,** 1635-1644.

RAMANAN, V., SHLOMAI, A., COX, D. B., SCHWARTZ, R. E., MICHAILIDIS, E., BHATTA, A., SCOTT, D. A., ZHANG, F., RICE, C. M. & BHATIA, S. N. 2015. CRISPR/Cas9 cleavage of viral DNA efficiently suppresses hepatitis B virus. *Scientific Reports,* 5**,** 1-9.

RAO, B. G., MURCKO, M., TEBBE, M. J. & KWONG, A. D. 2015. Discovery and development of Telaprevir (Incivek™)–a protease inhibitor to treat hepatitis C infection. *Successful Drug Discovery***,** 195-212.

REINA, G., PENG, S., JACQUEMIN, L., ANDRADE, A. F. & BIANCO, A. 2020. Hard nanomaterials in time of viral pandemics. *ACS Nano,* 14**,** 9364-9388.

RENZETTE, N., CAFFREY, D. R., ZELDOVICH, K. B., LIU, P., GALLAGHER, G. R., AIELLO, D., PORTER, A. J., KURT-JONES, E. A., BOLON, D. N. & POH, Y.-P. 2014. Evolution of the influenza A virus genome during development of oseltamivir resistance in vitro. *Journal of Virology,* 88**,** 272-281.

RICCIARDI, S., GUARINO, A. M., GIAQUINTO, L., POLISHCHUK, E. V., SANTORO, M., DI TULLIO, G., WILSON, C., PANARIELLO, F., SOARES, V. C. & DIAS, S. S. 2022. The role of NSP6 in the biogenesis of the SARS-CoV-2 replication organelle. *Nature,* 606**,** 761-768.

RICHARD, S. A. 2021. Exploring the pivotal immunomodulatory and anti-inflammatory potentials of glycyrrhizic and glycyrrhetinic acids. *Mediators of Inflammation,* 1, 1-15.

RICHMAN, D.D. AND NATHANSON, N. 2016. Antiviral therapy. *Viral Pathogenesis*, 12, 271–287.

ROBINSON, B. S., RICCARDI, K. A., GONG, Y.-F., GUO, Q., STOCK, D. A., BLAIR, W. S., TERRY, B. J., DEMINIE, C. A., DJANG, F. & COLONNO, R. J. 2000. BMS-232632, a highly potent human immunodeficiency virus protease inhibitor that can be used in combination with other available antiretroviral agents. *Antimicrobial Agents and Chemotherapy,* 44**,** 2093-2099.

RODRÍGUEZ-PÉREZ, R. & BAJORATH, J. 2022. Evolution of support vector machine and regression modeling in chemoinformatics and drug discovery. *Journal of Computer-Aided Molecular Design,* 36**,** 355-362.

ROTONDO, J. C., MAZZIOTTA, C., LANZILLOTTI, C., TOGNON, M. & MARTINI, F. 2021. Epigenetic dysregulations in merkel cell polyomavirus-driven merkel cell carcinoma. *International Journal of Molecular Sciences,* 22(21)**,** 1-19.

RUAN, S., TANG, J., QIN, Y., WANG, J., YAN, T., ZHOU, J., GAO, D., XU, E. & LIU, D. 2022. Mechanical force-induced dispersion of starch nanoparticles and nanoemulsion: Size control, dispersion behaviour, and emulsified stability. *Carbohydrate Polymers,* 275**,** 1-11.

RUTENBER, E. E. & STROUD, R. M. 1996. Binding of the anticancer drug ZD1694 to E. coli thymidylate synthase: assessing specificity and affinity. *Structure,* 4**,** 1317-1324.

RYOM, L., BOESECKE, C., GISLER, V., MANZARDO, C., ROCKSTROH, J. K., PUOTI, M., FURRER, H., MIRO, J., GATELL, J. M. & POZNIAK, A. 2016. Essentials from the 2015 European AIDS Clinical Society (EACS) guidelines for the treatment of adult HIV-positive persons. *HIV medicine,* 17**,** 83-88.

SAAG, M. S., BENSON, C. A., GANDHI, R. T., HOY, J. F., LANDOVITZ, R. J., MUGAVERO, M. J., SAX, P. E., SMITH, D. M., THOMPSON, M. A. & BUCHBINDER, S. P. 2018. Antiretroviral drugs for treatment and prevention of HIV infection in adults: 2018 recommendations of the International Antiviral Society–USA Panel. *Jama,* 320**,** 379-396.

SAIVISH, M. V., PACCA, C. C., DA COSTA, V. G., DE LIMA MENEZES, G., DA SILVA, R. A., NEBO, L., DA SILVA, G. C. D., DE AGUIAR MILHIM, B. H. G., DA SILVA TEIXEIRA, I. & HENRIQUE, T. 2023. Caffeic acid has antiviral activity against Ilheus virus *in vitro*. *Viruses,* 15(2)**,** 1-20.

SAMJI, H., CESCON, A., HOGG, R. S., MODUR, S. P., ALTHOFF, K. N., BUCHACZ, K., BURCHELL, A. N., COHEN, M., GEBO, K. A. & GILL, M. J. 2013. Closing the gap:

increases in life expectancy among treated HIV-positive individuals in the United States and Canada. *PloS One,* 8(12)**,** 1-8.

SARRAZIN, C., COOPER, C. L., MANNS, M. P., REDDY, K. R., KOWDLEY, K. V., ROBERTS, S. K., DVORY-SOBOL, H., SVAROVSKIA, E., MARTIN, R. & CAMUS, G. 2018. No impact of resistance-associated substitutions on the efficacy of sofosbuvir, velpatasvir, and voxilaprevir for 12 weeks in HCV DAA-experienced patients. *Journal of Hepatology,* 69**,** 1221-1230.

SAXENA, S. K., SAXENA, S., SAXENA, R., SWAMY, M. A., GUPTA, A. & NAIR, M. P. 2010. Emerging trends, challenges and prospects in antiviral therapeutics and drug development for infectious diseases. *Electronic Journal of Biology,* 6**,** 26-31.

SAXENA, S.K., MISHRA, N. AND SAXENA, R. 2009. Advances in antiviral drug discovery and development: Part I: Advancements in antiviral drug discovery. *Future Virology*, 4(2), 101-107.

SCHAMES, J. R., HENCHMAN, R. H., SIEGEL, J. S., SOTRIFFER, C. A., NI, H. & MCCAMMON, J. A. 2004. Discovery of a novel binding trench in HIV integrase. *Journal of Medicinal Chemistry,* 47**,** 1879-1881.

SCHNEIDER, P., WALTERS, W. P., PLOWRIGHT, A. T., SIEROKA, N., LISTGARTEN, J., GOODNOW JR, R. A., FISHER, J., JANSEN, J. M., DUCA, J. S. & RUSH, T. S. 2020. Rethinking drug design in the artificial intelligence era. *Nature Reviews Drug Discovery,* 19**,** 353-364.

SCHOEMAN, D. & FIELDING, B. C. 2019. Coronavirus envelope protein: current knowledge. *Virology Journal,* 16**,** 1-22.

SCHÖNING, V. & HAMMANN, F. 2018. How far have decision tree models come for data mining in drug discovery? *Expert Opinion on Drug Discovery,* 13**,** 1067-1069.

SCHOOF, M., FAUST, B., SAUNDERS, R. A., SANGWAN, S., REZELJ, V., HOPPE, N., BOONE, M., BILLESBØLLE, C. B., PUCHADES, C. & AZUMAYA, C. M. 2020. An ultrapotent synthetic nanobody neutralizes SARS-CoV-2 by stabilizing inactive Spike. *Science,* 370**,** 1473-1479.

SCOTT, T., MOYO, B., NICHOLSON, S., MAEPA, M. B., WATASHI, K., ELY, A., WEINBERG, M. S. & ARBUTHNOT, P. 2017. ssAAVs containing cassettes encoding SaCas9 and guides targeting hepatitis B virus inactivate replication of the virus in cultured cells. *Scientific Reports,* 7**,** 1-11.

SEEGER, C. & SOHN, J. A. 2014. Targeting hepatitis B virus with CRISPR/Cas9. *Molecular Therapy-Nucleic Acids,* 3, 1-7.

SEGALL, M. D. & BARBER, C. 2014. Addressing toxicity risk when designing and selecting compounds in early drug discovery. *Drug Discovery Today,* 19**,** 688-693.

SELIM, S., ALBQMI, M., ALANAZI, A., ALRUWAILI, Y., AL-SANEA, M. M., ALNUSAIRE, T. S., ALMUHAYAWI, M. S., AL JAOUNI, S. K., HUSSEIN, S. & WARRAD, M. 2023. Antiviral activities of olive oil apigenin and taxifolin against SARS-CoV-2 RNA-dependent RNA polymerase (RdRP): *in silico*, pharmacokinetic, ADMET, and *in vitro* approaches. *Cogent Food & Agriculture,* 9(1)**,** 1-16.

SEPTEMBRE-MALATERRE, A., BOUMENDJEL, A., SETEYEN, A.-L. S., BOINA, C., GASQUE, P., GUIRAUD, P. & SÉLAMBAROM, J. 2022. Focus on the high therapeutic potentials of quercetin and its derivatives. *Phytomedicine Plus,* 2(1)**,** 1-18.

SHAM, H. L., KEMPF, D. J., MOLLA, A., MARSH, K. C., KUMAR, G. N., CHEN, C.-M., KATI, W., STEWART, K., LAL, R. & HSU, A. 1998. ABT-378, a highly potent inhibitor of the human immunodeficiency virus protease. *Antimicrobial Agents and Chemotherapy,* 42**,** 3218-3224.

SHAN, T., YE, J., JIA, J., WANG, Z., JIANG, Y., WANG, Y., WANG, Y., ZHENG, K. & REN, Z. 2021. Viral UL8 is involved in the antiviral activity of oleanolic acid against HSV-1 infection. *Frontiers in Microbiology,* 12**,** 1-12.

SHAO, L., SU, Y., ZHANG, Y., YANG, F., ZHANG, J., TANG, T. & YU, F. 2023. Nine-valent oleanolic acid conjugates as potent inhibitors blocking the entry of influenza A virus. *European Journal of Medicinal Chemistry,* 258**,** 1-11.

SILICIANO, R. F. & GREENE, W. C. 2011. HIV latency. *Cold Spring Harbor Perspectives in Medicine,* 1**,** 1-20.

SIMM, J., KLAMBAUER, G., ARANY, A., STEIJAERT, M., WEGNER, J. K., GUSTIN, E., CHUPAKHIN, V., CHONG, Y. T., VIALARD, J. & BUIJNSTERS, P. 2018. Repurposing high-throughput image assays enables biological activity prediction for drug discovery. *Cell Chemical Biology,* 25**,** 611-618.

SINGH, L., KRUGER, H. G., MAGUIRE, G. E., GOVENDER, T. & PARBOOSING, R. 2017. The role of nanotechnology in the treatment of viral infections. *Therapeutic Advances in Infectious Disease,* 4**,** 105-131.

SINGH, S., VERMA, A. K., THAKUR, G., SHARMA, S. & AWASTHI, A. 2023. Quercetin: a putative eco-friendly wide spectrum antiviral against dengue. *Macromolecular Symposia*, 410, 1-5.

SONG, J., ZHANG, L., XU, Y., YANG, D., YANG, S., ZHANG, W., WANG, J., TIAN, S., YANG, S. & YUAN, T. 2021. The comprehensive study on the therapeutic effects of baicalein for the treatment of COVID-19 *in vivo* and *in vitro*. *Biochemical Pharmacology,* 183**,** 1-9.

SPECK, S. H. & GANEM, D. 2010. Viral latency and its regulation: lessons from the γ-herpesviruses. *Cell Host & Microbe,* 8**,** 100-115.

STEINER, M. C., GIBSON, K. M. & CRANDALL, K. A. 2020. Drug resistance prediction using deep learning techniques on HIV-1 sequence data. *Viruses,* 12(5)**,** 1-25.

STERNBERG, S. H. & DOUDNA, J. A. 2015. Expanding the biologist's toolkit with CRISPR-Cas9. *Molecular Cell,* 58**,** 568-574.

STOUCH, T. R., KENYON, J. R., JOHNSON, S. R., CHEN, X.-Q., DOWEYKO, A. & LI, Y. 2003. *In silico* ADME/Tox: why models fail. *Journal of Computer-Aided Molecular Design,* 17**,** 83-92.

STUMPFE, D., HU, H. & BAJORATH, J. R. 2019. Evolving concept of activity cliffs. *ACS Omega,* 4**,** 14360-14368.

SU, G., CHEN, Y., LI, X. & SHAO, J. W. 2024. Virus versus host: Influenza A virus circumvents the immune responses. *Frontiers in Microbiology*, 15(1394510), 1-11.

SUN, Y., TAO, Q., CAO, Y., YANG, T., ZHANG, L., LUO, Y. & WANG, L. 2023. Kaempferol has potential anti-coronavirus disease 2019 (COVID-19) targets based on bioinformatics analyses and pharmacological effects on endotoxin-induced cytokine storm. *Phytotherapy Research,* 37**,** 2290-2304.

SURNAR, B., KAMRAN, M. Z., SHAH, A. S., BASU, U., KOLISHETTI, N., DEO, S., JAYAWEERA, D. T., DAUNERT, S. & DHAR, S. 2019. Orally administrable therapeutic synthetic nanoparticle for Zika virus. *ACS Nano,* 13**,** 11034-11048.

SWARUP, V., GHOSH, J., GHOSH, S., SAXENA, A. & BASU, A. 2007. Antiviral and anti-inflammatory effects of rosmarinic acid in an experimental murine model of Japanese encephalitis. *Antimicrobial Agents and Chemotherapy,* 51**,** 3367-3370.

TALELE, T. T., KHEDKAR, S. A. & RIGBY, A. C. 2010. Successful applications of computer aided drug discovery: moving drugs from concept to the clinic. *Current Topics in Medicinal Chemistry,* 10**,** 127-141.

TEBAS, P., STEIN, D., TANG, W. W., FRANK, I., WANG, S. Q., LEE, G., SPRATT, S. K., SUROSKY, R. T., GIEDLIN, M. A. & NICHOL, G. 2014. Gene editing of CCR5 in autologous CD4 T cells of persons infected with HIV. *New England Journal of Medicine,* 370**,** 901-910.

THIRUMURUGAN, D., CHOLARAJAN, A., RAJA, S. & VIJAYAKUMAR, R. 2018. An introductory chapter: secondary metabolites. *Secondary metabolites-sources and applications,* 1-48.

THOMPSON, N. C., GREENEWALD, K., LEE, K. & MANSO, G. F. 2020. The computational limits of deep learning. *ArXiv, Cornell University,* 1-16.

TIAN, L., LI, X., JI, H., YU, Q., YANG, M., GUO, L., HUANG, L. & GAO, W. 2022. Melanin-like nanoparticles: advances in surface modification and tumour photothermal therapy. *Journal of Nanobiotechnology,* 20 (485), 1-29.

TON, A. T., GENTILE, F., HSING, M., BAN, F. & CHERKASOV, A. 2020. Rapid identification of potential inhibitors of SARS-CoV-2 main protease by deep docking of 1.3 billion compounds. *Molecular Informatics,* 39**,** 1-7.

TONG, T., HU, H., ZHOU, J., DENG, S., ZHANG, X., TANG, W., FANG, L., XIAO, S. & LIANG, J. 2020. Glycyrrhizic-acid-based carbon dots with high antiviral activity by multisite inhibition mechanisms. *Small,* 16**,** 1-12.

TRAYLEN, C. M., PATEL, H. R., FONDAW, W., MAHATME, S., WILLIAMS, J. F., WALKER, L. R., DYSON, O. F., ARCE, S. & AKULA, S. M. 2011. Virus reactivation: a panoramic view in human infections. *Future Virology,* 6**,** 451-463.

TROOSKIN, S. B., REYNOLDS, H. & KOSTMAN, J. R. 2015. Access to costly new hepatitis C drugs: medicine, money, and advocacy. *Clinical Infectious Diseases,* 61**,** 1825-1830.

TROPSHA, A. 2010. Best practices for QSAR model development, validation, and exploitation. *Molecular Informatics,* 29**,** 476-488.

TSENG, C.-K., HSU, S.-P., LIN, C.-K., WU, Y.-H., LEE, J.-C. & YOUNG, K.-C. 2017. Celastrol inhibits hepatitis C virus replication by upregulating heme oxygenase-1 via the JNK MAPK/Nrf2 pathway in human hepatoma cells. *Antiviral Research,* 146**,** 191-200.

TSUKUDA, S. & WATASHI, K. 2020. Hepatitis B virus biology and life cycle. *Antiviral Research,* 182**,** 1-10.

TUTUNCHI, H., NAEINI, F., OSTADRAHIMI, A. & HOSSEINZADEH-ATTAR, M. J. 2020. Naringenin, a flavanone with antiviral and anti-inflammatory effects: A promising treatment strategy against COVID-19. *Phytotherapy Research,* 34**,** 3137-3147.

UNTERTHINER, T., MAYR, A., KLAMBAUER, G., STEIJAERT, M., WEGNER, J. K., CEULEMANS, H. & HOCHREITER, S. Deep learning as an opportunity in virtual screening. Proceedings of the deep learning workshop at NIPS, 2014. MIT Press Cambridge, MA, United States, 1-9.

UTSUNOMIYA, H., ICHINOSE, M., IKEDA, K., UOZAKI, M., MORISHITA, J., KUWAHARA, T., KOYAMA, A. H. & YAMASAKI, H. 2014. Inhibition by caffeic acid of the influenza A virus multiplication in vitro. *International Journal of Molecular Medicine,* 34**,** 1020-1024.

UVA, M., MENCUCCINI, L., ATREI, A., INNOCENTI, C., FANTECHI, E., SANGREGORIO, C., MAGLIO, M., FINI, M. & BARBUCCI, R. 2015. On the mechanism of drug release from polysaccharide hydrogels cross-linked with magnetite nanoparticles by applying alternating magnetic fields: the case of doxo delivery. *Gels,* 1**,** 24-43.

VAMATHEVAN, J., CLARK, D., CZODROWSKI, P., DUNHAM, I., FERRAN, E., LEE, G., LI, B., MADABHUSHI, A., SHAH, P. & SPITZER, M. 2019. Applications of machine

learning in drug discovery and development. *Nature Reviews Drug Discovery,* 18**,** 463-477.

VAN DIEMEN, F. R., KRUSE, E. M., HOOYKAAS, M. J., BRUGGELING, C. E., SCHÜRCH, A. C., VAN HAM, P. M., IMHOF, S. M., NIJHUIS, M., WIERTZ, E. J. & LEBBINK, R. J. 2016. CRISPR/Cas9-mediated genome editing of herpesviruses limits productive and latent infections. *PLoS Pathogens,* 12(6)**,** 1-29.

VAN DRIE, J. H. 2007. Computer-aided drug design: the next 20 years. *Journal of Computer-Aided Molecular Design,* 21**,** 591-601.

VAUGHAN, H. J., GREEN, J. J. & TZENG, S. Y. 2020. Cancer-targeting nanoparticles for combinatorial nucleic acid delivery. *Advanced Materials,* 32**,** 1-36.

VERMA, A., UZUN, O., HU, Y., HU, Y., HAN, H.-S., WATSON, N., CHEN, S., IRVINE, D. J. & STELLACCI, F. 2008. Surface-structure-regulated cell-membrane penetration by monolayer-protected nanoparticles. *Nature Materials,* 7**,** 588-595.

VERMA, V., RYAN, K. M. & PADRELA, L. 2021. Production and isolation of pharmaceutical drug nanoparticles. *International Journal of Pharmaceutics,* 603**,** 1-22.

VIDAL, D., GARCIA-SERNA, R. & MESTRES, J. 2011. Ligand-based approaches to *in silico* pharmacology. *Chemoinformatics and Computational Chemical Biology***,** 489-502.

VON ITZSTEIN, M., WU, W.-Y., KOK, G. B., PEGG, M. S., DYASON, J. C., JIN, B., VAN PHAN, T., SMYTHE, M. L., WHITE, H. F. & OLIVER, S. W. 1993. Rational design of potent sialidase-based inhibitors of influenza virus replication. *Nature,* 363**,** 418-423.

WANG, Y., FAN, G., SALAM, A., HORBY, P., HAYDEN, F. G., CHEN, C., PAN, J., ZHENG, J., LU, B. & GUO, L. 2020. Comparative effectiveness of combined favipiravir and oseltamivir therapy versus oseltamivir monotherapy in critically ill patients with influenza virus infection. *The Journal of Infectious Diseases,* 221**,** 1688-1698.

WANG, Z., MA, W., FU, X., QI, Y., ZHAO, Y. & ZHANG, S. 2023. Development and applications of mRNA treatment based on lipid nanoparticles. *Biotechnology Advances,* 65**,** 1-23.

WEN, B. & GORYCKI, P. 2019. Bioactivation of herbal constituents: Mechanisms and toxicological relevance. *Drug Metabolism Reviews,* 51**,** 453-497.

WLODAWER, A. & VONDRASEK, J. 1998. Inhibitors of HIV-1 protease: a major success of structure-assisted drug design. *Annual Review of Biophysics and Biomolecular Structure,* 27**,** 249-284.

WOLFF, G., LIMPENS, R. W., ZEVENHOVEN-DOBBE, J. C., LAUGKS, U., ZHENG, S., DE JONG, A. W., KONING, R. I., AGARD, D. A., GRÜNEWALD, K. & KOSTER, A. J. 2020. A molecular pore spans the double membrane of the coronavirus replication organelle. *Science,* 369**,** 1395-1398.

WORLD HEALTH ORGANIZATION (2024). Hepatitis C. WHO Website. www.who.int/news-room/fact-sheets/detail/ hepatitis-c. Updated April 9, 2024 [Accessed October 10, 2024]

WRAPP, D., WANG, N., CORBETT, K. S., GOLDSMITH, J. A., HSIEH, C.-L., ABIONA, O., GRAHAM, B. S. & MCLELLAN, J. S. 2020. Cryo-EM structure of the 2019-nCoV spike in the prefusion conformation. *Science,* 367**,** 1260-1263.

WU, S., SKOLNICK, J. & ZHANG, Y. 2007. Ab initio modeling of small proteins by iterative TASSER simulations. *BMC Biology,* 5**,** 1-10.

XIAO-JIE, L., HUI-YING, X., ZUN-PING, K., JIN-LIAN, C. & LI-JUAN, J. 2015. CRISPR-Cas9: a new and promising player in gene therapy. *Journal of Medical Genetics,* 52**,** 289-296.

XIN, X., PEI, X., YANG, X., LV, Y., ZHANG, L., HE, W. & YIN, L. 2017. Rod-shaped active drug particles enable efficient and safe gene delivery. *Advanced Science,* 4**,** 1-11.

XIONG, P., HUANG, X., YE, N., LU, Q., ZHANG, G., PENG, S., WANG, H. & LIU, Y. 2022. Cytotoxicity of metal-based nanoparticles: from mechanisms and methods of evaluation to pathological manifestations. *Advanced Science,* 9**,** 1-22.

YADAVALLI, T. & SHUKLA, D. 2017. Role of metal and metal oxide nanoparticles as diagnostic and therapeutic tools for highly prevalent viral infections. *Nanomedicine: Nanotechnology, Biology and Medicine,* 13**,** 219-230.

YANG, L., WEN, K.-S., RUAN, X., ZHAO, Y.-X., WEI, F. & WANG, Q. 2018. Response of plant secondary metabolites to environmental factors. *Molecules,* 23**,** 1-26.

YANG, X., HE, Z., ZHENG, Y., WANG, N., MULINGE, M., SCHMIT, J.-C., STEINMETZ, A. & SEGUIN-DEVAUX, C. 2021. Chemical constituents of *Cassia abbreviata* and their anti-HIV-1 activity. *Molecules,* 26**,** 1-8.

YANG, X., LONG, F., JIA, W., ZHANG, M., SU, G., LIAO, M., ZENG, Z., CHEN, W. & CHEN, J. 2023. Artesunate inhibits PDE4 leading to intracellular cAMP accumulation, reduced ERK/MAPK signaling, and blockade of influenza A virus vRNP nuclear export. *Antiviral Research,* 215**,** 1-14.

YAZDI, A. S., GUARDA, G., RITEAU, N., DREXLER, S. K., TARDIVEL, A., COUILLIN, I. & TSCHOPP, J. 2010. Nanoparticles activate the NLR pyrin domain containing 3 (Nlrp3) inflammasome and cause pulmonary inflammation through release of IL-1α and IL-1β. *Proceedings of the National Academy of Sciences,* 107**,** 19449-19454.

YESHI, K., CRAYN, D., RITMEJERYTĖ, E. & WANGCHUK, P. 2022. Plant secondary metabolites produced in response to abiotic stresses has potential application in pharmaceutical product development. *Molecules,* 27**,** 1-31.

YIN, L., ZHAO, F., SUN, H., WANG, Z., HUANG, Y., ZHU, W., XU, F., MEI, S., LIU, X. & ZHANG, D. 2020a. CRISPR-Cas13a inhibits HIV-1 infection. *Molecular Therapy-Nucleic Acids,* 21**,** 147-155.

YIN, W., MAO, C., LUAN, X., SHEN, D.-D., SHEN, Q., SU, H., WANG, X., ZHOU, F., ZHAO, W. & GAO, M. 2020b. Structural basis for inhibition of the RNA-dependent RNA polymerase from SARS-CoV-2 by remdesivir. *Science,* 368**,** 1499-1504.

YU, J. S., TSENG, C. K., LIN, C. K., HSU, Y. C., WU, Y. H., HSIEH, C. L. & LEE, J. C. 2017. Celastrol inhibits dengue virus replication via up-regulating type I interferon and downstream interferon-stimulated responses. *Antiviral Research,* 137**,** 49-57.

YU, L., WANG, X., ZHU, D., DING, W., WANG, L., ZHANG, C., JIANG, X., SHEN, H., LIAO, S. & MA, D. 2015. Disruption of human papillomavirus 16 E6 gene by clustered regularly interspaced short palindromic repeat/Cas system in human cervical cancer cells. *OncoTargets and Therapy,* 8**,** 37-44.

YU, M., XU, J. & ZHENG, J. 2019. Renal clearable luminescent gold nanoparticles: from the bench to the clinic. *Angewandte Chemie International Edition,* 58**,** 4112-4128.

YUEN, K.-S., CHAN, C.-P., WONG, N.-H. M., HO, C.-H., HO, T. H., LEI, T., DENG, W., TSAO, S. W., CHEN, H. & KOK, K. H. 2015. CRISPR/Cas9-mediated genome editing of Epstein–Barr virus in human cells. *Journal of General Virology,* 96**,** 626-636.

ZAREIFOPOULOS, N., LAGADINOU, M., KARELA, A., KYRIAKOPOULOU, O. & VELISSARIS, D. 2020. Neuropsychiatric effects of antiviral drugs. *Cureus*, *12*(8), 1-12.

ZENG, L., LIU, Y., NGUYENLA, X. H., ABBOTT, T. R., HAN, M., ZHU, Y., CHEMPARATHY, A., LIN, X., CHEN, X. & WANG, H. 2022. Broad-spectrum CRISPR-mediated inhibition of SARS-CoV-2 variants and endemic coronaviruses *in vitro*. *Nature Communications,* 13**,** 1-16.

ZHANG, H., SARAVANAN, K. M., YANG, Y., HOSSAIN, M. T., LI, J., REN, X., PAN, Y. & WEI, Y. 2020. Deep learning based drug screening for novel coronavirus 2019-nCov. *Interdisciplinary Sciences: Computational Life Sciences,* 12**,** 368-376.

ZHANG, L., TAN, J., HAN, D. & ZHU, H. 2017. From machine learning to deep learning: progress in machine intelligence for rational drug discovery. *Drug Discovery Today,* 22**,** 1680-1685.

ZHANG, Y. & LI, M. 2021. Genome editing technologies as cellular defense against viral pathogens. *Frontiers in Cell and Developmental Biology,* 9**,** 1-9.

ZHANG, Y., YE, T., XI, H., JUHAS, M. & LI, J. 2021. Deep learning driven drug discovery: tackling severe acute respiratory syndrome coronavirus 2. *Frontiers in Microbiology,* 12**,** 1-8.

ZHAO, W. 2017. Research on the deep learning of the small sample data based on transfer learning. *AIP Conference Proceedings*, 1864, 1-8.

ZHEN, S., HUA, L., LIU, Y., GAO, L., FU, J., WAN, D., DONG, L., SONG, H. & GAO, X. 2015. Harnessing the clustered regularly interspaced short palindromic repeat (CRISPR)/CRISPR-associated Cas9 system to disrupt the hepatitis B virus. *Gene Therapy,* 22**,** 404-412.

ZHEN, S., HUA, L., TAKAHASHI, Y., NARITA, S., LIU, Y.-H. & LI, Y. 2014. *In vitro* and *in vivo* growth suppression of human papillomavirus 16-positive cervical cancer cells by CRISPR/Cas9. *Biochemical and Biophysical Research Communications,* 450**,** 1422-1426.

ZHENG, Y., YANG, X.-W., SCHOLS, D., MORI, M., BOTTA, B., CHEVIGNÉ, A., MULINGE, M., STEINMETZ, A., SCHMIT, J.-C. & SEGUIN-DEVAUX, C. 2021. Active components from *Cassia abbreviata* prevent HIV-1 entry by distinct mechanisms of action. *International Journal of Molecular Sciences,* 22(9)**,** 1-21.

ZHOU, H., GAO, S.-J., ZHANG, M.-T., JIA, J., CHEN, F.-X., CHEN, C.-L., YANG, P.-F. & MAO, J.-L. 2023. Synthesis, configurational analysis and antiviral activities of novel

diphenylacrylic acids with caffeic acid as the lead compound. *Journal of Molecular Structure,* 1291**,** 1-11.

ZHOU, J., SHEN, B., ZHANG, W., WANG, J., YANG, J., CHEN, L., ZHANG, N., ZHU, K., XU, J. & HU, B. 2014. One-step generation of different immunodeficient mice with multiple gene modifications by CRISPR/Cas9 mediated genome engineering. *The International Journal of Biochemistry & Cell Biology,* 46**,** 49-55.

ZHU, Y., SHAO, Y., QU, X., GUO, J., YANG, J., ZHOU, Z. & WANG, S. 2019. Sodium ferulate protects against influenza virus infection by activation of the TLR7/9-MyD88-IRF7 signaling pathway and inhibition of the NF-κB signaling pathway. *Biochemical and Biophysical Research Communications,* 512**,** 793-798.

ZUMLA, A., CHAN, J. F., AZHAR, E. I., HUI, D. S. & YUEN, K.-Y. 2016. Coronaviruses—drug discovery and therapeutic options. *Nature Reviews Drug discovery,* 15**,** 327-347.

References for section 2.1

ADAMSON, C. S., CHIBALE, K., GOSS, R. J., JASPARS, M., NEWMAN, D. J. & DORRINGTON, R. A. 2021. Antiviral drug discovery: preparing for the next pandemic. *Chemical Society Reviews*, 50, 3647-3655.

CHEN, L., DENG, Y., DONG, S., WANG, H., LI, P., ZHANG, H. & CHU, W. 2021. The occurrence and control of waterborne viruses in drinking water treatment: a review. *Chemosphere* 130728, 1–11.

CHEUNG, Y. Y. H., LAU, E. H. Y., YIN, G., LIN, Y., COWLING, B. J. & LAM, K. F. 2024. Effectiveness of vaccines and antiviral drugs in preventing severe and fatal COVID-19, Hong Kong. *Emerging Infectious Diseases*, 30(1), 70-78.

CLEMENTE, J. C., URSELL, L. K., PARFREY, L. W. & KNIGHT, R. 2012. The impact of the gut microbiota on human health: an integrative view. *Cell,* 148, 1258–1270.

CONTROL & PREVENTION 2013. Prevention and control of seasonal influenza with vaccines. Recommendations of the advisory committee on immunization practices--United States, 2013-2014. MMWR 62, 1–43.

CORTEZ, V., MELIOPOULOS, V. A., KARLSSON, E. A., HARGEST, V., JOHNSON, C., & SCHULTZ-CHERRY, S. 2017. Astrovirus biology and pathogenesis. *Annual Review of Virology*, 4, 327–348.

FANCELLO, L., RAOULT, D. & DESNUES, C. 2012. Computational tools for viral metagenomics and their application in clinical research. *Virology*, 434, 162-174.

FARKAS, K., HILLARY, L. S., MALHAM, S. K., MCDONALD, J. E. & JONES, D. L. 2020. Wastewater and public health: the potential of wastewater surveillance for monitoring COVID-19. *Current. Opinion in Environmental. Science and Health,* 17, 14–20.

GALL, A. M., MARIÑAS, B. J., LU, Y. & SHISLER, J. L. 2015. Waterborne viruses: a barrier to safe drinking water. *PLoS Pathogens*, 11(6), 1-7.

GARNER, E., DAVIS, B. C., MILLIGAN, E., BLAIR, M. F., KEENUM, I., MAILE-MOSKOWITZ, A., PAN, J., GNEGY, M., LIGUORI, K. & GUPTA, S. 2021. Next generation sequencing approaches to evaluate water and wastewater quality. *Water Research*, 194, 1-24.

GERETTI, A. M., ARMENIA, D. & CECCHERINI-SILBERSTEIN, F. 2012. Emerging patterns and implications of HIV-1 integrase inhibitor resistance. *Current Opinion in Infectious Diseases*, 25, 677-686.

GONZALES-GUSTAVSON, E., RUSIÑOL, M., MEDEMA, G., CALVO, M. & GIRONES, R. 2019. Quantitative risk assessment of norovirus and adenovirus for the use of reclaimed water to irrigate lettuce in Catalonia. *Water Research,* 153, 91–99.

IBRAHIM, Y., OUDA, M., KADADOU, D., BANAT, F., NADDEO, V., ALSAFAR, H., YOUSEF, A.F., BARCELO, D. & HASAN, S. W. 2021. Detection and removal of waterborne enteric viruses from wastewater: a comprehensive review. *Journal of Environmental Chemical Engineering,* 9(4), 1-25.

KAUSAR, S., SAID KHAN, F., ISHAQ MUJEEB UR REHMAN, M., AKRAM, M., RIAZ, M., RASOOL, G., HAMID KHAN, A., SALEEM, I., SHAMIM, S. & MALIK, A. 2021. A review: mechanism of action of antiviral drugs. *International Journal of Immunopathology and Pharmacology*, 35, 1-12.

LI, L.L., LIU, N., YU, J.M., AO, Y.Y., LI, S., STINE, O.C. & DUAN, Z.J. 2017. Analysis of Aichi virus and Saffold virus association with pediatric acute gastroenteritis. *Journal of Clinical Virology*, 87, 37-42.

LI, S., XIE, Y., YU, C., ZHENG, C. & XU, Z. 2024. The battle between host antiviral innate immunity and immune evasion by cytomegalovirus. *Cellular and Molecular Life Sciences*, *81*(1), 1-19.

LOCARNINI, S. A. & YUEN, L. 2010. Molecular genesis of drug-resistant and vaccine-escape HBV mutants. *Antiviral Therapy*, 15, 451-461.

MCCALL, C. & XAGORARAKI, I. 2019. Metagenomic approaches for detecting viral diversity in water environments. *Journal of Environmental Engineering*, 145(8), 1-9.

SCHOEMAN, D. & FIELDING, B. C. 2019. Coronavirus envelope protein: current knowledge. *Virology Journal*, 16, 1-22.

TANG, A., BI, X., LI, X., LI, F., LIAO, X., ZOU, J., SUN, W. & YUAN, B. 2020. The inactivation of bacteriophage MS2 by sodium hypochlorite in the presence of particles. *Chemosphere* 266, 1-8.

WORLD HEALTH ORGANIZATION, 2012. Global costs and benefits of drinking-water supply and sanitation interventions to reach the MDG target and universal coverage. Geneva: WHO

WORLD HEALTH ORGANIZATION, 2014. Waterborne outbreaks of Hepatitis E: recognition, investigation and control. World Health Organization.

WORLD HEALTH ORGANIZATION/UNITED NATIONS CHILDREN EMERGENCY FUND, 2021. Progress on household drinking water, sanitation, and hygiene 2000–2020: five years into the SDGs, Geneva, Switzerland. Retrieved from https://data.unicef.org/resources/progress-on-household-drinking-water-sanitation-and-hygiene-2000-2020/ (accessed September 02, 2022).

WU, Y., GUO, C., TANG, L., HONG, Z., ZHOU, J., DONG, X., YIN, H., XIAO, Q., TANG, Y., QU, X. & KUANG, L. 2020. Prolonged presence of SARS-CoV-2 viral RNA in faecal samples. *The Lancet Gastroenterology & Hepatology* 5, 434–435.

XAGORARAKI, I., YIN, Z. & SVAMBAYEV, Z. 2014. Fate of viruses in water systems. *Journal of Environmental Engineering*, 140, 04014021-040140218.

YEO, C., KAUSHAL, S. & YEO, D. 2020. Enteric involvement of coronaviruses: is faecal–oral transmission of SARS-CoV-2 possible? *The Lancet Gastroenterology & Hepatology,* 5, 335–337.

ZHU, H., YUAN, F., YUAN, Z., LIU, R., XIE, F., HUANG, L., LIU, X., JIANG, X., WANG, J., XU, Q. & SHEN, Z. 2018. Monitoring of Poyang lake water for sewage contamination using human enteric viruses as an indicator. *Virology Journal,* 15, 3–9.

ZWART, M. P., HEMERIK, L., CORY, J. S., DE VISSER, J. A. G., BIANCHI, F. J., VAN OERS, M. M., VLAK JM, HOEKSTRA R.F. & VAN DER WERF W. 2009. An experimental test of the independent action hypothesis in virus–insect pathosystems. *Proceedings of the Royal Society B: Biological Sciences* 276, 2233–2242.

CHAPTER THREE

3.0 Viral landscape of selected wastewater treatment plants and receiving river in eThekwini Municipality, Durban, South Africa: a metagenomic approach

Abstract…….....231

1.0 Introduction…….....232

2.0 Materials and methods……..…234

3.0 Results and discussion…….239

4.0 Conclusion……....…....265

References…….…….265

Supplementary information……....286

This chapter has been formatted for submission to BMC Genomics

Viral landscape of selected wastewater treatment plants and receiving river in eThekwini Municipality, Durban, South Africa: a metagenomic approach

Adedayo Ayodeji Lanrewaju[1], Abimbola Motunrayo Folami[1], James E. San[2], Martin M. Nyaga[3], Saheed Sabiu[1] and Feroz Mahomed Swalaha[1]*

[1]Department of Biotechnology and Food Science, Faculty of Applied Sciences, Durban University of Technology, P. O. Box 1334, Durban 4000, South Africa

[2]Nelson Mandela School of Medicine, KwaZulu-Natal Research Innovation and Sequencing platform unit, University of KwaZulu- Natal, 719 Umbilo Road, Durban 4001, South Africa

[3]Next Generation Sequencing Unit, Division of Virology, Faculty of Health Sciences, University of the Free State, P.O. Box 339, Bloemfontein 9300, South Africa

*Correspondence: fswalaha@dut.ac.za

Abstract

Wastewater treatment plants (WWTPs) reduce water scarcity via treatment before discharge to watercourses or reuse. However, the disinfection processes do not completely remove pathogens, especially viruses, which pose a significant public health threat owing to their low infectious doses and environmental persistence. The diversity and abundance of viruses in WWTPs and their receiving rivers are less investigated than other pathogens such as bacteria and protozoa. Therefore, for the first time, this study examined the viral diversity and distribution of four WWTPs and receiving waters within the eThekwini Municipality, Durban, KwaZulu-Natal, South Africa, using the metagenomic next-generation sequencing approach. A total of 30 viral families spanning broad host ranges including 26 human pathogenic viral species from eight families, were identified across the different sampling sites. The detection of common enteric viruses (Enteroviruses A, B, C, Hepatovirus A, Rotavirus A, Norwalk virus), the emerging neurotropic HMO Astrovirus A (VA1, linked to lethal encephalitis in neonates and immunocompromised patients) and less frequently reported pathogens like Cytomegalovirus emphasized that wastewater could provide insights into the health status of

individuals within a community. Conversely, plant viruses accounted for eight families dominated by the *Virgaviridae* associated with various plants. Most phytopathogenic reads belonged to the Tobamovirus genus with additional representation from the family *Bromoviridae*. Therefore, these findings highlight the significance of wastewater surveillance in tracking known viral infections and unveiling possible emerging viruses that could help in monitoring potential viral threats. Similarly, wastewater-based surveillance techniques might be used to track plant pathogenic viruses in agriculture to detect, study and curb viral spread to prevent potential drops in plant yields and accompanying economic losses. Quantitative and infectivity tests are necessary to build an early warning system of possible viral threats in future studies.

Keywords: Metagenomics; Pathogenic viruses; Public health; River; Viral diversity; Wastewater

1.0 Introduction

Access to safe water is a basic human right, although water shortage has become a constant global challenge (Kesari *et al.*, 2021). Thus, wastewater treatment plants (WWTPs) are crucial in reducing the water scarcity problem via treatment to supplement the finite supply of freshwater. These treatment plants are designed to remove contaminants, including bacteria, protozoa, and viruses to improve the safety of the discharged tertiary effluent into the environment or potential reuse (Wang *et al.*, 2021).

The occurrence of viruses in wastewater poses a significant public health threat owing to their low infectious doses, persistence in the environment (Milani and Bidhendi, 2022) and potential to cause disease outbreaks such as gastroenteritis, hepatitis and respiratory infections

(Bouseettine *et al.*, 2020). Despite their significance, there is still a paucity of data on the viral communities within wastewater treatment plants relative to the bacterial populations (Zhang *et al.*, 2024; Chen *et al.*, 2021). Recently, there have been remarkable efforts towards surveillance of viral pathogens in South Africa, especially monitoring enteric viruses. The prevalence of viruses such as noroviruses, rotaviruses, adenoviruses among others in various water sources has been reported and this further highlight the need for comprehensive viral surveillance (Omatola *et al.*, 2024; Osunmakinde *et al.*, 2018).

Apart from enteric viruses, plant viruses characterized by their extensive distribution have also been found in wastewater and reclaimed water, including several species that are known etiological agents of crop diseases (Rosario *et al.*, 2009). Unfortunately, research has revealed the ability of certain phytopathogenic viruses to retain their infectivity after undergoing treatments (Mehle *et al.*, 2023; Bačnik *et al.*, 2020; Jeżewska *et al.*, 2018). To make matters worse, water-borne transmission of these viruses via contaminated supplies has been documented (Mehle *et al.*, 2023; Bačnik *et al.*, 2020; Mehle and Ravnikar, 2012). Nevertheless, there is a dearth of information on the viral diversity at the WWTPs in eThekwini, Durban, South Africa.

Metagenomics next-generation sequencing (mNGS) has become a significant technique for viral surveillance as it circumvents the limitations of conventional culture-based and PCR-dependent techniques and do not adequately encompass the complete viral diversity (Batool and Galloway-Peña, 2023). The application of mNGS in wastewater virology not only enables viral pathogens identification but may entail the discovery of novel viruses, thus facilitating the comprehensive characterization of viral communities without the need for prior genomic

knowledge (McCall and Xagoraraki, 2019). Furthermore, wastewater-based epidemiology has surfaced as an economical method and early warning signal for monitoring viral diseases within a community, as revealed by the SARS-CoV-2 monitoring initiatives (Parkins *et al.*, 2024).

Therefore, for the first time, this study examined the viral diversity and distribution of selected WWTPs across eThekwini Municipality, Durban, KwaZulu-Natal, South Africa, using the NGS technique. This study offered insights into the diverse viral families of plants, insects, fungi and vertebrates while highlighting the human and plant pathogenic viruses of public health importance prevalent at the investigated WWTPs and their corresponding effluents-receiving rivers.

2.0 Materials and methods

Sample collection

Four WWTPs within eThekwini Municipality, Durban, KwaZulu-Natal, South Africa, were selected for this study. These treatment plants encompass Amanzimtoti WWTP (WWTP1), characterized by processing 50% domestic and 50% industrial influent; Isipingo WWTP (WWTP2), Shallcross WWTPs (WWTP3) and Kingsburgh WWTP (WWTP4), which processes entirely domestic influent (Supplementary Figure 1). The WWTPs employ the activated sludge process for biological treatment while subjecting the tertiary aqueous effluent to chlorination before its discharge into the receiving environment. A total of 44 samples were collected in 2L autoclaved polypropylene plastic bottles between March and June 2024. In summary, 32 wastewater samples comprising primary influent (n=16) and tertiary (chlorinated) effluent (n=16) were collected from the four WWTPs during the sampling period. Additionally, 12 water samples were obtained from the Isipingo (RIVER2), Shallcross (RIVER3) and

Kingsburgh (RIVER4) rivers where the WWTPs discharge their chlorinated effluents (Supplementary Figure 1). The Amanzimtoti River (RIVER1), which receives effluent from the Amanzimtoti WWTP, was not sampled due to inaccessibility at sampling time. The collected samples were conveyed on ice to the Department of Biotechnology and Food Science at the Durban University of Technology for concentration and subsequent analysis.

Viral particle concentration

Polyethylene glycol (PEG) precipitation method was adopted to concentrate all water samples, including highly turbid ones (Aw and Gin, 2010). Each sample was combined with 8% PEG 8000 (80 gL^{-1}) and NaCl (17.5 g/L^{-1}), then incubated at 4°C overnight with agitation at 150 rpm to facilitate viral precipitation. The mixture was first centrifuged at 6700 *g* for 30 min, followed by a subsequent centrifugation at 10,000 *g* for 30 min to collect the pellet. Pellets were resuspended in 10 mL phosphate buffer saline (PBS), after which an equal volume of chloroform was added and the suspension centrifuged at 1700 *g* for 30 min. The resulting supernatant was passed through a 0.22 µm syringe filter to remove residual bacteria. Concentrates were stored at -80°C for pending viral nucleic acids extraction until further analyses.

Nucleic acids extraction

Viral nucleic acids were extracted from the concentrated water samples using the RNeasy® PowerFecal® Pro Kit (Qiagen, Hilden, Germany) according to the manufacturer's guidelines. Briefly, 100 mL of concentrated water samples was combined with 650 µL CD1 and 100 µL Trizol solutions and subsequently introduced into PowerBead Pro Tubes for homogenization. Following centrifugation, the supernatant was mixed with a CD2 solution to remove inhibitors

and washed with ethanol. RNA purification was conducted using MB RNA spin columns integrated with on-column DNase digestion before eluting the RNA with 50 µL nuclease-free water. Viral RNA was quantified using the RNA-specific fluorometric method on the Qubit 3.0 utilizing the Qubit HS RNA reagent (Life Technologies, USA).

Library preparation and sequencing

The synthesis of cDNA and whole transcriptome amplification (WTA) of the RNA samples was conducted before library preparation. The reverse transcription of RNA into cDNA was the first stage in the WTA procedure, followed by flanking of the primer ligation sites and concludes with a final amplification phase of the cDNA library, which is independent of poly A-tailing and oligo d(t) priming. In addition, the QIASeq FX Single Cell RNA Library Preparation Kit (Qiagen, Hilden, Germany) was used for the library preparation of each sample due to its suitability for low-input nucleic acids characteristic of wastewater samples, enhancing amplification efficiency and recovery of low-abundance viral genomes. Thereafter, the concentrations of the resulting libraries for each sample were quantified fluorometrically while their fragment sizes were evaluated using the Agilent 2100 Bioanalyzer (Agilent Technologies, USA). The cDNA libraries were sequenced on a NextSeq 2000 platform (Illumina, San Diego) utilizing a P2 kit with 2 × 150 bp paired-end reads, at the NGS unit of the University of the Free State, Bloemfontein, South Africa.

Bioinformatics analyses

The processing of the resultant raw paired-end reads, obtained in FASTQ format was executed utilizing a cloud-based, open-source metagenomics bioinformatics tool; Chan Zuckerberg ID (CZ ID) platform (v6.6) for microbial community profiling and pathogen identification

(Kalantar *et al.*, 2020). This online bioinformatics tool facilitates the examination of metagenomic data by automating quality control, host filtering, taxonomic classification and genome coverage analysis, thereby enabling efficient virome surveillance. The pipeline starts with adapter trimming using Trimmomatic (Bolger *et al.*, 2014), where initial quality control included adapter trimming and removal of low-quality bases using a minimum Phred score cutoff of Q30, and reads shorter than 25 bp were discarded after trimming, before proceeding with duplicate removal with the CD-HIT-DUP tool v4.6.8 (Li and Godzik, 2006) and integrates low-complexity filtering based on Lempel-Ziv-Welch (LZW) compression scores for sequencing noise reduction. Initially, host-derived reads were aligned and removed utilizing the Spliced Transcripts Alignment to a Reference (STAR) aligner (Dobin *et al.*, 2013). Furthermore, another layer of host filtering was executed using Bowtie2 (Langmead and Salzberg, 2012) via the HG38 database to eliminate human sequences optimally, where host-derived reads were subtracted by alignment to the human reference genome (GRCh38) using a high-stringency approach, and all reads mapping to the host genome were removed prior to downstream analysis. The remaining non-host reads underwent nucleotide alignment with GSNAPL (Wu and Nacu, 2010) against the NCBI nt database after host sequences filtration, while translated alignment was conducted utilizing RAPSearch2 (Ye *et al.*, 2011) against the NCBI nr database, with an alignment e-value cutoff of $\leq 1 \times 10^{-5}$ applied to retain statistically significant matches. Thereafter, reads were assembled into contigs using SPAdes (Bankevich *et al.*, 2012), and aligned subsequently to a curated BLAST + database for improved taxonomic classification (Altschul *et al.*, 1990). Moreover, CZ ID identifies and measures External RNA Control Consortium (ERCC) RNA spike-in control which are synthetic transcripts integrated during sample processing. These are adopted to assess input nucleic acid concentrations, analyze amplification biases and guide downstream contamination correction models (Kalantar *et al.*, 2020; Zinter *et al.*, 2019). Detected taxa were then quantified using reads per million

(rPM) while z-scores are calculated using the internal control backgrounds to highlight statistically significant detections while filtering out environmental contaminants (Davis *et al.*, 2018; Ruppé and Schrenzel, 2018; Wilson *et al.*, 2018), and taxa were retained only if they met a minimum threshold of RPM ≥10 with at least 5 supporting reads. Residual host contamination was reduced by filtering out reads and mapping them to Deuterostomia. In addition, all pipeline steps, reference databases and parameters are version-controlled to ensure reproducibility.

Data visualization

The data visualizations and statistical analyses employed in this study were conducted using the R Package (version 4.1.0). Operational taxonomic unit (OTU) abundance data were normalized to relative abundance per sample using total sum scaling for compositional barplot visualization. Alpha diversity metrics (Observed, Shannon, and Simpson) were calculated with Wilcoxon rank-sum tests. PERMANOVA was employed to evaluate the group differences in centroid location (Anderson, 2001), while the betadisper/permutest method was used to assess the homogeneity of multivariate variances and examine the community dispersion (Anderson, 2006). Redundancy analysis (RDA) on the centered log-ratio (CLR) distance matrix was used to perform ordination while visualizing eigenvalues in a scree plot (Supplementary Figure 2), to verify that the first two axes accounted for more than 20% total variance, hence validating their usage in the PCA plot (Gower, 1966). CLR transformed OTU (Gloor *et al.*, 2017; Aitchison, 1982), were analyzed using Wilcoxon rank-sum tests while obtained p-values were adjusted with the Benjamini–Hochberg procedure (Benjamini and Hochberg, 1995) and reported OTUs with FDR < 0.05. The reads and taxonomy tables, which constitute the abundance data, were adopted as input files for visualization in R while employing a suite of packages such as Vegan (Oksanen *et al.*, 2013), ggplot2 (Wickham *et al.*, 2016), tidyverse

(Wickham 2019), phyloseq (McMurdie and Holmes, 2013). Redundancy analysis (RDA) was used to calculate ordination, and the results were visualized as scree and biplots.

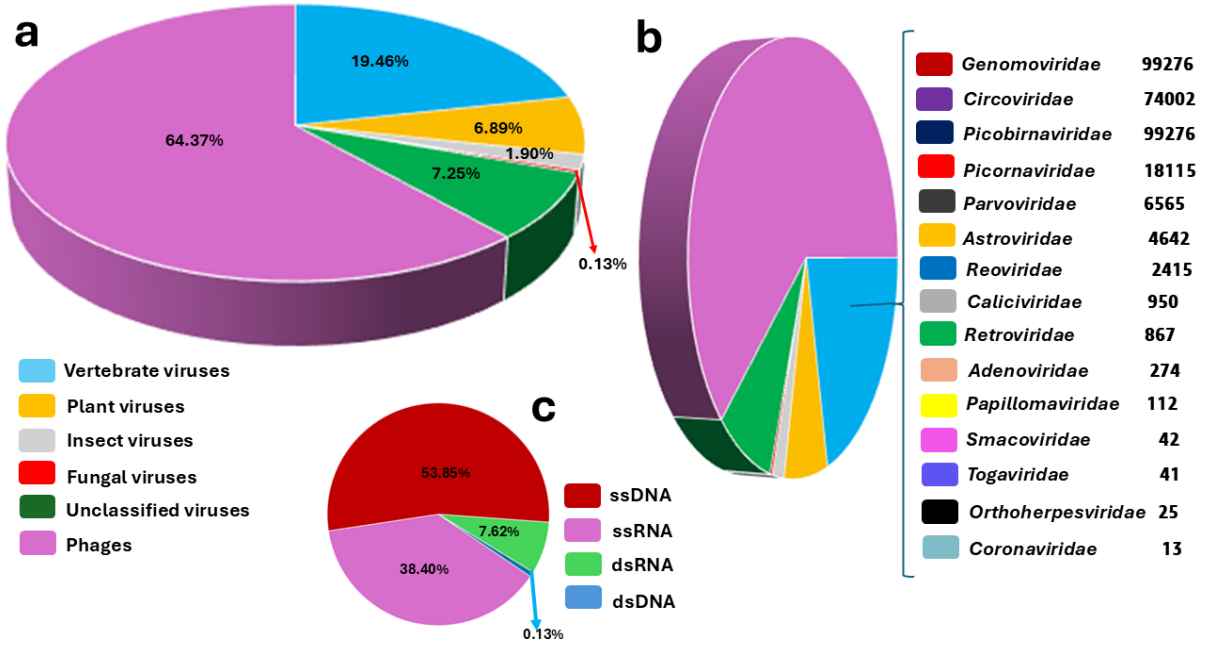


Figure 1 (a) Percentage host distribution of viral species identified in the study (b) Diversity of the different vertebrate viral families identified in this study based on reads (c) Pie chart of the genome type percentages of the viruses identified in this study.

3.0 Results and discussion

A total of 1,177,574 viral reads were obtained after quality control. Based on their known host specificity, the viral reads reported in this study have a wide host range; vertebrates viruses accounted for 19.46% reads followed by the plant viruses (6.89%) and insect viruses (1.90%), while the fungal viruses (0.13%) had the lowest proportion (Figure 1a). Furthermore, unclassified viruses accounted for 7.25% while more than half of the filtered reads (64.37%) were phages. This is partly similar to the report of McCall *et al.* (2023), where the highest

proportion of viral reads are linked with vertebrates and bacteria. Phages predominate wastewater virome owing to their natural abundance connected to higher bacterial populations (Kallies *et al.*, 2023; De Paepe *et al.*, 2014), ease of recovery via standard methods and dominant representations in viral databases. Moreover, RNA viruses are not easily detected relative to phages and humans shed lower viral quantities than phages shed by bacterial hosts (Gregory *et al.*, 2020; Paez-Espino *et al.*, 2016).

The most abundant phage family in this study is *Myoviridae*, which occurs across all the sampling sites, including WWTPs and rivers, except in WWTP3 effluent obtained in May. This absence may be attributed to a temporal reduction below the detection limit. These phages are characterized by double-stranded DNA (dsDNA) genomes, with bacteria and archaea being their natural hosts (Hantula and Vainio, 2021). *Microviridae* followed the order of prevalence with a marginal difference from *Siphoviridae*. Other phages families identified in this study include *Podoviridae*, *Drexlerviridae*, *Autographiviridae* and *Demerecviridae* in decreasing order. Recently, a global survey on viral abundance reported *Microviridae* as the most prevalent phage family, succeeded by *Siphoviridae*, *Myoviridae* and *Podoviridae* (Nieuwenhuijse *et al.*, 2020). On the contrary, *Myoviridae*, being the most abundant phage in this study, might be attributed to geographic variations and this being a pilot study relative to a global study. Notably, Korf *et al.* (2019), reported a higher prevalence of *Myoviridae* compared to *Siphoviridae,* which partly aligned with this study. Furthermore, a higher abundance of *Siphoviridae* compared to *Myoviridae* was observed by Jurczak-Kurek *et al.* (2016), with *Podoviridae* being the least prevalent. Thus, this finding further highlights the significant role of phages in shaping the microbial diversity within the investigated WWTPs and rivers.

A significant number of virions are being released by humans, livestock and wildlife channelled into the WWTPs and discharged subsequently into receiving waters after limited removal. A total of 15 viral families that infect vertebrates were detected in this study (Figure 1b), with *Genomoviridae* and *Coronaviridae* having the highest and lowest number of reads, respectively. Previously, Tisza *et al.* (2023) detected 28 different viral families connected to vertebrates in raw wastewater after one year surveillance, while viral families including *Circoviridae*, *Genomoviridae*, *Astroviridae* and *Hepeviridae,* which infect vertebrates among others, were identified in the Yangtze River, China (Lu *et al.*, 2022). The findings give a comprehensive perspective on the distribution and emergence of vertebrate viruses, as demonstrated by wastewater and river surveillance.

Although phages such as *Microviridae* are often reported as the most abundant ssDNA viral reads in previous studies (Tucker *et al.*, 2011), recent studies have also demonstrated that non-phage ssDNA viruses such as *Genomoviridae* and *Circoviridae* families are also prevalent viral reads in sewage (Kraberger *et al.*, 2015). Of the reported viral families in this study, the predominant viral reads belong to the ssDNA genome comprising *Genomoviridae*, *Circoviridae*, *Parvoviridae*, *Smacoviridae* and *Nanoviridae* (Figure 1c). Notably, previous viral wastewater surveillance studies (Li *et al*., 2024; Lu *et al*., 2022; Guerrero-Latorre *et al*., 2018), have reported the occurrence of DNA genomes despite adopting DNA removal procedures. Specifically, *Genomoviridae* entails a significant fraction of the reads aligning with recent investigation from Chinese WWTP where *Genomoviridae* accounted for more than 50% of the virome followed by *Circoviridae* as the next-largest family (Zhang *et al.*, 2024). Next is the ssRNA viruses with the family *Virgaviridae* linked with plants heavily dominating this genome group, similar to the viral wastewater surveillance study conducted in Spain (Cuevas-Ferrando *et al.*, 2025). The *Picorbirnaviridae* family dominated the dsRNA reads detected in

this study consistent with comprehensive sewage surveillance in the United Kingdom where the *Picorbirnaviridae* members were detected in every wastewater virome library investigated (Adriaenssens *et al.*, 2018). In contrast, this study observed limited viral reads of the dsDNA genomes with *Adenoviridae* accounting for less than one percent of the total viral reads. This observation is consistent with a previous WWTP monitoring where Adenovirus was the least commonly identified routine enteric virus (Wang *et al.*, 2020a). This similar pattern across different studies suggests a consistent hierarchy in wastewater and river virome that can be incorporated into surveillance initiatives.

Research has shown that WWTPs obtain water from multiple points and non-point sources, serving as a channel for accumulating diverse viral families (Chen *et al.*, 2021; Guajardo-Leiva *et al.*, 2020). A total of 30 different viral families were identified in this study (Figure 2). There is a relative division of the virome into two ecological signatures across the seven different sampling sites, as the WWTPs (WWTP1-4) demonstrate wider taxonomic diversity, showing a significant occurrence of ssRNA viruses associated with plants and insects. Expectedly, human enteric RNA families including *Picornaviridae*, *Caliciviridae* and *Astroviridae* were prevalent in the WWTPs with a notable decline in the receiving rivers, suggesting an efficiency of the WWTP processes; however, the viruses were not completely eradicated. This observation is consistent with Tisza *et al.* (2023), where more than 450 pathogenic viruses were detected in raw sewage. A notable occurrence of *Genomoviridae* and *Circoviridae* families was observed in the rivers relative to the WWTPs, corroborated by Lu *et al.* (2022), where these viral families were reported in Yangtze River. Moreover, *Retroviridae*, *Coronaviridae*, and *Togaviridae,* which are enveloped viruses, were less abundant in this study, and this emphasized the vulnerability of enveloped viruses to treatment processes and their reduced stability compared with non-enveloped counterparts (Ye *et al.*, 2016). The viral profiles illustrated distinct trends,

including persistent faecal pollution, transport of treated effluent downstream, and limited prevalence of enveloped viruses, suggesting their removal and reduced circulation within the community.

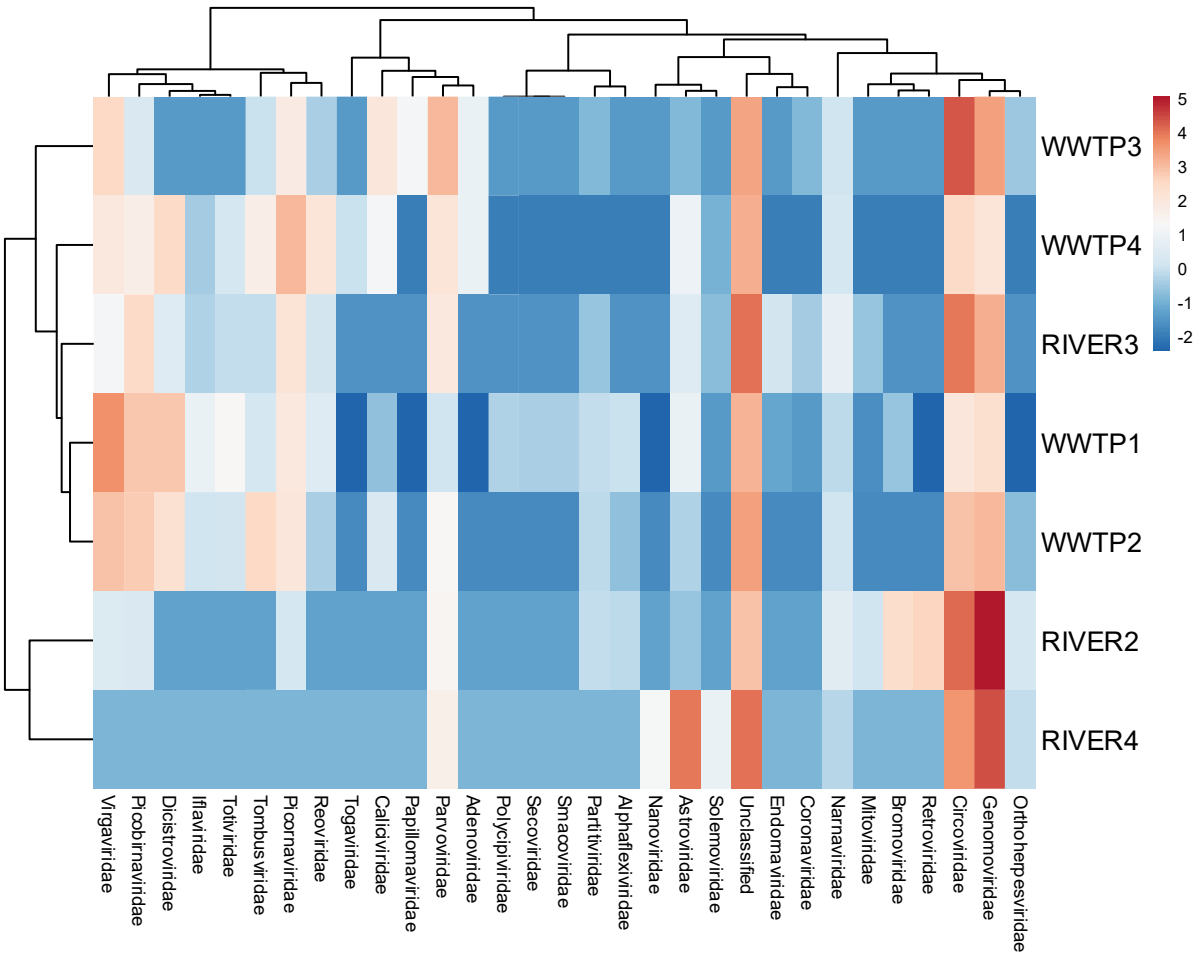


Figure 2. Overall read abundance of the identified 30 viral families across the examined wastewater treatment plants and effluents-receiving river within eThekwini, Durban, KwaZulu-Natal, South Africa.

Relative abundance

The relative abundance profile of the 20 top-most abundant viral species during the sampling period reveals a succession of viral species linked to the sampling season or sampling site from March to June (Figure 3). In March (autumn), Cyclovirus homa and a significant proportion of Gemycircularvirus were found to be the most abundant viral species. This observation suggested a consistent occurrence of animal-associated cycloviruses, which have been identified across diverse environments and hosts (Harding *et al.*, 2022). Their occurrence in WWTPs and effluents receiving river might result from human and livestock waste being discharged to WWTPs and waterways. Gemycircularvirus has been classified as a new viral genus detected globally in faecal and environmental samples. Notably, their detection in the environment has been detected previously where da Silva Assis *et al.* (2016), reported their prevalence in wastewater (97%) and river water samples (69%) from Rio de Janeiro and Manaus, Brazil. Furthermore, Pepper mild mottle virus (PMMoV), a common plant virus, proposed as an indicator of faecal pollution (Kitajima *et al.*, 2018), was predominant in one of the sampling sites, indicating an increase in food waste or agricultural runoff and faecal pollution with influence on other sites.

April signified a swing towards a wider range of viral compositions with an increase in the proportion of reads characterized as uncultured viruses and less-abundant species such as Bat cyclovirus, *Genomoviridae* sp., among others. Bat associated cycloviruses may pollute waterways due to heavy rainfall, illustrating wildlife-human interactions and land use (Harding *et al.*, 2022; Plowright *et al.*, 2015). The occurrence of irregular animal viral diversity suggests occasional influxes due to different community practices, including peri-urban farming, backyard poultry, different sanitation methods and ecological elements such as increased surface runoff attributed to the transition from summer to autumn. The detection of unclassified

viruses emphasized the essence of continuous wastewater monitoring to demonstrate community health status and early warning signals for potential emerging threats.

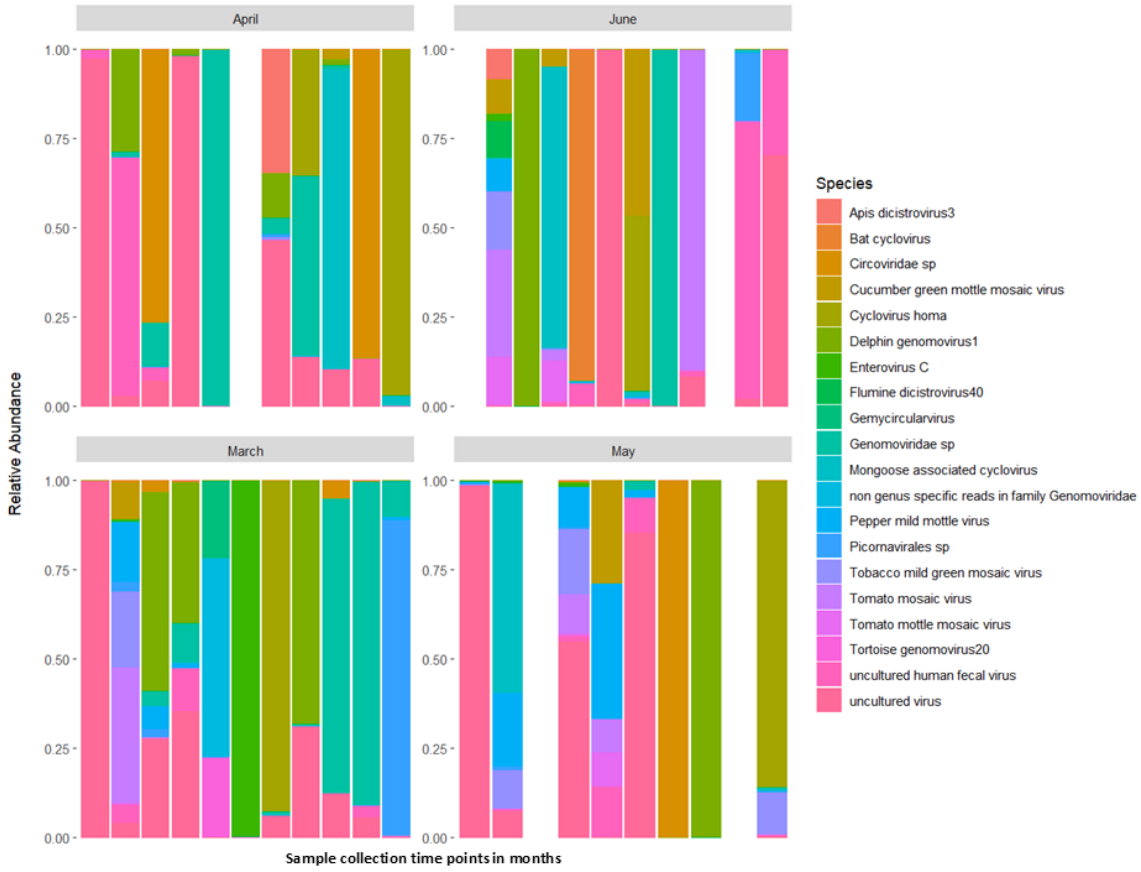


Figure 3: Relative abundance profile of 20 top-most abundant viral species during the sampling period.

Collectively, the monthly profiles demonstrated the prevalence of cycloviruses of the examined wastewater-river virome, followed by the tobamoviruses and other environmental viruses, which correlate with seasonal runoff and human activities. Furthermore, the consistently high proportion of reads detected as unclassified viruses revealed the knowledge gap in environmental virology, emphasizing the necessity of consistent wastewater surveillance to

unveil the unknown viral diversity and comprehensive databases to determine the ecological functions of these unidentified viruses.

Alpha diversity

The alpha diversity plot demonstrated notable variation from site to site, with distinction between the wastewater treatment plants (WWTP1-4) and river sites (RIVER2-4) (Figure 4). The observed richness, a straightforward count of viral operational taxonomic units (vOTUs), revealed the most notable variation across the different sites. The highest richness in WWTP1 ranges from a minimum of about 156 to a maximum of approximately 225, while the three river sites range from 15 to 32. The observed richness inflation at the plant collecting from mixed sources suggests that heterogenous influent introduces several low abundant taxa (Bibby and Peccia, 2013).

Similarly, Shannon diversity comprising richness and evenness (Jost, 2006), was also at the highest level at WWTP1, however it demonstrated a more limited dynamic range relative to richness. This might be due to the extreme samples from WWTP1 being offset by river communities, though lower in richness, yet relatively even. This dampening effect might indicate the responsiveness of the Shannon metrics to both the quantity of taxa and their relative abundances (Hill, 1973). Simpson's index (Simpson, 1949), highlighting evenness, illustrated the least variation across sites; samples from WWTP1-4 and RIVER2-4 were grouped within the range of 0.40 – 0.90. The convergence of Simpson indices, though they have varying richness, suggests that the dominant viral taxa were probably represented across the sampling sites. This observation emphasizes that wastewater treatment standardizes the abundance distribution of the most prevalent viruses (Farkas *et al.*, 2020). This convergence suggests that

the treatment processes equalize the dominant viral taxa across all sites while the rare ones differentiate effluents and receiving rivers. Collectively, WWTP1 illustrates high richness, while Shannon and Simpson index suggests diverse and evenly distributed viral species characteristic of mixed influent source flowing into a WWTP. A relatively moderate richness, lower Shannon index and moderate Simpson index, suggesting a smaller viral community dominated by a subset of taxa (García-Fontana *et al.*, 2020), was observed in WWTP2-4, possibly due to receiving just domestic influent. The difference in the different WWTPs can be linked to wastewater treatment efficiency, environmental conditions and external viral inputs or source of the influents which are site dependent. Conversely, RIVERS2-4, with a lower number of species, showed similar evenness to the WWTPs, resulting in intermediate Shannon values.

Furthermore, the observed jittered points suggested variation from month - month, especially richness spikes at WWTP1 in March and June which could be attributed to rainfall-related increases in viral communities or change in temperature (Ahmed *et al.*, 2020; Hata *et al.*, 2014). While weather changes may influence richness, the difference between wastewater and river conditions remained unchanged, suggesting the need for consistent sampling to comprehend transient events fully and not as continuous trends. Overall, Wilcoxon rank-sum tests showed no significant differences for richness ($W = 182.5$, $p = 0.812$), Shannon diversity ($W = 199$, $p = 0.864$), and Simpson evenness ($W = 201$, $p = 0.823$) did not exhibit significant differences between the wastewater and river categories; 95% confidence intervals for all the three metrics included zero. This indicated a relatively similar diversity level within wastewater samples and river water communities possibly due to similar treatment strategies adopted across the treatment plants. Summarily, the observed trends suggest a complex interplay between human

activities like wastewater discharge and environmental conditions in determining the viral diversity patterns.

Beta diversity

Principal Component Analysis (PCA) of viral diversity across investigated sampling sites indicated observable, although not sharply defined, clustering of samples according to the site (Figure 5). The scree plot demonstrated the proportion of total variance expressed by each principal component within the dataset (Supplementary Figure 2), while PCA condenses the CLR-transformed viral counts into a few principal components to illustrate the relationship between the viral communities. The largest variance was PC1, about 13%, followed by PC2, approximately 7%. Altogether, both components account for about 20% of the total variance, supporting their selection for the PCA biplot. Following PC1 and PC2, the variance attributed to each subsequent component diminished. Specifically, a significant decline was observed from PC1 to PC4 before the curve started to flatten, suggesting that the remaining components captured more subtle patterns or noise. The observed pattern is a known feature of complex biological datasets like metagenomic viral profiles, where variability is distributed across numerous dimensions. Although none singly dominated, PC1-PC10 collectively accounted for a substantial share of the overall variation and are possibly the most valuable for interpreting group differences. Overall, the scree plot validated that PC1 and PC2 offer an abridged yet accurate representation of the fundamental trends while highlighting the intricate nature of the data above these initial two dimensions.

The 95% confidence ellipses around the group centroids showed considerable overlap, suggesting similarity within the communities (Figure 5). Nevertheless, minimal shifts in the centroids indicated a shift in taxonomic composition rather than random variation. Specifically,

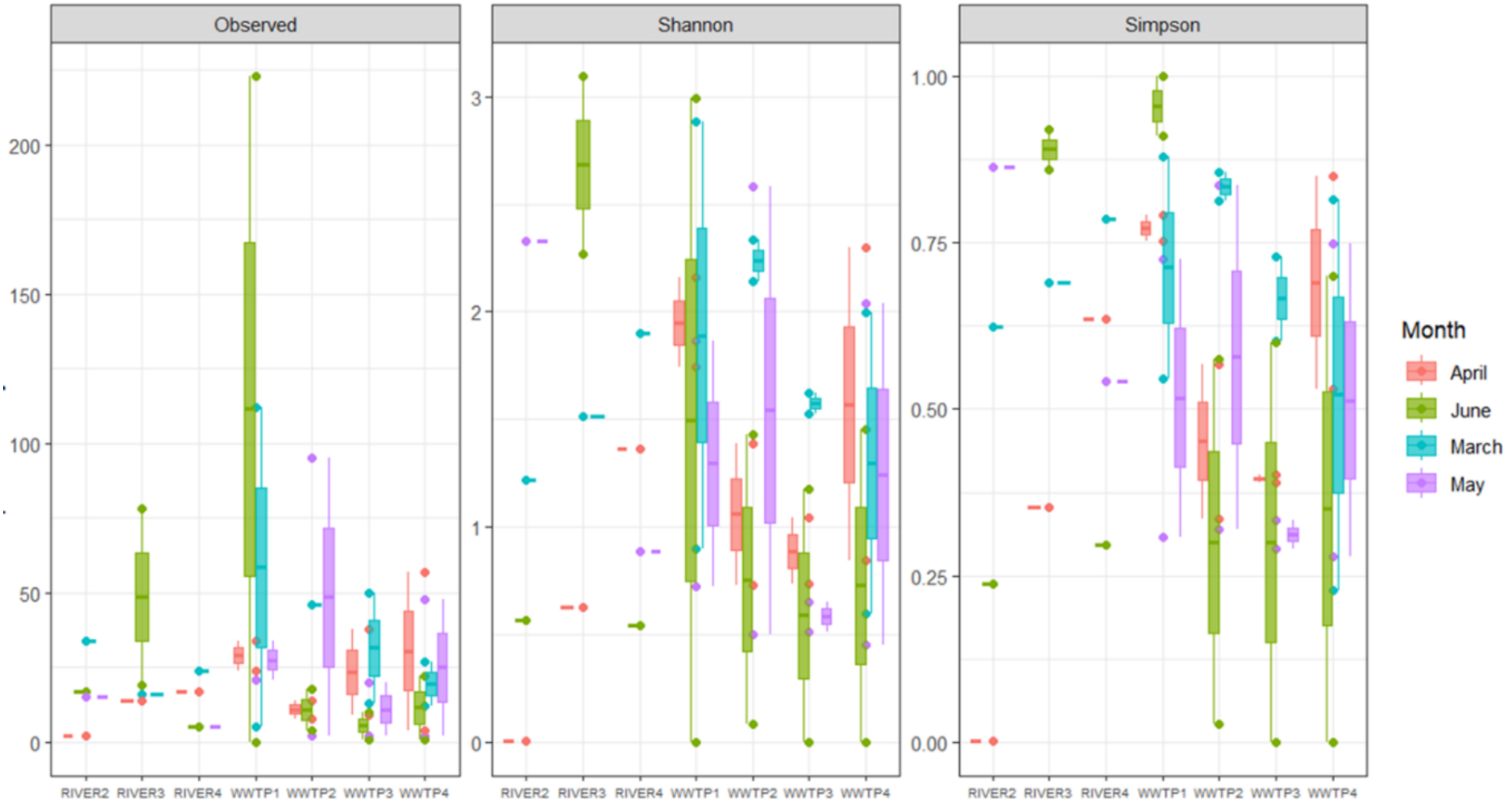


Figure 4: Alpha diversity metrics of the viral communities within the wastewater treatment plants and rivers: Observed (richness), Shannon (richness and evenness) and Simpson's index (evenness) illustrated as box-and-jitter plots.

WWTP1 revealed a broad distribution of the viral community, indicating a significant diversity in the viral profiles within this site. On the other hand, there was a more compact cluster in RIVER2 and RIVER4, suggesting greater uniformity in viral communities within those environments. There were notable patterns despite a modest variance accounted for by the PC1 and PC2. The intersecting ellipses demonstrated between some WWTPs and RIVER (WWTP1 and RIVER2) indicated common viral fingerprinting, suggesting the possible effects of effluent discharge and downstream transport into the receiving rivers, coupled with human or animal activities on the surrounding water bodies. Notably, few samples from WWTP1 emerge as outliers along PC1, potentially suggesting typical viral loads or possible occurrences of industrial discharge or incomplete treatment. This suggested further investigation to unveil factors responsible for the divergence.

The visual observation was validated by a one-factor PERMANOVA (Anderson, 2001), as the sampling period; month accounted for merely 7.9% of the variance in the CLR distances (R^2=0.079) with an insignificant corresponding pseudo-F value (F=1.15. P=0.111). Hence, there was no regular change in the viral assemblage from March to June. This permutation test is suitable for compositional NGS data because it is dependent on label assumptions and not parametric assumptions thus it is appropriate for assessing the observed groupings. Moreover, multivariate dispersion test was conducted using PERMDISP (Anderson, 2006), owing to the confounding influence of unequal within-group variances on PERMANOVA. The average distance to the group median was relatively consistent, ranging from 22.2 to 27.6. The seasonal groups displayed an equal level of dispersion because the permutation test was non-significant (F = 0.78, P = 0.494). Thus, the PERMANOVA result suggest authentic compositional similarity instead of variance heterogeneity. At the community level, a Wilcoxon rank-sum test

comparing CLR-transformed total abundance between river and WWTP samples yielded W = 194, p = 0.969, aligning with the ordination-based finding of negligible global differences.

Generally, both PCA and PERMANOVA suggest a stable core virome across the sampling sites and months, characterized by slight and temporary disturbances. The ordination, PERMANOVA and dispersion analyses suggest that the viral community composition demonstrated stability during the four sampling months despite notable rainfall at the WWTPs. Similar levels of temporal stability have been documented for prominent sewage-associated viruses such as crAssphage, Adenoviruses and Polyomaviruses which exhibited minimal titre differences across seasons and treatment stages (Farkas *et al.*, 2020). The absence of a notable month impact suggests that the spikes shown in alpha diversity richness especially in WWTP1 (March and June) were probably due to low-abundance taxa instead of a complete turnover of the core virome. Overall, this observation suggests that the most prevalent viruses are replenished by a significant human catchment regularly and are not eliminated completely during the treatment process. This analysis demonstrates the intricate and multidimensional features of viral communities in wastewater and surface water environments and the possible influence of human activities on downstream ecosystems.

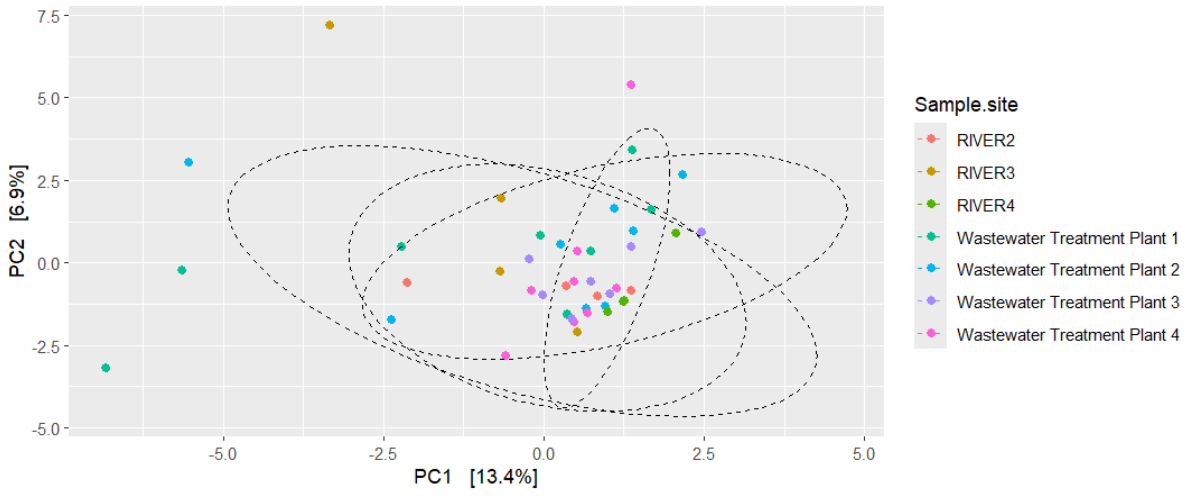


Figure 5: Principal Component Analysis (PCA) of viral diversity across investigated sampling sites: three river sites (RIVER2, RIVER3, RIVER4) and four wastewater treatment plants (WWTP1, WWTP2, WWTP3, WWTP4).

Human viral pathogens

In this study, 26 human pathogenic viral species from eight families were identified across the various sampling sites (Figure 6); however, none of the pathogenic virus was detected uniformly across all the sampling sites. Multiple members of the *Picornaviridae* family are prominent, including Enteroviruses A, B and C and human enterovirus (unclassified Enterovirus), single-stranded RNA genome belonging to the genus Enterovirus. They cause different illnesses including mild respiratory infections, severe neurological conditions: meningitis and acute flaccid myelitis (Wang *et al.*, 2020b). Of all the pathogenic human strains, Enterovirus C has the highest prevalence and was detected across the investigated WWTPs in the influent or effluent, except in WWTP3 and was undetected in the river samples. A similar trend of detection was observed for Enterovirus A, Enterovirus B and the unclassified human enterovirus, although Enterovirus B was undetected in WWTP2. Similarly, Guerrero-Latorre *et al.* (2018), reported the detection of Enteroviruses A, B and C, with Enterovirus C having the highest occurrence in Quito's river. Conversely, Tedcastle *et al.* (2022) identified several Enteroviruses, especially species A, B, C and D, with a notable occurrence of Enterovirus D68 strains from clade D and sub-clade B. Notably, this study demonstrated the diversity of enteroviruses circulating within the different communities. The human viral pathogen with the next highest abundance is another member of the *Picornaviridae* family referred to as Parechovirus A (PeV-A); a species in the *Parechovirus* genus is recently gaining attention as an important pathogen in children and infants, being linked to various clinical outcomes

ranging from mild gastrointestinal illness to severe symptoms including neonatal sepsis-like illness, meningitis, encephalitis, especially in children less than three months old (Deézsi-Magyar *et al.*, 2024). Within this age range, it is the second leading virus associated with central nervous system (CNS) infections (Fernandez-Garcia *et al.*, 2020). In this study, PeV-A was detected in all the sampling sites except in RIVER2 and RIVER4. Similarly, PeV-A has been detected in influent and effluent wastewater samples (Wang *et al.*, 2020a), while Guerrero-Latorre *et al.* (2018), reported its occurrence in urban river waters in Quito, Ecuador further indicating the utility of wastewater-based metagenomics for tracking enteric viruses at the community level. The non-detection of PeV-A in RIVER2 and RIVER4, despite its prevalence in effluent samples, might be due to factors such as RNA degradation and dilution leading to low viral loads below the detection threshold of metagenomic sequencing, highlighting the need for context-specific sampling strategies in wastewater surveillance.

Additionally, Hepatovirus A (HAV), designated as Hepatitis A virus until 2014 (Guerrero-Latorre *et al.*, 2018), belonging to the Hepatovirus genus is another member of the *Picornaviridae* family identified in this study. HAV is the causative agent of hepatitis A infection, which results in liver damage with accompanying symptoms including jaundice, nausea and fatigue (Li, 2023). Specifically, it was detected in the influents of WWTP1 and WWTP2 but not in their effluents or the receiving river (RIVER2). This suggests localized community transmission of the virus and effective viral removal at WWTP2. In addition, it was completely undetected in WWTP3, WWTP4 and receiving rivers (RIVER3 and RIVER4). This finding may indicate low community prevalence of the virus or low viral loads below the detection threshold. Previously, Fernandez-Cassi *et al.* (2018), reported a partly similar trend with the occurrence of HAV in raw sewage. On the contrary, Nasiri *et al.* (2021) reported the detection of HAV in all tested influent samples and 50% of the effluent samples while Chigor

and Okoh (2012) reported its detection in Buffalo River further suggesting environmental contamination.

Another common waterborne enteric virus identified in this study is the Rotavirus A (RVA) of the *Reoviridae* family, which is the causative agent of diarrhoea and consequently the main cause of diarrhoea-related mortality among children younger than five years (Lanrewaju *et al.*, 2022; Troeger *et al.*, 2018). RVA was detected in WWTP1 (influent), WWTP2, 3 and 4 (influent) and RIVER3, while it was undetected in RIVER 2 and 4. Previously, Guajardo-Leiva *et al.* (2020) had reported the occurrence of RVA in wastewater influents, while its prevalence has also been reported in both wastewater influent and effluent (Guajardo-Leiva *et al.*, 2025; Soltane and Allayeh, 2023). Mammalian orthoreovirus (MRV), another member of the *Reoviridae* family, has been recognized as a contributor to mild gastroenteritis and respiratory illness ranging from symptomatic to asymptomatic (Mao *et al.*, 2024). In this study, it was detected only in the influent of WWTP1. While MRVs are shed by infected hosts and considered environmentally stable, direct detention in water matrices has been rarely reported. Therefore, this study offers new evidence of MRV dissemination in wastewater, and considering its environmental resilience, conducting further research to understand its persistence and potential implications for public health is imperative.

Human astrovirus (HAstV) is a notable etiological agent of gastroenteritis affecting children, immunocompromised and the elderly (Lanrewaju *et al.*, 2022; Aguilar-Hernández *et al.*, 2020). Apart from gastrointestinal manifestations, HAstVs have recently been implicated in sudden central nervous system (CNS) infections in immunocompromised individuals highlighting the potential of these viruses to circumvent the gastrointestinal tract and induce other systemic

diseases (Lu *et al.*, 2023). The identification of diverse HAstV strains in wastewater and river underscores the genetic diversity of circulating strains and the need for continuous surveillance to understand their evolving clinical significance. Table 1 summarizes the HAstV species identified in this study, sampling source and associated human disease. Of all the detected astroviruses in this study, HMO Astrovirus A is the most abundant and dominating human pathogenic virus in RIVER4, suggesting ongoing circulation within the community. In contrast to the eight human astrovirus serotypes, VA-clade strains, especially genotype VA1 can infiltrate the central nervous system resulting in severe or fatal encephalitis in neonates and immunocompromised individuals, hence their designation as emerging neutrotropic pathogens (Maximova *et al.*, 2023; Brown *et al.*, 2015). A comprehensive analysis of 80 studies revealed the presence of Astrovirus in 56.8% of raw sewage, 48.5% of effluent and 28.6% of surface water with VA/MLB genotypes constituting a significant portion (Takuissu *et al.*, 2023), while Tao *et al.* (2022), reported the occurrence of VA1-3 in all influent and effluent samples from a year-long sequencing investigation conducted in Eastern China. Their constant identification in wastewater and surface waters emphasizes ongoing circulation and portends public health threats, especially for neonates and immunocompromised individuals at risk of VA1 encephalitis. Unfortunately, the lack of vaccines or specialized antiviral drugs highlights the need for regular wastewater monitoring as early warning signals of an impending viral pandemic.

Table 1: Overview of detected astroviruses, detection sources, genetic diversity and corresponding human disease

Species	Genus	Water matrix	Genetic lineage	Associated human disease and reference
Astrovirus MLB1	Mamaastrovirus	WWTP1 Influent	HAstV-MLB	Gastroenteritis, acute encephalopathy (Siqueira *et al.*, 2017)

Astrovirus MLB2	Unclassified Astroviridae	WWTP1 Influent	HAstV-MLB	Gastroenteritis (Wei *et al.*, 2021)
Human astrovirus	Unclassified Astroviridae	WWTP1 & WWTP4 Influent, RIVER3		Gastroenteritis (Li *et al.*, 2023)
Human astrovirus MLB2	Unclassified Astroviridae	WWTP1 Influent	HAstV-MLB	Gastroenteritis, meningitis (Cordey *et al.*, 2016)
Mamastrovirus 1	Mamastrovirus	WWTP1 & 4 Influent	Classic HAstVs	Gastroenteritis (Lu *et al.*, 2023)
Mamastrovirus 6	Mamastrovirus	WWTP1 Influent	Novel HAstV	Gastroenteritis (Lu *et al.*, 2023)
Mamastrovirus sp	Mamastrovirus	WWTP1, 4 Influent & RIVER 4	-	
HMO Astrovirus A	Mamastrovirus	WWTP4 & RIVER4	classic HAstVs/VA3	Gastroenteritis, severe extra-intestinal illnesses (Wohlgemuth *et al.*, 2019)

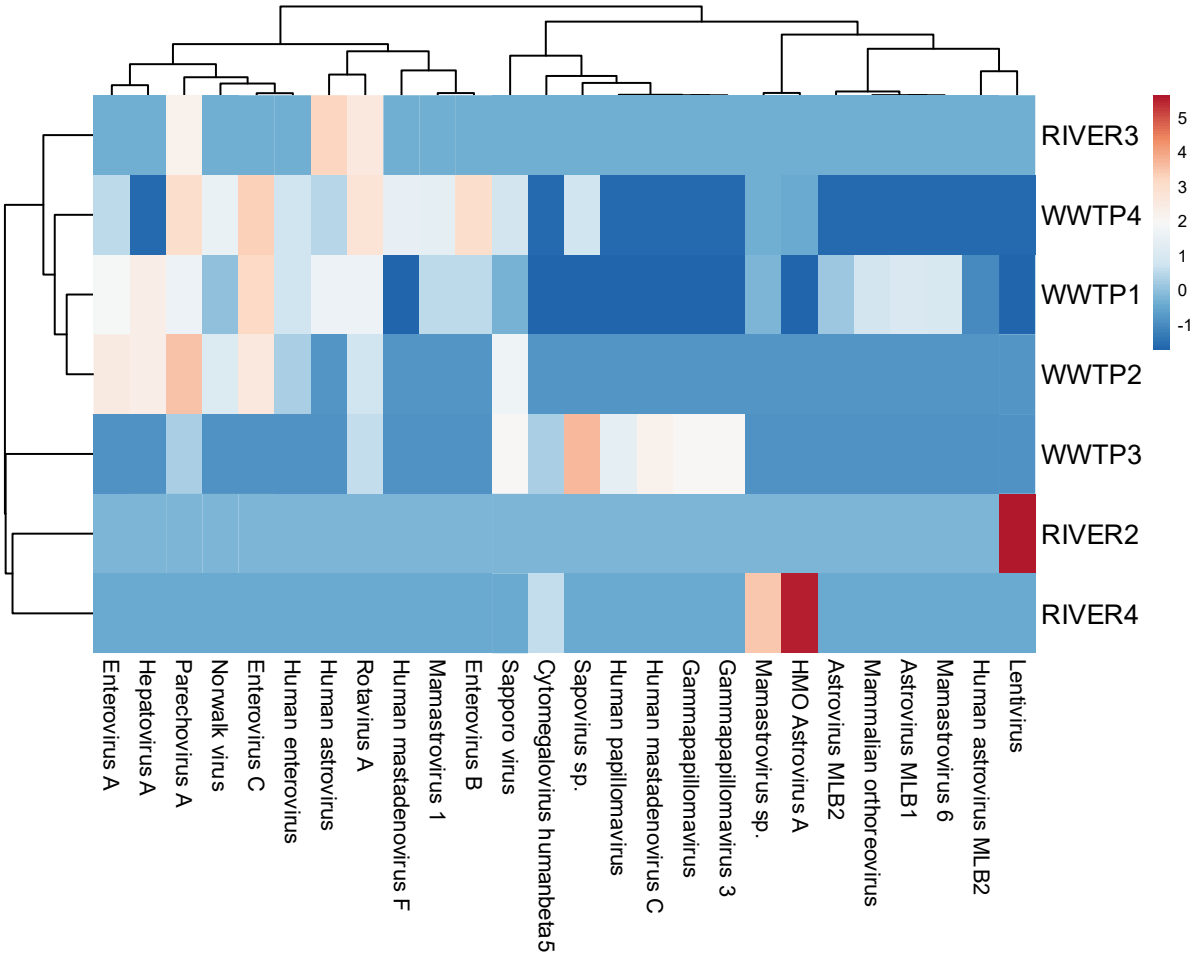


Figure 6: Overall read abundance of 26 human pathogenic viral species detected across the examined wastewater treatment plants and effluents-receiving rivers within eThekwini Durban, Kwazulu-Natal, South Africa.

Members of the *Caliciviridae* family identified in this study include Norwalk virus, Sapovirus sp., and Sapporo virus. Noroviruses, originally known as Norwalk viruses and Sapovirus referred to Sapporo virus has been reclassified within the genus Norovirus and Sapovirus respectively (Mayo, 2002). Noroviruses and sapoviruses are prevalent etiological agents of gastroenteritis and infectious diarrhea (Wright *et al.*, 2020). In this study none of these viruses were identified in the effluent-receiving rivers (RIVER2, RIVER3 and RIVER4) but they were detected across the influents of different investigated WWTPs: Norwalk virus in WWTP1, WWTP2 and WWTP4, Sapovirus sp. in WWTP3 and WWTP4 and Sapporo virus in WWTP1, WWTP2, WWTP3 and WWTP4. Norovirus and Sapovirus has been detected previously in wastewater (Li *et al.*, 2024), while Sapporo virus and Norwalk virus have been detected in river (Guerrero-Latorre *et al.*, 2018). In this study, detecting these viruses from the *Caliciviridae* family in influents and not in effluents and rivers might be due to effective viral reduction during treatment, coupled with their low prevalence in the inflow. Nevertheless, their occurrence across different WWTPs influents suggests ongoing community transmission and the need for constant surveillance to guide further public health interventions.

Cytomegalovirus humanbeta5 (CMV), classified under the genus Cytomegalovirus and of the *Orthoherpesviridae* family, is recognized as the leading cause of congenital viral infections (Lazzarotto *et al.*, 2011). This virus contributes to permanent disability significantly, particularly sensorineural hearing loss (Dreher *et al.*, 2014). In the current survey, CMV was

identified in only WWTP3 and RIVER4. There is a dearth of reports on its detection in wastewater, and this may constitute one of the earliest environmental detections of the virus. Due to the possible excretion of CMV in urine being routinely used for clinical isolation (Puget *et al.*, 2024), its detection in wastewater is biologically plausible and further validates the potential of wastewater surveillance for unveiling the viral dark matter in the environment.

Lentiviruses, a genus within the *Retroviridae* family, are known to infect different mammalian hosts, including humans (Stover and Watson, 2015). One notable feature of lentiviruses is their capacity to infect cells with macrophage-like phenotypes in the brain, leading to different neurological diseases with varying severity based on the specific virus and the host (Mohammadzadeh *et al.*, 2021). For instance, human immunodeficiency virus (HIV), categorised within the Lentivirus genus, compromises the immune system and can result in acquired immunodeficiency syndrome (AIDS). Of all the sampling sites examined in this study, lentivirus was detected in only RIVER2. Although their presence in the environment is scarcely documented, Li *et al.* (2024) reported their prevalence in raw sewage. Therefore, this finding suggests their potential occurrence in the environment and highlights the need for further investigation into their sources, persistence and public health importance.

Human papillomavirus (HPV), a member of the *Papillomaviridae* family has been linked to almost all cases of cervical cancer globally and is responsible for a significant proportion of anal cancer, penile cancer, vaginal cancer and oropharyngeal cancers. In this study, Gammapapillomavirus and Gammapapillomavirus 3 were identified in the influent of WWTP3, while Human papillomavirus (HPV) was detected in both influent and effluent of the same plant. Gammapapillomavirus have often been detected in histological normal skin across

several mucosal anatomical sites including oral, nasal, cervical mucosa and mucocutaneous epithelium of the penis and anal canal (Hošnjak *et al.*, 2021). Moreover, HPVs have been detected in urban wastewater, suggesting they enter sewage via skin washing, mucous membrane shedding and urine excretion (La Rosa *et al.*, 2013). The persistence of HPV in tertiary effluent indicated its environmental stability and further suggests the need for further investigation into its potential environmental transmission.

Human mastadenovirus classified within the *Adenoviridae* family contributes to diverse illnesses comprising acute gastroenteritis and epidemic keratoconjuctivitis affecting children and adults (Chen and Tian, 2018). Human mastadenoviruses A, B and C are associated with respiratory infections (Saasa *et al.*, 2024), while human mastadenovirus F comprising human adenovirus (HAdV) types 40 and 41 is considered a major cause of gastroenteritis globally (Brown *et al.*, 2016; Osborne *et al.*, 2015). In the present survey, Human mastadenovirus C was detected in the influent of WWTP3 while Human mastadenovirus F was identified in the influent of WWTP4. Earlier investigation has reported the occurrence of Human mastadenovirus B in raw sewage (Yoshitomi *et al.*, 2017) and Human mastadenovirus F in urban river waters in Quito, Ecuador (Guerrero-Latorre *et al.*, 2018). The occurrence of mastadenovirus in different WWTPs suggests their community circulation and the essence of wastewater surveillance in tracking respiratory and enteric adenovirus infections.

Overall, the prevalence of common human enteric viruses like Enterovirus C, Rotavirus A to lesser-known pathogens like Cytomegalovirus across wastewater and river samples emphasized that wastewater could provide a snapshot of community health. Therefore, these

findings highlight the significance of wastewater surveillance in not just tracking known infections but also to unveil emerging viral threats that may be latent.

Plant viral pathogens

Similar to human viruses, plant viruses are characterized by their broad geographic reach and diversity being the most prevalent eukaryotic viral group identified in wastewater (Rusiñol *et al.*, 2020; Fernandez-Cassi *et al.*, 2018; Furtak *et al.*, 2016). Therefore, pathogenic viruses within reclaimed or surface waters can trigger crop diseases and subsequently substantial economic losses (Cuevas-Ferrando *et al.*, 2025; Mehle *et al.*, 2018). In the current study, plant viruses accounted for 8 of the 30 viral families (Figure 2), including *Virgaviridae*, *Tombusviridae*, *Bromoviridae*, *Alphaflexiviridae*, *Secoviridae*, *Nanoviridae*, *Solemoviridae* and *Endornaviridae*. The most frequently detected family is the *Virgaviridae* family with the highest number of reads aligned with previous studies (Cuevas-Ferrando *et al.*, 2025; Lopez-Roblero *et al.*, 2024). However, the read counts for other families were lower, possibly due to a significant number of the *Virgaviridae* reads, which might have created a bias facilitating the sequencing of this family over others (Cuevas-Ferrando *et al.*, 2025). This is followed by *Tombusviridae* and *Bromoviridae* families. Specifically, the pathogenic viral species detected in this study belong to the *Virgaviridae* and *Bromoviridae* family (Figure 7).

Tomato mosaic virus (ToMV) is the most abundant plant virus, classified within the Tobamovirus genus and *Virgaviridae* family. ToMV is considered one of the most widespread and destructive viruses affecting tomatoes globally (Ullah *et al.*, 2019; King *et al.*, 2011) and extends beyond *Solanaceae* family owing to its broad host range (Lyu *et al.*, 2023). The virus spreads through contact with contaminated surfaces or soils, leading to several symptoms

influenced by environmental conditions or the host species affected (Cuevas-Ferrando *et al.*, 2025; Blancard, 2012). In this study, ToMV was detected in the influents of WWTP1, WWTP2, WWTP3, WWTP4 and RIVER2. Similarly, Maksimović *et al.* (2024) identified ToMV as the most abundant plant virus in their study while Lopez-Roblero *et al.* (2024) documented *Virgaviridae* as the most abundant plant viral family; however, ToMV was not the most abundant phytopathogenic viral species. In this study, the non-detection of ToMV in the effluents might suggest the efficiency of the selected WWTPs, while its high occurrence highlights the possibility of plant-virus transmission via wastewater, especially where raw or treated wastewater is used for irrigation.

Tobacco mild green mosaic virus (TMGMV) was the second most abundant viral phytopathogen identified in this study, though undetected in RIVER2 and RIVER4. TMGMV, also of the Tobamovirus genus, infects several economically significant plants including tobacco, pepper, eggplant, petunia and tomato (Zhao *et al.*, 2021). Previously, the occurrence of TMGMV has been reported in WWTP (Rothman and Whiteson, 2022) and the watershed (Demoliner *et al.*, 2025). Following TMGMV in abundance is Tomato mottle mosaic virus (TMMV), also of the Tobamovirus genus, and has recently emerged as one of the most economically important viruses affecting tomato plants (Tettey *et al.*, 2022). In the current study, TMMV was detected in the influents of WWTP1 and WWTP2 (influent and effluent). There is a potential risk of spreading this viral pathogen via water reuse, considering its detection in the effluent. Similarly, Rothman and Whiteson (2022) reported the prevalence of TMMV in wastewater, highlighting the need for further monitoring of the virus within the environment.

Another notable member of the *Tobamovirus* genus identified in this study is the Pepper mild mottle virus (PMMoV), which causes mild to severe symptoms in pepper, including leaf mosaic, distortion and stunting, along with fruit deformities and diminished yields (Kumari *et al.*, 2023). PMMoV was detected in WWTP1 (influent and effluent), WWTP2 (influent and effluent), RIVER2, WWTP3 (influent), RIVER3 and WWTP4 (influent and effluent). The detection of PMMoV across all investigated WWTPs in this study may be attributed to its previously reported high abundance in the human gut virome (Zhang *et al.*, 2006); hence, it is being considered as a potential faecal pollution indicator in water (Kitajima *et al.*, 2018). This demonstrates its relevance not just as a phytopathogen but also as an indicator of faecal contamination.

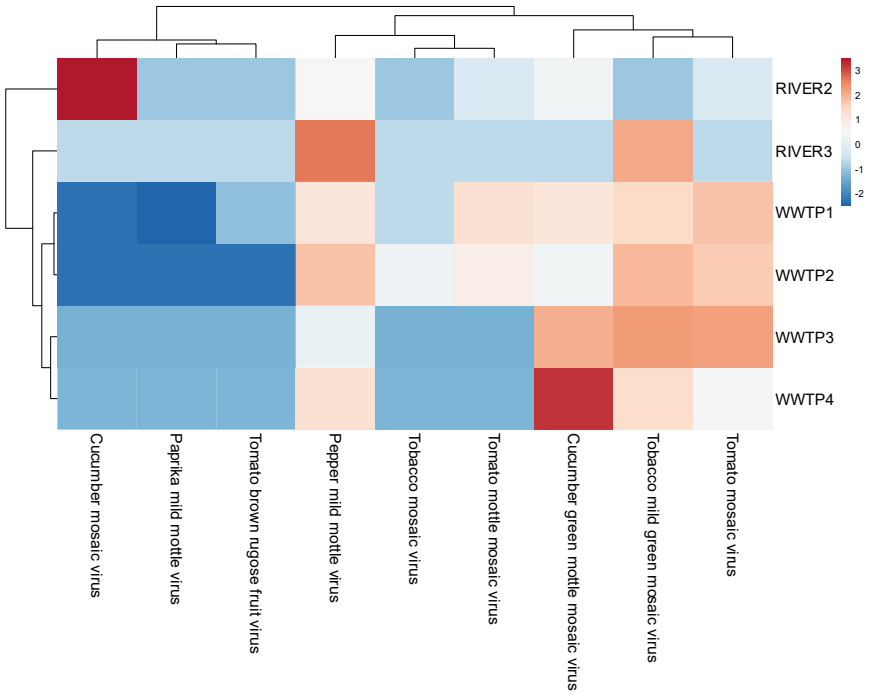


Figure 7: Overall read abundance of the 9 phytopathogenic viral species detected across the examined wastewater treatment plants and effluents-receiving rivers within eThekwini Durban, Kwazulu-Natal, South Africa.

Cucumber green mottle mosaic virus (CGMMV) is also of the Tobamovirus genus, which causes leaf mosaic, deformities, fruit mottling and plant stunting across several plant species, especially within the *Solanaceae*, *Cucurbitaceae* and *Cruciferae* families, resulting in substantial economic losses to the vegetable industry globally (Qi *et al.*, 2021). CGMMV was detected in the influents of WWTP1, WWTP2, WWTP3, WWTP4 and RIVER2 in this study. This observation agrees with Cuevas-Ferrando *et al.* (2025), where CGMMV was detected in wastewater, indicating the possibility of its spread via water. Furthermore, Tobacco mosaic virus (TMV), also of the Tobamovirus genus, infects an array of plants, particularly tobacco and a broad spectrum of hosts within the *Solanaceae*, resulting in several symptoms including foliar mosaic patterns, vein clearing and deformation (Chen *et al.*, 2023). In this study, TMV was identified in WWTP1 (influent and effluent), WWTP2 (influent). TMV has been detected in sewage since 1960 (Yarwood, 1960) and its presence in wastewater documented in recent studies (Tandukar *et al.*, 2020).

Other members of the *Virgaviridae* family and Tobamovirus genus that were less abundant in this study include Paprika mild mottle virus (PaMMV) and Tomato brown rugose fruit virus (ToBRFV). PaMMV known to infect pepper plants (Han *et al.*, 2024), was detected in only the influent of WWTP1. Nevertheless, it has been previously documented in environmental samples including wastewater, freshwater and sludge (Lopez-Roblero *et al.*, 2024). Therefore, less abundant pathogens may survive in aquatic environments and contaminate agricultural farmlands. Conversely, ToBRFV is an emerging viral phytopathogen that proliferates swiftly with tomato as its primary host while infecting other crops like pepper. It is responsible for considerable crop damage and fruit deformities, posing a serious risk to tomato production globally (Zhang *et al.*, 2022). In the current study, it was identified in the influent of WWTP1. Previously, it has been detected in both influent and effluent samples (Sherchan *et al.*, 2023)

while Nash *et al.* (2024) confirmed its prevalence in the influent, highlighting its environmental importance.

Unlike other phytopathogenic viruses detected in this study, Cucumber mosaic virus (CMV) does not belong to the *Virgaviridae* family and Tobamovirus genus, instead it is categorised under the Cucumovirus genus and *Bromoviridae* family as one of the most important agricultural viruses due to the economic and production losses linked with it (Scholthof *et al.*, 2011). CMV has infected more than 1200 species globally being the most common in pepper, tomato, cucumber and lettuce (Palukaitis and García-Arenal, 2003). Symptoms of its infection on the host plants include mosaic, reduction in leaf size and stunted growth (Kwon *et al.*, 2023). In this study, CMV was detected in the influent of WWTP1 and RIVER2. Although CMV is not commonly detected in aquatic environments, it has been identified in surface waters (Zhang *et al.*, 2023), while its presence has been previously reported in some rivers of Southern Italy (Piazzolla *et al.*, 1986). This finding underscores the need for wider viral environmental monitoring for other phytopathogenic viruses apart from the members of the *Virgaviridae* family that could be latent.

Overall, most viral phytopathogenic species detected across the sampling sites were of the *Virgaviridae* family and Tobamovirus genus (ToMV, TMGMV, PMMoV), while emerging pathogens (CMV, ToBRFV) were less frequent but significant owing to their economic importance in agriculture. No phytopathogenic viral species were identified in RIVER4, indicating possible differences in viral load, environmental persistence, or agricultural activity. Thus, these findings reiterate the significance of wastewater surveillance in monitoring known and emerging plant viruses.

4.0 Conclusion

This viral surveillance study of selected WWTPs and their receiving rivers in eThekwini Municipality, Durban, South Africa, using mNGS provides a baseline insight into the viral diversity and abundance of the investigated sites; though limited to March-June, it sets the stage for more comprehensive future studies. The findings from this study emphasize the effectiveness of mNGS for evaluating the virome of the aquatic environment as it highlights the viral diversity of the investigated WWTPs and receiving river before attention is turned to human viral pathogens and phytopathogenic viruses. Detecting common human enteric viruses (Enteroviruses A, B, C, Hepatovirus A, Rotavirus A, Norwalk virus), the emerging neurotropic HMO Astrovirus A (VA1, linked to lethal encephalitis in neonates and immunocompromised patients) and less frequently reported pathogens like Cytomegalovirus emphasized that wastewater could provide a snapshot of community health. Therefore, these findings highlight the significance of wastewater surveillance in tracking known viral infections and unveiling possible emerging viruses that could constitute viral threats. Similarly, wastewater-based surveillance techniques might be used to track plant pathogenic viruses in agriculture to detect, study and curb viral spread to prevent potential decreases in plant yields and accompanying economic losses. While the mNGS approach employed in this study revealed a comprehensive snapshot of the viral diversity for the investigated sites, absolute concentrations and information on the infectivity status of the detected viruses were not provided, which could have further guided targeted intervention. Thus, incorporating quantitative and infectivity assays in future studies will provide insights that can be a guide to safeguard human health and agricultural productivity further.

References

ADRIAENSSENS, E. M., FARKAS, K., HARRISON, C., JONES, D. L., ALLISON, H. E. & MCCARTHY, A. J. 2018. Viromic analysis of wastewater input to a river catchment reveals a diverse assemblage of RNA viruses. *mSystems*, 3(3), 10-1128.

AGUILAR-HERNÁNDEZ, N., MEYER, L., LÓPEZ, S., DUBOIS, R. M. & ARIAS, C. F. 2020. Protein disulfide isomerase A4 is involved in genome uncoating during human astrovirus cell entry. *Viruses*, 13(53), 1-12.

AHMED, W., PAYYAPPAT, S., CASSIDY, M., HARRISON, N. & BESLEY, C. 2020. Sewage-associated marker genes illustrate the impact of wet weather overflows and dry weather leakage in urban estuarine waters of Sydney, Australia. *Science of the Total Environment*, 705, 1-14.

AITCHISON, J. 1982. The statistical analysis of compositional data. *Journal of the Royal Statistical Society: Series B (Methodological)*, 44, 139–160.

ALTSCHUL, S. F., GISH, W., MILLER, W., MYERS, E. W. & LIPMAN, D. J. 1990. Basic local alignment search tool. *Journal of Molecular Biology*, 215, 403–410.

ANDERSON, M. J. 2001. A new method for non-parametric multivariate analysis of variance. *Austral Ecology*, 26, 32–46.

ANDERSON, M. J. 2006. Distance-based tests for homogeneity of multivariate dispersions. *Biometrics*, 62, 245–253.

AW, T. & GIN, K. H. 2010. Environmental surveillance and molecular characterization of human enteric viruses in tropical urban wastewaters. *Journal of Applied Microbiology*, 109, 716–730.

BAČNIK, K., KUTNJAK, D., PECMAN, A., MEHLE, N., ŽNIDARIČ, M. T., AGUIRRE, I. G. & RAVNIKAR, M. 2020. Viromics and infectivity analysis reveal the release of

infective plant viruses from wastewater into the environment. *Water Research*, 177, 1-11.

BANKEVICH, A., NURK, S., ANTIPOV, D., GUREVICH, A. A., DVORKIN, M., KULIKOV, A. S., LESIN, V. M., NIKOLENKO, S. I., PHAM, S. & PRJIBELSKI, A. D. 2012. SPAdes: a new genome assembly algorithm and its applications to single-cell sequencing. *Journal of Computational Biology*, 19, 455–477.

BATOOL, M. & GALLOWAY-PEÑA, J. 2023. Clinical metagenomics-challenges and future prospects. *Frontiers in Microbiology*, 14, 1-13.

BENJAMINI, Y. & HOCHBERG, Y. 1995. Controlling the false discovery rate: a practical and powerful approach to multiple testing. *Journal of the Royal Statistical Society: Series B (Methodological)*, 57, 289–300.

BIBBY, K. & PECCIA, J. 2013. Identification of viral pathogen diversity in sewage sludge by metagenome analysis. *Environmental Science & Technology*, 47, 1945–1951.

BLANCARD, D. 2012. Tomato Diseases: Identification, Biology and Control: A Colour Handbook, Second Edition. Academic Press, Cambridge, MA, USA.

BLINKOVA, O., ROSARIO, K., LI, L., KAPOOR, A., SLIKAS, B., BERNARDIN, F., BREITBART, M. & DELWART, E. 2009. Frequent detection of highly diverse variants of cardiovirus, cosavirus, bocavirus, and circovirus in sewage samples collected in the United States. *Journal of Clinical Microbiology*, 47, 3507–3513.

BOLGER, A. M., LOHSE, M. & USADEL, B. 2014. Trimmomatic: a flexible trimmer for Illumina sequence data. *Bioinformatics*, 30, 2114–2120.

BOUSEETTINE, R., HASSOU, N., BESSI, H. & ENNAJI, M. M. 2020. Waterborne transmission of enteric viruses and their impact on public health. In: *Emerging and Reemerging Viral Pathogens*. Elsevier, 907-932

BROWN, J. R., MORFOPOULOU, S., HUBB, J., EMMETT, W. A., IP, W., SHAH, D., BROOKS, T., PAINE, S. M., ANDERSON, G. & VIRASAMI, A. 2015. Astrovirus VA1/HMO-C: an increasingly recognized neurotropic pathogen in immunocompromised patients. *Clinical Infectious Diseases*, 60, 881–888.

BROWN, J. R., SHAH, D. & BREUER, J. 2016. Viral gastrointestinal infections and norovirus genotypes in a paediatric UK hospital, 2014–2015. *Journal of Clinical Virology*, 84, 1–6.

CHEN, H., HAN, Y., LIU, Y., LIU, D., JIANG, L., HUANG, K., WANG, H., GUO, L., WANG, X. & WANG, J. 2023. Classification models for Tobacco Mosaic Virus and Potato Virus Y using hyperspectral and machine learning techniques. *Frontiers in Plant Science*, 14, 1-15.

CHEN, S. & TIAN, X. 2018. Vaccine development for human mastadenovirus. *Journal of Thoracic Disease*, 10(19), S2280–S2294.

CHEN, Y., WANG, Y., PAEZ-ESPINO, D., POLZ, M. F. & ZHANG, T. 2021. Prokaryotic viruses impact functional microorganisms in nutrient removal and carbon cycle in wastewater treatment plants. *Nature Communications*, 12(5398), 1-11.

CHIGOR, V. N. & OKOH, A. I. 2012. Quantitative RT-PCR detection of hepatitis A virus, rotaviruses and enteroviruses in the Buffalo River and source water dams in the Eastern Cape Province of South Africa. *International Journal of Environmental Research and Public Health*, 9, 4017–4032.

CORDEY, S., VU, D.-L., SCHIBLER, M., L'HUILLIER, A. G., BRITO, F., DOCQUIER, M., POSFAY-BARBE, K. M., PETTY, T. J., TURIN, L. & ZDOBNOV, E. M. 2016. Astrovirus MLB2, a new gastroenteric virus associated with meningitis and disseminated infection. *Emerging Infectious Diseases*, 22, 846–849.

CUEVAS-FERRANDO, E., SÁNCHEZ, G. & PÉREZ-CATALUÑA, A. 2025. Exploring plant virus diversity in wastewater and reclaimed water through metagenomic analysis. *Water Research*, 270, 1-9.

DA SILVA ASSIS, M. R., VIEIRA, C. B., FIORETTI, J. M., ROCHA, M. S., DE ALMEIDA, P. I. N., MIAGOSTOVICH, M. P. & FUMIAN, T. M. 2016. Detection and molecular characterization of gemycircularvirus from environmental samples in Brazil. *Food and Environmental Virology*, 8, 305–309.

DAVIS, N. M., PROCTOR, D. M., HOLMES, S. P., RELMAN, D. A. & CALLAHAN, B. J. 2018. Simple statistical identification and removal of contaminant sequences in marker-gene and metagenomics data. *Microbiome*, 6, 1-14.

DE PAEPE, M., LECLERC, M., TINSLEY, C. R. & PETIT, M.-A. 2014. Bacteriophages: an underestimated role in human and animal health? *Frontiers in Cellular and Infection Microbiology*, 4, 1-11.

DEÉZSI-MAGYAR, N., NOVÁK, N., LUKÁCS, A., TARCSAI, K. R., HAJDU, Á., TAKÁCS, L., FARKAS, F. B., RIGÓ, Z., BARCSAY, E. & KIS, Z. 2024. First whole genome sequencing and analysis of human parechovirus type 3 causing a healthcare-associated outbreak among neonates in Hungary. *European Journal of Clinical Microbiology & Infectious Diseases*, 43, 2341–2350.

DEMOLINER, M., FILIPPI, M., GULARTE, J. S., DE ALMEIDA, P. R., DA SILVA, M. S., PEREIRA, V. M. D. A. G., HANSEN, A. W., GIRARDI, V., FERREIRA, H. L. &

SPILKI, F. R. 2025. Comparison of metagenomic protocols for virome data generation from environmental matrices and stool samples: insights into viral diversity and fecal contamination indicators. *Total Environment Microbiology*, 1, 1-16.

DOBIN, A., DAVIS, C. A., SCHLESINGER, F., DRENKOW, J., ZALESKI, C., JHA, S., BATUT, P., CHAISSON, M. & GINGERAS, T. R. 2013. STAR: ultrafast universal RNA-seq aligner. *Bioinformatics*, 29, 15–21.

DREHER, A. M., ARORA, N., FOWLER, K. B., NOVAK, Z., BRITT, W. J., BOPPANA, S. B. & ROSS, S. A. 2014. Spectrum of disease and outcome in children with symptomatic congenital cytomegalovirus infection. *The Journal of Pediatrics*, 164, 855–859.

FARKAS, K., WALKER, D. I., ADRIAENSSENS, E. M., MCDONALD, J. E., HILLARY, L. S., MALHAM, S. K. & JONES, D. L. 2020. Viral indicators for tracking domestic wastewater contamination in the aquatic environment. *Water Research*, 181, 1-20.

FERNANDEZ-CASSI, X., TIMONEDA, N., MARTÍNEZ-PUCHOL, S., RUSIÑOL, M., RODRIGUEZ-MANZANO, J., FIGUEROLA, N., BOFILL-MAS, S., ABRIL, J. F. & GIRONES, R. 2018. Metagenomics for the study of viruses in urban sewage as a tool for public health surveillance. *Science of the Total Environment*, 618, 870–880.

FERNANDEZ-GARCIA, M. D., SIMON-LORIERE, E., KEBE, O., SAKUNTABHAI, A. & NDIAYE, K. 2020. Identification and molecular characterization of the first complete genome sequence of Human Parechovirus type 15. *Scientific Reports*, 10, 1-9.

FURTAK, V., ROIVAINEN, M., MIROCHNICHENKO, O., ZAGORODNYAYA, T., LAASSRI, M., ZAIDI, S. Z., REHMAN, L., ALAM, M. M., CHIZHIKOV, V. & CHUMAKOV, K. 2016. Environmental surveillance of viruses by tangential flow filtration and metagenomic reconstruction. *Eurosurveillance*, 21(15), 1-11.

GARCÍA-FONTANA, C., RODRIGUEZ-SANCHEZ, A., MUÑOZ-PALAZON, B., GONZALEZ-MARTINEZ, A., VELA-CANO, M. & GONZALEZ-LOPEZ, J. 2020. Profile of the spatial distribution patterns of the human and bacteriophage virome in a wastewater treatment plant located in the south of Spain. *Water*, 12(8), 1-18.

GLOOR, G. B., MACKLAIM, J. M., PAWLOWSKY-GLAHN, V. & EGOZCUE, J. J. 2017. Microbiome datasets are compositional: and this is not optional. *Frontiers in Microbiology*, 8, 1-6.

GOWER, J. C. 1966. Some distance properties of latent root and vector methods used in multivariate analysis. *Biometrika*, 53, 325–338.

GREGORY, A. C., ZABLOCKI, O., ZAYED, A. A., HOWELL, A., BOLDUC, B. & SULLIVAN, M. B. 2020. The gut virome database reveals age-dependent patterns of virome diversity in the human gut. *Cell Host & Microbe*, 28, 724–734.

GUAJARDO-LEIVA, S., CHNAIDERMAN, J., GAGGERO, A. & DÍEZ, B. 2020. Metagenomic insights into the sewage RNA virosphere of a large city. *Viruses*, 12(9), 1-15.

GUAJARDO-LEIVA, S., DÍEZ, B., ROJAS-FUENTES, C., CHNAIDERMAN, J., CASTRO-NALLAR, E., CATRIL, V., AMPUERO, M. & GAGGERO, A. 2025. From sewage to genomes: expanding our understanding of the urban and semi-urban wastewater RNA virome. *Environmental Research*, 276, 1-15.

GUERRERO-LATORRE, L., ROMERO, B., BONIFAZ, E., TIMONEDA, N., RUSIÑOL, M., GIRONES, R. & RIOS-TOUMA, B. 2018. Quito's virome: metagenomic analysis of viral diversity in urban streams of Ecuador's capital city. *Science of the Total Environment*, 645, 1334–1343.

HAN, Z., GAO, M., YAN, Z., HONG, H., YIN, X., XU, S., PENG, J., YAN, F., LI, X. & JIANG, S. 2024. First report of Paprika mild mottle virus infecting pepper (*Capsicum annuum*) in China. *Plant Disease*, 108(12), 1.

HANTULA, J. & VAINIO, E. J. 2021. Viruses as components of forest microbiome. In: *Forest Microbiology*. Elsevier, 371-382.

HARDING, C., LARSEN, B. B., GRYSEELS, S., OTTO, H. W., SUAZO, C., KRABERGER, S., UPHAM, N. S., WOROBEY, M., VAN DOORSLAER, K. & VARSANI, A. 2022. Discovery of three cycloviruses in fecal samples from silver-haired bats (*Lasionycteris noctivagans*) in Arizona (USA). *Archives of Virology*, 167, 2771–2775.

HATA, A., KATAYAMA, H., KOJIMA, K., SANO, S., KASUGA, I., KITAJIMA, M. & FURUMAI, H. 2014. Effects of rainfall events on the occurrence and detection efficiency of viruses in river water impacted by combined sewer overflows. *Science of the Total Environment*, 468, 757–763.

HILL, M. O. 1973. Diversity and evenness: a unifying notation and its consequences. *Ecology*, 54, 427–436.

HOŠNJAK, L., KOCJAN, B. J., PIRŠ, B., SEME, K. & POLJAK, M. 2021. The genetic diversity of human papillomavirus types from the species *Gammapapillomavirus* 15: HPV135, HPV146, and HPV179. *Plos One*, 16(5), 1-18.

ITARTE, M., MARTÍNEZ-PUCHOL, S., FORÉS, E., HUNDESA, A., TIMONEDA, N., BOFILL-MAS, S., GIRONES, R. & RUSIÑOL, M. 2021. NGS techniques reveal a high diversity of RNA viral pathogens and papillomaviruses in fresh produce and irrigation water. *Foods*, 10, 1-21.

JEŻEWSKA, M., ZARZYŃSKA-NOWAK, A. & TRZMIEL, K. 2018. Detection of infectious tobamoviruses in irrigation and drainage canals in Greater Poland. *Journal of Plant Protection Research*, 58, 123–130.

JOST, L. 2006. Entropy and diversity. *Oikos*, 113, 363–375.

JURCZAK-KUREK, A., GĄSIOR, T., NEJMAN-FALEŃCZYK, B., BLOCH, S., DYDECKA, A., TOPKA, G., NECEL, A., JAKUBOWSKA-DEREDAS, M., NARAJCZYK, M. & RICHERT, M. 2016. Biodiversity of bacteriophages: morphological and biological properties of a large group of phages isolated from urban sewage. *Scientific Reports*, 6, 1-17.

KALANTAR, K. L., CARVALHO, T., DE BOURCY, C. F., DIMITROV, B., DINGLE, G., EGGER, R., HAN, J., HOLMES, O. B., JUAN, Y. F. & KING, R. 2020. IDseq—An open source cloud-based pipeline and analysis service for metagenomic pathogen detection and monitoring. *GigaScience*, 9, 1-14.

KALLIES, R., HU, D., ABDULKADIR, N. U., SCHLOTER, M. & ROCHA, U. 2023. Identification of huge phages from wastewater metagenomes. *Viruses*, 15, 1-15.

KESARI, K. K., SONI, R., JAMAL, Q. M. S., TRIPATHI, P., LAL, J. A., JHA, N. K., SIDDIQUI, M. H., KUMAR, P., TRIPATHI, V. & RUOKOLAINEN, J. 2021. Wastewater treatment and reuse: a review of its applications and health implications. *Water, Air, & Soil Pollution*, 232, 1–28.

KING, A. M., LEFKOWITZ, E., ADAMS, M. J. & CARSTENS, E. B. 2011. Virus taxonomy: ninth report of the International Committee on Taxonomy of Viruses. *Elsevier*, 1-1326.

KITAJIMA, M., SASSI, H. P. & TORREY, J. R. 2018. Pepper mild mottle virus as a water quality indicator. *NPJ Clean Water*, 1(19), 1-9.

KORF, I. H., MEIER-KOLTHOFF, J. P., ADRIAENSSENS, E. M., KROPINSKI, A. M., NIMTZ, M., ROHDE, M., VAN RAAIJ, M. J. & WITTMANN, J. 2019. Still something to discover: novel insights into Escherichia coli phage diversity and taxonomy. *Viruses*, 11, 1-29.

KRABERGER, S., ARGÜELLO-ASTORGA, G. R., GREENFIELD, L. G., GALILEE, C., LAW, D., MARTIN, D. P. & VARSANI, A. 2015. Characterisation of a diverse range of circular replication-associated protein encoding DNA viruses recovered from a sewage treatment oxidation pond. *Infection, Genetics and Evolution*, 31, 73–86.

KUMARI, N., SHARMA, V., PATEL, P. & SHARMA, P. 2023. Pepper mild mottle virus: a formidable foe of capsicum production—a review. *Frontiers in Virology*, 3, 1-20.

KWON, M.-J., KWON, S.-J., KIM, M.-H., CHOI, B., BYUN, H.-S., KWAK, H.-R. & SEO, J.-K. 2023. Visual tracking of viral infection dynamics reveals the synergistic interactions between cucumber mosaic virus and broad bean wilt virus 2. *Scientific Reports*, 13, 1-14.

LA ROSA, G., FRATINI, M., ACCARDI, L., D'ORO, G., DELLA LIBERA, S., MUSCILLO, M. & DI BONITO, P. 2013. Mucosal and cutaneous human papillomaviruses detected in raw sewages. *Plos One*, 8(1), 1-10.

LANGMEAD, B. & SALZBERG, S. L. 2012. Fast gapped-read alignment with Bowtie 2. *Nature Methods*, 9, 357–359.

LANREWAJU, A. A., ENITAN-FOLAMI, A. M., SABIU, S., EDOKPAYI, J. N. & SWALAHA, F. M. 2022. Global public health implications of human exposure to viral contaminated water. *Frontiers in Microbiology*, 13, 1-18.

LAZZAROTTO, T., GUERRA, B., GABRIELLI, L., LANARI, M. & LANDINI, M. P. 2011. Update on the prevention, diagnosis and management of cytomegalovirus infection during pregnancy. *Clinical Microbiology and Infection*, 17, 1285–1293.

LI, J. 2023. Transmission, pathology, and prevention strategies of Hepatitis A virus. *Molecular Pathogens*, 14(2), 1-14.

LI, J. X., LIU, S. S. & GU, Q. S. 2016. Transmission efficiency of cucumber green mottle mosaic virus via seeds, soil, pruning and irrigation water. *Journal of Phytopathology*, 164, 300–309.

LI, J., YANG, L., WANG, K., GAO, Z., LI, P., LIN, Y., JIA, L., WANG, Q., SONG, H. & LI, P. 2023. Characterisation of human astrovirus in a diarrhoea outbreak using nanopore and Sanger sequencing protocols. *Virology Journal*, 20(263), 1-8.

LI, W. & GODZIK, A. 2006. Cd-hit: a fast program for clustering and comparing large sets of protein or nucleotide sequences. *Bioinformatics*, 22, 1658–1659.

LI, Y., MIYANI, B., FAUST, R. A., DAVID, R. E. & XAGORARAKI, I. 2024. A broad wastewater screening and clinical data surveillance for virus-related diseases in the metropolitan Detroit area in Michigan. *Human Genomics*, 18(14), 1-18.

LOPEZ-ROBLERO, A., MARTÍNEZ CANO, D. J., DIEGO-GARCÍA, E., GUILLÉN-NAVARRO, G. K., IŠA, P. & ZARZA, E. 2024. Metagenomic analysis of plant viruses in tropical fresh and wastewater. *Environmental DNA*, 6(416), 1-13.

LU, J., YANG, S., ZHANG, X., TANG, X., ZHANG, J., WANG, X., WANG, H., SHEN, Q. & ZHANG, W. 2022. Metagenomic analysis of viral community in the Yangtze River expands known eukaryotic and prokaryotic virus diversity in freshwater. *Virologica Sinica*, 37, 60–69.

LU, L., ZHONG, H., XU, M., JIA, R., LIU, P., SU, L., CAO, L., ZHU, X. & XU, J. 2023. Diversity of classic and novel human astrovirus in outpatient children with acute gastroenteritis in Shanghai, China. *Frontiers in Microbiology*, 14, 1-10.

LYU, J., YANG, Y., SUN, X., JIANG, S., HONG, H., ZHU, X. & LIU, Y. 2023. Genetic variability and molecular evolution of tomato mosaic virus populations in three northern China provinces. *Viruses*, 15(7), 1-13.

MAKSIMOVIĆ, O., BAČNIK, K., RIVAREZ, M. P. S., VUČUROVIĆ, A., MEHLE, N., RAVNIKAR, M., GUTIÉRREZ-AGUIRRE, I. & KUTNJAK, D. 2024. Virome analysis of irrigation water sources provides extensive insights into the diversity and distribution of plant viruses in agroecosystems. *Water Research*, 249, 1-15.

MAO, L., LI, X., CAI, X., LI, W., LI, J., YANG, S., ZHAI, J., SUOLANG, S. & LI, B. 2024. First specific detection of mammalian orthoreovirus from goats using TaqMan real-time RT-PCR technology. *Veterinary Sciences*, 11(4), 1-10.

MAXIMOVA, O. A., WELLER, M. L., KROGMANN, T., STURDEVANT, D. E., RICKLEFS, S., VIRTANEVA, K., MARTENS, C., WOLLENBERG, K., MINAI, M. & MOORE, I. N. 2023. Pathogenesis and outcome of VA1 astrovirus infection in the human brain are defined by disruption of neural functions and imbalanced host immune responses. *PLoS Pathogens*, 19, 1-27.

MAYO, M. 2002. A summary of taxonomic changes recently approved by ICTV. *Archives of Virology*, 147, 1655–1656.

MCCALL, C. & XAGORARAKI, I. 2019. Metagenomic approaches for detecting viral diversity in water environments. *Journal of Environmental Engineering*, 145(8), 1-9.

MCCALL, C., LEO ELWORTH, R. A., WYLIE, K. M., WYLIE, T. N., DYSON, K., DOUGHTY, R., TREANGEN, T. J., HOPKINS, L., ENSOR, K. & STADLER, L. B. 2023. Targeted metagenomic sequencing for detection of vertebrate viruses in wastewater for public health surveillance. *ACS ES&T Water*, 3, 2955–2965.

MCMURDIE, P. J. & HOLMES, S. 2013. phyloseq: an R package for reproducible interactive analysis and graphics of microbiome census data. *Plos One*, 8(4), 1-11.

MEHLE, N. & RAVNIKAR, M. 2012. Plant viruses in aqueous environment—survival, water mediated transmission and detection. *Water Research*, 46, 4902–4917.

MEHLE, N., BAČNIK, K., BAJDE, I., BRODARIČ, J., FOX, A., GUTIÉRREZ-AGUIRRE, I., KITEK, M., KUTNJAK, D., LOH, Y. L. & MAKSIMOVIĆ CARVALHO FERREIRA, O. 2023. Tomato brown rugose fruit virus in aqueous environments—survival and significance of water-mediated transmission. *Frontiers in Plant Science*, 14, 1-15.

MEHLE, N., GUTIÉRREZ-AGUIRRE, I., KUTNJAK, D. & RAVNIKAR, M. 2018. Water-mediated transmission of plant, animal, and human viruses. *Advances in Virus Research*, 101, 85–128.

MILANI, J. S. & BIDHENDI, N. G. 2022. A review on the potential of common disinfection processes for the removal of virus from wastewater. *International Journal of Environmental Research*, 16(9), 1-11.

MOHAMMADZADEH, N., RODA, W., BRANTON, W. G., CLAIN, J., RABEZANAHARY, H., ZGHIDI-ABOUZID, O., GELMAN, B. B., ANGEL, J. B., COHEN, E. A. & GILL, M. J. 2021. Lentiviral infections persist in brain despite effective antiretroviral therapy and neuroimmune activation. *mBio*, 12(6), 1-16.

NASH, D., ELLMEN, I., KNAPP, J. J., MENON, R., OVERTON, A. K., CHENG, J., LYNCH, M. D., NISSIMOV, J. I. & CHARLES, T. C. 2024. A novel tiled amplicon sequencing assay targeting the tomato brown rugose fruit virus (ToBRFV) genome reveals widespread distribution in municipal wastewater treatment systems in the province of Ontario, Canada. *Viruses*, 16(3), 1-19.

NASIRI, M., GHALEJOOGH, Z. Y., ATAEI-PIRKOOH, A., BOKHARAEI-SALIM, F., MONAVARI, S. H., TAVAKOLI, A., ASADIFAR, B., ESGHAEI, M., PASALARI, H. & SAMIMI-RAD, K. 2021. Detection and phylogenetic analysis of Hepatitis A virus in the wastewater treatment plant of Ekbatan Town in Tehran, Iran. *Hepatitis Monthly*, 21(10), 1-6.

NIEUWENHUIJSE, D. F., OUDE MUNNINK, B. B., PHAN, M. V., MUNK, P., VENKATAKRISHNAN, S., AARESTRUP, F. M., COTTEN, M. & KOOPMANS, M. P. 2020. Setting a baseline for global urban virome surveillance in sewage. *Scientific Reports*, 10(1), 1-13.

OKSANEN, J., BLANCHET, F. G., KINDT, R., LEGENDRE, P., MINCHIN, P. R., O'HARA, R., SIMPSON, G. L., SOLYMOS, P., STEVENS, M. H. H. & WAGNER, H. 2013. Community ecology package. *R package version*, 2, 321–326.

OMATOLA, C. A., OLASEHINDE, T. A. & OLANIRAN, A. O. 2024. Relative abundance and the fate of human rotavirus in wastewater during treatment processes: identification of potential infectious rotavirus in the final effluents and receiving aquatic milieu in Durban area, South Africa. *Environmental Monitoring and Assessment*, 196, 1-15.

OSBORNE, C. M., MONTANO, A. C., ROBINSON, C. C., SCHULTZ-CHERRY, S. & DOMINGUEZ, S. R. 2015. Viral gastroenteritis in children in Colorado 2006–2009. *Journal of Medical Virology*, 87, 931–939.

OSUNMAKINDE, C. O., SELVARAJAN, R., SIBANDA, T., MAMBA, B. B. & MSAGATI, T. A. 2018. Overview of trends in the application of metagenomic techniques in the analysis of human enteric viral diversity in Africa's environmental regimes. *Viruses*, 10(8), 1-25.

PAEZ-ESPINO, D., ELOE-FADROSH, E. A., PAVLOPOULOS, G. A., THOMAS, A. D., HUNTEMANN, M., MIKHAILOVA, N., RUBIN, E., IVANOVA, N. N. & KYRPIDES, N. C. 2016. Uncovering Earth's virome. *Nature*, 536, 425–430.

PALUKAITIS, P. & GARCÍA-ARENAL, F. 2003. Cucumoviruses. *Advances in Virus Research*, 62, 241–323.

PARKINS, M. D., LEE, B. E., ACOSTA, N., BAUTISTA, M., HUBERT, C. R., HRUDEY, S. E., FRANKOWSKI, K. & PANG, X.-L. 2024. Wastewater-based surveillance as a tool for public health action: SARS-CoV-2 and beyond. *Clinical Microbiology Reviews*, 37(1), 1-60.

PHAN, T. G., MORI, D., DENG, X., RAJINDRAJITH, S., RANAWAKA, U., NG, T. F. F., BUCARDO-RIVERA, F., ORLANDI, P., AHMED, K. & DELWART, E. 2015. Small circular single stranded DNA viral genomes in unexplained cases of human encephalitis, diarrhea, and in untreated sewage. *Virology*, 482, 98–104.

PIAZZOLLA, P., CASTELLANO, M. & DE STRADIS, A. 1986. Presence of plant viruses in some rivers of southern Italy. *Journal of Phytopathology*, 116, 244–246.

PLOWRIGHT, R. K., EBY, P., HUDSON, P. J., SMITH, I. L., WESTCOTT, D., BRYDEN, W. L., MIDDLETON, D., REID, P. A., MCFARLANE, R. A. & MARTIN, G. 2015. Ecological dynamics of emerging bat virus spillover. *Proceedings of the Royal Society B: Biological Sciences*, 282, 1-9.

PUGET, L., NODE, J., CAËL, B., BAMOULID, J., COAQUETTE, A., PRÉTET, J.-L. & LEPILLER, Q. 2024. Urinary cytomegalovirus excretion: the unresolved issues. *Annales Pharmaceutiques Françaises*, 82, 45–53.

QI, Y.-H., HE, Y.-J., WANG, X., ZHANG, C.-X., CHEN, J.-P., LU, G. & LI, J.-M. 2021. Physical contact transmission of Cucumber green mottle mosaic virus by *Myzus persicae*. *Plos One*, 16(6), 1-13.

REMNANT, E. J., SHI, M., BUCHMANN, G., BLACQUIÈRE, T., HOLMES, E. C., BEEKMAN, M. & ASHE, A. 2017. A diverse range of novel RNA viruses in geographically distinct honey bee populations. *Journal of Virology*, 91(16), 1-19.

ROSARIO, K., NILSSON, C., LIM, Y. W., RUAN, Y. & BREITBART, M. 2009. Metagenomic analysis of viruses in reclaimed water. *Environmental Microbiology*, 11, 2806–2820.

ROTHMAN, J. A. & WHITESON, K. L. 2022. Sequencing and variant detection of eight abundant plant-infecting tobamoviruses across Southern California wastewater. *Microbiology Spectrum*, 10(6), 1-6.

RUPPÉ, E. & SCHRENZEL, J. 2018. Messages from the second international conference on clinical metagenomics (ICCMg2). *Microbes and Infection*, 20, 222–227.

RUSIÑOL, M., MARTÍNEZ-PUCHOL, S., TIMONEDA, N., FERNÁNDEZ-CASSI, X., PÉREZ-CATALUÑA, A., FERNÁNDEZ-BRAVO, A., MORENO-MESONERO, L., MORENO, Y., ALONSO, J. L. & FIGUERAS, M. J. 2020. Metagenomic analysis of viruses, bacteria and protozoa in irrigation water. *International Journal of Hygiene and Environmental Health*, 224, 1-11.

SAASA, N., M'KANDAWIRE, E., NDEBE, J., MWENDA, M., CHIMPUKUTU, F., MUKUBESA, A. N., NJOBVU, F., SHEMPELA, D. M., SIKALIMA, J. &

CHIYESU, C. 2024. Detection of human adenovirus and rotavirus in wastewater in Lusaka, Zambia: demonstrating the utility of environmental surveillance for the community. *Pathogens*, 13(6), 1-12.

SCHOLTHOF, K. B. G., ADKINS, S., CZOSNEK, H., PALUKAITIS, P., JACQUOT, E., HOHN, T., HOHN, B., SAUNDERS, K., CANDRESSE, T. & AHLQUIST, P. 2011. Top 10 plant viruses in molecular plant pathology. *Molecular Plant Pathology*, 12, 938–954.

SHERCHAN, S. P., MALLA, B. & HARAMOTO, E. 2023. First quantitative detection of tomato brown rugose fruit virus in wastewater in Louisiana. *Science of the Total Environment*, 888, 1-4.

SIMPSON, E. H. 1949. Measurement of diversity. *Nature*, 163, 688-688.

SIQUEIRA, J. A. M., DE SOUZA OLIVEIRA, D., DE CARVALHO, T. C. N., PORTAL, T. M., JUSTINO, M. C. A., DA SILVA, L. D., RESQUE, H. R. & GABBAY, Y. B. 2017. Astrovirus infection in hospitalized children: Molecular, clinical and epidemiological features. *Journal of Clinical Virology*, 94, 79–85.

SOLTANE, R. & ALLAYEH, A. K. 2023. Occurrence of enteroviruses, noroviruses, rotaviruses, and adenoviruses in a wastewater treatment plant. *Journal of Umm Al-Qura University for Applied Sciences*, 9, 449–454.

STOVER, M. G. & WATSON, R. R. 2015. Animal lentiviruses: models for human immunodeficiency viruses and nutrition. In: *Health of HIV Infected People*. Elsevier, 349-365.

TAKUISSU, G. R., KENMOE, S., EBOGO-BELOBO, J. T., KENGNE-NDÉ, C., MBAGA, D. S., BOWO-NGANDJI, A., NDZIE ONDIGUI, J. L., KENFACK-MOMO, R.,

TCHATCHOUANG, S. & KENFACK-ZANGUIM, J. 2023. Assessing the prevalence of astroviruses in water environments: a systematic review and meta-analysis. *ACS ES&T Water*, 3, 3782–3789.

TANDUKAR, S., SHERCHAN, S. P. & HARAMOTO, E. 2020. Applicability of crAssphage, pepper mild mottle virus, and tobacco mosaic virus as indicators of reduction of enteric viruses during wastewater treatment. *Scientific Reports*, 10, 1-9.

TAO, Z., LIN, X., LIU, Y., JI, F., WANG, S., XIONG, P., ZHANG, L., XU, Q., XU, A. & CUI, N. 2022. Detection of multiple human astroviruses in sewage by next generation sequencing. *Water Research*, 218, 1-9.

TEDCASTLE, A., WILTON, T., PEGG, E., KLAPSA, D., BUJAKI, E., MATE, R., FRITZSCHE, M., MAJUMDAR, M. & MARTIN, J. 2022. Detection of Enterovirus D68 in wastewater samples from the UK between July and November 2021. *Viruses*, 14(1), 1-11.

TETTEY, C. K., YAN, Z.-Y., ZHAO, M.-S., CHAO, G., TIAN, Y.-P. & LI, X.-D. 2022. Tomato mottle mosaic virus: characterization, resistance gene effectiveness, and quintuplex RT-PCR detection system. *Journal of Integrative Agriculture*, 21, 2641–2651.

TISZA, M., JAVORNIK CREGEEN, S., AVADHANULA, V., ZHANG, P., AYVAZ, T., FELIZ, K., HOFFMAN, K. L., CLARK, J. R., TERWILLIGER, A. & ROSS, M. C. 2023. Wastewater sequencing reveals community and variant dynamics of the collective human virome. *Nature Communications*, 14, 1-10.

TROEGER, C., KHALIL, I. A., RAO, P. C., CAO, S., BLACKER, B. F., AHMED, T., ARMAH, G., BINES, J. E., BREWER, T. G. & COLOMBARA, D. V. 2018. Rotavirus vaccination and the global burden of rotavirus diarrhea among children younger than 5 years. *JAMA Pediatrics*, 172, 958–965.

TUCKER, K. P., PARSONS, R., SYMONDS, E. M. & BREITBART, M. 2011. Diversity and distribution of single-stranded DNA phages in the North Atlantic Ocean. *The ISME Journal*, 5, 822–830.

ULLAH, N., AKHTAR, K. P., SALEEM, M. Y. & HABIB, M. 2019. Characterization of tomato mosaic virus and search for its resistance in *Solanum* species. *European Journal of Plant Pathology*, 155, 1195–1209.

WANG, H., NEYVALDT, J., ENACHE, L., SIKORA, P., MATTSSON, A., JOHANSSON, A., LINDH, M., BERGSTEDT, O. & NORDER, H. 2020a. Variations among viruses in influent water and effluent water at a wastewater plant over one year as assessed by quantitative PCR and metagenomics. *Applied and Environmental Microbiology*, 86(24), 1-14.

WANG, M., ZHU, J. & MAO, X. 2021. Removal of pathogens in onsite wastewater treatment systems: a review of design considerations and influencing factors. *Water*, 13(9), 1-30.

WANG, S.-H., WANG, K., ZHAO, K., HUA, S.-C. & DU, J. 2020b. The structure, function, and mechanisms of action of enterovirus non-structural protein 2C. *Frontiers in Microbiology*, 11, 1-14.

WEI, H., KHAMRIN, P., KUMTHIP, K., YODMEEKLIN, A. & MANEEKARN, N. 2021. High divergence of human astrovirus genotypes circulating in pediatric patients hospitalized with acute gastroenteritis in Chiang Mai, Thailand, 2017–2020. *Scientific Reports*, 11(1), 1-8.

WICKHAM, H., CHANG, W. & WICKHAM, M. H. 2016. Package 'ggplot2'. Create elegant data visualisations using the grammar of graphics. *Version*, 2, 1–189.

WILSON, M. R., O'DONOVAN, B. D., GELFAND, J. M., SAMPLE, H. A., CHOW, F. C., BETJEMANN, J. P., SHAH, M. P., RICHIE, M. B., GORMAN, M. P. & HAJJ-ALI, R. A. 2018. Chronic meningitis investigated via metagenomic next-generation sequencing. *JAMA Neurology*, 75, 947–955.

WOHLGEMUTH, N., HONCE, R. & SCHULTZ-CHERRY, S. 2019. Astrovirus evolution and emergence. *Infection, Genetics and Evolution*, 69, 30–37.

WRIGHT, S., KLEVEN, D., KAPOOR, R., KAVURI, S. & GANI, I. 2020. Recurring norovirus & sapovirus infection in a renal transplant patient. *IDCases*, 20, 1-5.

WU, T. D. & NACU, S. 2010. Fast and SNP-tolerant detection of complex variants and splicing in short reads. *Bioinformatics*, 26, 873–881.

YARWOOD, C. E. 1960. Release and preservation of virus by roots. *Phytopathology*, 50(2), 111-114.

YE, Y., CHOI, J.-H. & TANG, H. 2011. RAPSearch: a fast protein similarity search tool for short reads. *BMC Bioinformatics*, 12, 1–10.

YE, Y., ELLENBERG, R. M., GRAHAM, K. E. & WIGGINTON, K. R. 2016. Survivability, partitioning, and recovery of enveloped viruses in untreated municipal wastewater. *Environmental Science & Technology*, 50, 5077–5085.

YOSHITOMI, H., SERA, N., GONZALEZ, G., HANAOKA, N. & FUJIMOTO, T. 2017. First isolation of a new type of human adenovirus (genotype 79), species Human mastadenovirus B (B2) from sewage water in Japan. *Journal of Medical Virology*, 89, 1192–1200.

ZELL, R., GROTH, M., SELINKA, L. & SELINKA, H. C. 2022. Picorna-like viruses of the Havel River, Germany. *Frontiers in Microbiology*, 13, 1-13.

ZHANG, J., TANG, A., JIN, T., SUN, D., GUO, F., LEI, H., LIN, L., SHU, W., YU, P. & LI, X. 2024. A panoramic view of the virosphere in three wastewater treatment plants by integrating viral-like particle-concentrated and traditional non-concentrated metagenomic approaches. *iMeta*, 3, 1-21.

ZHANG, S., GRIFFITHS, J. S., MARCHAND, G., BERNARDS, M. A. & WANG, A. 2022. Tomato brown rugose fruit virus: an emerging and rapidly spreading plant RNA virus that threatens tomato production worldwide. *Molecular Plant Pathology*, 23, 1262–1277.

ZHANG, T., BREITBART, M., LEE, W. H., RUN, J.-Q., WEI, C. L., SOH, S. W. L., HIBBERD, M. L., LIU, E. T., ROHWER, F. & RUAN, Y. 2006. RNA viral community in human feces: prevalence of plant pathogenic viruses. *PLoS Biology*, 4(1), 1-11.

ZHANG, X., SUN, X., LIU, Y., QIAO, N., WANG, X., ZHAO, D., SHANG, K. & ZHU, X. 2023. Potential risk of plant viruses entering disease cycle in surface water in protected vegetable growing areas of Eastern China. *Plos One*, 18(1), 1-12.

ZHAO, W., WU, S., DU, L., LI, T., CHENG, Z., ZHOU, Y. & JI, Y. 2021. Development of a reverse-transcription loop-mediated isothermal amplification assay for the detection of Tobacco mild green mosaic virus (TMGMV). *Journal of Virological Methods*, 298, 1-7.

ZINTER, M., MAYDAY, M., RYCKMAN, K., JELLIFFE-PAWLOWSKI, L. & DERISI, J. 2019. Towards precision quantification of contamination in metagenomic sequencing experiments. *Microbiome*, 7, 1–10.

Supplementary Information

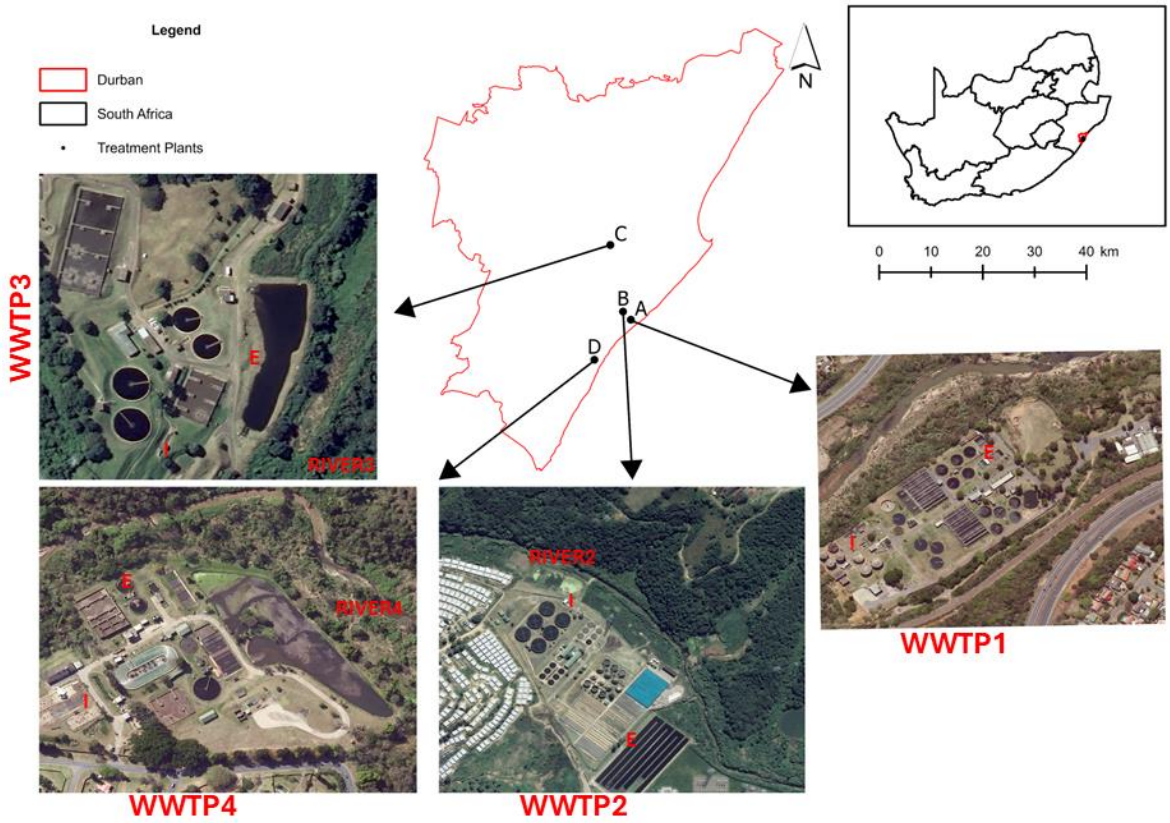


Figure 1: Overall map showing the investigated wastewater treatment plants and receiving rivers in eThekwini Municipality, Durban, South Africa. A. Amanzimtoti WWTP (WWTP1), B. Isipingo WWTP (WWTP2), C. Shallcross WWTPs (WWTP3) and D. Kingsburgh WWTP (WWTP4) and receiving rivers (RIVER1, RIVER2 and RIVER3). The sampling points are indicated as I (Influent), E (Effluent) RIVER2,3,4 (Effluent receiving river) in red colour.

Table 1: Differences in α-diversity metrics using Wilcoxon rank sum (two sided)

Parameter	Observed	Shannon	Simpson
W statistic	182.5	199	201
p-value	0.8124	0.864	0.8228
Alternative hypothesis	true location shift ≠ 0	true location shift ≠ 0	true location shift ≠ 0
95 % CI (lower)	–17.000050	–0.6130378	–0.1879805
95 % CI (upper)	9.999965	0.7052490	0.2332859
Estimated shift (difference in location)	–1.999916	0.0379717	0.01210414

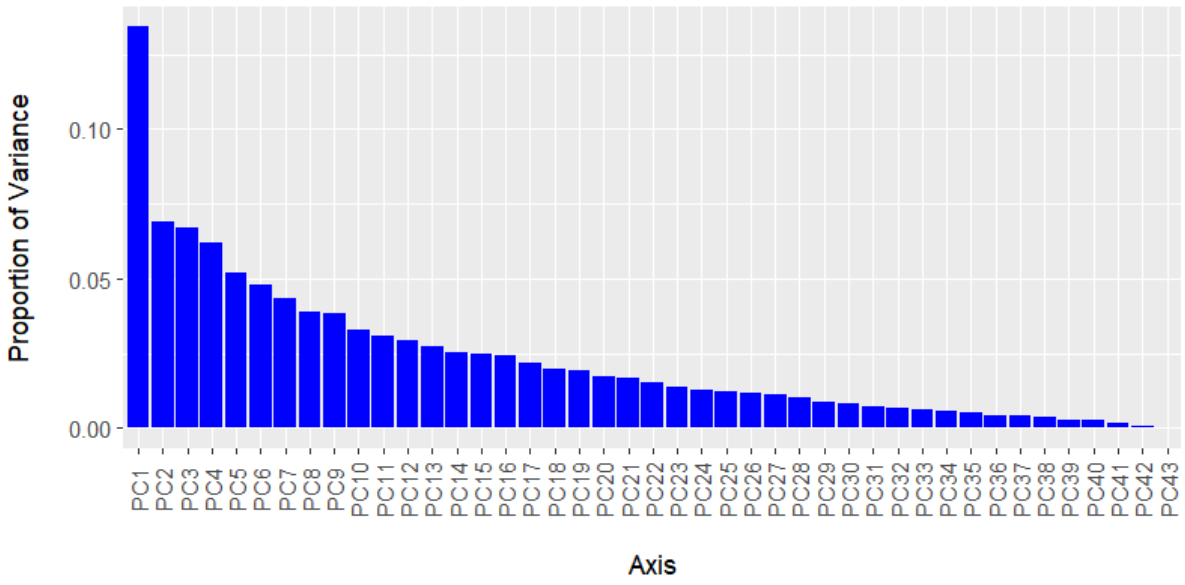


Figure 2: Scree plot showing the proportion of variance demonstrated by each of the first 43 principal components (PC1-PC43) derived from the PCA performed on centered and scaled viral abundance data generated from rivers and wastewater treatment plants samples.

CHAPTER FOUR

4.0 Metabolite profiling of selected medicinal plants and identification of lead compounds against selected druggable targets of SARS-CoV-2 and rotavirus A using computational techniques

4.1 Introduction…….289

4.2 Metabolites profiling and cheminformatics bioprospection of selected medicinal plants against the main protease and RNA-dependent RNA polymerase of SARS-CoV-2 **(Published in Journal of Biomolecular Structure and Dynamics)** …….293

4.3 Computational bioprospection of selected plant secondary metabolites against VP7 (capsid protein) of rotavirus A **(Published in Scientific African)**.…….……...……315

4.4 Bioprospection for antiviral compounds from selected medicinal plants against RNA polymerase of rotavirus A using molecular modelling and density functional theory **(Published in Chemical Physics Impact)** ……...……...337

4.5 Cheminformatics bioprospection of selected medicinal plants metabolites against trypsin cleaved VP4 (spike protein) of rotavirus A **(Published in Journal of Biomolecular Structure and Dynamics)**……..…….350

References……372

This chapter has been published as four separate articles in three different journals (Journal of Biomolecular Structure and Dynamics, Scientific African and Chemical Physics Impact). Each article focused on the identification of lead compounds against selected druggable targets of SARS-CoV-2 (main protease and RNA-dependent RNA polymerase) and rotavirus A (spike protein, capsid protein and RNA-dependent RNA polymerase).

4.1 Introduction

African medicinal plants and their metabolites have established therapeutic potential against various viral diseases (Beressa *et al*., 2021). For instance, metabolites from *Lindera aggregata*, *Artemisia annua*, *Lycoris radiata*, and *Pyrrosia lingua* have potentiated significant therapeutic effects against severe acute respiratory syndrome coronavirus (SARS-CoV) (Li *et al*., 2005). Specifically, the antiviral activity of *Spondias mombin* (Corthout *et al*., 1991; Siqueira *et al*., 2020) and *Macaranga barteri* (Ogbole *et al*., 2018; Segun *et al*., 2021) against diverse viruses has been established. Furthermore, *Dicerocaryum eriocarpum*, despite being a multipurpose plant with various ethnomedicinal benefits such as wound treatment, expulsion of retained placenta, antibacterial and anti-inflammatory properties (Luseba *et al*., 2007), and numerous ethnoveterinary uses (Van der Merwe *et al*., 2001) remains largely unexplored for its antiviral activity. Within this thesis, these medicinal plants provide bioactive chemicals that facilitate the synthesis of phyto-nanomaterials discussed in the next chapter. This chapter serves as a pivotal intermediary phase connecting natural product discovery to nanomaterial-based antiviral approaches.

A novel coronavirus named SARS-CoV-2, responsible for coronavirus disease (COVID-19), a respiratory disease, was initially identified in Wuhan, China in late 2019 (Wang *et al*., 2020; Lanrewaju *et al*., 2022). Subsequently, the World Health Organization (WHO) labelled COVID-19 a pandemic in March 2020, with the disease leading to an estimated 6.9 million fatalities as of June 2023 (World Health Organization, 2023). The WHO has authorized the use of different vaccines; however, none provide 100% efficacy yet (Vardhan and Sahoo, 2022). The Food and Drug Administration (FDA)-approved drugs for treating COVID-19, including remdesivir, olumiant, bebtelovimab, lagevrio, molnupiravir, and paxlovid (nirmatrelvir and

ritonavir), have usage restrictions to minimize potential adverse effects (Islam *et al*., 2022). As a result, developing targeted drugs for COVID-19 is imperative owing to its devastating consequences (Wrapp *et al*., 2020). Thus, identifying potent compounds with the potential to modulate key therapeutic targets in the virus, such as the main protease (MP) and RNA-dependent RNA polymerase (RP), is a worthwhile approach. However, computational exploration of *S. mombin*, *M. barteri*, and *D. eriocarpum* metabolites against these targets is currently lacking. Thus, this section profiles the metabolites of the three selected medicinal plants and subsequently employs computational bioprospection techniques to identify potential antiviral leads against the MP and the RP of SARS-CoV-2.

Rotavirus (RV) infections account for an estimated 258 million diarrhoea cases in children under five years globally (Troeger *et al*., 2018). RV-diarrhoea was implicated in approximately 122,000–215,000 deaths of children annually between 2013 and 2017 (Omatola and Olaniran 2022). Specifically, RVA continues to contribute to diarrhoea-induced mortality in children under age five significantly (Lanrewaju *et al*., 2022; Ugboko *et al*., 2020). Although implementing rotavirus vaccination schemes has led to a 60% reduction in mortality rates, vaccine efficacy remains comparatively low in developing nations (Parashar *et al*., 2016). Currently, oral and intravenous rehydration therapy is the basic treatment for RVA-induced diarrhoea; however, this therapy is simply symptomatic and does not alleviate the duration or severity of diarrhoea (Jiang *et al*., 2023). Unfortunately, no effective antiviral medication has been approved to treat RVA infection; hence, the urgency to prioritize developing anti-RVA drugs.

Rotavirus, a non-enveloped virus belonging to the Reoviridae family, is characterized by an icosahedral shape and segmented double-stranded RNA (dsRNA) genome containing 11 segments encoding six structural proteins (VP1-4, VP6 and VP7) and six non-structural proteins (NSP1-NSP6) (Nyaga *et al*., 2020). The external capsid glycoprotein VP7, which is highly immunogenic, induces antibodies, playing a crucial role in viral attachment to the host (Garuba *et al*., 2022). Due to its involvement in viral attachment, pathogenesis and abundance on the viral surface, targeting it could be a logical approach to disrupt its interaction with host cells (Asensio-Cob *et al*., 2023). Therefore, this section investigates the pooled metabolites of the selected medicinal plants to identify broad-spectrum antiviral lead compounds against RVA VP7 epitopes using advanced computational techniques.

Although RV VP1 encoding the RNA-dependent RNA polymerase (RdRp) domain has unique structural features, it functions like other viral RdRps (Tohmé *et al*., 2021). The RdRp protein which is highly conserved among different RNA viruses is important in viral replication and transcription (Elfiky, 2020). Thus, targeting RdRp offers a promising antiviral strategy for RV and other RNA viruses. Thus, this section explores the antiviral activity of the pooled metabolites from selected medicinal plants against RVA RdRp using molecular modelling and density functional theory methods.

The cell entry procedure of RV is initiated by interactions involving VP7 and VP4 (Amimo *et al*., 2021). The spike-like VP4 protein on the viral surface enhances entry by binding to the host's receptors (Shaikh *et al*., 2022). Trypsin-induced activation of VP4 cleaves the protein into two domains, VP5* and VP8* improving virus infectivity and cell entry (Omatola and Olaniran, 2022). Each domain executes distinct functions during this process (Amimo *et al*.,

2021). VP5* possesses membrane permeabilizing abilities (Kumar *et al*., 2020), because of its hydrophobic structural region enabling viral entry into cells (Jiang *et al*., 2023). Conversely, VP8* has a carbohydrate-recognition domain crucial for viral attachment and infection (Li *et al*., 2021). As a result, VP5* and VP8* represent promising anti-RVA therapeutic targets due to their significant functions in the viral pathogenesis. Consequently, this section of the study examines the metabolites of the selected medicinal plants to identify promising antiviral leads with broad spectrum activity against VP5* and VP8* using advanced computational techniques. Importantly, the lead compounds identified in this study via these computational studies provide a logical foundation for further conjugation with metallic nanoparticles, directly influencing the phyto-nanomaterial design and antiviral assessments discussed in Chapter Five.

This chapter of the thesis is divided into four parts with each section presented as an experimental article: (1) metabolites profiling and cheminformatics bioprospection of selected medicinal plants against the main protease and RNA-dependent RNA polymerase of SARS-CoV-2, (2) computational bioprospection of selected plant secondary metabolites against VP7 (capsid protein) of rotavirus A, (3) bioprospection for antiviral compounds from selected medicinal plants against RNA polymerase of rotavirus A using molecular modelling and density functional theory and (4) Cheminformatics bioprospection of selected medicinal plants metabolites against trypsin cleaved VP4 (spike protein) of RVA.

4.2 Metabolites profiling and cheminformatics bioprospection of selected medicinal plants against the main protease and RNA-dependent RNA polymerase of SARS-CoV-2

This article has been published in Journal of Biomolecular Structure and Dynamics and presented accordingly

JOURNAL OF BIOMOLECULAR STRUCTURE AND DYNAMICS
https://doi.org/10.1080/07391102.2023.2236718

Taylor & Francis
Taylor & Francis Group

Check for updates

Metabolites profiling and cheminformatics bioprospection of selected medicinal plants against the main protease and RNA-dependent RNA polymerase of SARS-CoV-2

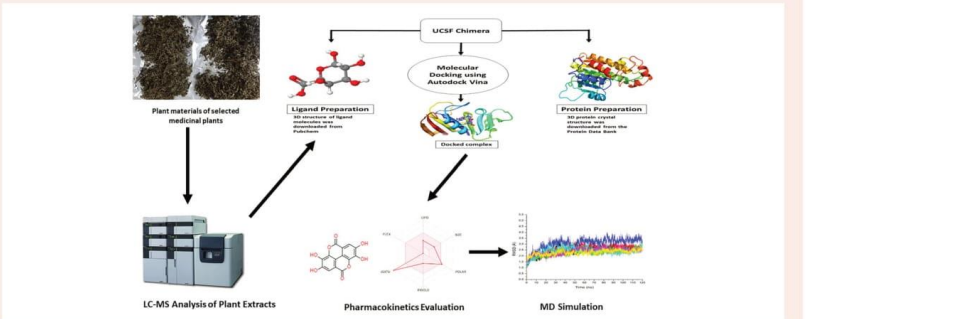
Adedayo Ayodeji Lanrewaju[a], Abimbola Motunrayo Enitan-Folami[a], Martin M. Nyaga[b], Saheed Sabiu[a] and Feroz Mahomed Swalaha[a]

[a]Department of Biotechnology and Food Science, Faculty of Applied Science, Durban University of Technology, Durban, South Africa; [b]Next Generation Sequencing Unit and Division of Virology, Faculty of Health Sciences, University of the Free State, Bloemfontein, South Africa

Communicated by Ramaswamy H. Sarma

ABSTRACT

Despite the existence of some vaccines, SARS-CoV-2 (S-2) infections persist for various reasons relating to vaccine reluctance, rapid mutation rate, and an absence of specific treatments targeted to the infection. Due to their availability, low cost and low toxicity, research into potentially repurposing phytometabolites as therapeutic alternatives has gained attention. Therefore, this study explored the antiviral potential of metabolites of some medicinal plants [*Spondias mombin*, *Macaranga barteri* and *Dicerocaryum eriocarpum* (Sesame plant)] identified using liquid chromatography-mass spectrometry (LCMS) as possible inhibitory agents against the S-2 main protease (S-2 MP) and RNA-dependent RNA polymerase (RP) using computational approaches. Molecular docking was used to identify the compounds with the best affinities for the selected therapeutics targets. Afterwards, compounds with poor physicochemical characteristics, pharmacokinetics, and drug-likeness were screened out. The top-ranked compounds were further subjected to a 120-ns molecular dynamics (MD) simulation. Only quercetin 3-O-rhamnoside (−48.77 kcal/mol) had higher binding free energy than the reference standard (zafirlukast) (−44.99 kcal/mol) against S-2 MP. Conversely, all the top-ranked compounds (ellagic acid hexoside, spiraeoside, apigenin-4′-glucoside and chrysoeriol 7-glucuronide) except gnetin L (−24.24 kcal/mol) had higher binding free energy (−55.19 kcal/mol, −52.75 kcal/mol, −47.22 kcal/mol and −43.35 kcal/mol) respectively, against S-2 RP relative to the reference standard (−34.79 kcal/mol). The MD simulations study further revealed that the investigated inhibitors are thermodynamically stable and form structurally compatible complexes that impede the regular operation of the respective S-2 therapeutic targets. Although, these S-2 therapeutic candidates are promising, further *in vitro* and *in vivo* evaluation is required and highly recommended.



ARTICLE HISTORY
Received 16 May 2023
Accepted 8 July 2023

KEYWORDS
Main protease; RNA-dependent RNA polymerase; phytochemicals; ADMET study; molecular dynamics simulation

1. Introduction

A novel coronavirus known as SARS-CoV-2 (S-2), responsible for coronavirus disease (COVID-19), a respiratory disease, was first reported in Wuhan, Hubei province in China in late 2019 (Wang et al., 2020; Lanrewaju et al., 2022). After that, the World Health Organization (WHO) designated COVID-19 as a pandemic in March 2020, and the illness has caused an

CONTACT Saheed Sabiu sabius@dut.ac.za
Supplemental data for this article can be accessed online at https://doi.org/10.1080/07391102.2023.2236718.
© 2023 Informa UK Limited, trading as Taylor & Francis Group

estimated 6.9 million fatalities as of June 2023 (World Health Organization, 2023). The WHO has authorized the use of different vaccines; however, none have a record of 100% effectiveness yet (Vardhan & Sahoo, 2022). The Food and Drug Administration (FDA)-approved drugs for treating COVID-19, including remdesivir, olumiant, bebtelovimab, lagevrio, molnupiravir, and paxlovid (nirmatrelvir and ritonavir), all come with restrictions on how they may be used to reduce the risk of adverse reactions (Islam et al., 2022). Thus, there is a critical need to develop specialized drugs for COVID-19 due to the devastating outcomes of the disease (Wrapp et al., 2020). In this regard, identifying potent compounds with the potential to inactivate important therapeutic targets in the virus such as the main protease (MP) and RNA-dependent RNA polymerase (RP) that are important for the organism's survival will be a viable approach.

The S-2 genome has 29,700 nucleotides, and the replicase gene has 21,000 nucleotides; this makes it significantly larger than the genome of a typical picornavirus (Abdallah et al., 2021). Two polyproteins, pp1ab (790 kDa) and pp1a (486 kDa) encoded by the replicase, overlap and stimulate all steps in viral transcription and replication (Thiel et al., 2001). The 33.8 kDa MP catalyzes a comprehensive proteolytic process that releases functional polypeptides from each polyprotein. Due to its central role in viral replication (Eltayb et al., 2023), MP is a promising therapeutic target for many CoV infections (Yang et al., 2003). Furthermore, two major non-structural polyproteins and the viral RP are encoded by two-third of the RNA genome of S-2. Four structural proteins (spike, envelope, membrane, and nucleocapsid) and additional auxiliary proteins are encoded by the remaining one-third of the genome (Luk et al., 2019). The RP protein is crucial in viral genome replication and transcription and is highly conserved across various RNA viruses. Because of its essential role in replicating RNA viruses like SARS-CoV-2, the RP has been the spotlight of antiviral drug development for several viruses, including hepatitis C, Zika, and the coronaviruses (Elfiky, 2020b; Elfiky et al., 2013; Elfiky & Ismail, 2019; Elfiky & Ismail, 2018). It has been observed that the active site of RP is significantly conserved amongst various coronaviruses (Elfiky, 2020a; Mir et al., 2022). Thus, S-2 and other coronaviruses share RP as a primary therapeutic target (Elfiky, 2020b, 2021).

Unfortunately, any drug's success rate during development (from phase I to drug approvals) is low, at around 6.2% (Vamathevan et al., 2019; Wong et al., 2019) and typically spans between 12 and 15 years of development (Delijewski & Haneczok, 2021; Vernon et al., 2010). As a result of the potential to drastically cut both development time and costs, drug repurposing or repositioning has emerged as a promising strategy. Interestingly, research indicating conventional medicine's effectiveness in managing COVID-19 (Ahmad et al., 2020) has made room for alternative treatments. For instance, phytochemicals are effective against viruses, making them a viable alternative treatment option (Ahmad et al., 2020; Rasool et al., 2021). Owing to their low cost, high efficiency, low risk of side effects, high cultural acceptability, and easy availability, numerous phytochemicals found in natural products are being researched as probable drug candidates against COVID-19 (Falang et al., 2020; Huang et al., 2020; Khaerunnisa et al., 2020; Osuntokun, 2020).

African medicinal plants and their metabolites have found therapeutic applications against viral diseases (Beressa et al., 2021). For instance, metabolites from *Lindera aggregata*, *Artemisia annua*, *Lycoris radiata*, and *Pyrrosia lingua* have potentiated significant therapeutic effect against SARS-associated coronavirus (Li et al., 2005). Specifically, the antiviral activity of *S. mombin* (Corthout et al., 1991; Siqueira et al., 2020) and *M. barteri* (Ogbole et al., 2018; Segun et al., 2021) against different viruses has been documented. Furthermore, *Dicerocaryum eriocarpum* (Sesame plant) is a multipurpose plant with various ethnomedicinal benefits such as wound treatment and retained placenta, antibacterial and anti-inflammatory ability (Luseba et al., 2007), ethnoveterinary benefits (Van der Merwe et al., 2001). However, there is dearth of information on the antiviral activity of *S. mombin*, *M. barteri* and *D. eriocarpum* against S-2 to date. Hence, this current study employed molecular docking approach to explore the antiviral potential of metabolites from the selected medicinal plants; *S. mombin*, *M. barteri* and *D. eriocarpum* as inhibitors of S-2 MP and RP. However, limitations associated with the approach include the generation of false-positive binding configuration as the most energy-minimized pose, the inaccurate prediction of energy interaction between two molecules and inability to assess the binding pose stability of the generated complexes. Therefore, in this study, in addition to validating the docking protocol, the thermodynamic binding free energy of the complex was evaluated using molecular mechanics/GB surface area approach while the stability, flexibility, and compactness of the protein connected with the putative inhibitory activity of the plants' metabolites were studied using molecular dynamics simulations. To reduce the risk of rejection during the pre- and clinical phases of drug development, *in silico* assessment of the ligand's pharmacological friendliness, bioavailability, and relative toxicity was conducted. The results of this study have the potential to facilitate the rapid and cost-effective development of anti-S-2 therapeutics.

2. Materials and methods

2.1. Plant collection, processing, and extraction

Healthy and young leaves of *S. mombin* and *M. barteri* were collected at Ibadan, Oyo State and Ago-Iwoye, Ogun State, Nigeria respectively. They were identified at Forest Herbarium Unit, Forestry Research Institute of Nigeria, Ibadan, Nigeria. In addition, fresh leaves, seeds, and stems of *Dicerocaryum eriocarpum* were collected from Siloam village in Limpopo Province and were identified at the Botany Department, University of Venda, South Africa. Plant materials were washed with water to get rid of any dirt, soil, or other debris that may have been accumulated from the soil or the environment. The materials were pulverized into a powder after being allowed to dry for two weeks in the shade. To prepare the extract, 2 g of each plant material was accurately weighed into a screw-capped 50 ml centrifuge tube. All the plant samples were extracted with 15 ml water, 100% methanol and 90% ethanol (Magangana et al., 2018). After vortexing for a minute, the samples were sonicated for

10 min at 4 °C with 35 kHz frequency. Then, 2 ml of each plant material was withdrawn and centrifuged at 14,000 rpm for 5 min. The clear supernatant was transferred into 1.5 ml glass vials for LCMS analysis.

2.2. Liquid chromatography-mass spectrometry (LCMS) analysis

A Waters Synapt G2 Quadrupole time-of-flight (QTOF) mass spectrometer (MS) connected to a Waters Acquity ultra-performance liquid chromatograph (UPLC) (Waters, Milford, MA, USA) was used for high-resolution UPLC-MS analysis. Data were collected by scanning in resolution mode and MSE mode between 150 and 1500 m/z. Two channels of MS data were captured in MSE mode, the first at a low collision energy (4 V), and the second at a collision energy ramp (40–100 V), which also allowed for the acquisition of fragmentation data. Waters HSS T3, 2.1 × 100 mm, 1.7 µm column was used for the separation. The injection volume used was 2 µl, and the mobile phase was composed of 0.1% formic acid (solvent A) and 0.1% formic acid-containing acetonitrile (solvent B). The sample was exposed to 40% B for 50 s, followed by a 1.5 min wash at 100% B and a 4 min re-equilibration to initial conditions. The temperature of the column was maintained at 55 °C, and the flow rate was 0.3 ml/min. The compounds were measured relative to a catechin calibration curve created by injecting different catechin standards ranging from 0.5 to 100 mg/L. Data were processed using MSDIAL and MSFINDER (Lai et al., 2018; Tsugawa et al., 2015).

2.3. Collection and preparation of S-2 MP and RP

The X-ray crystal structure of S-2 MP (7LOD) and RP (6M71) was retrieved from the Protein Data Bank (https://www.rcsb.orgs/, accessed on 11 September 2022) and were optimized for docking (Sabiu et al., 2021) using UCSF's Chimera program, version 1.14 (Pettersen et al., 2004).

2.4. Acquisition of ligands, preparation, and molecular docking

The 3D structures of the 77 ligands (metabolites obtained from the LCMS analysis) and the standards were retrieved from Pubchem (https://pubchem.ncbi.nlm.nih.gov/, accessed on 11 September 2022). While zafirlukast (Delijewski & Haneczok, 2021) and cefoperazone (Farhat & Khan, 2021) were used as reference standards for targeting S-2 MP, remdesivir (Beigel et al., 2020) and zafirlukast (Delijewski & Haneczok, 2021; Parab et al., 2021), were adopted as reference standards for targeting S-2 RP. The structures were prepared and optimized by adding Gasteiger charges through the Open Babel program plug-in on Python Prescription (PyRx) v 0.9.5. Then, using PyRx's AutoDock tool, the prepared protein and optimized ligands were docked (Aribisala & Sabiu, 2022). To guarantee docking at the protein's active site, amino acid residues whose grid box coordinates matched the predetermined x, y, and z positions were selected. The x-y-z coordinates, and amino acid residues at the active site of S-2 MP (11, −13, 18) and S-2 RP (124, 125, 110) were determined using Discovery Studio version 21.1.0 (BIOVIA, 2021) and thereafter validated from literature (Singh et al., 2021; Tumskiy & Tumskaia, 2021). The standard was used as a benchmark to identify the ligands with the highest binding affinity at the protein's active sites.

2.5. Pharmacokinetics properties prediction of the compounds with best docking score

In this study, the SwissADME web (http://swissadme.ch/index.php, accessed on 15 December 2022) was employed to predict physicochemical characteristics, pharmacokinetics, and drug-likeness of the ligands with the highest binding affinity (Abdalla et al., 2021). In addition, the Protox II webserver (https://tox-new.charite.de/protox_II/, accessed on 15 December 2022) was used to make similar predictions about the toxicological properties. The findings of these studies were used in conjunction with the binding affinity of the best compounds to reduce the number of compounds to be investigated further. Afterwards, the PDB files containing the docked systems of the top six compounds with the lowest energy minimization (highest binding affinity) were retrieved and used for molecular dynamics (MD) simulation.

2.6. Verification of docking procedure

The docking poses were assessed by overlaying the ligand on the crystal structure of S-2 MP (7L0D) and RP (6M71). All the ligands were docked into the native protein to see how well the AutoDock program could mimic the ligand's orientation and position in the crystal structure. The best conformational clusters from this dock were ranked based on the root-mean-square deviation (RMSD) between their docked position and the ligand's experimentally determined position (Al-Khodairy et al., 2013).

2.7. Molecular dynamics (MD) simulation

The MD simulation was conducted as previously described (Sabiu et al., 2021). The AMBER 18 program was used, and the simulation was performed for 120 ns using the FF18SB version of the AMBER force field to characterize the operating systems. Likewise, the ANTECHAMBER was used to make the ligand atomic partial charges by employing general amber force field (GAFF) measurements and constrained electrostatic potential (RESP). The systems were neutralized with hydrogen atoms, Na^+, and Cl^- counter ions from the Leap module. Each system was suspended inside an orthorhombic box of TIP3P water molecules, with all atoms positioned such that they were within 8 Å of any box edge, and the amino acid residues were appropriately numbered. All simulated system's hydrogen atom bonds were limited using the SHAKE technique. Each simulation used a step-size of 2 fs, corresponding to the isobaric-isothermal ensemble (NPT) with randomised seeding, 300 K temperature, 1 bar constant pressure, and a Langevin thermostat with a collision frequency of 1.0 ps and a pressure-coupling constant of

2 ps. After that, the 120 ns MDS results were observed and labelled as post-dynamic data.

2.8. Post-MD simulation analysis

The post-dynamic evaluation was executed as described previously (Aribisala et al., 2021). The AMBER 18 package's PTRAJ module was used to combine the simulated coordinates and trajectories of the systems and for evaluation throughout the simulation. The CPPTRAJ module of the AMBER 18 package was adopted to evaluate the root-mean-square deviation (RMSD), root-mean-square fluctuation (RMSF), the radius of gyration (ROG), and solvent-accessible surface area (SASA) while Origin v 6.0 was used to create their plots. The binding free energy was also estimated using the molecular mechanics generalized born surface area (MMGBSA) method, which averaged 100,000 snapshots from a 120 ns MD simulation trajectory and plugged the values into the equation DGbind = Gcomplex - (Greceptor + Gligand). To visualize the complexes' interaction at 120 ns MD simulation, Discovery Studio Version 21.1.0 used an MDmDiscoveryScript to offer functions, characteristics, constants, and data structures.

3. Results and discussion

3.1. LCMS analysis

Antiviral medications are known to elicit side effects and has led to a growing interest in developing plant-based drugs due to their reduced toxicity and minimal adverse reactions. Hence, researchers are currently employing different techniques towards drug development from plant-based products (Ghildiyal et al., 2020). The modulatory activity of *S. mombin* (Corthout et al., 1991; Siqueira et al., 2020) and *M barteri* (Ogbole et al., 2018; Segun et al., 2021) against different viruses have been reported. In addition, for the first time we evaluated the antiviral activity of the *D. eriocarpum in silico* owing to its previously reported pharmacological activity (Van der Merwe et al., 2001; Luseba et al., 2007). Therefore, the selected medicinal palnts were profiled using LCMS to identify their metabolites.The results of untargeted LC-QTOF-MS/MS, and MS/MS analysis of the three investigated plants revealed a total of 77 secondary metabolites belonging to different chemical chararcterization groups (Table S1).

3.2. Molecular docking

Molecular docking technique is one of the most widely used techniques in computer-aided drug design (CADD) for finding new drug leads (Talevi, 2018). In this kind of structure-based computer-generated screening, compounds are ranked according to their interactions and orientations at a target-binding site, with a higher negative value signifying a higher attraction for the target (Ramírez & Caballero, 2016), which suggests a better fitness of the molecule into the target-binding site (Kehinde et al., 2022). The docking scores of the selected plants' metabolites against S-2 MP vary between −4.4 kcal/mol to −9.8 kcal/mol, with 2-isopropylmalic acid and mallotusinic acid having the least and highest docking scores, respectively. A total of nine compounds with docking scores higher than zafirlukast against S-2 MP were selected for further investigations (-8.4 kcal/mol) (Table 1, Supplementary Table S2).

Table 1. Binding energy scores of top compounds and reference standards against S-2 MP and S-2 RP.

Ligands	Binding affinity (kcal/mol)
S-2 MP	
Mallotusinic acid	−9.8
Geraniin	−9.7
Miconioside A	−9.1
Corilagin	−9.1
Abacopterin D	−8.9
2TA	−8.9
Quercitrin	−8.7
kaempferol 7-O-glucoside	−8.6
Quercetin 3-O-rhamnoside	−8.5
Zafirlukast [standard]	−8.4
Cefoperazone [standard]	−7.8
S-2 RP	
Pelargoniin A	−10.9
Capinerin B	−10.5
Geraniin	−10.2
Mallotusinic acid	−10.2
Chebulagic acid	−9.8
29 C	−9.4
2TA	−9.3
Spiraeoside	−9.0
Miconioside A	−8.6
Apigenin-4-glucoside	−8.5
Orobanchoside	−8.5
Tetramethylquercetin-3-rutinoside	−8.5
Plantamajoside	−8.4
Ellagic acid hexoside	−8.3
Acteoside	−8.3
Gnetin L	−8.3
Chrysoeriol 7-glucuronide	−8.3
Abacopterin D	−8.2
Tricin 7-glucuronide	−8.2
Isomartynoside	−8.2
Zafirlukast [standard]	−7.9
Remdesivir [standard]	−7.1

2TA: 2-[14,18,19-Trihydroxy-2,3,11,15-tetraoxo-6,22-bis[(3,4,5-trihydroxybenzoyl)oxy]-8-[(3,4,5 trihydroxybenzoyl)oxymethyl]-4,7,10,16-tetraoxatetracyclo[11.7.1.15,9.017,21]-docosa-1(20),17(21),18-trien-12-yl]acetic acid; 29 C: 29-(Carboxymethyl)-13,14,15,18,19,20,29,34,35-nonahydroxy-2,10,23,28-tetraoxo-5-(3,4,5-trihydroxybenzoyl)oxy-3,6,9,24,27,32-hexaoxaheptacyclo[28.6.1.04,25.07,26.011,16.017,22.033,37]-heptatriaconta-1(36),11,13,15,17,19,21,33(37),34-nonaene-31-carboxylic acid.

Top twenty compounds with higher docking scores (-10.9 kcal/mol to −8.2 kcal/mol) (Table 1) compared to the reference standard (zafirlukast (-7.9 kcal/mol)) targeted against S-2 RP were selected (Supplementary Table S2). The higher docking score of the compounds relative to the standard could suggest their prospective affinity for S-2 RP. Zafirlukast (-7.9 kcal/mol), was designated as the benchmark for thermodynamic binding free energy calculation and subsequent MD simulation analysis because it showed higher affinity towards S-2 RP relative to remdesivir (-7.1 kcal/mol). Time-dependent structural and conformational changes on the S-2 MP and RP upon binding the phytochemical compounds were conducted using MD simulations, a dependable and widely used computational technique.

3.3. Docking technique validation

Docking studies necessitate validation because the method often generates false-positive binding configurations as the

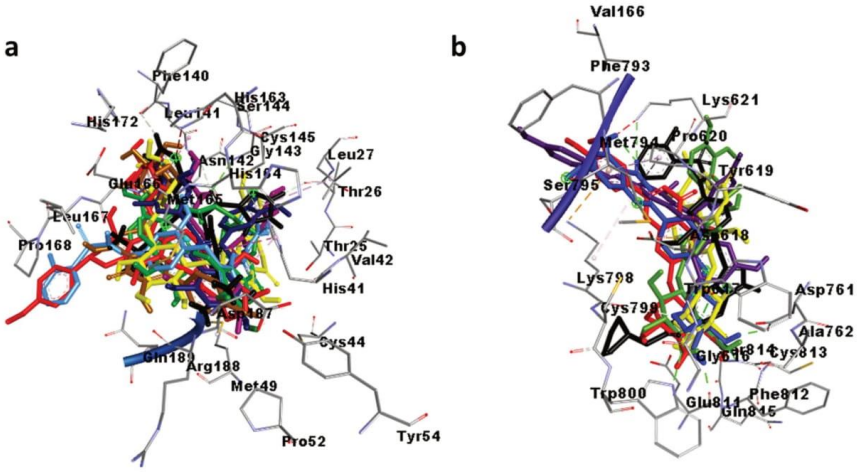


Figure 1. The superimposition and interactions of the top-ranked compounds at the active site of the crystal structure of (a) S-2 MP with (abacopterin D (red), corilagin (green), kaempferol 7-O-glucoside (brown), miconioside A (yellow), quercetin 3-O-rhamnoside (purple), Quercitrin (royal blue), and zafirlukast (light blue)) (b) S-2 RP with (apigenin-4′-glucoside (blue), chrysoeriol 7-glucuronide (red), ellagic acid hexoside (yellow), gnetin L (purple), spiraeoside (green), and zafirlukast (black).

most energy-minimized pose. Measuring the ligand's RMSD from its reference position in the complex after optimal superimposition is one of the most prevalent approaches for evaluating the precision of docking geometry. Figure 1 shows the overlaying and interactions of the top-rank compounds and reference standards at the active site of the respective S-2 targets. Each of the ligands' most energy-efficient conformations (highest binding free energy) was found to interact with more bonds, including hydrogen bonds with the residues in the S-2 MP binding site (Figure 1a) (His41, Asn142, Cys145, Glu166 and Gln189) (Lockbaum et al., 2021; Shode et al., 2022) and S-2 RP (Figure 1b) binding site (Asp618, Asp761, Ala762, Glu811 and Phe812) (Mir et al., 2022). The investigated compounds and reference standard; zafirlukast had an RMSD of less than 1 Å when superimposed on the crystal structure of S-2 MP and S-2 RP, suggesting that the compounds have similar binding orientation. This finding provides further evidence that the docking scores for the ligands and the standards are due to their contacts with the residues at the active site of the S-2 MP and S-2 RP, thereby verifying the docking methodology employed. The amino acid interactions of the top-ranked compounds and the reference standards against S-2 MP, including residues His41 and Cys145 (Tumskiy & Tumskaia, 2021), and S-2 RP, including residues Asp761 and Ala762 (Mir et al., 2022), are consistent with previous literatures.

3.4. Absorption, distribution, metabolism, excretion, and toxicity (ADMET) profile prediction

Absorption, distribution, metabolism, excretion, and toxicity (ADMET) properties perform essential functions in the search and development of novel medications as they are critical for the overall therapeutic efficacy of drugs. During the pre- and clinical phases of drug development, the risk of failure has been lessened by *in silico* analysis of a compound's ADMET characteristics, which offers details about the compound's *in vivo* pharmacological friendliness, bioavailability, and relative toxicity when administered orally.

According to the Lipinski's rule of five (Ro5), bioactive drugs must not exceed one violation of the following criteria: molecular weight (500 g/mol), hydrogen donor (5), hydrogen acceptor (10), and octanol co-efficient (5) (Lipinski et al., 2001). This rule allows pharmacologically active compounds to be evaluated for their potential as potential drugs. Unfortunately, most compounds with high docking scores against the S-2 MP in this study (Table 2A) failed the Ro5, except zafirlukast. However, zafirlukast and investigated compounds are all soluble in water and can readily move through the systemic circulation when administered (Remko et al., 2011). Conversely, twenty compounds with higher docking scores against the S-2 RP were selected for physicochemical and pharmacokinetic screening (Table 2B). Only apigenin-4′-glucoside, gnetin L and zafirlukast (reference standard) passed the Ro5 with 1, 0 and 1 violations respectively while spiraeoside, ellagic acid hexoside and chrysoeriol 7-glucuronide failed the Ro5 but with 2 violations. Unfortunately, all the other compounds failed the Ro5 with 3 violations. Thus, apigenin-4′-glucoside and gnetin L alongside spiraeoside, ellagic acid hexoside and chrysoeriol 7-glucuronide with 2 violations were selected because they will require lesser structural modifications to enhance their druggability compared to other compounds with 3 violations.

A drug's bioavailability score measures the quantity of a certain unmodified medication that reaches the systemic circulation and the degree or pace of absorption (Heaney, 2001). The bioavailability score of drugs administered intravenously is higher than that of oral drugs. It is an essential pharmacokinetic property to consider when determining the appropriate dosage for a drug. Interestingly, all the compounds targeted against

Table 2A. ADMET properties of all the high scoring compounds docked against S-2 MP.

Ligands	MW < 500 (g/mol)	HBA ≤ 10	HBD ≤ 5	Log P o/ w ≤ 5	WS	GI Abs	BBBP	Pgp	CYP1A2	CYP2C19	CYP2C9	CYP2D6	CYP3A4	LV (N)	BS	H	C	IM	M	CY	LD50 (mg/kg)	TC
Mallotusinic acid	1120.75	32	17	−1.48	S	Low	No	Yes	No	No	No	No	No	3	0.11	In	In	Ac	In	In	300	3
Geraniin	952.64	27	14	−1.70	S	Low	No	Yes	No	No	No	No	No	3	0.17	In	In	Ac	In	In	300	3
Miconioside A	608.59	14	7	−0.18	S	Low	No	Yes	No	No	No	No	No	3	0.17	In	In	Ac	In	Ac	2300	5
Corilagin	634.5	18	11	−0.55	S	Low	No	Yes	No	No	No	No	No	3	0.17	In	In	Ac	In	In	2260	5
Abacopterin D	638.6	15	8	−1.01	S	Low	No	Yes	No	No	No	No	No	3	0.17	In	In	Ac	In	Ac	3000	5
2TA	984.7	28	13	−0.77	S	Low	No	Yes	No	No	No	No	No	3	0.11	In	In	Ac	In	Ac	300	3
Quercitrin	448.4	11	7	0.16	S	Low	No	No	No	No	No	No	No	2	0.17	In	Ac	Ac	In	In	5000	5
kaempferol 7-O-glucoside	448.4	11	7	−0.04	S	Low	No	No	No	No	No	No	No	2	0.17	In	In	In	In	In	5000	5
Quercetin 3-O-rhamnoside	448.4	11	7	0.16	S	Low	No	No	No	No	No	No	No	2	0.17	In	A	Ac	In	In	5000	5
Zafirlukast	575.7	6	2	4.65	S	Low	No	No	No	Yes	Yes	Yes	Yes	1	0.55	Ac	In	Ac	In	In	300	3

the S-2 MP could be developed as oral drugs due to their low bioavailability score of 0.17 (Table 2A). In the same vein, all the compounds targeted against the S-2 RP equally had bioavailability scores of 0.17 except apigenin-4′-glucoside, gnetin L and zafirlukast with bioavailability scores of 0.55. A higher bioavailability score indicates a higher drug concentration in the body's circulatory system to reach its maximum therapeutic dosage (Shode et al., 2022).

Members of the isozyme's family; cytochrome P450, are responsible for the biotransformation of several drugs. Drug toxicity, diminished pharmacological impact, and adverse drug effects can all result from drug interactions and metabolism. A significant determinant of such reactions is the use of the cytochrome P450 system (Ogu & Maxa, 2000). Except for zafirlukast, none of the compounds targeted at S-2 MP inhibited the liver's CYP isoenzymes (CYP1A2, CYP2C19, CYP2C9, CYP2D6, and CYP3A4) involved in phase 1 drug detoxification (Table 2A) signifying their lack of capacity to initiate drug-drug interactions when used alongside other drugs. All the compounds were predicted to be immunotoxic except kaempferol 7-O-glucoside. In contrast, miconioside A was predicted to be active for cytotoxicity, while quercetin 3-O-rhamnoside and quercitrin were predicted to be active for carcinogenicity and zafirlukast for hepatotoxicity. All the compounds targeted at the S-2 RP were active for immunotoxicity except apigenin-4′-glucoside. In addition, only apigenin-4′-glucoside and ellagic acid hexoside were active for mutagenicity while miconioside A, tetramethylquercetin-3-rutinoside and abacopterin D were active for cytotoxicity. Only zafirlukast is active for hepatotoxicity.

Of all the compounds targeted at S-2 MP, mallotusinic acid, geraniin and 2TA belong to drug toxicity class three, just like zafirlukast (300 mg/kg), which is unsuitable for drug development. Therefore, the three compounds were excluded from further analysis. All the other compounds investigated in this study belong to the toxicity class five with LD_{50} values between 2260 and 5000 mg/kg making them suitable for use as medications (Table 2B). Interestingly, all the compounds targeted at S-2 RP belong to toxicity class 4–6 which is ideal for drug development (Verma et al., 2022), except pelargoniin A, geraniin, mallotusinic acid and 2TA, which belong to drug toxicity 2, 3, 3 and 3, respectively. Therefore, compounds selected for further analysis are apigenin-4′-glucoside and gnetin L which passed the Lipinski's Ro5, while spiraeoside, ellagic acid hexoside and chrysoeriol 7- glucuronide with two violations were also selected ahead of the rest of compounds with three violations. Remarkably, all five compounds belong to toxicity classes 5, 4, 5, 5, and 5, respectively, making them suitable for drug use. Summarily, fewer structural alterations can be made on the selected compounds for both targets to enhance their druggability compared to the others not selected.

3.5. Thermodynamic binding free energy of top-ranked compounds

The cutting-edge computational method of molecular mechanics generalized born surface area (MMGBSA) has been extensively investigated to study binding energy using a more refined

Table 28. ADMET properties of the high scoring compounds docked against 5-2.RP.

Ligands	MW < 500 (g/mol)	HBA ≤ 10	HBD ≤ 5	Log P o/ w ≤ 5	WS	GI Abs	BBBP	Pgp	CYP1A2	CYP2C19	CYP2C9	CYP2D6	CYP3A4	LV (N)	BS	H	C	IM	M	CY	LD50 (mg/kg)	TC
Pelargoniin A	926.65	26	14	−1.24	S	Low	No	Yes	No	No	No	No	No	3	0.17	In	In	Ac	In	In	30	2
Capinerin B	966.7	27	14	−1.16	S	Low	No	Yes	No	No	No	No	No	3	0.17	In	In	Ac	In	In	620	4
Geraniin	952.64	27	14	−1.70	S	Low	No	Yes	No	No	No	No	No	3	0.17	In	In	Ac	In	In	300	3
Mallotusinic acid	1120.75	32	17	−1.48	S	Low	No	Yes	No	No	No	No	No	3	0.11	In	In	Ac	In	In	300	3
Chebulagic acid	954.66	27	13	−0.88	S	Low	No	Yes	No	No	No	No	No	3	0.11	In	In	Ac	In	In	420	4
29C	970.66	28	14	−1.18	S	Low	No	Yes	No	No	No	No	No	3	0.11	In	In	Ac	In	In	419	4
2TA	984.7	28	13	−0.77	S	Low	No	Yes	No	No	No	No	No	3	0.11	In	In	Ac	In	Ac	300	3
Spiraeoside	464.38	12	8	−0.19	S	Low	No	Yes	No	No	No	No	No	2	0.17	In	In	Ac	In	In	5000	5
Miconioside A	608.59	14	7	−0.18	S	Low	No	Yes	No	No	No	No	No	3	0.17	In	In	Ac	In	Ac	2300	5
Apigenin-4′-glucoside	432.38	10	6	0.48	S	Low	No	Yes	No	No	No	No	No	1	0.55	In	In	In	Ac	In	5000	5
Orobanchoside	640.6	16	10	−1.32	S	Low	No	No	No	No	No	No	No	3	0.17	In	In	Ac	In	In	5000	5
Tetramethylquercetin-3-rutinoside	666.6	16	6	0.14	S	Low	No	Yes	No	No	No	No	No	3	0.17	In	In	Ac	In	Ac	1000	4
Plantamajoside	640.6	16	10	−1.04	S	Low	No	No	No	No	No	No	No	3	0.17	In	In	Ac	In	In	5000	5
Ellagic acid hexoside	464.33	13	7	−0.63	S	Low	No	No	No	No	No	No	No	2	0.17	In	In	Ac	Ac	In	5000	5
Acteoside	624.59	15	9	−0.43	S	Low	No	Yes	No	No	No	No	No	3	0.17	In	In	Ac	In	In	5000	5
Gnetin L	484.5	7	5	4.13	S	Low	No	No	No	No	No	Yes	No	0	0.55	In	Ac	Ac	In	In	500	4
Chrysoeriol 7-glucuronide	476.4	12	6	0.45	S	Low	No	Yes	No	No	No	No	No	2	0.11	In	In	Ac	In	In	5000	5
Abacopterin D	638.6	15	8	−1.01	S	Low	No	Yes	No	No	No	No	No	3	0.17	In	In	Ac	In	Ac	3000	5
Tricin 7-glucuronide	506.41	13	6	0.30	S	Low	No	Yes	No	No	No	No	No	3	0.11	In	In	Ac	In	In	5000	5
Isomartynoside	652.64	15	7	0.06	S	Low	No	Yes	No	No	No	No	No	3	0.17	In	In	Ac	In	In	5000	5
Zafirlukast	575.7	6	2	4.65	S	Low	No	No	No	Yes	Yes	Yes	Yes	1	0.55	Ac	In	Ac	In	In	300	3

MW: Molecular weight; BBB permeant: Blood-brain barrier permeation; HB-D: Hydrogen bond donor; Log P o/w: Partition coefficient; HB-A: Hydrogen bond acceptor; CY: Cytotoxicity; Pgp: Permeability glycoprotein substrate; WS: Water solubility; CYP: Cytochrome; LV: Lipinski violation; BS: Bioavailability score; H: Hepatotoxicity; C: Carcinogenicity; IM: Immunotoxicity; GI Abs: Gastrointestinal absorption; M: Mutagenicity; LD: Lethal dose; TC: Toxicity class; S: Soluble; Ac: Active; In: Inactive; N: Number of violation; 2TA: 2-[14,18,19-Trihydroxy-2,3,11,15-tetraoxo-6,22-bis[(3,4,5-trihydroxybenzoyl)oxy]-8-[(3,4,5 trihydroxybenzoyl)oxymethyl]-4,7,10,16-tetraoxatetracyclo[11.7.1.15,9.017,21]docosa-1(20),17(21),18-trien-12-yl]acetic acid; 29C: 29-(Carboxymethyl)-13,14,15,18,19,20,29,34,35-nonahydroxy-2,10,23,28-tetraoxo-5-[(3,4,5-trihydroxybenzoyl)oxy-3,6,9,24,27,32-hexaoxaheptacyclo[28.6.1.04,25.07,26.011,16.017,22.033,37]heptatriaconta-1(36),11,13,15,17,19,21,33(37),34-nonaene-31-carboxylic acid.

Table 3A. MMGBSA-based binding free energy outline (Kcal/mol) of the top-ranked compounds against S-2 MP.

Ligands	ΔE_{vdW}	ΔE_{elec}	ΔG_{gas}	ΔG_{solv}	ΔG_{bind}
Abacopterin D	−31.82 ± 9.89	−40.24 ± 13.95	−72.06 ± 14.92	45.76 ± 11.01	−26.30 ± 7.64
Corilagin	−40.12 ± 5.45	−27.03 ± 11.38	−67.15 ± 13.33	38.73 ± 8.37	−28.42 ± 6.26
Kaempferol 7-O-glucoside	−39.97 ± 4.59	−27.68 ± 15.37	−67.64 ± 15.66	33.32 ± 11.14	−34.32 ± 5.74
Miconioside A	−55.26 ± 4.54	−28.76 ± 9.57	−84.02 ± 10.77	39.47 ± 7.24	−44.55 ± 5.59
Quercetin 3-O-rhamnoside	−46.81 ± 5.97	−50.38 ± 11.02	−97.19 ± 11.43	48.42 ± 5.75	−48.77 ± 7.89
Quercitrin	−46.31 ± 4.76	−34.26 ± 12.09	−80.56 ± 11.17	37.41 ± 5.99	−43.16 ± 6.63
Zafirlukast	−62.09 ± 5.56	−19.22 ± 6.99	−81.32 ± 9.36	36.32 ± 5.40	−44.99 ± 5.41

algorithm and solvation model. Post-scoring compounds utilizing MMGBSA have been shown to have a stronger connection to their reported binding affinity of docked complexes than docking (Greenidge et al., 2013; Tripathi et al., 2013). The thermodynamic binding free energy quantifies the energy difference between a complex and its unbound constituent; the greater the negative value, the greater the attraction of the ligand for the protein (Acharya et al., 2020). The top-ranked compounds in this study, apart from quercetin 3-O-rhamnoside, showed lower binding free energy against S-2 MP compared to zafirlukast (Table 3A). Abacopterin D, corilagin, kaempferol 7-O-glucoside, miconioside A and quercitrin had −26.30 kcal/mol, −28.42 kcal/mol, −34.32 kcal/mol, −44.55 kcal/mol, and −43.16 kcal/mol respectively which were lower than that of zafirlukast (Table 3A). In other words, out of all the test compounds, only quercetin 3-O-rhamnoside (−48.77 kcal/mol) had a better affinity towards the S-2 MP compared to zafirlukast (−44.99 kcal/mol) (Table 3A). This observation may suggest that quercetin 3-O-rhamnoside had a better potential to inhibit S-2 MP than other test compounds. There is a need for further investigation of the compounds examined as potential inhibitors due to their binding affinity. The finding in this study regarding quercetin 3-O-rhamnoside is consistent with a previous study (Rakshit et al., 2022), where it was reported to have high binding affinity and form a stable complex with S-2 MP.

On the other hand, all the test compounds had higher binding free energy for the binding site of S-2 RP than zafirlukast (-34.79 kcal/mol) except gnetin L (-24.24 kcal/mol). Ellagic acid hexoside, spiraeoside, apigenin-4-glucoside and chrysoeriol 7-glucuronide when complexed with S-2 RP had −55.19 kcal/mol, −52.75 kcal/mol, −47.22 kcal/mol, and −43.35 kcal/mol respectively which were higher than −34.79 kcal/mol observed in zafirlukast + S-2 RP (Table 3B). This finding could mean that ellagic acid hexoside, spiraeoside, apigenin-4-glucoside and chrysoeriol 7-glucuronide have greater potential as inhibitors of S-2 RP, with ellagic acid hexoside being the most promising among the highest-scoring compounds. Furthermore, this observation partly agrees with the molecular docking study results and shows that these compounds could be superior to zafirlukast for the management/treatment of COVID-19. Consistent with previous studies, some of these compounds with high binding affinity relative to the standard have been reported as inhibitors S-2 therapeutic targets. For instance, ellagic acid hexoside has been earlier documented to have inhibitory activity against SARS-CoV-2 Mpro in a molecular docking study among phenolic compounds isolated from *Phyllanthus tenellus* (Supian et al., 2022). Also, spiraeoside has been previously reported to have good binding energy against SARS-CoV-2 spike protein in a molecular docking study (Manokaran et al., 2021). In addition, apigenin analogues have been reported to have high binding affinity against SARS-CoV-2 main protease (Farhat et al., 2022). Remarkably, this study went further to complement the results of those previous docking studies to measure the stability, flexibility, compactness and the negative free binding energy between the bound ligand and protein through MD simulation.

3.6. Thermodynamic stability, firmness, and flexibility of the top-ranked compounds

The structural and conformational changes caused by an inhibitor's binding to a biological target are thought to impact the target's biological activity (Sindhu & Srinivasan, 2015). The potential inhibitory action of the compounds may be influenced by any structural alterations found on the S-2 targets evaluated in this study. Therefore, through the 120 ns MD simulation executed, the RMSD, RMSF, ROG, SASA, angles, distances and numbers of hydrogen bonds were analyzed to determine the thermodynamic stability, flexibility and compactness of the highest-scoring compounds complexed individually with S-2 MP and RP. The RMSD assesses the alterations in the protein-ligand structure and offers insight on the steadiness of the complex (Martínez, 2015). To highlight how much the complex's structure deviates from its apo structure over time, the RMSD trajectory of the complex was assessed; a lower RMSD value implies better stability (Nasution et al., 2018). The ligand-protein complexes of the two targets (S-2 MP and S-2 RP) evaluated in this study and their apo-proteins were brought into equilibrium within the first 10 ns of the simulation with relatively more swaying in the ligand-S-2 MP complexes relative to the ligand-S-2 RP complexes. As a consequence, in the ligand-S-2 MP complexes, all the compounds except miconioside A (3.48 Å) had lesser average RMSD values than zafirlukast (2.49 Å) (Table 4A) owing to its higher fluctuation pattern (Figure 2a). After 10 ns of simulation, when the atoms in each system had equilibrated, the ligand-protein complexes and apo-proteins of the two targets showed significant swaying, with the swaying being more pronounced in the ligand-S-2 MP complexes than in the ligand complexes with S-2 RP (Figure 2a, b). This significant swaying in ligand-S-2 MP complexes could be responsible for a wider variation in the mean RMSD values reported for ligand-S-2 MP complexes relative to ligand-S-2 RP complexes (Table 4A, B). Remarkably, all the compounds investigated had average RMSD values less than 3.0 Å apart from one compound each with RMSD value above 3.0 Å for both S-2 MP and S-2 RP (Table 4A, B). Generally, this suggests

Table 3B. MMGBSA-based binding free energy outline (Kcal/mol) of the top-ranked compounds against S-2 RP.

Ligands	ΔE_{vdW}	ΔE_{elec}	ΔG_{gas}	ΔG_{solv}	ΔG_{bind}
Apigenin-4-glucoside	−37.59 ± 4.65	−75.11 ± 8.14	−112.70 ± 8.19	65.48 ± 5.88	−47.22 ± 4.60
Chrysoeriol 7-glucuronide	−33.53 ± 5.15	−104.40 ± 20.73	−137.94 ± 20.29	94.58 ± 15.27	−43.35 ± 7.30
Ellagic acid hexoside	−47.68 ± 5.15	−78.45 ± 11.19	−126.13 ± 9.36	70.94 ± 6.74	−55.19 ± 5.11
Gnetin L	−30.49 ± 4.93	−46.87 ± 11.60	−77.38 ± 12.44	53.15 ± 9.37	−24.24 ± 5.95
Spiraeoside	−22.73 ± 6.33	−208.90 ± 36.33	−231.65 ± 34.79	178.90 ± 27.81	−52.75 ± 9.44
Zafirlukast	−45.01 ± 7.04	−42.52 ± 12.79	−87.53 ± 14.69	52.74 ± 9.59	−34.79 ± 10.33

ΔE_{vdW} = van der Waals energy; ΔE_{elec} = electrostatic energy; ΔE_{gas} = gas phase free energy; ΔG_{sol} = solvation free energy; ΔG_{bind} = total binding free energy.

Table 4A. Mean RMSD, RMSF, ROG, SASA and hydrogen bonds of apo-MP protein, top-ranked compounds, and standard against S-2 MP.

Ligands	Mean RMSD (Å)	Mean RMSF (Å)	Mean ROG (Å)	Mean SASA (Å)	Mean number of H-bonds	Mean distance (Å) of H-bonds	Mean angle (°) of H-bonds
Abacopterin D	2.47 ± 0.50	1.64 ± 0.90	21.91 ± 0.19	14148.96 ± 350.22	136.95 ± 8.33	2.86 ± 0.06	151.75 ± 7.71
Corilagin	1.88 ± 0.29	1.31 ± 0.61	21.89 ± 0.11	13874.65 ± 267.03	139.06 ± 7.57	2.86 ± 0.06	151.68 ± 7.74
Kaempferol 7-O-glucoside	2.09 ± 0.22	1.28 ± 0.56	22.09 ± 0.16	13840.95 ± 326.75	137.59 ± 7.90	2.86 ± 0.06	151.60 ± 7.65
Miconioside A	3.48 ± 0.62	1.46 ± 0.65	21.99 ± 0.11	14180.20 ± 289.08	140.27 ± 7.70	2.86 ± 0.06	151.80 ± 7.71
Quercetin 3-O-rhamnoside	1.84 ± 0.28	1.41 ± 0.62	22.12 ± 0.15	14165.23 ± 259.58	137.15 ± 7.63	2.86 ± 0.06	151.79 ± 7.74
Quercitrin	2.02 ± 0.33	1.40 ± 0.55	22.25 ± 0.13	13971.67 ± 259.99	141.11 ± 7.99	2.86 ± 0.06	151.74 ± 7.56
Zafirlukast	2.49 ± 0.47	1.43 ± 0.64	21.97 ± 0.12	14154.08 ± 300.76	137.14 ± 7.91	2.86 ± 0.06	151.74 ± 7.50
S-2 MP	1.97 ± 0.32	1.45 ± 0.71	22.17 ± 0.16	14510.42 ± 327.83	136.11 ± 8.00	2.86 ± 0.06	151.45 ± 7.61

the compounds' structural stability and compatibility with the respective target (Ramírez & Caballero, 2016).

In the ligand-S-2 RP complexes, ellagic acid hexoside (3.05 Å), spiraeoside (2.60 Å) and chrysoeriol 7-glucuronide (2.43 Å) had mean RMSD values higher than zafirlukast (2.41 Å). Furthermore, there was an increase in the mean RMSD value due to ligand binding compared to the apo-S-2 MP (1.97 Å) except for corilagin (1.88 Å) and quercetin 3-O-rhamnoside (1.84 Å). This similar trend was observed in the ligand-S-2 RP complexes as well in which there was an increase in the average RMSD values owing to ligand binding except for gnetin L (2.30 Å) with similar RMSD value as the apo-S-2 RP (2.30 Å) (Table 4B). This observation is consistent with an earlier investigation in which an increase in the mean RMSD value was reported owing to the binding of verbascoside to the S-2 spike protein (Acharya et al., 2020). The highest free binding energy towards S-2 MP was observed with quercetin 3-O-rhamnoside, which had the lowest RMSD value. This further corroborates its advantage as a potential S-2 MP inhibitor. On the contrary, ellagic acid hexoside with the highest binding free energy has the highest mean RMSD value (3.05 Å) towards S-2 RP. The deviation observed from the satisfactory 3.0 Å in the binding of ellagic acid hexoside is negligible hence it confirms the stability of the protein and simultaneously suggests its possible prospects as a potential inhibitor of S-2 RP.

The thermodynamic flexibility of amino acid residues at the binding site of both investigated S-2 targets upon the binding of the ligands was elucidated by assessing their RMSF value (Balogun et al., 2022). Generally, the more stable the intra- and intermolecular bonds are, the lesser the RMSF value (Al-Khodairy et al., 2013). The stability of a protein structure is crucial for the protein to carry out its function (Boadu et al., 2022). The less fluctuation there is, particularly at the active site where ligand binding and catalysis occur, the stronger the bonds and the more attraction a ligand has for the protein (Aribisala & Sabiu, 2022). This fluctuation can be related to a protein's capacity to generate intra- and intermolecular stable bonds. This study observed high fluctuations in the amino acid residues of both investigated S-2 proteins throughout the simulation period. In S-2 MP, high fluctuation was more prominent in residues between 50 and 65, 185 and 200, 270 and 280 in which major swaying was observed. At the same time, there was a lesser fluctuation between residues 80 and 115, 225 and 275 with minimal swaying (Figure 3a). Out of the residues in the key binding domain of S-2 MP (41, 142, 145, 161, 166 and 189) (Gambacorta et al., 2022), only 189 is located in the zone of main swaying, while the rest are situated in the area of negligible swaying (Figure 3a). These findings could be responsible for the lesser average RMSF values observed at the key binding domain of S-2 MP relative to the protein in all the resulting complexes (Tables 4A, 5A). The reduced number of residues in the key binding site of S-2 MP found in the region of major fluctuations relative to the entire protein in all systems may account for the significant involvement of this zone in intra- and intermolecular binding and, consequently, a plus in the protein's inhibition. In the S-2 MP systems, the maximum average RMSF value in the bound protein (1.45 Å) and at the binding site (1.67 Å) was observed in the unbound S-2 MP (Tables 4A, 5A) for both cases indicating that the binding of the ligands at the active site of S-2 MP resulted in good intra- and intramolecular binding in the S-2 MP systems (1.45 Å). However, abacopterin D (1.64 Å) and miconioside A (1.46 Å), have higher average RMSF value upon binding to the whole protein compared to the apo-S-2 MP, which partly agrees with the RMSD results. The least mean RMSF value in the bound protein was observed in Kaempferol 7-O-glucoside (1.28 Å), suggesting that it forms stable bonds and is thus more effective as an inhibitor of S-2 MP than other investigated compounds. This deduction counters this study's thermodynamic binding free energy and RMSD results, in which quercetin 3-O-rhamnoside has the best binding free energy and least RMSD value against S-2 MP. Nevertheless, the average RMSF value observed in quercetin 3-O-rhamnoside both in the whole protein (1.41 Å)

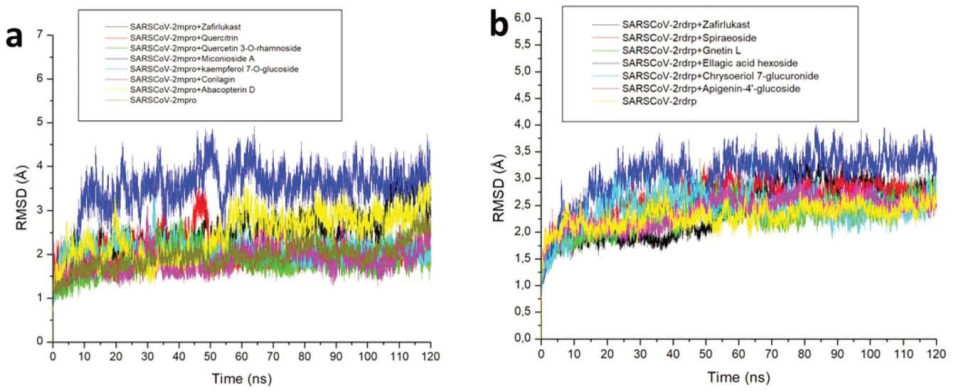


Figure 2. Comparative root mean square deviation (RMSD) plots of alpha-carbon, top-ranked compounds and reference standards against (a) S-2 MP and (b) S-2 RP after 120 ns MD simulation period.

Table 4B. Mean RMSD, RMSF, ROG, SASA and hydrogen bonds of apo-RP protein, top-ranked compounds, and standard against S-2 RP.

Ligands	Mean RMSD (Å)	Mean RMSF (Å)	Mean ROG (Å)	Mean SASA (Å)	Mean number of H-bonds	Mean distance (Å) of H-bonds	Mean angle (°) of H-bonds
Apigenin-4′-glucoside	2.39 ± 0.28	1.42 ± 0.75	30.04 ± 0.11	36873.86 ± 532.51	424.54 ± 14.01	2.85 ± 0.06	151.81 ± 7.55
Chrysoeriol 7-glucuronide	2.43 ± 0.33	1.47 ± 0.84	30.07 ± 0.14	36918.87 ± 734.62	426.69 ± 14.18	2.85 ± 0.06	152.23 ± 7.00
Ellagic acid hexoside	3.05 ± 0.48	1.48 ± 0.87	30.26 ± 0.15	36992.22 ± 573.85	427.94 ± 14.11	2.85 ± 0.06	151.96 ± 7.27
Gnetin L	2.30 ± 0.31	1.46 ± 0.73	30.06 ± 0.17	37047.43 ± 791.13	418.35 ± 15.50	2.85 ± 0.06	152.24 ± 7.00
Spiraeoside	2.60 ± 0.37	1.46 ± 0.78	29.99 ± 0.11	36524.18 ± 694.01	419.34 ± 15.24	2.85 ± 0.06	152.10 ± 7.11
Zafirlukast	2.41 ± 0.50	1.63 ± 0.84	29.94 ± 0.12	37215.45 ± 603.44	416.25 ± 15.58	2.85 ± 0.06	151.74 ± 7.56
S-2 RP	2.30 ± 0.21	1.39 ± 0.71	30.03 ± 0.10	37521.13 ± 509.48	420.04 ± 14.05	2.85 ± 0.06	151.73 ± 7.56

Table 5A. Average RMSF (Å) of S-2 MP key binding site residues upon binding with top-ranked compounds and zafirlukast.

KBS residues of S-2 MP	Abacopterin D	Corilagin	Kaempferol 7-O-glucoside	Miconioside A	Quercetin 3-O-rhamnoside	Quercitrin	Zafirlukast	S-2 MP
41	0.91	0.70	0.75	0.77	0.60	0.82	0.85	1.29
142	2.38	1.48	1.51	2.28	1.71	1.59	1.82	2.40
145	0.94	0.82	0.63	0.94	0.76	0.73	0.93	0.79
161	0.78	0.67	0.64	0.85	0.71	0.69	0.63	0.66
166	1.68	0.96	1.12	1.40	1.26	1.58	1.48	1.74
189	2.42	1.66	1.65	1.60	3.01	2.39	1.83	3.15
Total RMSF	1.52	1.05	1.05	1.31	1.34	1.30	1.26	1.67

Table 5B. Average RMSF (Å) of S-2 RP key binding site residues upon binding with top-ranked compounds and zafirlukast.

KBS residues of S-2 RP	Apigenin-4′-glucoside	Chrysoeriol 7-glucuronide	Ellagic acid hexoside	Gnetin L	Spiraeoside	Zafirlukast	S-2 RP
761	1.12	1.29	1.23	1.18	1.26	1.18	1.25
762	1.25	1.32	1.25	1.22	1.36	1.25	1.41
Total RMSF	1.19	1.31	1.24	1.20	1.31	1.21	1.33

and at the binding site (1.34 Å) is still within the satisfactory boundary of 3.0 Å which suggests its potential as a good inhibitor of S-2 RP.

In S-2 RP, high fluctuation was more pronounced in residues between 20 and 130, 180 and 230, 275 and 350, 780 and 860 with the observation of major swaying, while lesser fluctuation between residues 140 and 170, 410 and 770 with minimal swaying was observed (Figure 3b).

Both key residues at the binding site of S-2 RP, (761 and 762) (Ahmad et al., 2020; Elfiky, 2021) were situated in the zone of minimal swaying (Figure 3b). Similarly, this observation could indicate that they were actively involved in the intra- and intermolecular binding within the protein and consequently responsible for its structural stability. As a result, RMSF values were higher for the whole protein across all bound systems than at the binding site of S-2 RP (Tables 4B, 5B). The least mean RMSF value in the bound protein (1.39 Å) was noted in the apo-S-2 RP, illustrating that binding typically results in enhanced protein flexibility. Apigenin-4′-glucoside (1.42 Å) exhibited the least mean RMSF value in the bound systems and at the binding site of S-2 RP (1.19 Å), indicating that it was able to decrease the flexibility of S-2 RP amino acid residues than the other bound systems. In general, the RMSF values in the bound protein and the binding

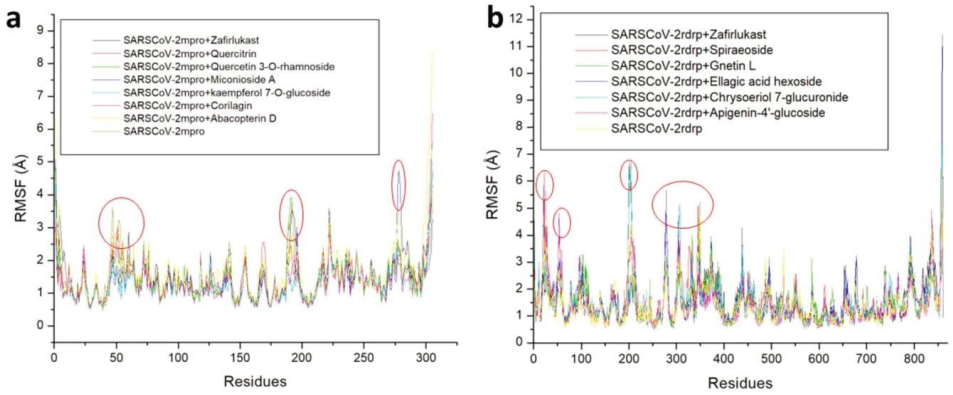


Figure 3. Comparative root mean Squares fluctuation (RMSF) plots of alpha-carbon, top-ranked compounds and reference standards against (a) S-2 MP and (b) S-2 RP after 120 ns MD simulation period.

site of both S-2 MP and S-2 RP are in the satisfactory boundary of 3 Å, which could indicate good intra- and intermolecular binding across all systems.

Another thermodynamic index, ROG, measures a complex's time-dependent compactness in an MD simulation, with smaller values indicating greater stability (Du et al., 2016). As a result, the ROG values of the simulated complexes were examined to see how easily the protein systems may be disrupted; a greater ROG value indicates a protein's mobility, while a lower value suggests the system's stability (Islam et al., 2020). According to the results of this investigation, the binding of the top-scoring compounds and zafirlukast to S-2 MP had minimal influence on its folding as there were fewer variations in compactness with this system (Figure 4a) throughout the 120 ns simulation period. Similarly, the respective average ROG values among all the systems equally support this observation with an overall variation of 0.1 Å as corilagin (21.89 Å) had the least average value (Table 4A). From the observation, it can be inferred that the top-ranked compounds are thermodynamically stable as they do not cause the S-2 MP to fold excessively and thus partly agrees with the RMSD values (Table 4A). In the same vein, because there were less differences in compactness within this system, the binding of the highest-scoring compounds and zafirlukast to S-2 RP had less effect on its folding (Figure 4b) during the simulation. In addition, there was an overall variation of 0.1 Å with zafirlukast (29.94 Å) having the least average value, similar to the findings in S-2 MP systems (Table 4B). It can also be deduced that the investigated compounds are stable thermodynamically as they partly agree with the RMSD values and do not make the S-2 RP to fold excessively. This is in harmony with the findings of Aribisala et al. (2022) in which an overall insignificant variation of 0.3 Å was reported in the binding of S-2 spike protein with investigated compounds. Corilagin, with the lowest average ROG value (21.89 Å), is close to having the least RMSD value (1.88 Å) but almost has the lowest binding free energy against S-2 MP. The average ROG values and the improved structural compatibility observed with the average RMSD values in this investigation could be influenced by various protein-specific features, including protein structure, size, length, point of interactions, and amino acid, supporting previous results that ROG may be influenced by these factors (Acharya et al., 2020; Lobanov et al., 2008).

An additional useful index for studying protein folding and surface area changes during simulation is the solvent-accessible surface area (SASA), where high values indicate more surface area and smaller values indicate a reduction in the protein volume (Mousavi et al., 2021). A protein's solvent-accessible surface area measures its amino acid residues' hydrophilic and hydrophobic properties upon contact with solvent or water (Khan et al., 2018), and the level of disparity in exposure might be attributed to modifications in the tertiary structure of the protein (Zhang & Lazim, 2017). Throughout the simulation period, minor fluctuations were observed in the SASA value in the S-2 MP systems (Figure 5a). Consequently, a slight variation of 670 Å was seen across all systems as the lowest SASA value was observed in kaempferol 7-O-glucoside S-2 MP (13840.95 Å). This observation is partly consistent with Aribisala et al. (2022), in which kaempferol 7-O-glucoside + S-2 wild-type spike protein was reported to have the lowest SASA value with a minimum variation of 700 Å across all the systems. This could be due to an insignificant effect of the test compounds on the surface area and volume of S-2 MP through the simulation period, like the ROG values showing that the thermodynamic entropy was not disturbed. This result does not agree with Mousavi et al. (Mousavi et al., 2021), in which the ligand-protein interactions largely influenced the SASA value. However, it is coherent with the results of Aribisala et al. (2022), where the binding of the test compounds to the S-2 wild-type spike protein had little effect on the SASA value.

In the S-2 RP systems, there was an initial increase in the SASA values up to 30 ns. There was a relatively steady continuous fluctuation in the SASA values until the end of the simulation (Figure 5b). In contrast to S-2 MP, there was a minimum variation of 1100 Å across all the S-2 RP systems. Interestingly, the least average SASA value (36524.18 Å) was

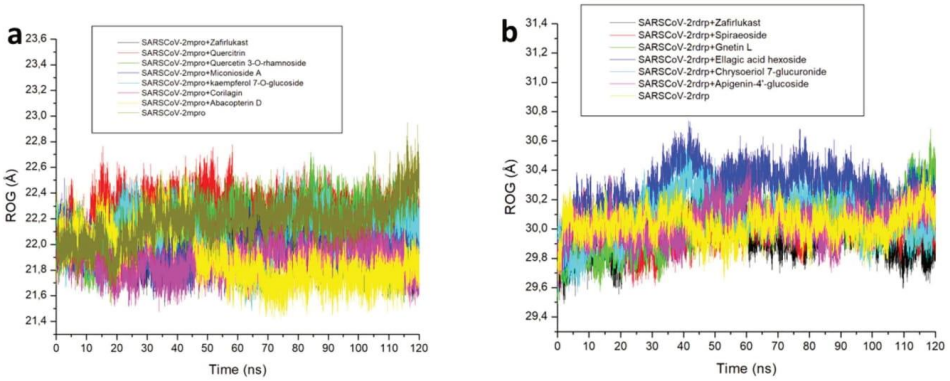


Figure 4. Comparative radius of gyration (ROG) plots of alpha-carbon, top-ranked compounds and reference standards against (a) S-2 MP and (b) S-2 RP after 120 ns MD simulation period.

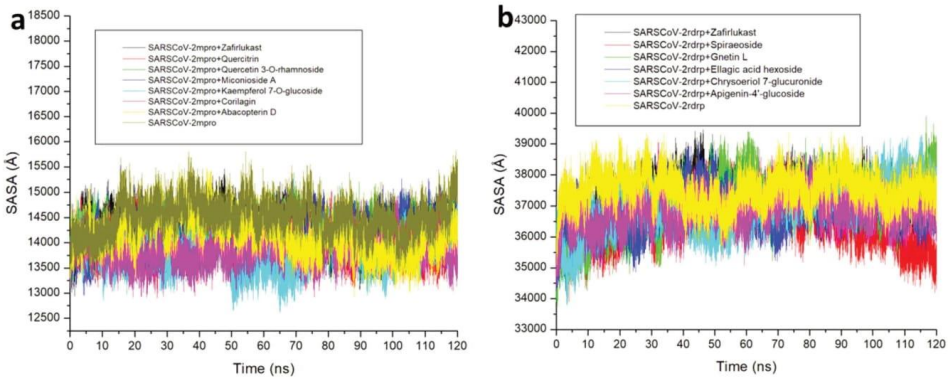


Figure 5. Comparative solvent-accessible surface area (SASA) plots of alpha-carbon, top-ranked compounds and reference standards against (a) S-2 MP and (b) S-2 RP after 120 ns MD simulation period.

observed in the spiraeoside + S-2 RP complex (Table 4B), which is in tandem with the ROG, RMSF value and its binding free energy is an indication that spiraeoside could be a suitable inhibitor of the S-2 RP. Conversely, kaempferol 7-O-glucoside with the lowest value in the S-2 MP complex (13840.95 Å) agrees with the average RMSF value but was inconsistent with the ROG and RMSD values. Generally, all the top-ranked compounds had lower average SASA values relative to their respective apo-proteins suggesting their ability to decrease the targets' surface area and limit protein residue interaction with immediate solvent molecules. This indicates their stable nature and probability of being effective as drugs against the investigated protein.

Protein-ligand hydrogen bonds were also investigated because of their importance in determining complex stability (Mondal et al., 2020). Hydrogen bonding is an essential factor in protein stability, and the effects of ligand binding on this factor may be studied by measuring the quantity and distance of hydrogen bonds formed throughout a simulation (Du et al., 2016). The number of hydrogen bonds formed in S-2 MP and S-2 RP shows a stable fluctuation pattern throughout the simulation, generally between 110 to 170 and 370 to 480, respectively (Figure 6a, b). This result reveals that both protein targets' thermodynamic entropy is unaffected by the protein's bindings with the top test compounds and their respective reference standards. Higher numbers of hydrogen bonds were observed in complexes of S-2 MP with the top test compounds and zafirlukast (136.95–141.11) compared to unbound S-2 MP (136.11). Similarly, a higher number of hydrogen bonds were equally observed in S-2 RP complexes relative to the apo-protein (420) as well, except in zafirlukast (416), gnetin L (418) and spiraeoside (419) with a reduced number of hydrogen bonds. This finding may suggest that the ligands have taken up some intramolecular space. The rise in hydrogen bonds could be linked to the contacts between the top test compounds, the reference standards, and the respective targets. Quercitrin complex was reported to have the highest number of hydrogen bonds (141.11) in the S-2 MP systems (Table 3A and Figure 6a). In contrast, the ellagic acid hexoside complex has the

highest number of hydrogen bonds (427.94) in the S-2 RP systems, which is in tandem with the compound's free binding energy result. This result emphasizes the role of hydrogen bonds in the high binding affinity of both compounds for S-2 MP and S-2 RP respectively.

The hydrogen-bond distance decreased steadily throughout the simulation (Figure 7a, b), a trend observed in both targets (S-2 MP and S-2 RP). The average hydrogen-bond distance across all systems was 2.86 Å against S-2 MP (Table 4A) and 2.85 Å against S-2 RP (Table 4B). This implies that the binding of both proteins with the top-scoring compounds and reference standards did not alter the proteins' structure but increased the force between the proteins' atoms and residues as the simulation continued. This result correlates with Aribisala and Sabiu, (2022), who reported a steady drop in the hydrogen bond distance in all systems (apo-protein and ligand-protein-complexed systems) and a mean hydrogen-bond length of 2.85 Å. Similarly, Aribisala et al. (2022) reported a mean hydrogen-bond length of 2.85 Å and 2.87 Å across all systems against S-2 wild type and omicron spike protein, respectively as a drop in the hydrogen bond distance as the simulation continued. The observed results prove that this study's top-ranked compounds and reference standards are thermodynamically compatible with their respective targets as defined by the RMSD findings.

Furthermore, there was a steady variation in the hydrogen bond angle as the simulation continued (Figure 8a, b). A significant swaying was shown between 137° and 168° at 0 ns, while the hydrogen bond angle sway between 154° and 164° at 120 ns in S-2 MP systems. Against S-2 RP, the swaying ranges between 136° and 169° at 0 ns while the fluctuation varies between 144° and 166° at 120 ns. It could be suggested that hydrogen bond angles would have an insignificant influence on the binding free energy, with all systems having average values between 151.45° and 151.80° with a variance of 0.35° against S-2 MP. However, there was a variance of 0.51° in S-2 RP where the average hydrogen bond angle of 151.73° and 152.24° was observed in S-2 RP. According to Kretschmer et al. (2012), a hydrogen bond angle of 180° is considered optimal therefore, this study's findings on hydrogen bond distance are consistent with the observation that the hydrogen bond angle fluctuates less toward 180° as the simulation continues, suggesting that the hydrogen bonds are becoming stronger.

3.7. Bond analysis of interaction plots

The study of receptor-ligand interactions elucidated the interactions between bound molecules and the amino acid residues at the enzyme's active site (Chetty et al., 2016; Kehinde et al., 2019). Figures 9–13 provide a time-dependent plot of interactions for the reference standards and the top-scoring compounds with the highest binding free energy against S-2 MP and S-2 RP. The number, kind and distance of bond interactions generated after 120 ns between the compounds under study and their respective targets, S-2 MP and S-2 RP were therefore analyzed in this study (Table 6A, B). Variations in binding free energy observed between compounds were linked to the differences in nature, bond lengths, and numbers of interactions between the ligands and the reference standard examined in this study against S-2 MP and S-2 RP. Many types of bonds were observed including conventional hydrogen bonds, carbon-based hydrogen bonds, Van der Waals, amide π-stacked, π-anion, π-sigma, π-cation, π-π t-cation, π-π t-shaped, π-π t-stacked, π-alkyl, alkyl, π-Sulphur, unfavourable donor-donor interactions among others.

Accordingly, abacopterin D, with the lowest free binding energy, has the lowest number of interactions (13) (Table 6A). Similarly, the number of interactions observed in corilagin (16) is also consistent with the binding free energy. Surprisingly, kaempferol 7-O-glucoside and miconioside A had an equal number of interactions (Table 6A); however, miconioside A had higher binding energy compared to kaempferol 7-O-glucoside (Table 4A). Miconioside A had a lower number of hydrogen bonds relative to kaempferol 7-

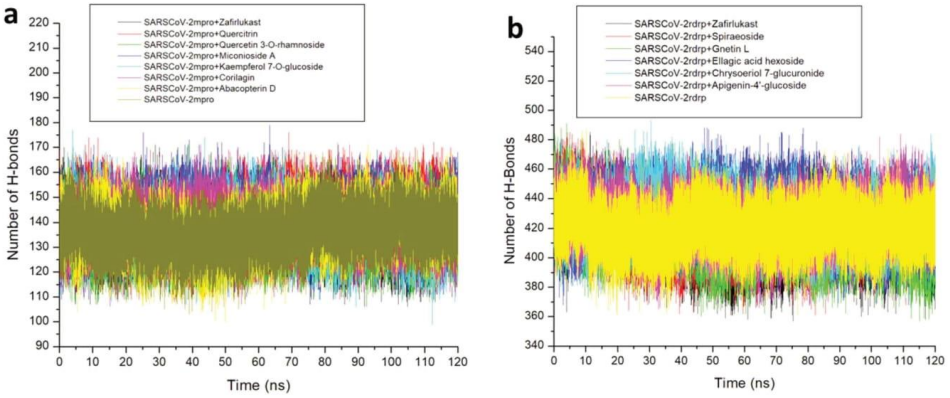


Figure 6. Time progression of the number of hydrogen bonds in (a) S-2 MP and (b) S-2 RP upon binding of the top-ranked compounds and gold standards during the 120 ns MD simulation period.

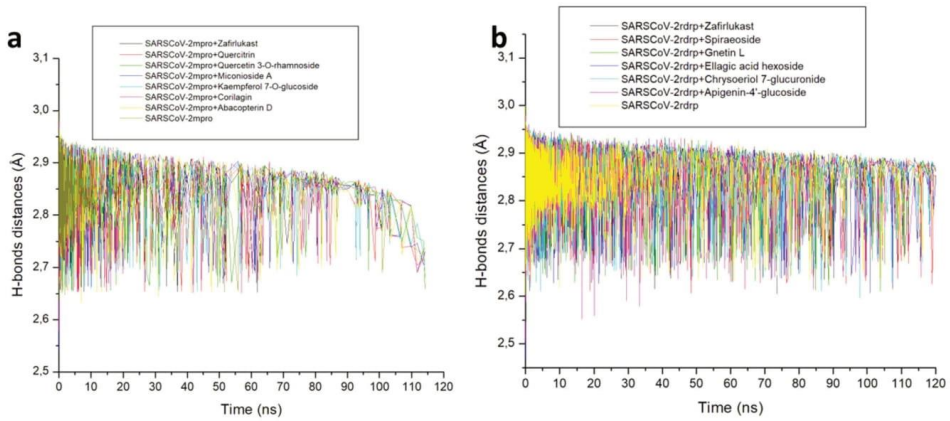


Figure 7. Time progression of the hydrogen bond distance in (a) S-2 MP and (b) S-2 RP upon binding of the top-ranked compounds and reference standards during the 120 ns MD simulation period.

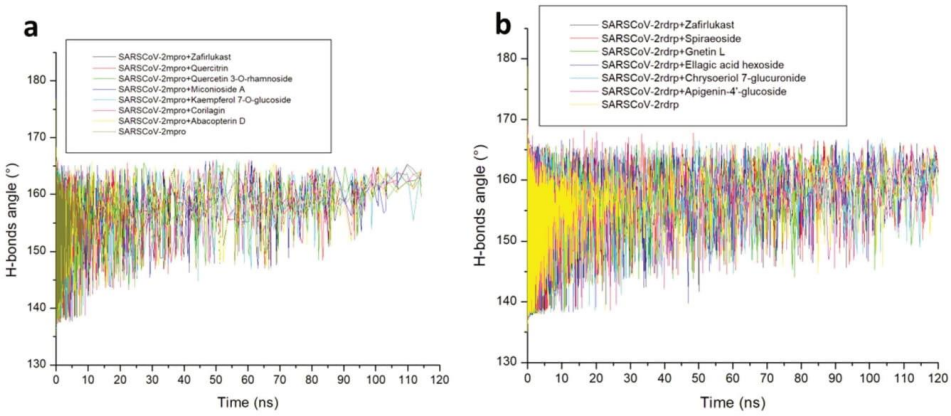


Figure 8. Time progression of the hydrogen bond angles in (a) S-2 MP and (b) S-2 RP upon binding of the top-ranked compounds and reference standards during the 120 ns MD simulation period.

O-glucoside; though, the latter was observed to form an unfavourable bond with the protein target. The formation of the unfavourable bond could imply that the S-2 MP + kaempferol 7-O-glucoside complex probably contains a repelling force, and the short length of the unfavourable bond indicates a robust repulsive force (Acharya et al., 2020; Bissantz et al., 2010). These could have significantly influenced the lower free binding energy reported in kaempferol 7-O-glucoside compared to miconioside A. Furthermore, this observation could be attributed to the presence of π-π stacked interactions within the aromatic ring of miconioside A and Hie41 (Supplementary Table S3). Acetylcholinesterase (AChE) inhibitors for the treatment of Alzheimer's disease have been developed using this interaction (π-π stacked) (da Silva et al., 2006), and this interaction had previously been described to be critical in drug development (Babine & Bender, 1997). Unfortunately, there is a deviation from this trend as quercetin 3-O-rhamnoside, with the highest free binding energy reported in this study has 19 interactions (Figure 9) compared to zafirlukast, with the highest interactions (32) (Figure 10, Table 6A) yet with lower free binding energy than quercetin 3-O-rhamnoside. However, the lowest average bond length found in this study was observed in quercetin 3-O-rhamnoside (4.32 Å) (Figure 9) and this could have been responsible for its higher free binding energy. A stronger force within two intramolecular or intermolecular entities has been observed to be correlated with shorter bond lengths; this may be because the atoms of the molecules are bound together more closely, leading to a higher affinity (Du et al., 2016). Furthermore, due to their unusually potent intermolecular interactions, hydrogen bond interactions are one of the most significant non-covalent bonds in designing new drugs (Patil et al., 2010). Specifically, quercetin 3-O-rhamnoside had the highest number of hydrogen bonds

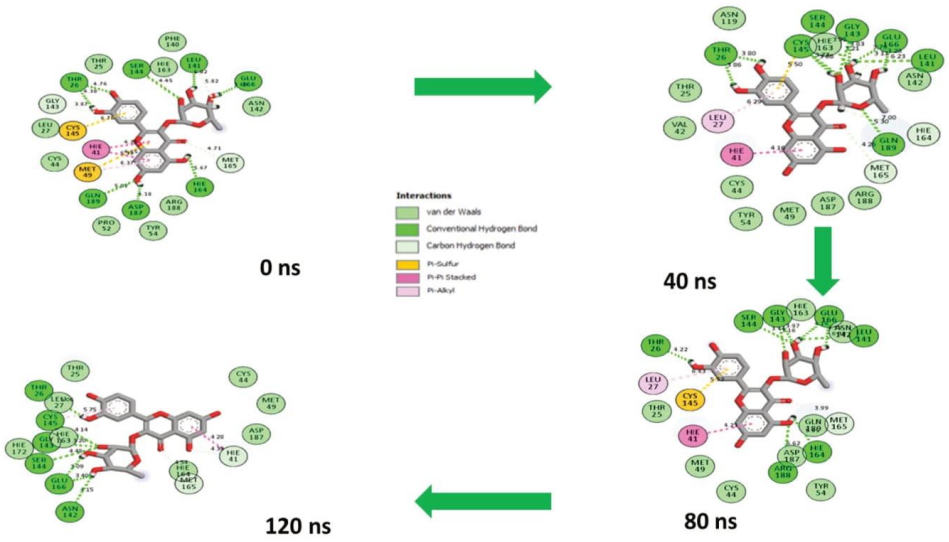


Figure 9. The plot of interactions of quercetin 3-O-rhamnoside against S-2 MP at various timeframes during the 120 ns simulation. Residues His41, Cys145, Glu166 and Gln189 reported in the active site of S-2 MP were observed in the interaction at 0 ns. Interaction frames at 40, 80, and 120 ns showed that the amino acid interactions evolved during the experiment. However, at 80 and 120 ns, common amino acids like Thr25, Thr26, Leu27, and Tyr54 are involved in the interactions.

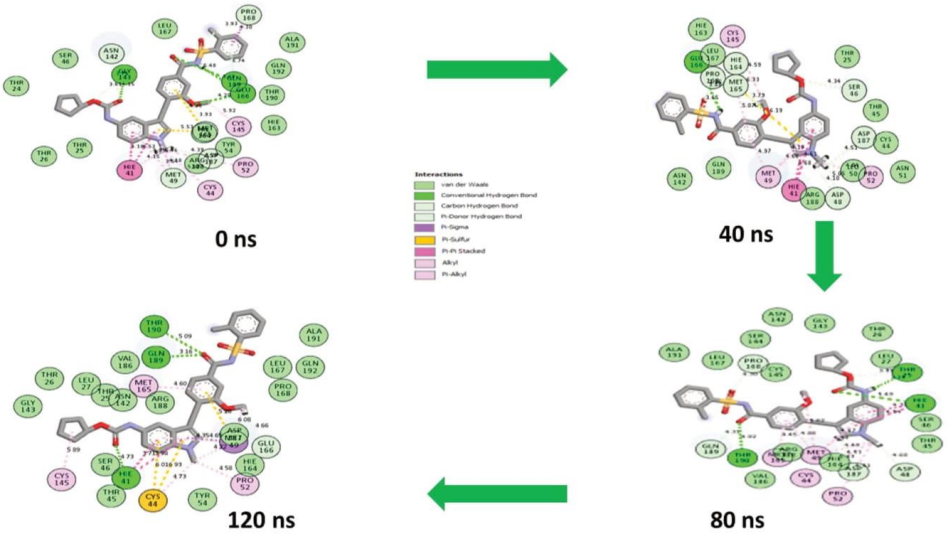


Figure 10. The plot of interactions of zafirlukast against S-2 MP at various timeframes during the 120 ns simulation. Residues His41, Asn142, Glu166 and Gln189 reported in the active site of S-2 MP were observed in the interaction at 0 ns. However, at timeframes 40, 80 and 120 ns, common amino acids observed as the interaction proceeds include Thr25, Thr26, Leu27, Asn51, Pro52, and Tyr54.

and consequently the highest free binding energy compared to other compounds investigated. The higher number of hydrogen bonds (11) observed in quercetin 3-O-rhamnoside (Table 6A) could be responsible for its high free binding energy.

Remarkably, just like the S-2 MP interactions, the compound with the lowest binding free energy (Table 3B) equally had the lowest number of interactions at 120 ns against S-2 RP (gnetin L) (Table 6B). Likewise, a higher number of interactions were observed in zafirlukast relative to

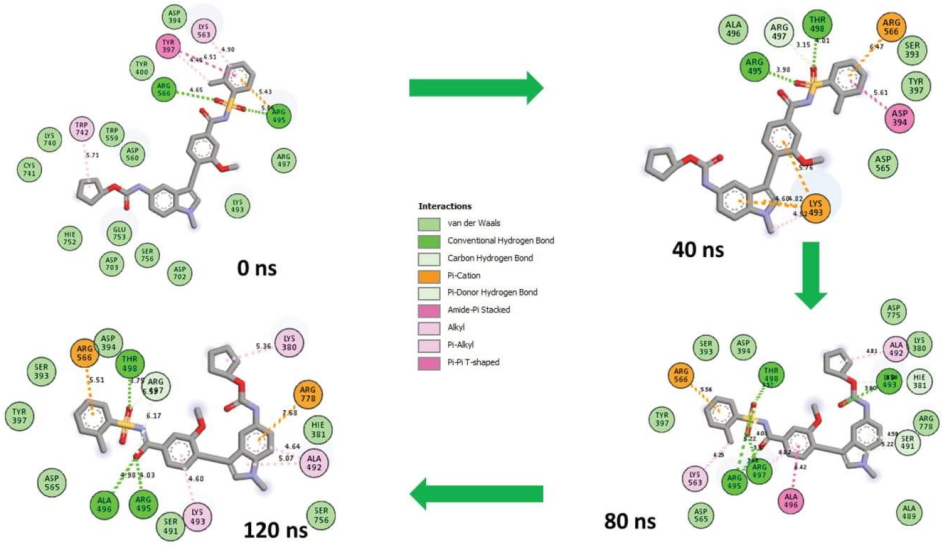


Figure 11. The plot of interactions of zafirlukast against S-2 RP at different timeframes during the 120 ns simulation. At 0 ns, residue Ser756 was noticed in the interaction plot of the complex. None of the residues at the protein's active site was observed to have interacted with the ligand at 40 ns and 80 ns however, residue Ser756 resurfaced at 120 ns. In addition, common amino acids noticed in the interactions at different timeframes include Arg495, Ala496, Arg497, Asp565, Arg566 among others.

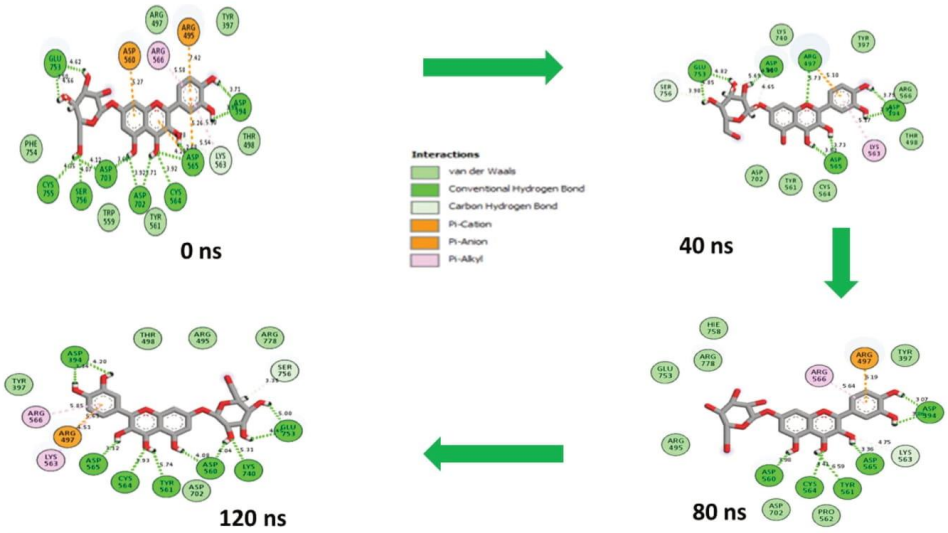


Figure 12. The plot of interactions of spiraeoside against S-2 RP at various timeframes during the 120 ns simulation. At 0 ns, residues Cys755 and Ser756 reported in the protein's active site were observed in the reaction. Several common amino acid residues were found throughout the simulation at the interaction timeframes of 40, 80 and 120 ns.

gnetin L (Figure 11). The observed number of interactions in zafirlukast is coherent with the resulting binding free energy (Table 3B). Interestingly, ellagic acid hexoside (Figure 12) with the highest binding free energy equally had the largest number of interactions (26) (Table 6B). Surprisingly, the highest number of interactions (26) also observed in apigenin-4′-glucoside is not in tandem with its binding free energy relative to ellagic acid hexoside. This lower binding free

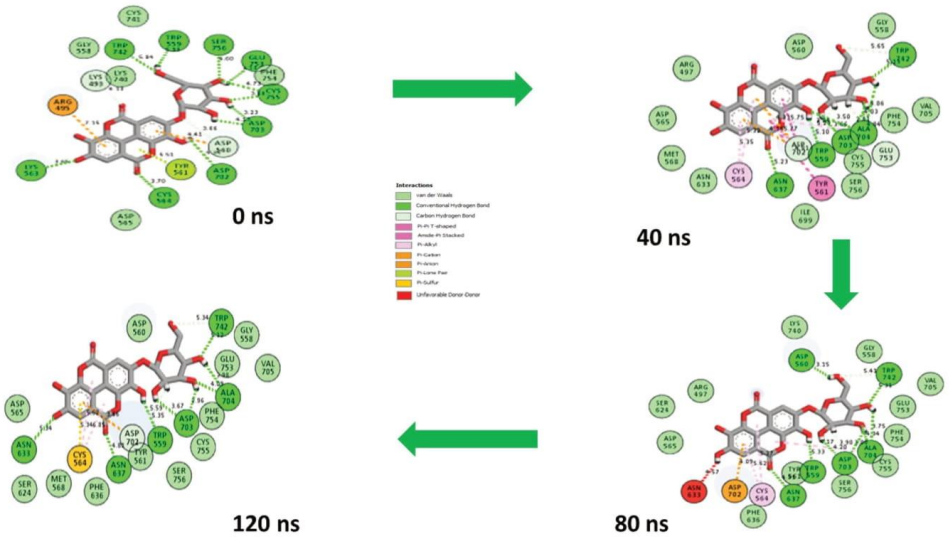


Figure 13. The plot of ellagic acid hexoside interactions against S-2 RP at different timeframes during the 120 ns simulation. At 0 ns, residues Cys755 and Ser756 reported in the protein's active site were observed in the reaction. Common amino acids observed as the simulation progresses at timeframes 40 and 80 ns include Arg497, Asp560, Asp565, and Asp703. The significant increase in the number of interactions from 40 ns could be responsible for the increased binding free energy found in the complex relative to spiraeoside against S-2 RP.

Table 6A. Molecular interactions between the top-ranked compounds against S-2 MP after 120 ns of simulation.

Top-ranked compounds	Total sum of interactions (mean bond length in Å)	Number of hydrogen bonds and interaction residues	Other vital interactions and residues	Unfavourable bonds (bond length in Å)
Abacopterin D	13 (4.38 Å)	9 (4.38 Å) [Glu166 (3), Met165, Gln192, Pro168 (3), Gln189]	2 (4.43 Å) [Pro168 (2)]	None
Corilagin	16 (4.42 Å)	7 (4.41 Å) [Met49, Asp187, Asn142, Gly143, Hie41(2), Hie163]	1 (4.50 Å) [Met165]	None
Kaempferol 7-O-glucoside	22 (4.68 Å)	10 (4.49 Å) [Glu166 (3), Gln192, Arg188, Gln189, Cys44(4)]	4 (5.81 Å) [Met49(3), Cys44 (1)]	1 (4.27 Å) Cys44
Miconioside A	22 (4.95 Å)	8 (4.71 Å), [Gln189 (2), Gln192 (2), Glu166, Thr190 (2), Arg188]	2 (5.77 Å) [Met49, Hie41]	None
Quercetin 3-O-rhamnoside	19 (4.32 Å)	11 (4.32 Å) [Thr26, Cys145(2), Gly143, Ser144, Glu166(2), Asn142, Met165, Hie41(2)]	2 (5.02 Å) [Hie41, Cys145]	None
Quercitrin	20 (4.76 Å)	5 (4.94 Å) [Thr26, Glu166(2), Hie164(2)]	2 (4.71 Å) [Hie41, Cys145]	1 (3.98 Å) [Cys44]
Zafirlukast	32 (4.86 Å)	6 (4.22 Å) [Thr190, Gln189, Hie41(3), Glu166]	8 (5.10 Å) [Hie41(2), Cys44(2), Cys145, Asp187, Met49(2)]	None

energy could be linked to the unfavourable bond formed with the protein, which suggests a strong repulsive force. Furthermore, owing to its higher binding free energy relative to chrysoeriol 7-glucuronide, a higher number of interactions (24) would have been expected in spiraeoside, but a lower number of interactions (19) (Figure 11) was observed (Table 6B). Moreover, more hydrogen bonds were observed in chrysoeriol 7-glucuronide (12) relative to spiraeoside (11). However, a closer examination of the observed interactions in both complexes revealed that the lower average bond length in the total number of interactions (4.47 and 4.58), number of hydrogen bonds (4.23 and 4.27) and other important interactions (5.32 and 5.37) was found in spiraeoside and chrysoeriol 7-glucuronide, respectively. There seems to be a correlation between the strength of the attraction between two intramolecular or intermolecular entities and the length of their bonds. This may be because there is a greater affinity between ligand and receptor with shorter bond lengths.

4. Conclusion

In light of the crucial functions of S-2 MP and RP in the replication and transcription of the virus, the identification of effective inhibitors of these therapeutic targets is essential for the treatment of COVID-19. Therefore, molecular docking

Table 6B. Molecular interactions between the top-ranked compounds against S-2 RP after 120 ns of simulation.

Top-ranked compounds	Total sum of interactions (mean bond length in Å)	Number of hydrogen bonds and interaction residues	Other vital interactions and residues	Unfavourable bonds (bond length in Å)
Apigenin-4′-glucoside	26 (4.71)	13 (4.39) [Asp560 (3), Trp742, Ala704 (2), Asp703, Asp702, Tyr561, Trp559 (3), Glu753]	5 (6.02) [Arg495 (2), Pro562 (2), Tyr561]	1 (5.26) [Lys563]
Chrysoeriol 7-glucuronide	24 (4.58)	12 (4.27) [Lys563 (2), Asp560 (3), Ser756, Asp703 (4), Asp 702 (2)]	4 (5.50) [Pro560, Lys740, Arg497(2)]	None
Ellagic acid hexoside	26 (4.84)	10 (4.63) [Asn633, Asn637, Trp559, Asp703 (2), Ala704 (2), Trp742 (2), Asp702]	4 (5.37) [Cys564 (3), Asp702]	None
Gnetin L	15 (4.88)	5 (3.98) [Asp565, Cys564, Lys563 (2), Pro562]	4 (6.01) [Arg495 (2), Ala739, Cys564]	None
Spiraeoside	19 (4.47)	11 (4.23) [Asp394 (2), Asp565, Cys564, Tyr561, Asp560 (2), Lys740, Glu753 (2), Ser756]	3 (5.32) [Arg497, Arg566, Lys563]	None
Zafirlukast	18 (5.21)	5 (4.89) [Thr498, Ala496, Arg495, Arg497 (2)]	6 (5.48) [Arg566, Lys493, Lys380, Arg778, Ala492 (2)]	None

and molecular dynamic simulation approaches were employed to find possible inhibitors of these targets. Quercetin 3-O-rhamnoside had a better binding affinity towards the S-2 MP relative to zafirlukast. In addition to its thermodynamic stability, it was compatible with the protein. Conversely, all the five compounds selected for further studies against S-2 RP had better binding affinity relative to zafirlukast except gnetin L. Remarkably, ellagic acid hexoside, spiraeoside, apigenin-4′-glucoside and chrysoeriol 7-glucuronide with higher binding free energy are thermodynamically stable and structurally compatible with the protein. The identified lead compounds cut across the three selected medicinal plants; quercetin 3-O-rhamnoside (*M. barteri*), ellagic acid hexoside (*S. mombin* and *M. barteri*), spiraeoside (*M. barteri*), apigenin-4′-glucoside (*M. barteri* and *D. eriocarpum*) and chrysoeriol 7-glucuronide (*D. eriocarpum*). They generally have favourable pharmacokinetic properties with none, or little structural alterations required to enhance their druggability. Therefore, owing to their affinity for the selected therapeutic targets, they are promising inhibitors of S-2 RP and could be considered potential therapeutic agents for the treatment of COVID-19. To further confirm their effectiveness against S-2 infection, *in vitro* and *in vivo* studies are strongly encouraged.

Acknowledgments

The DUT Doctoral Scholarship Scheme to A. A. Lanrewaju is duly acknowledged. The Centre for High-Performance Computing (CHPC), South Africa, is equally acknowledged for granting access to the computing systems used in this study.

Disclosure statement

No potential conflict of interest was reported by the authors.

Supplementary description

Additional information on the LCMS profiling of the metabolites from the selected plants, docking scores for 77 plant metabolites against S-2 MP and RP and 2D interaction plots of top rank compounds against S-2 MP and RP after 120 ns simulation (Supplementary Tables S1–S3).

Funding

This study was based on the financial assistance received from the Directorate of Research and Postgraduate Support, Durban University of Technology (DUT), and the South African Medical Research Council (SAMRC) under a Self-Initiated Research Grant as well as the National Research Foundation (NRF) Research Development Grant for Rated Researchers (Grant number 120433) and the Competitive Programme for Rated Researchers Support (SRUG2204193723) to S. Sabiu. We also acknowledge Water Research Commission (WRC) of South Africa for the grant (Project no. K5/C2020-2021-00181) awarded to am Enitan-Folami.

Data availability statement

The data is contained within the article or supplementary material.

Author's contributions

Conceptualization, S.S., A.M.E. and A.A.L.; methodology, A.A.L.; software, S.S.; validation, A.A.L. and S.S; formal analysis, A.A.L.; investigation, A.A.L; resources, S.S.; data curation, A.A.L. and S.S.; writing—original draft preparation, A.A.L.; writing—review and editing, A.M.E., M.M.N, F.M.S, S.S; supervision, A.M.E., F.M.S and S.S.; funding acquisition, A.M.E., F.M.S. and S.S. All authors read and contributed to the critical review of the manuscript for intellectual content and approved the submission for publication.

References

Abdalla, M., Mohapatra, R. K., Sarangi, A. K., Mohapatra, P. K., Eltayb, W. A., Alam, M., El-Arabey, A. A., Azam, M., Al-Resayes, S. I., Seidel, V., & Dhama, K. (2021). In silico studies on phytochemicals to combat the emerging COVID-19 infection. *Journal of Saudi Chemical Society*, *25*(12), 101367. https://doi.org/10.1016/j.jscs.2021.101367

Abdallah, H. M., El-Halawany, A. M., Sirwi, A., El-Araby, A. M., Mohamed, G. A., Ibrahim, S. R., Koshak, A. E., Asfour, H. Z., Awan, Z. A., & A. Elfaky, M. (2021). Repurposing of some natural product isolates as SARS-COV-2 main protease inhibitors via in vitro cell free and cell-based antiviral assessments and molecular modeling approaches. *Pharmaceuticals*, *14*(3), 213. https://doi.org/10.3390/ph14030213

Acharya, A., Agarwal, R., Baker, M. B., Baudry, J., Bhowmik, D., Boehm, S., Byler, K. G., Chen, S. Y., Coates, L., Cooper, C. J., Demerdash, O., Daidone, I., Eblen, J. D., Ellingson, S., Forli, S., Glaser, J., Gumbart, J. C., Gunnels, J., Hernandez, O., … Zanetti-Polzi, L. (2020). Supercomputer-based ensemble docking drug discovery pipeline with application to COVID-19. *Journal of Chemical Information and Modeling*, *60*(12), 5832–5852. https://doi.org/10.1021/acs.jcim.0c01010

Ahmad, J., Ikram, S., Ahmad, F., Rehman, I. U., & Mushtaq, M. (2020). SARS-CoV-2 RNA dependent RNA polymerase (RdRp)–a drug repurposing study. *Heliyon*, *6*(7), e04502. https://doi.org/10.1016/j.heliyon.2020.e04502

Ahmad, S., Zahiruddin, S., Parveen, B., Basist, P., Parveen, A., Parveen, R., Ahmad, M. (2020). Indian medicinal plants and formulations and their potential against COVID-19–preclinical and clinical research.*Frontiers in Pharmacology*, *11*, 578970. https://doi.org/10.3389/fphar.2020.578970

Al-Khodairy, F. M., Khan, M. K. A., Kunhi, M., Pulicat, M. S., Akhtar, S., & Arif, J. M. (2013). In Silico prediction of mechanism of Erysolin-induced apoptosis in human breast cancer cell lines. *American Journal of Bioinformatics Research*, *3*(3), 62–71. https://doi.org/10.5923/j.bioinformatics.20130303.03

Aribisala, J. O., Aruwa, C. E., Uthman, T. O., Nurain, I. O., Idowu, K., & Sabiu, S. (2022). Cheminformatics bioprospection of broad spectrum plant secondary metabolites targeting the spike proteins of omicron variant and wild-type SARS-CoV-2. *Metabolites*, *12*(10), 982. https://doi.org/10.3390/metabo12100982

Aribisala, J. O., Nkosi, S., Idowu, K., Nurain, I. O., Makolomakwa, G. M., Shode, F. O., & Sabiu, S. (2021). Astaxanthin-mediated bacterial lethality: Evidence from oxidative stress contribution and molecular dynamics simulation. *Oxidative Medicine and Cellular Longevity*, *2021*, 7159652. https://doi.org/10.1155/2021/7159652

Aribisala, J. O., & Sabiu, S. (2022). Cheminformatics identification of phenolics as modulators of penicillin-binding protein 2a of staphylococcus aureus: A structure–Activity-relationship-based study. *Pharmaceutics*, *14*(9), 1818. https://doi.org/10.3390/pharmaceutics14091818

Babine, R. E., & Bender, S. L. (1997). Molecular recognition of protein − Ligand complexes: Applications to drug design. *Chemical Reviews*, *97*(5), 1359–1472. https://doi.org/10.1021/cr960370z

Balogun, F. O., Naidoo, K., Aribisala, J. O., Pillay, C., & Sabiu, S. (2022). Cheminformatics identification and validation of dipeptidyl peptidase-IV modulators from shikimate pathway-derived phenolic acids towards interventive type-2 diabetes therapy. *Metabolites*, *12*(10), 937. https://doi.org/10.3390/metabo12100937

Beigel, J. H., Tomashek, K. M., Dodd, L. E., Mehta, A. K., Zingman, B. S., Kalil, A. C., Hohmann, E., Chu, H. Y., Luetkemeyer, A., Kline, S., Lopez de Castilla, D., Finberg, R. W., Dierberg, K., Tapson, V., Hsieh, L., Patterson, T. F., Paredes, R., Sweeney, D. A., Short, W. R., … Lane, H. C; ACTT-1 Study Group Members. (2020). Remdesivir for the treatment of Covid-19. *The New England Journal of Medicine*, *383*(19), 1813–1826. https://doi.org/10.1056/NEJMoa2007764

Beressa, T. B., Deyno, S., Mtewa, A. G., Aidah, N., Tuyiringire, N., Lukubye, B., Weisheit, A., Tolo, C. U., & Ogwang, P. E. (2021). Potential benefits of antiviral African medicinal plants in the management of viral infections: Systematic review. *Frontiers in Pharmacology*, *12*, 682794. https://doi.org/10.3389/fphar.2021.682794

Biovia, D. S. (2021). *Discovery studio. Version 21.1.0*. Dassault Systèmes.

Bissantz, C., Kuhn, B., & Stahl, M. (2010). A medicinal chemist's guide to molecular interactions. *Journal of Medicinal Chemistry*, *53*(14), 5061–5084. https://doi.org/10.1021/jm100112j

Boadu, A., Agoni, C., Karpoormath, R., Soliman, M., & Nlooto, M. (2022). Repurposing antiviral phytochemicals from the leaf extracts of Spondias mombin (Linn) towards the identification of potential SARSCOV-2 inhibitors. *Scientific Reports*, *12*(1), 10896. https://doi.org/10.1038/s41598-022-14558-3

Chetty, S., Bhakat, S., Martin, A. J., & Soliman, M. E. (2016). Multi-drug resistance profile of PR20 HIV-1 protease is attributed to distorted conformational and drug binding landscape: Molecular dynamics insights. *Journal of Biomolecular Structure & Dynamics*, *34*(1), 135–151. https://doi.org/10.1080/07391102.2015.1018326

Corthout, J., Pieters, L., Claeys, M., Berghe, D. V., & Vlietinck, A. (1991). Antiviral ellagitannins from Spondias mombin. *Phytochemistry*, *30*(4), 1129–1130. https://doi.org/10.1016/S0031-9422(00)95187-2

da Silva, C. H., Campo, V. L., Carvalho, I., & Taft, C. A. (2006). Molecular modeling, docking and ADMET studies applied to the design of a novel hybrid for treatment of Alzheimer's disease. *Journal of Molecular Graphics & Modelling*, *25*(2), 169–175. https://doi.org/10.1016/j.jmgm.2005.12.002

Delijewski, M., & Haneczok, J. (2021). AI drug discovery screening for COVID-19 reveals zafirlukast as a repurposing candidate. *Medicine in Drug Discovery*, *9*, 100077. https://doi.org/10.1016/j.medidd.2020.100077

Du, X., Li, Y., Xia, Y.-L., Ai, S.-M., Liang, J., Sang, P., Ji, X.-L., & Liu, S.-Q. (2016). Insights into protein–Ligand interactions: Mechanisms, models, and methods. *International Journal of Molecular Sciences*, *17*(2), 144. https://doi.org/10.3390/ijms17020144

Elfiky, A. A. (2020a). Anti-HCV, nucleotide inhibitors, repurposing against COVID-19. *Life Sciences*, *248*, 117477. https://doi.org/10.1016/j.lfs.2020.117477

Elfiky, A. A. (2020b). Ribavirin, remdesivir, sofosbuvir, galidesivir, and tenofovir against SARS-CoV-2 RNA dependent RNA polymerase (RdRp): A molecular docking study. *Life Sciences*, *253*, 117592. https://doi.org/10.1016/j.lfs.2020.117592

Elfiky, A. A. (2021). SARS-CoV-2 RNA dependent RNA polymerase (RdRp) targeting: An in silico perspective. *Journal of Biomolecular Structure & Dynamics*, *39*(9), 3204–3212. https://doi.org/10.1080/07391102.2020.1761882

Elfiky, A. A., Elshemey, W. M., Gawad, W. A., & Desoky, O. S. (2013). Molecular modeling comparison of the performance of NS5b polymerase inhibitor (PSI-7977) on prevalent HCV genotypes. *The Protein Journal*, *32*(1), 75–80. https://doi.org/10.1007/s10930-013-9462-9

Elfiky, A. A., & Ismail, A. (2019). Molecular dynamics and docking reveal the potency of novel GTP derivatives against RNA dependent RNA polymerase of genotype 4a HCV. *Life Sciences*, *238*, 116958. https://doi.org/10.1016/j.lfs.2019.116958

Elfiky, A. A., & Ismail, A. M. (2018). Molecular docking revealed the binding of nucleotide/side inhibitors to Zika viral polymerase solved structures. *SAR and QSAR in Environmental Research*, *29*(5), 409–418. https://doi.org/10.1080/1062936X.2018.1454981

Eltayb, W. A., Abdalla, M., & Rabie, A. M. (2023). Novel investigational anti-sars-cov-2 agent ensitrelvir "s-217622": A very promising potential universal broad-spectrum antiviral at the therapeutic frontline of coronavirus species. *ACS Omega*, *8*(6), 5234–5246. https://doi.org/10.1021/acsomega.2c03881

Falang, K. D., Poyi, C. O., Ajima, U., Bukar, B. B., Amagon, K. I., Damen, J. G., Agabi, Y., Kutshik, R. J., Longdet, I. Y., Gomerep, S. S., Shittu, I., Davou, S. D., Kolawole, J. A., & Wannang, N. N. (2020). Combinatorial evaluation of antiviral activity of some Nigerian medicinal plants on SARS-CoV-2. *Journal of Complementary and Alternative Medical Research*, *12*, 38–50. https://doi.org/10.9734/jocamr/2020/v12i130199

Farhat, A., Ben Hlima, H., Khemakhem, B., Ben Halima, Y., Michaud, P., Abdelkafi, S., & Fendri, I. (2022). Apigenin analogues as SARS-CoV-2 main protease inhibitors: In-silico screening approach. *Bioengineered*, *13*(2), 3350–3361. https://doi.org/10.1080/21655979.2022.2027181

Farhat, N., & Khan, A. U. (2021). Repurposing drug molecule against SARS-Cov-2 (COVID-19) through molecular docking and dynamics: A quick approach to pick FDA-approved drugs. *Journal of Molecular Modeling*, *27*(11), 312. https://doi.org/10.1007/s00894-021-04923-w

Gambacorta, N., Caputo, L., Quintieri, L., Monaci, L., Ciriaco, F., & Nicolotti, O. (2022). Rational discovery of antiviral whey protein-derived small peptides targeting the SARS-CoV-2 main protease. *Biomedicines*, *10*(5), 1067. https://doi.org/10.3390/biomedicines10051067

Ghildiyal, R., Prakash, V., Chaudhary, V. K., Gupta, V., & Gabrani, R. (2020). Phytochemicals as antiviral agents: Recent updates. In: Swamy, M. (Eds), *Plant-derived Bioactives* (pp. 279–295). Springer. https://doi.org/10.1007/978-981-15-1761-7_12

Greenidge, P. A., Kramer, C., Mozziconacci, J.-C., & Wolf, R. M. (2013). MM/GBSA binding energy prediction on the PDBbind data set: Successes, failures, and directions for further improvement. *Journal of*

Chemical Information and Modeling, *53*(1), 201–209. https://doi.org/10.1021/ci300425v

Heaney, R. P. (2001). Factors influencing the measurement of bioavailability, taking calcium as a model. *The Journal of Nutrition*, *131*(4 Suppl), 1344S–1348S. https://doi.org/10.1093/jn/131.4.1344S

Huang, F., Li, Y., Leung, E. L.-H., Liu, X., Liu, K., Wang, Q., Lan, Y., Li, X., Yu, H., Cui, L., Luo, H., & Luo, L. (2020). A review of therapeutic agents and Chinese herbal medicines against SARS-COV-2 (COVID-19). *Pharmacological Research*, *158*, 104929. https://doi.org/10.1016/j.phrs.2020.104929

Islam, M. S., Mahmud, S., Sultana, R., & Dong, W. (2020). Identification and in silico molecular modelling study of newly isolated Bacillus subtilis SI-18 strain against S9 protein of Rhizoctonia solani. *Arabian Journal of Chemistry*, *13*(12), 8600–8612. https://doi.org/10.1016/j.arabjc.2020.09.044

Islam, T., Hasan, M., Rahman, M. S., & Islam, M. R. (2022). Comparative evaluation of authorized drugs for treating Covid-19 patients. *Health Science Reports*, *5*(4), e671. https://doi.org/10.1002/hsr2.671

Kehinde, I., Ramharack, P., Nlooto, M., & Gordon, M. (2019). The pharmacokinetic properties of HIV-1 protease inhibitors: A computational perspective on herbal phytochemicals. *Heliyon*, *5*(10), e02565. https://doi.org/10.1016/j.heliyon.2019.e02565

Kehinde, I., Ramharack, P., Nlooto, M., & Gordon, M. (2022). Molecular dynamic mechanism (s) of inhibition of bioactive antiviral phytochemical compounds targeting cytochrome P450 3A4 and P-glycoprotein. *Journal of Biomolecular Structure & Dynamics*, *40*(3), 1037–1047. https://doi.org/10.1080/07391102.2020.1821780

Khaerunnisa, S., Kurniawan, H., Awaluddin, R., Suhartati, S., & Soetjipto, S. (2020). Potential inhibitor of COVID-19 main protease (Mpro) from several medicinal plant compounds by molecular docking study. *Preprints*, 2020030226. https://doi.org/10.20944/preprints202003.0226.v1

Khan, S., Bjij, I., Betz, R. M., & Soliman, M. E. (2018). Reversible versus irreversible inhibition modes of ERK2: A comparative analysis for ERK2 protein kinase in cancer therapy. *Future Medicinal Chemistry*, *10*(9), 1003–1015. https://doi.org/10.4155/fmc-2017-0275

Kretschmer, R., Kinzel, D., & González, L. (2012). The role of hydrogen bonds in protein–ligand interactions. DFT calculations in 1, 3-dihydrobenzimidazole-2 thione derivatives with glycinamide as model HIV RT inhibitors. *International Journal of Quantum Chemistry*, *112*(7), 1786–1795. https://doi.org/10.1002/qua.23001

Lai, Z., Tsugawa, H., Wohlgemuth, G., Mehta, S., Mueller, M., Zheng, Y., Ogiwara, A., Meissen, J., Showalter, M., Takeuchi, K., Kind, T., Beal, P., Arita, M., & Fiehn, O. (2018). Identifying metabolites by integrating metabolome databases with mass spectrometry cheminformatics. *Nature Methods*, *15*(1), 53–56. https://doi.org/10.1038/nmeth.4512

Lanrewaju, A. A., Enitan-Folami, A. M., Sabiu, S., Edokpayi, J. N., & Swalaha, F. M. (2022). Global public health implications of human exposure to viral contaminated water. *Frontiers in Microbiology*, *13*, 981896–981896. https://doi.org/10.3389/fmicb.2022.981896

Li, S.-Y., Chen, C., Zhang, H.-Q., Guo, H.-Y., Wang, H., Wang, L., Zhang, X., Hua, S.-N., Yu, J., Xiao, P.-G., Li, R.-S., & Tan, X. (2005). Identification of natural compounds with antiviral activities against SARS-associated coronavirus. *Antiviral Research*, *67*(1), 18–23. https://doi.org/10.1016/j.antiviral.2005.02.007

Lipinski, C. A., Lombardo, F., Dominy, B. W., & Feeney, P. J. (2001). Experimental and computational approaches to estimate solubility and permeability in drug discovery and development settings. *Advanced Drug Delivery Reviews*, *46*(1-3), 3–26. https://doi.org/10.1016/s0169-409x(00)00129-0

Lobanov, M. Y., Bogatyreva, N., & Galzitskaya, O. (2008). Radius of gyration as an indicator of protein structure compactness. *Molecular Biology*, *42*(4), 623–628. https://doi.org/10.1134/S0026893308040195

Lockbaum, G. J., Reyes, A. C., Lee, J. M., Tilvawala, R., Nalivaika, E. A., Ali, A., Kurt Yilmaz, N., Thompson, P. R., & Schiffer, C. A. (2021). Crystal structure of SARS-CoV-2 main protease in complex with the non-covalent inhibitor ML188. *Viruses*, *13*(2), 174. https://doi.org/10.3390/v13020174

Luk, H. K., Li, X., Fung, J., Lau, S. K., & Woo, P. C. (2019). Molecular epidemiology, evolution and phylogeny of SARS coronavirus. *Infection, Genetics and Evolution : journal of Molecular Epidemiology and Evolutionary Genetics in Infectious Diseases*, *71*, 21–30. https://doi.org/10.1016/j.meegid.2019.03.001

Luseba, D., Elgorashi, E., Ntloedibe, D., & Van Staden, J. (2007). Antibacterial, anti-inflammatory and mutagenic effects of some medicinal plants used in South Africa for the treatment of wounds and retained placenta in livestock. *South African Journal of Botany*, *73*(3), 378–383. https://doi.org/10.1016/j.sajb.2007.03.003

Magangana, T. P., Stander, M. A., & Makunga, N. P. (2018). Effect of nitrogen and phosphate on in vitro growth and metabolite profiles of Stevia rebaudiana Bertoni (Asteraceae). *Plant Cell, Tissue and Organ Culture (PCTOC)*, *134*(1), 141–151. https://doi.org/10.1007/s11240-018-1407-8

Manokaran, S., Ah, M. R., Keerthi, A. M., Kallapur, S. S., & Soujanya, R. (2021). Molecular docking and pharmacokinetic studies of naturally occurring flavonoid glycosides and their activity against COVID-19 viral proteins. *SPAST Abstracts*, *1*(01), 1.

Martínez, L. (2015). Automatic identification of mobile and rigid substructures in molecular dynamics simulations and fractional structural fluctuation analysis. *PloS One*, *10*(3), e0119264. https://doi.org/10.1371/journal.pone.0119264

Mir, S. A., Firoz, A., Alaidarous, M., Alshehri, B., Bin Dukhyil, A. A., Banawas, S., Alsagaby, S. A., Alturaiki, W., Bhat, G. A., Kashoo, F., & Abdel-Hadi, A. M. (2022). Identification of SARS-CoV-2 RNA-dependent RNA polymerase inhibitors from the major phytochemicals of Nigella sativa: An in silico approach. *Saudi Journal of Biological Sciences*, *29*(1), 394–401. https://doi.org/10.1016/j.sjbs.2021.09.002

Mondal, I., Basak, T., Banerjee, S., & Chattopadhyay, S. (2020). A theoretical insight on the rigid hydrogen-bonded network in the solid state structure of two zinc (ii) complexes and their strong fluorescence behaviors. *CrystEngComm*, *22*(17), 3005–3019. https://doi.org/10.1039/D0CE00125B

Mousavi, S. S., Karami, A., Haghighi, T. M., Tumilaar, S. G., Idroes, R., Mahmud, S., Celik, I., Ağagündüz, D., Tallei, T. E., & Emran, T. B. (2021). In silico evaluation of Iranian medicinal plant phytoconstituents as inhibitors against main protease and the receptor-binding domain of SARS-CoV-2. *Molecules*, *26*(18), 5724. https://doi.org/10.3390/molecules26185724

Nasution, M. A. F., Toepak, E. P., Alkaff, A. H., & Tambunan, U. S. F. (2018). Flexible docking-based molecular dynamics simulation of natural product compounds and Ebola virus Nucleocapsid (EBOV NP): A computational approach to discover new drug for combating Ebola. *BMC Bioinformatics*, *19*(Suppl 14), 419. https://doi.org/10.1186/s12859-018-2387-8

Ogbole, O. O., Akinleye, T. E., Segun, P. A., Faleye, T. C., & Adeniji, A. J. (2018). In vitro antiviral activity of twenty-seven medicinal plant extracts from Southwest Nigeria against three serotypes of echoviruses. *Virology Journal*, *15*(1), 110. https://doi.org/10.1186/s12985-018-1022-7

Ogu, C. C., & Maxa, J. L. (2000). Drug interactions due to cytochrome P450. *Proceedings (Baylor University. Medical Center)*, *13*(4), 421–423. https://doi.org/10.1080/08998280.2000.11927719

Osuntokun, O. T. (2020). Synergistic efficacy of Aframomum melegueta [Roscoe] K. Schum and Spondias mombin (Linn), A predictive treatment of SARS-CoV-2 (COVID-19) infection. *Journal of Bioscience & Biomedical Engineering (JB & Bio Engine*, *1*(2), 1–8.

Parab, A., Kaur, G., Sharma, A., Bhuller, G., Chitnis, S., Chindaliya, A., & Weta, M. (2021). Re-profiling of US-FDA approved drugs for COVID-19 by in-silico studies. *Journal of Bioinformatics and Systems Biology*, *04*(02), 50–73. https://doi.org/10.26502/jbsb.5107021

Patil, R., Das, S., Stanley, A., Yadav, L., Sudhakar, A., & Varma, A. K. (2010). Optimized hydrophobic interactions and hydrogen bonding at the target-ligand interface leads the pathways of drug-designing. *PloS One*, *5*(8), e12029. https://doi.org/10.1371/journal.pone.0012029

Pettersen, E. F., Goddard, T. D., Huang, C. C., Couch, G. S., Greenblatt, D. M., Meng, E. C., & Ferrin, T. E. (2004). UCSF Chimera—a visualization system for exploratory research and analysis. *Journal of Computational Chemistry*, *25*(13), 1605–1612. https://doi.org/10.1002/jcc.20084

Rakshit, M., Muduli, S., Srivastav, P. P., & Mishra, S. (2022). Pomegranate peel polyphenols prophylaxis against SARS-CoV-2 main protease by in-silico docking and molecular dynamics study. *Journal of Biomolecular Structure & Dynamics*, *40*(23), 12917–12931. https://doi.org/10.1080/07391102.2021.1979427

Ramírez, D., & Caballero, J. (2016). Is it reliable to use common molecular docking methods for comparing the binding affinities of enantiomer pairs for their protein target? *International Journal of Molecular Sciences*, *17*(4), 525. https://doi.org/10.3390/ijms17040525

Rasool, N., Bakht, A., & Hussain, W. (2021). Analysis of inhibitor binding combined with reactivity studies to discover the potentially inhibiting phytochemicals targeting Chikungunya viral replication. *Current Drug Discovery Technologies*, *18*(3), 437–450. https://doi.org/10.2174/1570163817666200312102659

Remko, M., Boháč, A., & Kováčiková, L. (2011). Molecular structure, pKa, lipophilicity, solubility, absorption, polar surface area, and blood brain barrier penetration of some antiangiogenic agents. *Structural Chemistry*, *22*(3), 635–648. https://doi.org/10.1007/s11224-011-9741-z

Sabiu, S., Balogun, F. O., & Amoo, S. O. (2021). Phenolics profiling of Carpobrotus edulis (L.) NE Br. and insights into molecular dynamics of their significance in type 2 diabetes therapy and its retinopathy complication. *Molecules*, *26*(16), 4867. https://doi.org/10.3390/molecules26164867

Segun, P. A., Ogbole, O. O., Akinleye, T. E., Faleye, T. O., & Adeniji, A. J. (2021). In vitro anti-enteroviral activity of stilbenoids isolated from the leaves of Macaranga barteri. *Natural Product Research*, *35*(11), 1909–1913. https://doi.org/10.1080/14786419.2019.1644505

Shode, F., Idowu, A., Uhomoibhi, O., & Sabiu, S. (2022). Repurposing drugs and identification of inhibitors of integral proteins (spike protein and main protease) of SARS-CoV-2. *Journal of Biomolecular Structure & Dynamics*, *40*(14), 6587–6602. https://doi.org/10.1080/07391102.2021.1886993

Sindhu, T., & Srinivasan, P. (2015). Exploring the binding properties of agonists interacting with human TGR5 using structural modeling, molecular docking and dynamics simulations. *RSC Advances*, *5*(19), 14202–14213. https://doi.org/10.1039/C4RA16617E

Singh, S., Sk, M. F., Sonawane, A., Kar, P., & Sadhukhan, S. (2021). Plant-derived natural polyphenols as potential antiviral drugs against SARS-CoV-2 via RNA-dependent RNA polymerase (RdRp) inhibition: an in-silico analysis. *Journal of Biomolecular Structure & Dynamics*, *39*(16), 6249–6264. https://doi.org/10.1080/07391102.2020.1796810

Siqueira, E. M. d S., Lima, T. L. C., Boff, L., Lima, S. G. M., Lourenço, E. M. G., Ferreira, É. G., Barbosa, E. G., Machado, P. R. L., Farias, K. J. S., Ferreira, L. d S., Rocha, H. A. d O., Simões, C. M. O., & Zucolotto, S. M. (2020). Antiviral potential of Spondias mombin L. leaves extract against herpes simplex virus type-1 replication using in vitro and in silico approaches. *Planta Medica*, *86*(7), 505–515. https://doi.org/10.1055/a-1135-9066

Supian, S., Ahmad, M. A., Rozano, L., Chandradevan, M., & Ab Rahman, Z. (2022). Phyllanthus tenellus Roxb. and Kaempferia parviflora Wall. ex Baker compounds as inhibitors of SARS-CoV-2 main protease and RNA-dependent RNA polymerase: A molecular docking study. *Journal of Pharmacy & Pharmacognosy Research*, *10*(6), 1103–1116. https://doi.org/10.56499/jppres22.1485_10.6.1103

Talevi, A. (2018). Computer-aided drug design: An overview. *Methods in Molecular Biology (Clifton, N.J.)*, *1762*, 1–19. https://doi.org/10.1007/978-1-4939-7756-7_1

Thiel, V., Herold, J., Schelle, B., & Siddell, S. G. (2001). Viral replicase gene products suffice for coronavirus discontinuous transcription. *Journal of Virology*, *75*(14), 6676–6681. https://doi.org/10.1128/JVI.75.14.6676-6681.2001

Tripathi, S. K., Muttineni, R., & Singh, S. K. (2013). Extra precision docking, free energy calculation and molecular dynamics simulation studies of CDK2 inhibitors. *Journal of Theoretical Biology*, *334*, 87–100. https://doi.org/10.1016/j.jtbi.2013.05.014

Tsugawa, H., Cajka, T., Kind, T., Ma, Y., Higgins, B., Ikeda, K., Kanazawa, M., VanderGheynst, J., Fiehn, O., & Arita, M. (2015). MS-DIAL: Data-independent MS/MS deconvolution for comprehensive metabolome analysis. *Nature Methods*, *12*(6), 523–526. https://doi.org/10.1038/nmeth.3393

Tumskiy, R. S., & Tumskaia, A. V. (2021). Multistep rational molecular design and combined docking for discovery of novel classes of inhibitors of SARS-CoV-2 main protease 3CLpro. *Chemical Physics Letters*, *780*, 138894. https://doi.org/10.1016/j.cplett.2021.138894

Vamathevan, J., Clark, D., Czodrowski, P., Dunham, I., Ferran, E., Lee, G., Li, B., Madabhushi, A., Shah, P., Spitzer, M., & Zhao, S. (2019). Applications of machine learning in drug discovery and development. *Nature Reviews. Drug Discovery*, *18*(6), 463–477. https://doi.org/10.1038/s41573-019-0024-5

Van der Merwe, D., Swan, G., & Botha, C. (2001). Use of ethnoveterinary medicinal plants in cattle by Setswana-speaking people in the Madikwe area of the North West Province of South Africa. *Journal of the South African Veterinary Association*, *72*(4), 189–196. https://doi.org/10.4102/jsava.v72i4.651

Vardhan, S., & Sahoo, S. K. (2022). Computational studies on the interaction of SARS-CoV-2 Omicron SGp RBD with human receptor ACE2, limonin and glycyrrhizic acid. *Computers in Biology and Medicine*, *144*, 105367. https://doi.org/10.1016/j.compbiomed.2022.105367

Verma, A. K., Ahmed, S. F., Hossain, M. S., Bhojiya, A. A., Mathur, A., Upadhyay, S. K., Srivastava, A. K., Vishvakarma, N. K., Barik, M., Rahaman, M. M., & Bahadur, N. M. (2022). Molecular docking and simulation studies of flavonoid compounds against PBP-2a of methicillin-resistant Staphylococcus aureus. *Journal of Biomolecular Structure & Dynamics*, *40*(21), 10561–10577. https://doi.org/10.1080/07391102.2021.1944911

Vernon, J. A., Golec, J. H., & DiMasi, J. A. (2010). Drug development costs when financial risk is measured using the Fama–French three-factor model. *Health Economics*, *19*(8), 1002–1005. https://doi.org/10.1002/hec.1538

Wang, C., Horby, P. W., Hayden, F. G., & Gao, G. F. (2020). A novel coronavirus outbreak of global health concern. *Lancet (London, England)*, *395*(10223), 470–473. https://doi.org/10.1016/S0140-6736(20)30185-9

Wong, C. H., Siah, K. W., & Lo, A. W. (2019). Estimation of clinical trial success rates and related parameters. *Biostatistics (Oxford, England)*, *20*(2), 273–286. https://doi.org/10.1093/biostatistics/kxx069

World Health Organization. (2023). Coronavirus disease (COVID-19) weekly epidemiological update and weekly operational update. *Weekly Epidemiological Update and Weekly Operational Update*. https://www.who.int/emergencies/diseases/novel-coronavirus-2019/situation-reports.

Wrapp, D., De Vlieger, D., Corbett, K. S., Torres, G. M., Wang, N., Van Breedam, W., Roose, K., van Schie, L., Hoffmann, M., Pöhlmann, S., Graham, B. S., Callewaert, N., Schepens, B., Saelens, X., & McLellan, J. S; VIB-CMB COVID-19 Response Team. (2020). Structural basis for potent neutralization of betacoronaviruses by single-domain camelid antibodies. *Cell*, *181*(5), 1004–1015. e1015. https://doi.org/10.1016/j.cell.2020.04.031

Yang, H., Yang, M., Ding, Y., Liu, Y., Lou, Z., Zhou, Z., Sun, L., Mo, L., Ye, S., Pang, H., Gao, G. F., Anand, K., Bartlam, M., Hilgenfeld, R., & Rao, Z. (2003). The crystal structures of severe acute respiratory syndrome virus main protease and its complex with an inhibitor. *Proceedings of the National Academy of Sciences of the United States of America*, *100*(23), 13190–13195. https://doi.org/10.1073/pnas.1835675100

Zhang, D., & Lazim, R. (2017). Application of conventional molecular dynamics simulation in evaluating the stability of apomyoglobin in urea solution. *Scientific Reports*, *7*(1), 44651. https://doi.org/10.1038/srep44651

4.3 Computational bioprospection of selected plant secondary metabolites against VP7 (capsid protein) of rotavirus A

This article has been published in Scientific African and presented accordingly

Scientific African 23 (2024) e02109

Contents lists available at ScienceDirect

Scientific African

journal homepage: www.elsevier.com/locate/sciaf

Computational bioprospection of selected plant secondary metabolites against VP7 (capsid protein) of rotavirus A

Adedayo Ayodeji Lanrewaju, Abimbola Motunrayo Enitan-Folami, Saheed Sabiu *, Feroz Mahomed Swalaha

Department of Biotechnology and Food Science, Faculty of Applied Science, Durban University of Technology, P. O. Box 1334, Durban 4000, South Africa

ARTICLE INFO

Editor: DR B Gyampoh

Keywords:
VP7 epitopes
Capsid protein
Binding free energy
Thermodynamic stability
Molecular dynamics simulation

ABSTRACT

Despite the global implementation of prequalified oral vaccines by the World Health Organization (WHO) in numerous countries, rotavirus A (RVA) have continued to be the principal cause of acute dehydrating diarrhoea in children under five years of age. Unfortunately, there are no authorized anti-rotaviral medications. Hence, it is crucial to prioritize the development of specialized therapeutics to combat rotaviral infections. For the first time, *Spondias mombin, Macaranga barteri* and *Dicerocaryum eriocarpum* metabolites were screened using computational techniques to identify potential novel modulators with broad-spectrum activity against VP7 epitopes (capsid protein) of RVA. Compounds with poor pharmacokinetics and drug-likeness were screened out from the initial top 20 metabolites identified using molecular docking. Thereafter, molecular dynamics (MD) simulation was used to assess the ability of the resulting compounds to modulate the selected VP7 epitopes. Remarkably, all the lead compounds had higher negative binding free energy than tizoxanide across the three epitopes of VP7, with apigenin-4′-glucoside having the highest affinity for VP7A (−24.13 kcal/mol) and VP7C (−43.67 kcal/mol) while the highest affinity for VP7D was observed in 2SG (−36.08 kcal/mol). Interestingly, 2SG (−18.24 kcal/mol, −31.21 kcal/mol, −36.08 kcal/mol), apigenin-4′-glucoside (−24.13 kcal/mol, −43.67 kcal/mol, −33.52 kcal/mol) and gnetin L (−21.21 kcal/mol, −27.56 kcal/mol, −32.48 kcal/mol) had better broad-spectrum affinities for VP7A, C and D relative to tizoxanide (−10.36 kcal/mol, −18.32 kcal/mol, −12.98 kcal/mol) respectively. Generally, the compounds are thermodynamically stable with 2SG (1.88 Å), ellagic acid (2.45 Å) and sericetin (2.22 Å) being the most stable against VP7A, C and D respectively. While this study unearths the lead compounds' promising ability to modulate the investigated VP7 epitopes, further confirmatory in vitro and in vivo studies are imperative, and efforts are underway towards achieving this task.

Introduction

Rotavirus (RV) infection is responsible for an estimated 258 million cases of infectious diarrhoea in children under five years, worldwide [1]. RV-diarrhoea was implicated in approximately 122,000–215,000 deaths of children annually between 2013 and 2017 [2]. Specifically, RVA remains a persistent cause of diarrhoea-mortality among children under five years [3,4]. Even though

* Corresponding author.
E-mail address: sabius@dut.ac.za (S. Sabiu).

https://doi.org/10.1016/j.sciaf.2024.e02109
Received 17 December 2023; Received in revised form 6 January 2024; Accepted 26 January 2024
Available online 2 February 2024
2468-2276/© 2024 The Author(s). Published by Elsevier B.V. This is an open access article under the CC BY-NC-ND license (http://creativecommons.org/licenses/by-nc-nd/4.0/).

implementing rotavirus immunization initiatives has resulted in a 60 % decrease in mortality, the vaccine's effectiveness in developing countries remains relatively low [5]. To date, the main approach for treating RVA-induced diarrhoea remains oral and intravenous rehydration; nevertheless, this method only provides symptomatic therapy and does not mitigate the duration or intensity of diarrhoea [6]. Unfortunately, there is currently no approved and effective antiviral medication to treat RVA infection; hence, there is a need to prioritize the development of anti-RVA drugs.

Rotavirus, a non-enveloped icosahedral-shaped double-stranded RNA (dsRNA) virus, belongs to the family Reoviridae with a multilayered virion composed of 11 segments coding for six structural proteins (VP1-4, VP6 and VP7) and six non-structural proteins (NSP1-NSP6) [7]. The highly immunogenic outer capsid glycoprotein VP7 stimulates the production of neutralizing antibodies and plays a crucial role in the attachment of the virus to the host cell [8]. Owing to the involvement of VP7 in the virus' attachment, pathogenesis and abundance on the viral surface, targeting and destabilizing it could be logical in deactivating RVA prior to its entry into host cells [9] and makes it an attractive therapeutic target for drug bioprospection and development.

Nature has provided humanity with useful products with low toxicity and minimal side effects to treat illnesses [10]. The possible antiviral capabilities of several plant species and constituents have been evaluated [11]. Studies have demonstrated the antiviral properties of *Rubia cordifolia* [12] and *Rindera lanata* [13] against RV *in vitro*. Furthermore, the notable antiviral activity of *Spondias mombin* against coxsackie and herpes simplex viruses [14,15] and *Macaranga barteri* against herpes simplex virus type-1viruses, echoviruses E7 and E19 [16,17] have been reported. In addition, *Dicerocaryum eriocarpum* exhibits a wide range of applications in traditional medicine, such as in treating wounds, facilitation of placenta expulsion, antibacterial activity [18], anti-inflammatory effects and ethnoveterinary uses [19]. Interestingly, the modulatory potential of the secondary metabolites of the three plants against VP5* and VP8* of RVA *in silico* has been reported [20]. Therefore, this study investigated the therapeutic potential of *S. mombin, M. barteri*, and *D. eriocarpum* secondary metabolites against the VP7 protein of RVA to identify promising compounds that could be further developed as drugs to manage/treat RVA-induced diarrhoea. The conventional approach to drug discovery involves the identification of potential drug candidates through trial-and-error screening procedure which is often characterized by its lengthy duration, substantial expenses, and significant likelihood of unsuccessful outcomes [21]. Consequently, by employing computational techniques, such as modern computer-aided molecular screening tools, researchers have successfully found lead compounds derived from plant secondary metabolites that exhibit noteworthy antiviral properties [8,22-24]. Therefore, this study forms part of the continuing efforts to develop anti-RVA drugs and adopted a computational structure-activity relationship approach on the secondary metabolites of the selected medicinal plants with proven antiviral activity through molecular docking, density functional theory (DFT), and MD simulation strategies (Fig. 1) to identify broad-spectrum compounds against the VP7 epitopes of RVA.

Materials and methods

Target protein acquisition and optimization

The X-ray crystal structure of VP7 (3FMG) was downloaded from the Protein Data Bank https://www.rcsb.orgs/ (accessed on 26 April

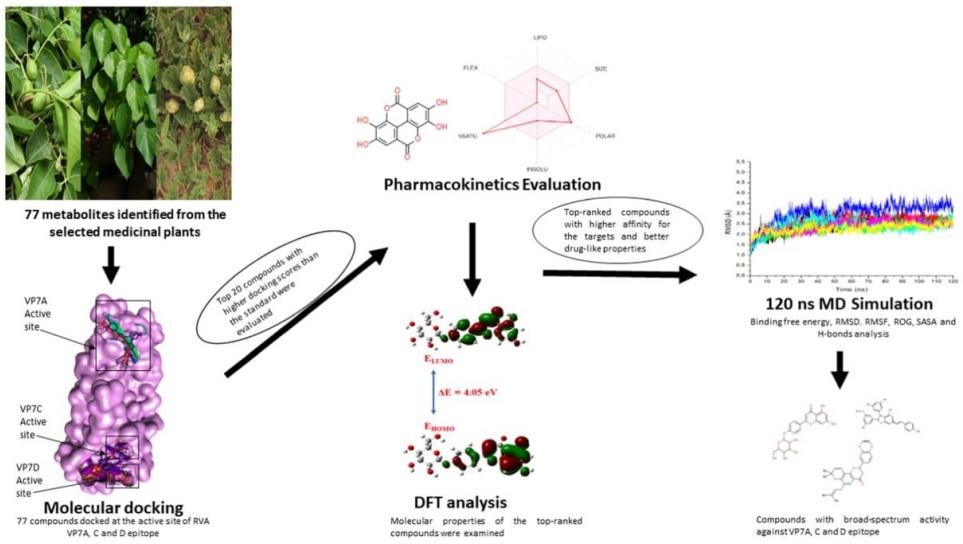


Fig. 1. Workflow of the concept adopted in this study.

2023). The VP7 protein exhibits a propensity for undergoing structural reconfiguration, while four prominent conserved polypeptide sequences (epitopes) have been identified within its chain A. Three epitopes (A, C and D) are potentially important for drug discovery and development due to their involvement in the interactions between the VP7 chains and the VP6 of RVA. By utilizing these conserved sequences, it is possible to disrupt the stability of VP7, prevent its interaction with VP6, and circumvent the structural reconfiguration of VP7 [25]. The protein structure was optimized as previously reported [26] using the UCSF Chimera v1.15 software [27].

Optimization of ligand

The 3D structures of the ligands; 77 secondary metabolites reported from the three selected plants (*S. mombin, M. barteri* and *D. eriocarpum*) [28] and the reference standard (tizoxanide) [29] were acquired from Pubchem (https://pubchem.ncbi.nlm.nih.gov/ (accessed on 11 September 2022)). The ligands and reference standard were optimized using the Open Babel plugin in Python Prescription (PyRx) v 0.9.5. and the universal force field (UFF) in 200 steps [30] before being saved in PDBQT format.

Molecular docking and validation

The optimized ligands and prepared protein were docked using PyRx v 0.9.5 [30]. The docking procedure entailed the selection of amino residues at the active site of the protein of the selected VP7 epitopes as previously reported [8,25] with the *x-y-z* coordinates; VP7A [centre (*X*: 24.02; *Y*: 96.82; *Z*: 18.38)], VP7C [centre (*X*: 3.34; *Y*: 114.16; *Z*: −3.73)] and VP7D [centre (*X*: −2.95; *Y*: 114.16; *Z*: 19.54)]. The standard was used as a point of reference for comparing the ligands that exhibited the greatest binding affinity at the receptor binding domain (RBD) of the protein and served as a criterion for choosing ligands with the greatest affinity for the respective epitopes. Thereafter, the techniques of redocking and superimposition were used to evaluate the docking process, ensuring its precision and reliability by mitigating the occurrence of false positive results. Briefly, the top-ranked ligands and tizoxanide (reference standard) were redocked into the RBD of the native protein to evaluate the ability of the AutoDock program to accurately replicate the ligand's orientation and location in the crystal structure [8].

Pharmacokinetic assessment

The physicochemical characteristics, pharmacokinetics, and drug-likeness of 20 compounds with the top docking score were predicted by using SwissADME web (http://swissadme.ch/index.php (accessed on 18 August 2023)). In addition, the Protox II webserver (https://tox-new.charite.de/protox_II/ (accessed on 18 August 2023)) was used to evaluate their toxicity profiles. The results of these assessments were employed to reduce the numbers to six, four and six for VP7A, C and D respectively. Subsequently, the docked complex of the top-scoring compounds with the lowest energy minimization was acquired from their corresponding PDB files and used for MD simulation.

Quantum chemical calculations

The reactivity of the top-ranked compounds was evaluated by conducting quantum chemical calculations using DFT. The electronic characteristics of the compounds were evaluated using the DFT approach in Gaussian 16 suite. Owing to its accuracy and lower computational requirements, the Becke3-Lee–Yang–Parr (B3LYP) method combined with the 6–31 + G(d,p) basis set was employed to optimize the top-ranked compounds [31]. Gauss View v 6.0 was used to view the output files. The energies of frontier highest occupied molecular orbital (HOMO) and lowest unoccupied molecular orbital (LUMO), taking into consideration the Parr and Pearson interpretation [32], were calculated. Thereafter, other chemical descriptors such as energy gap (ΔE), ionization energy (I), electron affinity (A), chemical hardness (η), softness (δ), electronegativity (χ), chemical potential (Cp), global electrophilicity (ω) were calculated using the equations below as described previously [33].

$$\Delta E = E_{\mathrm{LUMO}} - E_{\mathrm{HOMO}} \tag{1}$$

$$I = -E_{\mathrm{LUMO}} \tag{2}$$

$$A = -E_{\mathrm{HOMO}} \tag{3}$$

$$\eta = \frac{\Delta \mathrm{E}}{2} \tag{4}$$

$$\delta = 1/(\eta) \tag{5}$$

$$\chi = \frac{(I + A)}{2} \tag{6}$$

$$Cp = -\chi \tag{7}$$

$$\omega = \frac{\chi^2}{\Delta E} \tag{8}$$

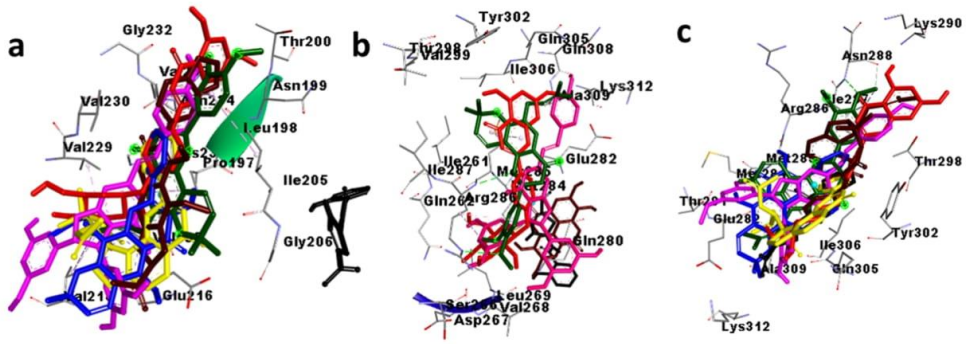


Fig. 2. The superimposition and interactions of the top-hit compounds at the active site of the crystal structure of (a) VP7A (2SG (green), apigenin-4′-glucoside (red), glabrescin (brown), glabratephrin (yellow), gnetin L (pink), sericetin (blue) and reference standard (black)) (b) C (2SG (green), apigenin-4′-glucoside (red), ellagic acid (brown), gnetin L (blue) and reference standard (black)) (c) D (2SG (green), apigenin-4′-glucoside (red), edulisin I (brown), glabratephrin (yellow), gnetin L (pink), sericetin (blue) and reference standard (black)). (For interpretation of the references to color in this figure legend, the reader is referred to the web version of this article.)

MD simulation

The MD simulation was conducted as previously reported [34]. The AMBER 18 software suite was utilized for the simulation conducted for 120 ns. The FF18SB variant of the AMBER 18 package was employed to depict the operating systems. The atomic partial charges of the ligands were generated through the utilization of ANTECHAMBER, which used the GAFF (general amber force field) and RESP (restrained electrostatic potential) methods for calculating measures, respectively. The systems were neutralized using the Leap Module's hydrogen atoms, Na^+ and Cl^- counter ions. The amino acid residues were numbered accordingly (1–312), and the systems were contained within a TIP3P orthorhombic box of water molecules to ensure that all atoms were within 10 Å of the box edge. A restriction potential of 500 kcal/mol was utilized for an initial minimization of 2000 steps in each simulation. The steepest descent technique was used for 990 steps, followed by 990 steps using conjugate degrees. An additional 990 steps of full minimization without any limitations were executed using the conjugate gradient method. The simulations involved gradually heating MD systems from 0 to 300 K for 50 ps while ensuring that the number of atoms and volume remained constant. The systems' solutes were subjected to a potential harmonic restraint of 10 kcal/mol and a collision frequency of 1.0 ps. Following this, every system was equilibrated for approximately 500 ps, during which the temperature was maintained consistently at 300 K. The SHAKE algorithm was adopted to impose restraints on the hydrogen bond atoms in every simulation. In each instance, the simulation was conducted with a 2 fs temporal resolution, consistent with the NPT (isobaric-isothermal ensemble) using randomised seeding with temperature at 300 K, constant pressure of 1 bar and a pressure-coupling constant of 2 ps (Langevin thermostat). Thereafter, the 120 ns MD simulation outcomes were adopted as post-dynamic data.

The post-MD simulation was conducted as previously described [34]. After conducting the simulation, the coordinates of the systems were combined and analyzed using the AMBER 18 PTRAJ module. The examination of root mean square fluctuation (RMSF), radius of gyration (ROG), root mean square deviation (RMSD), solvent-accessible surface area (SASA) and hydrogen bonds (H-bonds) analysis (number, distance and angle) were executed using the CPPTRAJ module and their plots were constructed with Origin v 6.0 [35]. Similarly, the binding free energy was determined using an average of 120,000 snapshots from a 120 ns MD simulation trajectory. The molecular mechanics generalized born surface area (MMGBSA) approach was employed, using the equation $\Delta Gbind = Gcomplex - (Greceptor + Gligand)$.

Results and discussion

Molecular docking

The molecular docking approach is often employed to assess the binding interactions of ligands and proteins. This technique evaluates compounds by their docking scores and discerns the crucial interactions between ligands and the binding domain of a target protein towards drug discovery and development [36]. In this study, the highest and lowest docking score against VP7A, VP7C and VP7D was observed in (2*S*)-6-(gamma,gamma-dimethylallyl)-3′,4′-dimethoxy-6″,6″-dimethylpyran[2″,3″:7,8]flavanone (2SG) (−7.2 kcal/mol) and 2-Isopropylmalic acid (−3.9 kcal/mol, mallotusinic acid (−8.8 kcal/mol) and bis(ethoxycarbonyloxymethyl) dodecanedioate (−4.6 kcal/mol), 3-(2,2-Dimethylpropoxymethoxy)-2-oxopropyl] 2-methylprop-2-enoate; [3-(3-methylbutan-2-yloxy)-2-oxopropyl] 2-methylprop-2-enoate; [3-(oxan-2-yloxy)-2-oxopropyl] 2-methylprop-2-enoate (3DO) (−8.1 kcal/mol) and 2-Isopropylmalic acid (−3.9 kcal/mol) respectively (Supplementary Table S1). The top twenty compounds with higher docking scores ranging from −7.2 to −6.2 kcal/mol (VP7A), −8.8 to −7.4 kcal/mol (VP7C) and −8.1 to 6.8 kcal/mol (VP7D) compared to the

Table 1
The cDFT parameters of top-ranked compounds against VP7A, C and D.

	cDFT parameters (eV)									
Ligands	LUMO	HOMO	Energy gap	Ionization energy	Electron affinity	Hardness	Softness	Electronegativity	Chemical potential	Global electrophilicity
Edulisin I	−1.89	−6.07	4.19	1.89	6.07	2.09	0.48	3.98	−3.98	3.78
Glabratephrin	−1.99	−6.52	4.52	1.99	6.52	2.26	0.44	4.26	−4.26	4.01
Glabrescin	−1.88	−5.51	3.64	1.88	5.51	1.82	0.55	3.69	−3.69	3.76

standard [tizoxanide (−5.5 kcal/mol), (−5.5 kcal/mol) and (−5.8 kcal/mol)] targeted against VP7A, C and D were selected respectively (Supplementary Table S2). The compounds' higher docking scores compared to the reference standard may indicate their potential affinity for the respective epitopes.

Verification of the docking protocol

The docking procedure pose was validated by superimposing the top-ranked compounds on the crystal structure of the native VP7 protein, though it lacks a co-crystallized ligand. Fig. 2 illustrates the overlapping and interplay between the highest-ranked compounds and the reference standard at the binding domain of the examined VP7 epitopes. All the top-hit compounds shared similar binding orientations against VP7A epitope except tizoxanide on the VP7 crystal structure (Fig. 1(a)). Of all the residues at the active site of the VP7A epitope (Lys194-Cys207), the top-ranked compounds shared a similar binding pose and interacted with Val195, Pro197, Leu 198, Asn199 and Thr200. Conversely, tizoxanide was observed to have partial occupancy at the binding pocket of the VP7A epitope, and interacted with Pro197, Ile205 and Gly206. Similarly, against VP7C, 2SG, apigenin-4′-glucoside and gnetin L shared a similar binding orientation interacting with Gln280, Glu282, Met284, Met285, Arg286 of all the residues at the active site of VP7C epitope (Ala273–Arg286) while ellagic and tizoxanide having a partial occupancy at the binding pocket of the VP7C interacted with Gln280, Gln282 and Met284 (Fig. 1(b)). Remarkably, all the top-ranked compounds and the reference standard had similar binding pose interacting with Tyr302, Gln305, Ile306, Ala309 and Lys312 of all the amino acids at the binding site of VP7D (Val300–Lys312) (Fig. 1 (c)). Interestingly, the observed amino acids interactions in VP7A, C and D against the investigated compounds are consistent with those reported in previous studies [8,25]. This observation establishes that the docking scores exhibited by the compounds and the reference standard could be a function of their interactions with the residues at the active site of the examined VP7 epitopes and consequently confirms the reliability of the employed docking procedure.

Prediction of pharmacokinetics, drug-likeness, physicochemical and toxicity properties

Apart from establishing favourable interaction with the intended target, an efficacious therapeutic molecule should possess good pharmacokinetic attributes while minimizing potential toxicities and adverse effects [37]. The identification of molecules with significant biological activity and favourable pharmacokinetic characteristics constitutes a paramount concern in drug design [38]. Despite the significant biological activity shown by several compounds, their therapeutic use is hindered by inadequate absorption, distribution, metabolism, excretion and toxicity (ADMET) characteristics. Therefore, ADMET prediction has emerged as a prominent research focus within the realm of computer-aided drug molecular design [39], owing to its significance in meeting the demands of drug design and reduction of several probable safety issues, thereby accelerating the drug development procedure.

According to Lipinski's rule of five (Ro5), bioactive molecules are required to adhere to limitations on their molecular weight (500 g/mol), hydrogen donor (5), hydrogen acceptor (10), and octanol co-efficient (5) as molecules with less than two violations would be orally accessible [40]. Of all the twenty top-scoring compounds against VP7A selected for ADMET analysis, 2SG, 6 MM, glabratephrin, gnetin L, sericetin, apigenin-4′-glucoside and glabrescin passed the Ro5 with 0, 1, 0, 0, 0, 1 and 0 violations respectively (Table 1) while gnetin L, 2SG, apigenin-4′-glucoside and ellagic acid passed the Ro5 with 0, 0, 1 and 0 violations respectively. Similarly, gnetin L, 6 MM, edulisin I, sericetin, 2SG, glabratephrin and apigenin-4′-glucoside passed the Ro5 with 0, 1, 0, 0, 0, 0 and 1 violations respectively, of all the top-scoring compounds against VP7D (Table 1) while tizoxanide (reference standard) passed the Ro5 with 0 violation. Therefore, these compounds with less than 2 violations display their potential to be orally bioavailable, indicating their capacity to reach target cells, tissues or organs and exert their pharmacological effects.

The assessment of a drug's bioavailability score is a crucial pharmacokinetic characteristic that must be considered when determining the right dosage for a medication. The quantity of the unaltered drug quantity that reaches the systemic circulation, based on a specific rate of absorption, is determined by the bioavailability score of a medication [41]. All the top-scoring compounds against the investigated targets that passed the Ro5 and tizoxanide (reference standard) had a bioavailability score of 0.55, indicating their potential to be developed as oral drugs [42].

To evaluate the toxicity profile of drugs, cytochrome P450 (CYP450), a key isoenzyme in drug metabolism, is crucial [43]. In this study, only apigenin-4′-glucoside is not an inhibitor of all the CYP450 isoenzymes, suggesting its inability to initiate any drug-drug interactions when co-administered with other drugs normally metabolised by the CYP450 isoenzymes of all the top-ranked compounds across the investigated targets. Conversely, other top-ranked compounds inhibited at least one or more CYP450 isoenzymes, indicating that they could interact with other medications processed by such enzymes. Furthermore, all the top-ranked compounds were active for at least one toxicity endpoint or the other (Supplementary Table S2).

In addition, the top-ranked compounds belonged to drug toxicity classes 4 and 5, suitable for drug development [44], however 6MM belonged to drug toxicity class 2, which is inappropriate for drug development; hence, it was excluded from subsequent investigations. These findings indicate the need for structural alterations of the top-ranked compounds to improve their druggability. In general, the top-ranked compounds exhibited favourable medicinal and pharmacokinetic characteristics, possess drug-like properties, and could be modified to enhance their suitability into being developed as drugs while reducing their toxicity.

Frontier molecular orbital properties

The cDFT parameters of the top-ranked compounds were calculated to investigate their molecular properties that could be of therapeutic significance. The HOMO and LUMO orbitals are widely acknowledged as significant indicators for predicting the chemical

and biological reactivity of chemical species. The HOMO is the electron-filled outermost orbital, which donates an electron to the protein to make a bond that blocks the active site of the protein in pathogens. Conversely, the LUMO is the first empty innermost orbital that is not filled with electrons, which acts as an electron acceptor or positive charge carrier to heavier parts where the nucleophilic part of a protein can be attacked [45]. A compound exhibiting a larger energy gap (LUMO-HOMO) indicates the less reactive nature of the compound, while a smaller energy gap corresponds to increased reactivity and heightened biological activity of the compound [46]. The cDFT parameters of 2SG, sericetin, apigenin-4′-glucoside, ellagic acid, gnetin L and tizoxanide have been previously reported [20], while that of edulisin I, glabratephrin and glabrescin are presented in Table 1.

The lowest energy gap was observed in sericetin (3.57 eV) and could have contributed to its reactivity, while glabratephrin (4.52 eV) exhibited the largest energy gap (Fig. 3), and could have been responsible for its low binding free energy after tizoxanide against VP7A and D. Chemical hardness linked to reactivity, measures the ability of a compound to withstand alterations in electron distribution. This parameter serves as a dependable measure for assessing chemical stability and holds significant importance in drug design [47]. An elevated level of chemical softness and a diminished level of chemical hardness are indicative of increased compound reactivity [48]. Therefore, the reactivity of sericetin against VP7A and D could be attributed to its chemical softness and hardness being the highest and lowest, respectively.

Another quantitative parameter is electronegativity, which measures the relative distribution of electrons in a molecule. The highest electronegativity value was observed in tizoxanide (5.07 eV), while ellagic acid (4.37 eV), glabratephrin (4.26 eV) and apigenin-4′-glucoside (4.23 eV) are next to tizoxanide against VP7 (Table 1). Remarkably, the lead compounds possess elevated electronegativity levels, indicating their effectiveness in accepting electrons. In addition, the electrophilicity index characterizes the propensity of an electrophile to attract a specific quantity of electron density and the capacity of a molecule to resist the transfer of electron density [48]. Molecules are classified into low (<0.8 eV), moderate (0.8–1.5 eV) and heavy (>1.5 eV) electrophiles based on their electrophilicity values [49]. Remarkably, all the top-hit compounds and tizoxanide are heavy electrophiles, thus implying a substantial presence of electrophiles.

MMGBSA-based binding free energy of the top-ranked compounds

Generally, the molecular docking approach ranks the feasible poses of a ligand in a binding pocket based on a scoring function, and the accuracy of these scoring functions has been improved using the MMGBSA approach [50]. This approach facilitates the integration of high-throughput MD simulations with the determination of binding free energies associated with protein-ligand interactions [51]. The thermodynamic binding free energy is a measure of the energy difference between a complex and its unbound components, as a more negative value indicates a stronger affinity of the ligand towards the protein [52]. In this study, all the lead compounds had higher negative binding free energy than tizoxanide across the three epitopes of VP7 with apigenin-4′-glucoside having the highest affinity for VP7A (−24.13 kcal/mol) and VP7C (−43.67 kcal/mol) while the highest affinity for VP7D was observed with 2SG (−36.08 kcal/mol). Interestingly, 2SG (−18.24 kcal/mol, −31.21 kcal/mol, −36.08 kcal/mol), apigenin-4′-glucoside (−24.13 kcal/mol, −43.67 kcal/mol, −33.52 kcal/mol) and gnetin L (−21.21 kcal/mol, −27.56 kcal/mol, −32.48 kcal/mol) had better broad-spectrum affinities for VP7A, C and D relative to tizoxanide (−10.36 kcal/mol, −18.32 kcal/mol, −12.98 kcal/mol) respectively (Table 2). This observation is in tandem with our previous study, where the secondary metabolites of selected medicinal plants exhibited different capacities at modulating both the VP5* and VP8* of RVA and specifically with sericetin and 2SG having a broad-spectrum affinity against both targets [20]. In general, the binding free energy results demonstrated the superiority of the top-ranked compounds over tizoxanide towards the management of RVA-induced diarrhoea.

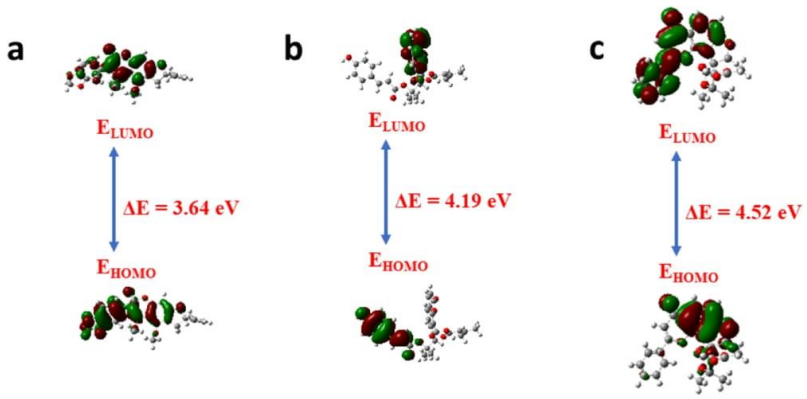


Fig. 3. Frontier molecular orbitals for (a) glabrescin (b) edulisin I (c) glabratephrin.

Stability, fluctuation compactness, protein surface conformation and H-bonds analysis of the simulated complexes

The RMSD is an essential metric used in the assessment of structural variations in protein structures, providing insights into the stability of the protein upon ligand binding over a certain period [53]. A reduced average RMSD value indicates enhanced stability of a protein-ligand combination during simulation, which implies a favourable capacity of the ligand to modulate the protein [54]. In this study, each complex exhibited unique pathways and varied patterns of variation, resulting in varying mean RMSD values after equilibrating at 4 ns, 10 ns and 3 ns for VP7A, C and D complexes, respectively (Fig. 4). Sericetin-VP7A and glabrescin-VP7A exhibited the highest fluctuation at 37 ns (4.9 Å) and 68 ns (5.8 Å) against VP7A while gnetin L-VP7C and 2SG-VP7C exhibited the highest fluctuation at 84 ns (6.1 Å) and 116 ns (5.4 Å) against VP7C (Fig. 3(a) and (b)). Also, the highest fluctuation against VP7D was observed in gnetin L-VP7D at 26 ns (6.0 Å) and edulisin I-VP7D at 75 ns (5.8 Å) (Fig. 4(c)). Expectedly, the observed fluctuations resulted in increased mean RMSD values in the highlighted ligands against VP7A (sericetin-3.56 Å and glabrescin-3.66 Å), VP7C (gnetin L-3.87 Å) and VP7D (gnetin L-4.14 Å and edulisin I-3.66 Å) except 2SG-VP7C (2.69 Å) which could be due to the short fluctuation moment exhibited by its complex during the simulation as opposed to other ligands (Table 3). Unfortunately, the observed increased average RMSD values were marginally above the acceptable 3 Å limit [55], suggesting probable reduced stability of those complexes. Other complexes with slightly higher average RMSD values above the acceptable limit of 3 Å but with considerable fluctuation patterns include VP7A (apigenin-4′-glucoside and glabratephrin) and VP7D (2SG, apigenin-4′-glucoside and tizoxanide). The lowest RMSD value against VP7A was observed in 2SG-VP7A (1.88 Å), followed by gnetin L-VP7A (2.33 Å), tizoxanide-VP7A (2.82 Å), apigenin-VP7A (3.09 Å) and glabratephrin-VP7A (3.11 Å) all of which are lower than the apo-VP7A (3.42 Å) suggesting their ability to confer reasonable stability on the protein upon binding (Table 3). Against VP7C, ellagic acid-VP7C (2.45 Å) had the lowest average RMSD value followed by 2SG-VP7C (2.69 Å), which are lesser than that of the unbound VP7C (2.87 Å) indicating their potential to enhance the stability of the protein. In addition, both glabratephrin-VP7D (2.82 Å) and sericetin-VP7D (2.22 Å) have lower mean RMSD values relative to the reference standard-tizoxanide (3.20 Å) and unbound VP7D (2.99 Å) (Table 3). This observation corroborates that of Aribisala et al. [21], in which ligand binding unto ParE resulted in reduced average RMSD value relative to the unbound ParE. This finding further suggests that these metabolites are better inhibitors compared to the reference standard and enhance the stability of the protein compared to the apo-protein. Conversely, apigenin-4′-glucoside-VP7C (2.91 Å) had a higher average RMSD value than the apo-protein (2.87 Å) (Table 3), but it is still within the 3.0 Å acceptable limit. This finding aligns with a previous study that revealed an increase in the mean RMSD value due to the binding of verbascoside and the SARS-CoV-2 spike protein [52]. Generally, the average RMSD values of the complexes are in-consistent with the binding free energy results against the three investigated epitopes however, most of the reported RMSD values were within the acceptable 3 Å limit while the complexes with RMSD values above the 3 Å limit show minor deviations from their respective unbound proteins.

The RMSF was evaluated to comprehend the structural flexibility of the amino acids at the RBD of the VP7 epitopes upon the binding of ligands (Table 3). This metric considers the mean volatility of atoms and residues in a receptor during a simulation period

Table 2
MMGBSA-based binding free energy framework (kcal/mol) of the top-ranked compounds against VP7A, C and D.

	Energy components (kcal/mol)				
Ligands	ΔE_{vdW}	ΔE_{elec}	ΔG_{gas}	ΔG_{solv}	ΔG_{bind}
VP7A					
2SG	−23.36 ± 6.95	−3.74 ± 4.30	−27.09 ± 8.39	8.85 ± 4.27	−18.24 ± 6.31
Apigenin-4′-glucoside	−29.38 ± 5.30	−24.58 ± 11.80	−53.96 ± 12.11	29.83 ± 9.02	−24.13 ± 5.54
Glabrescin	−25.87 ± 5.15	−6.94 ± 8.01	−32.81 ± 9.85	13.34 ± −19.47	−19.47 ± 4.54
Glabratephrin	−21.35 ± 3.97	−2.21 ± 4.74	−23.57 ± 6.28	8.07 ± 4.55	−15.50 ± 3.52
Gnetin L	−26.78 ± 3.57	−11.25 ± 10.56	−38.05 ± 11.47	16.83 ± 8.75	−21.21 ± 4.57
Sericetin	−24.13 ± 8.11	−5.56 ± 5.24	−29.69 ± 11.58	11.26 ± 5.06	−18.42 ± 7.15
Tizoxanide	−14.05 ± 6.37	−240.47 ± 70.59	−254.53 ± 74.45	244.17 ± 70.64	−10.36 ± 5.10
VP7C					
2SG	−39.72 ± 3.69	−3.57 ± 3.69	−43.29 ± 5.20	12.09 ± 3.20	−31.21 ± 3.63
Apigenin-4′-glucoside	−39.65 ± 3.68	−59.91 ± 10.27	−99.56 ± 9.91	55.89 ± 7.67	−43.67 ± 3.85
Ellagic acid	−22.16 ± 4.95	−57.33 ± 12.80	−79.50 ± 10.80	47.80 ± 7.91	−31.69 ± 4.30
Gnetin L	−33.55 ± 8.47	−20.63 ± 10.47	−54.20 ± 11.78	26.64 ± 7.90	−27.56 ± 7.28
Tizoxanide	−20.71 ± 5.40	−276.39 ± 29.00	−297.10 ± 28.76	278.79 ± 26.72	−18.32 ± 5.71
VP7D					
2SG	−43.40 ± 5.36	−7.36 ± 3.42	−50.76 ± 6.66	14.67 ± 2.84	−36.08 ± 5.46
Apigenin-4′-glucoside	−30.41 ± 4.72	−60.02 ± 16.94	−90.43 ± 16.76	56.91 ± 11.44	−33.52 ± 6.46
Edulisin I	−37.02 ± 2.86	−9.87 ± 6.65	−46.90 ± 6.61	19.48 ± 5.52	−27.42 ± 2.83
Glabratephrin	−29.54 ± 4.65	−17.65 ± 5.24	−47.19 ± 8.63	24.71 ± 5.25	−22.48 ± 4.44
Gnetin L	−37.23 ± 3.46	−22.27 ± 8.95	−59.52 ± 8.58	27.04 ± 6.55	−32.48 ± 3.73
Sericetin	−30.89 ± 4.87	−2.34 ± 4.34	−33.24 ± 7.02	9.26 ± 3.88	−23.98 ± 5.13
Tizoxanide	−18.80 ± 7.35	−181.63 ± 44.02	−200.42 ± 47.86	187.45 ± 43.88	−12.98 ± 6.10

ΔE_{vdW} = van der Waals energy; ΔE_{elec} = electrostatic energy; ΔE_{gas} = gas phase free energy; ΔG_{sol} = solvation free energy; ΔG_{bind} = total binding free energy.

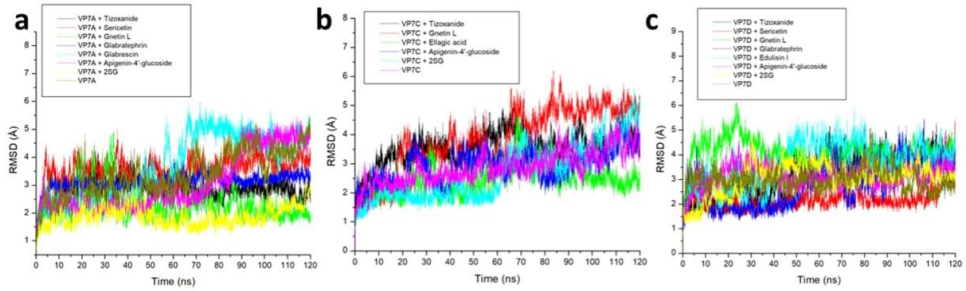


Fig. 4. Comparative RMSD plots of alpha-carbon, top-ranked compounds and reference standards against (a) VP7A (b) C and (c) D after 120 ns MD simulation period.

and can be associated with their ability to form stable intra and intermolecular bonds [56]. A reduction in volatility at the active site where ligand binding and catalysis take place corresponds to an increase in the strength of the binding and affinity between the ligand and the protein [54]. In this study, a relatively higher fluctuation between residues 180 and 245, 265 and 280 was observed in VP7A (Fig. 5(a)), suggesting the limited capacity of these residues to form stable bonds. Unfortunately, all the residues at the active site of VP7A were situated in the region of higher fluctuation (Fig. 5(a)); hence, the average RMSF values at the active site were higher than the whole VP7A (Tables 3 and 4). The unbound VP7A, tizoxanide, sericetin, gnetin L, glabratephrin, glabrescin, apigenin-4′-glucoside and 2SG had RMSF values of 3.05 and 1.74 Å, 2.22 and 1.67 Å, 2.01 and 1.83 Å, 2.39 and 1.74 Å, 1.97 and 1.57 Å, 4.81 and 2.53 Å, 3.19 and 2.11 Å, 2.09 and 1.70 Å respectively at the active site and in the whole protein (Tables 3 and 4). During the 120 ns simulation period, majority of the protein's active site fluctuation could be attributed to residues Asn199, Thr200, Gln201, Thr202, Leu203, Gly204, Ile205, Gly206 and Cys207 (Table 4).

Residues with high levels of fluctuations indicate increased flexibility and the presence of unstable bonds, while residues with minimal fluctuations are linked with less flexibility and enhanced structural stability [57]. The lesser RMSF value observed at the active site and whole VP7A protein upon ligand binding in gnetin L-VP7A, glabratephrin-VP7A and 2SG-VP7A compared to the unbound VP7A suggests the potential affinity of these compounds for VP7A. This observation implies that these compounds could reduce flexibility and form stable interactions with the amino acid residues of VP7A. However, both apigenin-4′-glucoside-VP7A and glabrescin-VP7A had higher mean RMSF values at the active site of the protein compared to the unbound VP7A, while higher mean RMSF values were observed in sericetin-VP7A and glabrescin-VP7A upon binding to the whole protein relative to the apo-VP7A and relatively consistent with the RMSD results. Glabratephrin-VP7A had the least RMSF value in the whole protein (1.57 Å) and at the active site (1.97 Å) of VP7A respectively, indicating its ability to form stable bonds and could be a better inhibitor of the epitope than other compounds. This observation opposes the binding free energy and RMSD results in which the lowest binding free energy was observed in apigenin-4′-glucoside-VP7A and 2SG-VP7A, respectively. Nonetheless, the mean RMSF value of 2SG-VP7A in the whole protein (1.70 Å) and at the active site (2.0 Å) is within the 3.0 Å satisfactory boundary, while apigenin-4′-glucoside-VP7A has 3.09 Å and 3.19 Å (Tables 3 and 4) which does not deviate much from the 3.0 Å satisfactory value indicating their potential as a good inhibitor of the VP7A epitope. Relatively reduced fluctuations in both the active site residues and the whole protein due to ligand binding suggest improved intra- and intermolecular bond stability. They are in tandem with the RMSD results, thereby suggesting the potential of the investigated compounds as VP7A epitope inhibitors. Leu198 had the lowest fluctuation of the residues at the active site of VP7A (Table 4), hence an indication of its significance in forming stable bonds with the studied compounds during the simulation.

Furthermore, a higher fluctuation was observed between residues 195 and 220, 260 and 280 in VP7C. Of the residues at the active site of VP7C, Ala273-Gln280 were situated in the region of high fluctuation (Fig. 5(b)), and this could have led to the higher average RMSF values at the active site relative to the whole VP7C. The unbound VP7C, tizoxanide, gnetin L, ellagic acid, apigenin-4′-glucoside and 2SG had mean RMSF values of 2.47 and 1.75 Å, 2.91 and 1.82 Å, 4.37 and 2.05 Å, 2.82 and 1.75 Å, 1.96 and 1.83 Å, 4.05 and 1.70 Å at the active site and in the whole protein respectively (Tables 3 and 5). Except for 2SG-VP7C complex, ligand binding unto VP7C resulted in increased RMSF value relative to the unbound VP7C; however, the average RMSF values recorded in the whole protein are all within the acceptable limit of 3.0 Å, indicating that the fluctuations in residues were conducive to maintaining stability. The lowest average RMSF value at the active site of VP7C exhibited by apigenin-4′-glucoside is consistent with its highest negative binding free energy, suggesting its potential as a better inhibitor compared to other compounds. The least fluctuation in the residues at the active site of VP7C was observed in Arg283, which portray its importance in the formation of stable bond with the metabolites.

Similar to VP7A, a relatively higher fluctuation was observed between residues 195 and 220, 260 and 280 in VP7D; however, none of the residues at the RBD is in the region of higher fluctuation (Fig. 5(c)) and consistent with expectations, the RMSF values of the amino acid residues at the active site were lesser compared to the values obtained for the whole protein. This finding indicates enhanced intra and intermolecular bonding at the binding domain of VP7D throughout the simulation. The unbound VP7D, tizoxanide, sericetin, gnetin L, glabratephrin, edulisin I, apigenin-4′-glucoside and 2SG had RMSF values of 1.38 and 1.59 Å, 1.43 and 2.04 Å, 1.51 and 2.06 Å, 1.38 and 1.98 Å, 1.47 and 2.17 Å, 1.44 and 1.77 Å, 1.41 and 1.73 Å, 1.72 and 2.04 Å, at the active site and in the whole protein respectively (Tables 3 and 6). The lowest mean RMSF value in the whole protein after the apo-protein was recorded in

Table 3
Mean RMSD, RMSF, ROG, SASA and hydrogen bonds of apo-VP7A, C and D proteins, top-ranked compounds, and the standard against VP7A, C and D.

Ligands	Mean RMSD (Å)	Mean RMSF (Å)	Mean ROG (Å)	Mean SASA (Å)	Mean Number of H-bonds	Mean distance (Å) of H-bonds	Mean angle (°) of H-bonds
				VP7A			
2SG	1.88 ± 0.34	1.70 ± 1.02	20.84 ± 0.20	12,598.49 ± 306.47	104.81 ± 7.04	2.85 ± 0.06	151.89 ± 7.67
Apigenin-4′-glucoside	3.09 ± 1.02	2.11 ± 0.83	20.64 ± 0.30	12,759.30 ± 241.39	107.25 ± 7.74	2.85 ± 0.06	152.27 ± 7.83
Glabrescin	3.66 ± 1.18	2.53 ± 1.20	20.42 ± 0.44	12,978.32 ± 324.86	102.52 ± 6.81	2.85 ± 0.06	152.27 ± 7.58
Glabratephrin	3.11 ± 0.28	1.57 ± 0.60	20.98 ± 0.13	12,796.71 ± 302.97	102.81 ± 6.97	2.85 ± 0.06	152.17 ± 7.54
Gnetin L	2.33 ± 0.57	1.74 ± 0.64	21.16 ± 0.22	12,904.61 ± 260.74	103.32 ± 6.90	2.85 ± 0.06	152.17 ± 7.54
Sericetin	3.56 ± 0.45	1.83 ± 1.27	20.90 ± 0.17	12,958.84 ± 309.23	104.93 ± 6.98	2.85 ± 0.06	151.79 ± 7.69
Tizoxanide	2.82 ± 0.37	1.67 ± 1.35	20.68 ± 0.17	12,535.76 ± 280.15	109.51 ± 6.90	2.85 ± 0.06	151.89 ± 7.58
VP7A	3.42 ± 0.77	1.74 ± 1.11	20.85 ± 0.17	12,864.65 ± 301.64	102.85 ± 7.12	2.85 ± 0.06	152.05 ± 7.80
				VP7C			
2SG	2.69 ± 0.96	1.70 ± 1.14	20.93 ± 0.18	13,101.72 ± 307.33	103.24 ± 6.94	2.85 ± 0.06	151.77 ± 7.74
Apigenin-4′-glucoside	2.91 ± 0.56	1.83 ± 0.68	20.71 ± 0.18	12,799.93 ± 314.38	107.73 ± 7.23	2.85 ± 0.06	151.88 ± 7.57
Ellagic acid	2.45 ± 0.51	1.75 ± 0.67	20.85 ± 0.17	12,585.80 ± 270.79	105.23 ± 6.98	2.85 ± 0.06	151.98 ± 7.68
Gnetin L	3.87 ± 1.07	2.05 ± 1.43	20.91 ± 0.23	12,985.99 ± 299.64	104.37 ± 7.02	2.85 ± 0.06	152.30 ± 7.56
Tizoxanide	3.55 ± 0.55	1.82 ± 0.80	20.76 ± 0.16	12,839.12 ± 270.76	107.65 ± 7.25	2.85 ± 0.06	152.17 ± 7.64
VP7C	2.87 ± 0.56	1.75 ± 0.61	20.92 ± 0.21	12,791.76 ± 253.44	101.25 ± 7.04	2.85 ± 0.06	152.13 ± 7.60
				VP7D			
2SG	3.07 ± 0.64	2.04 ± 0.91	20.87 ± 0.18	13,005.91 ± 290.79	103.73 ± 7.16	2.85 ± 0.06	152.04 ± 7.60
Apigenin-4′-glucoside	3.12 ± 0.45	1.73 ± 0.79	20.67 ± 0.20	12,622.74 ± 280.81	110.51 ± 7.50	2.85 ± 0.06	152.24 ± 7.60
Edulisin I	3.66 ± 0.86	1.77 ± 0.89	20.99 ± 0.19	12,957.04 ± 255.83	100.97 ± 7.36	2.85 ± 0.06	152.09 ± 7.72
Glabratephrin	2.82 ± 0.85	2.17 ± 0.83	20.87 ± 0.23	12,992.45 ± 251.45	105.76 ± 6.90	2.85 ± 0.06	152.07 ± 7.76
Gnetin L	4.14 ± 0.50	1.98 ± 1.13	20.74 ± 0.15	12,995.75 ± 255.13	105.65 ± 6.98	2.85 ± 0.06	152.20 ± 7.62
Sericetin	2.22 ± 0.51	2.06 ± 0.78	20.94 ± 0.21	12,904.16 ± 293.79	105.14 ± 7.23	2.85 ± 0.07	151.76 ± 7.53
Tizoxanide	3.20 ± 0.89	2.04 ± 1.42	20.90 ± 0.21	12,972.23 ± 378.50	106.90 ± 7.44	2.85 ± 0.07	151.82 ± 7.77
VP7D	2.99 ± 0.41	1.59 ± 0.60	20.67 ± 0.14	12,773.99 ± 226.46	105.75 ± 6.94	2.85 ± 0.06	151.87 ± 7.61

apigenin-4′-glucoside; however, at the active site, gnetin L had the lowest RMSF value (Table 6). However, the average RMSF value in both the whole protein and at the binding domain is still below the acceptable border of 3.0 Å, indicating the possibility of the compounds under study as good inhibitors. The lowest fluctuation in the active site of VP7D was found in Ile306, hence its contribution towards the stability of the investigated metabolites (Table 6). Among the lead compounds, glabratephrin-VP7A, 2SG-VP7C and apigenin-4′-glucoside-VP7D had the lowest average RMSF values in the whole protein against VP7A, C and D, respectively, indicating their potential to induce minimal distortion of the targets during the simulation however, it contradicts their free binding energy results and average RMSD values. Generally, ligand binding resulted in increased average RMSF values across the three studied epitopes and this contradicts Aribisala et al. [54], in which phenolics binding to PBP3 and PBP5 yielded reduced average RMSF values relative to the unbound protein.

Apart from the RMSF, ROG assesses the level of compactness and folding shown by a complex during a simulation. The presence of high compactness and folding in a complex indicates a higher degree of thermodynamic orderliness and, in some cases, instability. The VP7A system exhibited reduced fluctuations in compactness during the 120 ns simulation period (Fig. 6(a)), suggesting that the binding of the lead compounds and tizoxanide to apo-VP7A had little impact on its folding except in glabrescin-VP7A complex with noticeable protein unfolding between 60 and 85 ns indicating lower compactness within this period. Furthermore, only glabratephrin-

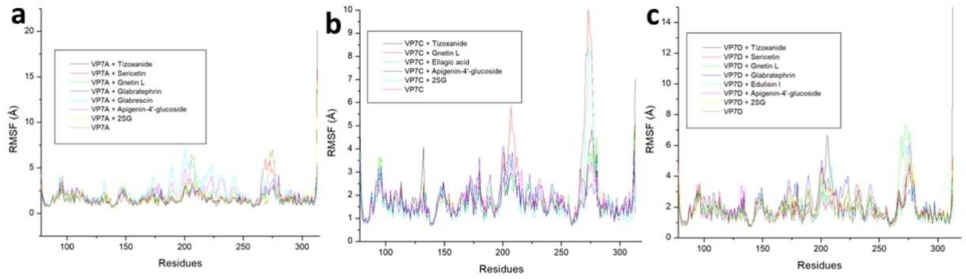


Fig. 5. Comparative RMSF plots of alpha-carbon, top-ranked compounds and reference standards against (a) VP7A (b) C and (c) D after 120 ns MD simulation period.

Table 4
Fluctuations of active residues within the VP7A epitope during the simulation.

KBS residues of VP7A	2SG	Apigenin-4′-glucoside	Glabrescin	Glabratephrin	Gnetin L	Sericetin	Tizoxanide	VP7A	Total RMSF
Lys194	1.34	1.79	2.25	1.23	1.48	1.42	1.37	1.24	1.52
Val195	1.29	1.68	2.49	1.26	1.39	1.26	1.23	1.20	1.48
Cys196	1.34	1.85	2.86	1.34	1.48	1.38	1.39	1.22	1.61
Pro197	1.39	2.56	3.82	1.26	1.78	1.46	1.59	1.35	1.90
Leu198	1.46	2.77	4.09	1.44	1.96	1.62	1.69	1.50	1.18
Asn199	1.95	3.99	5.85	2.00	2.64	2.17	2.32	2.09	2.88
Thr200	2.56	4.67	6.68	2.62	3.34	2.65	2.79	3.02	3.54
Gln201	2.91	4.91	7.12	2.89	3.46	3.00	3.04	3.41	3.84
Thr202	2.25	3.57	5.25	2.09	2.59	2.14	2.23	2.63	2.84
Leu203	2.38	3.75	5.59	2.10	2.57	2.30	2.43	3.57	3.09
Gly204	2.02	3.15	4.88	1.66	2.18	1.91	2.08	4.07	2.74
Ile205	2.37	3.87	5.51	2.07	2.65	2.11	2.51	4.91	3.25
Gly206	2.99	3.45	5.87	2.74	3.01	2.42	3.21	6.53	3.78
Cys207	2.95	2.63	5.01	2.92	2.97	2.31	3.26	6.00	3.51
Total RMSF	2.09	3.19	4.81	1.97	2.39	2.01	2.22	3.05	

Table 5
Fluctuations of active residues within the VP7C epitope during the simulation.

KBS residues of VP7C	2SG	Apigenin-4′-glucoside	Ellagic acid	Gnetin L	Tizoxanide	VP7C	Total RMSF
Ala273	8.41	2.37	3.64	10.12	3.61	3.31	5.24
Asp274	7.97	2.39	3.83	9.16	4.36	3.24	5.16
Pro275	8.21	2.34	3.30	8.86	4.33	3.01	5.03
Thr276	8.05	2.53	3.88	8.43	4.87	3.43	5.20
Thr277	5.55	2.31	3.62	5.72	4.31	2.97	4.08
Ala278	4.05	2.03	2.94	3.82	3.21	2.54	3.10
Pro279	3.17	2.20	2.78	3.19	2.95	2.68	2.83
Gln280	3.46	3.24	4.59	2.35	3.78	3.19	3.44
Thr281	1.61	1.47	2.70	1.47	1.88	1.92	1.84
Glu282	1.60	1.70	2.56	1.78	1.75	1.88	1.88
Arg283	1.31	1.26	1.53	1.10	0.98	1.33	1.25
Met284	1.22	1.13	1.23	1.53	1.62	1.63	1.39
Met285	1.01	1.14	1.41	1.46	1.40	1.55	1.33
Arg286	1.10	1.32	1.46	2.14	1.69	1.86	1.60
Total RMSF	4.05	1.96	2.82	4.37	2.91	2.47	

VP7A, gnetin L-VP7A and sericetin-VP7A have mean ROG values higher than that of the apo-VP7A (Table 3); however, a minimal overall difference of 0.74 Å was observed, which indicates that the ligand binding induced a minimal effect on the protein folding. Therefore, it can be inferred that ligand binding sustained the thermodynamic entropy of the protein, and this is partly corroborated by the RMSD values indicating their thermodynamic stability towards VP7A. The interaction between the highest-ranking compounds and tizoxanide with VP7C had little impact on its folding process, as revealed by the limited fluctuations in compactness (Fig. 6(b)) over the 120 ns simulation period. Expectedly, the corresponding ROG values across all the complexes corroborated this finding with an overall difference of 0.22 Å and the least value (20.71 Å) was exhibited by apigenin-4′-glucoside-VP7C (Table 3). Likewise, the binding of the investigated compounds and tizoxanide with VP7D had a negligible impact on the protein's folding process (Fig. 6(c)) throughout the simulation. This was evidenced in the overall difference of average ROG value of 0.32 Å across all the complexes, which

Table 6
Fluctuations of active residues within the VP7D epitope during the simulation.

KBS residues of VP7D	2SG	Apigenin-4′-glucoside	Edulisin I	Glabratephrin	Gnetin L	Sericetin	Tizoxanide	VP7D	Total RMSF
Val300	1.31	1.15	1.19	1.27	1.47	1.55	1.53	1.25	1.34
Asp301	1.46	1.24	1.32	1.59	1.66	1.86	1.57	1.47	1.52
Tyr302	1.24	1.26	1.06	1.50	1.25	1.92	1.63	1.57	1.43
Val303	1.26	1.27	1.05	1.14	1.07	1.13	1.22	1.07	1.15
Asn304	1.60	1.48	1.32	1.47	1.41	1.60	1.66	1.48	1.50
Gln305	1.66	1.49	1.25	1.56	1.23	1.59	1.80	1.82	1.55
Ile306	1.04	1.17	0.92	0.94	0.92	1.07	1.03	1.10	1.02
Ile307	1.19	1.05	0.97	1.00	0.88	1.09	1.08	1.00	1.03
Gln308	1.98	1.64	1.66	1.69	1.34	1.55	1.67	1.62	1.64
Ala309	1.37	1.05	1.13	1.24	0.97	1.11	0.99	1.02	1.11
Met310	1.25	1.05	1.04	1.21	0.98	1.08	0.99	0.89	1.06
Ser311	2.30	1.54	1.63	1.66	1.36	1.41	1.32	1.32	1.57
Lys312	4.73	2.98	4.23	2.80	3.37	2.68	2.15	2.30	3.16
Total RMSF	1.72	1.41	1.44	1.47	1.38	1.51	1.43	1.38	

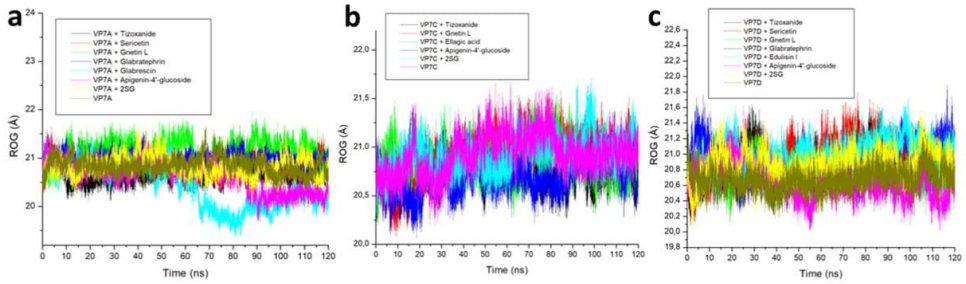


Fig. 6. Comparative ROG plots of alpha-carbon, top-ranked compounds and reference standard against (a) VP7A (b) C and (c) D after 120 ns MD simulation period.

is similar to the findings of Aribisala et al. [34] in which an overall variation of 0.3 Å was observed in the binding of SARS-CoV-2 wild-type spike protein with secondary metabolites among all the studied systems. Interestingly, the lowest mean ROG value was observed in apigenin-4′-glucoside-VP7D, just as in VP7C (Table 4). Generally, the structural compatibility observed in this study could be associated with various factors such as the topology, size, and length of the protein with the ligand's molecular weight and its contact with the target protein [56,58].

Another important thermodynamic stability index for evaluating protein folding and surface area changes throughout the simulation is the SASA, with higher values indicative of an expansion in the volume of the protein [57]. The degree of change in the SASA value is determined by the physicochemical characteristics of the amino acid residues that have been rearranged or altered [59] upon exposure to solvent or water [60] and the observed variation in exposure levels might potentially be ascribed to changes in the tertiary conformation of the protein [61]. During the simulation period, minor swaying was observed in the VP7A, C and D SASA plots (Fig. 7), suggesting a minimal effect owing to the binding of the studied metabolites to the targets. Against VP7A, an overall minimal difference of 442.56 Å was observed across all the complexes, with the lowest mean SASA value observed in tizoxanide-VP7A (12,535.76 Å)

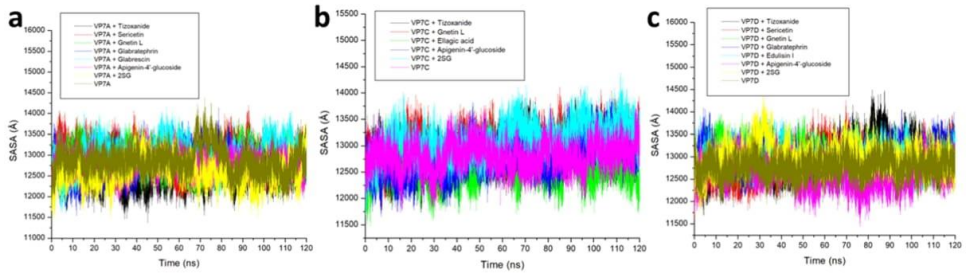


Fig. 7. Comparative SASA plots of alpha-carbon, top-ranked compounds and reference standard against (a) VP7A (b) C and (d) D after 120 ns MD simulation period.

followed by 2SG-VP7A (12,598.49 Å) (Table 3). The lowest SASA value observed in tizoxanide-VP7A complex suggests its potential to reduce the surface exposure of the protein to surrounding solvent compared to other investigated compounds; however, tizoxanide, 2SG, apigenin-4′-glucoside, and glabratephrin have lower SASA values relative to the unbound VP7A (Table 3) indicating that their binding to the protein reduced its volume though with a little effect. Furthermore, a minimum overall difference of 515.92 Å was observed in VP7C across all the complexes. The lowest average SASA value was found in ellagic acid-VP7C complex (12,585.80 Å), and this is consistent with the mean RMSD value, indicating that it could be a better inhibitor of VP7C compared to other compounds (Table 3). In addition, only ellagic acid-VP7C has lower mean SASA value relative to the apo-VP7C, indicating its capacity to reduce the target's surface area and limit its interaction with surrounding solvent molecules consistent with the RMSD finding. Similarly, a little overall difference of 383.17 Å was observed across all systems against VP7D with apigenin-4′-glucoside (12,622.74 Å) exhibiting the lowest average SASA value consistent with the RMSF and ROG findings. Also, only the apigenin-4′-glucoside-VP7D complex mean SASA value is lesser than that of VP7D unbound protein, suggesting its potential to decrease the protein's target surface area and limit exposure to solvent molecules. Generally, the minimal influence of ligand binding on the mean SASA values of the resulting complexes exhibits a partly similar trend to the findings of the average ROG values observed in this study, as the ligand binding did not significantly affect the folding of the protein, suggesting that the binding of the compounds and tizoxanide on VP7A, C and D does not disturb its thermodynamic entropy. This agrees with the findings of Moussaoui et al. [62], in which the mean SASA values for each complex did not vary significantly from one another.

Hydrogen bonds (H-bonds) indicators are essential for a protein's structural stability and compactness [63]. Consequently, H-bonds studies may be utilized to evaluate protein and protein-ligand complex stability during simulation [64]. Throughout the simulation, a steady variation in the form of the number of H-bonds formed in each system was observed against VP7A, C, and D (Fig. 8(a)–(c)). The observed stable fluctuation in the number of H-bonds formed upon ligand binding suggests that the thermodynamic entropy of the respective systems was unaffected, thereby retaining the protein geometry. Specifically, for glabrescin-VP7A and glabratephrin-VP7A complexes, ligand binding resulted in reduced intramolecular hydrogen bonds formation against VP7A, and a similar trend was observed in 2SG, edulisin I, gnetin L and sericetin with reduction of hydrogen bonds formation against VP7D relative to the apo-protein (Table 3). The observed reduction in the mean number of hydrogen bonds formed relative to the apo-protein could indicate breakage in some intramolecular hydrogen bonds formed owing to the ligand binding. This observation is similar to that of S'thebe et al. [65], in which the binding of the top three compounds and reference standards with the investigated target led to a reduction in the average number of intramolecular H-bonds. However, this observation contrasted the number of hydrogen bonds formed upon the binding of other metabolites to VP7A and VP7D. Interestingly, in VP7C, ligand binding resulted in the increased formation of intramolecular hydrogen bonds across all systems. This aligns with the findings of Lanrewaju et al. [28], where ligand binding to SARS-CoV-2 main protease resulted in the rise of hydrogen bonds compared to the unbound main protease. The observed increase in intramolecular H-bonds suggests that the ligands have occupied the intramolecular space of the proteins, as the rise in the number of H-bonds may imply the occurrence of H-bond interactions facilitated by the intermolecular bindings of ligands to the protein.

Evaluations of the intramolecular H-bond distance in VP7A, C and D during the simulation revealed a continuous reduction across all systems (Fig. 9(a)–(c)). Interestingly, an average H-bond distance of 2.85 Å was recorded in all the systems across VP7A, C and D (Table 3). This finding is consistent with our previous study [28], in which a consistent reduction in the distance of hydrogen bonds with an average hydrogen bond distance of 2.85 Å across all systems was observed. In addition, previous studies have documented an acceptable intramolecular H-bonds distance of 3.5 Å, with a lower value indicating a stronger hydrogen bonding interaction [54]. Thus, in the present investigation, a hydrogen bond distance below 3.5 Å indicates a favourable hydrogen bonding state throughout the simulation. Exhibiting identical average H-bonds distance across the apo-proteins and bonding systems in the investigated epitopes implies a state of thermodynamic orderliness upon ligand binding, and this provides further support to other thermodynamic metrics evaluated in this study.

Furthermore, as the simulation continued, this study showed a consistent variation in the H-bonds angle in VP7A, C and D (Fig. 10 (a)–(c)). At the outset of the simulation, a significant variation ranging from 138° to 166° was observed in the plots. Nevertheless, as the simulation proceeded, the variation significantly decreased to 180° in the systems across the targets (Fig. 10(a)–(c)). The

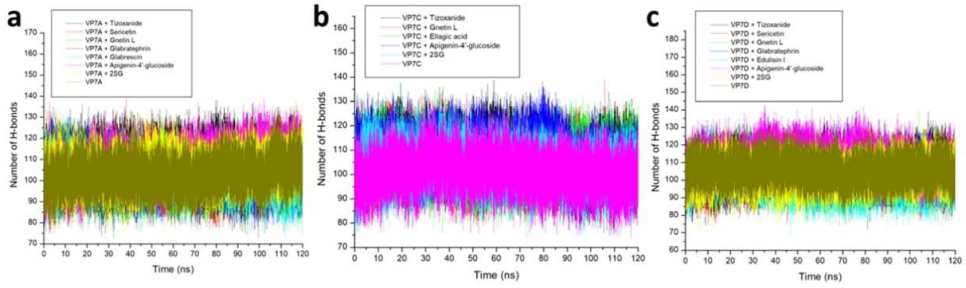


Fig. 8. Time progression of the number of H-bonds in (a) VP7A (b) C and (c) D upon binding with the top-ranked compounds and reference standards during the 120 ns MD simulation period.

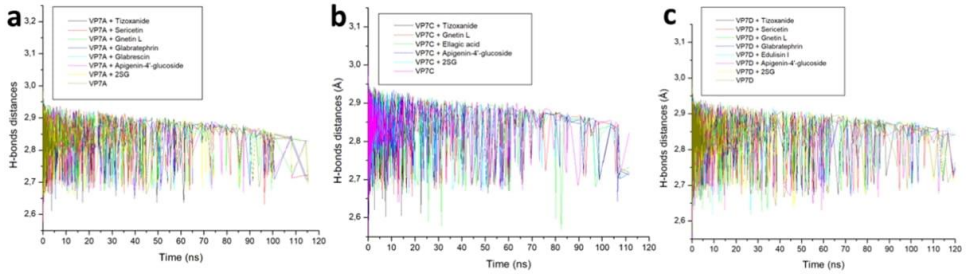


Fig. 9. Time progression of the H-bonds distance in (a) VP7A (b) C and (b) D upon binding of the top-ranked compounds and reference standards during the 120 ns MD simulation period.

diminishing degree of variation towards 180° which has been reported to be the ideal hydrogen bond angle [66], during the simulation signifies the enhanced strength of the bonding, and this aligns with the results obtained from the analysis of the H-bonds distance in this study. Generally, the observed average bond angles across the three targets are closely related, ranging from 151.79°–152.27°, 151.77°–152.30° and 151.76°–152.24° in VP7A, C and D respectively (Table 3). This observation suggests that the target protein VP7 is not in a disordered state upon ligand binding, and this is relatively consistent with other thermodynamic metrics examined in this study for stability, compactness, and flexibility. The fact that the H-bonds distance and angle values are similar across board for both targets suggests their negligible effect on the binding free energy reported in this study.

Bond analysis of interaction plots of the top-ranked compounds after 120 ns MD simulation

The binding affinity between a ligand and a receptor and the stability of the resulting complex are intricately linked to the kind of interactions, bond length, and the number of interactions occurring within the complex [57]. Therefore, this study evaluated the features in the binding of the highest-ranked compounds with VP7A, C, and D after a 120 ns simulation period. Figs. 11–16 illustrate the plot of interactions between tizoxanide and the top-ranked compounds which exhibited the highest negative binding free energy with VP7A, C and D. On the other hand, Supplementary Table S3 displays the plot of interactions for the remaining top-ranked compounds. Interactions observed in this study between the VP7 epitopes, and the top-ranked ligands include hydrogen bonds (conventional, π-donor, and carbon), van der Waals, amide π-stacked, π-anion, π-sigma, π-cation, π-π t-cation, π-π t-shaped, π-π t-stacked, π-alkyl, alkyl, π-Sulphur, unfavourable donor-donor interactions among others. Apigenin-4′-glucoside-VP7A complex with the highest negative binding free energy against VP7A had the highest number of interactions (17) with hydrogen bonds contacts with Ile149 and Asp151 (2) (Table 7 and Fig. 11). These observations established a correlation between the higher binding free energy in the apigenin-4′-glucoside-VP7A complex to the number, nature, and distance of interactions within the complex. The next highest negative binding free energy against VP7A was observed in gnetin L-VP7A complex but did not correlate with the observed sum of interactions (15). Analysis of the bond interactions revealed that gnetin L-VP7A made three hydrogen bond contacts with Pro120, Cys130 and Val118 and with shorter bond length compared to apigenin-4′-glucoside-VP7A (Table 7), and could be connected with the observed high binding free energy. Hydrogen bonds have been recognized as a significant class of non-covalent bonds in drug discovery due to their exceptional intermolecular interactions [67]. Glabrescin-VP7A complex has the highest number of interactions (16) after apigenin-4′-glucoside-VP7A but with no correlation with its binding free energy. Also, just one hydrogen bond contact with Leu121 was made and could be liable for the observed lesser binding free energy (Tables 7 and S3). A similar binding free energy was observed in sericetin-VP7A and 2SG-VP7A; unfortunately, a lesser number of interactions was observed in 2SG relative to sericetin (Tables 2 and

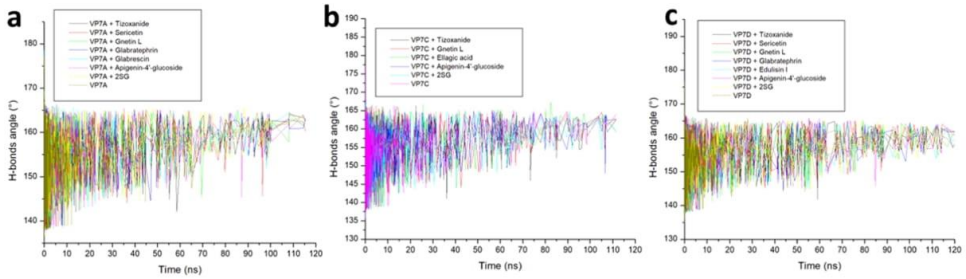


Fig. 10. Time progression of the H-bonds angle in (a) VP7A (b) C and (c) D upon binding of the top-ranked compounds and reference standards during the 120 ns MD simulation period.

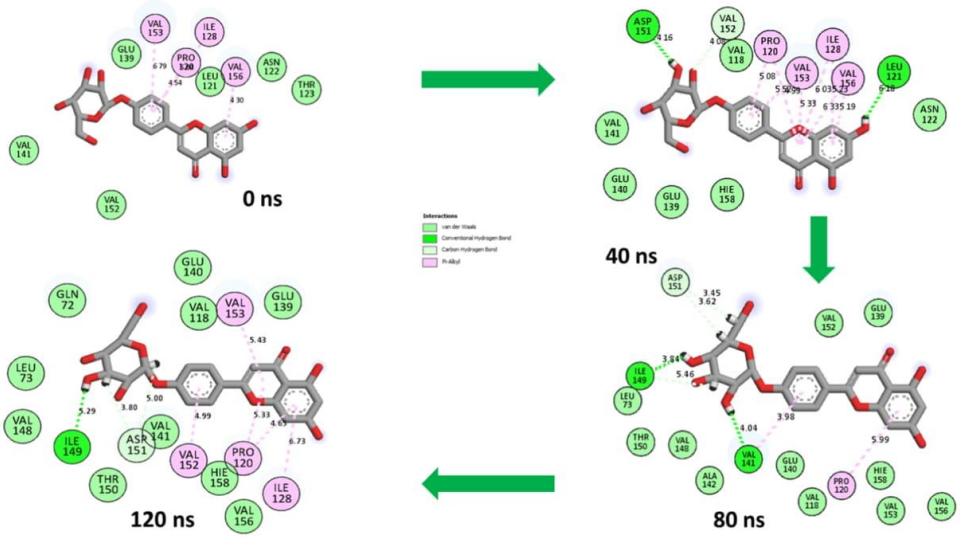


Fig. 11. Interaction plots of apigenin-4′-glucoside + VP7A at 0, 40, 80 and 120 ns.

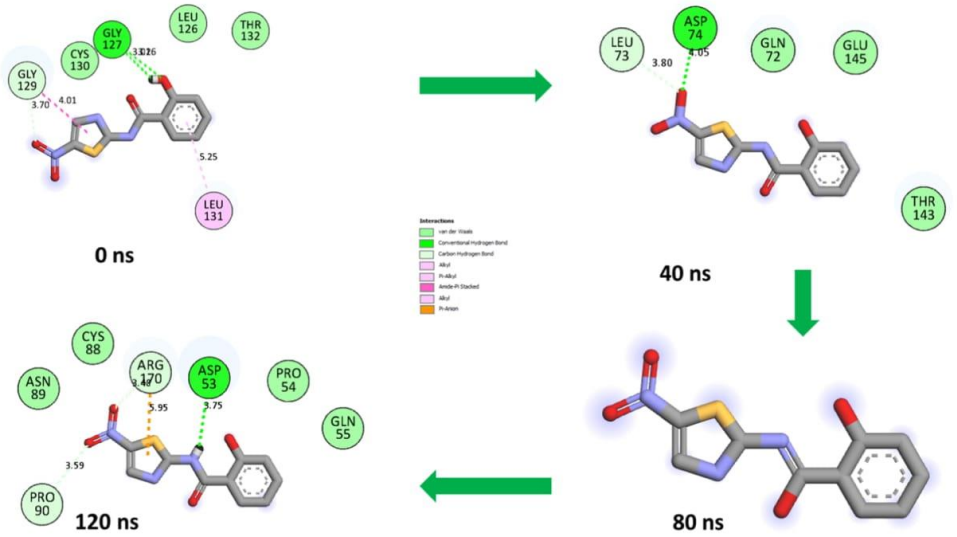


Fig. 12. Interaction plots of tizoxanide + VP7A at 0, 40, 80 and 120 ns.

7). A closer look at the interaction plot of 2SG-VP7A at 0, 40, and 80 ns (Supplementary Table S3) revealed a larger number of interactions compared to 120 ns, which could be associated with the free binding energy that was detected. In the same vein, the observed interactions in tizoxanide-VP7A relative to glabratephrin-VP7A does not justify its binding free energy, but a closer examination of tizoxanide-VP7A at 40 and 80 ns revealed lesser and no interactions respectively and could be liable for its binding free energy (Fig. 12).

Remarkably, all investigated top-ranked compounds against VP7C exhibited a higher number of interactions and hydrogen bonds contacts than tizoxanide which is consistent with the binding free energy results reported in this study. The higher number of

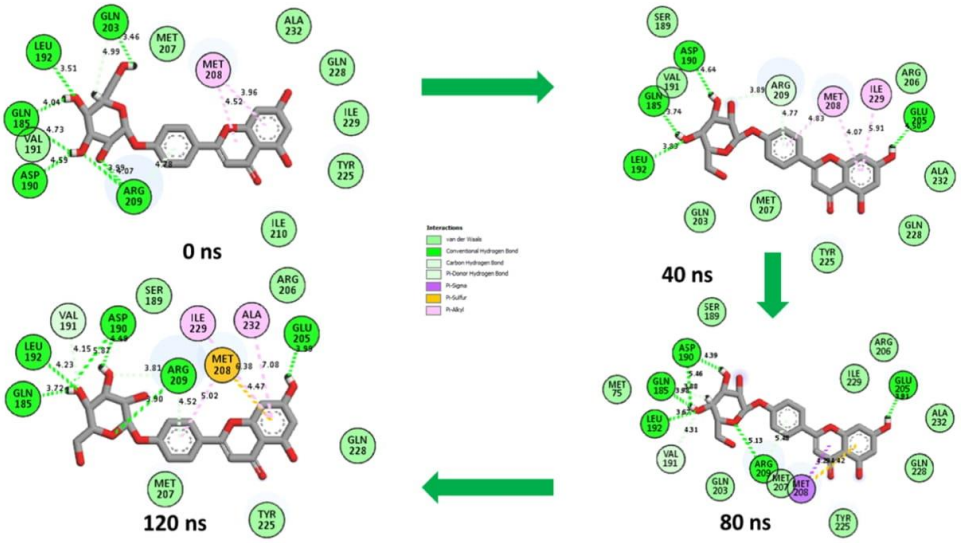


Fig. 13. Interaction plots of apigenin-4′-glucoside + VP7C at 0, 40, 80 and 120 ns.

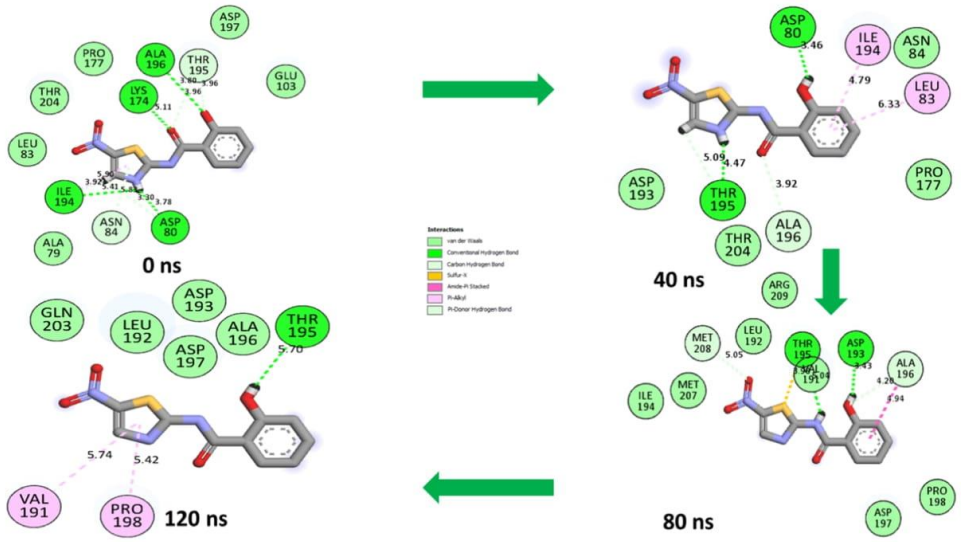


Fig. 14. Interaction plots of tizoxanide + VP7C at 0, 40, 80 and 120 ns.

interactions against VP7C observed in gnetin L-VP7C (20) and 2SG-VP7C (19) is not in sync with its binding free energy (Table 7) relative to apigenin-4′-glucoside-VP7C (18) with the highest negative binding free energy. The observed higher binding free energy in apigenin-4′-glucoside relative to other top-ranked compounds and the reference standard could be due to its higher number of hydrogen bonds (9) with Gln185, Leu192, Val191, Asp190 (2), Arg209 (3) and Glu205 (Fig. 13). As highlighted earlier, hydrogen bonds are one of the most vital non-covalent bonds in drug discovery and, in addition, are important in facilitating molecular recognition, enhancing the stability of protein-ligand interactions, and promoting the overall stability of drug-target complexes [67]. Therefore, the lesser number of hydrogen bonds observed in gnetin L (4) and 2SG (2), despite their higher number of interactions

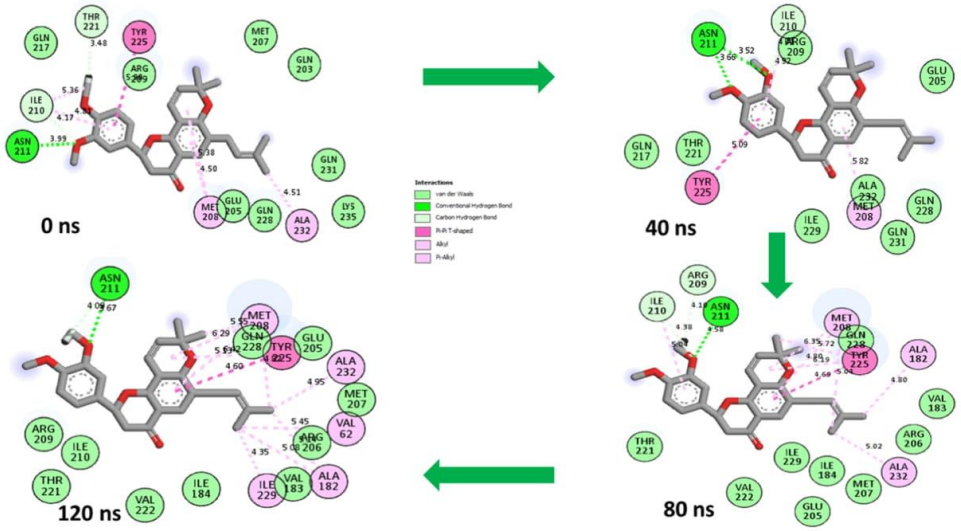


Fig. 15. Interaction plots of 2SG + VP7D at 0, 40, 80 and 120 ns.

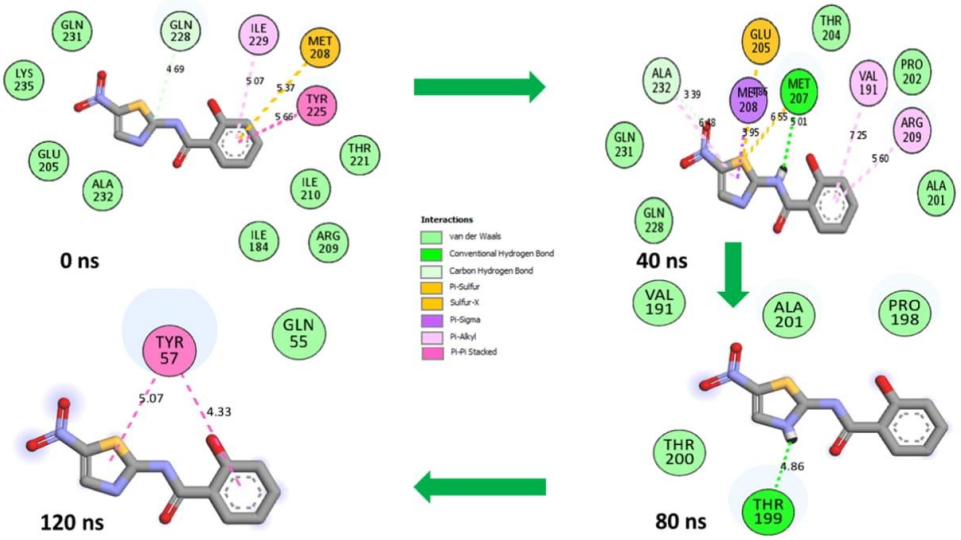


Fig. 16. Interaction plots of tizoxanide + VP7D at 0, 40, 80 and 120 ns.

relative to apigenin-4′-glucoside (9) (Table 7) could be responsible for their reduced binding free energy. Interestingly, the number of interactions and hydrogen bond contacts observed in ellagic acid-VP7C and tizoxanide+-VP7C (Fig. 14) is consistent with the binding free energy (Tables 3 and 7). Therefore, these observations indicate the significance of the number, length and nature of contacts in the calculation of binding free energy, as previously shown in the interactions with VP7A in this investigation.

The lowest and highest number of interactions against VP7D was exhibited by 2SG-VP7D (22) and tizoxanide-VP7D (3), and is consistent with their binding free energy (Figs. 15 and 16). Furthermore, gnetin L-VP7D (14) and sericetin-VP7D (14) shared equal numbers of interactions; however, they are different in terms of their binding free energy (Tables 3 and 7). The hydrogen bonds

Table 7
Bond interactions between the top-ranked compounds against VP7A, C and D after 120 ns simulation.

Top-ranked compounds	Total number of interactions and mean bond length (Å)	Number of hydrogen bonds [mean distance (Å)] and interaction residues	Other vital interactions and residues
VP7A			
2SG	4 (–)	None	None
Apigenin-4′-glucoside	17 (5.15)	3 (4.70) [Ile149, Asp151 (2)]	5 (5.43) [Val152, Val153, Pro120 (2), Ile128]
Glabrescin	16 (5.49)	1 (5.77) [Leu121]	9 (5.46) [Val153 (3), Val152, Pro120, Val156 (2), Ile128 (2)]
Glabratephrin	9 (4.69)	1 (4.67) [Asn122]	1 (4.71) [Val156]
Gnetin L	15 (4.75)	3 (4.34) [Pro120, Cys130, Val118]	3 (5.15) [Ile128, Val141 (2)]
Sericetin	10 (4.85)	1 (3.45) [Trp34]	4 (5.20) [Pro35, Trp34 (2), Gly33]
Tizoxanide	8 (4.19)	3 (3.61) [Pro90, Arg170, Asp53]	1 (5.95) [Arg170]
		VP7C	
2SG	19 (4.85)	2 (4.98) [Gln185, Met208]	11 (4.83) [Arg209 (2), Val191, Leu192, Met207 (2), Met208, Tyr225 (2), Ile229, Ala232]
Apigenin-4′-glucoside	18 (4.74)	9 (4.30) [Gln185, Leu192, Val191, Asp190 (2), Arg209 (3), Glu205]	4 (5.74) [Met208 (2), Ile229, Ala232]
Ellagic acid	14 (4.33)	5 (4.06) [Thr195, Thr204, Asp80 (2), Lys174]	4 (4.67) [Pro202, Arg206, Ile194 (2)]
Gnetin L	20 (4.70)	4 (4.61) [Ile210, Ala196, Tyr225, Glu205]	7 (4.76) [Ile210, Arg209, Ala196 (2), Met208, Pro198, Tyr225]
Tizoxanide	7 (5.62)	1 (5.70) [Thr195]	2 (5.58) [Val191, Pro198]
		VP7D	
2SG	22 (5.00)	2 (3.88) [Asn211 (2)]	11 (5.20) [Met208 (2), Gln228 (2), Tyr225 (1), Ala232, Ile229, Ala182 (2), Arg206, Val62]
Apigenin-4′-glucoside	13 (4.88)	6 (4.88) [Met207 (2), Met208, Arg209, Ile210, Asn211]	2 (4.88) [Met208, Tyr225]
Edulisin I	15 (5.24)	2 (3.87) [Val222, Thr221]	6 (5.70) [Met208, Ile210 (2) Tyr225 (3)]
Glabratephrin	12 (4.99)	4 (4.87) [Asn211, Arg209 (2), Met208]	4 (4.83) [Tyr225, Met208, Arg209, Ile210]
Gnetin L	14 (5.48)	2 (4.57) [Lys235, Glu205]	4 (5.95) [Ile184, Ile210, Tyr225, Met208]
Sericetin	14 (5.67)	None	7 (5.67) [Met208 (2), Tyr225 (2), Ile184, Ile210, Ala232]
Tizoxanide	3 (4.7)	None	3 (4.7) [Tyr57, Gln55]

analysis of the two complexes revealed that sericetin does not make hydrogen bond contact with any of the residues, while gnetin L was observed to make hydrogen bond contact with Lys235 and Glu205. The observed hydrogen bond contact, as highlighted earlier, could be associated with the higher binding free energy exhibited by gnetin L. In addition, a shorter bond length in gnetin L-VP7D compared to sericetin-VP7D (Table 7) could have resulted in its higher binding free energy against VP7D relative to sericetin. Moreover, the sum of interactions in edulisin I-VP7D (15) is insufficient to account for its binding free energy relative to apigenin-4′-glucoside-VP7D (13); however, a shorter bond length was observed in apigenin-4′-glucoside compared to edulisin I-VP7D. Shorter bond lengths have been reported to result in a stronger force between intermolecular or intramolecular entities owing to the proximity of the molecules, hence a higher affinity for the receptor [64]. This observation could be connected to the higher negative binding free energy in apigenin-4′-glucoside-VP7D coupled with a higher number of hydrogen bond contacts relative to edulisin I-VP7D. Conversely, the number of interactions in glabratephrin-VP7D (12) aligns with its binding free energy (Tables 3 and 7).

Overall, a conspicuous periodic shift was observed during the simulation period due to the inherent flexibility of the protein and ligand in the MD simulation, which is known for its dynamic nature [58,68]. Consequently, the amino acid residues in the interaction plots for the complexes in this study exhibit variations at regular intervals during the 120 ns simulation period (Figs. 11–16). Interestingly, no adverse donor-donor interactions, which might potentially result in a repulsive force [69], were detected in the molecular interactions between the top-ranked compounds against VP7A, C and D at 120 ns of simulation (Table 7) and such interactions were rarely identified over the whole simulation period (Figs. 11–16). Summarily, the enhanced broad-spectrum activity demonstrated by 2SG, apigenin-4′-glucoside, and gnetin L relative to tizoxanide against the VP7 epitopes can be ascribed to the number, type and bond lengths of contacts with the receptor.

Conclusion

This study has demonstrated the abilities of the lead compounds as potential inhibitors of the investigated VP7 epitopes. The lead compounds cut across all the three investigated medicinal plants: 2SG (*M. barteri*), apigenin-4′-glucoside and ellagic acid (*M. barteri* and *D. eriocarpum*), glabrescin, sericetin and glabratephrin (*D. eriocarpum*), gnetin L (*S. mombin*), and edulisin I (*M. barteri*) which further validates the antiviral abilities of these plants. The top-ranked compounds exhibited satisfactory pharmacokinetics and toxicity properties utilized in this investigation for screening, enhancing their potential to be developed as drug candidates with further improvements and structural alterations. Remarkably, all the lead compounds had higher negative binding free energy than tizoxanide

across the three epitopes of VP7 ascribed to the number, type, and bond length formed with the targets as apigenin-4′-glucoside had the highest affinity for VP7A and C while the highest affinity for VP7D was observed in 2SG indicating their better potential at inhibiting the protein relative to other compounds. Interestingly, 2SG, apigenin-4′-glucoside and gnetin L had better broad-spectrum affinities for VP7A, C and D relative to tizoxanide (reference standard) respectively. This observation denotes that 2SG, apigenin-4′-glucoside, and gnetin L exhibit superior advantages compared to other lead compounds in the management of RVA-induced diarrhoea, which any of the VP7 epitopes can cause. Furthermore, the thermodynamic information obtained from a 120 ns simulation confirmed the stability, flexibility, and compactness of the hit compounds with 2SG, ellagic acid and sericetin being the most stable against VP7A, C and D respectively. Although this study's findings unearth the lead compounds' promising ability to modulate the investigated VP7 epitopes, further confirmatory in vitro and in vivo studies are recommended to validate the findings and efforts are being made to pursue this approach.

Funding

The study is based on the financial assistance received from the Directorate of Research and Postgraduate Support, DUT, and the South African Medical Research Council (SAMRC) under a Self-Initiated Research Grant as well as the National Research Foundation (NRF) Research Development Grant for Rated Researchers (Grant number 120433) and the Competitive Programme for Rated Researchers Support (SRUG2204193723) to S. Sabiu. We also acknowledge Water Research Commission (WRC) of South Africa for the grant (K5/C2020-2021-00181) awarded to A.M. Enitan-Folami.

CRediT authorship contribution statement

Adedayo Ayodeji Lanrewaju: Methodology, Validation, Formal analysis, Investigation, Data curation, Writing – original draft. **Abimbola Motunrayo Enitan-Folami:** Conceptualization, Writing – review & editing, Supervision, Funding acquisition. **Saheed Sabiu:** Conceptualization, Software, Validation, Resources, Data curation, Writing – review & editing, Supervision, Funding acquisition. **Feroz Mahomed Swalaha:** Writing – review & editing, Supervision, Funding acquisition.

Declaration of competing interest

The authors declare that they have no conflict of interest.

Data availability

The data is contained within the article or supplementary material.

Acknowledgments

The Durban University of Technology (DUT) Doctoral Scholarship Scheme administered by the Directorate of Research and Postgraduate Support to A. A. Lanrewaju is duly acknowledged. The Centre for High-Performance Computing (CHPC), South Africa, is equally acknowledged for granting access to the computing systems used in this study.

Supplementary materials

Supplementary material associated with this article can be found, in the online version, at doi:10.1016/j.sciaf.2024.e02109.

References

[1] C. Troeger, I.A. Khalil, P.C. Rao, S. Cao, B.F. Blacker, T. Ahmed, G. Armah, J.E. Bines, T.G. Brewer, D.V. Colombara, Rotavirus vaccination and the global burden of rotavirus diarrhea among children younger than 5 years, JAMA Pediatr. 172 (10) (2018) 958–965, https://doi.org/10.1001/jamapediatrics.2018.1960.
[2] C.A. Omatola, A.O. Olaniran, Rotaviruses: from pathogenesis to disease control—A critical review, Viruses 14 (5) (2022) 875, https://doi.org/10.3390/v14050875.
[3] H.U. Ugboko, O.C. Nwinyi, S.U. Oranusi, J.O. Oyewale, Childhood diarrhoeal diseases in developing countries, Heliyon 6 (4) (2020) e03690, https://doi.org/10.1016/j.heliyon.2020.e03690.
[4] A.A. Lanrewaju, A.M. Enitan-Folami, S. Sabiu, J.N. Edokpayi, F.M. Swalaha, Global public health implications of human exposure to viral contaminated water, Front. Microbiol. 13 (2022) 981896, https://doi.org/10.3389/fmicb.2022.981896.
[5] U.D. Parashar, H. Johnson, A.D. Steele, J.E. Tate, Health impact of rotavirus vaccination in developing countries: progress and way forward, Clin. Infect. Dis. 62 (suppl_2) (2016) S91–S95, https://doi.org/10.1093/cid/civ1015.
[6] L. Jiang, A. Tang, L. Song, Y. Tong, H. Fan, Advances in the development of antivirals for rotavirus infection, Front. Immunol. 14 (2023), https://doi.org/10.3389/fimmu.2023.1041149.
[7] M.M. Nyaga, S. Sabiu, V.N. Ndze, F.E. Dennis, K.C. Jere, Report of the 1st African enteric viruses genome initiative (AEVGI) data and bioinformatics workshop on whole-genome analysis of some African rotavirus strains held in bloemfontein, South Africa, Vaccine 38 (34) (2020) 5402–5407, https://doi.org/10.1016/j.vaccine.2020.06.010.

[8] T. Garuba, R. Govender, H.A. Isah, S. Sabiu, Metabolites profiling and molecular docking identification of putative leads from endophytic *Phyllosticta capitalensis* as modulators of key druggable structural targets of rotavirus A, Trans. R. Soc. South Africa 77 (3) (2022) 207–217, https://doi.org/10.1080/0035919X.2022.2158387.

[9] D. Asensio-Cob, J.M. Rodríguez, D. Luque, Rotavirus particle disassembly and assembly in vivo and in vitro, Viruses 15 (8) (2023) 1750, https://doi.org/10.3390/v15081750.

[10] A.E. Fadiji, I. Omomowo, O. Omomowo, A. Lanrewaju, D. Akande, Antimicrobial efficacy and phytochemical screening of aqueous and ethanolic extracts of *Ocimum gratissimum* (scent leaf) leaf against some clinical isolates, J. Basic Pharmacol. Toxicol. 2 (2) (2018) 19–24.

[11] R. Sharma, M. Bhattu, A. Tripathi, M. Verma, R. Acevedo, P. Kumar, V.D. Rajput, J. Singh, Potential medicinal plants to combat viral infections: a way forward to environmental biotechnology, Environ. Res. (2023) 115725, https://doi.org/10.1016/j.envres.2023.115725.

[12] Y. Sun, X. Gong, J.Y. Tan, L. Kang, D. Li, Vikash, J. Yang, G Du, In vitro antiviral activity of *Rubia cordifolia* aerial part extract against rotavirus, Front. Pharmacol. 7 (2016) 308, https://doi.org/10.3389/fphar.2016.00308.

[13] A. Civra, R. Francese, D. Sinato, M. Donalisio, V. Cagno, P. Rubiolo, R. Ceylan, A. Uysal, G. Zengin, D. Lembo, In vitro screening for antiviral activity of Turkish plants revealing methanolic extract of *Rindera lanata* var. lanata active against human rotavirus, BMC Complement. Altern. Med. 17 (2017) 1–8, https://doi.org/10.1186/s12906-017-1560-3.

[14] J. Corthout, L. Pieters, M. Claeys, D.V. Berghe, A. Vlietinck, Antiviral ellagitannins from *Spondias mombin*, Phytochemistry 30 (4) (1991) 1129–1130, https://doi.org/10.1016/S0031-9422(00)95187-2.

[15] E.M.d.S. Siqueira, T.L. Lima, L. Boff, S.G. Lima, E.M. Lourenço, É.G. Ferreira, E.G. Barbosa, P.R. Machado, K.J. Farias, L.d.S. Ferreira, Antiviral potential of *Spondias mombin* L. leaves extract against herpes simplex virus type-1 replication using in vitro and in silico approaches, Planta Med. 86 (07) (2020) 505–515, https://doi.org/10.1055/a-1135-9066.

[16] O.O. Ogbole, T.E. Akinleye, P.A. Segun, T.C. Faleye, A.J. Adeniji, In vitro antiviral activity of twenty-seven medicinal plant extracts from Southwest Nigeria against three serotypes of echoviruses, Virol. J. 15 (1) (2018) 1–8, https://doi.org/10.1186/s12985-018-1022-7.

[17] P.A. Segun, O.O. Ogbole, T.E. Akinleye, T.O. Faleye, A.J. Adeniji, In vitro anti-enteroviral activity of stilbenoids isolated from the leaves of *Macaranga barteri*, Nat. Prod. Res. (2019) 1–5, https://doi.org/10.1080/14786419.2019.1644505.

[18] D. Luseba, E. Elgorashi, D. Ntloedibe, J. Van Staden, Antibacterial, anti-inflammatory and mutagenic effects of some medicinal plants used in South Africa for the treatment of wounds and retained placenta in livestock, S. Afr. J. Bot. 73 (3) (2007) 378–383, https://doi.org/10.1016/j.sajb.2007.03.003.

[19] D. Van der Merwe, G. Swan, C. Botha, Use of ethnoveterinary medicinal plants in cattle by Setswana-speaking people in the Madikwe area of the North West Province of South Africa, J. S. Afr. Vet. Assoc. 72 (4) (2001) 189–196.

[20] A.A. Lanrewaju, A.M. Enitan-Folami, M.M. Nyaga, S. Sabiu, F.M. Swalaha, Cheminformatics bioprospection of selected medicinal plants metabolites against trypsin cleaved VP4 (spike protein) of rotavirus A, J. Biomol. Struct. Dyn. (2023) 1–20, https://doi.org/10.1080/07391102.2023.2258405.

[21] J.O. Aribisala, R.A. Abdulsalam, Y. Dweba, K. Madonsela, S. Sabiu, Identification of secondary metabolites from *Crescentia cujete* as promising antibacterial therapeutics targeting type 2A topoisomerases through molecular dynamics simulation, Comput. Biol. Med. 145 (2022) 105432, https://doi.org/10.1016/j.compbiomed.2022.105432.

[22] F.O. Shode, J.O.-o. Uhomoibhi, K.A. Idowu, S. Sabiu, K.K. Govender, Molecular dynamics study on selected bioactive phytochemicals as potential inhibitors of HIV-1 subtype C protease, Metabolites 12 (11) (2022) 1155, https://doi.org/10.3390/metabo12111155.

[23] J.O.-O. Uhomoibhi, F.O. Shode, K.A. Idowu, S. Sabiu, Molecular modelling identification of phytocompounds from selected African botanicals as promising therapeutics against druggable human host cell targets of SARS-CoV-2, J. Mol. Graph. Model. 114 (2022) 108185, https://doi.org/10.1016/j.jmgm.2022.108185.

[24] J.J. Oloche, B.B. Oluremi, C.E. Aruwa, S. Sabiu, Molecular modeling identification of key secondary metabolites from *Xylopia aethiopica* as promising therapeutics targeting essential measles viral proteins, Evidence-Based Complement. Altern. Med. (2023) 1575358, https://doi.org/10.1155/2023/1575358.

[25] A. Ghosh, S. Chattopadhyay, M. Chawla-Sarkar, P. Nandy, A. Nandy, In silico study of rotavirus VP7 surface accessible conserved regions for antiviral drug/vaccine design, PLoS One 7 (7) (2012) e40749, https://doi.org/10.1371/journal.pone.0040749.

[26] S. Sabiu, F.O. Balogun, S.O. Amoo, Phenolics profiling of *Carpobrotus edulis* (L.) NE Br. and insights into molecular dynamics of their significance in type 2 diabetes therapy and its retinopathy complication, Molecules 26 (16) (2021) 4867, https://doi.org/10.3390/molecules26164867.

[27] E.F. Pettersen, T.D. Goddard, C.C. Huang, G.S. Couch, D.M. Greenblatt, E.C. Meng, T.E. Ferrin, UCSF Chimera—A visualization system for exploratory research and analysis, J. Comput. Chem. 25 (13) (2004) 1605–1612, https://doi.org/10.1002/jcc.20084.

[28] A.A. Lanrewaju, A.M. Enitan-Folami, M.M. Nyaga, S. Sabiu, F.M. Swalaha, Metabolites profiling and cheminformatics bioprospection of selected medicinal plants against the main protease and RNA-dependent RNA polymerase of SARS-CoV-2, J. Biomol. Struct. Dyn. (2023) 1–21, https://doi.org/10.1080/07391102.2023.2236718.

[29] J.-F. Rossignol, M. Abu-Zekry, A. Hussein, M.G. Santoro, Effect of nitazoxanide for treatment of severe rotavirus diarrhoea: randomised double-blind placebo-controlled trial, Lancet 368 (9530) (2006) 124–129, https://doi.org/10.1016/S0140-6736(06)68852-1.

[30] S. Dallakyan, A.J. Olson, Small-molecule library screening by docking with PyRx, Chem. Biol. (2015) 243–250, https://doi.org/10.1007/978-1-4939-2269-7_19.

[31] H. Kruse, L. Goerigk, S. Grimme, Why the standard B3LYP/6–31G* model chemistry should not be used in DFT calculations of molecular thermochemistry: understanding and correcting the problem, J. Org. Chem. 77 (23) (2012) 10824–10834, https://doi.org/10.1021/jo302156p.

[32] Calais, J.-L. (1993). Density-Functional Theory of Atoms and Molecules. R.G. Parr and W. Yang, Oxford University Press, New York, Oxford, 1989. IX+ 333 pp. Price£ 45.00. International Journal of Quantum Chemistry, 47(1), 101-101. 10.1002/qua.560470107.

[33] C.U. Ibeji, D.C. Akintayo, H.O. Oluwasola, E.O. Akintemi, O.G. Onwukwe, O.M. Eziomume, Synthesis, experimental and computational studies on the anti-corrosion performance of substituted Schiff bases of 2-methoxybenzaldehyde for mild steel in HCl medium, Sci. Rep. 13 (1) (2023) 3265, https://doi.org/10.1038/s41598-023-30396-35.

[34] J.O. Aribisala, C.E. Aruwa, T.O. Uthman, I.O. Nurain, K. Idowu, S. Sabiu, Cheminformatics bioprospection of broad spectrum plant secondary metabolites targeting the spike proteins of omicron variant and wild-type SARS-CoV-2, Metabolites, 12 (10) (2022) 982, https://doi.org/10.3390/metabo12100982.

[35] L. Deschenes, D. Bout, Origin 6.0: scientific data analysis and graphing software origin lab corporation. University of Texas, Austin, J. Am. Chem. Soc. 122 (39) (2000) 9567–9568, https://doi.org/10.1021/ja004761d.

[36] N.S. Pagadala, K. Syed, J. Tuszynski, Software for molecular docking: a review, Biophys. Rev. 9 (2017) 91–102, https://doi.org/10.1007/s12551-016-0247-1.

[37] T. Jian-Bo, X. Zhang, L. Ding, B. Shuai, Molecular design, molecular docking and ADMET study of cyclic sulfonamide derivatives as SARS-CoV-2 inhibitors, Chin. J. Anal. Chem. 49 (12) (2021) 63–73, https://doi.org/10.1016/j.cjac.2021.09.006.

[38] C. Prashantha, K. Gouthami, L. Lavanya, S. Bhavanam, A. Jakhar, R. Shakthiraju, V. Suraj, K. Sahana, H. Sujana, N. Guruprasad, Molecular screening of antimalarial, antiviral, anti-inflammatory and HIV protease inhibitors against spike glycoprotein of coronavirus, J. Mol. Graph. Model. 102 (2021) 107769, https://doi.org/10.1016/j.jmgm.2020.107769.

[39] Y. Wang, J. Xing, Y. Xu, N. Zhou, J. Peng, Z. Xiong, X. Liu, X. Luo, C. Luo, K. Chen, In silico ADME/T modelling for rational drug design, Q. Rev. Biophys. 48 (4) (2015) 488–515, https://doi.org/10.1017/S0033583515000190.

[40] C.A. Lipinski, F. Lombardo, B.W. Dominy, P.J. Feeney, Experimental and computational approaches to estimate solubility and permeability in drug discovery and development settings, Adv. Drug Deliv. Rev. 64 (2001) 4–17, https://doi.org/10.1016/s0169-409x(00)00129-0.

[41] R.P. Heaney, Factors influencing the measurement of bioavailability, taking calcium as a model, J. Nutr. 131 (4) (2001) 1344S–1348S, https://doi.org/10.1093/jn/131.4.1344S.

[42] O.A. Ojo, A.E. Adegboyega, G.I. Johnson, N.L. Umedum, K. Onuh, M.N. Adeduro, V.O. Nwobodo, A.O. Elekan, T.E. Alemika, T.O. Johnson, Deciphering the interactions of compounds from Allium sativum targeted towards identification of novel PTP 1B inhibitors in diabetes treatment: a computational approach, Inform. Med. Unlocked 26 (2021) 100719, https://doi.org/10.1016/j.imu.2021.100719.

[43] C.C. Ogu, J.L. Maxa, Drug interactions due to cytochrome P450, Baylor Univ. Med. Center Proc. (2000), https://doi.org/10.1080/08998280.2000.11927719.

[44] A.K. Verma, S.F. Ahmed, M.S. Hossain, A.A. Bhojiya, A. Mathur, S.K. Upadhyay, A.K. Srivastava, N.K. Vishvakarma, M. Barik, M.M. Rahaman, Molecular docking and simulation studies of flavonoid compounds against PBP-2a of methicillin-resistant *Staphylococcus aureus*, J. Biomol. Struct. Dyn. 40 (21) (2022) 10561–10577, https://doi.org/10.1080/07391102.2021.1944911.
[45] F.M. Ahamed, S. Chinnam, M. Challa, G. Kariyanna, A. Kumer, S. Jadoun, A. Salawi, A. G Al-Sehemi, U. Chakma, M.A.A Mashud, Molecular dynamics simulation, QSAR, DFT, molecular docking, ADMET, and synthesis of ethyl 3-((5-bromopyridin-2-yl) imino) butanoate analogues as potential inhibitors of SARS-CoV-2, Polycycl. Aromat. Compd. (2023) 1–19, https://doi.org/10.1080/10406638.2023.2173618.
[46] E.O. Akintemi, K.K. Govender, T. Singh, A DFT study of the chemical reactivity properties, spectroscopy and bioactivity scores of bioactive flavonols, Comput. Theor. Chem. 1210 (2022) 113658, https://doi.org/10.1016/j.comptc.2022.113658.
[47] B.Y.G. Mountessou, A.W. Ngouonpe, A.S.W. Mbobda, E.O. Akintemi, H.-G. Stammler, S.F. Kouam, J.C. Tchouankeu, B.N. Lenta, N. Sewald, T. Singh, Structural analysis and molecular docking study of pachypodostyflavone: a potent anti-onchocerca, J. Mol. Struct. (2023) 136003, https://doi.org/10.1016/j.molstruc.2023.136003.
[48] A. Rampadarath, J.O. Aribisala, N.P. Makunga, S. Mazibuko-Mbeje, S. Sabiu, Molecular bioprospection of *Helianthus annuus* L.(sunflower) cypsela for antidiabetic therapeutics through network pharmacology, density functional theory and molecular dynamics simulation, S. Afr. J. Bot. 162 (2023) 72–95, https://doi.org/10.1016/j.sajb.2023.08.045.
[49] S. Lakhera, K. Devlal, A. Ghosh, P. Chowdhury, M. Rana, Modelling the DFT structural and reactivity study of feverfew and evaluation of its potential antiviral activity against COVID-19 using molecular docking and MD simulations, Chem. Pap. 76 (5) (2022) 2759–2776, https://doi.org/10.1007/s11696-022-02067-6.
[50] N. Forouzesh, N. Mishra, An effective MM/GBSA protocol for absolute binding free energy calculations: a case study on SARS-CoV-2 spike protein and the human ACE2 receptor, Molecules 26 (8) (2021) 2383, https://doi.org/10.3390/molecules26082383.
[51] U. Dasmahapatra, C.K. Kumar, S. Das, P.T. Subramanian, P. Murali, A.E. Isaac, K. Ramanathan, B. Mm, K. Chanda, In-silico molecular modelling, MM/GBSA binding free energy and molecular dynamics simulation study of novel pyrido fused imidazo [4,5-c] quinolines as potential anti-tumor agents, Front. Chem. 10 (2022) 991369, https://doi.org/10.3389/fchem.2022.991369.
[52] A. Acharya, R. Agarwal, M.B. Baker, J. Baudry, D. Bhowmik, S. Boehm, K.G. Byler, S. Chen, L. Coates, C.J. Cooper, Supercomputer-based ensemble docking drug discovery pipeline with application to COVID-19, J. Chem. Inf. Model. 60 (12) (2020) 5832–5852, https://doi.org/10.1021/acs.jcim.0c01010.
[53] E. Singh, R.K. Jha, R.J. Khan, A. Kumar, M. Jain, J. Muthukumaran, A.K. Singh, A computational essential dynamics approach to investigate structural influences of ligand binding on Papain like protease from SARS-CoV-2, Comput. Biol. Chem. 99 (2022) 107721, https://doi.org/10.1016/j.compbiolchem.2022.107721.
[54] J.O. Aribisala, K. Idowu, T.R. Makhanya, S. Sabiu, Cheminformatics identification of phenolics as modulators of key penicillin—binding proteins of *Escherichia coli* towards interventive antibacterial therapy, Mol. Simul. (2023) 1–17, https://doi.org/10.1080/08927022.2023.2228423.
[55] D. Ramírez, J. Caballero, Is it reliable to use common molecular docking methods for comparing the binding affinities of enantiomer pairs for their protein target? Int. J. Mol. Sci. 17 (4) (2016) 525, https://doi.org/10.3390/ijms17040525.
[56] M.H. Baig, D.R. Sudhakar, P. Kalaiarasan, N. Subbarao, G. Wadhawa, M. Lohani, M.K.A. Khan, A.U. Khan, Insight into the effect of inhibitor resistant S130G mutant on physico-chemical properties of SHV type beta-lactamase: a molecular dynamics study, PLoS One 9 (12) (2014) e112456, https://doi.org/10.1371/journal.pone.0112456.
[57] S.S. Mousavi, A. Karami, T.M. Haghighi, S.G. Tumilaar, R. Idroes, S. Mahmud, I. Celik, D. Ağagündüz, T.E. Tallei, T.B. Emran, In silico evaluation of Iranian medicinal plant phytoconstituents as inhibitors against main protease and the receptor-binding domain of SARS-CoV-2, Molecules 26 (18) (2021) 5724, https://doi.org/10.3390/molecules26185724.
[58] L. Stella, S. Melchionna, Equilibration and sampling in molecular dynamics simulations of biomolecules, J. Chem. Phys. 109 (23) (1998) 10115–10117, https://doi.org/10.1063/1.477703.
[59] D. Gilis, M. Rooman, Stability changes upon mutation of solvent-accessible residues in proteins evaluated by database-derived potentials, J. Mol. Biol. 257 (5) (1996) 1112–1126, https://doi.org/10.1006/jmbi.1996.0226.
[60] S. Khan, I. Bjij, R.M. Betz, M.E. Soliman, Reversible versus irreversible inhibition modes of ERK2: a comparative analysis for ERK2 protein kinase in cancer therapy, Future Med. Chem. 10 (9) (2018) 1003–1015, https://doi.org/10.4155/fmc-2017-0275.
[61] D. Zhang, R. Lazim, Application of conventional molecular dynamics simulation in evaluating the stability of apomyoglobin in urea solution, Sci. Rep. 7 (1) (2017) 44651, https://doi.org/10.1038/srep44651.
[62] M. Moussaoui, M. Baassi, S. Baammi, H. Soufi, M. Salah, R. Daoud, A. El Allali, M. Belghiti, S. Belaaouad, In silico design of novel CDK2 inhibitors through QSAR, ADMET, molecular docking and molecular dynamics simulation studies, J. Biomol. Struct. Dyn. (2023) 1–17, https://doi.org/10.1080/07391102.2023.2212304.
[63] J. Kataria, P. Rani, P. Devi, Evaluation of molecular interactions in binary mixtures comprising ethylene and di-ethylene glycol with ethyl lactate through thermophysical and spectroscopic studies, J. Mol. Liq. 343 (2021) 117626, https://doi.org/10.1016/j.molliq.2021.117626.
[64] X. Du, Y. Li, Y.-L. Xia, S.-M. Ai, J. Liang, P. Sang, X.-L. Ji, S.-Q. Liu, Insights into protein–ligand interactions: mechanisms, models, and methods, Int. J. Mol. Sci. 17 (2) (2016) 144, https://doi.org/10.3390/ijms17020144.
[65] N.W. S'thebe, J.O. Aribisala, S. Sabiu, Cheminformatics bioprospection of sunflower seeds' oils against quorum sensing system of *Pseudomonas aeruginosa*, Antibiotics 12 (3) (2023) 504, https://doi.org/10.3390/antibiotics12030504.
[66] R. Kretschmer, D. Kinzel, L. González, The role of hydrogen bonds in protein–ligand interactions. DFT calculations in 1, 3-dihydrobenzimidazole-2 thione derivatives with glycinamide as model HIV RT inhibitors, Int. J. Quantum Chem. 112 (7) (2012) 1786–1795, https://doi.org/10.1002/qua.23001.
[67] R. Patil, S. Das, A. Stanley, L. Yadav, A. Sudhakar, A.K. Varma, Optimized hydrophobic interactions and hydrogen bonding at the target-ligand interface leads the pathways of drug-designing, PLoS One 5 (8) (2010) e12029, https://doi.org/10.1371/journal.pone.0012029.
[68] J.O. Aribisala, S. Sabiu, Cheminformatics identification of phenolics as modulators of penicillin-binding protein 2a of *Staphylococcus aureus*: a structure–activity-relationship-based study, Pharmaceutics 14 (9) (2022) 1818, https://doi.org/10.3390/pharmaceutics14091818.
[69] J.O. Aribisala, S. Sabiu, Cheminformatics identification of phenolics as modulators of penicillin-binding protein-3 of *Pseudomonas aeruginosa* towards interventive antibacterial therapy, J. Biomol. Struct. Dyn. (2023) 1–16, https://doi.org/10.1080/07391102.2023.2192808.

4.4 Bioprospection for antiviral compounds from selected medicinal plants against RNA polymerase of rotavirus A using molecular modelling and density functional theory

This article has been published in Chemical Physics Impact and presented accordingly

Chemical Physics Impact 9 (2024) 100745



Contents lists available at ScienceDirect

Chemical Physics Impact

journal homepage: www.sciencedirect.com/journal/chemical-physics-impact



Full Length Article

Bioprospection for antiviral compounds from selected medicinal plants against RNA polymerase of rotavirus A using molecular modelling and density functional theory

Adedayo Ayodeji Lanrewaju, Abimbola Motunrayo Folami, Saheed Sabiu *, Feroz Mahomed Swalaha

Department of Biotechnology and Food Science, Faculty of Applied Science, Durban University of Technology, P. O. Box 1334, Durban 4000, South Africa

ARTICLE INFO

Keywords:
Anti-rotavirus metabolites
Catalytic residues
Density functional theory
RNA-dependent RNA polymerase
Thermodynamic metrics

ABSTRACT

Rotavirus A (RVA) infection remains a significant global health challenge, especially in developing countries, causing severe dehydrating diarrhoea in children under five years of age. Despite the availability of four World Health Organization (WHO) pre-qualified vaccines, their availability, particularly in low-income countries, pose significant challenges. Currently, there are no specific anti-rotaviral medications hence, the urgency to develop novel therapeutics against rotavirus infection. Thus, this study explored the potential of secondary metabolites of *Spondias mombin, Macaranga barteri* and *Dicerocaryum eriocarpum* as novel inhibitors of the RNA-dependent RNA polymerase (VP1) of rotavirus A using computational techniques. Pharmacokinetics parameters were adopted to screen the top 20 metabolites with high affinity for the target, initially identified through a docking study. Furthermore, the ability of the resulting compounds to modulate the investigated target was assessed using molecular dynamics (MD) simulation, while density functional theory (DFT) calculations were conducted to predict the molecular properties of the top-ranked compounds. Except for ellagic acid hexoside (-33.14 kcal/mol), all the leads had higher binding free energy values relative to sofosbuvir (-36.58 kcal/mol) following a 120 ns MD simulation. Overall, the resulting complexes with the lead compounds demonstrated acceptable stability, reduced flexibility and compactness, with spiraeoside (-51.02 kcal/mol) displaying more favourable thermodynamics metrics, albeit with a lesser binding free energy relative to chrysoeriol 7-glucuronide (-58.36 kcal/mol). The binding free energy and thermodynamic parameters of the top-hit compounds could be attributed to their respective bond interactions and molecular orbital properties except chrysoeriol 7-glucuronide, with a need for additional structural adjustment to enhance its thermodynamic properties. Thus, these findings indicate the potential modulatory ability of the lead compounds against the VP1 protein of RVA, underscoring the importance of further *in vitro* and *in vivo* studies to validate the predicted activity, and ongoing efforts are being made to pursue this line of investigation.

1. Introduction

Rotavirus A (RVA) is the primary etiological agent of diarrhoea and remains the foremost cause of mortality associated with diarrhoea in children under five years of age, resulting in approximately 130,000 fatalities globally in 2016 [1]. Approximately 190,000 children <5 years old died in 2015 owing to RVA-induced diarrhoea, with major fatalities observed in countries with low-income economies in Africa and Asia [2]. Earlier in 2009, a global immunization initiative utilizing the RVA vaccine was implemented with the support of the WHO focused on reducing the incidence of mortality associated with diarrhoea diseases [3]. Despite the vaccines' widespread use in about 106 countries, RVA remains a primary factor contributing to the death of children under 5 years of age worldwide [1,4]. The primary approach to managing RVA-induced diarrhoea in children involves the use of oral rehydration solutions (ORS) containing a combination of glucose and electrolytes, which facilitate water absorption and control dehydration [5]. Currently, there exists no established therapeutic intervention for the management of RVA-induced diarrhoea; hence, it is imperative to prioritize the development of potential drugs with anti-RVA properties.

* Corresponding author.
E-mail address: sabius@dut.ac.za (S. Sabiu).

https://doi.org/10.1016/j.chphi.2024.100745
Received 17 August 2024; Received in revised form 15 September 2024; Accepted 18 September 2024
Available online 23 September 2024
2667-0224/© 2024 The Authors. Published by Elsevier B.V. This is an open access article under the CC BY-NC license (http://creativecommons.org/licenses/by-nc/4.0/).

Rotaviruses is a member of the family Reoviridae composed of 11 segments of double-stranded RNA (dsRNA) coding for six structural proteins (VP1-VP4, VP6, VP7) and six non-structural proteins (NSP1–6) [6,7]. Although the RV VP1, which codes for RNA-dependent RNA polymerase (RdRp) domain, has a distinct organization, its functionality closely mirrors that of other viral RdRps [5]. The RdRp protein plays a critical role in the replication and transcription of viral genomes, and it is highly conserved among different RNA viruses. Hence, targeting the viral polymerase presents a promising avenue for antiviral intervention, not only in the case of RV but also regarding other RNA viruses.

Plants serve as a rich reservoir of diverse secondary metabolites exhibiting a multitude of therapeutic properties [8], including antiviral properties [9]. For instance, *Spondias mombin* (hog plum, amra or cajazeira), which has been used traditionally for treating cold sores, diarrhoea, dysentery, conjunctivitis and to relieve stomach pain has demonstrated antiviral activity against coxsackie and herpes simplex viruses *in vitro* [10,11]. Similarly, *Macaranga barteri* (Agbasa or Aarasa) with reported antiviral activity against herpes simplex virus type-1viruses, echoviruses E7 and E19 [12,13], has been previously used in African traditional medicine to cure various illnesses such as cough, diabetes bronchitis and wound treatment [13]. Also, *Dicerocaryum eriocarpum* (Devil's thorn) has shown different applications in traditional medicine, such as in wound treatment, placenta expulsion, antibacterial activity [14], abdominal pains [15], anti-inflammatory effects and ethnoveterinary uses [16]. Notably, the *in silico* modulatory potential of the secondary metabolites from *S. mombin, M. barteri*, and *D. eriocarpum* against VP5* and VP8* [17] and VP7 epitopes [18], of RVA have been demonstrated. The conventional procedure for drug discovery is often associated with prolonged timelines, huge financial costs, and a high probability of unfavourable outcomes [19]. As a result, current emerging studies are now employing advanced computational approaches such as modern computer-aided molecular screening tools to effectively identify lead compounds with notable antiviral characteristics [20-23]. To advance ongoing effort in the development of anti-RVA therapeutics, this study employed computational techniques [molecular docking, density functional theory (DFT) and MD simulation] (Fig. 1) to elucidate the secondary metabolites of selected medicinal plants (*S. mombin, M. barteri*, and *D. eriocarpum*) with proven antiviral potentials [11,13,17] to identify compounds with modulatory activity against the VP1 protein of RVA.

2. Materials and methods

2.1. Protein sourcing and optimization

The X-ray crystal structure of VP1 (2R7Q) was acquired from the Protein Data Bank [https://www.rcsb.orgs/ (accessed on 20 April 2023)], and subsequently optimized as previously reported [24] using UCSF Chimera v1.15 [25].

2.2. Ligand acquisition and preparation

The 3D structures of the ligands; 77 secondary metabolites previously identified in *S. mombin, M. barteri* and *D. eriocarpum* [26] and the reference standards (sofosbuvir and remdesivir) were retrieved from PubChem [https://pubchem.ncbi.nlm.nih.gov/ (accessed on 23 July 2022)]. Sofosbuvir and remdesivir, two nucleotide analogues, were chosen as reference standards in this study because they can disrupt the RdRps of RNA viruses [27]. Thereafter, gasteiger charges were added to optimize the ligands and reference standards through the Open Babel plugin on Python Prescription (PyRx) v 0.9.5 [28].

2.3. Molecular docking and validation

The cleaned protein and optimized ligands were docked using the PyRx AutoDock tool [28]. The amino acid residues at the binding domain of VP1 crystal structure of RVA were selected for docking as previously reported [29,30], with the x-y-z coordinates; centre (X: 54.61, Y: 66.14, Z: 89.59). The ligands with the highest affinity for the protein's binding site were selected by employing the standard as a

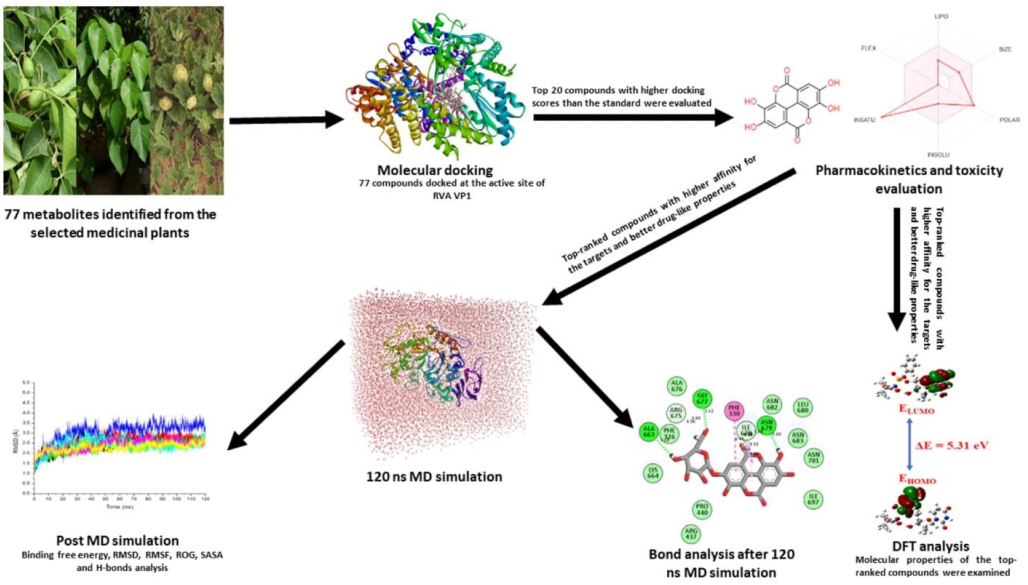


Fig. 1. Workflow of the strategy adopted in this study.

reference point. The capacity of AutoDock to accurately replicate the orientation and positioning of top-ranked metabolites and the reference standard was evaluated by re-docking the top-ranked metabolites into the binding domain of the protein's co-crystal structure while simultaneously mitigating the occurrence of false positives [28].

2.4. Pharmacokinetics and toxicity analysis

The physicochemical properties, pharmacokinetics, and drug-likeness of the top 20 compounds with the lowest docking scores out of the 77 metabolites were predicted through the SwissADME website [https://swissadme.ch/index.php, (accessed on 07 June 2023)]. Moreover, the Protox II web server [https://tox-new.charite.de/protox_II/, (accessed on 07 June 2023)] was utilized to generate predictions pertaining to the toxicological characteristics. The findings from these investigations were utilized to narrow down the selection to five compounds for further investigations.

2.5. MD simulation of the top-ranked complexes

The AMBER 18 software suite of the Centre for High Performance Computing (CHPC), Cape Town, South Africa, was adopted for the 120 ns simulation performed as earlier reported [31]. The FF18SB variant of the AMBER 18 package was employed to describe the operating systems. The atomic partial charges of the ligands were generated using ANTECHAMBER, which made use of the general amber force field (GAFF) and restrained electrostatic potential (RESP) techniques. The Na^+, Cl^- counter ions and hydrogen atoms of the Leap Module were adopted to neutralize the systems. The amino acid residues were numbered appropriately (1–1087), and the systems were contained within a TIP3P orthorhombic box of water molecules to ensure that all atoms were within 10 Å of the box edge. Prior to each simulation, an initial minimization of 2000 steps were conducted with a restriction potential of 500 kcal/mol. The steepest descent technique was employed for 990 steps, after which the conjugate degrees method was utilized for another 990 steps. An additional 990 steps of full (unlimited) minimization were executed using the conjugate gradient method. The study conducted involved gradually heating molecular dynamics simulations from 0 to 300 K for 50 ps. The systems under observation were kept at a constant number of atoms and volume throughout the simulation. The systems' solutes are subjected to a potential harmonic restraint of 10 kcal/mol and a collision frequency of 1.0 ps. Thereafter, every system was brought to equilibrium for approximately 500 ps, with the temperature maintained at a constant of 300 K. The SHAKE algorithm was employed to constrain the hydrogen bonds atom in each simulation conducted with a 2 fs step size, in tandem with the isobaric-isothermal ensemble (NPT) with randomized seeding. The temperature was maintained at 300 K, a constant pressure of 1 bar and a pressure-coupling constant of 2 picoseconds, a Langevin thermostat with a collision frequency of 1.0 ps. The post-dynamic data were obtained from the results of the 120 ns MD simulation. Following the completion of the simulation, the systems' coordinates were consolidated and subjected to analysis utilizing the AMBER 18 PTRAJ module. The root mean square fluctuation (RMSF), radius of gyration (ROG), root mean square deviation (RMSD), solvent-accessible surface area (SASA) and hydrogen bonds (H-bonds) analysis (number, distance and angle) were evaluated using the CPPTRAJ module, while their respective graphical representations were plotted with Origin v 6.0 [32]. An average of 120,000 snapshots from a 120 ns MD simulation trajectory was used to determine the binding free energy through the molecular mechanics generalized born surface area (MMGBSA) approach using the equation ΔGbind = Gcomplex - (Greceptor + Gligand) [33].

2.6. Quantum chemical calculations for the top-ranked compounds

Quantum chemical calculation was adopted to forecast the molecular features of therapeutic importance for the top-ranked compounds through DFT [34]. The Gaussian 16 suite of the Centre for High Performance Computing (CHPC), Cape Town, South Africa, was used to investigate their electronic properties by optimizing through the Becke3-Lee–Yang–Parr (B3LYP) method combined with the 6–31 + G(d,p) basis set [35], while the resulting files were viewed using GaussView 6 software V. 6.0.16. The frontier molecular orbitals that were evaluated using DFT include the highest occupied molecular orbital (HOMO) and lowest unoccupied molecular orbital (LUMO) [36] taking into account the Parr and Pearson interpretation of DFT and Koopmans theorem [37]. The equations below were used to calculate additional chemical descriptors such as energy gap (ΔE), ionization energy (I), electron affinity (A), chemical hardness (η), softness (δ), electronegativity (χ), chemical potential (Cp), global electrophilicity (ω).

$$\Delta E = E_{LUMO-}E_{HOMO} \tag{1}$$

$$I = -E_{LUMO} \tag{2}$$

$$A = -E_{HOMO} \tag{3}$$

$$\eta = \frac{\Delta E}{2} \tag{4}$$

$$\delta = \frac{1}{\eta} \tag{5}$$

$$\chi = \frac{(I+A)}{2} \tag{6}$$

$$Cp = -\chi \tag{7}$$

$$\omega = \frac{\chi 2}{\Delta E} \tag{8}$$

3. Results and discussion

3.1. Molecular docking

Molecular docking is a valuable tool which facilitates the prediction and positioning of drug candidates' binding to their protein targets [38], with a higher negative docking score of the bound complexes indicating better fitness of the ligand into the active site of the protein [34,39]. In the present study, geraniin and mallotusinic acid exhibited the highest negative docking score against VP1, (−11.0 kcal/mol), while azelaic acid had the least negative docking score at (−5.2 kcal/mol) (Supplementary Table S1). The top twenty compounds with higher negative docking scores (−11.0 kcal/mol to −9.2 kcal/mol) (Supplementary Table S2) relative to the reference standard (sofosbuvir (−8.8 kcal/mol)) were selected for further analysis. The compounds' higher docking scores compared to the reference compound suggest their better fitness into the active site of the RVA's VP1. Therefore, sofosbuvir (−8.8 kcal/mol) was selected as the reference standard for calculating thermodynamic binding free energy and conducting subsequent MD simulation study owing to its better fitness into the binding domain of the protein relative to remdesivir (−7.3 kcal/mol).

3.2. Docking pose validation

The result of docking validation conducted using the redocking approach depicts the interactions between the lead compounds and the reference standard within the binding domain of the VP1 protein crystal void of a co-crystallized ligand and is presented in Fig. 2. Chrysoeriol 7-glucuronide, spiraeoside, kaempferol 7-O-glucoside and sofosbuvir shared similar binding orientation and interacted with Arg457, Asp520, Ser522, Asp631, Asp632, Lys679. Conversely, gnetin L and ellagic acid hexoside, with partial occupancy of the catalytic site, interacted more

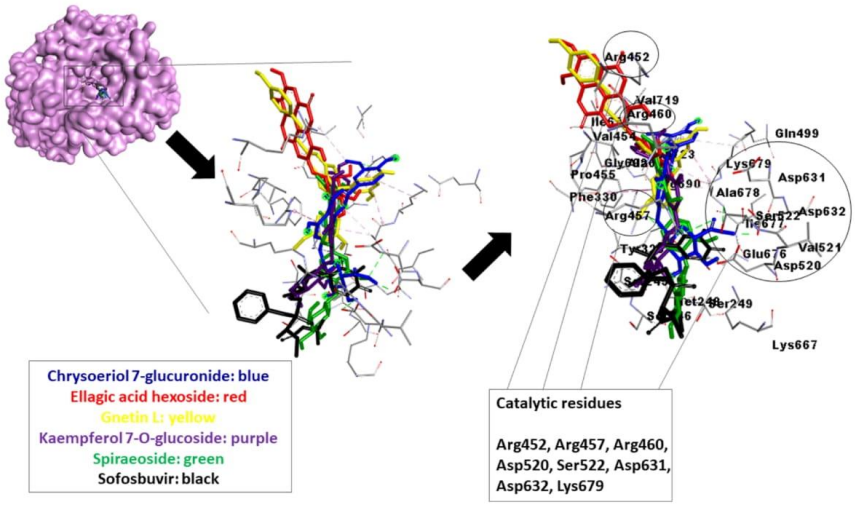


Fig. 2. Superimposition and interactions of the lead compounds and reference standard against the crystal structure of VP1.

with Arg452, Arg457 and Arg460 (Fig. 2). These observed interactions with amino acids are in line with previous investigations [29,30] thus reinforcing the dependability and consistency of the employed docking methodology.

3.3. ADMET properties of the top-ranked compounds

Early prediction of drug candidates' properties could play a significant role in streamlining the drug discovery process, resulting in cost and time savings, leading to notable cost and time savings, as many potential drug candidates have not progressed to clinical trials due to their unfavourable pharmacokinetic and toxicity features [40]. Hence, the accurate prediction of absorption, distribution, metabolism, excretion and toxicity (ADMET) properties holds significant importance in drug discovery and development due to their substantial contribution to approximately 60% of clinical trial failures associated with drug candidates [41].

Based on the Lipinski's rule of five (Ro5), [42], it was observed that only gnetin L and 6 MM passed the rule with 0 and 1 violation respectively while[(1S,3R,6S,7S,8S,9S,10S,11S,14S,16S)−6-acetyl-14-[(2R,4R,5R,6R)−5-[(2S,3R,4R,5R,6R)−3,5-dihydroxy-4-methoxy-6-methyloxan-2-yl]oxy-4-methoxy-6-methyloxan-2-yl]oxy-8-hydroxy-7,11-dimethyl-2-oxapentacyclo[8.8.0.01,3.03,7.011,16]octadecan-9-yl] acetate (1SR), chrysoeriol 7- glucuronide, kaempferol 7-O-glucoside, ellagic acid hexoside and spiraeoside failed the Ro5 but with 2 violations (Supplementary Table S2). Unfortunately, all other compounds failed to meet Lipinski's criteria, with three violations. Therefore, 1SR, chrysoeriol 7-glucuronide, kaempferol 7-O-glucoside, ellagic acid hexoside and spiraeoside were chosen due to their potential oral bioavailability and would require less structural alterations to improve their druggability compared to other compounds with 3 violations (Supplementary Table S2). The bioavailability score of a drug, which refers to the fraction of a therapeutic dose that remains unaltered and enters the systemic circulation, is a crucial factor in pharmacological dosage calculations [43]. The bioavailability score of all the top-scoring compounds and sofosbuvir was either 0.11 or 0.17, except for gnetin L and 6 MM, which exhibited a higher bioavailability score of 0.55 (Supplementary Table S2). A higher bioavailability score signifies a substantial medication concentration required to provide optimal therapeutic effects at the intended site of action. Specifically, the low bioavailability score of some of the selected metabolites correlates with their low oral bioavailability. However, they remain viable for administration via non-oral routes (Heaney, 2001).

Cytochrome P450s (CYPs) are a superfamily of haem-containing proteins that are mostly produced in the liver and perform a crucial role in facilitating the metabolic processes of a diverse array of exogenous and endogenous chemicals [44]. Metabolic clearance, drug-drug interactions (DDI), and interpatient heterogeneity in pharmacokinetics include the prominent characteristics associated with the isoenzymes [45]. Many drug-like substances that undergo clearance primarily by cytochrome P450-mediated oxidation are metabolized by isoforms 1A2, 2C9, 2C19, 2D6, and 3A4 [46]. The potential inhibition of any of these CYP isoforms raises issues for concurrent use with other drugs. Remarkably, only gnetin L (1), sofosbuvir and 6 MM (3) inhibited 1, 1 and 3 CYP450 isoenzymes respectively, suggesting their potential to trigger DDI when administered with other medications (Supplementary Table S2).

In addition, all the top-scoring compounds and the reference standard showed activity in at least one toxicity endpoint apart from kaempferol 7-O-glucoside, which demonstrated inactivity across all toxicity endpoints. Moreover, of all the compounds with <3 Ro5 violations selected earlier, only 6 MM belonged to toxicity class 2, which is unsuitable for drug development. Therefore, 6 MM was excluded from further investigations. Chrysoeriol 7-glucuronide, gnetin L, kaempferol 7-O-glucoside, ellagic acid hexoside, spiraeoside and sofosbuvir belong to toxicity class 5, 4, 5, 5, 5 and 6, respectively with LD_{50} values ranging from 500 – 12,000 mg kg^{-1} which is acceptable for drug development [47]. In general, the selected compounds exhibited promising characteristics, requiring fewer structural adjustments to amend their druggability compared to the eliminated compounds.

3.4. Binding free energy analysis of the top-ranked compounds

The use of the MMGBSA method in the molecular dynamics (MD) trajectory facilitated the calculation of the binding free energy associated with protein-ligand complexes due to its superiority over several molecular docking scoring functions in terms of accuracy [48]. The level of attraction between the ligand and the protein is directly correlated

with the magnitude of the negative value of the thermodynamic binding free energy [49]. All the lead compounds except ellagic acid hexoside (−33.14 kcal/mol) have higher negative binding free energy compared to the reference standard (−36.58 kcal/mol) (Table 1). This observation regarding the binding free energy in this study could imply that chrysoeriol 7-glucuronide, gnetin L, kaempferol 7-O-glucoside and spiraeoside exhibit higher potential as inhibitors of VP1, with chrysoeriol 7-glucuronide displaying the most favourable effect among the lead compounds. Furthermore, this observation indicates that these metabolites might potentially exhibit superior efficacy in the disruption of the VP1 protein of RVA compared to sofosbuvir. The binding free energy results obtained in this study are partly similar to a previous observation [26], where ellagic acid hexoside, spiraeoside, apigenin-4′-glucoside and chrysoeriol 7-glucuronide had higher negative binding free energy than sofosbuvir against the RdRp of SARS-CoV-2.

3.5. Thermodynamic stability, flexibility, compactness, protein surface conformation and hydrogen bonds analysis

The MD simulation approach provides valuable insights into the thermodynamic alterations occurring within protein-ligand complexes, elucidating conformational and stability changes induced by ligand binding [50]. Therefore, a 120 ns MD simulation was conducted to assess the RMSD, RMSF, ROG, SASA and H-bonds analysis to gain insights into the stability of the complex, the compactness of the protein, and the flexibility of the amino acid residues. The RMSD was computed to assess the overall stability of the resulting complexes during the simulation [51]. The ligand-VP1 complexes and the apo-protein did not significantly fluctuate after the atoms of each system reached equilibrium within the first 5 ns of the simulation, which lasted until the simulation was completed (Fig. 3). As expected, there was only a marginal deviation in the average RMSD value of the apo-protein relative to the simulated complexes (Table 3). For instance, a higher mean RMSD value relative to the unbound VP1 (1.88 Å) was observed in chrysoeriol 7-glucuronide-VP1 (1.92 Å), ellagic acid hexoside-VP1 (1.94 Å), spiraeoside-VP1 (1.89 Å) and sofosbuvir-VP1 (1.94 Å), indicating that the ligand binding resulted in increased average RMSD value and hence reduced stability of the protein. This observation aligns with an earlier investigation that reported an increased mean RMSD value due to the interaction between verbascoside and the SARS-CoV-2 spike protein [49]. Conversely, the binding of gnetin L (1.87 Å) and kaempferol 7-O-glucoside (1.81 Å) resulted in a lower average RMSD value compared to the apo-VP1 (1.88 Å) (Table 3), suggesting that ligand binding resulted in reduced mean RMSD value hence increased stability of the protein and further confirms their capability as better VP1 inhibitors compared to other top-ranked compounds and the reference

Table 1
MMGBSA-based binding free energy framework of the top-ranked compounds.

Energy framework (kcal/mol)					
VP1					
Complex	ΔE_{vdW}	ΔE_{elec}	ΔG_{gas}	ΔG_{solv}	ΔG_{bind}
Chrysoeriol 7-glucuronide	−46.91 ±4.39	−80.27 ±12.26	−127.18 ±12.22	68.81 ±8.46	−58.36 ±6.91
Ellagic acid hexoside	−47.67 ±3.30	−26.97 ±9.57	−74.64 ±9.62	41.50 ±7.69	−33.14 ±4.01
Gnetin L	−49.98 ±5.08	−54.79 ±15.60	−104.80 ±14.21	60.09 ±11.07	−44.71 ±5.72
Kaempferol 7-O-glucoside	−47.78 ±4.28	−55.99 ±22.30	−103.77 ±20.02	59.24 ±13.59	−44.53 ±8.13
Spiraeoside	−50.17 ±4.28	−52.72 ±11.23	−102.89 ±10.44	51.87 ±6.70	−51.02 ±6.05
Sofosbuvir	−50.37 ±3.97	−27.01 ±9.88	−77.39 ±11.47	40.80 ±7.73	−36.58 ±6.68

ΔE_{vdW} = van der Waals energy; ΔE_{elec} = electrostatic energy; ΔE_{gas} = gas phase free energy; ΔG_{sol} = solvation free energy; ΔG_{bind} = total binding free energy.

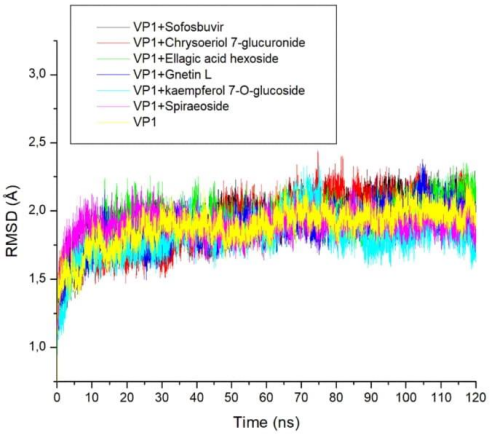


Fig. 3. Comparative RMSD plots of alpha-carbon, top-ranked compounds and reference standard against VP1 after 120 ns MD simulation period.

standard. This finding agrees with an earlier report [52], where the binding of emblicanin A unto SARS-CoV-2 RdRp resulted in enhanced stability of the complex. In general, the binding free energy results do not align with the mean RMSD values of the complexes; nevertheless, all the RMSD values are within the acceptable 3 Å limit [53], suggesting that the ligand binding does not really disturb the stability of the protein and, hence, are potential inhibitors of the protein.

The median variation of all residues during the simulation was examined by analyzing the RMSF. The RMSF is a measure of the flexibility exhibited by amino acid residues in a molecule, which is assessed by overlaying a reference conformation with the trajectory conformations of specific amino acids. A low RMSF value indicates less mobility, while a higher RMSF value suggests more flexibility of the protein-ligand combination [54]. Specifically, a decrease in volatility at the active site where ligand binding and catalysis take place results in a stronger binding and affinity between the ligand and the protein [55]. A higher swaying was observed between residues 10 and 70, 80 and 90, 140 and 160, 320 and 355, 385 and 410, 565 and 580, 770 and 805, 990 and 1020 (Fig. 4), which imply a reduced capacity of these residues to form stable bonds. Remarkably, none of the catalytic residues within the protein are positioned in the high swaying zone, and this could explain the higher mean RMSF values observed in the whole VP1 compared to the values at the catalytic sites of the protein (Tables 2 and 3) suggesting stronger intra and intermolecular bonding at the catalytic site of VP1. In the whole protein, higher average RMSF was observed in chrysoeriol 7-glucuronide-VP1 (1.19 Å), ellagic acid hexoside-VP1 (1.16 Å) and gnetin L-VP1 (1.18 Å), relative to the apo-protein (1.15 Å) due to ligand binding implying weaker intra and intermolecular bonding.

In contrast, lesser mean average RMSF values were reported in kaempferol 7-O-glucoside-VP1 (1.14 Å), spiraeoside-VP1 (1.10 Å) and sofosbuvir-VP1 (1.10 Å), indicating stronger intra and intermolecular bonding (Table 3). At the catalytic site of VP1, gnetin L (0.83 Å), spiraeoside (0.85 Å) and the reference standard (0.80 Å) exhibited lesser average RMSF value relative to the apo-protein (0.86 Å) suggesting reduced flexibility and consequently stronger intra and intermolecular bonding at the catalytic domain (Table 3). On the other hand, chrysoeriol 7-glucuronide (0.90 Å), ellagic acid hexoside (0.87 Å), and kaempferol 7-O-glucoside (0.87 Å) had higher mean RMSF value at the catalytic site compared to the unbound protein denoting increased flexibility at the catalytic site. Therefore, there is a need for additional structural adjustment of the compounds, especially chrysoeriol 7-

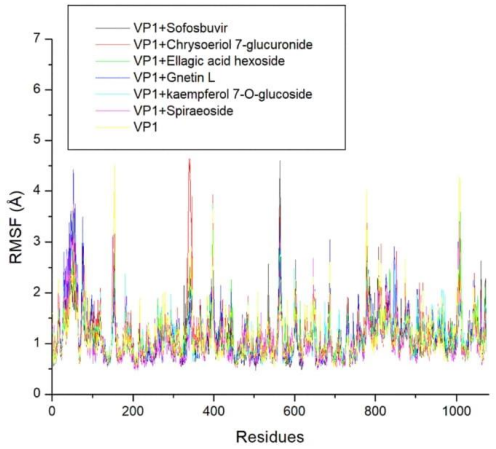


Fig. 4. Comparative RMSF plots of alpha-carbon top-ranked compounds and reference standard against VP1 after 120 ns MD simulation period.

glucuronide, to enhance its thermodynamic abilities. Among the catalytic residues in the protein, Asp520, which is one of the conserved acidic residues [30], had the lowest degree of variation, suggesting that the residue played a crucial role in establishing stable bonds with the compounds under investigation during the simulation. These observations are inconsistent with Pundir et al. [56], in which the binding of remdesivir, CHEMBL1276156, PubChem135548348 to the RdRp of SARS-CoV-2 does not affect the average RMSF value of the complex. On the contrary, the binding of geraniin to SARS-CoV-2 RdRp resulted in an increased average RMSF value (32.01 Å) relative to the unbound RdRp (21.70 Å) as previously reported [57]. Generally, the mean RMSF values in the whole protein and at the catalytic site were within the acceptable deviation limit of < 3 Å, indicating that the observed fluctuations do not affect the stability of the protein significantly.

Another thermodynamic metric ROG assesses the degree of compactness and folding by a complex in a simulation. This phenomenon has been associated with various parameters related to the protein, such as protein topology, size, and length, and parameters connected to the ligand, such as molecular weight and the specific contact point on the target [58]. Complexes with a high ROG value are more prone to exhibiting flexibility, hence rendering them unstable, while lower ROG values indicate a more compact and densely packed configuration [59]. The average ROG values for the investigated metabolites range from 30.41 Å to 30.56 Å with sofosbuvir-VP1 (reference standard) having a mean ROG value of 30.51 Å and chrysoeriol 7-glucuronide-VP1 being the highest (30.56 Å) (Table 2). The lowest ROG value was observed in spiraeoside-VP1 (30.41 Å), which is equal to the apo-VP1 and lower than that of the reference standard (30.51 Å), and this further confirms its potential as a novel VP1 inhibitor as it was able to maintain the compactness of the protein (Table 2 and Fig. 5). This corroborates the RMSF result in which it exhibited a lower average RMSF value relative to the unbound VP1. The ROG findings in this study are partly consistent with Khan et al. [60], in which a negligible difference in average ROG

Table 2
Mean RMSD, RMSF, ROG, SASA and hydrogen bonds of apo-VP1 protein, top-ranked compounds, and the standard.

Ligands	Mean RMSD (Å)	Mean RMSF (Å)	Mean ROG (Å)	Mean SASA (Å)	Mean Number of H-Bonds	Mean Distance (Å) of H-Bonds	Mean Angle (°) of H-Bonds
VP1							
Chrysoeriol 7-glucuronide	1.92±0.19	1.19±0.53	30.56±0.16	43,290.91 ±897.66	575.42±16.34	2.86±0.06	151.92±7.57
Ellagic acid hexoside	1.94±0.15	1.16±0.45	30.49±0.10	43,595.91 ±683.88	564.47±15.88	2.86±0.06	151.97±7.57
Gnetin L	1.87±0.16	1.18±0.54	30.50±0.08	43,323.76 ±664.22	571.51±16.14	2.86±0.06	151.97±7.59
Kaempferol 7-O-glucoside	1.81±0.16	1.14±0.45	30.45±0.11	43,069.24 ±633.97	577.57±15.82	2.86±0.06	151.88±7.63
Spiraeoside	1.89±0.10	1.10±0.49	30.41±0.07	42,509.72 ±548.80	578.69±16.22	2.86±0.06	151.92±7.65
Sofosbuvir	1.94±0.15	1.10±0.47	30.51±0.11	43,967.71 ±759.48	577.48±16.62	2.86±0.06	151.79±7.66
VP1	1.88±0.14	1.15±0.49	30.41±0.08	43,557.14 ±640.52	572.54±15.96	2.86±0.06	151.99±7.57

Table 3
Catalytic residues fluctuations (Å) in VP1.

Catalytic residues of VP1	Chrysoeriol 7-glucuronide	Ellagic acid hexoside	Gnetin L	Kaempferol 7-O-glucoside	Spiraeoside	Sofosbuvir	VP1	Total RMSF
Arg452	0.71	0.74	0.79	0.69	0.67	0.60	0.60	0.69
Arg457	0.72	0.74	0.73	0.73	0.66	0.60	0.64	0.69
Arg460	0.79	0.77	0.67	0.75	0.65	0.62	0.62	0.70
Glu492	0.80	0.81	0.73	0.77	0.61	0.74	0.90	0.77
Asp520	0.72	0.67	0.61	0.58	0.66	0.59	0.62	0.64
Ser522	0.74	0.65	0.61	0.60	0.68	0.62	0.63	0.65
Gln523	0.84	0.77	0.77	0.72	0.74	0.72	0.73	0.76
Asp525	1.12	0.89	0.99	1.03	1.08	0.93	0.94	0.99
Ser591	0.72	0.81	0.63	0.66	0.80	0.57	0.74	0.70
Lys594	1.09	0.98	0.82	0.88	1.31	0.89	1.08	1.01
Lys597	0.84	0.86	0.79	0.92	1.01	0.88	0.90	0.89
Asp631	1.75	1.75	1.73	1.50	1.58	1.68	1.73	1.67
Asp632	1.10	1.10	1.11	1.11	0.92	1.15	1.16	1.09
Lys679	0.60	0.62	0.63	1.20	0.56	0.65	0.74	0.71
Total RMSF	0.90	0.87	0.83	0.87	0.85	0.80	0.86	

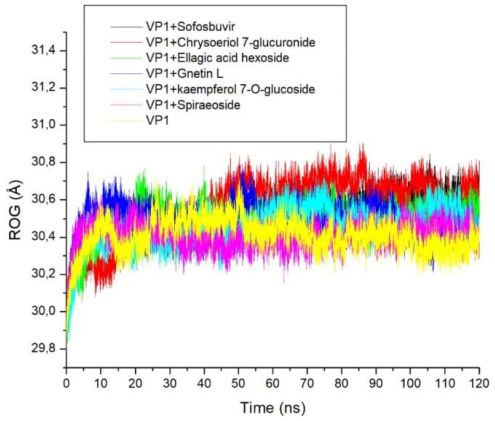


Fig. 5. Comparative ROG plots of alpha-carbon, top-ranked compounds and reference standard against VP1 after 120 ns MD simulation period.

values was reported between apo-RdRP and remdesivir-RdRp of SARS-CoV-2. Generally, an overall difference of 0.15 Å was observed in the ROG values between the investigated compounds and sofosbuvir, indicating that the ligand binding had a negligible effect on the compactness of the target, hence further confirming the affinity of the top hit compounds for the VP1 protein.

The surface characteristics of proteins, such as polar, nonpolar, exposed, and buried residue, were examined by analyzing the solvent accessible surface area (SASA). The SASA profile of each system evaluates the extent of structural modification in protein accessibility to solvent due to ligand binding [40], with higher SASA values suggesting an increased surface area, whereas lower SASA values portend a reduction in protein volume [61]. A progressive decline with minor fluctuations in SASA against VP1 was observed during the simulation for all systems and was more noticeable in the spiraeoside-VP1 complex (Fig. 6). Consequently, the lowest mean SASA value was reported in spiraeoside-VP1 complex (42,509.72 Å), suggesting that fewer VP1 residues are available for solvent interaction. This observation is consistent with the RMSF and ROG result and further validates its potential as a VP1 inhibitor and partly supports its binding free energy outcome. Apart from the spiraeoside-VP1 complex, a reduction in SASA value was equally observed in chrysoeriol 7-glucuronide-VP1 (43,290.91 Å), gnetin L-VP1 (43,323.76 Å), kaempferol 7-O-glucoside-VP1 (43,069.24 Å) suggesting their potential to inhibit the protein. These observations contradict that of Ahmed et al. [62], in which the binding of remdesivir analogues with SARS-CoV-2 RdRp protein resulted in higher average SASA values relative to the unbound protein. Similarly, ellagic acid hexoside-VP1 (43,595.91 Å) and sofosbuvir-VP1 (43,967.71 Å) exhibited higher average SASA values compared to the apo-protein; however, the ellagic acid hexoside-VP1 complex's mean SASA value is lower compared to the standard portraying it as a better inhibitor relative to the reference standard.

The formation of H-bonds, their associated distance and angle play a crucial role in maintaining the stability of a complex, and these parameters may be assessed via simulation to get insights into the effects of ligand binding on the overall stability of the protein [61,63]. A steady fluctuation pattern was observed in the number of H-bonds between 494 and 652 before and after the binding of the ligands to VP1 during the stimulation (Fig. 7). These findings indicate the relative consistency in H-bonds formation in VP1, thereby maintaining the protein's structure with or without ligand binding. In addition, similar conclusions in the results of the RMSF and ROG analysis were reported in this study, indicating that the stability of VP1 was relatively unaffected upon binding of the lead compounds and sofosbuvir.

Higher mean number of H-bonds was observed in spiraeoside-VP1 (578), kaempferol 7-O-glucoside-VP1 (577), sofosbuvir-VP1 (577), chrysoeriol 7-glucuronide-VP1 (575) relative to unbound VP1 (572) (Table 3), while lower number of H-bonds were observed in ellagic acid hexoside-VP1 (564) and gnetin L-VP1 (571). Based on the observed overall difference of 7 hydrogen bonds in the intramolecular bonds of VP1 subsequent to the binding of the leads and sofosbuvir, it can be deduced that the geometry of VP1 was not compromised upon ligand binding. These findings are partly similar to Lanrewaju et al. [17] report, where an overall difference of 5 hydrogen bonds was observed across the investigated metabolites upon binding to RVA VP8* protein.

Furthermore, during the 120 ns simulation, the binding of the top-ranked compounds and sofosbuvir resulted in a consistent decrease in the distance of H-bonds generated within VP1 (Fig. 8). A mean H-bond distance of 2.86 Å was observed in the apo-protein and the bound complexes, which is considered good because it is lesser than the

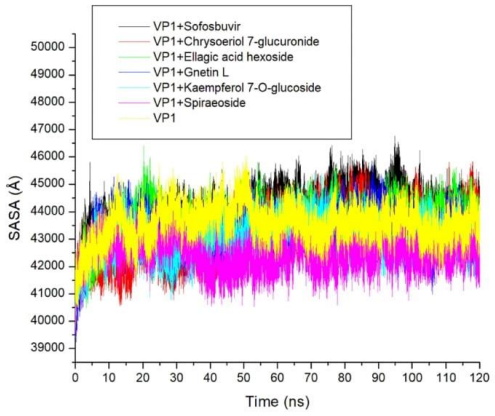


Fig. 6. Comparative SASA plots of alpha-carbon, top-ranked compounds and reference standard against VP1 after 120 ns MD simulation period.

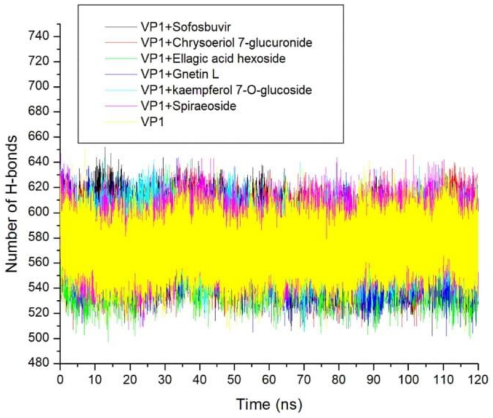


Fig. 7. Time evolution of the number of H-bonds in VP1 upon binding with the top-ranked compounds and reference standard during the 120 ns MD simulation period.

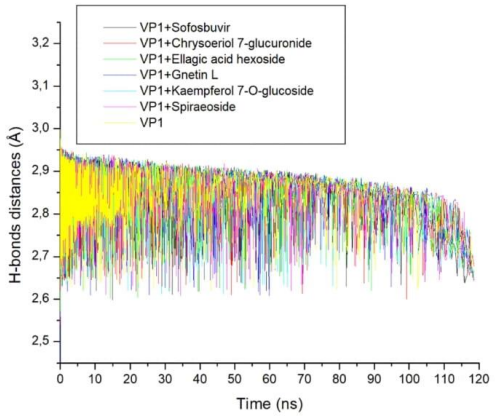


Fig. 8. Time evolution of the H-bonds distance in VP1 upon binding of the top-ranked compounds and reference standard during the 120 ns MD simulation period.

satisfactory 3.5 Å for H-bonds distance during simulation [61,63]. This is similar to findings by Aribisala et al. [64], in which an average H-bond distance of 2.87 Å was reported in the apo-omicron spike protein of SARS-CoV-2 and the bound complexes. A shorter bond length denotes a more stable bond and an intensified attraction between two entities resulting in a tighter cohesion of their constituent atoms [63]. In addition, observing identical hydrogen bonds distance across the unbound-protein and the bound complexes systems suggests thermodynamic orderliness upon ligand binding is relatively coherent with the thermodynamic metrics evaluated in this investigation. The third component of the H-bonds analysis is the bond angle, where values approaching 180° indicate a stronger H-bond [65].

A steady fluctuation in the H-bonds angle was observed during the simulation, while a significant variation was observed at the start of the simulation, spanning from 137° to 168°, with a reduction in the fluctuation towards 180° as the simulation continues (Fig. 9). The average

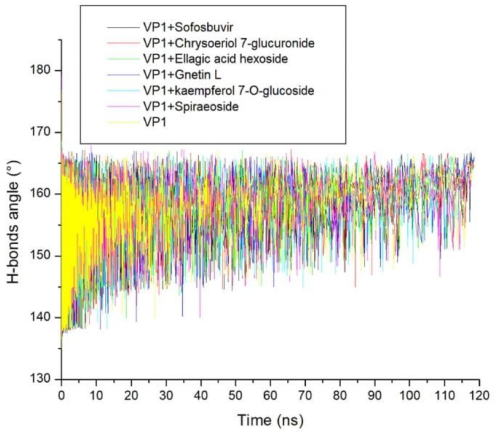


Fig. 9. Time evolution of the H-bonds angles in VP1 upon binding of the top-ranked compounds and reference standard during the 120 ns MD simulation period.

H-bonds angles fluctuate between 151.92° and 151.99° (Table 2), with an intangible overall difference of 0.07° revealing proximity between the reported values for all the complexes and the unbound protein, which is in sync with other thermodynamic metrics. Summarily, the H-bonds distance and angle values for all systems are closely similar, suggesting their minimal or no impact on their binding free energy.

3.6. Bond analysis of the top-ranked compounds after 120 ns MD simulation

The kind of contacts, bond lengths, and number of interactions in a complex influence a compound's affinity for a target and the stability of the resultant complex [55]. Consequently, following the 120 ns simulation time, the type of contacts, bond lengths, and number of interactions with the top-ranked compounds' binding to VP1 were evaluated in this investigation. Different interactions, including hydrogen bonds, Van der Waals, amide π-stacked, π-anion, π-sigma, π-cation, π-π t-cation, π-π t-shaped, π-π t-stacked, π-alkyl, alky, π-Sulphur and unfavourable donor−donor interactions were detected between the top-hit compounds and VP1. Therefore, the interactions plot of the top-ranked compounds and sofosbuvir with VP1 were further analysed in this investigation and are shown in Supplementary Table S3.

In this study, the kind, bond length, and number of interactions between the compounds had a significant influence on their resultant stability and binding free energy. Unfortunately, the highest negative binding free energy in chrysoeriol 7-glucuronide is not in sync with the observed number of interactions (22) (Table 4). Furthermore, spiraeoside, with the next highest negative binding free energy, exhibited the highest number of interactions (29), which is inconsistent with its binding free energy. However, a shorter bond length was (4.96 Å) noticed in chrysoeriol 7-glucuronide relative to spiraeoside (5.11 Å). This aligns with that of Du et al. [63], which indicated that the variation in interaction bond length might account for the differences in binding affinity. A reduced bond length signifies enhanced bond stability and increased intermolecular attraction, resulting in a stronger cohesive force that closely binds the atoms of two entities. Therefore, this could be linked to the higher negative binding free energy observed in chrysoeriol 7-glucuronide compared to spiraeoside. Meanwhile, unfavourable donor-donor interaction, a repulsive force [64], was observed in spiraeoside at 0, 40 and 80 ns but was reported in chrysoeriol 7-glucuronide only at 120 ns and could be connected to a lesser negative binding free energy observed in spiraeoside relative to chrysoeriol 7-glucuronide (Supplementary Table S3 and Table 4). Of the 29 interactions observed in spiraeoside, 9 were van der Waals [Ile662, Asp505, Ser245, Tyr322, Ser242, Lys238, Phe326, Ser511 and Arg443] while of the 22 interactions observed in chrysoeriol 7-glucuronide, 5 were van der Waals [Ile678, Lys664, Ser241, Ser245, Asp505]. Therefore, the higher number of interactions observed in spiraeoside which was partly due to the formation of van der Waals; a weak attractive force could be responsible for the higher number of interactions, which could not account for the binding free energy compared to chrysoeriol 7-glucuronide.

Remarkably, both gnetin L and kaempferol 7-O-glucoside exhibited similar binding free energy accompanied by an equal number of interactions and the absence of unfavourable donor-donor interaction at 120 ns. However, a shorter bond length was observed in gnetin L (4.87 Å, 4.07 Å) compared to kaempferol 7-O-glucoside (5.24 Å, 4.63 Å) (Table 4) in the total sum of interactions and hydrogen bonds respectively. A higher negative binding free energy would have been noticed in gnetin L relative to kaempferol 7-O-glucoside due to its shorter bond length but unfavourable donor-donor interaction, which is a repulsive force in gnetin L at 80 ns. In addition, a higher number of H-bonds was detected in kaempferol 7-O-glucoside (6) compared to gnetin L (5) (Supplementary Table S3). It could have covered up for the unfavourable donor-donor interaction observed in gnetin L, hence a similar binding free energy.

Table 4
Bond analysis of the top-ranked compounds against VP1 after 120 ns simulation.

Top-ranked compounds	Total sum of interactions (Mean length in Å)	Number of H-bonds and interaction residues	Other vital interactions and residues	Unfavourable Bonds
Chrysoeriol 7-glucuronide	22 (4.96 Å)	11 (4.57 Å) [Arg708, Arg442, Ala663(3) Asp617, Ile662, Lys652, Glu661(3)]	5 (5.54 Å) [Arg675, Phe326, Val439, Arg442, Ala663]	1 (6.31 Å) Tyr322
Ellagic acid hexoside	20 (4.84 Å)	6 (4.73 Å) [Asn683, Asn701, Asn682, Asn679 (2), Ile678]	4 (5.00 Å) [Ile678 (2), Pro440, Phe330]	None
Gnetin L	26 (4.87 Å)	5 (4.07 Å) [Lys238, Gly441, Glu661, Arg675, Glu684]	10 (5.28 Å) [Lys238 (2), Arg442 (2), Arg675, Phe326 (2), Pro440 (2), Phe330]	None
Kaempferol 7-O-glucoside	26 (5.24 Å)	6 (4.63 Å) [Arg442, Ser241, Tyr322, Glu661 (2), Lys652]	9 (5.69 Å) [Pro440, Phe326, Arg442 (2), Val439, Arg675 (2), Ala663 (2)]	None
Spiraeoside	29 (5.11 Å)	11(4.50 Å) [Ser241 (2), Ala237, Arg442 (2), Arg445, Ser507, Lys652, Asp617, Glu661 (2)]	9 (5.85 Å) [Arg442, Ala663, Arg445 (2), Arg437 (2), Asp616 (2), Val439]	None
Sofosbuvir	22 (4.70 Å)	10 (3.99 Å) [Ala663, Glu661, Gly441, Ser241 (2), Ser242 (2), Lys238 (3)]	4 (6.19 Å) [Arg675, Arg331, Arg443, Arg442]	1 (5.81 Å) [Tyr322]

The number of interactions exhibited by ellagic acid hexoside (20) and sofosbuvir (22) agrees with their reported binding free energy (Tables 3 and 5). Apart from the number of interactions, higher negative binding free energy in sofosbuvir could be due to its shorter bond length (4.70 Å) relative to ellagic acid hexoside with longer bond length (4.84 Å) because short bond length has been linked with strong cohesive force which closely binds atoms together. In addition, a higher number of H-bonds was noticed in sofosbuvir (10) compared to ellagic acid hexoside (6) (Supplementary Table S3). The hydrogen bond plays a crucial role in determining the binding affinity and contributes significantly to the binding interaction between ligands and proteins. In addition, these bonds govern drug selectivity, metabolization, and adsorption [45]. Therefore, the higher number of H-bonds and their shorter bond length in sofosbuvir (10, 3.99 Å) could be connected to its higher negative binding free energy compared to ellagic acid hexoside (6, 4.73 Å) (Table 4).

The simulation period revealed a noticeable variation as a result of the intrinsic flexibility shown by both ligand and protein in the MD simulation, which is renowned for its dynamic characteristics [64]. Consequently, there are consistent fluctuations in the amino acid residues shown in the interaction plots for the complexes examined in this study over the 120 ns simulation period (Supplementary Table S3). Generally, the significance of the number, length and type of contacts in determining the binding free energy is therefore shown by the interaction plots analysis, as demonstrated in the interactions with VP1 in this study.

3.7. Molecular orbital properties of the top-ranked compounds

The use of the quantum approach of DFT is prevalent in computational investigations to comprehend the pharmacological impact of the lead compounds. The HOMO and LUMO of a compound contribute significantly to its biological processes as its kinetic resilience, electrochemical stability, chemical hardness, and softness are all connected to the HOMO-LUMO energy gap that exists between the atoms of the molecule. A larger energy gap indicates notable kinetic stability but limited electrochemical stability; however, a comparatively lower energy difference and increased softness indicate a higher degree of polarity and chemical conductivity in the molecules. Furthermore, a compound's reactivity decreases as its energy gap widens, suggesting a reduction in electronic transition within the compound, while a narrow energy gap indicates a higher degree of atomic system and greater electrochemical stability [66], which are crucial in facilitating the binding of molecules to specific protein receptors [67].

The cDFT parameters of the top-ranked compounds and the reference standard are presented in Table 5, while that of gnetin L has been previously reported [17]. The lowest energy gap in this study was observed in spiraeoside (3.86 eV), while chrysoeriol 7-glucuronide (4.04 eV), with the highest negative binding free energy has a higher energy gap (Table 1, 5 and Fig. 10). The next negative higher binding free energy was observed in spiraeoside and could be linked to its energy gap; its reactivity which is a function of its reduced energy gap, was more evident in its higher number of interactions (Table 4) and more favourable thermodynamic features relative to other lead compounds (Table 2).

The cDFT descriptors evaluated in this study, including the ionization potential, electron affinity, hardness, softness, electronegativity, chemical potential and electrophilicity, offer vital chemical insights pertinent to the potential therapeutics application of the investigated compounds. Among these descriptors, chemical hardness of a molecule, which is inversely proportional to softness, holds significance in evaluating chemical stability and plays a crucial role in drug design studies [68]. This hardness reflects a molecule's ability to withstand changes in its electron configuration and indicates less reactivity because as the energy gap widens, reactivity diminishes. In contrast, softness indicates a smaller energy gap and an increased polarization due to chemical changes, leading to higher reactivity [69]. Therefore, the higher chemical softness (0.52 eV) and lower chemical hardness (1.93 eV) of spiraeoside, compared to other investigated compounds (Table 5), suggests that spiraeoside is highly reactive and could have influenced its affinity for the compound. More importantly, the less flexibility and high compactness, reduced surface for solvent interaction and higher number

Table 5
The cDFT parameters of the top-ranked compounds.

cDFT parameters (eV)										
Ligands	LUMO	HOMO	Energy gap	Ionization energy	Electron affinity	Hardness	Softness	Electronegativity	Chemical potential	Global electrophilicity
Chrysoeriol 7-glucuronide	−2.08	−6.12	4.04	2.08	6.12	2.02	0.50	4.10	−4.10	4.17
Ellagic acid hexoside	−2.13	−6.50	4.37	2.13	6.50	2.18	0.46	4.31	−4.31	4.26
Kaempferol 7-O-glucoside	−2.04	−5.94	3.90	2.04	5.94	1.95	0.51	3.99	−3.99	4.08
Spiraeoside	−2.43	−6.29	3.86	2.43	6.29	1.93	0.52	4.36	−4.36	4.92
Sofosbuvir	−1.49	−6.80	5.31	1.49	6.80	2.66	0.38	4.14	−4.14	3.23

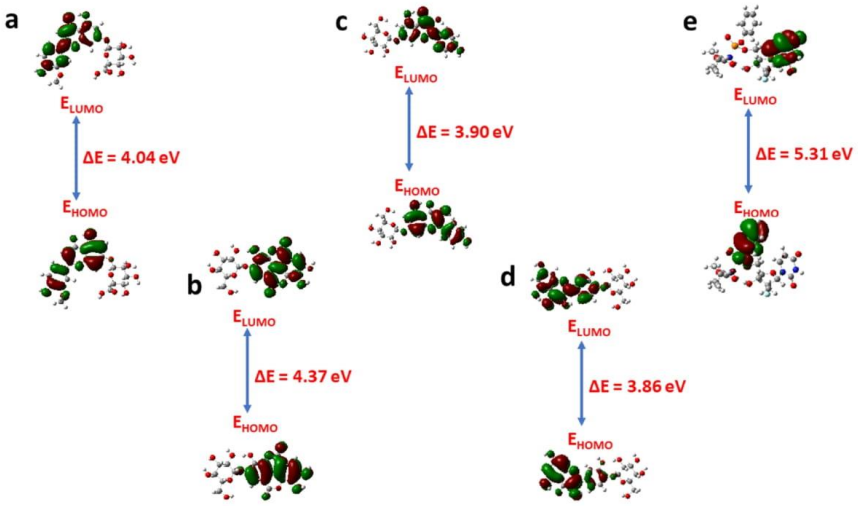


Fig. 10. Frontier molecular orbitals for (a) chrysoeriol 7-glucuronide (b) ellagic acid hexoside (c) kaempferol 7-O-glucoside (d) spiraeoside (e) sofosbuvir (reference standard).

of hydrogen bonds (Table 3) observed upon the binding of spiraeoside to the protein could be attributed to its lower chemical hardness and higher chemical softness values compared to other top-ranked compounds.

Electronegativity and chemical potential are metrics that assess the capacity of an atom or functional group to attract electrons [34]. Specifically, a negative chemical potential provides support for the molecule's stability by inhibiting spontaneous breakdown [68], and the extent of decomposition of compounds into elements is inversely proportional to the magnitude of their negative chemical potential values [69]. The stability of the top-ranked compounds and the reference compound (sofosbuvir) is further supported by their chemical potential's negative value, which inhibits spontaneous breakdown with spiraeoside (−4.36 eV) having the highest negative chemical potential value (Table 5), suggesting it has the most electron attracting ability. Expectedly, this trend is also supported by the observed electronegativity values in which spiraeoside (4.36 eV) had the highest electronegativity value (Table 5). The possibility of an electrophile to acquire a certain amount of electron density and the resistance of a molecule to exchange electron density are both defined by the electrophilicity index. A trend partly similar to the chemical potential and electronegativity values was observed in the top-ranked compounds, with spiraeoside (4.92 eV) having the highest value; however, the lowest electrophilicity index was exhibited by the reference standard (3.23 eV) (Table 5). Based on their electrophilicity values, molecules are classified into low (< 0.8 eV), moderate (0.8 – 1.5 eV) and heavy (>1.5 eV) electrophiles [70]. Remarkably, all the lead compounds and sofosbuvir are heavy electrophiles, signifying a substantial presence of electrophiles.

4. Conclusion

The results of this investigation have demonstrated the potential capabilities of the identified top-hit compounds belonging to different classes of secondary metabolites ranging from flavone (chrysoeriol 7-glucuronide), flavonol (spiraeoside, kaempferol 7-O-glucoside), polyphenol (gnetin L) and tannin (ellagic acid hexoside) in modulating the VP1 of RVA. Four of the identified hits exhibited significantly higher binding free energy than sofosbuvir after MD simulation, emphasizing their potential as promising candidates. These lead compounds span across the three distinct investigated medicinal plants: chrysoeriol 7-glucuronide (*D. eriocarpum*), ellagic acid hexoside (*S. mombin* and *M. barteri*), gnetin L and kaempferol 7-O-glucoside (*S. mombin*) and spiraeoside (*M. barteri*), which further confirms the antiviral potentials of the selected plants. The utilization of DFT yielded significant insights into the electronic characteristics of the top-ranked compounds, which could profoundly influence their biological functionality. Although, chrysoeriol 7-glucuronide had the highest negative binding free energy relative to other lead compounds, spiraeoside demonstrated more favourable thermodynamic abilities. This could be linked to its superior molecular properties, suggesting better reactivity relative to the other investigated compounds. Moreover, spiraeoside's favourable pharmacological features might be associated with its higher number of bond interactions compared to other identified hits. These observations collectively indicate the inhibitory potential of the hit compounds, especially spiraeoside against the VP1 protein of RVA, offers promising advantages in the management of RV infection. However, there is a need for structural refinement of chrysoeriol 7-glucuronide to enhance its druggability. Furthermore, complementary *in vitro* and *in vivo* studies are strongly recommended to validate the therapeutic potential of the profiled lead metabolites in combating RVA infections. The collective insights from this study thus contribute valuable information for the continued exploration and development of potential antiviral agents against RVA.

Disclosure statement

No potential conflict of interest was reported by the authors.

CRediT authorship contribution statement

Adedayo Ayodeji Lanrewaju: Writing – original draft, Validation, Methodology, Investigation, Formal analysis, Data curation. **Abimbola Motunrayo Folami:** Writing – review & editing, Supervision, Funding acquisition, Conceptualization. **Saheed Sabiu:** Writing – review & editing, Validation, Supervision, Software, Resources, Funding acquisition, Data curation, Conceptualization. **Feroz Mahomed Swalaha:** Writing – review & editing, Supervision, Funding acquisition.

Declaration of competing interest

The authors declare that they have no known competing financial interests or personal relationships that could have appeared to influence the work reported in this paper.

Data availability

The data is contained within the article or supplementary material.

Acknowledgements

The Durban University of Technology (DUT) Doctoral Scholarship Scheme to A. A. Lanrewaju is duly acknowledged. The Centre for High-Performance Computing (CHPC), South Africa, is equally acknowledged for granting access to the computing systems used in this study.

Funding

The study is based on the financial assistance received from the Directorate of Research and Postgraduate Support, Durban University of Technology (DUT), and the South African Medical Research Council (SAMRC) under a Self-Initiated Research Grant and the National Research Foundation (NRF) Competitive Programme for Rated Researchers Support (SRUG2204193723) to S. Sabiu. We also acknowledge Water Research Commission (WRC) of South Africa for the grant (Project no K5/C2020–2021–00181) awarded to A.M. Enitan-Folami.

Supplementary materials

Supplementary material associated with this article can be found, in the online version, at doi:10.1016/j.chphi.2024.100745.

References

[1] C. Troeger, et al., Rotavirus vaccination and the global burden of rotavirus diarrhea among children younger than 5 years, JAMA Pediatr 172 (10) (2018) 958–965.
[2] M.M. Nyaga, et al., Report of the 1st African Enteric Viruses Genome Initiative (AEVGI) Data and Bioinformatics Workshop on whole-genome analysis of some African rotavirus strains held in Bloemfontein, South Africa, Vaccine 38 (34) (2020) 5402–5407.
[3] A. Bhuinya, et al., A tale of antiviral counterattacks in rotavirus infection, Microbiol. Res. (2022) 127046.
[4] A.A. Lanrewaju, et al., Global public health implications of human exposure to viral contaminated water, Front. Microbiol. 13 (2022) 981896. -981896.
[5] M.J. Tohmé, L.R. Delgui, Advances in the development of antiviral compounds for rotavirus infections, MBio 12 (3) (2021) e00111–e00121.
[6] R. Yamashiro, A. Sakudo, M. Nagatsu, Efficient recovery and enrichment of infectious rotavirus using separation with antibody-integrated graphite-encapsulated magnetic nanobeads produced by argon/ammonia gas plasma technology, Int. J. Nanomed. 14 (2019) 1865.
[7] Enitan-Folami, A., A. Lanrewaju, and F. Swalaha, Inactivation of waterborne pathogens using medicinal plants. 2022.
[8] A.E. Fadiji, et al., Antimicrobial efficacy and phytochemical screening of aqueous and ethanolic extracts of Ocimum gratissimum (scent leaf) leaf against some clinical isolates, J. Basic Pharmacol. Toxicol. 2 (2) (2018) 19–24.
[9] M. Akram, et al., Antiviral potential of medicinal plants against HIV, HSV, influenza, hepatitis, and coxsackievirus: a systematic review, Phytother. Res. 32 (5) (2018) 811–822.
[10] J. Corthout, et al., Antiviral ellagitannins from Spondias mombin, Phytochemistry 30 (4) (1991) 1129–1130.
[11] E.M.d.S. Siqueira, et al., Antiviral potential of spondias mombin L. leaves extract against herpes simplex virus type-1 replication using in vitro and in silico approaches, Planta Med. 86 (07) (2020) 505–515.
[12] O.O. Ogbole, et al., *In vitro* antiviral activity of twenty-seven medicinal plant extracts from Southwest Nigeria against three serotypes of echoviruses, Virol. J. 15 (1) (2018) 1–8.
[13] P.A. Segun, et al., *In vitro* anti-enteroviral activity of stilbenoids isolated from the leaves of Macaranga barteri, Nat. Prod. Res. (2019) 1–5.
[14] D. Luseba, et al., Antibacterial, anti-inflammatory and mutagenic effects of some medicinal plants used in South Africa for the treatment of wounds and retained placenta in livestock, South African J. Botany 73 (3) (2007) 378–383.
[15] I.C. Du Preez, D.R. Mumbengegwi, Phytochemical investigation on Namibian plants for anti-malaria compounds, J. Stud. Humanit. Soc. Sci. (2014) 147–158.
[16] D. Van der Merwe, G. Swan, C. Botha, Use of ethnoveterinary medicinal plants in cattle by Setswana-speaking people in the Madikwe area of the North West Province of South Africa, J S Afr. Vet. Assoc 72 (4) (2001) 189–196.
[17] A.A. Lanrewaju, et al., Cheminformatics bioprospection of selected medicinal plants metabolites against trypsin cleaved VP4 (spike protein) of rotavirus A, J. Biomol. Struct. Dynam. (2023) 1–20.
[18] A.A. Lanrewaju, et al., Computational bioprospection of selected plant secondary metabolites against VP7 (capsid protein) of rotavirus A, Scientific African (2024) e02109.
[19] D. Sun, et al., Why 90% of clinical drug development fails and how to improve it? Acta Pharmaceutica. Sinica B 12 (7) (2022) 3049–3062.
[20] J.O.-O. Uhomoibhi, et al., Molecular modelling identification of phytocompounds from selected African botanicals as promising therapeutics against druggable human host cell targets of SARS-CoV-2, J. Mol. Graphics Modell. 114 (2022) 108185.
[21] J.J. Oloche, et al., Molecular modeling identification of key secondary metabolites from Xylopia aethiopica as promising therapeutics targeting essential measles viral proteins, Evidence-Based Complem. Altern. Med. 2023 (2023).
[22] T. Garuba, et al., Metabolites profiling and molecular docking identification of putative leads from endophytic Phyllosticta capitalensis as modulators of key druggable structural targets of rotavirus A, Transac. Royal Soc. South Africa 77 (3) (2022) 207–217.
[23] F.O. Shode, et al., Molecular dynamics study on selected bioactive phytochemicals as potential inhibitors of HIV-1 subtype C protease, Metabolites 12 (11) (2022) 1155.
[24] S. Sabiu, F.O. Balogun, S.O. Amoo, Phenolics profiling of Carpobrotus edulis (L.) NE Br. and insights into molecular dynamics of their significance in type 2 diabetes therapy and its retinopathy complication, Molecules 26 (16) (2021) 4867.
[25] E.F. Pettersen, et al., UCSF Chimera—a visualization system for exploratory research and analysis, J. Comput. Chem. 25 (13) (2004) 1605–1612.
[26] A.A. Lanrewaju, et al., Metabolites profiling and cheminformatics bioprospection of selected medicinal plants against the main protease and RNA-dependent RNA polymerase of SARS-CoV-2, J. Biomol. Struct. Dynam. (2023) 1–21.
[27] S. Khan, et al., A review on the interaction of nucleoside analogues with SARS-CoV-2 RNA dependent RNA polymerase, Int. J. Biol. Macromol. 181 (2021) 605–611.
[28] S. Dallakyan, A.J. Olson, Small-molecule library screening by docking with PyRx, Chem. Biol. (2015) 243–250.
[29] S.M. McDonald, et al., Shared and group-specific features of the rotavirus RNA polymerase reveal potential determinants of gene reassortment restriction, J. Virol. 83 (12) (2009) 6135–6148.
[30] X. Lu, et al., Mechanism for coordinated RNA packaging and genome replication by rotavirus polymerase VP1, Structure 16 (11) (2008) 1678–1688.
[31] J.O. Aribisala, S. Sabiu, Cheminformatics identification of phenolics as modulators of penicillin-binding protein 2a of staphylococcus aureus: a structure–activity-relationship-based study, Pharmaceutics 14 (9) (2022) 1818.
[32] L. Deschenes, D. Bout, Origin 6.0: scientific data analysis and graphing software origin lab corporation. University of Texas, Austin, J. Am. Chem. Soc. 122 (39) (2000) 9567–9568.
[33] M. Ylilauri, O.T. Pentikäinen, MMGBSA as a tool to understand the binding affinities of filamin–peptide interactions, J. Chem. Inf. Model 53 (10) (2013) 2626–2633.
[34] A. Rampadarath, et al., Molecular bioprospection of Helianthus annuus L. (sunflower) cypsela for antidiabetic therapeutics through network pharmacology, density functional theory and molecular dynamics simulation, South African J. Botany 162 (2023) 72–95.
[35] H. Kruse, L. Goerigk, S. Grimme, Why the standard B3LYP/6-31G* model chemistry should not be used in DFT calculations of molecular thermochemistry: understanding and correcting the problem, J. Org. Chem. 77 (23) (2012) 10824–10834.
[36] J.-L. Calais, Density-functional theory of atoms and molecules. RG Parr and W. Yang, Oxford University press, New York, Oxford, 1989. IX+ 333 pp. Price£ 45.00, Int. J. Quantum Chem. 47 (1) (1993) 101. -101.
[37] J. Luo, et al., Koopmans' theorem for large molecular systems within density functional theory, J. Phys. Chem. A 110 (43) (2006) 12005–12009.
[38] T.G. Mashamba, et al., Quorum sensing modulation and inhibition in biofilm forming foot ulcer pathogens by selected medicinal plants, Heliyon 8 (4) (2022).
[39] A. Akoonjee, et al., Waste to medicine: evidence from computational studies on the modulatory role of corn silk on the therapeutic targets implicated in type 2 diabetes mellitus, Biology (Basel) 12 (12) (2023) 1509.
[40] S. Aziz, et al., Identifying non-nucleoside inhibitors of RNA-dependent RNA-polymerase of SARS-CoV-2 through per-residue energy decomposition-based pharmacophore modeling, molecular docking, and molecular dynamics simulation, J. Infect. Public Health 16 (4) (2023) 501–519.
[41] S. Anandan, et al., Integrated approach for studying bioactive compounds from Cladosporium spp. against estrogen receptor alpha as breast cancer drug target, Sci. Rep. 12 (1) (2022) 22446.
[42] C.A. Lipinski, et al., Experimental and computational approaches to estimate solubility and permeability in drug discovery and development settings, Adv. Drug Deliv. Rev. 64 (2012) 4–17.
[43] R.P. Heaney, Factors influencing the measurement of bioavailability, taking calcium as a model, J. Nutr. 131 (4) (2001) 1344S–1348S.
[44] A.P. Hill, R.J. Young, Getting physical in drug discovery: a contemporary perspective on solubility and hydrophobicity, Drug Discov. Today 15 (15–16) (2010) 648–655.

[45] M. Moussaoui, et al., In silico design of novel CDK2 inhibitors through QSAR, ADMET, molecular docking and molecular dynamics simulation studies, J. Biomol. Struct. Dynam. (2023) 1–17.
[46] N.A. Meanwell, Improving drug candidates by design: a focus on physicochemical properties as a means of improving compound disposition and safety, Chem. Res. Toxicol. 24 (9) (2011) 1420–1456.
[47] A.K. Verma, et al., Molecular docking and simulation studies of flavonoid compounds against PBP-2a of methicillin-resistant Staphylococcus aureus, J. Biomol. Struct. Dynam. 40 (21) (2022) 10561–10577.
[48] E. Wang, et al., End-point binding free energy calculation with MM/PBSA and MM/GBSA: strategies and applications in drug design, Chem. Rev. 119 (16) (2019) 9478–9508.
[49] A. Acharya, et al., Supercomputer-based ensemble docking drug discovery pipeline with application to COVID-19, J. Chem. Inf. Model 60 (12) (2020) 5832–5852.
[50] T.A. Wani, et al., A potential anticancer dihydropyrimidine derivative and its protein binding mechanism by multispectroscopic, molecular docking and molecular dynamic simulation along with its in-silico toxicity and metabolic profile, Europ. J. Pharmaceut. Sci. 158 (2021) 105686.
[51] S.A. Khan, et al., Identification of chymotrypsin-like protease inhibitors of SARS-CoV-2 via integrated computational approach, J. Biomolecul. Struct. Dynam. 39 (7) (2021) 2607–2616.
[52] A. Sharma, et al., Identification of natural inhibitors against prime targets of SARS-CoV-2 using molecular docking, molecular dynamics simulation and MM-PBSA approaches, J. Biomolecul. Struct. Dynam. 40 (7) (2022) 3296–3311.
[53] D. Ramírez, J. Caballero, Is it reliable to use common molecular docking methods for comparing the binding affinities of enantiomer pairs for their protein target? Int. J. Mol. Sci. 17 (4) (2016) 525.
[54] V.J. Reeda, V.B. Jothy, Vibrational spectroscopic, quantum computational (DFT), reactivity (ELF, LOL and Fukui), molecular docking studies and molecular dynamic simulation on (6-methoxy-2-oxo-2H-chromen-4-yl) methyl morpholine-4-carbodithioate, J. Mol. Liq. 371 (2023) 121147.
[55] J.O. Aribisala, et al., Cheminformatics identification of phenolics as modulators of key penicillin– binding proteins of Escherichia coli towards interventive antibacterial therapy, Mol. Simul. (2023) 1–17.
[56] H. Pundir, et al., Identification of SARS-CoV-2 RNA dependent RNA polymerase inhibitors using pharmacophore modelling, molecular docking and molecular dynamics simulation approaches, J. Biomolecul. Struct. Dynam. 40 (24) (2022) 13366–13377.
[57] A. Boadu, et al., Repurposing antiviral phytochemicals from the leaf extracts of Spondias mombin (Linn) towards the identification of potential SARSCOV-2 inhibitors, Sci. Rep. 12 (1) (2022) 1–14.
[58] M.Y. Lobanov, N. Bogatyreva, O. Galzitskaya, Radius of gyration as an indicator of protein structure compactness, Mol. Biol. (N.Y.) 42 (2008) 623–628.
[59] R. Islam, et al., A molecular modeling approach to identify effective antiviral phytochemicals against the main protease of SARS-CoV-2, J. Biomolecul. Struct. Dynam. 39 (9) (2021) 3213–3224.
[60] F.I. Khan, et al., Remdesivir strongly binds to RNA-dependent RNA polymerase, membrane protein, and main protease of SARS-CoV-2: indication from molecular modeling and simulations, Front. Pharmacol. 12 (2021) 710778.
[61] S.S. Mousavi, et al., In silico evaluation of Iranian medicinal plant phytoconstituents as inhibitors against main protease and the receptor-binding domain of SARS-CoV-2, Molecules 26 (18) (2021) 5724.
[62] S. Ahmed, et al., Remdesivir analogs against SARS-CoV-2 RNA-dependent RNA polymerase, J. Biomolecul. Struct. Dynam. 40 (21) (2022) 11111–11124.
[63] X. Du, et al., Insights into protein–ligand interactions: mechanisms, models, and methods, Int. J. Mol. Sci. 17 (2) (2016) 144.
[64] J.O. Aribisala, et al., Cheminformatics Bioprospection of Broad Spectrum Plant Secondary Metabolites Targeting the Spike Proteins of Omicron Variant and Wild-Type SARS-CoV-2, Metabolites 12 (10) (2022) 982.
[65] R. Kretschmer, D. Kinzel, L. González, The role of hydrogen bonds in protein–ligand interactions. DFT calculations in 1, 3-dihydrobenzimidazole-2 thione derivatives with glycinamide as model HIV RT inhibitors, Int. J. Quantum. Chem. 112 (7) (2012) 1786–1795.
[66] J.A. Agwupuye, et al., Molecular modeling, DFT studies and biological evaluation of methyl 2, 8-dichloro-1, 2-dihydroquinoline-3-carboxylate, Chem. Phys. Impact 6 (2023) 100146.
[67] S. Akash, et al., Anti-viral drug discovery against monkeypox and smallpox infection by natural curcumin derivatives: a Computational drug design approach, Front. Cell Infect. Microbiol. 13 (2023) 272.
[68] B.Y.G. Mountessou, et al., Structural analysis and molecular docking study of pachypodostyflavone: a potent anti-onchocerca, J. Mol. Struct. (2023) 136003.
[69] S. Kumar, et al., In-silico identification of small molecule benzofuran-1, 2, 3-triazole hybrids as potential inhibitors targeting EGFR in lung cancer via ligand-based pharmacophore modeling and molecular docking studies, Silico Pharmacol. 11 (1) (2023) 20.
[70] S. Lakhera, et al., Modelling the DFT structural and reactivity study of feverfew and evaluation of its potential antiviral activity against COVID-19 using molecular docking and MD simulations, Chemical Papers 76 (5) (2022) 2759–2776.

4.5 Cheminformatics bioprospection of selected medicinal plants metabolites against trypsin cleaved VP4 (spike protein) of rotavirus A

This article has been published in Journal of Biomolecular Structure and Dynamics and presented accordingly

Taylor & Francis
Taylor & Francis Group

Journal of Biomolecular Structure and Dynamics

ISSN: (Print) (Online) Journal homepage: https://www.tandfonline.com/loi/tbsd20

Cheminformatics bioprospection of selected medicinal plants metabolites against trypsin cleaved VP4 (spike protein) of rotavirus A

Adedayo Ayodeji Lanrewaju, Abimbola Motunrayo Enitan-Folami, Martin M. Nyaga, Saheed Sabiu & Feroz Mahomed Swalaha

To cite this article: Adedayo Ayodeji Lanrewaju, Abimbola Motunrayo Enitan-Folami, Martin M. Nyaga, Saheed Sabiu & Feroz Mahomed Swalaha (20 Sep 2023): Cheminformatics bioprospection of selected medicinal plants metabolites against trypsin cleaved VP4 (spike protein) of rotavirus A, Journal of Biomolecular Structure and Dynamics, DOI: 10.1080/07391102.2023.2258405

To link to this article: https://doi.org/10.1080/07391102.2023.2258405

View supplementary material

Published online: 20 Sep 2023.

Submit your article to this journal

View related articles

View Crossmark data

Full Terms & Conditions of access and use can be found at
https://www.tandfonline.com/action/journalInformation?journalCode=tbsd20

JOURNAL OF BIOMOLECULAR STRUCTURE AND DYNAMICS
https://doi.org/10.1080/07391102.2023.2258405

Taylor & Francis
Taylor & Francis Group

Check for updates

Cheminformatics bioprospection of selected medicinal plants metabolites against trypsin cleaved VP4 (spike protein) of rotavirus A

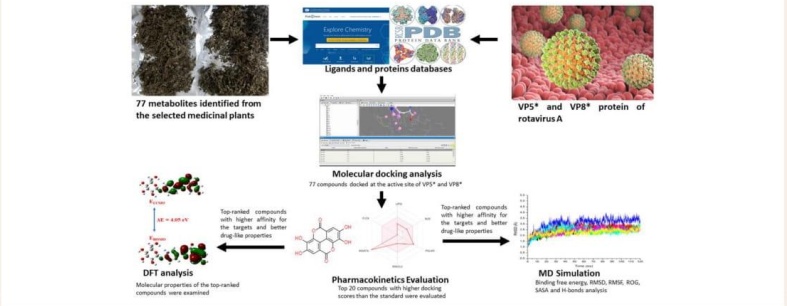
Adedayo Ayodeji Lanrewaju[a], Abimbola Motunrayo Enitan-Folami[a], Martin M. Nyaga[b], Saheed Sabiu[a] and Feroz Mahomed Swalaha[a]

[a]Department of Biotechnology and Food Science, Durban University of Technology, Durban, South Africa; [b]Next Generation Sequencing Unit and Division of Virology, University of the Free State, Bloemfontein, South Africa

Communicated by Ramaswamy H. Sarma

ABSTRACT

Rotaviruses have continued to be the primary cause of acute dehydrating diarrhoea in children under five years of age despite the global introduction of four World Health Organization (WHO) prequalified oral vaccines in over 106 countries. Currently, no medication is approved by the Food and Drug Administration (FDA) specifically for treating rotavirus A-induced diarrhoea. Consequently, it is important to focus on developing prophylactic and curative therapeutics to combat rotaviral infections. For the first time, this study computationally screened and identified metabolites from *Spondias mombin*, *Macaranga barteri* and *Dicerocaryum eriocarpum* as potential novel inhibitors with broad-spectrum activity against VP5* and VP8* (spike protein) of rotavirus A (RVA). The initial top 20 metabolites identified through molecular docking were further filtered using drug-likeness and pharmacokinetics parameters. The molecular properties of the resulting top-ranked compounds were predicted by conducting density functional theory (DFT) calculations, while molecular dynamics (MD) simulation revealed their thermodynamic compatibility with a significant affinity towards VP8* than VP5*. Except for ellagic acid (−11.78 kcal/mol), the lead compounds had higher binding free energy than the reference standard (VP5* (−11.81 kcal/mol), VP8* (−14.12 kcal/mol)) with 2SG (−20.98 kcal/mol) and apigenin-4′-glucoside (−23.56 kcal/mol) having the highest affinity towards VP5* and VP8*, respectively. Of all the top-ranked compounds, better broad-spectrum affinities for both VP5* and VP8* than tizoxanide were observed in 2SG (VP5* (−20.98 kcal/mol), VP8* (−20.13 kcal/mol)) and sericetin (VP5* (−20.46 kcal/mol), VP8* (−18.31 kcal/mol)). While the identified leads could be regarded as potential modulators of the investigated therapeutic targets for effective management of rotaviral infection, additional *in vitro* and *in vivo* evaluation is strongly recommended, and efforts are on-going in this regard.



ARTICLE HISTORY
Received 25 July 2023
Accepted 7 September 2023

KEYWORDS
Rotavirus; spike protein; phyto-metabolites; density functional theory; pharmacokinetics; molecular dynamics simulation

1. Introduction

Globally, rotaviruses have been the predominant cause of acute dehydrating diarrhoea in children under 5 years of age since their initial discovery in human cases nearly four decades ago (Omatola & Olaniran, 2022). There are over 258 million rotavirus (RV) infection-caused diarrhoea cases globally, and approximately 1.3 million deaths of all ages were attributed to complications from diarrhoeal illness (Tohmé &

CONTACT Saheed Sabiu sabius@dut.ac.za Department of Biotechnology and Food Science, Durban University of Technology, P. O. Box 1334, Durban, 4000, South Africa.

Supplemental data for this article can be accessed online at https://doi.org/10.1080/07391102.2023.2258405.

© 2023 Informa UK Limited, trading as Taylor & Francis Group

Delgui, 2021). Three of the seven RV groups; group A (RVA), group B (RVB), and group C (RVC), have strains that may infect humans. The RVA strain is a constant cause of diarrhoea, and diarrhoea-related deaths in children under five years old and was specifically responsible for 130, 000 deaths in 2016 globally (Troeger et al., 2018). Despite the global implementation of four World Health Organization (WHO) prequalified oral vaccines in more than 106 countries (WHO, 2021), RVA is still the leading cause of diarrhoea-related mortality in children to date (Kim et al., 2020; Lanrewaju et al., 2022). This could be due to the effectiveness of vaccines estimated to be 50–90% in preventing severe diarrhoea, with moderate efficacy in countries with poorer living standards (Troeger et al., 2018). Other obstacles hindering the realization of the complete potential of the vaccines for worldwide rotavirus disease prevention include age-based limitations on vaccine usage, safety concerns related to intussusception and reversion to virulence in malnourished or immunocompromised individuals owing to the live attenuated virus nature of the vaccine and the necessity for cold chain storage, which is challenging to maintain in poor socio-economic settings. The primary treatment for RVA-induced gastroenteritis is oral rehydration therapy (ORT) for replacing fluids and electrolytes lost in stool and vomit, complemented with zinc tablets to aid the mucosal epithelial lining repair (Omatola & Olaniran, 2022). Regrettably, there is currently no FDA-approved medication for the treatment/management of RVA-induced diarrhoea; hence, developing novel prophylactic and curative therapeutics against rotaviral infection is a global imperative.

Rotaviruses belong to the Reoviridae family and are characterized by their 11-segmented double-stranded RNA (dsRNA) genome that encodes six non-structural proteins (NSP1-NSP6) and six structural proteins (VP1-4, VP6, and VP7) (Nyaga et al., 2020). To launch the cell entry process, RVs rely on interactions between VP7 and VP4 (Amimo et al., 2021). The VP4 protein, a spike-like protrusion on the floor of the virus, aids the virus in penetrating the cell by binding to the host's receptors (Shaikh et al., 2022). Trypsin stimulates VP4 by cleaving it to two domains, VP5* and VP8*, which improves the virus's ability to infect and enter host cells (Omatola & Olaniran, 2022). Each domain performs a discrete responsibility in the cell entry process (Amimo et al., 2021). Due to a hydrophobic structural region facilitating RV entry into cells (Jiang et al., 2023), VP5* has been predicted to have membrane permeabilization properties (Kumar et al., 2020). On the other hand, the carbohydrate-recognition domain located in VP8* plays a crucial role in viral attachment and infection (Li et al., 2021). Therefore, both VP5* and VP8* represent promising therapeutic targets for developing viable drug candidates against RV infections because they play a significant role in the pathogenesis of RVA.

Natural products are a rich source of bioactive compounds for various infectious illnesses (Fadiji et al., 2018; Newman & Cragg, 2016). For instance, the potential antiviral properties of various plant species and isolated compounds have been investigated (Hudson, 2018; Reichling, 2010). Specifically, the antiviral activity of *Artocarpus integrifolia*, *Myristica fragrans,* and *Spondias lutea* against RV has been reported (Gonçalves et al., 2005). In addition, the significant modulatory activity of *Spondias mombin* (Corthout et al., 1991; Siqueira et al., 2020) and *Macaranga barteri* (Ogbole et al., 2018; Segun et al., 2021) against different viruses has been documented. Also, *Dicerocaryum eriocarpum* is a versatile plant with several ethnomedicinal uses, including treating wounds, assisting in expelling retained placentas, antibacterial activity (Luseba et al., 2007), anti-inflammatory properties, and ethnoveterinary uses (Van der Merwe et al., 2001). However, there is a dearth of information on the modulatory potential of *S. mombin*, *M. barteri* and *D. eriocarpum* against RVA. Hence, there is a need to investigate their antiviral activity against RVA owing to their promising bioactivities. This study is part of an ongoing attempt to discover effective drug candidates against the therapeutic targets of RVA and employed a computational approach to explore the antiviral potential of secondary metabolites from *S. mombin*, *M. barteri* and *D. eriocarpum* against the VP5* and VP8* proteins to identify lead compounds that could be developed as therapeutics against diarrhoea caused by RVA. Computational techniques have been adopted in several studies involving protein-ligand interactions in the search for effective antiviral drug candidates against SARS-CoV-2 (Aribisala et al., 2022; Uhomoibhi et al., 2022), human immunodeficiency virus (HIV) (Shode et al., 2022) and RVA (Garuba et al., 2022) as it reduces the time and cost associated with the conventional drug discovery and development approach. Therefore, molecular docking was adopted to screen the most promising compounds with abilities to modulate the activity of VP5* and VP8* of RVA. Pharmacokinetic screening was carried out using *in silico* methods to mitigate the common hindrances encountered in the conventional drug discovery process, wherein compounds exhibit exceptional performance *in vitro* but do not satisfy the necessary criteria for a drug to be deemed appropriate for delivery. Furthermore, density functional theory calculations were conducted to gain insights into the top-ranked compounds' composition characteristics. Molecular dynamics (MD) simulation provided information on the protein's stability, compactness, and flexibility upon binding with the phytometabolites (Figure 1). Hence, for the first time, this study offered computational insights into identifying broad-spectrum metabolites with modulatory ability against VP5* and VP8* that could be further developed as anti-RVA drugs.

2. Methodology

2.1. Library of phytoconstituents

A total of 77 secondary metabolites isolated from *S. mombin*, *M. barteri* and *D. eriocarpum* as previously reported (Lanrewaju et al., 2023), were used in this study.

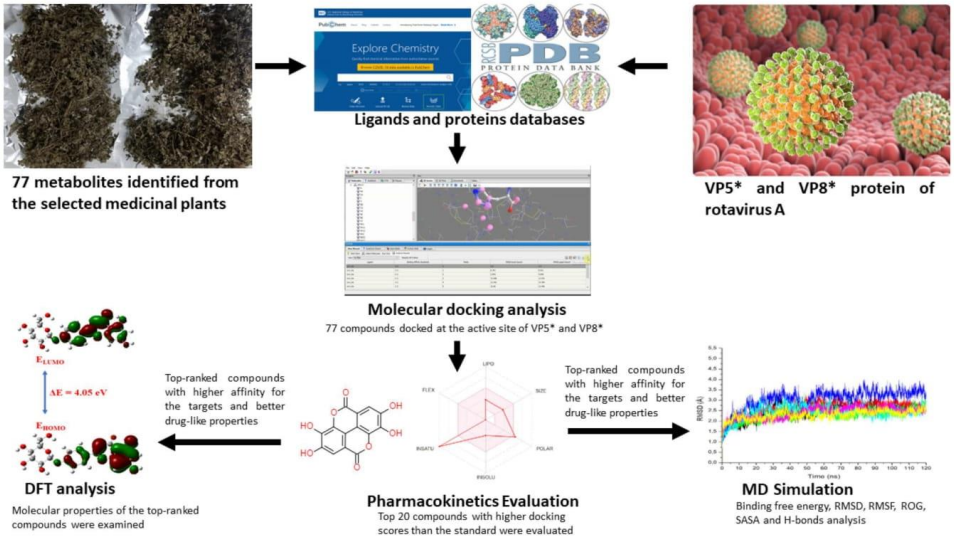


Figure 1. Workflow of the concept adopted in this study.

2.2. Protein acquisition and preparation

The X-ray crystal structure of VP5* (2B4I) and VP8* (2P3I) of RVA were retrieved from the Protein Data Bank [https://www.rcsb.orgs/(accessed on 16 January 2023)]. In preparation for molecular docking, the structures were optimized by removing water molecules and non-standard amino acids using the UCSF Chimera v1.15 software (Sabiu et al., 2021).

2.3. Ligand preparation

The 3D structures of the ligands and the reference standards were retrieved from Pubchem [https://pubchem.ncbi.nlm.nih.gov/ (accessed on 11 September 2022)]. Tizoxanide, the bioactive form of nitazoxanide, has been shown to have the capacity to control RVA infection (Rossignol et al., 2006); hence, it was adopted as the reference standard for targeting VP5* and VP8* in this investigation. Using the Open Babel plugin on Python Prescription (PyRx) v 0.9.5 (Aribisala & Sabiu, 2022), the ligands and reference standards were prepared and optimized by adding Gasteiger charges (Dallakyan & Olson, 2015). The Universal Force Field (UFF) was used to optimize the energy level, which was minimized for 200 steps with a fixed number of updates for a step as 1 and energy difference for stop as 0.1. The UFF is known for its high compatibility with a wide range of atom type in the periodic table, making it a promising choice for various simulations (Artemova et al., 2016). It is a non-reactive force field, meaning that it does not allow for the formation or dissolution of covalent bonds and hence assumes a constant topology for the studied system (Jaillet et al., 2017). All ligands were saved in PDBQT format.

2.4. Molecular docking

Python Prescription v 0.9.5. AutoDock tool was used to dock the prepared protein and optimized ligands (Aribisala & Sabiu, 2022). Docking was performed at the active site of the protein by selecting amino acid residues at the active site of the proteins as reported previously in literature for VP5* (Yoder & Dormitzer, 2006) with the x-y-z coordinates [centre (X: 9.77; Y: 39.94; Z: 3.08)]. The amino acid residues of the binding domain of VP8* were determined using Discovery Studio 21.1.0 and validated from literature (Kraschnefski et al., 2009) with the x-y-z coordinates [centre (X: 42.12; Y: 11.68; Z: 13.89)]. The reference standard was utilized as a reference against which the ligands with the highest binding affinity at the protein's active sites could be compared. It was used as a criterion for selecting ligands that exhibit the highest affinity for the protein's active sites.

2.5. Pharmokinetics properties predictions of top-scoring compounds

The SwissADME web (http://swissadme.ch/index.php, accessed on 18 January 2023) was used to forecast the physicochemical characteristics, pharmacokinetics, and drug-likeness of 20 compounds with the top docking score. Similarly, their toxicological characteristics were predicted using the Protox II webserver (https://tox-new.charite.de/protox_II/, accessed on 18 January 2023). The observations of these investigations were adopted to reduce the numbers to three compounds for VP5* and five compounds for VP8*. The docked systems of the top-ranked compounds with the lowest energy minimization (highest binding affinity) were obtained from their respective PDB files and utilized for MD.

2.6. Validation of docking protocol

Redocking and superimposition were used to test the docking process, assure its accuracy and dependability while eliminating false positive outcomes. Ligands were superimposed over VP5* (2B4I) and VP8* (2P3I) crystal structures to assess the docking poses. Top-ranked metabolites and tizoxanide (reference standard) were re-docked into their original protein's binding domain to test AutoDock's ability to reproduce the ligand's orientation and location from the crystal structure. The root-mean-square deviation (RMSD) between the docked location of the ligand and its experimentally obtained position was used to rank the best conformational clusters from this dock (Al-Khodairy et al., 2013). The docking protocol is validated generally by an RMSD value of < 2 Å (Katuwal et al., 2023).

2.7. Quantum chemical calculations

The molecular properties of the top-ranked compounds were predicted by conducting related quantitative calculations (Medjahed et al., 2016). Density functional theory (DFT) has been widely used to evaluate molecular properties and compute electronic structure properties. The DFT method in Gaussian 16 suite was adopted to assess the electronic properties of the compounds. The Becke3-Lee–Yang–Parr (B3LYP) method, in combination with the 6-31 + G(d,p) basis set, was adopted for the optimization of the investigated compounds and calculations due to its superior accuracy and relatively lower computational requirements (Ma et al., 2022) while the output files were viewed using Gauss View v 6.0 (Ibeji et al., 2023). The primary conceptual DFT (cDFT) properties evaluated in this study were the energies of the lowest unoccupied molecular orbital (E_{LUMO}) and the highest occupied molecular orbital (E_{HOMO}). Additional cDFT parameters were derived based on previously described fundamental properties (Ibeji et al., 2023) and highlighted in Equations (1)–(8) below.

$$\text{Energy gap}, \Delta E = E_{LUMO} - E_{HOMO} \quad (1)$$

$$\text{Ionization energy}, I = -E_{LUMO} \quad (2)$$

$$\text{Electron affinity}, A = -E_{HOMO} \quad (3)$$

$$\text{Hardness}, \eta = \frac{\Delta E}{2} \quad (4)$$

$$\text{Softness}, \delta = \frac{1}{\eta} \quad (5)$$

$$\text{Electronegativity}, \chi = \frac{(I + A)}{2} \quad (6)$$

$$\text{Chemical potential}, Cp = -\chi \quad (7)$$

$$\text{Global electrophilicity}, \omega = \frac{\chi 2}{\Delta E} \quad (8)$$

2.8. Molecular dynamics simulation

The MD simulation was carried out as described previously (Aribisala & Sabiu, 2022). In short, the AMBER 18 package was used for a 120 ns simulation period in which the system was characterized using the FF18SB variant (Nair & Miners, 2014). Likewise, the atomic partial charges of the ligands were generated using the ANTECHAMBER by adopting general amber force field (GAFF) and restrained electrostatic potential (RESP) methods. All the systems were neutralized by adding hydrogen atoms, Na^+ and Cl^- counter ions of the Leap module. The amino acids were numbered appropriately in each simulation case, and each system was suspended so that all atoms were within 8 Å of any box edge in an orthorhombic box of TIP3P water molecules (Jorgensen et al., 1983). Thereafter, the SHAKE approach was used to limit each simulated system's hydrogen atom bonds (Ryckaert et al., 1977). After applying a constraint potential of 500 kcal/mol to both solutes and performing a 2000-step minimization using the steepest descent technique, the system was subjected to 1000 steps of conjugate gradients. An additional 990 steps of full minimization were carried out using the conjugate gradient method (without restraint). For 50 ps, MD simulation in which the temperature was gradually increased from 0 K to 300 K were run, keeping the number of atoms and volume of the system's constant. After the systems were heated, an equilibration lasting about 500 ps was performed as the working temperature was maintained at 300 K. Other parameters, including a few atoms and pressure, were held constant to simulate an isobaric-isothermal ensemble. The Berendsen barostat kept the pressure at 1 bar throughout the system (Basconi & Shirts, 2013; Gonnet, 2007). In each MD run, the step size was 2 fs, which corresponded to the isobarisothermic ensemble (NPT) with random seeding, 300 K temperature, 1 bar constant pressure, a Langevin thermostat with a collision frequency of 1.0 ps (Izaguirre et al., 2001), and a pressure-coupling constant of 2 ps. The data from the MD simulation, which lasted 120 ns were considered post-dynamic.

The post-MD simulation was carried out as described earlier (Aribisala & Sabiu, 2022). The coordinates and trajectories of the systems were recorded during the simulation and analyzed after the simulation was completed using the PTRAJ module of the AMBER 18 software package for post-dynamic analysis. With the use of the CPPTRAJ module included in the AMBER 18 suite, root mean square deviation (RMSD), root mean square fluctuation (RMSF), solvent accessible surface area (SASA), and radius of gyration (ROG) were all analyzed. Thereafter, Origin v 6.0 (Aribisala et al., 2022) was used to generate the individual plots. Similarly, binding free energy was further determined using a mean of 120,000 snapshots recorded during a 120 ns MD simulation trajectory using the molecular mechanics generalized born surface area (MMGBSA) technique with the equation DGbind = Gcomplex – (GReceptor + Gligand).

3. Results and discussion

3.1. Antiviral potentials of the selected medicinal plants

Despite substantial advancements in immunization and preventive medicine, vaccines and targeted antiviral therapies are still unavailable for many viruses. Natural products are a new source of antiviral compounds, with about 40% of the existing medications being traced back to plant derivatives, either directly or indirectly (Ali et al., 2021). Medicinal plants

provide diverse therapeutic antiviral chemotypes that can hinder viral reproduction by impeding viral adsorption, binding to cell receptors, blocking virus penetration into host cells, and interfering with intracellular signal activation pathways. The antiviral activity of *S. mombin* (Corthout et al., 1991; Siqueira et al., 2020) and *M. barteri* (Ogbole et al., 2018; Segun et al., 2021) against different viruses have been documented. Specifically, the pharmacological activity of *D. eriocarpum* (Van der Merwe et al., 2001; Luseba et al., 2007) and its *in silico* antiviral activity against SARS-CoV-2 have been reported (Lanrewaju et al., 2023). Therefore, this study investigated the modulatory activity of *S. mombin*, *M. barteri* and *D. eriocarpum* against RVA *in silico*.

3.2. Molecular docking

The molecular docking model is based on a scoring function that calculates the free energy shift upon binding. It is a useful tool for assessing the biochemical activities of a single ligand bound to a single receptor target protein or enzyme (Tri et al., 2023). The secondary metabolites of the selected medicinal plant extracts and reference standard were docked against VP5* and VP8* binding domains. The highest and lowest docking score against VP5* was observed in 2alpha-hydroxymaprounic acid 2, 3-bis-p-hydroxybenzoate (−6.4 kcal/mol) and azelaic acid (−3.9 kcal/mol) respectively (Supplementary Table S1). On the other hand, 3-(2,2-Dimethylpropoxymethoxy)-2-oxopropyl] 2-methylprop-2-enoate; [3-(3-methylbutan-2-yloxy)-2-oxopropyl] 2-methylprop-2-enoate; [3-(oxan-2-yloxy)-2-oxopropyl] 2-methylprop-2-enoate (−8.3 kcal/mol) had the highest docking score against VP8*, while the lowest docking score was observed in azelaic acid (-4.4 kcal/mol) (Supplementary Table S1). The top twenty compounds with higher docking scores (−6.4 kcal/mol to −5.7 kcal/mol) (Table 1) and (−8.3 kcal/mol to −6.9 kcal/mol) (Table 1) relative to the standard (tizoxanide (−5.0 kcal/mol and −5.5 kcal/mol) targeted against VP5* and VP8* were selected respectively.

3.3. Docking protocol validation

The redocking method was adopted to verify the accuracy of the docking procedure used in this study. This was essential for ensuring that the binding pocket of the individual protein was consistent with the orientation of the top-scoring compounds obtained from docking experiments because the technique often produces false-positive binding configurations as the position with the least energy.

The superimposition of the top-ranked metabolites on the crystal structure of VP5* revealed that both sericetin and 2SG have similar binding positions, while sacranoside A and tizoxanide also share similar binding orientation on the crystal structure (Figure 2(a)). Interestingly, the observed amino acids interactions of the investigated metabolites revealed Trp262, Tyr367 and Leu473, which are residues at the binding domain of the VP5* protein and in tandem with a previous report (Yoder & Dormitzer, 2006). The docking protocol validation revealed a similar binding orientation for the investigated compounds and the native inhibitor against VP8* (Figure 2(b)). In addition, the superimposition of the investigated metabolites and tizoxanide (reference standard) had an RMSD value of < 1 Å from each other, indicating the preferred docking position for all the compounds tested against VP8* protein. Furthermore, the amino acid interactions of the top-ranked compound and tizoxanide at the active site of VP8* protein, such as Arg101, Tyr155, Lys187, Tyr188 and Ser190 corresponds with those previously reported (Garuba et al., 2022; Kraschnefski et al., 2009). In summary, this observation reveals that the docking scores obtained for the compounds and the standard are attributable to their interactions with the residues at the active site of the crystal structure of both VP5* and VP8*; hence, it confirms the validity of the utilized docking protocol. Figure 2 depicts the superimposition and interactions of the top-ranked compounds and tizoxanide at the binding site of the investigated RVA therapeutic targets.

3.4. Pharmacokinetic prediction of the top-scoring compounds and the reference standard

A drug's potential to inhibit a particular protein is depicted by assessing its inhibitory activity against the target protein and evaluating other properties, including absorption, distribution, metabolism, excretion, and toxicity (ADMET). By reducing the number of possible safety issues, the drug development process may be sped up considerably using in-silico ADMET profiling, which provides information about the compound's *in vivo* pharmacological friendliness, bioavailability, and relative toxicity when administered orally.

The Lipinski's rule of five (Ro5) stipulates that bioactive substances must abide by restrictions on their molecular weight (500 g/mol), hydrogen donor (5), hydrogen acceptor (10), and octanol co-efficient (5) (Lipinski et al., 2001). These restrictions are critical to ensure the screened metabolites access their druggable targets in the body at therapeutically relevant concentrations. Of all the twenty top-scoring compounds against VP5* selected for physicochemical and pharmacokinetic analysis, 6MM, sericetin, 2SG and sacranoside A passed the Ro5 with 1, 0, and 0 violations respectively (Table 1). Similarly, twenty top-scoring compounds against VP8* were selected for physicochemical and pharmacokinetic analysis, out of which 6MM, gnetin L, 2SG, sericetin, apigenin-4′-glucoside, and ellagic acid passed the Ro5 with 1, 0, 0, 0, 1, and 0 respectively (Table 1). Interestingly, tizoxanide (reference standard) passed the Ro5 with 0 violation.

A drug's bioavailability score measures the amount of an unmodified drug that enters the systemic circulation at a particular absorption rate (Heaney, 2001). The bioavailability score of drugs administered intravenously is higher than that of oral drugs. It is an essential pharmacokinetic feature to consider when calculating the optimum dose for a medicine. All the compounds that passed the Ro5 against VP5* and VP8* including the reference standard had a bioavailability score of 0.55 (Table 1). A high bioavailability score corresponds with a high drug concentration in the systemic circulation to attain its maximum therapeutic dosage (Shode et al., 2022).

Table 1. Binding affinity and ADMET properties of all the top compounds docked against VP5* and VP8*

Ligands	BA (kcal/mol)	MW < 500 (g/mol)	HBA ≤ 10	HBD ≤ 5	Log P o/ w ≤ 5	WS	GI Abs	BBB P	Pgp	CYP1A2	CYP2C19	CYP2C9	CYP2D6	CYP3A4	LV (N)	BS	H	C	IM	M	CY	LD_{50} (mg/kg)	TC
VP5*																							
2alpha-Hydroxymaprounic acid 2, 3-bis-p-hydroxybenzoate	−6.4	712.91	8	3	7.55	PS	Low	No	No	No	No	No	No	Yes	2	0.56	In	Ac	Ac	In	In	5000	5
Chrysoeriol 7-glucuronide	−6.4	476.4	12	6	0.45	S	Low	No	Yes	No	No	No	No	No	2	0.11	In	In	Ac	In	In	5000	5
Mallotusinic acid	−6.2	1120.75	32	17	−1.48	S	Low	No	Yes	No	No	No	No	No	3	0.11	In	In	Ac	In	In	300	3
3DO	−6.0	728.86	25	14	4.44	S	Low	No	Yes	No	No	No	No	Yes	2	0.17	In	In	In	In	In	8000	6
Acteoside	−6.0	624.59	15	9	−0.43	S	Low	No	Yes	No	No	No	No	No	3	0.17	In	In	Ac	In	In	5000	5
Miconioside A	−6.0	608.59	14	7	−0.18	S	Low	No	Yes	No	No	No	No	No	3	0.17	In	In	Ac	In	Ac	2300	5
6MM	−6.0	422.6	1	0	6.17	PS	Low	No	Yes	Yes	Yes	No	No	Yes	1	0.55	In	In	Ac	Ac	In	200	2
Ellagic acid hexoside	−6.0	464.33	13	7	−0.63	S	Low	No	No	No	No	No	No	No	2	0.17	In	In	Ac	Ac	In	5000	5
Capinerin B	−5.9	966.7	27	14	−1.16	S	Low	No	Yes	No	No	No	No	No	3	0.17	In	In	Ac	In	In	620	4
Sericetin	−5.9	404.46	5	2	4.78	PS	High	No	No	No	Yes	Yes	No	No	0	0.55	In	In	Ac	In	In	2500	5
kaempferol 7-O-glucoside	−5.9	448.4	11	7	−0.04	S	Low	No	No	No	No	No	No	No	2	0.17	In	In	In	In	In	5000	5
Tricin 7-glucuronide	5.9	506.41	13	6	0.30	S	Low	No	Yes	No	No	No	No	No	3	0.11	In	In	Ac	In	In	5000	5
2SG	−5.9	434.52	5	0	6.30	PS	High	Yes	Yes	No	No	Yes	Yes	Yes	0	0.55	In	In	Ac	In	In	2000	4
Isomartynoside	−5.9	652.64	15	7	0.06	S	Low	No	Yes	No	No	No	No	No	3	0.17	In	In	Ac	In	In	5000	5
1SR	−5.9	710.8	13	3	2.07	S	Low	No	Yes	No	No	No	No	No	2	0.17	In	In	Ac	In	Ac	180	3
Menthiafolin	−5.9	540.56	12	5	0.79	S	Low	No	No	No	No	No	No	No	2	0.11	In	In	Ac	In	In	2000	4
Chebulagic acid	−5.8	954.66	27	13	−0.88	S	Low	No	Yes	No	No	No	No	No	3	0.11	In	In	Ac	In	In	420	4
Geraniin	−5.8	952.64	27	14	−1.70	S	Low	No	Yes	No	No	No	No	No	3	0.17	In	In	Ac	In	In	300	3
Pelargoniin A	−5.8	926.65	26	14	−1.24	S	Low	No	Yes	No	No	No	No	No	3	0.17	In	In	Ac	In	In	30	2
Sacranoside A	−5.7	432.5	10	6	−0.93	S	Low	No	Yes	No	No	No	No	No	1	0.55	In	In	In	In	In	4000	5
Tizoxanide	−5.0	265.25	5	2	1.11	S	High	No	No	No	No	No	No	No	0	0.55	In	Ac	In	Ac	In	1000	4
VP8*																							
3DO	−8.3	728.86	25	14	4.44	S	Low	No	Yes	No	No	No	No	Yes	2	0.17	In	In	In	In	In	8000	6
6MM	−8.2	422.6	1	0	6.17	PS	Low	No	Yes	Yes	Yes	No	No	Yes	1	0.55	In	In	Ac	Ac	In	200	2
Isomartynoside	−8.0	652.64	15	7	0.06	S	Low	No	Yes	No	No	No	No	No	3	0.17	In	In	Ac	In	In	5000	5
Miconioside A	−7.5	608.59	14	7	−0.18	S	Low	No	Yes	No	No	No	No	No	3	0.17	In	In	Ac	In	Ac	2300	5
Capinerin B	−7.4	966.7	27	14	−1.16	S	Low	No	Yes	No	No	No	No	No	3	0.17	In	In	Ac	In	In	620	4
Abacopterin D	−7.4	638.6	15	8	−1.01	S	Low	No	Yes	No	No	No	No	No	3	0.17	In	In	Ac	In	Ac	3000	5
Gnetin L	−7.4	484.5	7	5	4.13	S	Low	No	No	No	No	Yes	No	No	0	0.55	In	Ac	Ac	In	In	500	4
Geraniin	−7.2	952.64	27	14	−1.70	S	Low	No	Yes	No	No	No	No	No	3	0.17	In	In	Ac	In	In	300	3
Mallotusinic acid	−7.2	1120.75	32	17	−1.48	S	Low	No	Yes	No	No	No	No	No	3	0.11	In	In	Ac	In	In	300	3
Chebulagic acid	−7.2	954.66	27	13	−0.88	S	Low	No	Yes	No	No	No	No	No	3	0.11	In	In	Ac	In	In	420	4
Pelargoniin A	−7.1	926.65	26	14	−1.24	S	Low	No	Yes	No	No	No	No	No	3	0.17	In	In	Ac	In	In	30	2
Orobanchoside	−7.1	640.6	16	10	−1.32	S	Low	No	No	No	No	No	No	No	3	0.17	In	In	Ac	In	In	5000	5
1SR	−7.1	710.8	13	3	2.07	S	Low	No	Yes	No	No	No	No	No	2	0.17	In	In	Ac	In	Ac	180	3
Chrysoeriol 7-glucuronide	−7.1	476.4	12	6	0.45	S	Low	No	Yes	No	No	No	No	No	2	0.11	In	In	Ac	In	In	5000	5
2SG	−7.1	434.52	5	0	6.30	PS	High	Yes	Yes	No	No	Yes	Yes	Yes	0	0.55	In	In	Ac	In	In	2000	4
2alpha-Hydroxymaprounic acid 2, 3-bis-p-hydroxybenzoate	−7.0	712.91	8	3	7.55	PS	Low	No	No	No	No	No	No	Yes	2	0.56	In	Ac	Ac	In	In	5000	5
Sericetin	−7.0	404.46	5	2	4.78	PS	High	No	No	No	Yes	Yes	No	No	0	0.55	In	In	Ac	In	In	2500	5
Apigenin-4′-glucoside	−6.9	432.38	10	6	0.48	S	Low	No	Yes	No	No	No	No	No	1	0.55	In	In	In	Ac	In	5000	5
Ellagic acid	−6.9	302.19	8	4	1.00	S	High	No	No	Yes	No	No	No	No	0	0.55	In	Ac	In	In	In	2991	4
Scrophenoside D	−6.9	654.61	16	9	−0.89	S	Low	No	Yes	No	No	No	No	No	3	0.17	In	In	Ac	In	In	5000	5
Tizoxanide	−5.5	265.25	5	2	1.11	S	High	No	No	No	No	No	No	No	0	0.55	In	Ac	In	Ac	In	1000	4

Notes: MW: Molecular weight; BBB permeant: Blood-brain barrier permeation; HB-D: Hydrogen bond donor; Log P o/w: Partition coefficient; HB-A: Hydrogen bond acceptor; CY: Cytotoxicity; Pgp: Permeability glycoprotein substrate; WS: Water solubility; CYP: Cytochrome; LV: Lipinski violation; BS: Bioavailability score; H: Hepatotoxicity; C: Carcinogenicity; IM: Immunotoxicity; GI abs: Gastrointestinal absorption; M: Mutagenicity; LD: Lethal dose; TC: Toxicity class; S: Soluble; PS: Poorly soluble; Ac: Active; In: Inactive; N: Number of violation. 3DO; 3-(2,2-Dimethylpropoxymethoxy)-2-oxopropyl] 2-methylprop-2-enoate;[3-(3-methylbutan-2-yloxy)-2-oxopropyl] 2-methylprop-2-enoate;[3-(oxan-2-yloxy)-2-oxopropyl] 2-methylprop-2-enoate, 6MM; 6-Methyl-7-(4-methylnaphtho[2,3-b][1]benzofuran-3-yl)-3-propan-2-ylthieno[2,3-c]pyridin-6-ium, 2SG; (2S)-6-(gamma,gamma-dimethylallyl)-3′,4′-dimethoxy-6″,6″-dimethylpyran[2″,3″:7,8]flavanone, 1SR; [(1S,3R,6S,7S,8S,9S,10S,11S,14S,16S)-6-acetyl-14-[(2R,4R,5R,6R)-5-[(2S,3R,4R,5R,6R)-3,5-dihydroxy-4-methoxy-6-methyloxan-2-yl]oxy-4-methoxy-6-methyloxan-2-yl]oxy-8-hydroxy-7,11-dimethyl-2-oxapentacyclo[8.8.0.01,3.03,7.011,16]octadecan-9-yl] acetate.

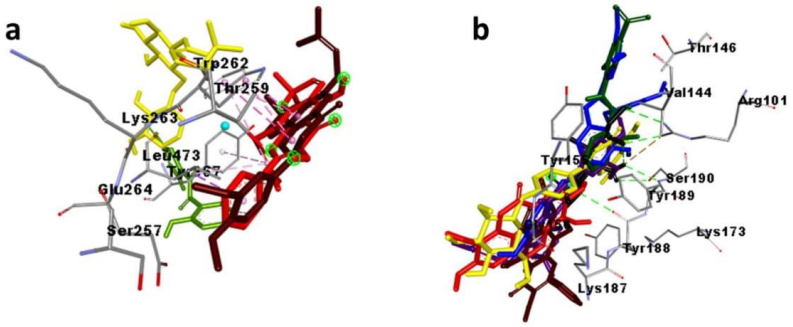


Figure 2. The superimposition and interactions of the investigated compounds with the highest binding affinity at the active site of the crystal structure of (a) VP5* with (sericetin (red), 2SG (brown), sacranoside A (yellow), reference standard (green)). although VP5* has no co-crystallized ligand, the investigated ligands interacted with some amino acids at the binding domain of the protein, such as Trp262, Tyr367 and Leu473; (b) VP8* with (co-crystallized ligand (black), ellagic acid (red), sericetin (brown), apigenin-4′-glucoside (yellow), gnetin L (blue), 2SG (purple), and reference standard (green).

Several drugs undergo biotransformation by cytochrome P450 isoenzyme family members as they are known for their critical roles in drug metabolism. Because of their crucial involvement in drug metabolism, cytochrome P450 (CYP) isoenzymes are often considered among the most significant determinants of drug toxicity (Verma et al., 2022). Of all the compounds that passed the Ro5 against VP5* and VP8*, only sacranoside A, apigenin-4′-glucoside and tizoxanide were observed to be a non-inhibitor of all the CYP isoenzymes while 6MM, sericetin, 2SG and ellagic acid inhibited at most three isoenzymes. This suggests that drug-drug interactions are unlikely to occur when sacranoside A, apigenin-4′-glucoside and tizoxanide are given alongside drugs processed by these isoenzymes. Furthermore, except for sacranoside A predicted for non-toxicity of all the toxicity profiles examined, sericetin 2SG, ellagic acid and apigenin-4′-glucoside were predicted for one toxicity endpoint, while 6MM, gnetin L and tizoxanide (reference standard) were predicted for two toxicity endpoints.

The selected compounds can be developed into drugs because they are in toxicity classes 4 and 5 with LD_{50} values ranging between 500 to 5000 mg/kg, which is appropriate for drug development. However, 6MM is an exception because it belongs to toxicity class 2 with LD_{50} value of 200 mg/kg both of which are not ideal for drug development; hence, it was excluded from further assessment in this study. Generally, the screening parameters used in this study are crucial in drug development, significantly lowering the proportion of failures attributed to toxicology and pharmacokinetics in both the preclinical and clinical stages (Lipinski et al., 2001; Verma et al., 2022). To summarize, fewer structural changes may be performed on the selected compounds for both targets to improve their druggability than the excluded compounds.

3.5. Molecular orbital properties

This study analyzed the top-ranked compounds' structural and chemical reactivity characteristics using DFT (Table 2). The frontier molecular orbitals (FMOs); the LUMO and HOMO are the most important orbitals within a given molecule as they perform significant functions in intermolecular interactions and the electronic spectrum of a molecule (Prasad et al., 2010). The HOMO energy level indicates a molecule's capacity to donate electrons, whereas the LUMO energy level provides insight into the molecule's propensity to accept electrons. A molecule's chemical reactivity, kinetic stability, optical polarizability, and chemical hardness-softness are all influenced by the energy gap between its HOMO and LUMO. Specifically, a molecule's reactivity is directly proportional to its energy gap, implying that a smaller molecule is more prone to reacting with other molecular species, including proteins and enzymes (Akintemi et al., 2022). In this study, the lowest energy gap in the compounds against both targets were observed in sericetin (3.57 eV) (Figure 3) hence suggesting its higher reactivity compared to other compounds, while sacranoside A and 2SG had the highest energy gap (6.33 eV and 4.21 eV) against VP5* and VP8* respectively (Table 2).

Furthermore, molecules with a larger HOMO-LUMO energy gap exhibit increased hardness, resulting in diminished reactivity. Chemical hardness is a reliable metric for assessing chemical stability and is pivotal in drug design investigations (Mountessou et al., 2023). Soft molecules exhibit a higher degree of polarizability than hard molecules due to their lower energy requirement for excitation. Sericetin (0.56 eV) has the highest chemical softness and could have contributed to its higher chemical reactivity against both targets (Table 2). Conversely, the highest chemical hardness value was observed in sacranoside A (3.16 eV) and 2SG (2.11 eV) against VP5* and VP8*, respectively, indicating their resistance to charge transfer and being the least reactive. Moreover, the observed low value of the chemical potential across all the compounds suggests a molecule with reduced polarization and enhanced resistance to electronic deformation when subjected to minor disturbances during a chemical reaction. The negative value of the chemical potential also lends credence to the stability of the molecule as it prevents spontaneous decomposition (Mountessou et al., 2023).

Electronegativity is a quantitative parameter that characterizes the relative distribution of electrons within a molecule. The reference standard exhibited the highest electronegativity

Table 2. The cDFT parameters in eV of top-ranked compounds against VP5* and VP8*.

Ligands	LUMO	HOMO	Energy gap	Ionization energy	Electron affinity	Hardness	Softness	Electronegativity	Chemical potential	Global electrophilicity
VP5*										
2SG	−1.46	−5.67	4.21	1.46	5.67	2.11	0.47	3.56	−3.56	3.01
Sericetin	−2.13	−5.70	3.57	2.13	5.70	1.79	0.56	3.91	−3.91	4.28
Sacranoside A	0.58	−5.75	6.33	−0.58	5.75	3.16	0.32	2.58	−2.58	1.06
Tizoxanide	−3.18	−6.94	3.76	3.18	6.94	1.88	0.53	5.06	−5.06	6.81
VP8*										
2SG	−1.46	−5.67	4.21	1.46	5.67	2.11	0.47	3.56	−3.56	3.01
Apigenin-4′-glucoside	−2.20	−6.25	4.05	2.20	6.25	2.02	0.49	4.23	−4.23	4.41
Ellagic acid	−2.27	−6.47	4.20	2.27	6.47	2.10	0.48	4.37	−4.37	4.56
Gnetin L	−1.47	−5.47	4.00	1.47	5.47	2.00	0.50	3.47	−3.47	3.01
Sericetin	−2.13	−5.70	3.57	2.13	5.70	1.79	0.56	3.91	−3.91	4.28
Tizoxanide	−3.18	−6.94	3.76	3.18	6.94	1.88	0.53	5.06	−5.06	6.81

Notes: LUMO: Lowest unoccupied molecular orbital; HOMO: Highest occupied molecular orbital; 2SG: (2S)-6-(gamma,gamma-dimethylallyl)-3′,4′-dimethoxy-6″,6″-dimethylpyran[2″,3″:7,8]flavanone.

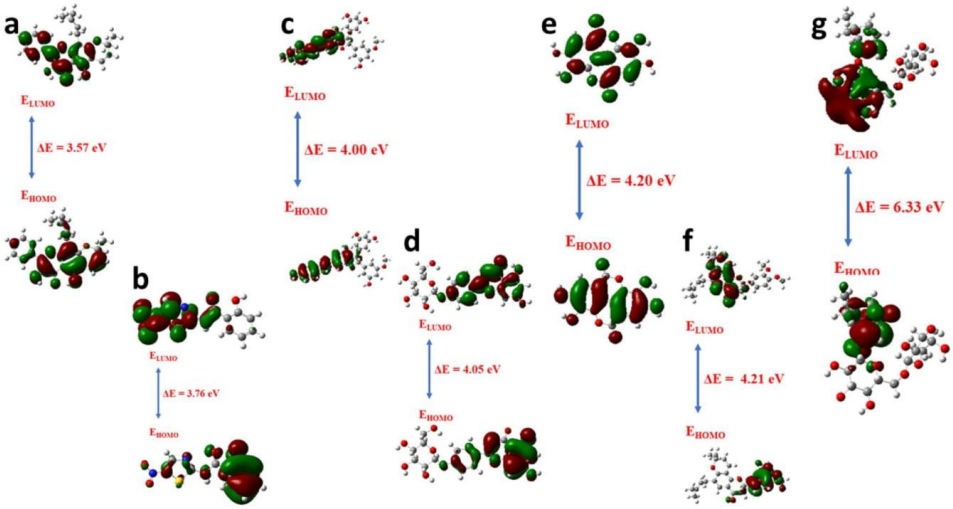


Figure 3. Frontier molecular orbitals for (a) sericetin; (b) tizoxanide; (c) gnetin L; (d) apigenin-4′-glucoside; (e) ellagic acid; (f) 2SG; (g) sacranoside A.

value; tizoxanide (5.07 eV), while sericetin (3.91 eV) and apigenin-4′-glucoside (4.23 eV) are next to tizoxanide against VP5* and VP8*, respectively (Table 2). Generally, the top-ranked compounds exhibited high electronegativity values, suggesting their proficiency in accepting electrons (Akintemi et al., 2022). The electrophilicity index measures the capacity of a molecule to acquire electrons from the environment, thereby indicating its potential to function as an electrophile (Mountessou et al., 2023). A molecule can be classified as a low electrophile if its electrophilicity value is below 0.8 eV, while a moderate electrophile has an electrophilicity value within the range of 0.8 to 1.5 eV and is considered a heavy electrophile if its electrophilicity value exceeds 1.5 eV (Lakhera et al., 2022). Of all the top-ranked compounds, only sacranoside A (1.06 eV) is a moderate electrophile, while others are heavy electrophiles, indicating a significant electrophile presence.

3.6. Thermodynamic binding free energy of top-ranked compounds

One of the most common approaches for calculating the affinity of ligands for binding to protein is the MMGBSA. The MMGBSA method determines the total energy of an optimized protein, ligand, and complex. The quantification of the energy difference between a complex and its unbound component is known as the thermodynamic binding free energy. The degree of affinity of the ligand for the protein is directly proportional to the magnitude of the negative value of the thermodynamic binding free energy (Acharya et al., 2020). All the top-ranked compounds had higher binding free energy against VP5* (Table 3). Sericetin, 2SG and sacranoside A on binding with VP5* had −20.46 kcal/mol, −20.98 kcal/mol and −16.96 kcal/mol respectively, which were higher than −11.81 kcal/mol observed in tizoxanide (reference standard).

This finding could mean that sericetin, 2SG and sacranoside A have greater potential as inhibitors of VP5*, with 2SG demonstrating the most promising inhibitory capacity among the top-ranked compounds. In addition, this finding is consistent with the outcomes of the molecular docking investigation, suggesting that these metabolites may be more effective than tizoxanide in managing RVA infection.

Conversely, all the top-ranked compounds had higher binding free energy for the binding domain of VP8* relative to tizoxanide (-14.12 kcal/mol) except ellagic acid (-11.78 kcal/mol). Apigenin-4′-glucoside, gnetin L, 2SG and sericetin upon binding with VP8*, had −23.56 kcal/mol, −20.63 kcal/mol, −20.13 kcal/mol and −18.31 kcal/mol respectively which were higher than −14.12 kcal/mol observed in tizoxanide + VP8* (Table 3). This observation, which partly agrees with the molecular docking results, could portend that apigenin-4′-glucoside, gnetin L, 2SG and sericetin have higher potential at inhibiting VP8* compared to the standard. Remarkably, two compounds (sericetin and 2SG) had broad-spectrum affinities against both targets (VP5* and VP8*) relative to tizoxanide (Table 3). The better affinity of sericetin and 2SG indicates their possible ability to impede the regular operation of both targets, hence their advantage as possible novel inhibitors of VP5* and VP8* compared to tizoxanide. These findings suggest the unique properties of the top-ranked compounds, with sericetin and 2SG as the best owing to their broad-spectrum ability to inhibit both VP5* and VP8*.

3.7. Thermodynamic stability, firmness, and flexibility of the top-ranked compounds

Structural and conformational changes may occur upon inhibitor binding to a biological target, potentially affecting the target's biological function (Sindhu & Srinivasan, 2015). Therefore, additional investigation was conducted to understand the complex's stability, the protein's compactness, and the flexibility of amino acid residues. For 120 ns, the RMSD trajectory was evaluated to examine the structural stability of the resulting complexes at the binding site of the proteins because the stability of a complex structure is a function of its proximity to the unbound protein (Du et al., 2016). The RMSD value should not exceed 3.0 Å to be considered desirable and typically acceptable (Ramírez & Caballero, 2016). The atoms were observed to be equilibrating in the first 5 ns of the simulation in the RMSD plot of ligands + VP5* complexes (Figure 4(a)). After that, there was no significant fluctuation while the simulation lasted for all the compounds. Within the initial 10 ns of the simulation, the ligand-protein complexes of VP8* reached equilibrium, while a major fluctuation was observed at 65 ns for the apo-protein and 2SG (Figure 4(b)), followed by a stable fluctuation for the rest of the simulation. Remarkably, all the investigated top-ranked metabolites in this study had a mean RMSD value within the acceptable limit of less than 3 Å, with values ranging from 1.30 Å to 1.93 Å for VP5* (Table 4) and 1.00 Å to 1.27 for VP8* (Table 4). This observation indicates the general stability of the complexes upon binding with the proteins. Sericetin (1.93 Å), sacranoside A (1.50 Å) and 2SG (1.88 Å) had higher average RMSD values relative to the unbound VP5* (1.45 Å), while the standard [tizoxanide (1.30 Å)] had lower RMSD value than the unbound VP5* (Table 3). Ligand binding typically increased RMSD values as compared to the apo-VP5*, which is in tandem with a previous work in which verbascoside binding to SARS-CoV-2 SP induced higher RMSD value (Uhomoibhi et al., 2022). This observation indicates that the standard is a better inhibitor; nevertheless, the higher RMSD values are still within the desirable and acceptable deviation limit of 3.0 Å. Conversely, all the compounds complexed with VP8*; 2SG (1.00 Å), apigenin-4′-glucoside (1.14 Å), ellagic acid (1.00 Å), gnetin L (1.04 Å), sericetin (1.27 Å), and the standard [tizoxanide (1.19 Å)] had average RMSD values lower than the unbound VP8* (1.28 Å) (Table 4). This finding demonstrates the potential of the compounds to boost the structural stability of VP8*.

Additionally, the RMSF values of the complexes were investigated to comprehend the flexibility of amino acid residues across the proteins. The RMSF measures the fluctuations of amino residues in VP5* and VP8* proteins, which can be linked to the stability of intra- and inter-molecular bonds within the complexes, and it determines the binding efficiency of ligands to the protein, as the stability increases with decreasing fluctuations at the catalytic location (Mousavi et al., 2021). Random variations, perhaps resulting from structural conformational alterations, were observed when the investigated compounds were bound to VP5* and VP8* (Figure 5(a,b)). For both targets, the RMSF values of the

Table 3. MMGBSA-based binding free energy Outline (kcal/mol) of the top-ranked compounds against VP5* and VP8*

Energy components (kcal/mol)					
Ligands	ΔE_{vdW}	ΔE_{elec}	ΔG_{gas}	ΔG_{solv}	ΔG_{bind}
VP5*					
2SG	−27.01 ± 3.93	−4.41 ± 2.77	−31.42 ± 5.15	10.44 ± 2.44	−20.98 ± 3.42
Sericetin	−25.84 ± 5.38	−5.39 ± 5.37	−31.22 ± 6.88	10.74 ± 3.37	−20.46 ± 4.39
Sacranoside A	−15.58 ± 9.47	−17.15 ± 14.18	−32.73 ± 21.26	15.77 ± 10.12	−16.96 ± 11.50
Tizoxanide	−18.11 ± 4.06	−9.84 ± 16.17	−27.95 ± 18.41	16.14 ± 16.56	−11.81 ± 3.35
VP8*					
2SG	−27.11 ± 9.45	−5.20 ± 5.50	−32.31 ± 12.44	12.18 ± 5.32	−20.13 ± 7.99
Apigenin-4′-glucoside	−30.84 ± 3.57	−17.00 ± 7.34	−47.84 ± 8.67	24.28 ± 5.02	−23.56 ± 5.21
Ellagic acid	−14.95 ± 3.73	−14.25 ± 9.56	−29.20 ± 10.54	17.42 ± 6.79	−11.78 ± 4.33
Gnetin L	−31.32 ± 4.69	−11.37 ± 6.78	−42.71 ± 9.81	22.08 ± 4.95	−20.63 ± 5.70
Sericetin	−27.09 ± 2.57	−3.55 ± 3.08	−30.63 ± 3.84	12.31 ± 2.46	−18.31 ± 2.32
Tizoxanide	−15.86 ± 6.04	−98.26 ± 27.23	−114.12 ± 30.11	99.99 ± 24.94	−14.12 ± 6.61

ΔE_{vdW} = van der Waals energy; ΔE_{elec} = electrostatic energy; ΔE_{gas} = gas phase free energy; ΔG_{sol} = solvation free energy; ΔG_{bind} = total binding free energy; 2SG; (2S)-6-(gamma,gamma-dimethylallyl)-3′,4′-dimethoxy-6″,6″-dimethylpyran[2″,3″:7,8]flavanone.

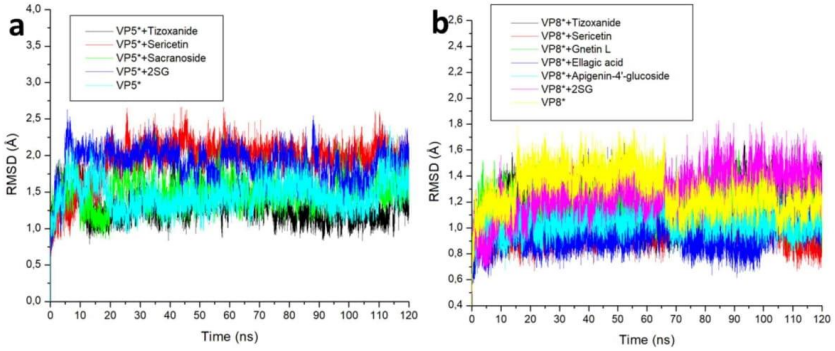


Figure 4. Comparative root mean square deviation (RMSD) plots of alpha-carbon, top-ranked compounds and reference standards against (a) VP5* and (b) VP8* after 120 ns MD simulation period.

Table 4. Mean RMSD, RMSF, ROG, SASA and hydrogen bonds of apo-VP5* and VP8* proteins, top-ranked compounds, and standard against VP5* and VP8*

Ligands	Mean RMSD (Å)	Mean RMSF (Å)	Mean ROG (Å)	Mean SASA (Å)	Mean number of H-Bonds	Mean distance (Å) of H-Bonds	Mean angle (°) of H-Bonds
VP5*							
2SG	1.88 ± 0.22	1.18 ± 0.77	22.37 ± 0.15	11664.45 ± 274.12	120.56 ± 7.29	2.85 ± 0.06	151.62 ± 7.59
Sericetin	1.93 ± 0.27	1.10 ± 0.69	22.29 ± 0.15	11278.12 ± 238.96	127.16 ± 7.19	2.85 ± 0.06	151.85 ± 7.47
Sacranoside A	1.50 ± 0.20	1.24 ± 1.52	22.43 ± 0.28	11463.81 ± 314.76	123.61 ± 7.10	2.85 ± 0.06	151.86 ± 7.71
Tizonamide	1.30 ± 0.18	1.08 ± 0.72	22.19 ± 0.15	11294.41 ± 239.36	124.79 ± 7.04	2.85 ± 0.06	151.74 ± 7.64
Rota VP5	1.45 ± 0.19	1.05 ± 0.55	22.12 ± 0.11	11103.43 ± 227.37	124.79 ± 6.82	2.85 ± 0.06	151.84 ± 7.65
VP8*							
2SG	1.00 ± 0.09	1.05 ± 0.09	15.13 ± 0.23	7373.72 ± 327.92	80.88 ± 5.86	2.85 ± 0.06	151.96 ± 7.84
Apigenin-4′-glucoside	1.14 ± 0.11	0.87 ± 0.03	14.96 ± 0.05	7135.33 ± 176.18	84.73 ± 5.73	2.85 ± 0.06	152.07 ± 7.64
Ellagic acid	1.00 ± 0.11	0.91 ± 0.07	15.05 ± 0.06	7211.25 ± 179.80	79.40 ± 5.65	2.85 ± 0.06	152.00 ± 7.63
Gnetin L	1.04 ± 0.08	0.88 ± 0.03	15.03 ± 0.06	7225.18 ± 186.49	82.37 ± 5.70	2.85 ± 0.06	151.99 ± 7.66
Sericetin	1.27 ± 0.16	0.83 ± 0.02	14.95 ± 0.05	7255.67 ± 168.55	82.04 ± 5.63	2.85 ± 0.06	151.88 ± 7.73
Tizoxanide	1.19 ± 0.13	1.01 ± 0.09	15.09 ± 0.15	7324.05 ± 189.37	80.59 ± 5.63	2.85 ± 0.06	151.67 ± 8.01
RotaVP8	1.28 ± 0.15	0.95 ± 0.03	15.03 ± 0.06	7244.67 ± 169.62	78.86 ± 5.52	2.85 ± 0.06	152.07 ± 7.76

2SG; (2S)-6-(gamma,gamma-dimethylallyl)-3′,4′-dimethoxy-6″,6″-dimethylpyran[2″,3″:7,8]flavanone.

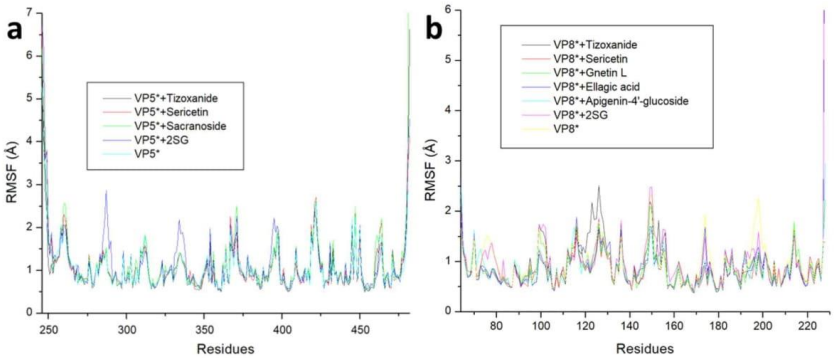


Figure 5. Comparative root mean Squares fluctuation (RMSF) plots of alpha-carbon top-ranked compounds and reference standards against (a) VP5* and (b) VP8* after 120 ns MD simulation period.

active site amino acid residues (Tables 5 and 6) were higher than the average RMSF values observed for the whole protein (Table 4). The unbound VP5*, 2SG, sericetin, sacranoside, tizoxanide had average RMSF values of 1.32 and 1.05 Å, 1.38 and 1.18 Å, 1.43 and 1.10 Å, 1.53 and 1.24 Å, 1.37 and 1.08 Å respectively at the active site and in the whole protein (Tables 5 and 4). Similarly, the unbound VP8*, 2SG, apigenin-4′-glucoside, ellagic acid, gnetin L, sericetin, tizoxanide had average RMSF values of 0.99 and 0.95 Å, 1.12 and 1.05 Å, 0.89 and 0.87 Å, 1.27 and 0.91 Å, 0.91 and 0.88 Å, 0.85 and 0.83 Å, 1.06 and 1.01 Å (Tables 6 and 4). This observation implies more fluctuations in the amino acid residues at the protein's

active site than in other protein regions. High fluctuations of residues mean that the bonds are more flexible and less stable, while low fluctuations mean that the bonds are less flexible and the structure is more stable (Mousavi et al., 2021).

Of the amino acids residues at the binding domain of VP5* (Lys261, Trp262, Val366, Tyr367, Phe415 and Leu473) (Yoder & Dormitzer, 2006), Lys261, Trp262, Tyr367 and Phe415 were responsible for the increased average RMSF value relative to the whole protein (Table 4) while at the active site of VP8*, (Asp100, Arg101, Tyr155, Asn178, Lys187, Tyr188, Ser190) (Kraschnefski et al., 2009), Asp100, Arg101, and Tyr155 were responsible for the increased average RMSF value compared to the whole protein (Table 6). Against VP5* whole protein, sericetin had the lowest mean RMSF value (1.10 Å) after the reference standard (1.08 Å), which suggests the ability of sericetin as a better inhibitor compared to other investigated metabolites. Conversely, at the binding site of VP5*, the lowest RMSF value (1.38 Å) was observed in 2SG after the reference standard and the unbound protein, although with a negligible difference. With VP8, the lowest average RMSF value in the whole protein (0.83 Å) and at the active site (0.85 Å) is sericetin, which suggests its better ability to form stable bonds both at the active site and with the whole protein compared to other investigated metabolites and the reference standard. All investigated metabolites and reference standard against VP5* and VP8* generally had mean RMSF values within the good deviation limit of less than 3.0 Å (Ramírez & Caballero, 2016). This implies that these compounds can form stable bonds and induce minimal distortion of these targets during simulation. The finding aligns with the observed RMSD values in this study, suggesting that the molecular structures of the identified compounds are compatible with the targets; hence, they are promising inhibitors.

The ROG was also computed to assess the proteins' structural compactness after ligand binding. A lower ROG value signifies a more stable system, which is important as ligand binding may modify the structural compactness of a protein, which in turn affects the protein's biological activity (Sindhu & Srinivasan, 2015). In this study, the relative compactness of the complexes revealed that the binding of the top-ranked metabolites and the reference standard to VP5* and VP8* had a minimal impact on the mean ROG values compared to the unbound protein. Lesser fluctuation in ROG was observed in (Figure 6(a)) VP5* + sericetin, VP5* + 2SG and VP5* + tizoxanide relative to VP5* + sacranoside A which exhibited noticeable fluctuation between 20 and 60 ns. The average ROG values of each system supported this finding which varied by 0.25 Å, with the sacranoside A + VP5* complex having the highest average ROG value. This suggests that VP5* was not affected by any thermodynamic disruption due to the binding of metabolites and is in tandem with the RMSD and

Table 5. Average RMSF (Å) of VP5* key binding site residues upon binding with top-ranked compounds and tizoxanide

KBS residues of RV VP5	2SG	Sericetin	Sacranoside A	Tizoxanide	RV VP5
261	2.01	2.20	2.55	2.21	1.85
262	1.60	1.60	1.95	1.76	1.46
366	0.69	0.69	0.69	0.72	0.74
367	2.09	2.26	2.09	1.63	1.98
415	1.05	1.06	1.05	1.06	1.07
473	0.84	0.78	0.83	0.86	0.83
Average RMSF	1.38	1.43	1.53	1.37	1.32

Table 6. Average RMSF (Å) of VP8* key binding site residues upon binding with top-ranked compounds and tizoxanide.

KBS residues of RV VP8	2SG	Apigenin-4′-glucoside	Ellagic acid	Gnetin L	Sericetin	Tizoxanide	RV VP8
100	1.63	1.18	0.98	1.36	1.13	1.62	1.50
101	1.74	0.99	0.90	1.24	0.95	1.59	1.38
155	1.65	1.39	1.26	1.23	1.20	1.45	1.24
178	0.59	0.56	0.56	0.56	0.57	0.61	0.61
187	0.79	0.84	0.74	0.72	0.79	0.77	0.78
188	0.88	0.79	0.73	0.79	0.81	0.82	0.82
190	0.57	0.50	0.45	0.45	0.50	0.54	0.61
Average RMSF	1.12	0.89	1.27	0.91	0.85	1.06	0.99

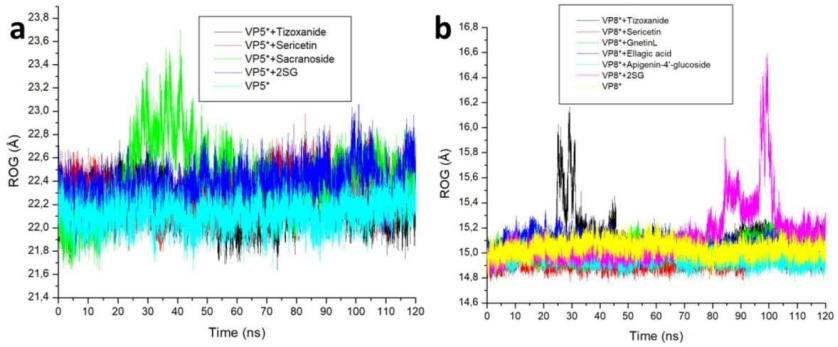


Figure 6. Comparative radius of gyration (ROG) plots of alpha-carbon, top-ranked compounds and reference standard against (a) VP5* and (b) VP8* after 120 ns MD simulation period.

RMSF value findings, indicating that the protein is thermodynamically stable. However, between 20 and 60 ns, VP5* unfolded under the influence of sacranoside A, indicating less or reduced compactness and stability. Just like in VP5, there was lesser fluctuations in VP8* + sericetin, VP8* + gnetin L, VP8* + ellagic acid and VP8* + apigenin-4′-glucoside (Figure 6(b)). However, VP8* + 2SG showed a noticeable fluctuation between 80 and 105 ns, while VP8* + tizoxanide (reference standard) displayed noticeable fluctuations between 25 and 45 ns in VP8* + tizoxanide (reference standard) (Figure 6(b)). Consequently, the highest average ROG values were observed in 2SG (15.13 Å), followed by tizoxanide (15.09 Å). Furthermore, all the top-ranked compounds had higher average ROG values relative to the unbound protein (15.03 Å) except sericetin (14.95 Å) and apigenin-4′-glucoside (14.96 Å), which indicates that their binding to the protein did not alter its compactness though a negligible difference was observed. Generally, there is a little variance of 0.24 Å and 0.18 Å in ROG values between the top-ranked compounds and the standard upon binding with VP5* and VP8* respectively. This suggests that there is no significant difference resulting from the ligand binding which highlights the potential of the top-ranked compounds as stable inhibitors of the investigated therapeutics targets. Another crucial metric for evaluating protein folding and changes in surface area during simulation is the solvent-accessible surface area (SASA). Higher SASA values indicate increased surface area, while reduced values suggest decreased protein volume (Mousavi et al., 2021). The degree of variation in the SASA value is determined by the physicochemical characteristics of the rearranged or altered amino acid residues (Gilis & Rooman, 1996). During this study's 120 ns simulation period, there were slight variations in SASA in the VP5* systems (Figure 7(a,b)). These findings indicate that the surface area and volume of VP5* were slightly affected by the test compounds' and tizoxanide's binding. This observation is reflected in the overall mean SASA values as the apo-VP5* (11103 Å) has lesser average SASA value than the investigated systems [2SG (11664 Å), sericetin (11278 Å), sacranoside A (11463 Å)] and the standard (11294 Å) (Table 4). Similar to the ROG findings, a higher variation of SASA was found in the complex plots of VP8* + 2SG and VP8* + tizoxanide (reference standard) throughout the 120 ns simulation period, indicating that both 2SG and tizoxanide had a greater influence on the surface expansion of VP8* protein. Consequently, both complexes; VP8* + 2SG (7373 Å) and VP8* + tizoxanide (7324 Å), had the highest mean ROG values. Furthermore, apigenin-4′-glucoside (7135 Å), ellagic acid (7211 Å), gnetin L (7225 Å) had mean ROG values lower than the unbound protein (7244 Å), which portends protein compactness, this suggests that a more significant proportion of the unbound protein residues are exposed to the solvent. Conversely, sericetin (7255 Å), 2SG (7373 Å) and tizoxanide (7324 Å) had higher mean ROG values compared to the unbound protein (7244 Å), though with a little impact on the protein's folding. This could mean that their binding does not significantly disrupt the thermodynamic entropy of the protein. Generally, the findings on the SASA values for the two targets align with those of Aribisala and Sabiu (2022), who reported that the interactions of lead phenolics with penicillin-binding protein 2a had minimal influences on the SASA values of the resulting complexes. These findings contrast the findings of Mousavi et al. (2021), who opined that the ligand-protein interactions can substantially affect SASA values.

Hydrogen bonds are essential in various biological processes, such as recognition, structural stability, enzyme catalysis, drug partition, and permeability (Morozov & Kortemme, 2005; S'thebe et al., 2023). Understanding the effect of ligand binding on protein stability requires considering intramolecular hydrogen bonding and distance, which may be measured during simulation (Du et al., 2016). Generally, the relatively stable progression of the number of hydrogen bonds formed in VP5* and VP8* before and after binding to the top-ranked compounds and reference standard shows that VP5* and VP8*'s thermodynamic entropy was not affected by binding to the investigated compounds (Figure 8(a,b)). The reduction in the mean number of intramolecular hydrogen bonds generated in VP5* + 2SG, VP5* + sacranoside A and VP5* + tizoxanide (reference standard) complexes (Table 4) suggest that some intramolecular hydrogen bonds are broken due to

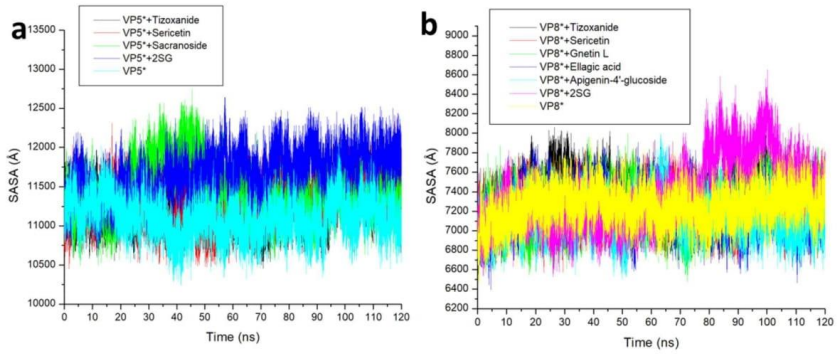


Figure 7. Comparative solvent-accessible surface area (SASA) plots of alpha-carbon, top-ranked compounds and reference standard against (a) VP5* and (b) VP8* after 120 ns MD simulation period.

ligand binding. On the other hand, an increase in the average number of intramolecular hydrogen bonds generated in VP5* + sericetin (127) compared to the apo-protein (124) could mean that the ligands have occupied space in the proteins, and the enhanced hydrogen bonds may indicate that these interactions are a consequence of intermolecular binding. Remarkably, the mean intramolecular bonds in VP8* upon the binding of 2SG (80.88), apigenin-4′-glucoside (84.73), ellagic acid (79.40), gnetin L (82.37), sericetin (82.04) and tizoxanide (80.59) were higher than that of unbound apo-VP8* (78.86) with apigenin-4′-glucoside having the highest value (Table 4). There was a little change of just 5 hydrogen bonds between intramolecular bonds of VP8* upon binding with the investigated metabolites and tizoxanide, suggesting that the thermodynamic parameters of VP8* were not altered by the ligand binding. As shown in Figure 9(a,b), the hydrogen bond distance between VP5* and VP8* complexes continues to decrease during the simulation, a trend that holds for both the unbound proteins and the top-ranked complexed systems. A similar average hydrogen bond distance was observed for all systems against VP5* and VP8* (2.85 Å) (Table 4), indicating that binding of both targets does not induce changes in the arrangement and geometry of both targets rather results in increased internal pull between atoms and residues of the targets as the simulation continues. Furthermore, this observation agrees with RMSD and RMSF results in that the top-ranked compounds and tizoxanide are thermodynamically compatible with the targets examined in this study. Figure 10(a,b) illustrate a steady variation in the hydrogen bond angle in VP5* and VP8*, respectively, as the simulation advances. Both VP5* and VP8* graphs showed significant swaying at 0 ns, with values ranging from 138° to 166°, although this effect diminished throughout the experiment. In the VP5* plot systems, the hydrogen bond angle fluctuated between 164° and 166° at 120 ns, while in the VP8* systems, the range was from 158° to 163°. With the optimum hydrogen bond angle set at 180° (Kretschmer et al., 2012), the hydrogen bond angle in this study, which steadily fluctuates towards 180° throughout the 120 ns simulation, implies that the hydrogen bonds are becoming stronger and agrees with the results of the distance measurements. Average hydrogen bond angle values observed in all systems against VP5* and VP8* range from 151.62° to 151.86° and 151.67° to 152.07°

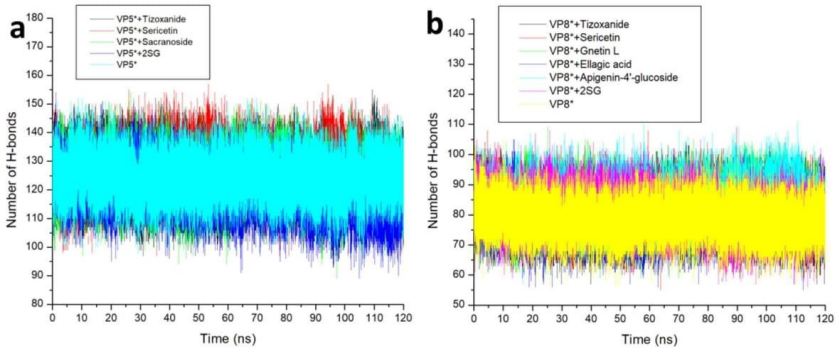


Figure 8. Time progression of the number of hydrogen bonds in (a) VP5* and (b) VP8* upon binding with the top-ranked compounds and reference standards during the 120 ns MD simulation period.

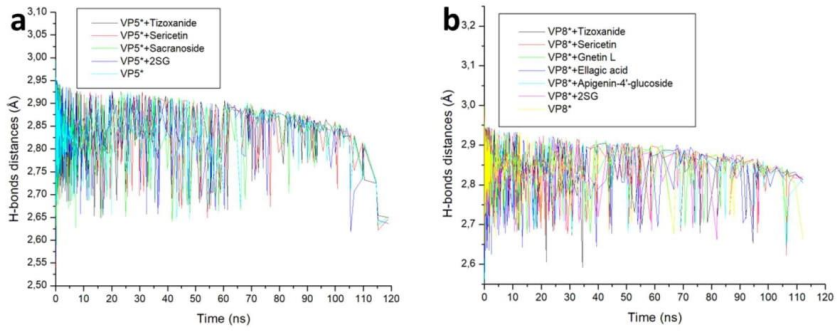


Figure 9. Time progression of the hydrogen bond distance in (a) VP5* and (b) VP8* upon binding of the top-ranked compounds and reference standards during the 120 ns MD simulation period.

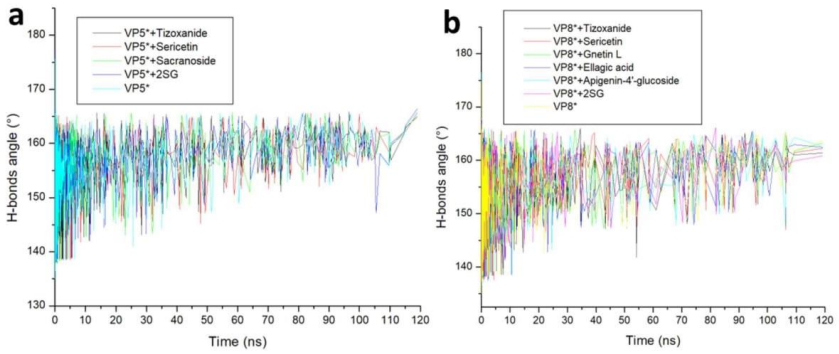


Figure 10. Time progression of the hydrogen bond angles in (a) VP5* and (b) VP8* upon binding of the top-ranked compounds and reference standards during the 120 ns MD simulation period.

Table 7. Mean bond length and molecular interactions between the top-ranked compounds against VP5* and VP8* after 120 ns simulation.

Top-ranked compounds	Total sum of interactions and mean bond length (Å)	Number of hydrogen bonds and interaction residues	Other vital interactions and residues
VP5*			
2SG	13 (5.88)	1 (4.56) [Trp17]	5 (5.53) [Tyr122 (2), Leu228 (2), Trp17]
Sacranoside A	8 (5.41)	1 (5.24) [Trp17]	None
Sericetin	13 (5.51)	None	4 (5.37) [Trp17 (3), Leu228]
Tizoxanide	4 (5.80)	None	2 (6.29) [Trp17, Leu228]
VP8*			
2SG	14 (4.64)	4 (4.39) [Thr9 (2), Thr10, Phe139]	4 (5.26) [Pro8 (4)]
Apigenin-4′-glucoside	14 (4.55)	5 (4.27) [Lys124, Tyr125 (3), Thr83]	2 (5.53) [Tyr92, Val81]
Ellagic acid	11 (5.54)	1 (3.97) [Asp3]	6 (5.81) [Ile144 (3), Pro14 (2), Tyr6]
Gnetin L	13 (5.31)	3 (4.93) [Tyr92, Tyr126, Ser127]	4 (5.66) [Tyr92 (2), Tyr126, Lys124]
Sericetin	8 (5.54)	1 (5.47) [Asn115]	1 (6.03) [Lys124]
Tizoxanide	13 (5.23)	1 (5.13) [Gln91]	5 (5.26) [Ile65 (2), Val80, Ile43, Ile78]

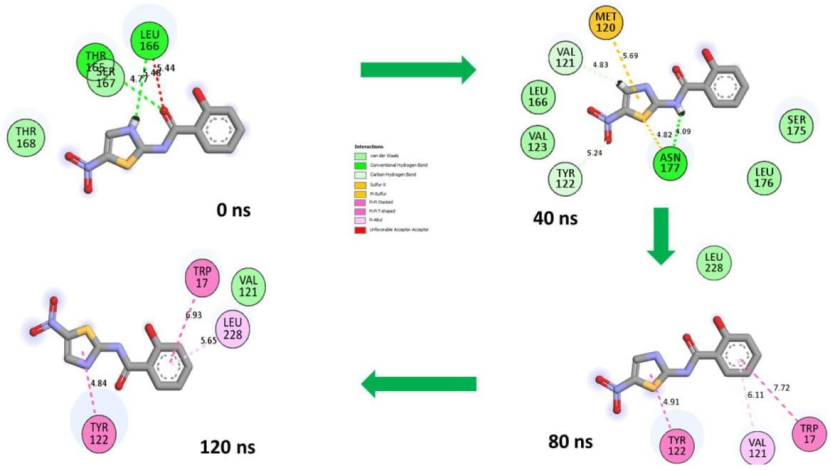


Figure 11. 2D interactions plots of tizoxanide against VP5* at various timeframes during the 120 ns simulation.

(Table 4) with 0.24 and 0.40 variance, respectively, which reveal the minimal effect of the parameter on the differences in the binding free energy observed in this study.

3.8. Bond analysis of interaction plots

The stability, flexibility, and compactness of a protein are not just the determinants that influence the capacity of a ligand to bind and inactivate a protein but also the kind of interactions between the ligand and the essential amino acids of a protein (Nasution et al., 2018). Therefore, time-dependent interactions for the top-ranked compounds and tizoxanide against VP5* and VP8* were further elucidated and plotted as depicted in Figures 11–17. These figures showed different types, lengths, and numbers of bonds formed between the ligands and the protein and were found to have a noticeable impact on their stability and free binding energy in this study (Table 7). The time-dependent interaction plots revealed the presence of various bond interactions between the top-ranked compounds and the proteins. These include hydrogen bonds (conventional, π-donor, and carbon), van der Waals, amide π-stacked, π-anion, π-sigma, π-cation, π-π t-cation, π-π t-shaped, π-π t-stacked, π-alkyl, alkyl, π-Sulphur, unfavourable donor-donor interactions among others (Figures 11–17).

Accordingly, 2SG and sericetin showed the highest interactions (Table 7) against VP5* (13) with consistent binding

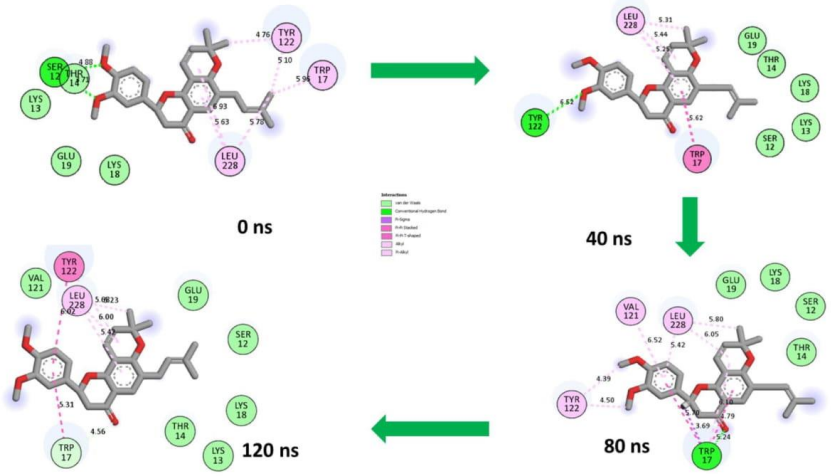


Figure 12. 2D interactions plots of 2SG against VP5* at various timeframes during the 120 ns simulation.

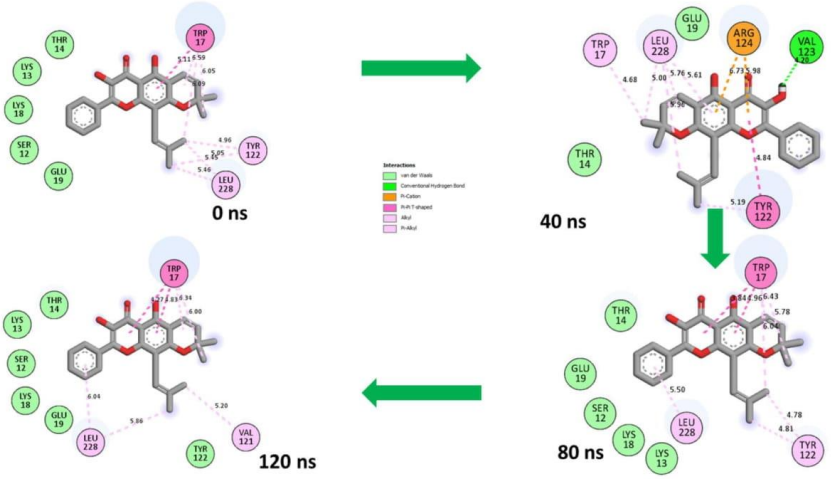


Figure 13. 2D interactions plots of sericetin against VP5* at various timeframes during the 120 ns simulation.

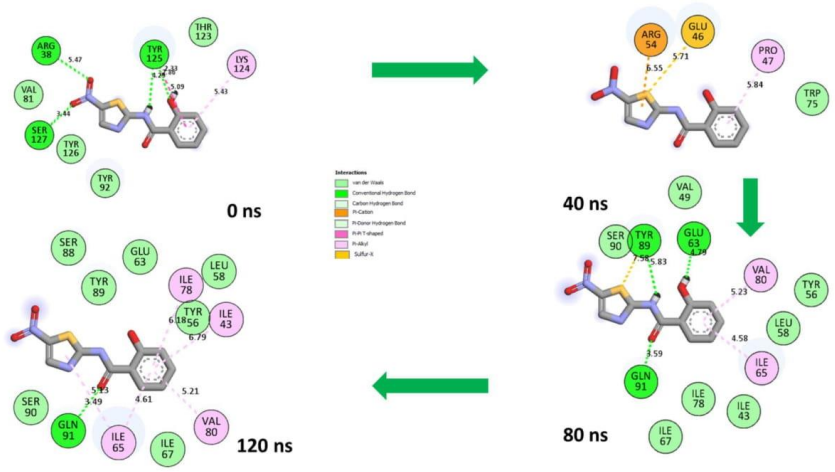


Figure 14. 2D interactions plots of tizoxanide against VP8* at various timeframes during the 120 ns simulation.

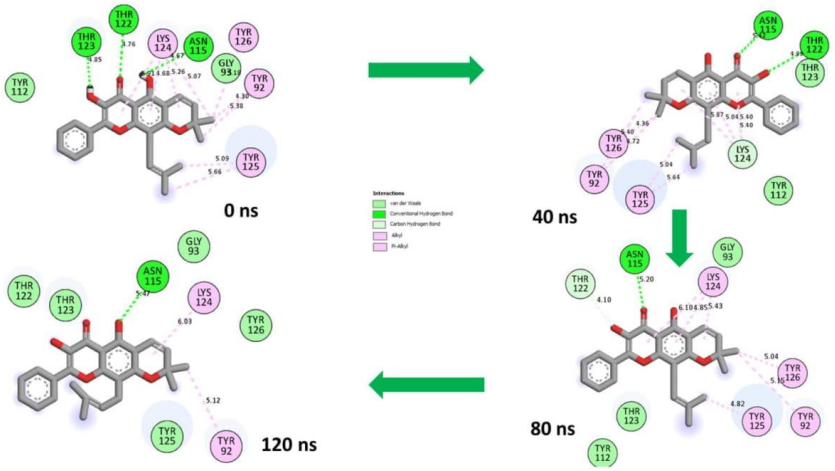


Figure 15. 2D interactions plots of sericetin against VP8* at various timeframes during the 120 ns simulation.

free energy. There is an insignificant difference in their bond length, which their respective binding free energy does not justify. The absence of hydrogen bonds in sericetin + VP5* could be responsible for the difference in the binding free energy of both sericetin and 2SG. Also noticeable between the two is the comparatively higher number of vital interactions and residues in 2SG than in sericetin, which could be responsible for its higher binding free energy. On the other hand, sacranoside A has a lesser binding free energy than 2SG and sericetin, which agrees with its number of interactions. The presence of hydrogen bonds in its interaction plot could have increased the binding free energy, but the bond length is higher than 2SG. Expectedly, tizoxanide has the lowest number of interactions and consequently the lowest binding free energy among the compounds investigated against VP5*.

Both 2SG and apigenin-4′-glucoside have equal interactions (14) against VP5* (Table 7); however, apigenin-4′-glucoside had higher binding free energy relative to 2SG. Interestingly, apigenin-4′-glucoside has a lesser bond length than 2SG, which could be responsible for its higher binding free energy. Shorter bond lengths are linked to greater force between intramolecular or intermolecular entities. This may be because molecules with shorter bond lengths have a greater affinity for one another since their atoms are more tightly bonded together (Du et al., 2016). Indeed, hydrogen bond interactions play a

vital role in developing new drugs. These interactions are characterized by their extraordinary strength and are among the most essential non-covalent bonds in drug discovery and design. Hydrogen bonds provide a crucial framework for molecular recognition, stabilization of protein-ligand binding, and greater stability of the drug-target complexes (Patil et al., 2010). Specifically, apigenin-4′-glucoside has the highest number of hydrogen bonds compared to other compounds investigated in this study (Table 7). This suggests the contribution of hydrogen bonds to its highest binding free energy. The results further underscore the importance of hydrogen bonds in discovering and developing new drugs.

Furthermore, the analysis revealed that gnetin L had the second-highest number of interactions (13) against VP8* relative to 2SG and apigenin-4′-glucoside, consistent with its free energy. Also, a lower number of hydrogen bonds observed in gnetin L relative to 2SG, and apigenin-4′-glucoside could have equally influenced its binding free energy. Unfortunately, the number of interactions observed in sericetin at 120 ns could not be linked with its binding free energy. However, an in-depth view of the interaction plot of sericetin at 0, 40 and 80 ns (Figure 15) showed a higher number of interactions relative to 120 ns and could be linked to the observed high free binding energy. Generally, the

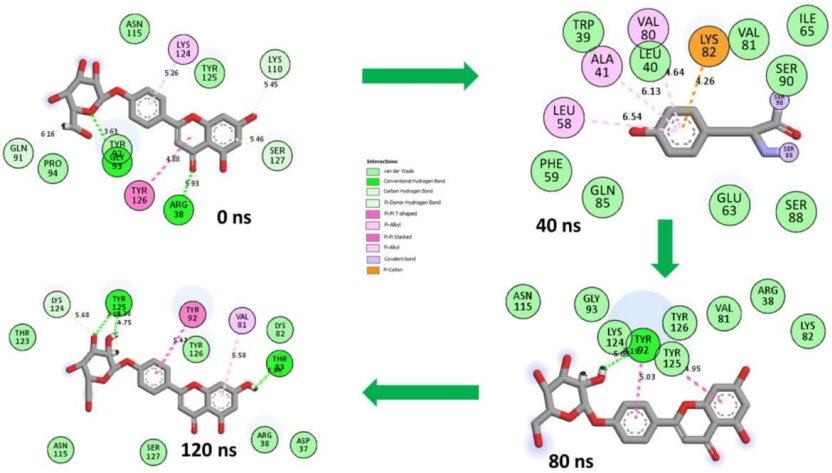


Figure 16. 2D interactions plots of apigenin-4′-glucoside against VP8* at various timeframes during the 120 ns simulation.

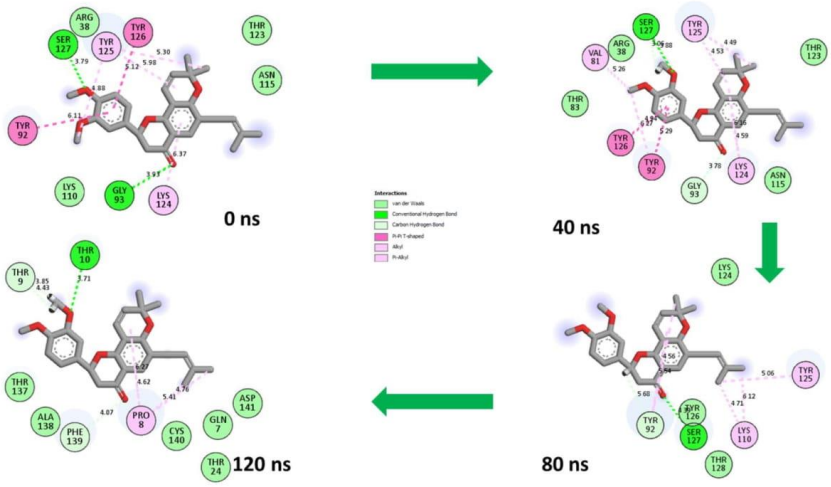


Figure 17. 2D interactions plots of 2SG against VP8* at various timeframes during the 120 ns simulation.

investigated compounds displayed a substantial periodic shift during the simulation period (Figures 11–17) owing to the dynamic character of MD simulation, where both components are flexible (Stella & Melchionna, 1998). As a result, over the 120 ns simulation period, the amino acid residues in the interaction plots for the complexes in this investigation vary at intervals (Figures 11–17). Furthermore, equal interactions (13) were observed in both tizoxanide and gnetin L, but they differ in free binding energy. Higher binding free energy observed in gnetin L relative to tizoxanide could be linked to more hydrogen bonds observed in gnetin L coupled with a shorter bond length than tizoxanide. The number of interactions observed in both tizoxanide (13) and ellagic acid (11) were justified by their respective free binding energy. Thus, the better broad-spectrum activities exhibited by 2SG and sericetin compared to tizoxanide against VP5* and VP8* may be ascribed to the quantity, nature, and bond distance of interactions with both proteins. Remarkably, unfavourable donor-donor interactions that could portend a repelling force were not observed in the molecular interactions between the top-ranked compounds against VP5* and VP8* at 120 ns of simulation and were hardly observed during the simulation (Table 7).

4. Conclusion

This study has identified lead compounds from *S. mombin*, *M. barteri* and *D. eriocarpum* plant that can impede the activity of VP5* and VP8*. Specifically, the best affinity towards VP5* and VP8* was observed with 2SG and apigenin-4′-glucoside, respectively. Furthermore, of all the top-ranked compounds, only 2SG and sericetin had better broad-spectrum affinities for both VP5* and VP8* than tizoxanide. This observation implies that 2SG and sericetin exhibit superior efficacy compared to other top-ranked metabolites analyzed in this study for treating RVA infection. Generally, the investigated top-ranked compounds were more thermodynamically compatible with VP8* than with VP5*, with 2SG and ellagic acid being the most thermodynamically compatible with VP8* while sacranoside A was the most compatible with VP5* which further confirms their affinity for the therapeutic targets. Remarkably, the top-ranked metabolites have satisfactory pharmacokinetic features with minimal structural modifications necessary to improve their druggability. Therefore, these molecules could be exploited in developing novel therapeutic candidates to combat RVA. The study's findings need further *in vitro* and *in vivo* validation, and work is already being undertaken in this regard.

Acknowledgments

The DUT Doctoral Scholarship Scheme to A. A. Lanrewaju is duly acknowledged. The Centre for High-Performance Computing (CHPC), South Africa, is equally acknowledged for granting access to the computing systems used in this study.

Disclosure statement

No potential conflict of interest was reported by the authors.

Funding

The study is based the financial assistance received from the Directorate of Research and Postgraduate Support, Durban University of Technology (DUT), and the South African Medical Research Council (SAMRC) under a Self-Initiated Research Grant as well as and the National Research Foundation (NRF) Research Development Grant for Rated Researchers (Grant number 120433) and the Competitive Programme for Rated Researchers Support (SRUG2204193723) to S. Sabiu. We also acknowledge Water Research Commission (WRC) of South Africa for the grant (Project no. K5/C2020-2021-00181) awarded to am Enitan-Folami.

Authors' contribution

Conceptualization, S.S. and A.M.E.; methodology, A.A.L.; software, S.S.; validation, A.A.L. and S.S; formal analysis, A.A.L.; investigation, A.A.L; resources, S.S.; data curation, A.A.L. and S.S.; writing—original draft preparation, A.A.L.; writing—review and editing, A.M.E., M.M.N., F.M.S, S.S; supervision, A.M.E., F.M.S and S.S.; funding acquisition, A.M.E., F.M.S. and S.S. All authors read and contributed to the critical review of the manuscript for intellectual content and approved the submission for publication.

Data availability statement

The data are contained within the article or supplementary material.

References

Acharya, A., Agarwal, R., Baker, M. B., Baudry, J., Bhowmik, D., Boehm, S., Byler, K. G., Chen, S. Y., Coates, L., Cooper, C. J., Demerdash, O., Daidone, I., Eblen, J. D., Ellingson, S., Forli, S., Glaser, J., Gumbart, J. C., Gunnels, J., Hernandez, O., … Zanetti-Polzi, L. (2020). Supercomputer-based ensemble docking drug discovery pipeline with application to COVID-19. *Journal of Chemical Information and Modeling*, *60*(12), 5832–5852. https://doi.org/10.1021/acs.jcim.0c01010

Akintemi, E. O., Govender, K. K., & Singh, T. (2022). A DFT study of the chemical reactivity properties, spectroscopy and bioactivity scores of bioactive flavonols. *Computational and Theoretical Chemistry*, *1210*, 113658. https://doi.org/10.1016/j.comptc.2022.113658

Ali, S. I., Sheikh, W. M., Rather, M. A., Venkatesalu, V., Muzamil Bashir, S., & Nabi, S. U. (2021). Medicinal plants: Treasure for antiviral drug discovery. *Phytotherapy Research : PTR*, *35*(7), 3447–3483. https://doi.org/10.1002/ptr.7039

Al-Khodairy, F. M., Khan, M. K. A., Kunhi, M., Pulicat, M. S., Akhtar, S., & Arif, J. M. (2013). In silico prediction of mechanism of erysolin-induced apoptosis in human breast cancer cell lines. *American Journal of Bioinformatics Research*, *3*(3), 62–71. https://doi.org/10.5923/j.bioinformatics.20130303.03

Amimo, J. O., Raev, S. A., Chepngeno, J., Mainga, A. O., Guo, Y., Saif, L., & Vlasova, A. N. (2021). Rotavirus interactions with host intestinal epithelial cells. *Frontiers in Immunology*, *12*, 793841. https://doi.org/10.3389/fimmu.2021.793841

Aribisala, J. O., Aruwa, C. E., Uthman, T. O., Nurain, I. O., Idowu, K., & Sabiu, S. (2022). Cheminformatics bioprospection of broad spectrum plant secondary metabolites targeting the spike proteins of omicron variant and wild-type SARS-CoV-2. *Metabolites*, *12*(10), 982. https://doi.org/10.3390/metabo12100982

Aribisala, J. O., & Sabiu, S. (2022). Cheminformatics identification of phenolics as modulators of penicillin-binding protein 2a of Staphylococcus aureus: A structure–activity-relationship-based study. *Pharmaceutics*, *14*(9), 1818. https://doi.org/10.3390/pharmaceutics14091818

Artemova, S., Jaillet, L., & Redon, S. (2016). Automatic molecular structure perception for the universal force field. *Journal of Computational Chemistry*, *37*(13), 1191–1205. https://doi.org/10.1002/jcc.24309

Basconi, J. E., & Shirts, M. R. (2013). Effects of temperature control algorithms on transport properties and kinetics in molecular dynamics

simulations. *Journal of Chemical Theory and Computation*, *9*(7), 2887–2899. https://doi.org/10.1021/ct400109a

Corthout, J., Pieters, L., Claeys, M., Berghe, D. V., & Vlietinck, A. (1991). Antiviral ellagitannins from Spondias mombin. *Phytochemistry*, *30*(4), 1129–1130. https://doi.org/10.1016/S0031-9422(00)95187-2

Dallakyan, S., & Olson, A. J. (2015). Small-molecule library screening by docking with PyRx. *Methods in Molecular Biology (Clifton, N.J.)*, *1263*, 243–250. https://doi.org/10.1007/978-1-4939-2269-7_19

Du, X., Li, Y., Xia, Y.-L., Ai, S.-M., Liang, J., Sang, P., Ji, X.-L., & Liu, S.-Q. (2016). Insights into protein–ligand interactions: Mechanisms, models, and methods. *International Journal of Molecular Sciences*, *17*(2), 144. https://doi.org/10.3390/ijms17020144

Fadiji, A. E., Omomowo, I. O., Omomowo, O. I., Lanrewaju, A. A., & Akande, D. (2018). Antimicrobial efficacy and phytochemical screening of aqueous and ethanolic extracts of Ocimum gratissimum (scent leaf) leaf against some clinical isolates. *Journal of Basic Pharmacology and Toxicology*, *2*(2), 19–24.

Garuba, T., Govender, R., Isah, H. A., & Sabiu, S. (2022). Metabolites profiling and molecular docking identification of putative leads from endophytic Phyllosticta capitalensis as modulators of key druggable structural targets of rotavirus A. *Transactions of the Royal Society of South Africa*, *77*(3), 207–217. https://doi.org/10.1080/0035919X.2022.2158387

Gilis, D., & Rooman, M. (1996). Stability changes upon mutation of solvent-accessible residues in proteins evaluated by database-derived potentials. *Journal of Molecular Biology*, *257*(5), 1112–1126. https://doi.org/10.1006/jmbi.1996.0226

Gonçalves, J., Lopes, R., Oliveira, D., Costa, S., Miranda, M., Romanos, M., Santos, N., & Wigg, M. (2005). In vitro anti-rotavirus activity of some medicinal plants used in Brazil against diarrhea. *Journal of Ethnopharmacology*, *99*(3), 403–407. https://doi.org/10.1016/j.jep.2005.01.032

Gonnet, P. (2007). P-SHAKE: A quadratically convergent SHAKE in O (n2). *Journal of Computational Physics*, *220*(2), 740–750. https://doi.org/10.1016/j.jcp.2006.05.032

Heaney, R. P. (2001). Factors influencing the measurement of bioavailability, taking calcium as a model. *Journal of Nutrition*, *131*(4 Suppl), 1344S–1348S. https://doi.org/10.1093/jn/131.4.1344S

Hudson, J. B. (2018). *Antiviral compounds from plants* (pp. 1–35). CRC Press.

Ibeji, C. U., Akintayo, D. C., Oluwasola, H. O., Akintemi, E. O., Onwukwe, O. G., & Eziomume, O. M. (2023). Synthesis, experimental and computational studies on the anti-corrosion performance of substituted Schiff bases of 2-methoxybenzaldehyde for mild steel in HCl medium. *Scientific Reports*, *13*(1), 3265. https://doi.org/10.1038/s41598-023-30396-3

Izaguirre, J. A., Catarello, D. P., Wozniak, J. M., & Skeel, R. D. (2001). Langevin stabilization of molecular dynamics. *Journal of Chemical Physics*, *114*(5), 2090–2098. https://doi.org/10.1063/1.1332996

Jaillet, L., Artemova, S., & Redon, S. (2017). IM-UFF: Extending the universal force field for interactive molecular modeling. *Journal of Molecular Graphics & Modelling*, *77*, 350–362. https://doi.org/10.1016/j.jmgm.2017.08.023

Jiang, L., Tang, A., Song, L., Tong, Y., & Fan, H. (2023). Advances in the development of antivirals for rotavirus infection. *Frontiers in Immunology*, *14*, 1041149. https://doi.org/10.3389/fimmu.2023.1041149

Jorgensen, W. L., Chandrasekhar, J., Madura, J. D., Impey, R. W., & Klein, M. L. (1983). Comparison of simple potential functions for simulating liquid water. *Journal of Chemical Physics*, *79*(2), 926–935. https://doi.org/10.1063/1.445869

Katuwal, S., Upadhyaya, S. R., Marahatha, R., Shrestha, A., Regmi, B. P., Khadayat, K., Basnet, S., Basnyat, R. C., & Parajuli, N. (2023). In silico study of coumarins: Wedelolactone as a potential inhibitor of the spike protein of the SARS-CoV-2 variants. *Journal of Tropical Medicine*, *2023*, 1–19. https://doi.org/10.1155/2023/4771745

Kim, A. H., Hogarty, M. P., Harris, V. C., & Baldridge, M. T. (2020). The complex interactions between rotavirus and the gut microbiota. *Frontiers in Cellular and Infection Microbiology*, *10*, 586751. https://doi.org/10.3389/fcimb.2020.586751

Kraschnefski, M. J., Bugarcic, A., Fleming, F. E., Yu, X., von Itzstein, M., Coulson, B. S., & Blanchard, H. (2009). Effects on sialic acid recognition of amino acid mutations in the carbohydrate-binding cleft of the rotavirus spike protein. *Glycobiology*, *19*(3), 194–200. https://doi.org/10.1093/glycob/cwn119

Kretschmer, R., Kinzel, D., & González, L. (2012). The role of hydrogen bonds in protein–ligand interactions. DFT calculations in 1, 3-dihydrobenzimidazole-2 thione derivatives with glycinamide as model HIV RT inhibitors. *International Journal of Quantum Chemistry*, *112*(7), 1786–1795. https://doi.org/10.1002/qua.23001

Kumar, D., Singh, A., Kumar, P., Uversky, V. N., Rao, C. D., & Giri, R. (2020). Understanding the penetrance of intrinsic protein disorder in rotavirus proteome. *International Journal of Biological Macromolecules*, *144*, 892–908. https://doi.org/10.1016/j.ijbiomac.2019.09.166

Lakhera, S., Devlal, K., Ghosh, A., Chowdhury, P., & Rana, M. (2022). Modelling the DFT structural and reactivity study of feverfew and evaluation of its potential antiviral activity against COVID-19 using molecular docking and MD simulations. *Chemicke Zvesti*, *76*(5), 2759–2776. https://doi.org/10.1007/s11696-022-02067-6

Lanrewaju, A. A., Enitan-Folami, A. M., Nyaga, M. M., Sabiu, S., & Swalaha, F. M. (2023). Metabolites profiling and cheminformatics bioprospection of selected medicinal plants against the main protease and RNA-dependent RNA polymerase of SARS-CoV-2. *Journal of Biomolecular Structure & Dynamics*, 1–21. https://doi.org/10.1080/07391102.2023.2236718

Lanrewaju, A. A., Enitan-Folami, A. M., Sabiu, S., Edokpayi, J. N., & Swalaha, F. M. (2022). Global public health implications of human exposure to viral contaminated water. *Frontiers in Microbiology*, *13*, 981896–981896. https://doi.org/10.3389/fmicb.2022.981896

Li, D., Wang, M., Qi, J., Zhang, Q., Wang, H., Pang, L., Sun, X., & Duan, Z. (2021). Human group A rotavirus P [25] VP8* specifically binds to A-type histo-blood group antigen. *Virology*, *555*, 56–63. https://doi.org/10.1016/j.virol.2020.12.016

Lipinski, C. A., Lombardo, F., Dominy, B. W., & Feeney, P. J. (2001). Experimental and computational approaches to estimate solubility and permeability in drug discovery and development settings. *Advanced Drug Delivery Reviews*, *46*(1–3), 3–26. https://doi.org/10.1016/s0169-409x(00)00129-0

Luseba, D., Elgorashi, E., Ntloedibe, D., & Van Staden, J. (2007). Antibacterial, anti-inflammatory and mutagenic effects of some medicinal plants used in South Africa for the treatment of wounds and retained placenta in livestock. *South African Journal of Botany*, *73*(3), 378–383. https://doi.org/10.1016/j.sajb.2007.03.003

Ma, Y., Tao, Y., Qu, H., Wang, C., Yan, F., Gao, X., & Zhang, M. (2022). Exploration of plant-derived natural polyphenols toward COVID-19 main protease inhibitors: DFT, molecular docking approach, and molecular dynamics simulations. *RSC Advances*, *12*(9), 5357–5368. https://doi.org/10.1039/d1ra07364h

Medjahed, S., Belaidi, S., Djekhaba, S., Tchouar, N., & Kerassa, A. (2016). Computational study of molecular electrostatic potential, drug likeness screening and structure-activity/property relationships of thiazolidine-2, 4-dione derivatives. *Journal of Bionanoscience*, *10*(2), 118–126. https://doi.org/10.1166/jbns.2016.1358

Morozov, A. V., & Kortemme, T. (2005). Potential functions for hydrogen bonds in protein structure prediction and design. *Advances in Protein Chemistry*, *72*, 1–38. https://doi.org/10.1016/S0065-3233(05)72001-5

Mountessou, B. Y. G., Ngouonpe, A. W., Mbobda, A. S. W., Akintemi, E. O., Stammler, H.-G., Kouam, S. F., Tchouankeu, J. C., Lenta, B. N., Sewald, N., Singh, T., & Mbouombouo, I. N. (2023). Structural analysis and molecular docking study of pachypodostyflavone: A potent anti-onchocerca. *Journal of Molecular Structure*, *1291*, 136003. https://doi.org/10.1016/j.molstruc.2023.136003

Mousavi, S. S., Karami, A., Haghighi, T. M., Tumilaar, S. G., Idroes, R., Mahmud, S., Celik, I., Ağagündüz, D., Tallei, T. E., Emran, T. B., Capasso, R., Fatimawali. (2021). In silico evaluation of Iranian medicinal plant phytoconstituents as inhibitors against main protease and the receptor-binding domain of SARS-CoV-2. *Molecules (Basel, Switzerland)*, *26*(18), 5724. https://doi.org/10.3390/molecules26185724

Nair, P. C., & Miners, J. O. (2014). Molecular dynamics simulations: From structure function relationships to drug discovery. *In Silico Pharmacology*, *2*(1), 4. https://doi.org/10.1186/s40203-014-0004-8

Nasution, M. A. F., Toepak, E. P., Alkaff, A. H., & Tambunan, U. S. F. (2018). Flexible docking-based molecular dynamics simulation of

natural product compounds and Ebola virus nucleocapsid (EBOV NP): A computational approach to discover new drug for combating Ebola. *BMC Bioinformatics*, *19*(Suppl 14), 419. https://doi.org/10.1186/s12859-018-2387-8

Newman, D. J., & Cragg, G. M. (2016). Natural products as sources of new drugs from 1981 to 2014. *Journal of Natural Products*, *79*(3), 629–661. https://doi.org/10.1021/acs.jnatprod.5b01055

Nyaga, M. M., Sabiu, S., Ndze, V. N., Dennis, F. E., & Jere, K. C. (2020). Report of the 1st African Enteric Viruses Genome Initiative (AEVGI) data and bioinformatics workshop on whole-genome analysis of some African rotavirus strains held in Bloemfontein, South Africa. *Vaccine*, *38*(34), 5402–5407. https://doi.org/10.1016/j.vaccine.2020.06.010

Ogbole, O. O., Akinleye, T. E., Segun, P. A., Faleye, T. C., & Adeniji, A. J. (2018). In vitro antiviral activity of twenty-seven medicinal plant extracts from Southwest Nigeria against three serotypes of echoviruses. *Virology Journal*, *15*(1), 110. https://doi.org/10.1186/s12985-018-1022-7

Omatola, C. A., & Olaniran, A. O. (2022). Rotaviruses: From pathogenesis to disease control—A critical review. *Viruses*, *14*(5), 875. https://doi.org/10.3390/v14050875

Patil, R., Das, S., Stanley, A., Yadav, L., Sudhakar, A., & Varma, A. K. (2010). Optimized hydrophobic interactions and hydrogen bonding at the target-ligand interface leads the pathways of drug-designing. *PloS One*, *5*(8), e12029. https://doi.org/10.1371/journal.pone.0012029

Prasad, O., Sinha, L., Misra, N., Narayan, V., Kumar, N., & Pathak, J. (2010). Molecular structure and vibrational study on 2, 3-dihydro-1H-indene and its derivative 1H-indene-1, 3 (2H)-dione by density functional theory calculations. *Journal of Molecular Structure: THEOCHEM*, *940*(1–3), 82–86. https://doi.org/10.1016/j.theochem.2009.10.011

Ramírez, D., & Caballero, J. (2016). Is it reliable to use common molecular docking methods for comparing the binding affinities of enantiomer pairs for their protein target? *International Journal of Molecular Sciences*, *17*(4), 525. https://doi.org/10.3390/ijms17040525

Reichling, J. (2010). Plant-microbe interactions and secondary metabolites with antibacterial, antifungal and antiviral properties. *Annual Plant Reviews Volume 39: Functions and Biotechnology of Plant Secondary Metabolites*, *39*, 214–347. https://doi.org/10.1002/9781444318876.ch4

Rossignol, J.-F., Abu-Zekry, M., Hussein, A., & Santoro, M. G. (2006). Effect of nitazoxanide for treatment of severe rotavirus diarrhoea: Randomised double-blind placebo-controlled trial. *Lancet (London, England)*, *368*(9530), 124–129. https://doi.org/10.1016/S0140-6736(06)68852-1

Ryckaert, J.-P., Ciccotti, G., & Berendsen, H. J. (1977). Numerical integration of the Cartesian equations of motion of a system with constraints: Molecular dynamics of n-alkanes. *Journal of Computational Physics*, *23*(3), 327–341. https://doi.org/10.1016/0021-9991(77)90098-5

S'thebe, N. W., Aribisala, J. O., & Sabiu, S. (2023). Cheminformatics bioprospection of sunflower seeds' oils against quorum sensing system of Pseudomonas aeruginosa. *Antibiotics (Basel, Switzerland)*, *12*(3), 504. https://doi.org/10.3390/antibiotics12030504

Sabiu, S., Balogun, F. O., & Amoo, S. O. (2021). Phenolics profiling of Carpobrotus edulis (L.) NE Br. and insights into molecular dynamics of their significance in type 2 diabetes therapy and its retinopathy complication. *Molecules (Basel, Switzerland)*, *26*(16), 4867. https://doi.org/10.3390/molecules26164867

Segun, P. A., Ogbole, O. O., Akinleye, T. E., Faleye, T. O., & Adeniji, A. J. (2021). In vitro anti-enteroviral activity of stilbenoids isolated from the leaves of Macaranga barteri. *Natural Product Research*, *35*(11), 1909–1913. https://doi.org/10.1080/14786419.2019.1644505

Shaikh, I. A., Muddapur, U. M., Kulkarni, M., Badiger, S., Krithika, C., Mahnashi, M. H., Mannasaheb, B. A., Alsaikhan, F., Bahafi, A., Iqubal, S. M. S., Khan, A. A., Shaikh, M. A. K., & Maqbul, M. S. (2022). In-silico analysis of VP4 protein causing pathogenesis in rotavirus and its interaction studies. *Science of Advanced Materials*, *14*(1), 67–79. https://doi.org/10.1166/sam.2022.4193

Shode, F., Idowu, A., Uhomoibhi, O., & Sabiu, S. (2022). Repurposing drugs and identification of inhibitors of integral proteins (spike protein and main protease) of SARS-CoV-2. *Journal of Biomolecular Structure & Dynamics*, *40*(14), 6587–6602. https://doi.org/10.1080/07391102.2021.1886993

Shode, F. O., Uhomoibhi, J. O-o., Idowu, K. A., Sabiu, S., & Govender, K. K. (2022). Molecular dynamics study on selected bioactive phytochemicals as potential inhibitors of HIV-1 subtype C protease. *Metabolites*, *12*(11), 1155. https://doi.org/10.3390/metabo12111155

Sindhu, T., & Srinivasan, P. (2015). Exploring the binding properties of agonists interacting with human TGR5 using structural modeling, molecular docking and dynamics simulations. *RSC Advances*, *5*(19), 14202–14213. https://doi.org/10.1039/C4RA16617E

Siqueira, E. M. D. S., Lima, T. L. C., Boff, L., Lima, S. G. M., Lourenço, E. M. G., Ferreira, É. G., Barbosa, E. G., Machado, P. R. L., Farias, K. J. S., Ferreira, L. D. S., Rocha, H. A. D. O., Simões, C. M. O., & Zucolotto, S. M. (2020). Antiviral potential of Spondias mombin L. leaves extract against herpes simplex virus type-1 replication using in vitro and in silico approaches. *Planta Medica*, *86*(7), 505–515. https://doi.org/10.1055/a-1135-9066

Stella, L., & Melchionna, S. (1998). Equilibration and sampling in molecular dynamics simulations of biomolecules. *Journal of Chemical Physics*, *109*(23), 10115–10117. https://doi.org/10.1063/1.477703

Tohmé, M. J., & Delgui, L. R. (2021). Advances in the development of antiviral compounds for rotavirus infections. *mBio*, *12*(3), e00111–00121. https://doi.org/10.1128/mBio.00111-21

Tri, M. D., Phat, N. T., Minh, P. N., Chi, M. T., Hao, B. X., Minh An, T. N., Alam, M., Van Kieu, N., Dang, V.-S., Mai, T. T. N., & Duong, T.-H. (2023). In vitro anti-inflammatory, in silico molecular docking and molecular dynamics simulation of oleanane-type triterpenes from aerial parts of Mussaenda recurvata. *RSC Advances*, *13*(8), 5324–5336. https://doi.org/10.1039/d2ra06870b

Troeger, C., Khalil, I. A., Rao, P. C., Cao, S., Blacker, B. F., Ahmed, T., Armah, G., Bines, J. E., Brewer, T. G., Colombara, D. V., Kang, G., Kirkpatrick, B. D., Kirkwood, C. D., Mwenda, J. M., Parashar, U. D., Petri, W. A., Riddle, M. S., Steele, A. D., Thompson, R. L., … Reiner, R. C. (2018). Rotavirus vaccination and the global burden of rotavirus diarrhea among children younger than 5 years. *JAMA Pediatrics*, *172*(10), 958–965. https://doi.org/10.1001/jamapediatrics.2018.1960

Uhomoibhi, J. O.-O., Shode, F. O., Idowu, K. A., & Sabiu, S. (2022). Molecular modelling identification of phytocompounds from selected African botanicals as promising therapeutics against druggable human host cell targets of SARS-CoV-2. *Journal of Molecular Graphics & Modelling*, *114*, 108185. https://doi.org/10.1016/j.jmgm.2022.108185

Van der Merwe, D., Swan, G., & Botha, C. (2001). Use of ethnoveterinary medicinal plants in cattle by Setswana-speaking people in the Madikwe area of the North West Province of South Africa. *Journal of the South African Veterinary Association*, *72*(4), 189–196. https://doi.org/10.4102/jsava.v72i4.651

Verma, A. K., Ahmed, S. F., Hossain, M. S., Bhojiya, A. A., Mathur, A., Upadhyay, S. K., Srivastava, A. K., Vishvakarma, N. K., Barik, M., Rahaman, M. M., & Bahadur, N. M. (2022). Molecular docking and simulation studies of flavonoid compounds against PBP-2a of methicillin-resistant Staphylococcus aureus. *Journal of Biomolecular Structure & Dynamics*, *40*(21), 10561–10577. https://doi.org/10.1080/07391102.2021.1944911

WHO. (2021). *World Health Organization. Summary of key characteristics of WHO prequalified rotavirus vaccines*. https://www.who.int/publications/i/item/WHO-IVB-2021.03

Yoder, J. D., & Dormitzer, P. R. (2006). Alternative intermolecular contacts underlie the rotavirus VP5* two-to three-fold rearrangement. *The EMBO Journal*, *25*(7), 1559–1568. https://doi.org/10.1038/sj.emboj.7601034

References for section 4.1

AMIMO, J. O., RAEV, S. A., CHEPNGENO, J., MAINGA, A. O., GUO, Y., SAIF, L. & VLASOVA, A. N. 2021. Rotavirus interactions with host intestinal epithelial cells. *Frontiers in Immunology*, 12, 1-17.

ASENSIO-COB, D., RODRÍGUEZ, J. M. & LUQUE, D. 2023. Rotavirus particle disassembly and assembly *in vivo* and *in vitro*. *Viruses*, 15(8), 1-23.

BERESSA, T. B., DEYNO, S., MTEWA, A. G., AIDAH, N., TUYIRINGIRE, N., LUKUBYE, B., WEISHEIT, A., TOLO, C. U. & OGWANG, P. E. 2021. Potential benefits of antiviral African medicinal plants in the management of viral infections: systematic review. *Frontiers in Pharmacology*, 12, 1-13.

CORTHOUT, J., PIETERS, L., CLAEYS, M., BERGHE, D. V. & VLIETINCK, A. 1991. Antiviral ellagitannins from *Spondias mombin*. *Phytochemistry*, 30(4), 1129-1130.

ELFIKY, A. A. 2020. Ribavirin, remdesivir, sofosbuvir, galidesivir and tenofovir against SARS-CoV-2 RNA-dependent RNA polymerase (RdRp): a molecular docking study. *Life Sciences*, 253, 1-8.

GARUBA, T., GOVENDER, R., ISAH, H. A. & SABIU, S. 2022. Metabolites profiling and molecular docking identification of putative leads from endophytic *Phyllosticta capitalensis* as modulators of key druggable structural targets of rotavirus A. *Transactions of the Royal Society of South Africa*, 77(3), 207-217.

ISLAM, T., HASAN, M., RAHMAN, M. S. & ISLAM, M. R. 2022. Comparative evaluation of authorized drugs for treating COVID-19 patients. *Health Science Reports*, 5(4), 1-9.

JIANG, L., TANG, A., SONG, L., TONG, Y. & FAN, H. 2023. Advances in the development of antivirals for rotavirus infection. *Frontiers in Immunology*, 14, 1-16.

KUMAR, D., SINGH, A., KUMAR, P., UVERSKY, V. N., RAO, C. D. & GIRI, R. 2020. Understanding the penetrance of intrinsic protein disorder in rotavirus proteome. *International Journal of Biological Macromolecules*, 144, 892-908.

LANREWAJU, A. A., ENITAN-FOLAMI, A. M., SABIU, S., EDOKPAYI, J. N. & SWALAHA, F. M. 2022. Global public health implications of human exposure to viral-contaminated water. *Frontiers in Microbiology*, 13, 1-18.

LI, D., WANG, M., QI, J., ZHANG, Q., WANG, H., PANG, L., SUN, X. & DUAN, Z. 2021. Human group A rotavirus P[25] VP8* specifically binds to A-type histo-blood group antigen. *Virology*, 555, 56-63.

LI, S. Y., CHEN, C., ZHANG, H. Q., GUO, H. Y., WANG, H., WANG, L., ZHANG, X., HUA, S. N., YU, J., XIAO, P. G., LI, R. S. & TAN, X. 2005. Identification of natural compounds with antiviral activities against SARS-associated coronavirus. *Antiviral Research*, 67(1), 18-23.

LUSEBA, D., ELGORASHI, E., NTLOEDIBE, D. & VAN STADEN, J. 2007. Antibacterial, anti-inflammatory and mutagenic effects of some medicinal plants used in South Africa for the treatment of wounds and retained placenta in livestock. *South African Journal of Botany*, 73(3), 378-383.

NYAGA, M. M., SABIU, S., NDZE, V. N., DENNIS, F. E. & JERE, K. C. 2020. Report of the 1st African Enteric Viruses Genome Initiative (AEVGI) data and bioinformatics workshop on whole-genome analysis of some African rotavirus strains held in Bloemfontein, South Africa. *Vaccine*, 38(34), 5402-5407.

OGBOLE, O. O., AKINLEYE, T. E., SEGUN, P. A., FALEYE, T. C. & ADENIJI, A. J. 2018. *In vitro* antiviral activity of twenty-seven medicinal plant extracts from southwest Nigeria against three echovirus serotypes. *Virology Journal*, 15(1), 1-8.

OMATOLA, C. A. & OLANIRAN, A. O. 2022. Rotaviruses: from pathogenesis to disease control—a critical review. *Viruses*, 14(5), 1-34.

PARASHAR, U. D., JOHNSON, H., STEELE, A. D. & TATE, J. E. 2016. Health impact of rotavirus vaccination in developing countries: progress and way forward. *Clinical Infectious Diseases*, 62(Suppl 2), S91-S95.

SEGUN, P. A., OGBOLE, O. O., AKINLEYE, T. E., FALEYE, T. O. & ADENIJI, A. J. 2021. *In vitro* anti-enteroviral activity of stilbenoids isolated from the leaves of *Macaranga barteri*. *Natural Product Research*, 35(11), 1909-1913.

SHAIKH, I. A., MUDDAPUR, U. M., KULKARNI, M., BADIGER, S., KRITHIKA, C., MAHNASI, M. H., MANNASaheb, B. A., ALSAIKHAN, F., BAHAFI, A., IQUBAL, S. M. S., KHAN, A. A., SHAIKH, M. A. K. & MAQBUL, M. S. 2022. *In silico* analysis of VP4 protein causing pathogenesis in rotavirus and its interaction studies. *Science of Advanced Materials*, 14(1), 67-79.

SIQUEIRA, E. M. D. S., LIMA, T. L., BOFF, L., LIMA, S. G., LOURENÇO, E. M., FERREIRA, É. G., BARBOSA, E. G., MACHADO, P. R., FARIAS, K. J. & FERREIRA, L. D. S. 2020. Antiviral potential of *Spondias mombin* leaves extract against herpes simplex virus type 1: *in vitro* and *in silico* approaches. *Planta Medica*, 86(7), 505-515.

TOHMÉ, M. J. & DELGUI, L. R. 2021. Advances in the development of antiviral compounds for rotavirus infections. *mBio*, 12(3), e00111-21.

TROEGER, C., KHALIL, I. A., RAO, P. C., CAO, S., BLACKER, B. F., AHMED, T., ARMAH, G., BINES, J. E., BREWER, T. G. & COLOMBARA, D. V. 2018. Rotavirus vaccination and the global burden of rotavirus diarrhoea among children younger than 5 years. *JAMA Pediatrics*, 172, 958-965.

UGBOKO, H. U., NWINYI, O. C., ORANUSI, S. U. & OYEWALE, J. O. 2020. Childhood diarrhoeal diseases in developing countries. *Heliyon*, 6(4), 1-12.

VAN DER MERWE, D., SWAN, G. & BOTHA, C. 2001. Ethnoveterinary medicinal plant use in cattle by Setswana-speaking people in the Madikwe area, North-West Province, South Africa. *Journal of the South African Veterinary Association*, 72(4), 189-196.

VARDHAN, S. & SAHOO, S. K. 2022. Computational studies on the interaction of SARS-CoV-2 Omicron SGp RBD with human receptor ACE2, limonin and glycyrrhizic acid. *Computers in Biology and Medicine*, 144(105367), 1-8.

WANG, C., HORBY, P. W., HAYDEN, F. G. & GAO, G. F. 2020. A novel coronavirus outbreak of global health concern. *The Lancet*, 395(10223), 470-473.

WORLD HEALTH ORGANIZATION. 2023. Coronavirus disease (COVID-19) weekly epidemiological update and weekly operational update. https://www.who.int/emergencies/diseases/novel-coronavirus-2019/situation-reports (accessed 2023).

WRAPP, D., DE VLIEGER, D., CORBETT, K. S., TORRES, G. M., WANG, N., VAN BREEDAM, W., ROOSE, K., VAN SCHIE, L., HOFFMANN, M., PÖHLMANN, S., GRAHAM, B. S., CALLEWAERT, N., SCHEPENS, B., SAELENS, X., MCLELLAN, J. S. & VIB-CMB COVID-19 RESPONSE TEAM. 2020. Structural basis for potent neutralization of betacoronaviruses by single-domain camelid antibodies. *Cell*, 181(5), 1004-1015.

CHAPTER FIVE

5.0 Computational bioprospection of silver-complexed leads against trypsin-cleaved spike protein of rotavirus A……..……...……...375

Abstract…….. 376

1.0Introduction……..... 378

2.0 Materials and methods…….....… 380

3.0 Results and discussion……...…….. 387

4.0 Conclusion……....415

References……...…….. 415

Supplementary information……....426

This chapter has been formatted for submission to Computational Biology and Chemistry

Computational bioprospection of silver-complexed antiviral leads against spike proteins of rotavirus A

Adedayo Ayodeji Lanrewaju[1], Abimbola Motunrayo Folami[1], Olatomide Ayodeji Fadare[2], Lukman Olawale Olasunkanmi[2,3], Saheed Sabiu[1*] and Feroz Mahomed Swalaha[1]

[1]Department of Biotechnology and Food Science, Faculty of Applied Science, Durban University of Technology, P. O. Box 1334, Durban 4000, South Africa

[2]Department of Chemistry, Faculty of Science, Obafemi Awolowo University, Ile Ife, Nigeria

[3]Department of Chemical Sciences, University of Johannesburg, P.O. Box 17011, Doornfontein Campus, 2028 Johannesburg, South Africa

*Correspondence: sabius@dut.ac.za

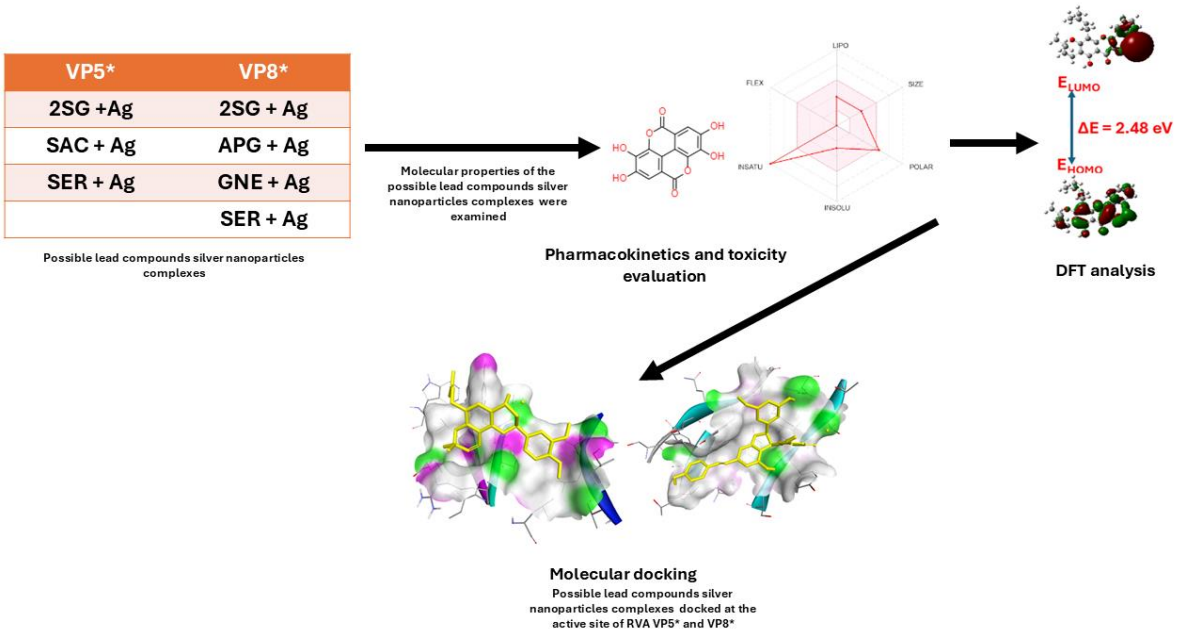
Abstract

Optimization of identified lead compounds from plants' secondary metabolites through silver complexation is a promising strategy for improving their drug-like properties and activity. This study used a silver complexation approach to enhance the binding affinity of previously identified lead compounds against trypsin-cleaved spike protein of rotavirus A; VP5* and VP8*. To comprehend the effect of the complexation, quantum chemical calculations (density functional theory, DFT model M06/def2TZVP) were used to compare the molecular features of silver-complexed leads and the lead compounds while assessing their drug-like properties and toxicity profiles through *in silico* techniques. Thereafter, the silver complexes were docked against VP5* and VP8*, followed by a comparative interaction analysis of the lead compounds and silver-complexed leads. Notably, the silver-complexed leads exhibited enhanced quantum molecular properties, suggesting better reactivity than their corresponding lead compounds without significantly altering their pharmacokinetics properties and toxicity profiles; hence, they remain suitable for drug development. Remarkably, higher negative docking scores were observed in all silver complexes docked against VP5* compared to their corresponding lead

compounds except in the sacranoside A series. Conversely, lower negative docking scores were reported in the apigenin-4'-glucoside series, gnetin L A-E, and sericetin B relative to their parent compounds, while the remaining silver-complexed leads exhibited improved binding affinity. Thereafter, comparative interactions analysis identified (2S)-6-(gamma,gamma-dimethylallyl)-3',4'-dimethoxy-6'',6''-dimethylpyran[2'',3'':7,8]flavanone C (2SGC) [-6.59 kcal/mol] and 2SGA [-6.77 kcal/mol] against VP5* and 2SGC [-8.06 kcal/mol] and sericetin A (SERA) [-7.26 kcal/mol] against VP8* as promising candidates. Further computational analysis including molecular dynamics simulation, is recommended to explore the thermodynamics profile of the resulting protein and silver-complexed leads and this is being considered for future study.

Keywords: Silver complexes; Lead compounds; Binding affinity; Frontier molecular orbitals; Molecular docking

Graphical Abstract



1.0 Introduction

Rotavirus A (RVA) is the predominant cause of viral acute gastroenteritis (AGE) in children under five years of age, responsible for approximately 128 500 deaths and several million hospital admissions annually (Lanrewaju *et al.*, 2022; Troeger *et al.*, 2018). Despite the global expansion of RVA vaccines, RVA infection continues to be a significant contributor to diarrhea-related illnesses and fatalities among young children (Cohen *et al.*, 2023; Clark *et al.*, 2017) which may be attributed to the relatively low efficacy of the vaccines, limited vaccine coverage and cold chain infrastructure challenges in low income countries (Troeger *et al.*, 2018). Specifically, these vaccines demonstrate significant efficacy in alleviating the effect of RVA-associated AGE, including reducing deaths, hospitalizations and severe diseases, particularly in high-income regions, while reduced effectiveness was reported in low and middle-income countries (Henschke *et al.*, 2022; Saha *et al.*, 2021). Unfortunately, the principal strategy for treating RVA-induced diarrhoea in children is administering oral rehydration solutions (ORS), a blend of glucose and electrolytes for enhancing water uptake and mitigating dehydration (Tohmé and Delgui, 2021). At present, there is a lack of approved therapeutic intervention for managing RVA-associated diarrhoea. Consequently, it is essential to focus on the discovery of novel agents with direct anti-RVA activity.

RVA belongs to the *Reoviridae* family and contains a triple-layered capsid encasing a genome comprising 11 segment double-stranded RNA (dsRNA), which codes for 6 structural proteins (VP1-VP4, VP6 and VP7) and six non-structural proteins (NSP1-NSP6) (Gutierrez *et al.*, 2023; Greenberg and Estes, 2009). The VP4 protein is characterized by its spike-like structure on the virus surface, and it is essential for both cellular entry and the virulence of the virus (Hu *et al.*, 2022; Ijaz *et al.*, 1994). More so, it is sensitive to trypsin, resulting in its cleavage to VP5* and

VP8* distinct functionality in the cell entry process (Amimo *et al.*, 2021). Owing to a hydrophobic structural region that enables the virus entry into cells (Jiang *et al.*, 2023), VP5* has been posited to possess membrane permeabilization properties (Kumar *et al.*, 2020). VP8* has a globular structure with a hemagglutinin domain linked to the host carbohydrate recognition (Pang *et al.*, 2018; Liu *et al.*, 2012) and encompasses the principal antigenic site of VP4 with a critical role in serum-specific neutralization (Trask *et al.*, 2012). Therefore, VP5* and VP8* represent compelling therapeutic targets for the development of anti-RVA drugs because they are indispensable for viral entry and immunogenicity.

The antiviral activities of plant secondary metabolites (PSMs) against herpes simplex virus (Zhou *et al.*, 2023; Astani and Schnitzler, 2014), dengue virus (Kaushik *et al.*, 2021; Yu *et al.*, 2017), human immunodeficiency virus (Esimone *et al.*, 2010), hepatitis c virus (Dey *et al.*, 2023; Kong *et al.*, 2013) and others have been reported. Recently *in silico* study has identified (2S)-6-(gamma,gamma-dimethylallyl)-3',4'-dimethoxy-6'',6''-dimethylpyran[2'',3'':7,8]flavanone (2SG), sericetin, sacranoside A, and 2SG, apigenin-4'-glucoside, gnetin L, sericetin as probable drug candidates against VP5* and VP8* of RVA respectively (Lanrewaju *et al.*, 2023). These leads can be optimized to boost their antiviral potency while minimizing toxicity (Barcelos *et al.*, 2022). One promising approach for such enhancement is by conjugating bioactive metal ions such as silver with organic ligands. This approach amplifies their activity through the combined effects while mitigating drug resistance, extends their spectrum of action and reduces the required dosage as demonstrated *in silico* (Kucuk *et al.*, 2022). Previously, metal complexes have been synthesized through the interaction of organic ligands with a range of metal ions such as zinc, nickel, cobalt, iron, manganese and silver (Veena *et al.*, 2024; da Silva *et al.*, 2022; Kucuk *et al.*, 2022), exploring their properties extensively through molecular docking, molecular dynamics (MD) simulation

and quantum chemical calculations. Specifically, silver is recognized as a broad-spectrum microbicide with considerable pharmacological effectiveness in addressing various challenges in disease treatment; thus, there is a growing interest in developing novel silver complexes (Kucuk *et al.*, 2022). Therefore, in response to the recurrent occurrence of RVA in the investigated wastewater treatment plants in Durban (chapter three), this study applies computational structure-activity relationship (SAR) approach to design anti-RVA drugs with improved activity, reduced toxicity and favorable pharmacokinetic profiles by complexing silver with previously identified lead compounds against VP5* and VP8*.

2.0 Materials and methods

The overall methodology involved geometry optimization of the silver complexes of the lead compounds, analysis of their quantum molecular properties, molecular docking against the VP5* and VP8* as well as toxicity evaluation. The workflow adopted in the study is summarized in Figure 1.

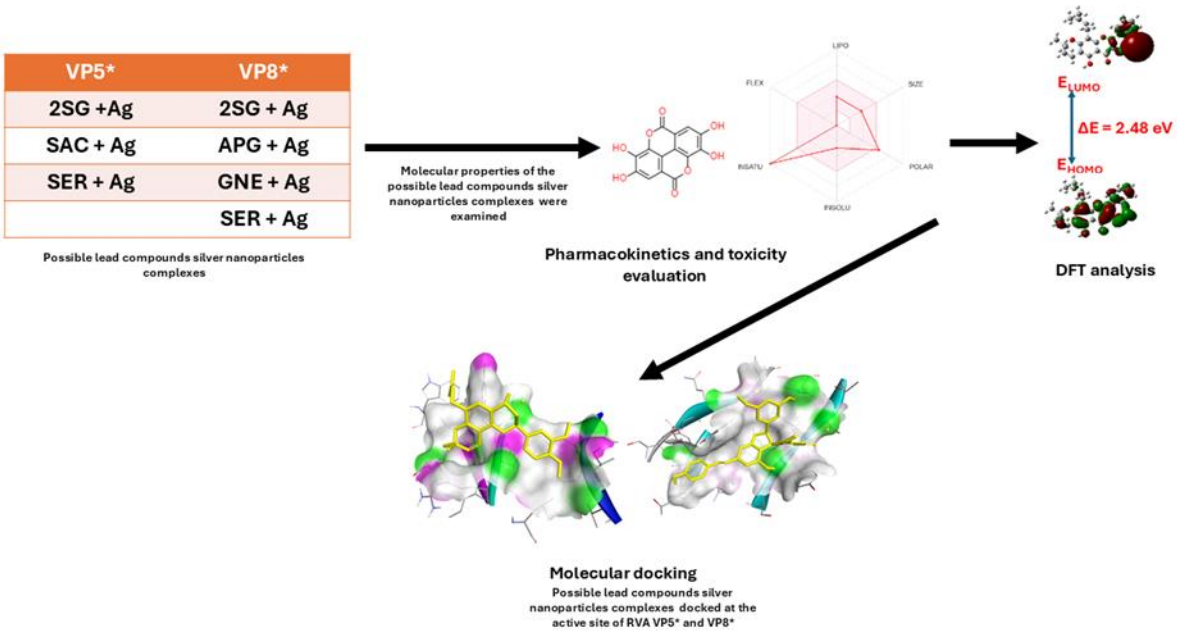


Figure 1: Workflow adopted in this study.

Silver-complexed leads

The 2D structure of the previously identified lead compounds [VP5*((2S)-6-(gamma,gamma-dimethylallyl)-3',4'-dimethoxy-6'',6''-dimethylpyran[2'',3'':7,8]flavanone (2SG), sericetin, sacranoside A) and VP8* (2SG, apigenin-4'-glucoside, gnetin L, sericetin)] were optimized by complexing with silver (Ag) (Figure 2-6) and converted into a 3D structure for further analysis using ChemDraw Professional 15.0 (PerkinElmer, Massachusetts, USA).

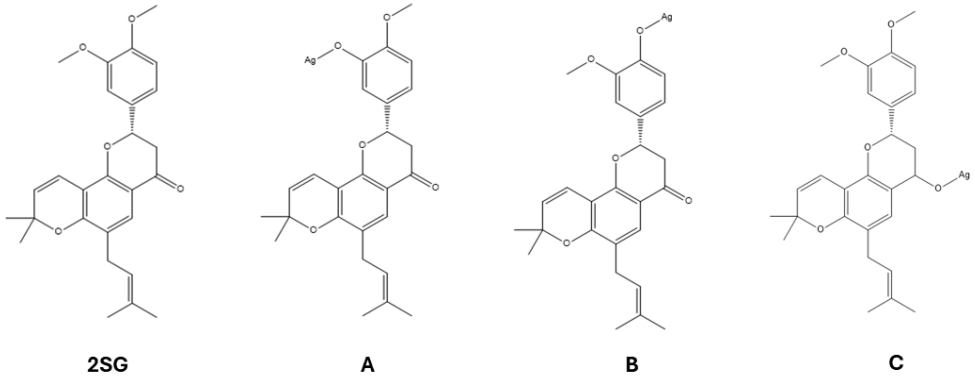


Figure 2: Structures of (2S)-6-(gamma,gamma-dimethylallyl)- 3',4'-dimethoxy-6'',6''-dimethylpyran[2'',3'':7,8]flavanone-Ag complexes.

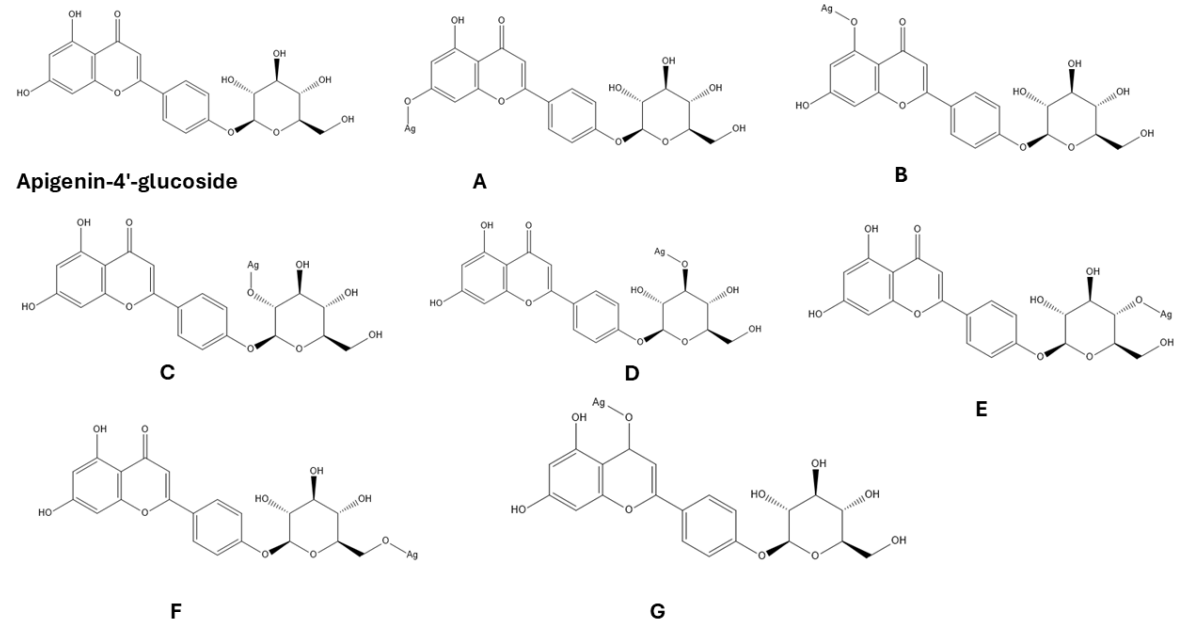


Figure 3: Structures of apigenin-4'-glucoside-Ag complexes.

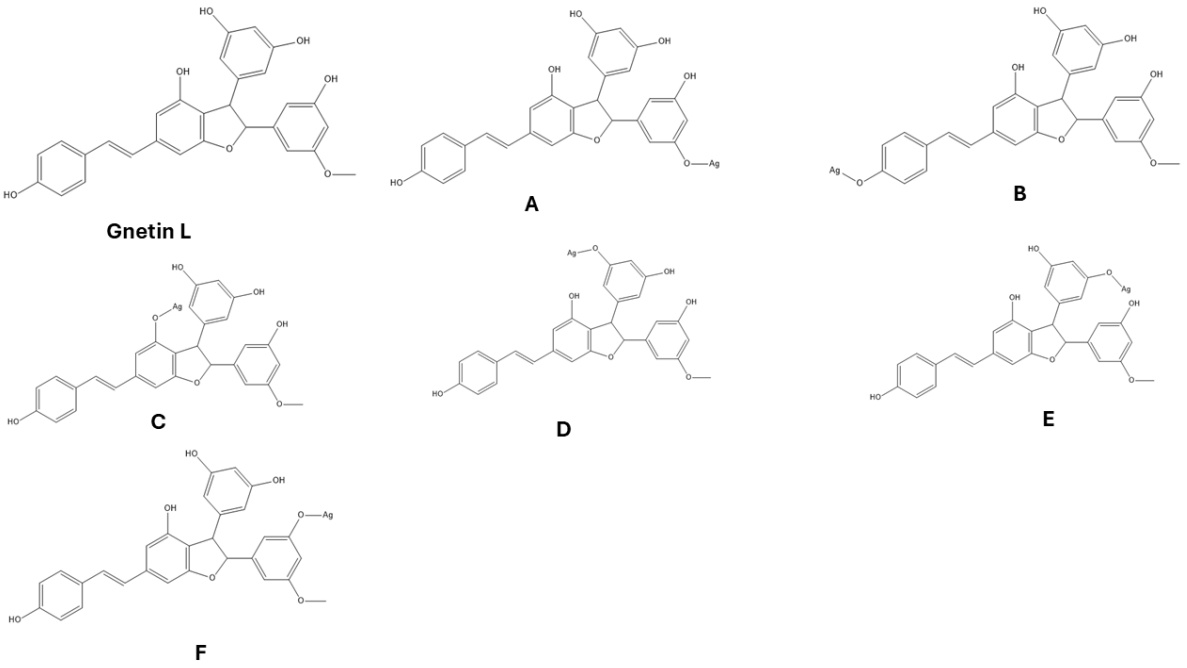


Figure 4: Structures of gnetin L-Ag complexes.

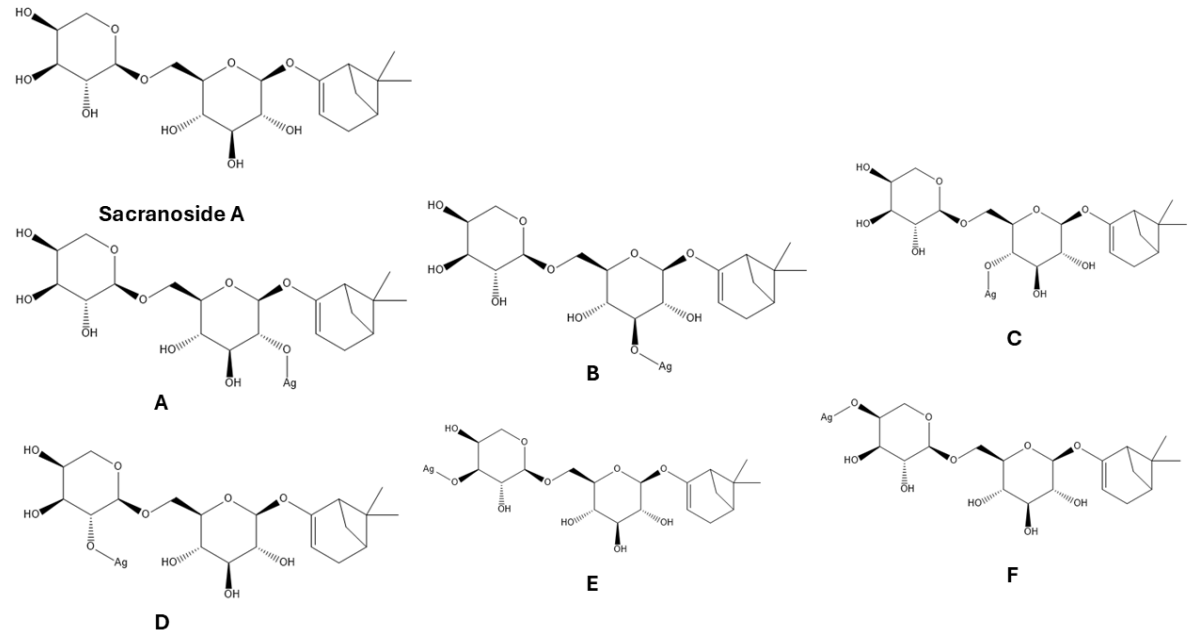


Figure 5: Structures of sacranoside A-Ag complexes.

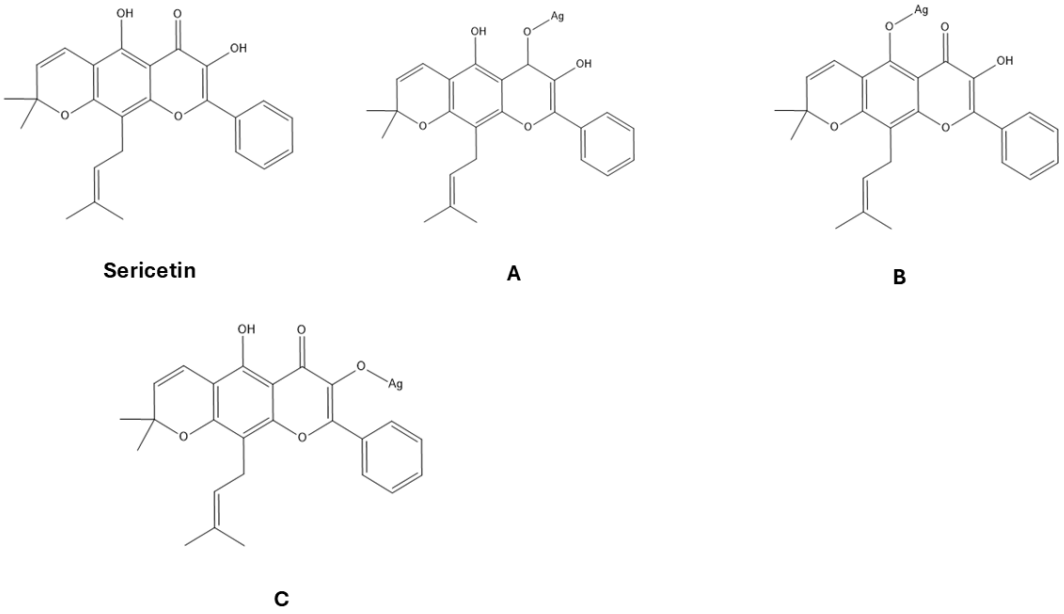


Figure 6: Structures of sericetin-Ag complexes.

Pharmacokinetic and physicochemical prediction

The physicochemical properties, pharmacokinetics and drug-likeness of the silver-complexed leads were predicted via the SwissADME website [https://swissadme.ch/index.php, (accessed on 27 November 2024)]. In addition, their toxicological features were predicted using the Protox II web server [https://tox-new.charite.de/protox_II/, (accessed on 27 November 2024)].

Quantum chemical calculations

Quantum chemical calculations were carried to predict therapeutically relevant molecular attributes of the silver-complexed leads using density functional theory (DFT) (Orio *et al.*, 2009). Their electronic properties were examined with the Gaussian 16 package on the Centre for High Performance Computing (CHPC), Cape Town, South Africa, employing the M06 functional (Zhao and Truhlar, 2008), combined with the def2-TZVP basis set (Alongamo *et al.*, 2019; Zhigulin *et al.*, 2019), while the optimized structures were visualized in GaussView 6

software V. 6.0.16. Frontier orbital analysis yielded highest occupied molecular orbital (HOMO) and lowest unoccupied molecular orbital (LUMO) (Calais, 1993), interpreted within the Parr and Pearson framework and Koopmans theorem (Luo *et al.*, 2006). Further molecular descriptors including energy gap (ΔE), ionization energy (I), electron affinity (A), chemical hardness (ŋ), softness (δ), electronegativity (χ), chemical potential (Cp), global electrophilicity (ω) were calculated as described previously (Lanrewaju *et al*., 2023).

Protein acquisition and preparation

X-ray crystal structure of VP5* (2B4I) and VP8* (2P3I) of RVA were retrieved from the Protein Data Bank [https://www.rcsb.orgs/ (accessed 16 January 2023)] and subsequently optimized using the PyMol software (DeLano, 2002).

Molecular docking and validation

Using AutoDock Tools, the optimized silver-complexed leads were docked into the active sites of the prepared targets as defined previously (Lanrewaju *et al.*, 2023; Kraschnefski *et al.*, 2009; Yoder and Dormitzer, 2006). The protein molecule (without associated water molecules) was loaded into AutoDock tools, where polar hydrogens and Gasteiger charges were added to show hydrogen-bond donors and acceptors and supply per-atom partial charges essential for accurate electrostatic scoring. A grid box with dimensions (Angstrom units), x = 62, y = 62, z = 56 and centre coordinates, x = 17.320, y = 15.092, z = 8.328 was set up for VP5* while x = 42, y = 48, z = 40 and centre coordinates, x = 36.906, y = 15.092, z = 8.328 was set up in the case of VP8*. The redocking approach was employed to validate the docking protocol by superimposing the top silver-complexed leads into the binding domain of the investigated

protein crystal structures (VP5* and VP8*) while the root mean square deviation (RMSD) between the docked and re-docked complexes (Figure 7-10) calculated were less than 2 (Katuwal *et al.*, 2023). Moreover, the silver-complexed leads interacted with key amino acid residues of the proteins, further validating the docking procedure.

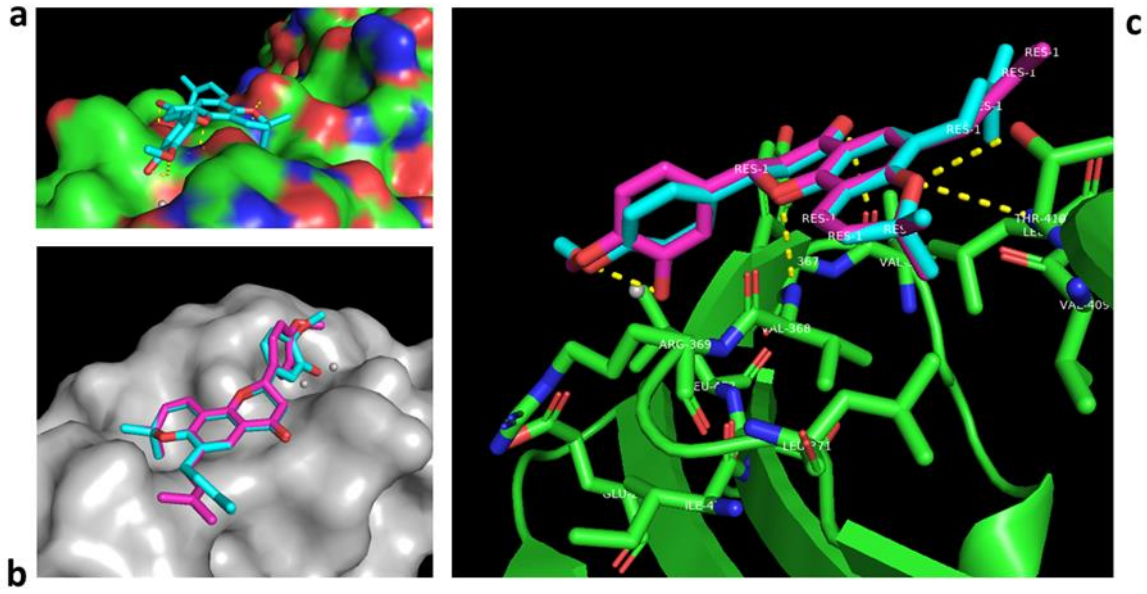


Figure 7: Docking technique validation conducted via the superimposition of the docked (2S)-6-(gamma,gamma-dimethylallyl)- 3',4'-dimethoxy-6'',6''-dimethylpyran[2'',3'':7,8]flavanone A on the VP5* protein docked complex (a) (2S)-6-(gamma,gamma-dimethylallyl)- 3',4'-dimethoxy-6'',6''-dimethylpyran[2'',3'':7,8]flavanone A docked to the VP5* surface (b) (2S)-6-(gamma,gamma-dimethylallyl)- 3',4'-dimethoxy-6'',6''-dimethylpyran[2'',3'':7,8]flavanoneA docked and re-docked to the VP5* surface (RMSD: 0.94) (c) the visualization of the (2S)-6-(gamma,gamma-dimethylallyl)- 3',4'-dimethoxy-6'',6''-dimethylpyran[2'',3'':7,8]flavanone A docked and re-docked at the binding pocket of VP5* while displaying the active site amino acids (Tyr367).

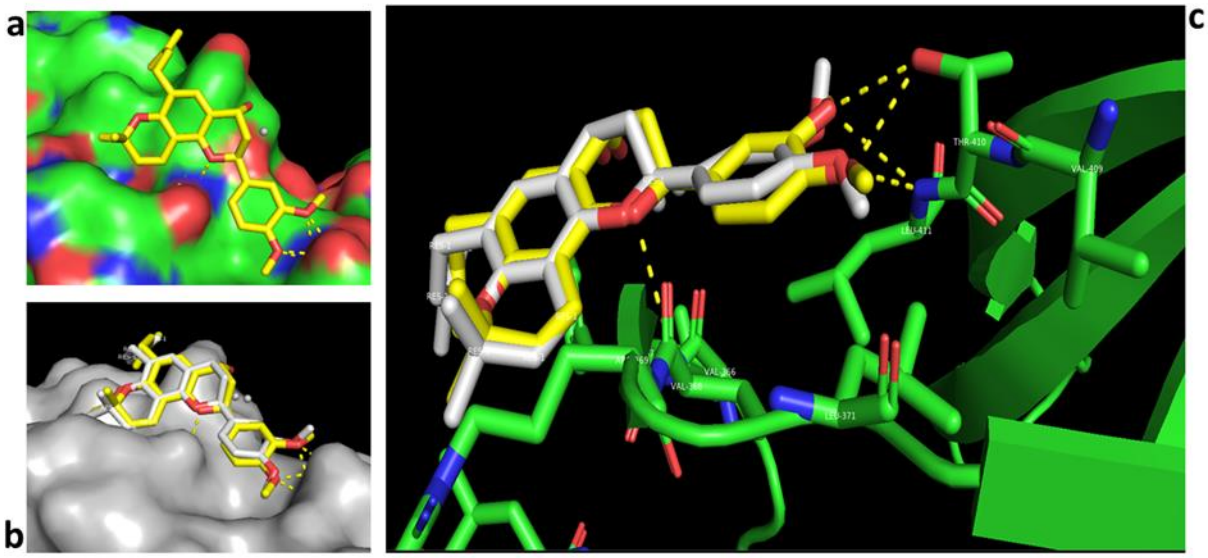


Figure 8: Docking technique validation conducted via the superimposition of the docked (2S)-6-(gamma,gamma-dimethylallyl)- 3',4'-dimethoxy-6'',6''-dimethylpyran[2'',3'':7,8]flavanone C on the VP5* protein docked complex (a) (2S)-6-(gamma,gamma-dimethylallyl)- 3',4'-dimethoxy-6'',6''-dimethylpyran[2'',3'':7,8]flavanone C docked to the VP5* surface (b) (2S)-6-(gamma,gamma-dimethylallyl)- 3',4'-dimethoxy-6'',6''-dimethylpyran[2'',3'':7,8]flavanone C docked and re-docked to the VP5* surface (RMSD: 0.66) (c) the visualization of the (2S)-6-(gamma,gamma-dimethylallyl)- 3',4'-dimethoxy-6'',6''-dimethylpyran[2'',3'':7,8]flavanone C docked and re-docked at the binding pocket of VP5* while displaying the active site amino acids (Val366, Tyr367).

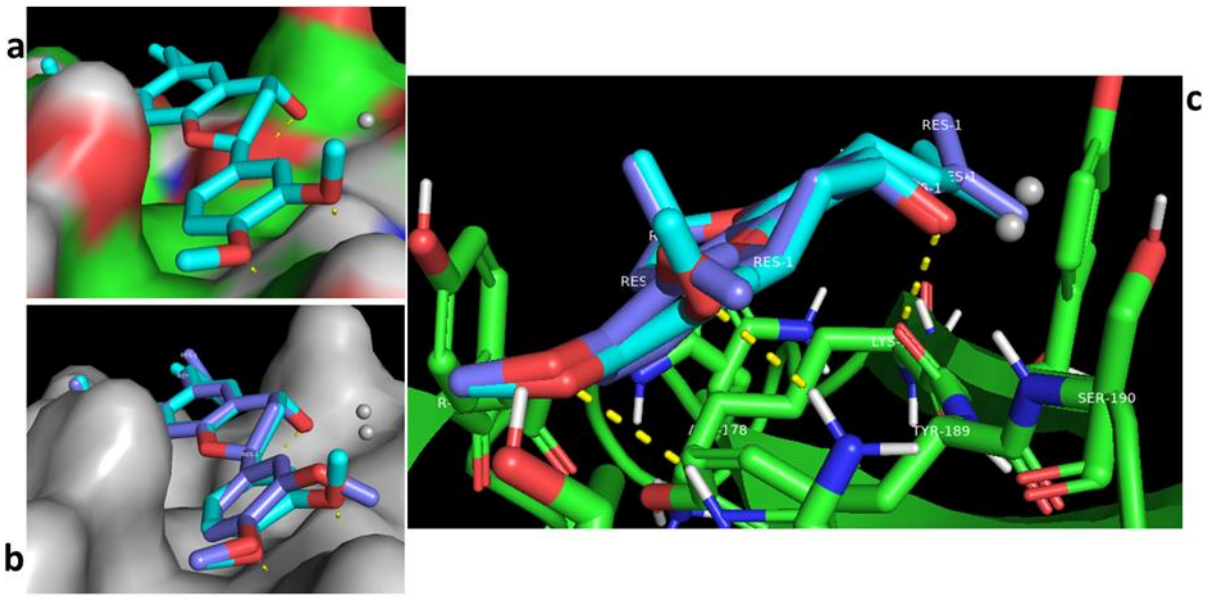


Figure 9: Docking technique validation conducted via the superimposition of the docked (2S)-6-(gamma,gamma-dimethylallyl)- 3',4'-dimethoxy-6'',6''-

dimethylpyran[2'',3'':7,8]flavanone C on the VP8* protein docked complex (a) (2S)-6-(gamma,gamma-dimethylallyl)- 3',4'-dimethoxy-6'',6''-dimethylpyran[2'',3'':7,8]flavanone C docked to the VP8* surface (b) (2S)-6-(gamma,gamma-dimethylallyl)- 3',4'-dimethoxy-6'',6''-dimethylpyran[2'',3'':7,8]flavanone C docked and re-docked to the VP8* surface (RMSD: 0.41) (c) the visualization of the (2S)-6-(gamma,gamma-dimethylallyl)- 3',4'-dimethoxy-6'',6''-dimethylpyran[2'',3'':7,8]flavanone C docked and re-docked at the binding pocket of VP8* while displaying the active site amino acids (Asn178, Ser190).

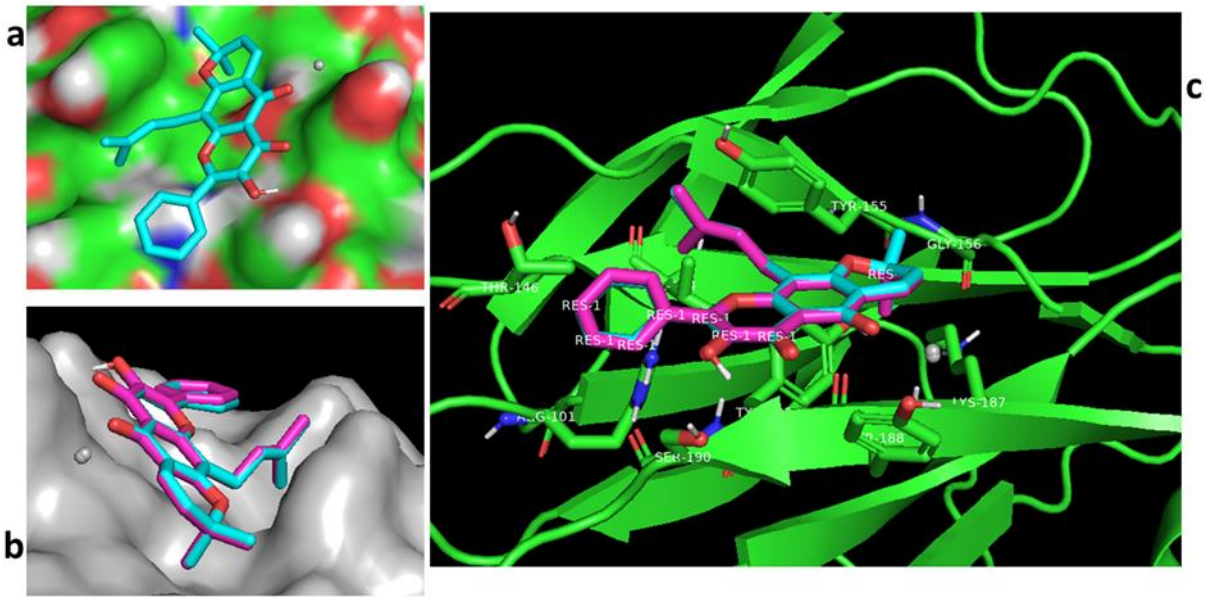


Figure 10: Docking technique validation conducted via the superimposition of the docked sericetin A on the VP8* protein docked complex (a) sericetin A docked to the VP8* surface (b) sericetin A docked and re-docked to the VP8* surface (RMSD: 0.12) (c) the visualization of the sericetin A docked and re-docked at the binding pocket of VP8* while displaying the active site amino acids (Arg101, Tyr155, Lys187, Tyr188, Ser190).

3.0 Results and discussion

Pharmacokinetics and toxicity properties of the silver-complexed leads

In drug discovery, the effective biological activity of the compounds under study is a critical criterion; however, it is insufficient to validate these compounds as drug candidates because numerous compounds with potential biological activity cannot progress to clinical trials owing to their poor pharmacokinetic profile. Consequently, evaluating the pharmacokinetic profiles

of the investigated molecules is essential to identify those with favorable features for potential therapeutic use before further analysis to save cost and time (Haloui *et al.*, 2024).

As per the Lipinski's rule of 5 (Ro5) (Lipinski *et al.*, 2012), while all the 2SG, gnetin L and sericetin derivatives satisfied the guideline except for a single parameter breach, this deviated from the 0 violation observed in their respective parent structures (2SG, gnetin L and sericetin) (Lanrewaju *et al.*, 2023). This observation might be attributed to Ag conjugation resulting in increased molecular weight beyond the 500 Da boundary, according to Ro5 (Table 1). All the predicted silver-complexed leads passed the rule as expected, similar to the parent compound. However, APGG breached the guideline with 2 violations owing to the increased number of hydrogen bond donors from 5 to 6. This violation suggests that it would be less orally bioavailable relative to other predicted complexes. Expectedly, the bioavailability score of this complex reduced from 0.55 to 0.17 compared to other predicted silver-APG complexes. The bioavailability score which is essential in pharmacological dosage calculations, quantifies the proportion of an administered therapeutic dose that remains unchanged and reaches systemic circulation. A high bioavailability score implies that therapeutically relevant concentrations can be reached orally, while a low bioavailability score is connected to their reduced oral bioavailability. Nonetheless, they can be administered via non-oral routes (Heaney, 2001). This observed deviation in APGG relative to other derivatives might be due to the conversion of a double bond to a single bond through the attachment of silver metal and can be described as a coordination interaction or complexation reaction involving the oxygen and silver metal (Van Santen *et al.*, 2015). This phenomenon arises from the electrophilic nature of silver and the nucleophilic lone pairs on oxygen (Kaichev *et al.*, 2003).

Cytochrome P450s enzymes (CYPs) represent a haem-containing superfamily predominantly synthesized in the liver, pivotal to the metabolism of various exogenous and endogenous chemicals (Hill and Young, 2010). The characteristics associated with isoenzymes include metabolic clearance, drug-drug interactions (DDI), and interpatient variability in pharmacokinetics (Moussaoui *et al.*, 2023). Possible inhibition of these CYP isoforms indicates significant concerns regarding simultaneous administration with other drugs. Of all the derivatives, minor differences were exhibited concerning the CYP isoforms inhibited by the silver complexes relative to the lead compounds except in SACA, where the conjugation of Ag does not inhibit the CYPs isoenzymes like the lead compound. Specifically, there was a reduction in the numbers of isoforms inhibited by the 2SG-silver complexes relative to 2SG, while the reverse was observed in the APG series where the silver complexes inhibited CYP3A4 as opposed to the lead compound in which none of the CYP isoforms was inhibited. Moreover, a partly similar trend was observed in the SER series, where there is a reduction in the number of isoforms inhibited relative to the lead compound, suggesting that Ag conjugation resulted in reduced toxicity except in SERA with an equal number of inhibitions as in the parent structure. There is not much difference between GNE and the GNE-silver complexes, as just one of the CYP isoenzymes was inhibited across board (Table 2). Remarkably, none of the isoenzymes in the SAC series were inhibited in the lead compound and the silver complexes, suggesting that Ag conjugation will not lead to DDI.

Considering their toxicological profile, in the 2SG series, only 2SGC has a lower lethal dose (500 mg/kg) relative to other silver complexes and the lead compound (Table 1). Nevertheless, it falls within toxicity class 4, which is suitable for drug development. In the APG series, the silver complexes retain toxicity class 5 with a lethal dose of 5000 mg/kg, just as in the lead compound; however, Ag conjugation in APGG led to a change in toxicity class 5 to 6 and a

Table 1. Physicochemical, pharmacokinetics and toxicity profile of all the silver-complexed leads

Ligands	MoW < 500 (g/mol)	HBA ≤ 10	HBD ≤ 5	LogP o/ w ≤ 5	WS	GI Abs	BBBP	Pgp	CYP1A2	CYP2C19	CYP2C9	CYP2D6	CYP3A4	LV (N)	BS	H	C	IM	M	CY	LD50 (mg/kg)	TC
2SGA	542.39	5	0	4.18	PS	Hh	Ye	Ye	No	No	No	No	Ye	1	0.55	Ia	Ia	At	Ia	Ia	2000	4
2SGB	527.36	5	0	3.87	PS	Hh	Ye	Ye	No	No	No	No	Ye	1	0.55	Ia	Ia	At	Ia	Ia	2000	4
2SGC	543.40	5	0	4.03	PS	Hh	Ye	Ye	No	No	No	Ye	Ye	1	0.55	Ia	Ia	At	Ia	Ia	500	4
APGA	539.24	10	5	-0.10	S	Lo	No	No	No	No	No	No	Ye	1	0.55	Ia	Ia	At	At	Ia	5000	5
APGB	539.24	10	5	-0.21	S	Lo	No	No	No	No	No	No	Ye	1	0.55	Ia	Ia	At	At	Ia	5000	5
APGC	539.24	10	5	0.02	S	Lo	No	Ye	No	No	No	No	Ye	1	0.55	Ia	Ia	At	At	Ia	5000	5
APGD	539.24	10	5	0.02	S	Lo	No	Ye	No	No	No	No	Ye	1	0.55	Ia	Ia	Ia	At	Ia	5000	5
APGE	539.24	10	5	-0.09	S	Lo	No	No	No	No	No	No	Ye	1	0.55	Ia	Ia	At	At	Ia	5000	5
APGF	539.24	10	5	-0.09	S	Lo	No	No	No	No	No	No	Ye	1	0.55	Ia	Ia	Ia	Ia	Ia	5000	5
APGG	541.25	10	6	-0.46	S	Lo	No	Ye	No	No	No	No	No	2	0.17	Ia	Ia	At	Ia	Ia	12000	6
GNEA	577.33	7	5	3.21	PS	Lo	No	No	No	No	No	No	Ye	1	0.55	Ia	Ia	At	Ia	Ia	3000	5
GNEB	591.36	7	4	3.48	PS	Hh	No	No	No	No	No	No	Ye	1	0.55	Ia	Ia	At	Ia	Ia	3000	5
GNEC	591.36	7	4	3.48	PS	Hh	No	No	No	No	No	No	Ye	1	0.55	Ia	Ia	At	Ia	Ia	3000	5
GNED	606.39	7	4	3.78	PS	Lo	No	Ye	No	No	No	No	Ye	1	0.55	Ia	Ia	At	Ia	Ia	500	4
GNEE	591.36	7	4	3.48	PS	Hh	No	No	No	No	No	No	Ye	1	0.55	Ia	Ia	At	Ia	Ia	3000	5
GNEF	591.36	7	4	3.48	PS	Hh	No	No	No	No	No	No	Ye	1	0.55	Ia	Ia	At	Ia	Ia	3000	5
SACA	539.32	10	5	-1.34	S	Lo	No	Ye	No	No	No	No	No	1	0.55	Ia	Ia	At	Ia	Ia	2000	4
SACB	539.32	10	5	-1.34	S	Lo	No	Ye	No	No	No	No	No	1	0.55	Ia	Ia	At	Ia	Ia	2000	4
SACC	539.32	10	5	-1.34	S	Lo	No	Ye	No	No	No	No	No	1	0.55	Ia	Ia	At	Ia	Ia	2000	4
SACD	539.32	10	5	-1.34	S	Lo	No	Ye	No	No	No	No	No	1	0.55	Ia	Ia	At	Ia	Ia	2000	4
SACE	539.32	10	5	-1.34	S	Lo	No	Ye	No	No	No	No	No	1	0.55	Ia	Ia	At	Ia	Ia	2000	4
SACF	539.32	10	5	-1.34	S	Lo	No	Ye	No	No	No	No	No	1	0.55	Ia	Ia	At	Ia	Ia	2000	4
SERA	513.33	5	2	3.45	PS	Hh	No	Ye	Ye	No	No	No	Ye	1	0.55	Ia	Ia	At	Ia	Ia	2500	5
SERB	511.32	5	1	3.83	PS	Hh	No	Ye	No	Ye	No	No	No	1	0.55	Ia	Ia	At	Ia	Ia	2500	5
SERC	511.32	5	1	3.94	PS	Hh	No	Ye	No	Ye	No	No	No	1	0.55	Ia	Ia	At	Ia	Ia	2500	5

Keys: MoW: Molecular weight; BBB permeant: Blood-brain barrier permeation; HBD: Hydrogen bond donor; LogP o/w: Partition coefficient; HBA: Hydrogen bond acceptor; CY: Cytotoxicity; Pgp: Permeability glycoprotein substrate; WS: Water solubility; CYP: Cytochrome; LV: Lipinski violation; BS: Bioavailability score; H: Hepatotoxicity; C: Carcinogenicity; IM: Immunotoxicity; GI abs: Gastrointestinal absorption; M: Mutagenicity; LD: Lethal dose; TC: Toxicity class; S: Soluble; PS: Poorly soluble; Hh: High; Lo: Low; At: Active; Ia: Inactive; Ye: Yes; N: Number of violations; 2SG: (2S)-6-(gamma,gamma-dimethylallyl)-3',4'-dimethoxy-6",6"-dimethylpyran[2",3":7,8]flavanone; APG: Apigenin-4'-glucoside; GNE: Gnetin L; SAC: Sacranoside A; SER: Sericetin

lethal dose of 12000 mg/kg. Of all the GNE series, only GNED retained toxicity class 4 and a lethal dose of 500 mg/kg, just like the lead compound, while other silver-complexed leads changed to toxicity class 5 and an increased lethal dose of 3000 mg/kg owing to their Ag conjugation.

On the contrary, Ag conjugation led to a reduction in the lethal dose from 4000 to 2000 mg/kg and toxicity class 5 to 4 which is still suitable for drug development. Interestingly, Ag conjugation does not affect the lethal dose and toxicity class in the SER series. Generally, the Ag conjugation onto the lead compounds did not significantly affect their pharmacokinetics and toxicity profiles except in a few cases, as highlighted earlier; thus, they are suitable for drug development. Recent developments in drug discovery have revealed that combining ADMET predictions with quantum chemistry calculations via DFT may provide further insight into a drug molecule as DFT offers information into the molecule's reactivity and stability.

Molecular orbital properties of the silver-complexed leads

Understanding the electronic properties of a complex system necessitates evaluating the frontier molecular orbital (FMO), which can yield essential chemical insights that could suggest medicinal properties of the molecules (Ayers *et al.*, 2006; Pearson, 1986). The HOMO pertains to a compound’s propensity to donate or release electrons, whereas the LUMO is linked to a compound’s capacity to accept electrons. Consequently, evaluating the HOMO and LUMO of leads may yield significant insights into the mechanisms of actions and facilitate the identification of their active sites (Ayers *et al.*, 2006). Additionally, the energy gap (LUMO-HOMO) of a compound provides valuable insight into its stability, with a larger energy gap

indicating higher stability, potentially hindering ligand binding to a protein, whereas a smaller energy gap suggests compound reactivity (Aihara, 1999).

In this study, the smallest energy gap within each series were measured in 2SGB (1.98 eV), APGA (2.30 eV), GNEB (1.59 eV), SACC (3.34 eV) and SERB (2.47 eV) (Table 2, Figure 11-15). Conversely, all the parent compounds exhibited higher energy gaps relative to their respective series, as previously reported (Lanrewaju *et al.*, 2023), suggesting a higher reactivity status of the silver-complexed leads relative to their corresponding lead compound. This observation agrees with Kucuk (2023), in which the compound exhibited a higher energy gap than the silver-compound complex. The reduced energy gap in the silver-complexed leads might be attributed to the orbital hybridization during complexation, resulting in the alterations of both occupied and virtual orbitals (Jadoon *et al.*, 2021). However, a different trend was observed in APGD with a higher energy gap value than the lead compound, possibly due to possible orbital overlap between the metal and the compound (Tosato *et al.*, 2020). Therefore, across all the series and their corresponding lead compounds, a similar trend was observed in the investigated parameters because the parameters are dependent on the energy gaps. Overall, the lowest energy gap was observed in GNEB (1.59 eV), suggesting its higher reactivity than other silver-complexed leads (Table 2, Figure 13).

The chemical hardness of a molecule which is inversely correlated with softness is significant in assessing chemical stability and signifies a molecule's resilience to alterations in electron configuration, which ultimately indicates a reduction in reactivity (Kumar *et al.*, 2023), resulting from increased energy gap. As Pearson (1986) noted, reduced chemical hardness and increased chemical softness indicate increased compound reactivity owing to a smaller energy

gap. Interestingly, lower chemical hardness was observed in 2SGB (0.99 eV), APGA (1.15 eV), GNEB (0.79 eV), SACC (1.67 eV), SERB (1.23 eV) in their respective series (Table 1). Expectedly, 2SGB (1.01 eV), APGA (0.87 eV), GNEB (1.26 eV) exhibited the highest chemical softness in their respective series. Contrarily, an opposite trend was observed in the SAC and SER series with similar chemical softness values observed in SACA (0.60 eV), SACC (0.59 eV) and SERB (0.81 eV), SERC (0.81 eV) which might be attributed to a similar spatial position of the Ag atom in their respective structures and consequently influence uniform electron distribution. Overall, GNEB exhibited the lowest chemical hardness (0.79 eV) and the highest chemical softness (1.26 eV) (Table 2).

In addition, the capacity of an atom or a functional group within a compound to attract electrons can be evaluated by assessing the electronegativity and chemical potential. Specifically, a negative chemical potential enhances molecular stability by preventing spontaneous degradation (Mountessou *et al.*, 2023). Moreover, the degree of dissociation of compounds into their elemental components decreases as the magnitude of its negative chemical potential increases (Kumar *et al.*, 2023). Higher electronegativity and higher negative chemical potential values were observed in 2SGB (4.43 eV, -4.43 eV), APGC (4.80 eV, -4.80 eV), GNED and GNEE (4.52 eV, -4.52 eV), SACC (4.99 eV, -4.99 eV) and SERB (4.10 eV, -4.10 eV) (Table 2). This suggests an enhanced capacity of the atoms and functional groups to attract electrons at the binding domain of the target proteins and might result in a higher affinity than other compounds with lower electronegativity and lower negative chemical potential values (Aribisala *et al.*, 2024).

Table 2: The cDFT parameters of the silver-complexed leads

Ligands	cDFT parameters (eV)									
	LUMO	HOMO	Energy gap	Ionization energy	Electron affinity	Hardness	Softness	Electronegativity	Chemical potential	Global electrophilicity
2SGA	-3.40	-5.41	2.01	3.40	5.41	1.01	0.99	4.41	-4.41	9.63
2SGB	-3.43	-5.42	1.98	3.43	5.42	0.99	1.01	4.43	-4.43	9.87
2SGC	-2.95	-5.63	2.69	2.95	5.63	1.34	0.74	4.29	-4.29	6.85
APGA	-3.52	-5.82	2.30	3.52	5.82	1.15	0.87	4.67	-4.67	9.45
APGB	-2.42	-5.53	3.11	2.42	5.53	1.56	0.64	3.98	-3.98	5.08
APGC	-3.16	-6.43	3.28	3.16	6.43	1.64	0.61	4.80	-4.80	7.02
APGD	-2.59	-6.77	4.18	2.59	6.77	2.09	0.48	4.68	-4.68	5.24
APDE	-2.81	-6.41	3.59	2.81	6.41	1.80	0.56	4.61	-4.61	5.91
APGF	-2.53	-5.99	3.45	2.53	5.99	1.73	0.58	4.26	-4.26	5.25
APGG	-2.87	-5.98	3.11	2.87	5.98	1.56	0.64	4.43	-4.43	6.30
GNEA	-3.37	-5.43	2.07	3.37	5.43	1.03	0.97	4.40	-4.40	9.37
GNEB	-3.42	-5.01	1.59	3.42	5.01	0.79	1.26	4.22	-4.22	11.19
GNEC	-3.35	-5.38	2.03	3.35	5.38	1.01	0.99	4.37	-4.37	9.39
GNED	-3.59	-5.45	1.86	3.59	5.45	0.93	1.08	4.52	-4.52	10.99
GNEE	-3.60	-5.45	1.85	3.60	5.45	0.92	1.08	4.52	-4.52	11.07
GNEF	-2.16	-5.28	3.12	2.16	5.28	1.56	0.64	3.72	-3.72	4.43
SACA	-3.11	-6.62	3.51	3.11	6.62	1.76	0.60	4.86	-4.86	6.74
SACB	-2.79	-6.58	3.79	2.79	6.58	1.89	0.53	4.68	-4.68	5.79
SACC	-3.32	-6.66	3.34	3.32	6.66	1.67	0.59	4.99	-4.99	7.46
SACD	-1.19	-6.06	4.87	1.19	6.06	2.43	0.41	3.63	-3.63	2.70
SACE	-2.80	-6.56	3.76	2.80	6.56	1.88	0.53	4.68	-4.68	5.82
SACF	-2.60	-6.23	3.63	2.60	6.23	1.81	0.55	4.41	-4.41	5.37
SERA	-2.70	-5.22	2.52	2.70	5.22	1.26	0.79	3.96	-3.96	6.23
SERB	-2.87	-5.33	2.47	2.87	5.33	1.23	0.81	4.10	-4.10	6.81
SERC	-2.80	-5.27	2.48	2.80	5.27	1.24	0.81	4.03	-4.03	6.57

LUMO: Lowest unoccupied molecular orbital; HOMO: Highest occupied molecular orbital; 2SG: (2S)-6-(gamma,gamma-dimethylallyl)-3',4'-dimethoxy-6",6"-dimethylpyran[2",3":7,8]flavanone; APG: Apigenin-4'-glucoside; GNE: Gnetin L; SAC: Sacranoside A; SER: Sericetin

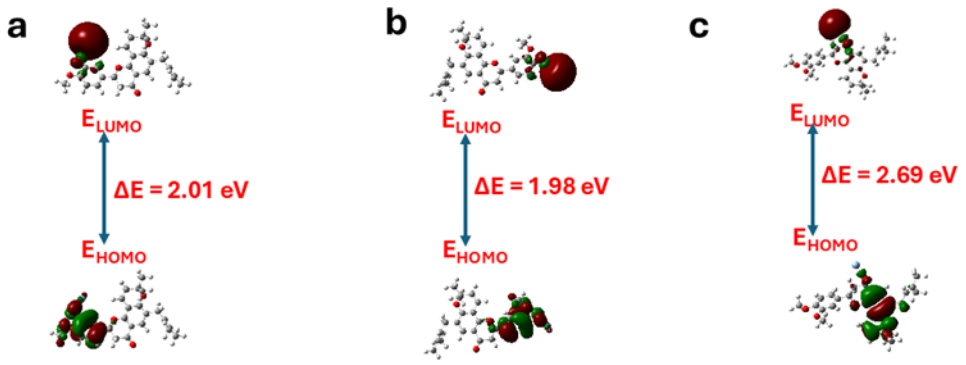


Figure 11: Frontier molecular orbitals of (2S)-6-(gamma,gamma-dimethylallyl)- 3',4'-dimethoxy-6'',6''-dimethylpyran[2'',3'':7,8]flavanone-Ag complexes (a) (2S)-6-(gamma,gamma-dimethylallyl)- 3',4'-dimethoxy-6'',6''-dimethylpyran[2'',3'':7,8]flavanone A (b) (2S)-6-(gamma,gamma-dimethylallyl)- 3',4'-dimethoxy-6'',6''-dimethylpyran[2'',3'':7,8]flavanone B (c) (2S)-6-(gamma,gamma-dimethylallyl)- 3',4'-dimethoxy-6'',6''-dimethylpyran[2'',3'':7,8]flavanone C.

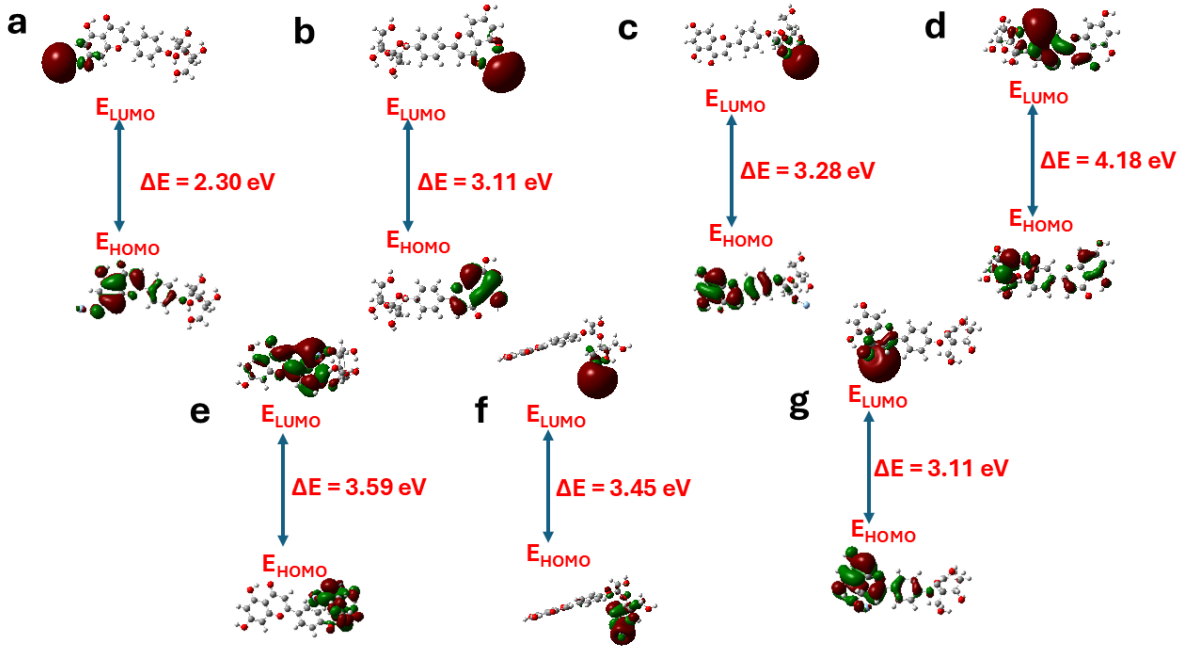


Figure 12: Frontier molecular orbitals of apigenin-4'-glucoside-Ag complexes (a) apigenin-4'-glucoside A (b) apigenin-4'-glucoside B (c) apigenin-4'-glucoside C (d) apigenin-4'-glucoside D (e) apigenin-4'-glucoside E (f) apigenin-4'-glucoside F (g) apigenin-4'-glucoside G.

Furthermore, the electrophilicity index delineates the capacity of an electrophile to gain a specific quantity of electron density and the extent to which a molecule resists the transfer of electron density. Values below 0.8 eV denote low electrophiles, 0.8 – 1.5 eV indicate moderate strength and anything above 1.5 eV defines a heavy electrophile (Lakhera *et al.*, 2022). The heaviest electrophiles across the different series include 2SGB (9.87 eV), APGA (9.45 eV), GNEB (11.19 eV), SACC (7.46 eV), SERB (6.81 eV) which is in tandem with other cDFT descriptors (Table 2). Notably, all the silver-complexed leads qualify as heavy electrophiles, indicating a significant abundance of electrophiles and might enhance their binding potential at the binding domain of the receptor. In essence, silver complexation resulted into reduced energy gaps, boosting softness while enhancing their heavy electrophiles position suggesting their ability to exchange electrons unhindered translating to stronger affinity for the target.

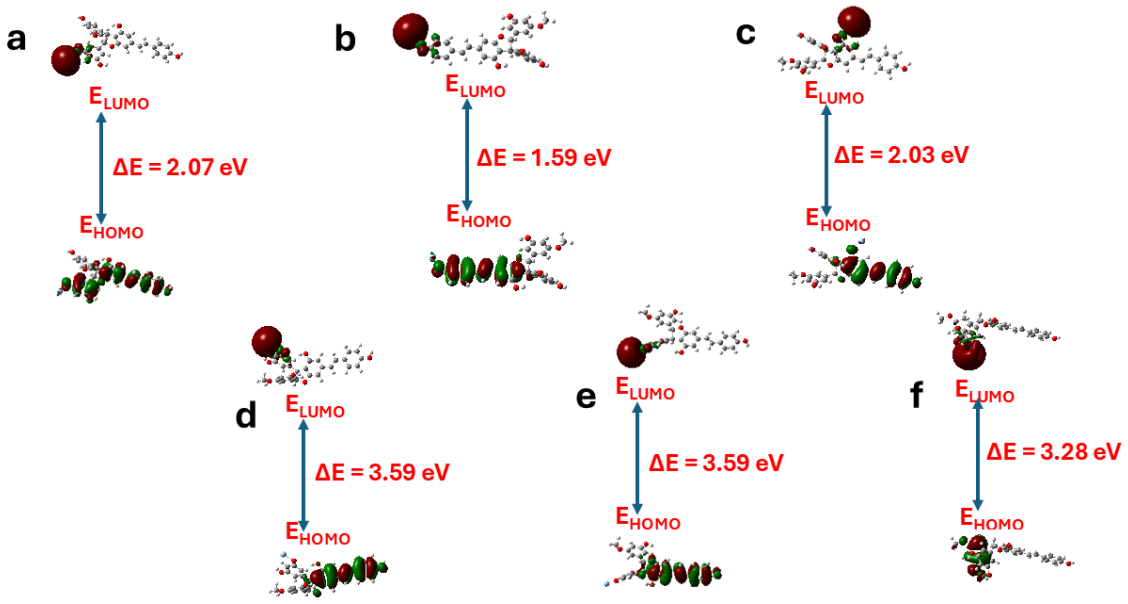


Figure 13: Frontier molecular orbitals of gnetin L-Ag complexes (a) gnetin L A (b) gnetin L B (c) gnetin L C (d) gnetin L D (e) gnetin L E (f) gnetin L F.

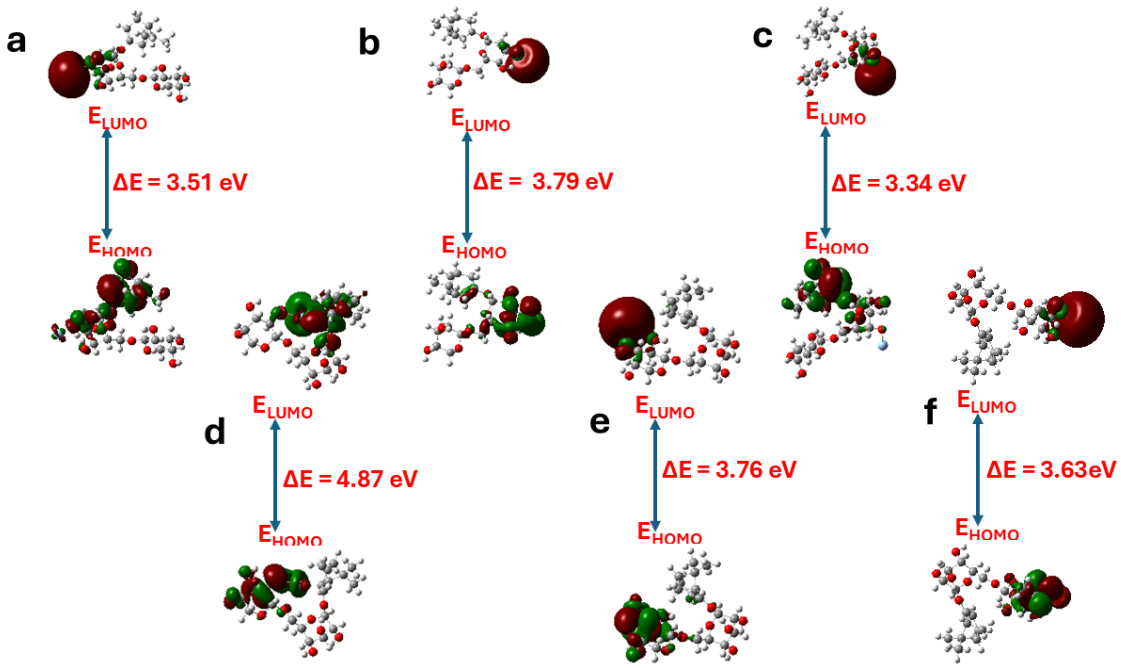


Figure 14: Frontier molecular orbitals of sacranoside A-Ag complexes (a) sacranoside A A (b) sacranoside A B (c) sacranoside A C (d) sacranoside A D (e) sacranoside A E (f) sacranoside A F.

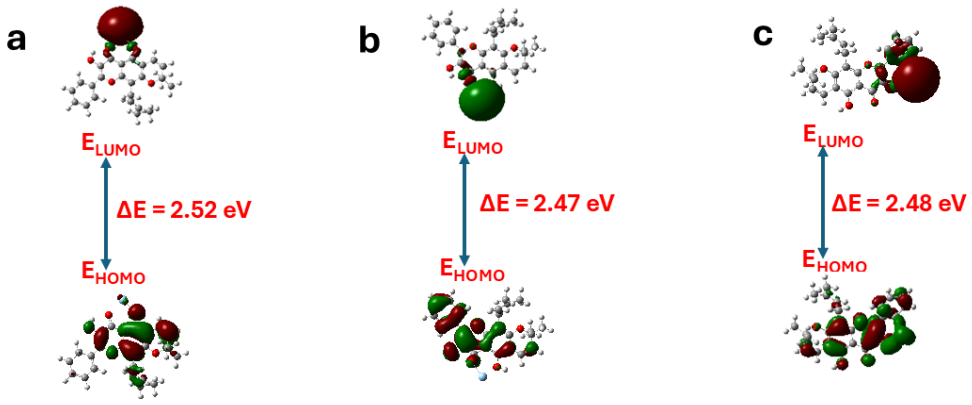


Figure 15: Frontier molecular orbitals of sericetin-Ag complexes (a) sericetin A (b) sericetin B (c) sericetin C.

Molecular docking

Molecular docking is a common method for examining the interactions between ligands and their targets. It positions a small molecule at the predefined binding domain of a target protein to enable the formation of a stable complex. Generally, the docking algorithm ascertains the most favourable binding pose of a small molecule to a target protein via negative binding scores. The degree to which a ligand fits within the binding domain of the receptor and its interactions is expressed in the docking score (Adedirin *et al.*, 2025; Akoonjee *et al.*, 2023). In this work, the docking scores of the possible silver-complexed leads ranged from -6.95 to -4.23 kcal/mol and -8.21 to -5.85 kcal/mol against VP5* and VP8*, respectively (Table 3 and 4). Previously, we have reported the docking scores of the lead compounds ranging from -5.70 to -5.90 kcal/mol and -6.90 to -7.40 kcal/mol against VP5* and VP8* respectively (Lanrewaju *et al.*, 2023). Notably, 2SGA (-6.77 kcal/mol), 2SGB (-6.95 kcal/mol), 2SGC (-6.59 kcal/mol) SERA (-6.25 kcal/mol), SERB (-6.41 kcal/mol) and SERC (-6.22 kcal/mol) exhibited higher negative docking scores against VP5* relative to their corresponding parent compounds [2SG (-5.90 kcal/mol) and SER (-5.90 kcal/mol)]. Similarly, against VP8*, 2SGA (-8.16 kcal/mol), 2SGB (-8.21 kcal/mol), 2SGC (-8.06 kcal/mol), GNEF (-7.61 kcal/mol), SERA (-7.26 kcal/mol), SERC (-7.47 kcal/mol) outperformed their respective lead compounds [2SG (-7.1 kcal/mol), GNE (-7.4 kcal/mol) and SER (-7.0 kcal/mol)]. This observation suggests that silver complexation resulted in a more negative docking score than the lead compound and is consistent with that of Hkiri *et al.* (2022), where silver complexation leads to a lower docking score than the compound. The improved binding affinity might be attributed to enhanced molecular rigidity and stability of the silver complex, decreasing its flexibility and leading to a better fit at the binding domain of the receptor due to silver complexation.

However, SACA (-4.43 kcal/mol), SACB (-5.17 kcal/mol), SACC (-4.23 kcal/mol), SACD (-5.14 kcal/mol), SACE (-4.99 kcal/mol) and SACF (-4.80 kcal/mol) had lower negative docking scores against VP5* compared to the lead compound [SAC (-5.7 kcal/mol)]. Also, APGA (-5.85 kcal/mol), APGB (-6.45 kcal/mol), APGC (-6.42 kcal/mol), APGD (-6.28 kcal/mol), APGE (-6.08 kcal/mol), APGF (-4.93 kcal/mol), APGG (-6.75 kcal/mol), GNEA (-6.65 kcal/mol), GNEB (-6.63 kcal/mol), GNED (-7.21 kcal/mol), GNEE (-6.81 kcal/mol) had higher docking score against VP8* relative to lead compound [APG (-6.90 kcal/mol) and GNE (-7.40 kcal/mol)]. This finding agrees with the report of Siqueira *et al.,* (2021), where sulfamethoxazole-silver complex (SMTZ)Ag (-8.18 kcal/mol) had a lower negative docking score compared to SMTZ (-8.70 kcal/mol) against *Pseudomonas aeruginosa* PqsR. The observed reduced binding affinity might be linked to spatial constraints due to silver coordination interfering with docking compared to the compound void of silver. Unfortunately, a positive score observed in gnetin L C (GNEC) against VP8* may be due to the inability of the silver-lead compound complex to bind at the binding domain of the receptor effectively and hence excluded from further analysis (Table 4).

A correlation analysis between the docking scores and the orbital descriptors of the silver-complexed leads showed a strong correlation between electron affinity (0.907) and the obtained docking scores against VP5* (Supplementary Table S1). The strongest positive correlation was demonstrated in the electron affinity, which showed its critical role in predicting changes to the docking score. This indicates that increasing the electron affinity of the molecule may result in higher negative docking scores (Wheeler and Bloom, 2014; Hunter and Sanders, 1990). Furthermore, the strong negative correlation (-0.907) of the HOMO suggests that higher negative docking scores might be associated with a corresponding higher HOMO energy value. Conversely, against VP8*, a strong negative correlation between the docking scores of the

silver-complexed leads and LUMO (-0,256) was demonstrated (Supplementary Table S2). Specifically, a higher LUMO energy value resulted in higher negative docking scores of the investigated complexes.

Further examination of binding affinities and interactions observed in the docking study is essential to the drug discovery process. Therefore, the pose ranking is conducted to identify the ligand orientation that demonstrates the highest affinity (lowest binding free energy) to the receptor, while accounting for the physical forces mediating the ligand-receptor contacts (Kitchen *et al.*, 2004).

Table 3: Molecular docking results of the silver-complexed leads at the active site of VP5*

Silver-lead compound complex	Docking score (kcal/mol)
2SGA	-6.77
2SGB	-6.95
2SGC	-6.59
Sacranoside A A	-4.43
Sacranoside A B	-5.17
Sacranoside A C	-4.23
Sacranoside A D	-5.14
Sacranoside A E	-4.99
Sacranoside A F	-4.80
Sericetin A	-6.25
Sericetin B	-6.41
Sericetin C	-6.22

2SG: (2S)-6-(gamma,gamma-dimethylallyl)-3',4'-dimethoxy-6",6"-dimethylpyran[2",3":7,8]flavanone

Table 4: Molecular docking results of the silver-complexed leads at the active site of VP8*

Silver-lead compound complex	Docking score (kcal/mol)
2SGA	-8.16
2SGB	-8.21
2SGC	-8.06
Apigenin-4'-glucoside A	-5.85
Apigenin-4'-glucoside B	-6.45
Apigenin-4'-glucoside C	-6.42
Apigenin-4'-glucoside D	-6.28
Apigenin-4'-glucoside E	-6.08
Apigenin-4'-glucoside F	-4.93

Apigenin-4'-glucoside G	-6.75
Gnetin L A	-6.65
Gnetin L B	-6.63
Gnetin L C	**+2.21**
Gnetin L D	-7.21
Gnetin L E	-6.81
Gnetin L F	-7.61
Sericetin A	-7.26
Sericetin B	-6.55
Sericetin C	-7.47

2SG: (2S)-6-(gamma,gamma-dimethylallyl)-3',4'-dimethoxy-6",6"-dimethylpyran[2",3":7,8]flavanone

Comparative bond analysis of interaction plots after molecular docking of the silver-complexed leads against VP5* and VP8*

Ligand binding to protein depends on non-covalent interactions between the interacting molecules encompassing electrostatic interactions, including hydrogen bonds, van der Waals contacts and hydrophobic effects (Shahidi and Dissanayaka, 2023). In this study, the interaction maps revealed the presence of alkyl, pi-alkyl, pi-Sigma, pi-pi stacked and pi-pi T-shaped contacts (Figures 16-22). Alkyl and pi-alkyl interactions represent short yet attractive hydrophobic bonds critical in determining ligand-receptor binding affinities. They also play a role in specificity, although in a less geometrically constrained manner relative to hydrogen bonds (Motiejunas and Wade, 2007). Specifically, the presence of alkyl and pi-alkyl bonds enhances the hydrophobic interactions of the ligand within the binding domain of the receptor (Arthur and Uzairu, 2019). Furthermore, pi-pi interactions are distinct dispersion forces between planar functional groups characterized by significant electron delocalization such as aromatic rings (de Freitas and Schapira, 2017; Pérez and Martín, 2015). The significance of these interactions is in their ability to stabilize the protein-ligand complex, offering further specificity for ligand binding (Bissantz *et al.*, 2010). Given that pi-pi interactions rank as the

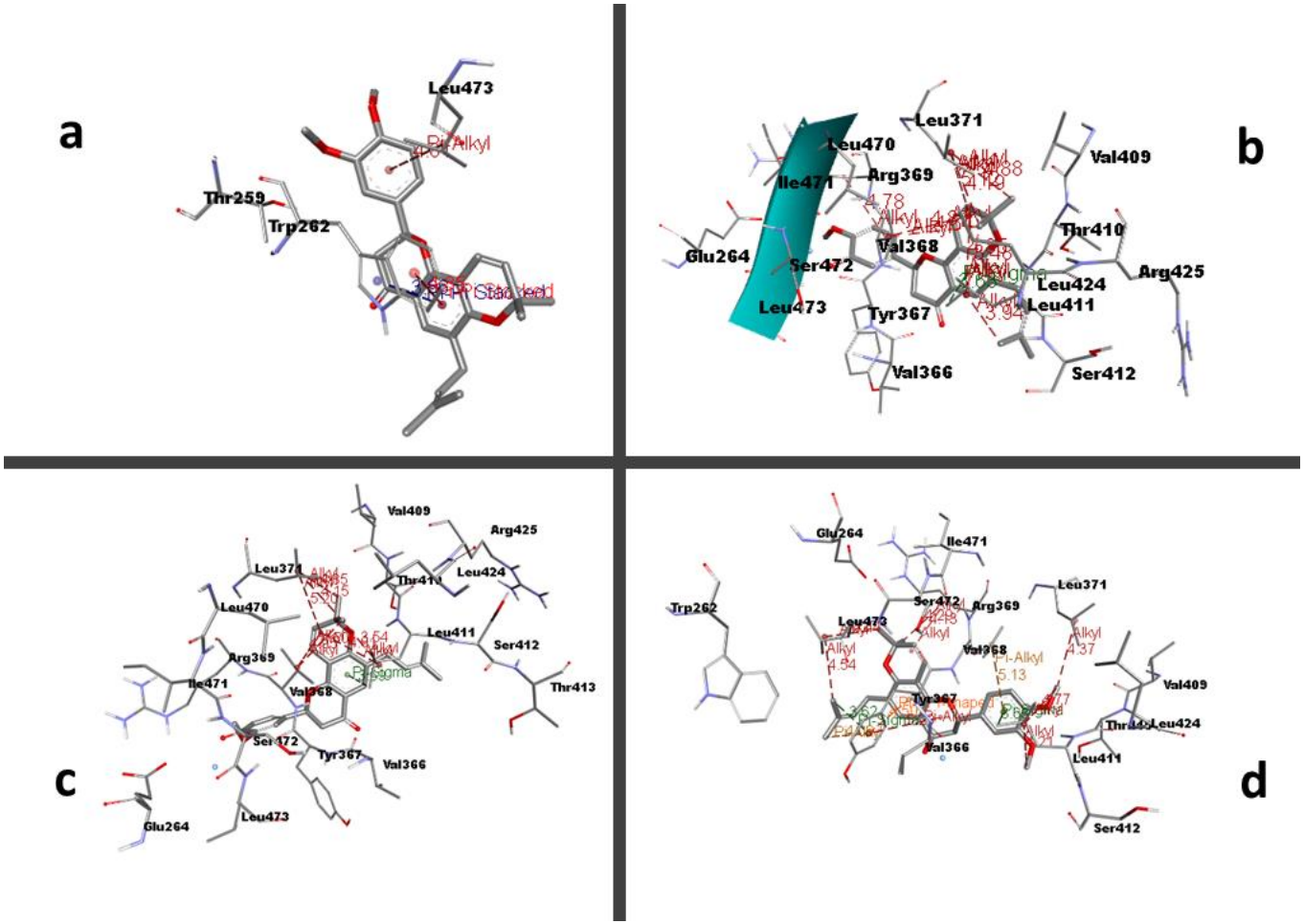


Figure 16: 3D interaction plots of (2S)-6-(gamma,gamma-dimethylallyl)- 3',4'-dimethoxy-6'',6''-dimethylpyran[2'',3'':7,8]flavanone-Ag complex (a) (2S)-6-(gamma,gamma-dimethylallyl)- 3',4'-dimethoxy-6'',6''-dimethylpyran[2'',3'':7,8]flavanone (b) (2S)-6-(gamma,gamma-dimethylallyl)- 3',4'-dimethoxy-6'',6''-dimethylpyran[2'',3'':7,8]flavanone A (c) (2S)-6-(gamma,gamma-dimethylallyl)- 3',4'-dimethoxy-6'',6''-dimethylpyran[2'',3'':7,8]flavanone B (d) (2S)-6-(gamma,gamma-dimethylallyl)- 3',4'-dimethoxy-6'',6''-dimethylpyran[2'',3'':7,8]flavanone C against VP5* after molecular docking.

most prevalent type of protein-ligand interaction, identifying the various forms of these interactions including pi-sigma, pi-pi stacked and pi-pi T-shaped for a detailed analysis of binding complexes is crucial (de Freitas and Schapira, 2017).

Against VP5*, 2SG had a total interaction of six, of which 1 is a pi-alkyl interaction while 2 are pi-pi stacked interactions while also interacting with two active site residues (Trp262, Leu473) (Table 5, Figure 16). In contrast, the 2SG-silver complexes had a higher number of interactions, 2SGA (25), 2SGB (24), 2SGC (28) and interacted with more active site residues relative to 2SG all of which could be responsible for their higher negative docking scores as the interaction of a ligand with important amino acids in a protein is essential for its inactivation (Bissantz *et al.*, 2010). Therefore, higher negative docking scores observed in the 2SG derivatives relative to 2SG might be attributed to the number of observed interactions and, more importantly, interaction with the active site residues. Despite having the highest number of contacts (28) and consequently interacting with a higher number of active site residues (5), 2SGC exhibited lower negative docking scores relative to other 2SG-silver complexes; this could be due to the limitation inherent in the scoring function of molecular docking software's (Table 3) (Kitchen *et al.*, 2004; Taylor *et al.*, 2002), which may not fully account for the enthalpic and entropic contributions of many contacts.

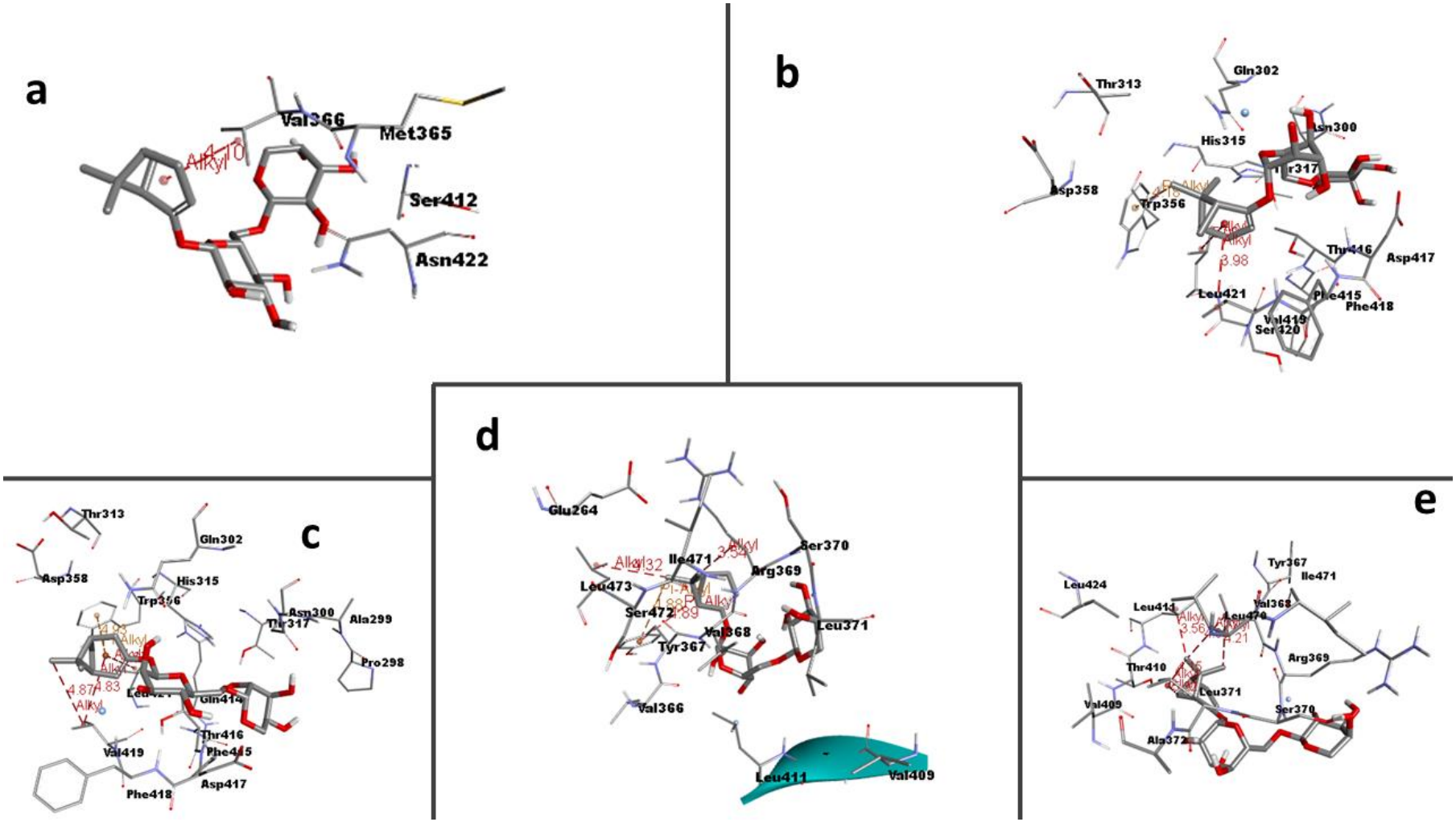


Figure 17: 3D interaction plots of sacranoside A-Ag complex (a) sacranoside A (b) sacranoside A A (c) sacranoside A B (d) sacranoside A C (e) sacranoside A D against VP5* after molecular docking.

All the SAC-silver complexes docked against VP5* have lower negative docking scores [SACA (-4.4), SACB (-5.1), SACC (-4.2), SACD (-5.1), SACE (-4.9), SACF (-4.8) kcal/mol] with a larger interaction network than the parent SAC molecule (-5.7 kcal/mol) (Table 5). However, a shorter bond length was observed in SAC-VP5* interactions relative to the SAC-silver complexes, which could be responsible for its higher negative docking score. A reduced bond length suggests enhanced stability and a stronger attraction between two entities, leading to a more cohesive arrangement of their constituent atoms (Du *et al.*, 2016). Additionally, SAC interacts with two active site residues as opposed to SACA, SACB, SACD and SACF, which interacts with just one active site residue (Figure 17). On the contrary, SACE interacts with two active site residues (Val366, Tyr367) partly like SAC (Val366, Ser412), while SACA interacted with three (Val366, Tyr367, Leu473). Unfortunately, the observed interactions could not sufficiently justify their docking scores.

All the SER derivatives have higher negative docking scores [SERA (-6.25), SERB (-6.41), SERC (-6.22) kcal/mol] with corresponding interactions compared to SER (-5.9 kcal/mol) except SERC with an equal number of interactions (11). Unfortunately, SERC does not interact with any active site residues, while SER interacts with 3 active site residues (Figure 18). Therefore, the observed docking scores in SERA might have emanated from interactions with other residues apart from the active site residues. Meanwhile, the higher docking scores in SERC relative to SER despite an equal number of interactions may be due to its shorter bond length (Table 5), tighter atomic engagement and consequently, stronger intermolecular attraction (Du *et al.*, 2016). Generally, 2SGC (28) and 2SGA (25) exhibited the greatest number of contacts, suggesting higher affinity for the target relative to other derivatives as they also interacted with the VP5* active site residues.

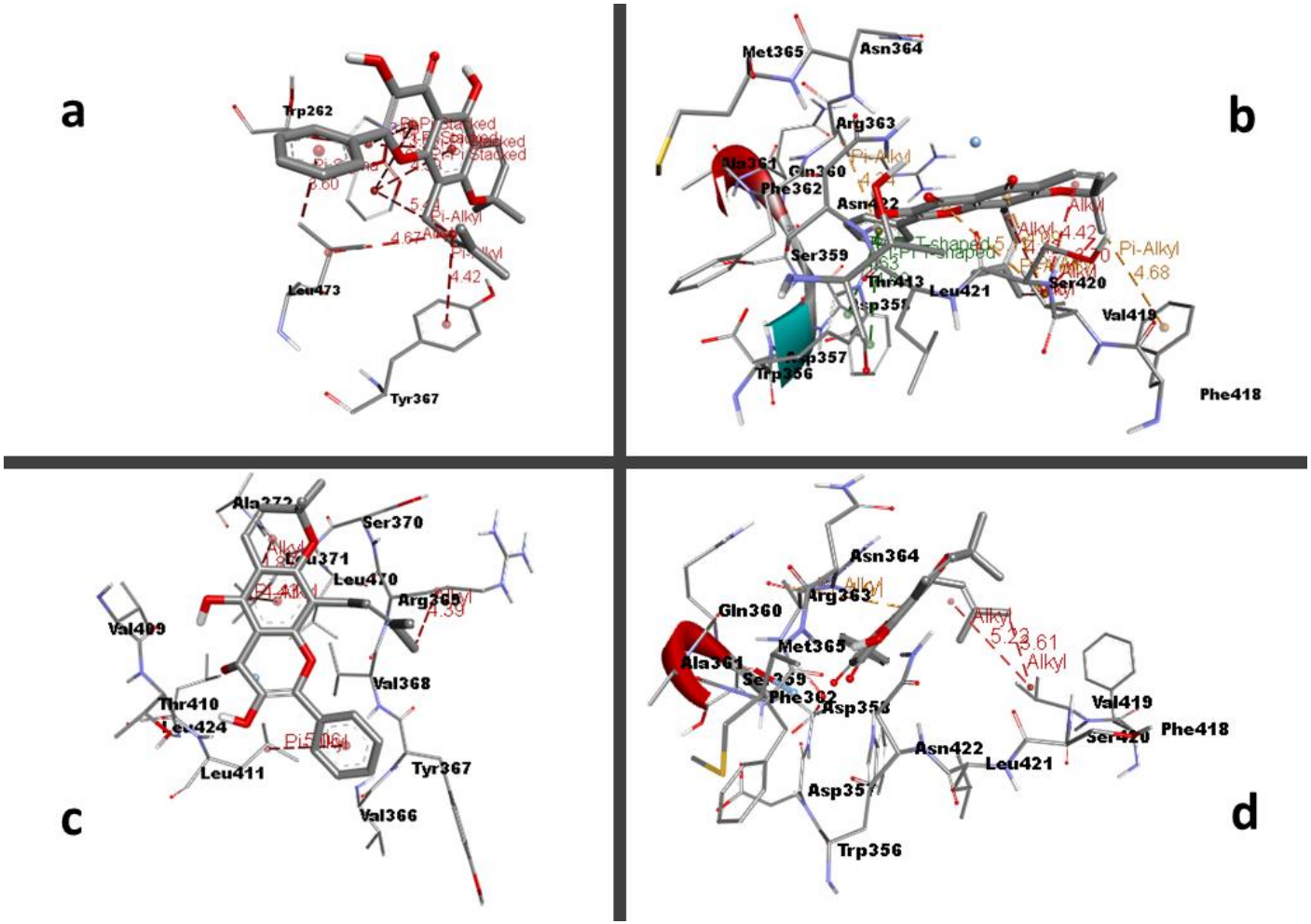


Figure 18: 3D interaction plots of sericetin-Ag complex (a) sericetin (b) sericetin A (c) sericetin B (d) sericetin C against VP5* after molecular docking.

Table 5: Comparative interactions analysis of the silver-complexed leads against VP5* after molecular docking

VP5*+ silver-complexed lead	Total number of interactions and mean bond length (Å)	Types of interactions observed [number/average distance (Å)]	Active site residue interacted with
2SG	6(4.54)	Pi-Alkyl (1/4.81), Pi-Pi Stacked (2/4.41)	Trp262, Leu473
2SGA	25(4.50)	Alkyl (8/4.61), Pi-Sigma (1/3.63)	Val366, Tyr367, Ser412, Leu473
2SGB	24(4.61)	Alkyl (4.76), Pi-Sigma (1/3.69)	Val366, Tyr367, Ser412, Leu473
2SGC	28(4.37)	Alkyl (6/4.36), Pi-Alkyl (4/4.75), Pi-Sigma (2/3.63), Pi-Pi Tshaped (1/4.50)	Trp262, Val366, Tyr367, Ser412, Leu473
Sacranoside A	5(4.10)	Alkyl (1/4.10)	Val366, Ser412
Sacranoside A A	17(4.39)	Alkyl (2/4.49), Pi-Alkyl (1/4.18)	Phe415
Sacranoside A B	20(4.83)	Alkyl (3/4.79), Pi-Alkyl (1/4.93)	Phe415
Sacranoside A C	17(4.41)	Alkyl (3/4.25), Pi-Alkyl (1/4.88)	Val366, Tyr367, Leu473
Sacranoside A D	17(4.27)	Alkyl (5/4.27)	Tyr367
Sacranoside A E	9	None	Val366, Tyr367
Sacranoside A F	14	None	Val366
Sericetin	11(4.42)	Alkyl (1/4.67), Pi-Alkyl (2/4.93), Pi-Sigma (1/3.60), Pi-Pi Stacked (4/4.31)	Trp262, Tyr367, Leu473,
Sericetin A	26(4.44)	Alkyl (4/4.14), Pi-Alkyl (4/4.56), Pi-Pi T-shaped (2/4.81)	None
Sericetin B	16(4.69)	Alkyl (2/4.63), Pi-Alkyl (2/4.75)	Val366, Tyr367
Sericetin C	11(4.58)	Alkyl (2/4.42), Pi-Alkyl (1/4.91)	None

2SG: (2S)-6-(gamma,gamma-dimethylallyl)-3',4'-dimethoxy-6",6"-dimethylpyran[2",3":7,8]flavanone

Table 6: Comparative interactions analysis of the silver-complexed leads against VP8* after molecular docking

VP8*+ silver-complexed leads	Total number of interactions and mean bond length (Å)	Types of interactions observed [number/average distance (Å)]	Active site residue interacted with
2SG	11(4.77)	Pi-Alkyl (2/4.53), Pi-Pi T-shaped (2/5.02)	Arg101, Tyr155, Lys187, Tyr188, Ser190
2SGA	20(4.46)	Alkyl (1/5.26), Pi-Alkyl (5/4.30)	Arg101, Tyr155, Asn178, Lys187, Tyr188, Ser190
2SGB	20(4.38)	Alkyl (1/5.47), Pi-Alkyl (3/4.16), Pi-sigma (1/3.93)	Arg101, Tyr155, Asn178, Lys187, Tyr188, Ser190

2SGC	28(4.80)	Alkyl (3/4.00), Pi-Alkyl (6/5.09), Pi-Pi T-shaped (2/5.14)	Arg101, Tyr155, Asn178, Lys187, Tyr188, Ser190
Apigenin-4'-glucoside	10(5.51)	Pi-Alkyl (1/5.39), Pi-Pi Stacked (1/5.42), Pi-Pi T-shaped (1/5.73)	Arg101, Tyr155, Asn178, Lys187, Ser190
Apigenin-4'-glucoside A	19(4.68)	Pi-Alkyl (1/5.21), Pi-Pi T-shaped (1/4.15)	Arg101, Tyr155, Asn178, Lys187, Tyr188, Ser190
Apigenin-4'-glucoside B	20(4.78)	Pi-Alkyl (3/4.90), Pi-Pi T-shaped (1/5.55), Pi-Sigma (1/3.67)	Arg101, Tyr155, Lys187, Tyr188, Ser190
Apigenin-4'-glucoside C	18(5.05)	Pi-Alkyl (1/5.41), Pi-Pi T-shaped (2/5.6), Pi-Sigma (1/3.58)	Arg101, Tyr155, Ser190
Apigenin-4'-glucoside D	18(5.05)	Pi-Alkyl (1/5.47), Pi-Pi T-shaped (2/5.58), Pi-Sigma (1/3.57)	Arg101, Tyr155, Lys187, Tyr188, Ser190
Apigenin-4'-glucoside E	17(4.35)	Pi-Alkyl (1/5.20), Pi-Sigma (1/3.49)	Arg101, Tyr155, Tyr188, Ser190
Apigenin-4'-glucoside F	19(4.76)	Pi-Alkyl (2/4.78), Pi-Pi T-shaped (3/4.75)	Arg101, Tyr155, Asn178, Lys187, Tyr188, Ser190
Apigenin-4'-glucoside G	20(4.86)	Pi-Alkyl (2/5.21), Pi-Pi stacked (1/4.22), Pi-Pi T-shaped (1/4.80)	Arg101, Tyr155, Lys187, Tyr188, Ser190
Gnetin L	7(4.10)	Pi-Sigma (1/3.41), Pi-Pi T-shaped (1/4.92), Pi-Alkyl (1/3.98)	Arg101, Tyr155, Lys187
Gnetin L A	18(4.35)	Pi-Alkyl (1/5.12), Pi-Sigma (1/3.58)	Arg101, Tyr155, Asn178, Lys187, Tyr188, Ser190
Gnetin L B	17(4.05)	Pi-Sigma (1/3.32), Pi-Pi T-shaped (2/4.41)	Arg101, Tyr155, Lys187, Tyr188, Ser190
Gnetin L D	26(4.50)	Alkyl (1/4.68), Pi-Alkyl (4/4.76), Pi-Sigma (1/3.30)	Arg101, Tyr155, Asn178, Lys187, Tyr188, Ser190
Gnetin L E	14(4.81)	Pi-Pi T-shaped (1/4.81)	Arg101, Tyr155, Asn178, Tyr188, Ser190
Gnetin L F	21(4.30)	Pi-Sigma (1/3.68), Pi-Pi T-shaped (1/4.92)	Arg101, Tyr155, Asn178, Lys187, Tyr188, Ser190
Sericetin	6(4.51)	Pi-Alkyl (2/4.23), Pi-Pi T-shaped (1/5.09)	Asn178, Lys187, Tyr188
Sericetin A	26(4.27)	Alkyl (3/4.02), Pi-Alkyl (5/4.54), Pi-Sigma (1/3.66)	Asp100, Arg101, Tyr155, Asn178, Lys187, Tyr188, Ser190
Sericetin B	19(4.40)	Alkyl (1/5.50), Pi-Alkyl (2/4.41), Pi-Sigma (2/3.84)	Arg101, Tyr155, Asn178, Lys187, Tyr188, Ser190
Sericetin C	21(4.40)	Alkyl (2/4.08), Pi-Alkyl (5/4.64), Pi-Sigma (1/3.89)	Arg101, Tyr155, Asn178, Lys187, Tyr188, Ser190

2SG: (2S)-6-(gamma,gamma-dimethylallyl)-3',4'-dimethoxy-6",6"-dimethylpyran[2",3":7,8]flavanone

Against VP8*, the sum of the interactions exhibited in the 2SG-silver complexes is in consonance with their binding affinity relative to the parent structure (2SG) [Table (4,6)].

Furthermore, all the 2SG-silver complexes interacted with six active site residues (Arg101, Tyr155, Asn178, Lys187, Tyr188, Ser190) while 2SG interacted with five active site residues (Arg101, Tyr155, Lys187, Tyr188, Ser190) (Figure 19). The additional interaction made with Asn178 in the derivatives may indicate that Ag conjugation is responsible for the increased affinity of the derivatives for the investigated protein compared to 2SG. Also, the longer average bond length observed in 2SG (4.77) relative to the derivatives [2SGA (4.46), 2SGB (4.38)] might be responsible for their higher docking score except in 2SGC (4.80) with longer average bond length and consequently a more positive docking score of all the 2SG-silver complexes. This further emphasize the influence of bond length and active site engagement on binding affinity in docking studies.

A different trend was observed in the APG series against VP8*, where a higher negative docking score was observed in the lead compound relative to the APG-silver complexes; nevertheless, a higher number of interactions was observed in the silver complexes (Table 6). Additionally, APGA and APGF interacted with six active site residues (Arg101, Tyr155, Asn178, Lys187, Tyr188, Ser190), as opposed to the parent structure interacting with five active site amino acid residues (Arg101, Tyr155, Asn178, Lys187, Ser190) though with a higher negative docking score as opposed to APGA and APGF. Furthermore, APGB, APGD, and APGG interacted with an equal number of active site residues similar to APG, which did not correlate with their docking scores (Figure 20). Interestingly, a lesser number of active site residues observed in the interaction plot of APGC (Arg101, Tyr155, Ser190) and APGE (Arg101, Tyr155, Tyr188, Ser190) agree with their docking score relative to the parent structure-APG. Moreover, the higher negative docking score observed in the parent structure does not correspond to the total longer bond length observed in the parent structure (5.51) relative to the shorter bond length in the silver complexes ranging from 4.35 - 5.05 (Table 6).

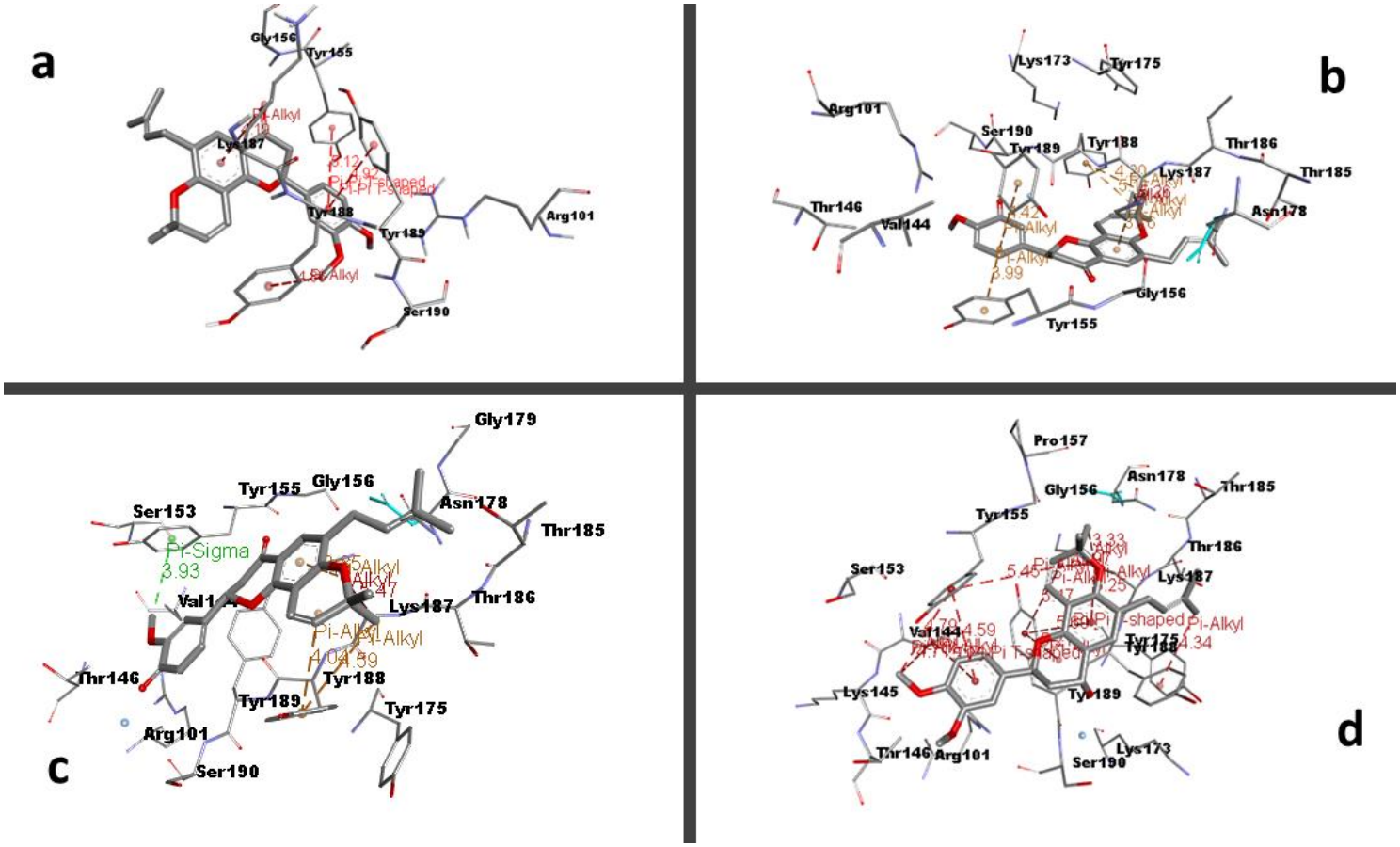


Figure 19: 3D interaction plots of possible (2S)-6-(gamma,gamma-dimethylallyl)- 3',4'-dimethoxy-6'',6''-dimethylpyran[2'',3'':7,8]flavanone-Ag complexes (a) (2S)-6-(gamma,gamma-dimethylallyl)- 3',4'-dimethoxy-6'',6''-dimethylpyran[2'',3'':7,8]flavanone (b) (2S)-6-(gamma,gamma-dimethylallyl)- 3',4'-dimethoxy-6'',6''-dimethylpyran[2'',3'':7,8]flavanone A (c) (2S)-6-(gamma,gamma-dimethylallyl)- 3',4' dimethoxy-6'',6''-dimethylpyran[2'',3'':7,8]flavanone B (d) (2S)-6-(gamma,gamma-dimethylallyl)- 3',4'-dimethoxy-6'',6''-dimethylpyran[2'',3'':7,8]flavanone C against VP8* after molecular docking.

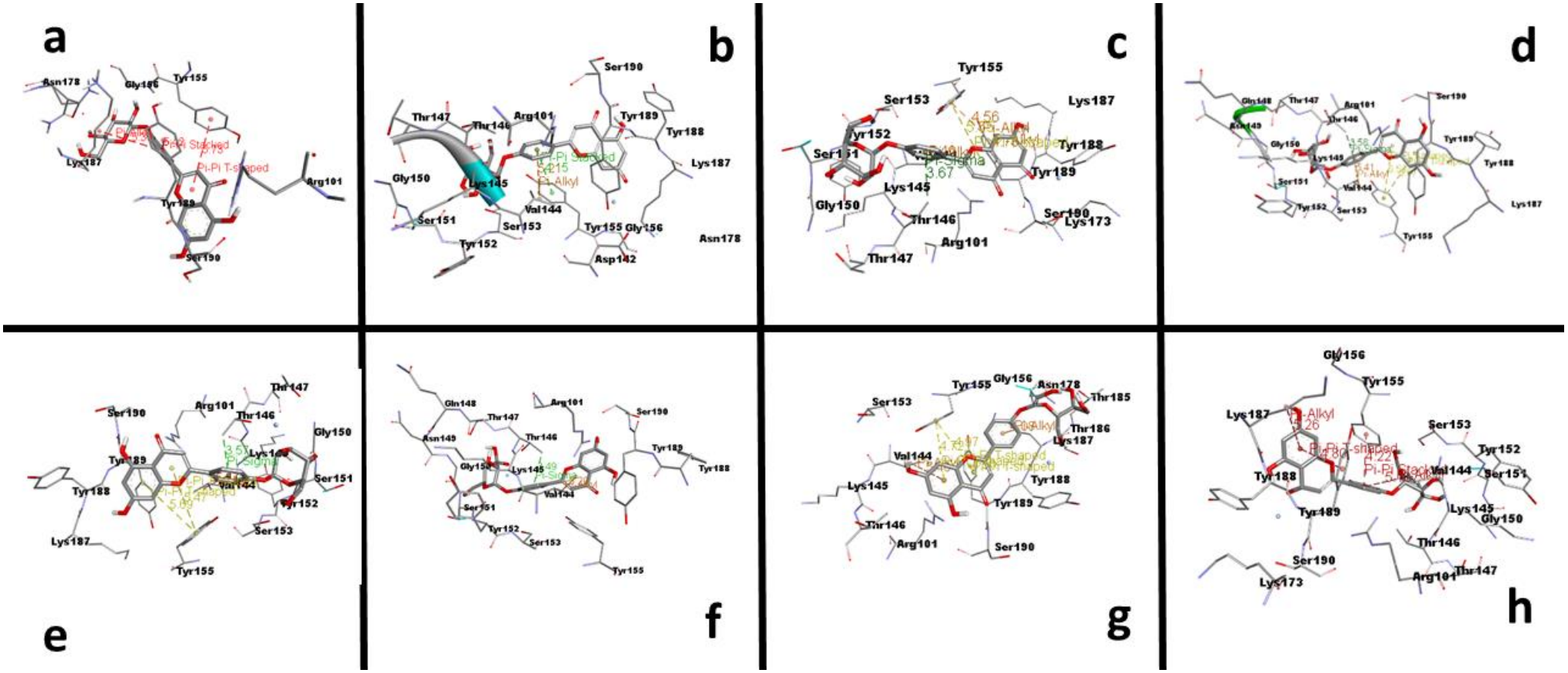


Figure 20: 3D interaction plots of apigenin-4'-glucoside-Ag complexes (a) apigenin-4'-glucoside (b) apigenin-4'-glucoside A (c) apigenin-4'-glucoside B (d) apigenin-4'-glucoside C (e) apigenin-4'-glucoside D (f) apigenin-4'-glucoside E (g) apigenin-4'-glucoside F (h) apigenin-4'-glucoside G against VP8* after molecular docking.

A similar trend was observed in the GNE-silver complexes, wherein the lead compound exhibited higher a negative docking score and fewer interactions relative to the silver complexes against VP8*. This observation contradicts their docking scores except for GNEF, which has a higher negative docking score (Table 4). In addition, a shorter bond length in GNEB (4.05) does not align with its docking score relative to the lead compound (4.10). Specifically, GNE interacted with just three active site residues (Arg101, Tyr155, Lys187) as opposed to the GNE-silver complexes interacting with between five to six active site residues, which does not justify their corresponding docking scores except in GNEF with a higher negative docking score (Figure 21). This discrepancy may be attributed to the inherent limitations of the scoring function in the molecular docking software.

The observed number of interactions in the SER series is consistent with their docking scores relative to the parent structure, except in SERB, with a lower negative docking score (Table 6). Similarly, the silver complexes reacted with more active site residues ranging between six and seven essential amino acids relative to the lead compound interacting with three active site residues (Asn178, Lys187, Tyr188) (Figure 22). Furthermore, the enhanced binding capacity of the silver complexes may be linked to their shorter bond length relative to the lead compound with a longer bond length, except SERB whose bond length does not align. Overall, against VP8*, the highest number of interactions was observed in 2SGC (28) and SERA (26), suggesting a better affinity for the investigated target while interacting with the active site amino acids.

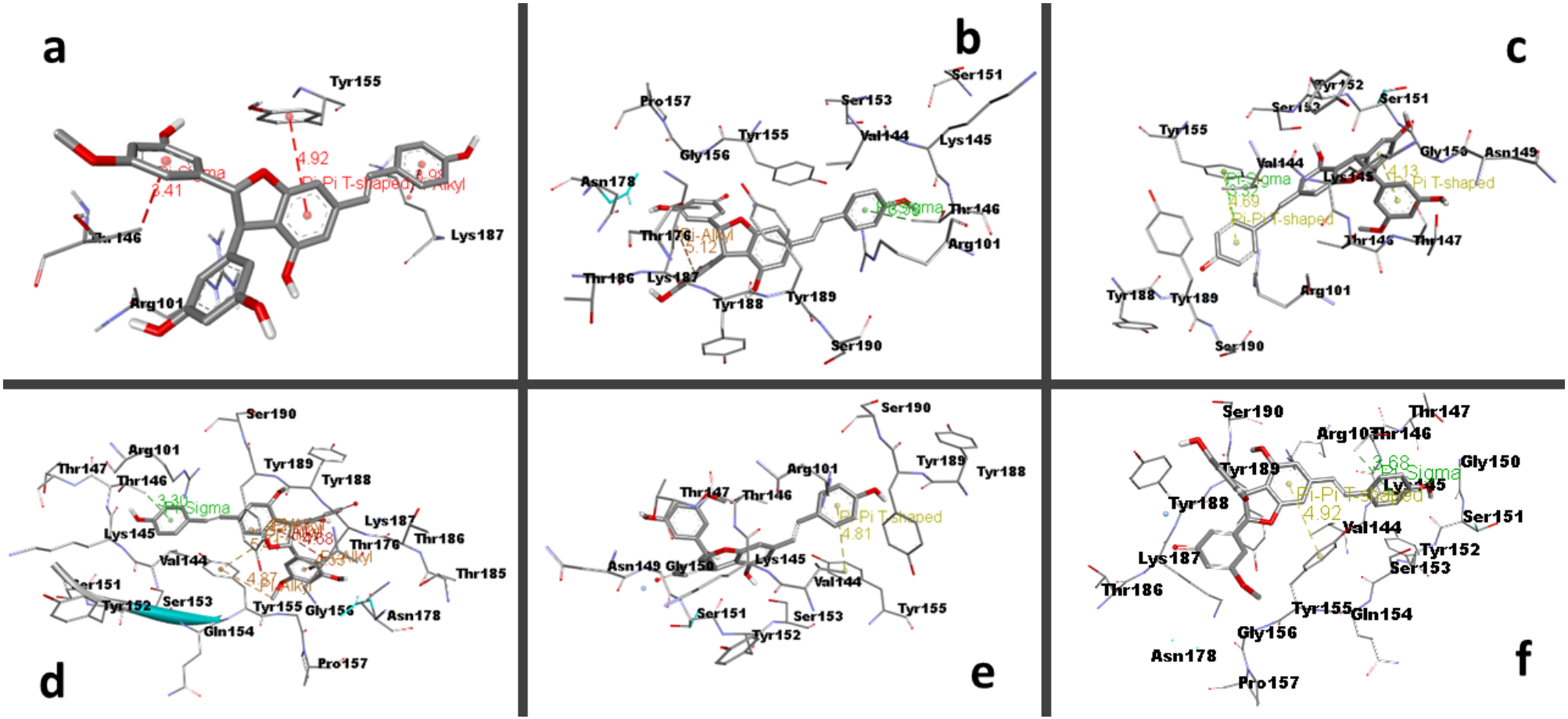


Figure 21: 3D interaction plots of gnetin L-Ag complexes (a) gnetin L (b) gnetin L A (c) gnetin L B (d) gnetin L D (e) gnetin L E (f) gnetin L F against VP8* after molecular docking.

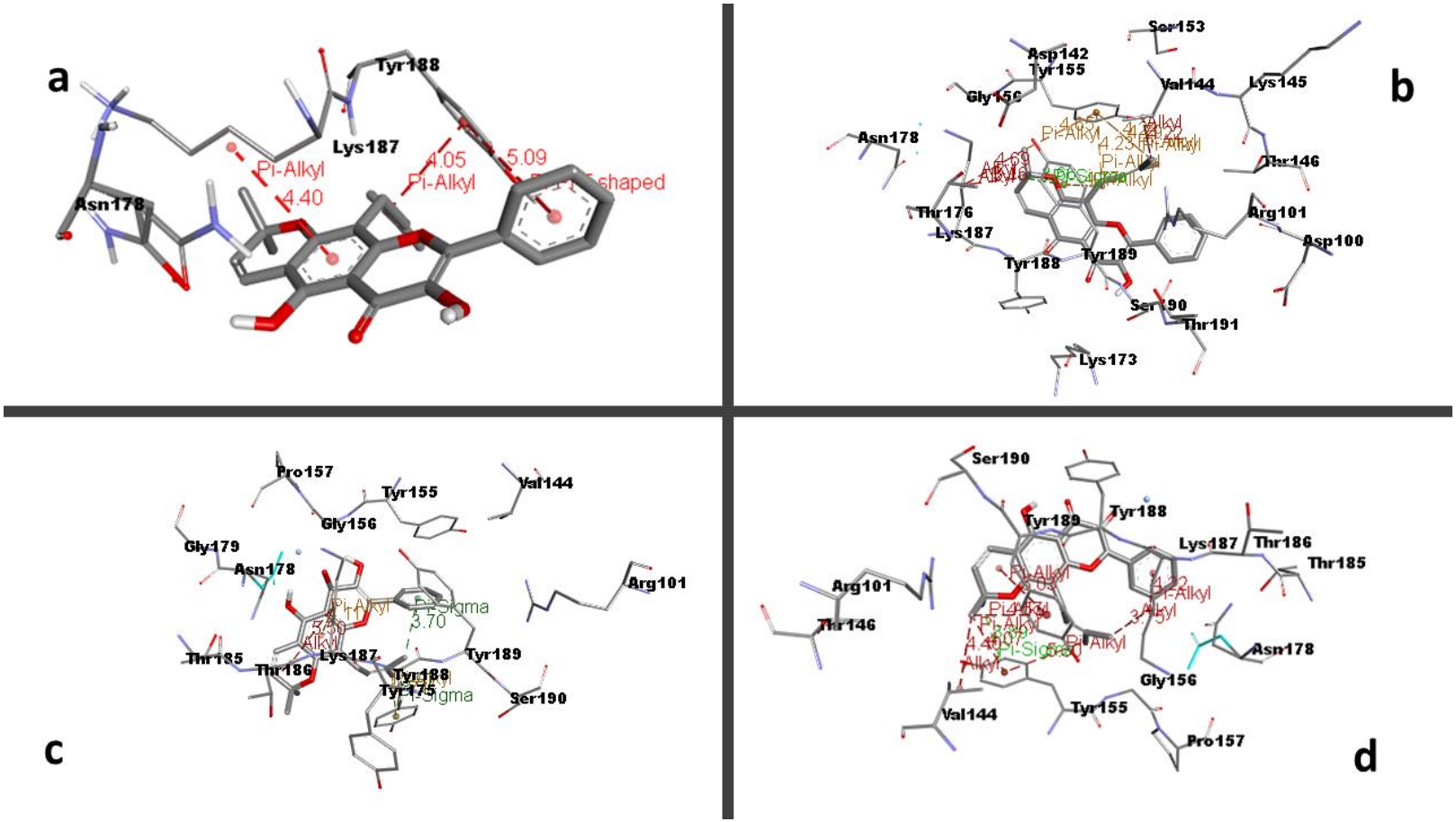


Figure 22: 3D interaction plots of sericetin-Ag complexes (a) sericetin (b) sericetin A (c) sericetin B (d) sericetin C against VP8* after molecular docking.

4.0 Conclusion

The silver-complexed leads exhibited enhanced molecular properties, suggesting better reactivity than their corresponding parent compounds. Generally, the silver complexation did not significantly alter the pharmacokinetics and toxicity profiles of the possible silver-complexed leads investigated hence, they are fit for drug development. Notably, all silver-complexed leads docked against VP5* exhibited stronger binding affinity than their corresponding lead compounds except for the sacranoside A series. On the contrary, the apigenin-4'-glucoside series, Gnetin L A -E, and sericetin B demonstrated reduced affinity than their corresponding lead compounds, while other derivatives exhibited higher negative docking score. 2SGC and 2SGA, as well as 2SGC and SERA have been identified as better possible silver-complexed leads considering their molecular properties, pharmacokinetics and toxicity profiles, docking scores and number of interactions against VP5* and VP8* respectively. Owing to the recurrent detection of RVA in the investigated wastewater treatment plants in Durban (chapter three), the promising results in this study warrant further computational investigation, including molecular dynamics simulation, to provide insights into the thermodynamics profile of the resulting protein and silver-complexed leads and this is being considered for future study.

References

ADEDIRIN, O., ABDULSALAM, R. A., NASIR-NAEEM, K. O., OKE, A. A., JUBRIL, A. O . & SABIU, S. 2025. Density functional theory and molecular dynamics simulation-based bioprospection of *Agathosma betulina* essential-oil metabolites against protein tyrosine phosphatase-1B for interventive antidiabetic therapy. *Heliyon*, 11(3), 1-20.

AIHARA, J. I. 1999. Reduced HOMO–LUMO gap as an index of kinetic stability for polycyclic aromatic hydrocarbons. *The Journal of Physical Chemistry A*, 103(35), 7487-7495.

AKOONJEE, A., LANREWAJU, A. A., BALOGUN, F. O., MAKUNGA, N. P. & SABIU, S. 2023. Waste to medicine: evidence from computational studies on the modulatory role of corn silk on therapeutic targets implicated in type-2 diabetes mellitus. *Biology*, 12(12), 1-40.

ALONGAMO, C. H. A., NKUNGLI, N. K. & GHOGOMU, J. N. 2019. DFT study on transition-metal coordination effects in charge transport and nonlinear-optical properties of 2-{[5-(4-nitrophenyl)-1,3,4-thiadiazol-2-ylimino]methyl}phenol. *Molecular Physics*, 117(19), 2577-2592.

AMIMO, J. O., RAEV, S. A., CHEPNGENO, J., MAINGA, A. O., GUO, Y., SAIF, L. & VLA SOVA, A. N. 2021. Rotavirus interactions with host intestinal epithelial cells. *Frontiers in Immunology*, 12, 1-17.

ARIBISALA, J. O., S'THEBE, N. W. & SABIU, S. 2024. *In silico* exploration of phenolics as modulators of penicillin-binding protein 2X of *Streptococcus pneumoniae*. *Scientific Reports*, 14(1), 1-21.

ARTHUR, D. E. & UZAIRU, A. 2019. Molecular docking of NCI anticancer analogues with human phosphatidylinositol-4,5-bisphosphate 3-kinase catalytic subunit. *Journal of King Saud University – Science*, 31(4), 1151-1166.

ASTANI, A. & SCHNITZLER, P. 2014. Antiviral activity of monoterpenes β-pinene and limonene against herpes simplex virus *in vitro*. *Iranian Journal of Microbiology*, 6(3), 149-155.

AYERS, P. W., PARR, R. G. & PEARSON, R. G. 2006. Elucidating the hard/soft acid–base principle: a perspective based on half-reactions. *The Journal of Chemical Physics*, 124(19), 194107-194107-8.

BARCELOS, M. P., GOMES, S. Q., FEDERICO, L. B., FRANCISCHINI, I. A. G., HAGE-M ELIM, L. I. D. S., SILVA, G. M. & DE PAULA DA SILVA, C. H. T. 2022. Lead optimization in drug discovery. In: *Research Topics in Bioactivity, Environment and Energy: Experimental and Theoretical Tools*. Springer, 481-500.

BISSANTZ, C., KUHN, B. & STAHL, M. 2010. A medicinal-chemist's guide to molecular interactions. *Journal of Medicinal Chemistry*, 53(14), 5061-5084.

CALAIS, J.-L. 1993. Density-Functional Theory of Atoms and Molecules. *International Journal of Quantum Chemistry*, 47(1), 101-101.

CLARK, A., BLACK, R., TATE, J., ROOSE, A., KOTLOFF, K., LAM, D., BLACKWELDE R, W., PARASHAR, U., LANATA, C. & KANG, G. 2017. Estimating global, regional and national rotavirus deaths in children < 5 years: approaches, analyses and improvements. *PLoS one*, 12(9), 1-18.

COHEN, R., MARTINÓN-TORRES, F., POSIUNIENE, I., BENNINGHOFF, B., OH, K.-B. & POELAERT, D. 2023. The value of rotavirus vaccination in Europe: A call for action. *Infectious Diseases and Therapy*, 12(1), 9-29.

DA SILVA, T. U., DA SILVA, E. T., DE CARVALHO POUGY, K., DA SILVA LIMA, C. H. & DE PAULA MACHADO, S. 2022. Molecular modelling of indazole-3-carboxylic acid and its metal complexes (Zn, Ni, Co, Fe, Mn) as NO-synthase inhibitors. *Inorganic Chemistry Communications*, 135, 1-9.

DE FREITAS, R. F. & SCHAPIRA, M. 2017. Systematic analysis of atomic protein–ligand interactions in the PDB. *MedChemComm*, 8(10), 1970-1981.

DELANO, W. L. 2002. PyMOL: An open-source molecular-graphics tool. *CCP4 Newsletter on Protein Crystallography*, 40, 82-92.

DEY, D., BISWAS, P., PAUL, P., MAHMUD, S., EMA, T. I., KHAN, A. A., AHMED, S. Z., HASAN, M. M., SAIKAT, A. S. M. & FATEMA, B. 2023. Natural flavonoids block CD81 receptor of hepatocytes and inhibit HCV infection: A computational approach. *Molecular Diversity*, 27(3), 1309-1322.

DU, X., LI, Y., XIA, Y.-L., AI, S.-M., LIANG, J., SANG, P., JI, X.-L. & LIU, S.-Q. 2016. Insights into protein–ligand interactions: mechanisms, models and methods. *International Journal of Molecular Sciences*, 17(144), 1-34.

ESIMONE, C. O., ECK, G., NWORU, C. S., HOFFMANN, D., ÜBERLA, K. & PROKSCH, P. 2010. Dammarenolic acid, a secodammarane triterpenoid from *Aglaia* sp., shows potent antiretroviral activity *in vitro*. *Phytomedicine*, 17(7), 540-547.

GREENBERG, H. B. & ESTES, M. K. 2009. Rotaviruses: From pathogenesis to vaccination. *Gastroenterology*, 136(6), 1939-1951.

GUTIERREZ, M. B., DE ASSIS, R. M. S., ANDRADE, J. D. S. R., FIALHO, A. M. & FUMI AN, T. M. 2023. Rotavirus A during the COVID-19 pandemic in Brazil, 2020–2022: Emergence of the G6P[8] genotype. *Viruses*, 15(8), 1-17.

HALOUI, R., ELKHATTABI, K., MKHAYAR, K., DAOUI, O., CHTITA, S., HAOUDI, A. & ELKHATTABI, S. 2024. Design of styrylpyridine-derived HDAC1 inhibitors for gastric cancer: 3D-QSAR, ADMET, docking and MD studies. *Scientific African*, 23, 1-13.

HEANEY, R. P. 2001. Factors influencing the measurement of bioavailability, using calcium as a model. *The Journal of Nutrition*, 131(4 Suppl.), 1344S-1348S.

HENSCHKE, N., BERGMAN, H., HUNGERFORD, D., CUNLIFFE, N., GRAIS, R., KANG, G., PARASHAR, U., WANG, S. & NEUZIL, K. 2022. Efficacy and safety of

rotavirus vaccines in high-mortality countries of Africa and Asia. *Vaccine*, 40(13), 1707-1711.

HILL, A. P. & YOUNG, R. J. 2010. Getting physical in drug discovery: Contemporary perspectives on solubility and hydrophobicity. *Drug Discovery Today*, 15(15-16), 648-655.

HKIRI, S., COŞKUN, K. A., ÜSTÜN, E., SAMARAT, A., TUTAR, Y., ŞAHIN, N. & SÉME RIL, D. 2022. Silver(I) complexes of oxadiazole-functionalized α-aminophosphonates: Synthesis, structure and biological activity. *Molecules*, 27(23), 1-15.

HU, C. T., DIAZ, K., YANG, L. C., SHARMA, A., GREENBERG, H. B. & SMITH, J. G. 202 2. VP4 determines α-defensin modulation of rotavirus infection. *Journal of Virology*, 96(4), e02053-21.

HUNTER, C. A. & SANDERS, J. K. M. 1990. The nature of π–π interactions. *Journal of the American Chemical Society*, 112(14), 5525-5534.

IJAZ, M., SABARA, M., ALKARMI, T., FRENCHICK, P., READY, K., DAR, F. & BABIU K, L. 1994. Molecular determinants of rotavirus virulence: Localization of a potential virulence site in murine rotavirus VP4. *Comparative Immunology, Microbiology & Infectious Diseases*, 17(2), 99-110.

JADOON, T., AHSIN, A., ULLAH, F., MAHMOOD, T. & AYUB, K. 2021. Adsorption mechanism of *p*-aminophenol on silver-graphene composite: A first-principles study. *Journal of Molecular Liquids*, 341, 1-12.

JIANG, L., TANG, A., SONG, L., TONG, Y. & FAN, H. 2023. Advances in developing antivirals for rotavirus infection. *Frontiers in Immunology*, 14, 1-16.

KAICHEV, V., BUKHTIYAROV, V., HÄVECKER, M., KNOP-GERCKE, A., MAYER, R. & SCHLÖGL, R. 2003. Nature of electrophilic and nucleophilic oxygen adsorbed on silver. *Kinetics and Catalysis*, 44(4), 432-440.

KATUWAL, S., UPADHYAYA, S. R., MARAHATHA, R., SHRESTHA, A., REGMI, B. P., KHADAYAT, K., BASNET, S., BASNYAT, R. C. & PARAJULI, N. 2023. *In silico* study of coumarins: wedelolactone as a potential inhibitor of SARS-CoV-2 spike variants. *Journal of Tropical Medicine*, 4756730, 1-19.

KAUSHIK, S., DAR, L., KAUSHIK, S. & YADAV, J. P. 2021. Anti-dengue activity of supercritical extract and oleanolic acid from *Leucas cephalotes*: *in vitro* and *in silico* evaluation. *BMC Complementary Medicine and Therapies*, 21(227), 1-15.

KITCHEN, D. B., DECORNEZ, H., FURR, J. R. & BAJORATH, J. 2004. Docking and scoring in virtual screening: methods and applications. *Nature Reviews Drug Discovery*, 3(11), 935-951.

KONG, L., LI, S., LIAO, Q., ZHANG, Y., SUN, R., ZHU, X., ZHANG, Q., WANG, J., WU, X . & FANG, X. 2013. Oleanolic and ursolic acids: novel hepatitis C virus antivirals inhibiting NS5B polymerase. *Antiviral Research*, 98(1), 44-53.

KRASCHNEFSKI, M. J., BUGARCIC, A., FLEMING, F. E., YU, X., VON ITZSTEIN, M., C OULSON, B. S. & BLANCHARD, H. 2009. Effects of sialic-acid-binding cleft mutations in rotavirus spike protein on glycan recognition. *Glycobiology*, 19(2), 194-200.

KUCUK, C. 2023. Silver-nitrate complex of 5-benzimidazole carboxylic acid: Synthesis, DFT, and docking as targeted anticancer agent. *Journal of Molecular Structure*, 1293, 1-14.

KUCUK, C., YURDAKUL, S., CELIK, S. & ERDEM, B. 2022. Experimental and DFT studies of 2-methyl-quinoxaline and its silver(I) complex: non-covalent interactions, antimicrobial and docking. *Inorganic Chemistry Communications*, 145, 1-17.

KUMAR, D., SINGH, A., KUMAR, P., UVERSKY, V. N., RAO, C. D. & GIRI, R. 2020. Penetrance of intrinsic disorder in the rotavirus proteome. *International Journal of Biological Macromolecules*, 144, 892-908.

KUMAR, S., ALI, I., ABBAS, F., KHAN, N., GUPTA, M. K., GARG, M., KUMAR, S. & KUMAR, D. 2023. *In silico* identification of benzofuran-1,2,3-triazoles as EGFR inhibitors via pharmacophore modelling and docking. *In Silico Pharmacology*, 11(20), 1-27.

LAKHERA, S., DEVLAL, K., GHOSH, A., CHOWDHURY, P. & RANA, M. 2022. DFT structural and reactivity study of feverfew and evaluation of antiviral potential against COVID-19. *Chemical Papers*, 76(6), 2759-2776.

LANREWAJU, A. A., ENITAN-FOLAMI, A. M., NYAGA, M. M., SABIU, S. & SWALAHA, F. M. 2023. Cheminformatics bioprospection of medicinal-plant metabolites against trypsin-cleaved VP4 of rotavirus A. *Journal of Biomolecular Structure and Dynamics*, 41(17), 7227-7246.

LANREWAJU, A. A., ENITAN-FOLAMI, A. M., SABIU, S., EDOKPAYI, J. N. & SWALAHA, F. M. 2022. Global public health implications of human exposure to virus-contaminated water. *Frontiers in Microbiology*, 13, 1-18.

LIPINSKI, C. A., LOMBARDO, F., DOMINY, B. W. & FEENEY, P. J. 2012. Experimental and computational estimation of solubility and permeability in drug discovery. *Advanced Drug Delivery Reviews*, 64(1-2), 4-17.

LIU, Y., HUANG, P., TAN, M., LIU, Y., BIESIADA, J., MELLER, J., CASTELLO, A. A., JIANG, B. & JIANG, X. 2012. Rotavirus VP8: phylogeny, host range and interaction with histo-blood-group antigens. *Journal of Virology,* 86(18), 9899-9910.

LUO, J., XUE, Z. Q., LIU, W. M., WU, J. L. & YANG, Z. Q. 2006. Koopmans' theorem for large molecular systems within density-functional theory. *The Journal of Physical Chemistry A*, 110(40), 12005-12009.

MOTIEJUNAS, D. & WADE, R. C. 2007. Structural, energetic and dynamic aspects of ligand–receptor interactions. *Current Computer-Aided Drug Design*, 3(3), 211-221.

MOUNTESSOU, B. Y. G., NGOUONPE, A. W., MBOBDA, A. S., AKINTEMI, E. O., STA MMLER, H.-G., KOUAM, S. F., TCHOUANKEU, J. C., LENTA, B. N., SEWALD, N. & SINGH, T. 2023. Structural analysis and docking of pachypodostyflavone: a potent anti-*Onchocerca* agent. *Journal of Molecular Structure*, 136003.

MOUSSAOUI, M., BAASSI, M., BAAMMI, S., SOUFI, H., SALAH, M., DAOUD, R., EL A LLALI, A., BELGHITI, M. & BELAAOUAD, S. 2023. *In silico* design of novel CDK2 inhibitors: QSAR, ADMET, docking and MD simulations. *Journal of Biomolecular Structure and Dynamics*, 41(15), 6358-6374.

ORIO, M., PANTAZIS, D. A. & NEESE, F. 2009. Density-functional theory in bioinorganic chemistry. *Photosynthesis Research*, 102(2-3), 443-453.

PANG, L.-L., WANG, M.-X., SUN, X.-M., YUAN, Y., QING, Y., XIN, Y., ZHANG, J.-Y., LI , D.-D. & DUAN, Z.-J. 2018. Glycan-binding patterns of human rotavirus P[10] VP8. *Virology Journal,* 15(161), 1-6.

PEARSON, R. G. 1986. Absolute electronegativity and hardness correlated with molecular-orbital theory. *Proceedings of the National Academy of Sciences*, 83(22), 8440-8441.

PÉREZ, E. M. & MARTÍN, N. 2015. π–π interactions in carbon nanostructures. *Chemical Society Reviews*, 44(18), 6425-6433.

SAHA, D., OTA, M. O., PEREIRA, P., BUCHY, P. & BADUR, S. 2021. Rotavirus vaccine performance: dynamic interdependence of host, pathogen and environment. *Expert Review of Vaccines*, 20(7), 945-957.

SHAHIDI, F. & DISSANAYAKA, C. S. 2023. Phenolic-protein interactions: Insights from *in silico* analyses – A review. *Food Production, Processing and Nutrition*, 5(2), 1-21.

SIQUEIRA, F. S., ALVES, C. F. S., MACHADO, A. K., SIQUEIRA, J. D., SANTOS, T. D., MIZDAL, C. R., MOREIRA, K. S., TEIXEIRA CARVALHO, D., BONEZ, P. C. & URQUHART, C. G. 2021. Docking, quorum-quenching, antibiofilm and safety profile of silver-complexed sulfonamide on *Pseudomonas aeruginosa*. *Biofouling*, 37(5), 555-571.

TAYLOR, R. D., JEWSBURY, P. J. & ESSEX, J. W. 2002. Review of protein–small-molecule docking methods. *Journal of Computer-Aided Molecular Design*, 16(3), 151-166.

TOHMÉ, M. J. & DELGUI, L. R. 2021. Advances in developing antiviral compounds for rotavirus infections. *mBio*, 12(3), e00111-21.

TOSATO, M., ASTI, M., DALLA TIEZZA, M., ORIAN, L., HÄUSSINGER, D., VOGEL, R., KÖSTER, U., JENSEN, M., ANDRIGHETTO, A. & PASTORE, P. 2020. Highly stable silver(I) cyclen-based complexes bearing sulfide arms: Toward ^{111}Ag radiopharmaceuticals. *Inorganic Chemistry*, 59(15), 10907-10919.

TRASK, S. D., OGDEN, K. M. & PATTON, J. T. 2012. Capsid-protein interactions orchestrate rotavirus functions. *Current Opinion in Virology*, 2(4), 373-379.

TROEGER, C., KHALIL, I. A., RAO, P. C., CAO, S., BLACKER, B. F., AHMED, T., ARMA H, G., BINES, J. E., BREWER, T. G. & COLOMBARA, D. V. 2018. Rotavirus vaccination and global burden of diarrhoea in children < 5 years. *JAMA Pediatrics*, 172(10), 958-965.

VAN SANTEN, R. A., TRANCA, I. & HENSEN, E. J. 2015. Theory of surface chemistry and reactivity of reducible oxides. *Catalysis Today*, 244, 63-84.

VEENA, V., SHIVAPRASAD, K., SHARANAGOUDA, H. & LAGASHETTY, A. 2024. Synthesis, characterization and *in silico* modelling of dimercapto-triazole-functionalized silver nanoparticles. *Results in Chemistry*, 7, 1-12.

WHEELER, S. E. & BLOOM, J. W. 2014. Toward a complete understanding of non-covalent interactions involving aromatic rings. *The Journal of Physical Chemistry A*, 118(28), 6133-6147.

YODER, J. D. & DORMITZER, P. R. 2006. Alternative intermolecular contacts underlying the VP5 two-to-three-fold rearrangement in rotavirus. *The EMBO Journal,* 25(7), 1559-1568.

YU, J.-S., TSENG, C.-K., LIN, C.-K., HSU, Y.-C., WU, Y.-H., HSIEH, C.-L. & LEE, J.-C. 2017. Celastrol inhibits dengue virus replication via up-regulating type-I interferon responses. *Antiviral Research*, 137, 49-57.

ZHAO, Y. & TRUHLAR, D. G. 2008. The M06 suite of density functionals: main-group thermochemistry, non-covalent interactions and transition metals. *Theoretical Chemistry Accounts*, 120(1-3), 215-241.

ZHIGULIN, G. Y., ZABRODINA, G., KATKOVA, M. & KETKOV, S. Y. 2019. Electron-density distribution and donor–acceptor interactions in water-soluble Ca II and Y III aminohydroximate metallamacrocycles: a DFT study. *Russian Chemical Bulletin*, 68(4), 743-750.

ZHOU, H., GAO, S.-J., ZHANG, M.-T., JIA, J., CHEN, F.-X., CHEN, C.-L., YANG, P.-F. & MAO, J.-L. 2023. Synthesis, configurational analysis and antiviral activity of novel diphenylacrylic acids derived from caffeic acid. *Journal of Molecular Structure*, 1291, 1-11.

Supplementary Information

Table 1: Correlation analysis of the docking scores and the orbital descriptors of complexes docked against VP5*

VP5*	Docking score	LUMO	HOMO	Energy gap	Ionization energy	Electron affinity	Hardness	Softness	Electronegativity	Chemical potential	Global electrophilicity
Docking score	1										
LUMO	0.083607	1									
HOMO	-0.90714	0.062949	1								
Energy gap	0.493447	0.888928	-0.40116	1							
Ionization energy	-0.08361	-1	-0.06295	-0.88893	1						
Electron affinity	0.907144	-0.06295	-1	0.401162	0.062949	1					
Hardness	0.493981	0.888776	-0.40143	0.999976	-0.88878	0.401435	1				
Softness	-0.67148	-0.73186	0.567292	-0.93268	0.731855	-0.56729	-0.93279	1			
Electronegativity	0.320857	-0.90085	-0.48994	-0.60197	0.900849	0.489937	-0.60173	0.393367	1		
Chemical potential	-0.32086	0.900849	0.489937	0.601974	-0.90085	-0.48994	0.60173	-0.39337	-1	1	
Global electrophilicity	-0.31621	-0.91341	0.138856	-0.90279	0.913413	-0.13886	-0.90276	0.891493	0.738469	-0.73847	1

Table 2: Correlation analysis of the docking scores and the orbital descriptors of complexes docked against VP8*

VP8*	Docking score	LUMO	HOMO	Energy gap	Ionization energy	Electron affinity	Hardness	Softness	Electronegativity	Chemical potential	Global electrophilicity
Docking score	1										
LUMO	-0.25633	1									
HOMO	-0.0489	0.044258	1								
Energy gap	-0.10435	0.146529	-0.66489	1							
Ionization energy	0.17116	-0.22863	0.17058	-0.84938	1						
Electron affinity	0.048904	-0.04426	-1	0.664892	-0.17058	1					
Hardness	-0.10579	0.147489	-0.66482	0.999963	-0.84942	0.66482	1				
Softness	0.109323	-0.12967	0.643011	-0.96892	0.82321	-0.64301	-0.96938	1			
Electronegativity	0.184956	-0.22967	-0.47801	-0.33819	0.78389	0.478013	-0.33827	0.328723	1		
Chemical potential	-0.18496	0.229671	0.478013	0.338193	-0.78389	-0.47801	0.338273	-0.32872	-1	1	

Global electrophilicity	0.146804	-0.17691	0.364143	-0.91373	0.947433	-0.36414	-0.91406	0.941363	0.614955	-0.61496	1

CHAPTER SIX

6.0 General discussion, conclusion and recommendations

6.1 General discussion……..…..429

6.2 Conclusion and recommendation……..……...439

References…….....443

6.1 General discussion

Wastewater surveillance of pathogenic viruses enables tracking of enteric viruses' prevalence within a community and supports outbreak prediction via wastewater-based epidemiology (Zahedi *et al*., 2021). This approach relies on analysing community wastewater as an indicator of public health status. Globally, Hepatitis A viruses, Adenoviruses, Astroviruses, Noroviruses, Enteroviruses, Rotaviruses (RVs), Aichi viruses and bacteriophages have been identified in different water matrices (Lanrewaju *et al*., 2022; Chen *et al*., 2021; Corpuz *et al*., 2020). Specifically in South Africa, these viruses have been reported in surface waters (Altintas *et al*., 2015), treated effluent (Sibanda and Okoh, 2013; Okoh *et al*., 2010) and raw sewage (Onosi *et al*., 2019). Generally, PCR-based techniques have been preferred as standard molecular tools for viral detection due to their rapid turnaround and high sensitivity, without the need for cell culture. Unfortunately, PCR-based assays are often vulnerable to inhibitory substances, cannot distinguish between infectious and non-infectious virions, and do not provide comprehensive insights into viral diversity or enable novel pathogens discovery within an ecosystem (Haramoto *et al*., 2018).

Globally, next generation sequencing (NGS), a high-throughput sequencing technique, has transformed molecular approaches for understanding complex microbial communities (Garner *et al*., 2021). Thus, this study adopted metagenomics next generation sequencing (mNGS) approach to characterize the viral diversity and abundance of selected wastewater treatment plants (WWTP1, WWTP2, WWTP3 and WWTP4) and receiving rivers (RIVER2, RIVER3 and RIVER4) in eThekwini Municipality, Durban, South Africa to assess potential community transmission of pathogenic viruses and the impact of effluent discharge on receiving water bodies.

Rotavirus A (RVA) being one of the commonest waterborne enteric viruses detected in this study, is a leading cause of acute gastroenteritis (AGE) in children under five years, responsible for approximately 128, 500 deaths annually and several million hospital admissions globally (Lanrewaju *et al*., 2022; Troeger *et al*., 2018). Despite increased global vaccine coverage, RVA infection continues to be a significant contributor to diarrhoea-related illnesses and fatalities among young children (Cohen *et al*., 2023; Clark *et al*., 2017). At present, no approved antiviral therapy exists for RVA-associated diarrhoea, highlighting the need for new anti-RVA compounds. Although SARS-CoV-2 was not identified in this survey, probably due to low community circulation during sampling, effective therapeutic options remain limited. Although the WHO has authorized several vaccines as a preventive measure, none offers complete protection (Vardhan & Sahoo, 2022). Unfortunately, approved therapeutics are also subject to usage restrictions due to potential adverse effects (Islam *et al*., 2022). Thus, there is an urgent need to develop specialized drugs for COVID-19 to address disease burden and future outbreaks (Wrapp *et al*., 2020).

For about six decades, extensive scientific research has identified several synthetic antiviral medicines that demonstrate efficacy against viral infectious illnesses. Regrettably, these agents have been shown to generate detrimental consequences. These consequences may include neuropsychiatric complications, comprising a continuum of symptoms like irritability and sleep disruptions such as depression, psychosis, painful neuropathy and side effects that may necessitate discontinuing the treatment (Zareifopoulos *et al*., 2020). They may lose their effectiveness against emerging virus strains that have developed resistance (Kurokawa *et al*., 2010). Given the worldwide prevalence of viral infections, drug resistance and the high expense of treatment, it is imperative to develop inexpensive and efficient antiviral medications. Bioactive plant secondary metabolites have demonstrated antiviral activity and can be

combined with pre-existing medicines, as well as other delivery modalities, to improve antiviral efficiency and bioavailability (Kapoor *et al*., 2017). Notably, *Spondias mombin* exhibits significant antiviral activity against coxsackievirus and herpes simplex virus (Siqueira *et al*., 2020; Corthout *et al*., 1991) while *Macaranga barteri* is effective against herpes simplex virus type-1 and suppresses echoviruses E7 and E19 (Segun *et al*., 2019; Ogbole *et al*., 2018). In addition, *Dicerocaryum eriocarpum* has been utilized for wound care, placenta expulsion, antibacterial activity (Luseba *et al*., 2007), anti-inflammatory effects and ethnoveterinary applications (Van der Merwe *et al*., 2001).

Unfortunately, a significant demand for labour, time and rising costs hinder conventional drug discovery pipelines, while the associated costs and lengthy procedures can be reduced via computational techniques in drug discovery and development (Diakou *et al*., 2022). Therefore, this study adopted *in silico* techniques in bioprospecting plant metabolites as modulators of druggable targets of SARS-CoV-2 and RVA. Computational techniques employed in this study such as molecular docking, molecular dynamics simulation and density functional theory, were selected for their proven utility in early-stage drug discovery especially in lead identification from a library of compounds derived from *S. mombin, M. barteri* and *D. eriocarpum*. Furthermore, the antiviral activity of silver-complexed leads showed increased activity compared to individual lead compounds *in silico*. The findings from this study form part of ongoing antiviral-development efforts by identifying silver-complexed leads against VP5* and VP8* of RVA.

6.1.1 Identification of enteric viruses from selected WWTPs (WWTP1, WWTP2, WWTP3 and WWTP4) and receiving river (RIVER2, RIVER3 and RIVER4) in eThekwini Municipality, Durban, South Africa using mNGS

The detection of diverse viral families with a wide range of hosts including vertebrates (19.46%) plants (6.89%), insects (1.90%), fungal (0.13%), unclassified (7.25%) and phages (64.37%) accounting for more than half of the filtered reads suggests the effectiveness of methods from sample collection to downstream processes adopted in this study. These findings confirm WWTPs and receiving rivers as hotspots for diverse viral communities that influence human health, agriculture and ecosystem stability. Similar observations have been reported, with the highest proportion of viral reads linked to vertebrates and bacteria (McCall *et al*., 2023).

Furthermore, this study identified 30 distinct viral families validating that WWTPs obtain water from multiple point and non-point sources, serving as channels for accumulating diverse viral families. The virome shows a division into two ecological signatures across the seven sampling sites, with the WWTPs (WWTP1-4) demonstrating wider taxonomic diversity, including a higher occurrence of ssRNA viruses associated with plants and insects. Human enteric RNA families including *Picornaviridae*, *Caliciviridae*, *Astroviridae* and *Reoviridae* were prevalent in the WWTPs with a notable decline in the receiving rivers, suggesting that the treatment processes are effective, although the viruses were not completely eradicated. Specifically, common human enteric viruses like Enteroviruses A, B, C, Hepatovirus A, Rotavirus A, Norwalk virus, the emerging neurotropic HMO Astrovirus A (VA1, linked to lethal encephalitis in neonates and immunocompromised patients) and lesser-known pathogens like Cytomegalovirus were detected across wastewater and river samples, emphasizing the

significance of wastewater surveillance in providing insights into community health status. This is consistent with earlier studies reporting human pathogenic viruses in sewage and rivers (Li *et al*., 2024; Tisza *et al*., 2023; Lu *et al*., 2022; Guerrero-Latorre *et al*., 2018).

Conversely, most viral phytopathogenic species detected across the sampling sites were of the *Virgaviridae* family and Tobamovirus genus (Tomato mosaic virus, Tobacco mild green mosaic virus, Pepper mild mottle virus), while emerging pathogens (Cucumber mosaic virus, Tomato brown rugose fruit virus) were less frequent but remain significant due to their economic importance in agriculture. The detection of the *Virgaviridae* family as the most abundant plant viral family might be due to the high number of the *Virgaviridae* reads, which may have introduced a sequencing toward this family, in agreement with previous studies (Cuevas-Ferrando *et al*., 2025; Lopez-Roblero *et al*., 2024).

These findings highlight the significance of wastewater surveillance in tracking known infections and unveiling emerging viral threats. Similarly, wastewater-based surveillance techniques can be used to monitor plant pathogenic viruses in agriculture to detect, study and curb viral spread to prevent decline in plant yields and accompanying economic losses. While Rotavirus A was detected as one of the common human enteric viral threats identified in this study, SARS-CoV-2 was undetected, likely due to low circulation during sampling, reflecting the community health status. Nevertheless, there is a need to prioritize the discovery of antiviral drug candidates as countermeasures ahead of future viral pandemics.

6.1.2 Metabolites profiling and identification of lead compounds from selected medicinal plants against druggable targets of SARS-CoV-2 and RVA using *in silico* methods

This part of the study focused on the metabolite profiling of the selected medicinal plants (*S. mombin, M. barteri* and *D. eriocarpum*) using untargeted liquid chromatography–quadrupole time-of-flight tandem mass spectrometry (LC-QTOF-MS/MS), which revealed 77 distinct secondary metabolites across the three species. The pooled metabolites were then screened *in silico* against SARS-CoV-2 [main protease and RdRp] and RVA [capsid protein (VP7A, VP7C, VP7D), RdRp (VP1), spike protein (VP5*, VP8*)] for the identification of lead compounds. The identification of the top 20 metabolites with higher negative docking scores against each of the investigated targets compared to the reference standards (Zafirlukast, Cefoperazone, Remdesivir, Tizoxanide and Sofosbuvir) suggests the effectiveness of the docking method applied to the 77 pooled metabolites from the selected medicinal plants. However, only nine metabolites had higher negative docking scores relative to the reference standard against SARS-CoV-2 main protease. The observed higher negative docking scores of the top metabolites suggest improved binding within the target regions of SARS-CoV-2 and RVA and support their potential as drug candidates. Thereafter, a minimum of three top-ranked metabolites were identified owing to their physicochemical, pharmacokinetic and toxicological profiles suitable for drug development.

The observed features in the top-ranked compounds suggest their potential oral bioavailability and ability to reach druggable targets, exert pharmacological effects and exhibit reduced toxicity. Previous studies have documented these features in molecules that progressed successfully through the preclinical and clinical phases of drug development (Mousavi *et al*., 2021; Sabe *et al*., 2021; Reichel and Lienau, 2016; Lipinski *et al*., 2001). However, molecular docking has several shortcomings, including flexibility challenges, inadequate resolutions of crystallographic targets, pseudo-positive binding conformations, difficulties in quantifying hydrogen bonding accurately, directional interactions, effects of solvent and entropy (Kitchen

et al., 2004, Taylor *et al*., 2002). To address these limitations, molecular dynamics simulation, was employed to provide insight into the stability, fluctuation, compactness, interatomic interactions and binding free energies of the top-ranked protein-ligand complexes (Menchon *et al*., 2018).

At least three of the top five compounds exhibited higher negative binding free energy against each of the evaluated druggable targets suggesting that the compounds are structurally and thermodynamically compatible at the binding domain of these targets indicating their suitability for drug development, consistent with previous antiviral reports (Aribisala *et al*., 2022; Uhomoibhi *et al*., 2022), and further validates the antiviral potential of the examined medicinal plants. However, for the SARS-CoV-2 main protease, only quercetin 3-O-rhamnoside exhibited higher negative binding free energy indicating the need to optimize other metabolites while broadening main-protease targeted leads.

Overall, the identified lead compounds, especially those with higher negative binding free energies, are relatively thermodynamically stable and form structurally compatible complexes. In cases where their thermodynamic metrics exceeded those of the reference standard, they remained within the less than 3.0 Å limit for acceptable deviation (Ramirex and Caballero, 2016). This stability may be attributed to the greater frequency of hydrogen-bond contacts and other significant interactions of the lead compounds during the 120-ns MD simulation, as highlighted in previous studies as critical factors in drug discovery (Du *et al*., 2016; Kretschmer *et al*., 2010). Notably, chrysoeriol7-glucuronide and spiraeoside demonstrated broad-spectrum affinity for the RNA-dependent RNA polymerase (RdRp) of SARS-CoV-2 and RVA VP1, outperforming the reference standard. Furthermore, 2SG and sericetin showed stronger broad-

spectrum affinity for both RVA VP5* and VP8*, while 2SG, apigenin-4 ′-glucoside and gnetin L exhibited better broad-spectrum affinities for RVA VP7A, VP7C and VP7D relative to the reference standard. These findings align with previous reports (Yi *et al.*, 2024; Aribisala *et al*., 2022), and suggest their potential as multitarget antiviral candidates.

Despite the promising characteristics exhibited by some of these compounds, higher thermodynamic metrics associated with the resulting complexes of certain compounds, particularly those surpassing the reference standard, may indicate an increased induction of thermodynamic entropy within the target proteins. For example, against VP5*, 2SG, sericetin and sacranoside, despite having higher negative binding free energies, exhibited higher RMSD and RMSF values compared to the standard and unbound VP5*. Similarly, against VP8*, sericetin, despite having higher negative binding free energies, exhibited a higher RMSD value compared to the standard and unbound VP8*. These observations highlight the need to optimize these leads to improve stability while enhancing their affinity for the target proteins. Therefore, a silver complexation approach was used to model possible silver nanoparticle conjugates for each lead compound, treating the compound as the reducing and capping agent to enhance their binding affinity for RVA VP5* and VP8* through *in silico* modelling.

6.1.3 *In silico* antiviral potential of silver-complexed leads against the spike protein of rotavirus A

Despite their promising antiviral potential, one of the primary challenges associated with developing natural compounds into drugs is their low solubility, bioavailability and toxicity following bioactivation (Giordano *et al*., 2023; Ponticelli *et al*., 2023). Consequently, this has renewed interest in nanotechnology, particularly in the development of advanced drug delivery

systems that maintain optimal drug concentration at target sites, reducing dosing frequency, enhance bioavailability, limit drug metabolism, inhibit cellular efflux mechanisms and improve targeted delivery (Pradhan *et al*., 2021). Demonstrating this *in silico* entails conjugating bioactive metal ions such as silver with organic ligands. This approach enhances activity through the combined effects, mitigates drug resistance, extends the spectrum of action and reduces the required dosage, as previously reported (Kucuk *et al*., 2022).

Of all investigated targets, RVA entry into the host cell is primarily mediated by the spike protein VP4 cleavage products; VP5* and VP8* (Omatola and Olaniran, 2022). Specifically, VP5* is responsible for membrane penetration (Kumar *et al*., 2020), while VP8* plays a key role in viral attachment and infection (Li *et al*., 2021). Furthermore, VP7 neutralizing antibodies production (Nyaga *et al*., 2020), while VP1 is essential for viral replication and transcription (Tohmé and Delgui 2021). Similarly, both RdRp and the main protease of SARS-CoV-2 are involved in viral replication (Eltayb *et al*., 2023; Elfiky, 2020). Due to their critical roles in viral entry and early infection, silver complexation optimization was focused on VP5* and VP8* to target this initial and vulnerable stage. The previously identified lead compounds targeting VP5* and VP8* were subsequently complexed with silver to evaluate changes in toxicity and pharmacokinetic profiles, reactivity and binding affinity accordingly.

Notably, conjugating silver to the VP5* and VP8* lead compounds largely preserved their pharmacokinetics and toxicity profiles except in a few cases due to increased molecular weight, an increase in hydrogen bond donors from 5 to 6, and the conversion of a double bonds to single bonds following silver coordination involving oxygen atoms (Van Santen *et al*., 2015). Furthermore, the frontier molecular orbitals of the silver-complexed leads were examined using

density functional theory and compared with those of the lead compounds. Interestingly, all the lead compounds exhibited higher energy gaps than their respective silver complexes, suggesting greater reactivity of the silver-complexed leads relative to their corresponding lead compounds. Silver complexation resulted in reduced energy gaps, increasing molecular softness while enhancing their heavy electrophiles' status, suggesting their ability to exchange electrons more readily, translating to a stronger affinity for the target. This observation agrees with previous findings reporting higher energy gaps in parent compounds compared to their silver complexes (Kucuk 2023).

Moreover, higher negative docking scores observed in the silver-complexed leads of the 2SG and SER series against VP5* and VP8* relative to the corresponding lead molecules may be attributed to enhanced molecular rigidity and stability of the ligand, decreasing its flexibility and improved fit within the receptor binding domain following silver complexation. This is consistent with a previous study showing more negative docking scores following silver complexation (Hkiri *et al*., 2022). However, lower negative docking scores were observed in some sacranoside derivatives against VP5*, and in all APG-silver complexes and some gnetin L-silver complexes against VP8*. This observation agrees with a previous study where silver complexation reduced the affinity of the complexes (Siqueira *et al*., 2021). This reduced binding affinity may be associated with spatial constraints arising from silver coordination interfering with docking compared to the unbound compound void of silver. Notably, a positive score observed in gnetin L C (GNEC) against VP8* may result from the inability of the silver complex to bind effectively within the receptor binding domain.

Higher negative docking scores observed in the derivatives relative to the parent compound may be attributed to the number of interactions and, more importantly, their interactions with the active site residues. Overall, the findings indicate that 2SGC and 2SGA, as well as 2SGC and SERA are the most promising silver-complexed leads based on their molecular properties, pharmacokinetics and toxicity profiles, docking scores and interaction profiles against VP5* and VP8* respectively.

6.2 Conclusions and recommendations

Waterborne enteric viruses, which are mostly transmitted by the faecal-oral channel, either through direct contact between individuals or by consuming contaminated water or food, may provide a significant health risk to workers at WWTPs and the surrounding community. Thus, regular wastewater surveillance is critical and imperative in tracking known infections and unveiling possible emerging viral threats. Given the worldwide prevalence of viral infections, development of resistance to conventional drugs and the high expense of treatment, it is imperative to urgently devise novel approaches to identify inexpensive and efficient antiviral medications. Thus, this study adopted mNGS approach to provide insights on the possible ongoing community transmission of pathogenic viruses in eThekwini Municipality, Durban, South Africa and contributes to the ongoing initiative to design antiviral therapeutics against SARS-CoV-2 and RVA.

The mNGS viral surveillance investigation of WWTP1, WWTP2, WWTP3 and WWTP4 and RIVER2, RIVER3 and RIVER4 in eThekwini Municipality, Durban, South Africa identified diverse viral families with a wide range of hosts including vertebrates (19.46%), plant (6.89%), insect (1.90%), fungal (0.13%), unclassified (7.25%) and phages (64.37%). These findings

confirm WWTPs and receiving rivers as hotspots for diverse viral communities that influence human health, agriculture and ecosystem stability. This study identified 30 different viral families, revealing two ecological signatures across the seven different sampling sites, as the WWTPs demonstrate wider taxonomic diversity relative to their receiving rivers. Specifically, common human enteric viruses like Enteroviruses A, B, C, Hepatovirus A, Rotavirus A, Norwalk virus, the emerging neurotropic HMO Astrovirus A (VA1, linked to lethal encephalitis in neonates and immunocompromised patients) and lesser-known pathogens like Cytomegalovirus were detected across wastewater and river samples, emphasizing the significance of wastewater surveillance in providing insights on the health status of a community.

Most viral phytopathogenic species detected across the sampling sites were of the *Virgaviridae* family and Tobamovirus genus (Tomato mosaic virus, Tobacco mild green mosaic virus, Pepper mild mottle virus), emerging pathogens (Cucumber mosaic virus, Tomato brown rugose fruit virus) were less frequent but significant owing to their economic importance in agriculture. These findings highlight the significance of wastewater surveillance in tracking known infections and unveiling possible emerging viral threats. Similarly, wastewater-based surveillance techniques might be used to track plant pathogenic viruses in agriculture to detect, study and curb viral spread to prevent potential decreases in plant yields and accompanying economic losses.

While the mNGS approach employed in this study was confined to March-June, it revealed a snapshot of the viral diversity for the investigated sites, absolute concentrations and information on the infectivity status of the detected viruses were not provided, which could

have further guided targeted intervention. Thus, it is recommended that quantitative and infectivity assays be integrated in subsequent year-round studies to provide insights that can guide in safeguarding human health and agricultural productivity.

Considering the detection of pathogenic viruses in this study from the surveyed WWTPs and receiving rivers, there is a need to prioritize the discovery of antiviral drug candidates ahead of time as countermeasures before the next viral pandemic. A significant demand for labour, time and rising costs are obstacles to conventional drug discovery pipelines; however, the associated costs and lengthy procedures can be significantly reduced via computational techniques in drug discovery and development. The lead compounds, especially those with higher negative binding free energies identified from the *in silico* screening of the 77 pooled metabolites from the selected medicinal plants (*S. mombin*, *M. barteri* and *D. eriocarpum*), are relatively thermodynamically stable and form structurally compatible complexes. These compounds, ranging from a minimum of three top-ranked metabolites screened from the 20 metabolites with higher negative docking scores against investigated targets of SARS-CoV-2 and RVA, owing to their physicochemical, pharmacokinetic and toxicological profiles, are suitable for drug development. They are considered orally bioavailable with the potential to reach druggable targets and exert pharmacological effects with reduced toxicity, which further validates the antiviral activity of the selected medicinal plants. Nevertheless, against VP5*, 2SG, sericetin and sacranoside, despite having higher negative binding free energies, exhibited higher RMSD and RMSF values than the standard and unbound VP5*.

Similarly, against VP8*, sericetin and 2SG, despite having higher negative binding free energies, have higher RMSD and RMSF values, respectively, compared to the standard and

unbound VP8*. This observation highlights the need for optimizing these leads to improve their characteristics while boosting their affinity for the target proteins. While the lead compounds with higher negative binding free energy against VP5* and VP8* were optimized via the silver complexation approach, it is recommended that other lead compounds with higher binding free energy against other targets be investigated as outlined below. Notably, chrysoeriol7-glucuronide and spiraeoside demonstrated broad-spectrum affinity for the RNA-dependent RNA polymerase (RdRp) of SARS-CoV-2 and RVA VP1, outperforming the reference standard. Furthermore, 2SG and sericetin had better broad-spectrum affinities for both RVA VP5* and VP8* while 2SG, apigenin-4 ′-glucoside and gnetin L exhibited better broad-spectrum affinities for RVA VP7A, VP7C and VP7D. Exploration of these lead compounds via silver complexation may identify novel complexes with improved activity and as multitarget antiviral candidates.

Conjugating silver to the VP5* and VP8* lead compounds of did not affect their pharmacokinetics and toxicity negatively except in few cases owing to increased molecular weight, increased number of hydrogen bond donors from five to six, conversion of a double bond to a single bond through the attachment of silver metal described as a coordination interaction or complexation reaction involving the oxygen and silver metal. Moreover, the lead compounds exhibited higher energy gaps relative to the derivatives, suggesting a higher reactivity status of the silver complexed compounds relative to their corresponding parent compound. In essence, silver complexation reduces energy gaps, boosting softness while enhancing the heavy electrophiles' position, suggesting their ability to exchange electrons unhindered, translating to a stronger affinity for the target.

Generally, higher negative docking scores observed in the silver-complexed leads relative to the lead compounds might be attributed to the number of observed interactions and, more importantly, interactions with the active site residues. Overall, this study showed that 2SGC and 2SGA, as well as 2SGC and SERA are better possible silver-complexed leads considering their molecular properties, pharmacokinetics and toxicity profiles, docking scores and number of interactions against VP5* and VP8* respectively. However, there is a need for further computational investigation, including molecular dynamics simulation, to provide insights into the thermodynamics profile of the resulting protein and silver-complexed leads.

Summarily, the observed enhanced binding capability of the best derivatives could be attributed to their higher reactivity and increased interactions with essential amino acids at the binding pocket of the investigated targets. Ultimately, complementary *in vitro* and *in vivo* assessments are required to confirm the antiviral potential of these silver-complexed leads, alongside further evaluation of their pharmacokinetic properties and optimization of delivery strategies to support potential real-world application.

References

ALTINTAS, Z., GITTENS, M., POCOCK, J. & TOTHILL, I. E. 2015. Biosensors for waterborne viruses: detection and removal. *Biochimie*, 115, 144-154.

ARIBISALA, J. O., ARUWA, C. E., UTHMAN, T. O., NURAIN, I. O., IDOWU, K. & SABIU, S. 2022. Cheminformatics bioprospection of broad spectrum plant secondary metabolites targeting the spike proteins of Omicron variant and wild-type SARS-CoV-2. *Metabolites*, 12(982), 1-26.

CHEN, L., DENG, Y., DONG, S., WANG, H., LI, P., ZHANG, H. & CHU, W. 2021. The occurrence and control of waterborne viruses in drinking water treatment: a review. *Chemosphere*, 281(130728), 1-11.

CLARK, A., BLACK, R., TATE, J., ROOSE, A., KOTLOFF, K., LAM, D., BLACKWELDER, W., PARASHAR, U., LANATA, C. & KANG, G. 2017. Estimating global, regional and national rotavirus deaths in children <5 years: approaches, analyses and improvements. *PLoS One*, 12(9), 1-18.

COHEN, R., MARTINÓN TORRES, F., POSIUNIENE, I., BENNINGHOFF, B., OH, K. B. & POELAERT, D. 2023. The value of rotavirus vaccination in Europe: a call for action. *Infectious Diseases and Therapy*, 12(1), 9-29.

CORPUZ, M. V. A., BUONERBA, A., VIGLIOTTA, G., ZARRA, T., BALLESTEROS JR, F., CAMPIGLIA, P., BELGIORNO, V., KORSHIN, G. & NADDEO, V. 2020. Viruses in wastewater: occurrence, abundance and detection methods. *Science of the Total Environment*, 745(140910), 1-26.

CORTHOUT, J., PIETERS, L., CLAEYS, M., VAN BERGHE, D. V. & VLIETINCK, A. 1991. Antiviral ellagitannins from *Spondias mombin*. *Phytochemistry*, 30(4), 1129–1130.

CUEVAS-FERRANDO, E., SÁNCHEZ, G. & PÉREZ-CATALUÑA, A. 2025. Exploring plant virus diversity in wastewater and reclaimed water through metagenomic analysis. *Water Research*, 270, 1-9.

DIAKOU, I., PAPAKONSTANTINOU, E., PAPAGEORGIOU, L., PIEROULI, K., DRAGOUMANI, K., SPANDIDOS, D. A., BACOPOULOU, F., CHROUSOS, G. P., ELIOPOULOS, E. & VLACHAKIS, D. 2022. Novel computational pipelines in antiviral structure-based drug design. *Biomedical Reports*, 17, 1-5.

DU, X., LI, Y., XIA, Y. L., AI, X. M., LIANG, J., SANG, P., JI, X. L. & LIU, S. Q. 2016. Insights into protein-ligand interactions: mechanisms, models, and methods. *International Journal of Molecular Sciences*, 17(144), 1-34.

ELFIKY, A. A. 2020. Ribavirin, remdesivir, sofosbuvir, galidesivir and tenofovir against SARS-CoV-2 RNA-dependent RNA polymerase (RdRp): a molecular docking study. *Life Sciences*, 253, 1-8.

ELTAYB, W. A., ABDALLA, M. & RABIE, A. M. 2023. Novel investigational anti-SARS-CoV-2 agent ensitrelvir "S-217622": a very promising potential universal broad-spectrum antiviral at the therapeutic frontline of coronavirus species. *ACS Omega*, 8(6), 5234-5246.

GARNER, E., DAVIS, B. C., MILLIGAN, E., BLAIR, M. F., KEENUM, I., MAILE-MOSKOWITZ, A., PAN, J., GNEGY, M., LIGUORI, K. & GUPTA, S. 2021. Next generation sequencing approaches to evaluate water and wastewater quality. *Water Research*, 194, 1-24.

GIORDANO, D., FACCHIANO, A. & CARBONE, V. 2023. Food plant secondary metabolites antiviral activity and their possible roles in SARS-CoV-2 treatment: an overview. *Molecules*, 28(2470), 1-29.

GUERRERO-LATORRE, L., ROMERO, B., BONIFAZ, E., TIMONEDA, N., RUSIÑOL, M., GIRONES, R. & RIOS-TOUMA, B. 2018. Quito's virome: metagenomic analysis of viral diversity in urban streams of Ecuador's capital city. *Science of the Total Environment*, 645, 1334-1343.

HARAMOTO, E., KITAJIMA, M., HATA, A., TORREY, J. R., MASAGO, Y., SANO, D. & KATAYAMA, H. 2018. A review on recent progress in the detection methods and prevalence of human enteric viruses in water. *Water Research*, 135, 168-186.

HKIRI, S., COŞKUN, K. A., ÜSTÜN, E., SAMARAT, A., TUTAR, Y., ŞAHIN, N. & SÉMERIL, D. 2022. Silver(I) complexes of oxadiazole-functionalized α-aminophosphonates: synthesis, structure and biological activity. *Molecules*, 27(23), 1-15.

ISLAM, T., HASAN, M., RAHMAN, M. S. & ISLAM, M. R. 2022. Comparative evaluation of authorized drugs for treating COVID-19 patients. *Health Science Reports*, 5(4) 1-9.

KAPOOR, R., SHARMA, B. & KANWAR, S. 2017. Antiviral phytochemicals: an overview. *Biochemistry & Physiology*, 6, 1-7.

KITCHEN, D. B., DECORNEZ, H., FURR, J. R. & BAJORATH, J. 2004. Docking and scoring in virtual screening for drug discovery: methods and applications. *Nature Reviews Drug Discovery*, 3, 935-949.

KRETSCHMER, R., KINZEL, D. & GONZÁLEZ, L. 2010. The role of hydrogen bonds in protein-ligand interactions: DFT calculations in 1,3-dihydrobenzimidazole-2-thione derivatives with glycinamide as model HIV RT inhibitors. *International Journal of Quantum Chemistry*, 112, 1787-1795.

KUCUK, C. 2023. Silver nitrate complex of 5-benzimidazole carboxylic acid: synthesis, DFT, and docking as targeted anticancer agent. *Journal of Molecular Structure*, 1293, 1-14.

KUCUK, C., YURDAKUL, S., CELIK, S. & ERDEM, B. 2022. Experimental and DFT studies of 2-methyl quinoxaline and its silver(I) complex: noncovalent interactions, antimicrobial and docking. *Inorganic Chemistry Communications*, 145, 1-15.

KUMAR, D., SINGH, A., KUMAR, P., UVERSKY, V. N., RAO, C. D. & GIRI, R. 2020. Understanding the penetrance of intrinsic protein disorder in rotavirus proteome. *International Journal of Biological Macromolecules*, 144, 892-908.

KUROKAWA, M., SHIMIZU, T., WATANABE, W. & SHIRAKI, K. 2010. Development of new antiviral agents from natural products. *The Open Antimicrobial Agents Journal*, 2, 49-57.

LANREWAJU, A. A., ENITAN-FOLAMI, A. M., SABIU, S., EDOKPAYI, J. N. & SWALAHA, F. M. 2022. Global public health implications of human exposure to viral contaminated water. *Frontiers in Microbiology*, 13, 1-18.

LI, D., WANG, M, QI, J., ZHANG, Q., WANG, H., PANG, L., SUN, X. & DUAN, Z. 2021. Human group A rotavirus P[25] VP8* specifically binds to A-type histo-blood group antigen. *Virology*, 555, 56-63.

LI, Y., MIYANI, B., FAUST, R. A., DAVID, R. E. & XAGORARAKI, I. 2024. A broad wastewater screening and clinical data surveillance for virus-related diseases in the metropolitan Detroit area in Michigan. *Human Genomics*, 18(14), 1-18.

LIPINSKI, C. A., LOMBARDO, F. & DOMINY, B. W. 2001. Experimental and computational approaches to estimate solubility and permeability in drug discovery and development settings. *Advanced Drug Delivery Reviews*, 46, 3-26.

LOPEZ-ROBLERO, A., MARTÍNEZ CANO, D. J., DIEGO-GARCÍA, E., GUILLÉN-NAVARRO, G. K., IŠA, P. & ZARZA, E. 2024. Metagenomic analysis of plant viruses in tropical fresh and wastewater. *Environmental DNA*, 6(416), 1-13.

LU, J., YANG, S., ZHANG, X., TANG, X., ZHANG, J., WANG, X., WANG, H., SHEN, Q. & ZHANG, W. 2022. Metagenomic analysis of viral community in the Yangtze River expands known eukaryotic and prokaryotic virus diversity in freshwater. *Virologica Sinica*, 37, 60-69.

LUSEBA, D., ELGORASHI, E., NTLOEDIBE, D. & VAN STADEN, J. 2007. Antibacterial, anti-inflammatory and mutagenic effects of some South African medicinal plants used

for wounds and retained placenta in livestock. *South African Journal of Botany*, 73(3), 378–383.

MCCALL, C., LEO ELWORTH, R. A., WYLIE, K. M., WYLIE, T. N., DYSON, K., DOUGHTY, R., TREANGEN, T. J., HOPKINS, L., ENSOR, K. & STADLER, L. B. 2023. Targeted metagenomic sequencing for detection of vertebrate viruses in wastewater for public health surveillance. *ACS ES&T Water*, 3(9), 2955-2965.

MENCHON, G., MAVEYRAUD, L. & CZAPLICKI, G. 2018. Molecular dynamics as a tool for virtual ligand screening. *Computational Drug Discovery and Design*, 1762, 145-178.

MOUSAVI, S. S., KARAMI, A., HAGHIGHI, T. M., TUMILAAR, S. G., IDROES, R., MAHMUD, S., CELIK, I., AĞAĞÜNDÜZ, D., TALLEI, T. E., EMRAN, T. B. & CAPASSO, R. 2021. *In silico* evaluation of Iranian medicinal plant phytoconstituents as inhibitors against main protease and the receptor-binding domain of SARS-CoV-2. *Molecules*, 26(5724), 1-23.

NYAGA, M. M., SABIU, S., NDZE, V. N., DENNIS, F. E. & JERE, K. C. 2020. Report of the 1st African Enteric Viruses Genome Initiative (AEVGI) data and bioinformatics workshop on whole-genome analysis of some African rotavirus strains held in Bloemfontein, South Africa. Vaccine, 38(34), 5402-5407.

OGBOLE, O. O., AKINLEYE, T. E., SEGUN, P. A., FALEYE, T. C. & ADENIJI, A. J. 2018. *In vitro* antiviral activity of twenty-seven medicinal plant extracts from southwest Nigeria against three echovirus serotypes. *Virology Journal*, 15(1), 1-8.

OKOH, A. I., SIBANDA, T. & GUSHA, S. S. 2010. Inadequately treated wastewater as a source of human enteric viruses in the environment. *International Journal of Environmental Research and Public Health*, 7, 2620-2637.

OMATOLA, C. A. & OLANIRAN, A. O. 2022. Rotaviruses: from pathogenesis to disease control—a critical review. *Viruses*, 14(5), 1-34.

ONOSI, O., UPFOLD, N. S., JUKES, M. D., LUKE, G. A. & KNOX, C. 2019. The first molecular detection of Aichi virus 1 in raw sewage and mussels collected in South Africa. *Food and Environmental Virology*, 11, 96-100.

PONTICELLI, M., BELLONE, M. L., PARISI, V., IANNUZZI, A., BRACA, A., DE TOMMASI, N., RUSSO, D., SILEO, A., QUARANTA, P. & FREER, G. 2023. Specialized metabolites from plants as a source of new multi-target antiviral drugs: a systematic review. *Phytochemistry Reviews*, 22, 615-693.

PRADHAN, D., BISWASROY, P., GOYAL, A., GHOSH, G. & RATH, G. 2021. Recent advancement in nanotechnology-based drug delivery system against viral infections. AAPS *PharmSciTech*, 22, 1-19.

RAMIREX, D. & CABALLERO, J. 2016. Is it reliable to use common molecular docking methods for comparing the binding affinities of enantiomer pairs for their protein target. *International Journal of Molecular Sciences*, 17, 525-545.

REICHEL, A. & LIENAU, P. 2016. Pharmacokinetics in drug discovery: an exposure-centred approach to optimising and predicting drug efficacy and safety. *Handbook of Experimental Pharmacol*ogy, 232, 235-260.

SABE, V. T., NTOMBELA, T., JHAMBA, L. A., MAGUIRE, G. E., GOVENDER, T., NAICKER, T. & KRUGER, H. G. 2021. Current trends in computer aided drug design and a highlight of drugs discovered via computational techniques: a review. *European Journal of Medicinal Chemistry*, 224, 1-21.

SEGUN, P. A., OGBOLE, O. O., AKINLEYE, T. E., FALEYE, T. O. & ADENIJI, A. J. 2019. In vitro anti-enteroviral activity of stilbenoids isolated from the leaves of *Macaranga barteri*. *Natural Product Research*, 33, 1-5.

SIBANDA, T. & OKOH, A. I. 2013. Real-time PCR quantitative assessment of hepatitis A virus, rotaviruses and enteroviruses in the Tyume River located in the Eastern Cape Province, South Africa. *Water SA*, 39, 295-304.

SIQUEIRA, E. M. D. S., LIMA, T. L., BOFF, L., LIMA, S. G., LOURENÇO, E. M., FERREIRA, É. G., BARBOSA, E. G., MACHADO, P. R., FARIAS, K. J. & FERREIRA, L. D. S. 2020. Antiviral potential of *Spondias mombin* leaves extract against herpes simplex virus type 1: *in vitro* and *in silico* approaches. *Planta Medica*, 86(7), 505-515.

SIQUEIRA, F. S., ALVES, C. F. S., MACHADO, A. K., SIQUEIRA, J. D., SANTOS, T. D., MIZDAL, C. R., MOREIRA, K. S., TEIXEIRA CARVALHO, D., BONEZ, P. C. & URQUHART, C. G. 2021. Docking, quorum quenching, antibiofilm and safety profile of silver complexed sulfonamide on *Pseudomonas aeruginosa*. *Biofouling*, 37(5), 555-571.

TAYLOR, R. D., JEWSBURY, P. J. & ESSEX, J. W. 2002. A review of protein-small molecule docking methods. *Journal of Computer-Aided Molecular Design*, 16, 151-166.

TISZA, M., JAVORNIK CREGEEN, S., AVADHANULA, V., ZHANG, P., AYVAZ, T., FELIZ, K., HOFFMAN, K. L., CLARK, J. R., TERWILLIGER, A. & ROSS, M. C. 2023. Wastewater sequencing reveals community and variant dynamics of the collective human virome. *Nature Communications*, 14(6878), 1-10.

TOHMÉ, M. J. & DELGUI, L. R. 2021. Advances in the development of antiviral compounds for rotavirus infections. *mBio*, 12(3), e00111-21.

TROEGER, C., KHALIL, I. A., RAO, P. C., CAO, S., BLACKER, B. F., AHMED, T., ARMAH, G., BINES, J. E., BREWER, T. G. & COLOMBARA, D. V. 2018.

Rotavirus vaccination and the global burden of rotavirus diarrhea among children younger than 5 years. *JAMA Pediatrics*, 172, 958-965.

UHOMOIBHI, J., IDOWU, K., SHODE, F. & SABIU, S. 2022. Molecular modeling identification of potential drug candidates from selected African plants against SARS-CoV-2 key druggable proteins. *Scientific African*, 17, 1-11.

VAN DER MERWE, D., SWAN, G. & BOTHA, C. 2001. Ethnoveterinary medicinal plant use in cattle by Setswana-speaking people in the Madikwe area, North-West Province, South Africa. *Journal of the South African Veterinary Association*, 72(4), 189–196.

VAN SANTEN, R. A., TRANCA, I. & HENSEN, E. J. 2015. Theory of surface chemistry and reactivity of reducible oxides. *Catalysis Today*, 244, 63-84.

VARDHAN, S. & SAHOO, S. K. 2022. Computational studies on the interaction of SARS-CoV-2 Omicron SGp RBD with human receptor ACE2, limonin and glycyrrhizic acid. *Computers in Biology and Medicine*, 144(105367), 1-8.

WRAPP, D., DE VLIEGER, D., CORBETT, K. S., TORRES, G. M., WANG, N., VAN BREEDAM, W., ROOSE, K., VAN SCHIE, L., HOFFMANN, M., PÖHLMANN, S., GRAHAM, B. S., CALLEWAERT, N., SCHEPENS, B., SAELENS, X., MCLELLAN, J. S. & VIB-CMB COVID-19 Response Team. 2020. Structural basis for potent neutralization of betacoronaviruses by single-domain camelid antibodies. *Cell*, 181(5), 1004-1015.

YI, Y., YU, R., XUE, H., JIN, Z., ZHANG, M., BAO, Y.-O., WANG, Z., WEI, H., QIAO, X. & YANG, H. 2024. Chrysin 7-O-β-D-glucuronide, a dual inhibitor of SARS-CoV-2 3CLpro and PLpro, for the prevention and treatment of COVID-19. *International Journal of Antimicrobial Agents*, 63, 1-6.

ZAHEDI, A., MONIS, P., DEERE, D. & RYAN, U. 2021. Wastewater-based epidemiology—surveillance and early detection of waterborne pathogens with a focus on SARS-CoV-2, Cryptosporidium and Giardia. *Parasitology Research*, 120(12), 4167-4188.

ZAREIFOPOULOS, N., LAGADINOU, M., KARELA, A., KYRIAKOPOULOU, O. & VELISSARIS, D. 2020. Neuropsychiatric effects of antiviral drugs. *Cureus*, 12(8), 1-12.